The University Of Sheffield.

Radiosensitising agents for non-small cell lung cancer (NSCLC)

By:

Thomas Luke Jones

A thesis submitted in partial fulfilment of the requirements for the degree of
Doctor of Philosophy

The University of Sheffield
Faculty of Medicine, Dentistry and Health
Department of Oncology and Metabolism

April 2019

Acknowledgments

I would firstly like to thank Dr Helen Bryant for her constant support, guidance and mentorship throughout the PhD, I leave the lab a far superior scientist and much of this is due to her. Furthermore, this work wouldn't have been achievable without her incessant drive and determination. I think she would agree that we made a good partnership and I will keep a favorable eye on any developments from the Bryant lab.

I would also like to thank Prof Sarah Danson and Prof Matthew Hatton for their brilliant clinical expertise to support a patient study as part of my PhD. It wasn't easy not always having the answer to clinical and logistical questions, but Sarah and Matthew's enduring support meant that no obstacle couldn't be overcome. I hope they enjoyed our collaboration as much as I did.

I express my gratitude to Yorkshire Cancer Research and all of its donors for funding this research project. Me and Helen have experienced firsthand how painstaking fundraising can be, so enormous credit is due.

I thank Dr Spencer Collis for his penetrating questions and advice in many a lab meeting, he is owed credit for many successful experiments. Additionally, I would like to express my gratitude to Dr Karen Sisley and Dr Sally Thomas for the opportunity of work whilst I was writing my thesis.

I must give credit to all my excellent and talented colleagues from the Bryant, Collis and Thompson labs. Your friendship and support, especially through the most stressful times, made coming to work a pleasure. I would like to thank Luke, Fatma, Leona, Callum, Hannah, Christian, Charlotte, Clair, Rachel, Connor and Nikita for their valuable friendship. Hannah, the Queen of IHC, needs mention for her help in

analyzing *in vivo* tumour tissues. Extra special mentions to Emma, Chris, Polly, Katie, Ola and Natasha for their sarcasm and support. Extra extra special mentions to David and Dan for their enduring friendship and wit, reveling in the lows of science has never been so much fun. I wish them all the best for the future.

I need to thank Prof Gill Tozer and Dr Will English for their excellent expertise and advice regarding our *in vivo* work. I would also like to thank their lab members Jack and Ruth for their support and friendship. Lastly, I must pay credit to the brilliant Matt Fisher, whom without much of the *in vivo* work in this thesis would not have been possible. Matt, thanks for being a patient and wise teacher and for going above and beyond your duties in collaboration with me and Helen. It was steep a learning curve but was never as daunting with you in our corner.

Honorable mentions also go to Janet Horsman, Carol Crabtree and Greg Wells for their support associated with the clinical study of this PhD project. Greg, in particular, was a vital source of advice and friendship. Gill Brown and the western park hospital research radiography team also deserve immense credit. Without their hard work consenting patients the clinical study would not have been able to flourish, there is no amount of chocolates that can repay my debt to them. Maggie Glover of the histology lab is also needing of mention. Maggie has created a welcoming, efficient and knowledgeable set-up for IHC and made endless tissue staining both generally successful and pleasant. Dr Jonathan Bury and Tracy Sanderson also contributed greatly to the optimisation of patient sample IHC staining.

As ever, I owe to my everlasting support from my parents. Everything I achieve is due to them. And finally, I pay tribute to my loving girlfriend Antonia. You provided sanctuary after the hardest of days and your consistent warmth and encouragement

is always appreciated, even when I’m too grumpy to mention it. Some would argue that the biggest reward for coming to Sheffield was the PhD, I would argue it was finding you.

Abstract

Over 60% of non-small cell lung cancer (NSCLC) patients receive radiotherapy, however outcomes are limited by tumour resistance and normal tissue toxicity. The mitotic kinase aurora kinase A (AURKA) is overexpressed in NSCLC. We hypothesised that increased expression of AURKA in NSCLC determines radioresistance and thus inhibitors of AURKA can sensitise to ionising radiation (IR).

We demonstrate that AURKA inhibition or depletion radiosensitises NSCLC cells *in vitro* in a p53-dependent manner. The radiosensitising effect is time-dependent with inhibition required post-irradiation.

We establish that treatment combination results in loss of the mitotic population in p53 proficient NSCLC cells but not in p53 deficient cells which become increasingly polyploid. Additionally, mitotic progression is perturbed, is more likely to result in intra-mitotic death or multipolar mitosis and is associated with increased mitotic catastrophe. Cooperative increases in senescence are observed in p53 proficient but not in p53 deficient NSCLC cells following Alisertib IR combination, implicating senescence in treatment response. We find that the addition of Alisertib has no effect on DNA damage repair or on checkpoint kinase activation in the initial hours post-irradiation but was associated with increased residual DNA damage 24 hours post-treatment.

Further, we present that Alisertib radiosensitises NSCLC xenograft models *in vivo,* inducing temporary tumour regressions. We demonstrate that mitotic elimination of p53 proficient NSCLC cells occurs *in vivo* following treatment combination and that proliferative fraction of cells is reduced.

Finally, we show using public datasets that high AURKA mRNA expression is associated with poorer clinical outcomes following radiotherapy. We also present data that indicate that AURKA protein detection in cell line pellets, and with further optimisation in NSCLC patient biopsies, is both adequately sensitive and specific.

Commercial Disclosure

Alisertib was provided by Takeda Pharmaceutical Company Limited for all *in vivo* experimentation

Publications and Presentations

The following presentations detailing work from this thesis were performed:

Jones, T., Hatton, M. Q., Danson, S. & Bryant, H. E. Radiosensitising agents for Non-small cell lung cancer (NSCLC). Sheffield Cancer Research Centre Research Day. March 2017.

Jones, T., Hatton, M. Q., Danson, S. & Bryant, H. E. Inhibition of Aurora kinase A (AURKA) radiosensitizes non-small cell lung cancer (NSCLC). Association for Radiation Research Meeting. June 2018.

Table of Contents

List of Figures

List of Tables

Abbreviations

ABC	Avidin-biotin complex
ADC	Adenocarcinoma
ALK	Anaplastic lymphoma kinase
APC	Anaphase-promoting complex
APS	Ammonium persulphate
ATCC	American type culture collection
ATM	Ataxia telangiectasia mutated
ATR	Ataxia telangiectasia and rad3 related
AURK	Aurora kinase
AURKA	Aurora kinase a
AURKAIP1	Aurora kinase a-interacting protein 1
AURKB	Aurora kinase b
AURKC	Aurora kinase c
BAK	BCL2 homologous antagonist/killer
BAX	BCL2-associated X protein
BCL2	B-cell lymphoma 2
BRCA1	Breast cancer 1, early onset
BRCA2	Breast cancer 2, early onset

BSA	Bovine serum albumin
Cdc20	Cell division cycle 20
CDC25	Cell division cycle 25
Cdh1	Cadherin 1
CDK	Cyclin-dependent kinase
CEP192	Centromeric protein 192
CHART	Continuous hyperfractionated accelerated radiotherapy
CHK1	Checkpoint kinase 1
CHK2	Checkpoint kinase 2
CI	Confidence interval
CR	Complete response
CS-137	Caesium-137
DAB	Diaminobenzidine
DAPI	4′,6-Diamidine-2′-phenylindole dihydrochloride
DER_{10}	Dose enhancement ratio for 10% survival fraction
ddH_2O	Deionised water
DNA	Deoxyribonucleic acid
DNA-PK	DNA-dependent protein kinase
DMEM	Dulbecco’s modified Eagle’s medium

DTT	Dithiothreitol
DSBs	Double strand breaks
ECL	Enhanced chemiluminescence
EDTA	Ethylenediaminetetraacetic acid
EGFR	Epidermal growth factor receptor
ERCC1	Excision repair cross-complementation group 1
FACS	Fluorescence-activated cell sorting
FCS	Foetal calf serum
FSC-H	Forward scatter height
γH2AX	(phosphorylated) H2A histone family, member X
HBC	Hydroxypropyl-β-cyclodextrin
HEF1	Human enhancer of filamentation 1
hnRNPK	Heterogeneous nuclear ribonucleoprotein K
HR	Hazard ratio
HRR	Homologous recombination repair
HRP	Horseradish peroxidise
HURP	Human hepatoma upregulated protein
HUVEC	Human umbilical vein endothelial cells
IF	Immunofluorescence

IHC	Immunohistochemistry
IMS	Industrial methylated spirit
INCENP	Inner centromeric protein
IR	Ionising radiation
IRAS	Integrated research application system
KM	Kaplan-Meier
LATS2	Large tumour suppressor 2
LCC	Large cell carcinoma
LCNEC	Large cell neuroendocrine carcinoma
LD50	Median lethal dose
MAPK	Mitogen-activated protein kinase
MDM2	Mouse double minute homolog 2
MTD	Maximum tolerated dose
mTOR	Mammalian target of rapamycin
mRNA	Messenger ribonucleic acid
NDEL1	NudE-like 1
NEAA	Non-essential amino acids
c-NHEJ	Canonical non-homologous end joining
Alt-NHEJ	Alternative non-homologous end joining

NIHR	National Institute for Health Research
Noc	Nocodazole
NOS	Not otherwise specified
NPM1	Nucleophosmin
NSCLC	Non-small cell lung cancer
NS	Non-statistically significant
OD	Optical density
PAGE	Polyacrylamide gel electrophoresis
PAK1	P21-activated kinase 1
PARP	Poly (ADP-ribose) polymerase
PBS	Phosphate buffered saline
PD	Progressive disease
PD-1	Programmed cell death protein 1
PDK1	Phosphoinositide-dependent kinase 1
PD-L1	Programmed death ligand 1
PHE	Public health England
PI	Propidium iodide
PI3K	Phosphatidylinositol 3-kinase
PKD2	Protein kinase D2

Plk1	Polo-like kinase 1
PMSF	Phenylmethanesulfonyl fluoride
PP1	Protein phosphatase 1
PP2A	Protein phosphatase 2 A
PR	Partial response
PTEN	Phosphatase and tensin homolog
PUMA	p53-upregulated modulator of apoptosis
RASSF1A	Ras association domain family protein 1 A
RECIST	Response evaluation criteria in solid tumours
RNA	Ribonucleic acid
ROS	Reactive oxygen species
RPM	Revolutions per minute
RPMI	Roswell Park Memorial Institute medium
SABR	Stereotactic ablative radiotherapy
SAC	Spindle assembly checkpoint
SAF-A	Scaffold-associated protein A
SBD	Stable disease
SCC	Squamous cell carcinoma
SCLC	Small-cell lung cancer

SD	Standard deviation
SDS	Sodium dodecyl sulphate
SDS-PAGE	SDS-polyacrylamide gel electrophoresis
SEM	Standard error of the mean
SF2	Survival fraction after 2 Gy
SF4	Survival fraction after 4 Gy
siRNA	Short-interfering RNA
SMC1	Structural maintenance of chromosomes 1
SNP	Single nucleotide polymorphism
SSA	Single strand annealing
SSBs	Single-strand breaks
SSC-H	Side scatter height
TACC3	Transforming acid coiled coil family member 3
TBS	Tris-buffered saline
TEMED	Tetramethylethylenediamine
TNM	Tumour node metastases
TPX2	Targeted protein for xklp2
T195	Threonine 195
T232	Threonine 232

T288	Threonine 288
WB	Western blot
XIAP	X-linked inhibitor of apoptosis
53BP1	P53-binding protein 1

1. Introduction

1.1. Non-small cell lung carcinoma (NSCLC)

1.1.1. Survival statistics and pathology of lung cancer

Lung cancer is overall the third most commonly diagnosed cancer in the UK, with approximately 46,700 new cases per year, only behind prostate cancer in men and breast cancer in women respectively (clinicalCRUK 2017). Importantly, lung cancer is the greatest cause of cancer related death in the UK and was responsible for 21% of all cancer deaths in 2016 (CRUK 2017). This is echoed by worldwide cancer statistics which indicate that lung cancer is the third most commonly diagnosed cancer and the most common cancer killer, accounting for an average of 18.6 deaths per 100,000 globally in 2018 (International Agency for Research on Cancer 2019). In fact, lung cancer has the second lowest survival rates amongst twenty of the most common cancers in the UK, with 10% and 5% of patients surviving 5 years and 10 years respectively, and much of this is attributed to late stage diagnosis (CRUK 2017).

Lung cancer is generally divided into non-small cell lung carcinoma (NSCLC) and small cell lung carcinoma (SCLC) which represent approximately 85% and 15% of lung cancers respectively (Jemal *et al.* 2011). NSCLC itself is further sub-divided histologically into squamous cell carcinoma (SCC), adenocarcinoma (ADC), large cell carcinoma (LCC) and large cell neuroendocrine carcinoma (LCNEC) with implications for disease management (Wistuba and Gazdar 2006; Nicholson *et al.* 2015). Furthermore, NSCLC not otherwise specified (NOS) represents a small subset of the disease which cannot be histologically categorised (Nicholson *et al.* 2015). ADC accounts for approximately 50% of NSCLC and is associated with

development in the more distal regions of the lung and has a tendency to display the glandular features of alveolar (and their precursor) cells (Chen *et al.* 2014; Cane *et al.* 2015). ADC may, but not always, develop from a pre-malignant state known as atypical adenomatous hyperplasia which develops in the peripheral airways and is characterised by localised thickening and fibrosis of the alveolar septa with cytological atypia (Westra 2000). SCC meanwhile accounts for approximately 40% of NSCLC and is believed to develop from the columnar epithelium of the proximal lung and has a stronger association with cigarette smoking than ADC (Chen *et al.* 2014; Cane *et al.* 2015). SCC may develop in a step-wise fashion histologically, typically progressing from squamous cell hyperplasia (Wistuba and Gazdar 2006). A diagnosis of LCC is typified by large undifferentiated lung epithelial cells that lack the morphological traits of ADC and SCC respectively, whilst a LCNEC diagnosis occurs when NSCLC cells display neuroendocrine morphology and traits (Nicholson *et al.* 2015). Given that UK survival statistics for NSCLC itself are poor (CRUK 2017) and globally approximately 40% of NSCLC patients present with unresectable disease (Jemal *et al.* 2011), lung cancer and even more specifically NSCLC present a major clinical challenge.

1.1.2. Radiotherapy and NSCLC

1.1.2.1. The staging of NSCLC and implications for radiotherapy

Primarily, patient management in NSCLC is highly dependent upon the clinical and pathological stage of disease (Detterbeck *et al.* 2017). The clinical staging system for NSCLC is based upon a TNM classification system (Detterbeck *et al.* 2017) which accounts for primary **T**umour extent and local invasion, lymph **N**ode metastases and distant **M**etastases. TNM descriptor scoring of NSCLC provides prognostic

information and affects disease management. The staging system for NSCLC is summarised in Table 1.1.

<table>
<tr><th colspan="8">TNM Stage groupings & 5-year survival (%)</th></tr>
<tr><td>Any T
Any N</td><td colspan="6">IVB (0)</td><td>M1c</td></tr>
<tr><td></td><td colspan="6">IVA (10)</td><td>M1b
M1a</td></tr>
<tr><td>N3</td><td colspan="4">IIIB (26)</td><td colspan="2">IIIC (13)</td><td>M0</td></tr>
<tr><td>N2</td><td colspan="4">IIIA (36)</td><td colspan="2">IIIB</td><td></td></tr>
<tr><td>N1</td><td colspan="5">IIB</td><td colspan="2">IIIA</td><td></td></tr>
<tr><td>N0</td><td>IA1 (92)</td><td>IA2 (83)</td><td>IA3 (77)</td><td>IB (68)</td><td>IIA (60)</td><td>IIB (53)</td><td>IIIA</td><td></td></tr>
<tr><td></td><td>T1a</td><td>T1b</td><td>T1c</td><td>T2a</td><td>T2b</td><td>T3</td><td>T4</td><td></td></tr>
</table>

Table 1.1. **The 8th Edition staging strategy for NSCLC established by the International Association for the Study of Lung Cancer**. Average stage-associated 5-year survival statistics (%) for NSCLC following clinical staging are displayed in brackets. Stage I patients have tumours of ≤4 cm in the greatest dimension with no lymph node or distant metastases. Stage II patients can have primary tumours of >4-≤7 cm in the greatest dimension or moderate local invasion and some local lymph node involvement. Stage III patients have tumours >7 cm in the greatest dimension or with extensive localised invasion or display significant lymph node involvement but do not exhibit evidence of distant metastases. Stage IV patients are defined by the presence of distant metastases, including pleural dissemination or tumour nodules in a contralateral lobe (M1a). A, B and C notations allow for sub-stage stratification based on these characteristics (Detterbeck *et al.* 2017). Adapted with permission from: Tsim *et al* (2010).

Early stage I-IIA NSCLC patients in the UK may be offered surgical resection with or without adjuvant cisplatin-based chemotherapy depending performance status (NICE 2019), whilst IIB and IIIA tumours may also be amenable to surgery in combination with other treatment modalities depending on tumour and patient factors such as

anatomical location and performance status (Weaver and Coonar 2017). Surgical resection of early stage NSCLC is considered the gold standard of treatment, and increasing rates of resection in the UK are partially attributed with improvements in 1-year survival rates since 1990 (Weaver and Coonar 2017). Also, surgery may also be of use in a palliative context in advanced NSCLC, although the potential risks and benefits of treatment require consideration (Weaver and Coonar 2017).

In advanced stage IIIB-IV NSCLC systemic therapies are an important treatment option. In stage IIIB-IV squamous NSCLC chemotherapy of gemcitabine is offered with platinum-agents as first line therapy (NICE 2019). Additionally, when programmed death ligand-1 (PD-L1) expression of ≥50% programmed cell death protein 1 (PD-1) targeted immunotherapy in the form of pembrolizumab can be offered (NICE 2019). Upon progression from pembrolizumab or when tumours are ≤50% positive for PD-L1 expression gemcitabine platinum agent combination is preferred (NICE 2019). The standard first line therapy for stage IIIB-IV non-squamous NSCLC is pemetrexed in combination with platinum-based chemotherapy. However, the systemic treatment of stage IIIB-IV non-squamous NSCLC can also be led by gene expression. The presence of epidermal growth factor receptor (EGFR) mutation may indicate treatment with first-line targeted inhibitors afatinib, erlotinib or gefitinib, presence of anaplastic lymphoma kinase (ALK) gene rearrangement may indicate first-line crizotinib, ceritinib or alectinib treatment, and ROS1 gene arrangement may indicate first-line crizotinib treatment respectively (NICE 2019). In the absence of the above mutations and gene rearrangements pemetrexed and platinum chemotherapy is standard and may be offered with pembrolizumab (NICE 2019). Pemetrexed is also used as maintenance therapy if progression does not occur quickly after chemotherapy (NICE 2019).

Radiotherapy is also an important treatment modality in NSCLC with >60% of patients receiving radiotherapy at least once during their disease (Vinod 2015). Radical (curative) radiotherapy is offered to patients with stages I-III NSCLC in the UK (NICE 2019) and highlights the flexibility of the treatment modality. When stage I-II NSCLC patients are deemed medically inoperable but suitable for curative radiotherapy stereotactic ablative radiotherapy (SABR) or continuous hyperfractionated accelerated radiotherapy (CHART) is offered as standard in the UK (NICE 2019). SABR is an emerging approach to treating inoperable stage I/II NSCLC. SABR as a modality of radiotherapy works by focussing multiple, small and accurate radiation beams to a discrete area. Each of the multiple beams of SABR deliver a small dose of radiation such that the collective dose at the point of beam intersection is much greater therefore delivering high doses of radiation to a target whilst reducing the dosing of non-targeted tissue (Timmerman et al. 2010). Compared to conventional radiotherapy SABR is more conformed with superior dose fall off in the surrounding normal tissues and delivers more dose per fraction, thus requiring reduced time on treatment and resulting in a higher radiobiological equivalent dose (Ball *et al.* 2019). Subsequently, in a phase III clinical trial, SABR has demonstrated superior local control rates without increased toxicity compared to conventional radiotherapy in inoperable stage I NSCLC patients (Ball *et al.* 2019). SABR in inoperable early-stage NSCLC has also shown comparable performance to surgical resection and highlights the role for radiotherapy in certain early-stage NSCLC patients (Timmerman *et al.* 2010; Yalman and Selek 2015). In operable stage IIIa NSCLC patients chemoradiotherapy and surgery may be offered and is associated with improved overall and progression-free survival (NICE 2019). In NSCLC patients with stage II or III disease that is unsuitable for surgery, concurrent

platinum chemotherapy can be offered in combination with radiotherapy in the UK when balanced against pre-existing patient morbidities (NICE 2019). Concurrent platinum chemotherapy with radiotherapy has yielded small but significant survival benefits in NSCLC (Aupérin *et al.* 2010). Stage III NSCLC patients eligible for radical radiotherapy but unsuitable for chemoradiotherapy are also offered CHART (NICE 2019). Alternatively, wherever CHART cannot be provided, conventionally fractionated radical radiotherapy (64-66 Gy in 32-33 fractions) is offered in the UK (NICE 2019).

When NSCLC patients in the UK cannot be treated curatively, but are suitable for palliative radiotherapy, radiotherapy can be given immediately or upon the onset of symptoms (NICE 2019). This may include stage III patients with circumstances that do not favour radical therapy taking factors such as age, performance status, pulmonary function and weight loss into account (Rodrigues *et al.* 2012). In oligometastatic stage IV NSCLC aggressive local radiotherapy at both the primary and metastatic tumour sites, such as bone, in order to achieve localised disease control is well supported (Folkert and Timmerman 2015; NICE 2019). Indeed, there is evidence supporting the use of SABR in the treatment of metastatic NSCLC (Iyengar *et al.* 2014) and several clinical trials are investigating the use of SABR in this context further (Gaya *et al.* 2016; Basler *et al.* 2017; Conibear *et al.* 2018). Also, palliative radiotherapy can be used to manage endobronchial and vena cava obstructions (NICE 2019). Thus, radiotherapy is an important treatment modality that has a role throughout the different stages of NSCLC, albeit in different contexts.

1.1.2.2. The weaknesses of current radiotherapy strategies in NSCLC

1.1.2.2.1. NSCLC heterogeneity in response to radiotherapy

Variability in NSCLC response to radiation increases the difficulty in identifying NSCLC patients who will benefit best from radiotherapy. In addition, there are currently no validated biomarkers of radiation response with clinical utility in NSCLC. Both varied response to radiation and lack of predictive biomarkers are likely a consequence of both the biological heterogeneity of NSCLC and our lack of understanding of how this relates to radiation response. The baseline radiosensitivity of the disease varies greatly for example. This is illustrated by the *in vitro* survival of a panel of NSCLC cell lines whereby survival fraction values after 2 Gy (SF2) range from 0.02 and 0.9 (Das *et al.* 2010). Variability in radio-response is not restricted to *in vitro* models however and is also true in NSCLC patients. For example, historical data in potentially curable but medically inoperable stage I and II NSCLC treated with high dose conventional radiotherapy showed that the number of complete and partial tumour regressions varied between 42% and 75% depending on a range of factors such as tumour stage and histology (Perez Carlos *et al.* 1987). Additionally, intra-thoracic tumour control rates varied between 35% and 20% depending on histological subtype (Perez Carlos *et al.* 1987). Finally, there was also histology dependent variability in local failure rates (in the form of tumour recurrence and progression) and these were associated with mortality rates (Perez Carlos *et al.* 1987). Providing overwhelming evidence that tumour biology, in this case tumour histology, and thus genotypic subtype is implicated in NSCLC radiation response.

1.1.2.2.2. NSCLC resistance to radiotherapy

The success of radiotherapy in the treatment of NSCLC is also hampered by inherent or acquired radio-resistance – a phenomena highlighted by the failure of conventional external beam radiation in achieving local tumour control in 60-70% of early stage NSCLC patients (Timmerman *et al.* 2010). One of the most established negative predictors of tumour response to radiotherapy, and thus by implication a factor in resistance, is tumour-associated hypoxia as molecular oxygen is involved in the fixation of cytotoxic DNA damage following irradiation (Quintiliani 1986). Indeed, as in many cancers, low oxygen concentration or hypoxia is a common phenomenon in NSCLC tumours (Le *et al.* 2006; Trinkaus *et al.* 2013) and is associated with poor clinical outcomes following radiotherapy (Li *et al.* 2006). Investigations into imaging approaches that can identify hypoxia and adapt radiotherapy are underway (Vera *et al.* 2017; Salem *et al.* 2018), but hypoxia is not routinely used to predict radiotherapy response in NSCLC.

However, radio-resistance in NSCLC is multifactorial with other suggested mechanisms including: an inherently resistant cancer stem cell population (Gomez-Casal *et al.* 2013), cancer-stroma interactions (Ji *et al.* 2015), dysregulated anti-apoptotic protein expression (Whitsett *et al.* 2014; Yang *et al.* 2015) and varied DNA repair response after irradiation (Cron *et al.* 2013). Preclinical data has identified dysregulated phosphatidylinositol 3-kinase (PI3K), Ras and EGFR signalling as potential molecular mediators of radioresistance in NSCLC (Brognard *et al.* 2001; Kriegs *et al.* 2015). One study has shown that tumour expression of excision repair cross-complementation group 1 (ERCC1) in stage III N2 positive NSCLC treated with neoadjuvant platinum chemoradiotherapy conferred poorer overall and progression-free survival (Hwang In *et al.* 2008). Another study, the RADAR study, evaluated the

expression of plasma biomarkers in NSCLC patients undergoing radical radiotherapy using mass spectrometry (Walker *et al.* 2015). Importantly Walker *et al* (2015) took plasma samples prior to and during radiotherapy given allowing the identification of treatment-related biomarkers. This approach identified plasma C-reactive protein (CRP) and Leucine-rich alpha-2-glycoprotein (LRG1) upregulation one-week post-radiotherapy, which when combined predicted worse overall survival (Walker *et al.* 2015). Neither plasma CRP and/or LRG1 expression is currently used with clinical utility in NSCLC radiotherapy, but these markers do show promise.

1.1.2.2.3. Normal tissue toxicity following thoracic irradiation

Normal tissue toxicities further restrict the success of radiotherapy in the treatment of NSCLC. Normal tissue responses to radiation are generally divided into the early tissue responses and late tissue responses. It is accepted that early tissue responses occur within days or weeks of irradiation within the most proliferative tissues and that these responses are generally resolvable. In contrast, the late tissue responses to irradiation can take weeks, months or years to manifest and are generally non-resolvable, hence meaning they are dose-limiting. Early tissue responses to thoracic irradiation include radiation pneumonitis and radiation oesophagitis and are both common, associated with significant patient morbidity and have potential to be dose-limiting (Kwint *et al.* 2012; Palma *et al.* 2013; Simone 2017). Furthermore, radiation pneumonitis is associated with mortality in a small number of cases (Palma *et al.* 2013). Late tissue responses to thoracic irradiation include pulmonary fibrosis and cardiac toxicity, of which the former may develop from radiation pneumonitis, and both constrain the dose of radiotherapy that can be given to the thorax (Simone 2017). Hence, both the early and late normal tissue

effects of thoracic irradiation are clinically important and affect radiotherapy treatment in NSCLC. Additionally, the specific site of the lung tumour and adjacent structures can prove too challenging for radiotherapy with regards to toxicity, especially in centrally located tumours that sit within 2cm of the proximal bronchial tree (Chaudhuri *et al.* 2015).

Given that not all patients develop toxicities such as radiation pneumonitis (Palma *et al.* 2013) there are ongoing studies investigating assays that can predict the normal tissue response to thoracic irradiation. The REQUITE study for example will be investigating if NSCLC patient radiation-induced lymphocyte apoptosis correlates with the development of radiation pneumonitis one-year post-radiotherapy (West *et al.* 2014). Currently, there is no marker predicting likelihood of normal tissue toxicity after thoracic irradiation in clinical use.

Resistance to radiotherapy in tumour cells and sensitivity to radiotherapy in normal tissues together contribute to a poor therapeutic response to radiotherapy in NSCLC. Hence, there is a clinical need for approaches in NSCLC that enhance the difference between tumour response to radiotherapy and likelihood of normal tissue toxicity, otherwise known as the therapeutic ratio summarised in Figure 1.1.

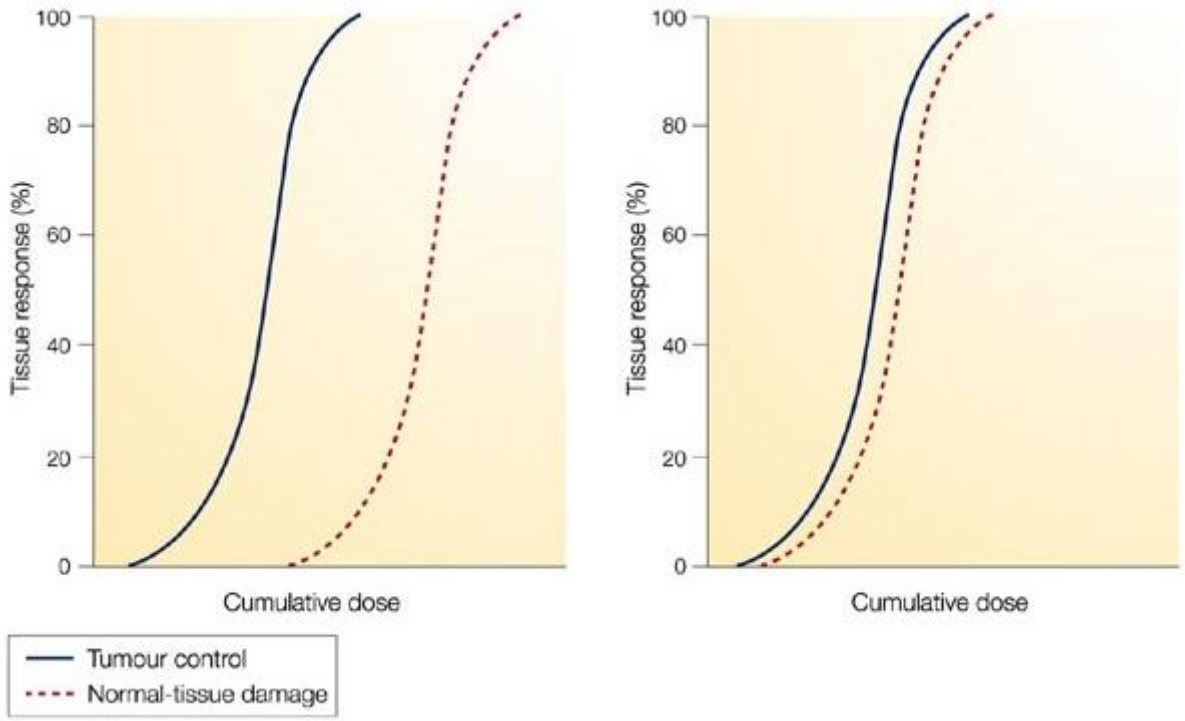

Figure 1.1. **Example therapeutic ratios with increasing radiotherapy dose**. The graph on the left illustrates the ideal therapeutic scenario whereby the difference between tumour response and normal tissues response to radiotherapy is maximal. Conversely, the graph on the right illustrates a scenario whereby the radiotherapy dose required to achieve tumour control also causes significant normal tissue toxicity. Taken with permission from: Bernier *et al* (2004).

One approach to improving the therapeutic ratio of radiotherapy in NSCLC is to selectively protect the normal tissues from radiation damage (reviewed by (Prasanna *et al.* 2012)). Strategies include the use of free-radical scavengers such as amifostine to reduce the cytotoxicity of ionising radiation (IR) in the non-neoplastic lung (Sarna *et al.* 2008). The converse approach to improving the therapeutic ratio of radiotherapy in NSCLC is through targeting the molecular determinants of radio-resistance, concurrently with irradiation, to enhance the response to radiotherapy or "radiosensitise" tumour cells (Franken *et al.* 2013). The radiosensitisation effect is highlighted in Figure 1.2 whereby the same cytotoxic killing effect in the A549 NSCLC cell line is achieved using a reduced dose of radiation in the same cell line

pre-treated with increasing concentrations of the Poly (ADP-ribose) polymerase (PARP) inhibitor Olaparib (Senra *et al.* 2011).

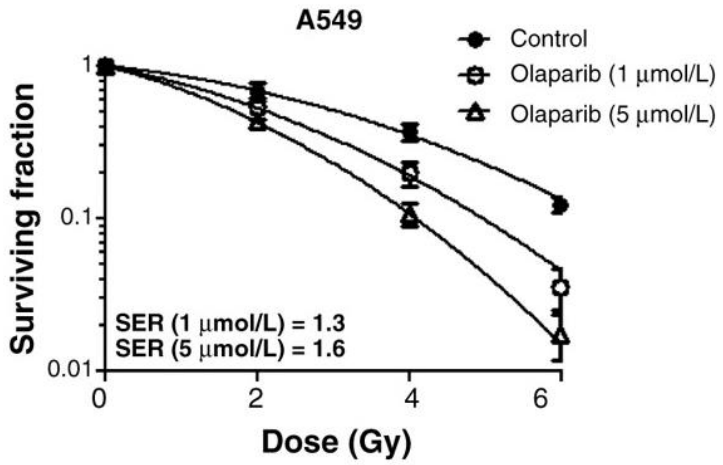

Figure 1.2. **Survival fraction of the A549 NSCLC cell line treated with Olaparib 2 hours before and 22 hours after radiation.** Taken with permission from: Senra *et al* (2011).

The effect in the case of Figure 1.2 is hypothesised to be due to Olaparib pre-treatment reducing the DNA repair capabilities of a cell and thus enhancing the persistence and cytotoxicity of genomic damage received during irradiation (Senra *et al.* 2011).

1.1.2.3. Drug radiation combinations in NSCLC

Combining systemically delivered chemotherapies or biological agents that synergise with radiation has promise as molecular dependencies or deficiencies present in the tumour population can be specifically targeted, with potential to radiosensitise tumours without exacerbating normal tissue toxicities. In addition, radiation enhancement will likely only occur locally within the irradiated volume. As previously discussed, combining platinum agents with radiation has yielded survival benefits in NSCLC (Aupérin *et al.* 2010) and is a standard of care for stage III NSCLC patients receiving curative radiotherapy in the UK (NICE 2019). Biological agents have

potential as radiosensitising agents as they are more likely to act specifically on tumour cells preferentially over non-neoplastic tissues. However, currently the EGFR-targeted antibody therapy cetuximab is the only biological agent known to receive approval for use in combination with radiotherapy in the UK, in head and neck squamous carcinoma (NICE 2008). Despite much interest in combining biological agents with radiotherapy in NSCLC there is no approved biological agent for such use. A consensus statement on the investigation of novel biological agent radiation combinations in NSCLC in the UK has now been published (Harrow *et al.* 2016). DNA damage response inhibitors will be combined with radical radiotherapy in stage III NSCLC patients whilst immune-modulating agents will be combined with palliative radiotherapy in stage IV NSCLC patients respectively (Harrow *et al.* 2016). PARP, Wee1, ataxia telangiectasia and rad3 related (ATR) and ataxia telangiectasia mutated (ATM) inhibitors are planned to be combined with conventionally fractionated radiotherapy in stage III NSCLC patients in the phase I CONCORDE platform trial in the UK (Hanna *et al.* 2017). Recent phase III evidence has showed that use of the PD-L1 blocking antibody durvalumab after platinum chemoradiotherapy in NSCLC patients statistically extends median progression-free survival from 5.6 months to 16.8 months compared to placebo with no significant increase in toxicity (Antonia *et al.* 2017). This highlights the potential of combining biological agents with radiotherapy in NSCLC and furthermore demonstrates that understanding the biological fate of NSCLC cells following irradiation provides therapeutic opportunities.

1.2. The molecular response to radiation

1.2.1. Radiation and DNA repair

IR induces DNA damage through direct ionising events and indirectly through reactive oxygen species (ROS) that form through the radiolysis of water. Doses of 1-2 Grays of radiation are estimated to cause >1000 damaged bases, ~1000 DNA single strand breaks and ~40 DNA double strand breaks (DSBs) (International Atomic Energy Agency 2010). Cellular DNA repair pathways exist to maintain genomic integrity and are subsequently activated following IR. Damaged bases and DNA single strand breaks are repaired efficiently by the base excision/single strand repair pathway and are generally considered inconsequential to the cell (Maier *et al.* 2016). In contrast, the induction of DNA DSBs largely mediates the cytotoxic effect of IR (Mladenov et al. 2013) and the cellular response to DNA DSBs post-IR is important in determining cellular fate.

ATM is attracted to and activated at sites of DNA DSBs and locally phosphorylates a range of substrates to orchestrate stabilisation of DNA DSBs and facilitate their repair (Smith *et al.* 2010). ATR can also be attracted to sites of DNA damage but is more important for the repair of DNA single strand breaks and resolution of stalled replication forks (Smith *et al.* 2010). Canonical non-homologous end joining (c-NHEJ) can repair DNA DSBs, occurs throughout the cell cycle and functions in an error-prone fashion through using DNA microhomologies to guide repair (Lieber 2010). Another method of DNA DSB repair is homologous recombination repair (HRR) which utilises homologous sister chromatid sequence to guide repair in an error-free fashion but through the requirement for sister chromatid homology only occurs in S and G2 phases of the cell cycle (Sung and Klein 2006). HRR of DNA DSBs requires resection of double stranded DNA ends to generate single stranded

DNA. This single stranded DNA can then undergo a process called strand invasion, annealing to homologous sister chromatid DNA that can be used as a template for repair (Sung and Klein 2006). Alternatively, DNA DSB repair can also occur through the single strand annealing (SSA) and alternative NHEJ (Alt-NHEJ) pathways. Both the SSA and Alt-NHEJ pathways, like HRR, require end DNA DSB end resection that expose flanking homologies that can anneal to form an intermediate DNA synapse (Bhargava *et al.* 2016). This DNA intermediate is cleaved at non-homologous 3' single strand tails prior to gap filling by DNA polymerases and ligation of ends (Bhargava *et al.* 2016). SSA requires significant end resection and long stretches of homologous sequence whilst Alt-NHEJ requires minor end resection and short sequence homologies to occur (Bhargava *et al.* 2016).

The cellular decision between c-NHEJ, HRR, SSA and Alt-NHEJ is determined by the balance of protection and resection of DNA DSB ends (Chapman *et al.* 2012) and is coordinated by cell cycle dependent phosphorylation of CtIP (Huertas and Jackson 2009). CtIP phosphorylation occurs in S-G2 phases through cyclin-dependent kinases and promotes CtIP-mediated DNA DSB end resection, whilst end resection does not occur in G1 (Huertas and Jackson 2009). Therefore, c-NHEJ, which does not require end resection, predominates in G1 whilst c-NHEJ, HRR, SSA and Alt-NHEJ can all occur in S-G2 phases depending on the relative protection DNA DSB ends and extent of end resection (Bhargava *et al.* 2016). c-NHEJ can result in sequence insertions, c-NHEJ, SSA and Alt-NHEJ can all result in sequence deletions whilst HRR, however, can fully re-establish DNA sequence information using the sister chromatid template (Bhargava *et al.* 2016). Improperly repaired DNA following IR can result in mutations that have potential for deleterious effects in any

cellular progeny. Given this, cell cycle progression is intimately linked to the DNA DSB repair processes.

1.2.2. Radiation and cell cycle checkpoints

Cell cycle checkpoints exist to regulate cellular progression through the cell cycle, ensuring appropriate division with faithful duplication of the genome and segregation of the duplicated chromosomes into two daughter cells. IR induces activation of DNA repair mechanisms which interact with the enforcers of cell cycle checkpoints and impact upon cell cycle progression. The G1-S checkpoint exists to regulate the irreversible commitment to duplicate the cellular DNA in the presence of extracellular mitogens (Pardee 1989). Radiation-induced DNA damage can prevent G1-S transition. A biphasic response to radiation-induced DNA damage in G1 has been suggested (Bartek and Lukas 2001) whereby an immediate transient response via ATM/ATR recognition of genomic damage leads to degradation of cell division cycle 25A (CDC25A) in a checkpoint kinase 1 (Chk1) dependant manner (Xiao *et al.* 2003). This causes loss of de-repression of cyclin dependant kinase 2 (CDK2) activity required for G1-S transition (Xiao *et al.* 2003). A slower but more long-lived G1-S block occurs via ATM-mediated stabilisation of p53 (Khosravi *et al.* 1999; Zhang *et al.* 2011) which subsequently results in the transcriptional activation of p21 expression and p21-dependant inhibition of cyclin-dependant kinases (Bartek and Lukas 2001).

Intra-S phase checkpoints exist to ensure that DNA replication does not occur in the presence of damaged DNA bases and stabilises stalled replication forks allowing recovery of replication after damage resolution (Kastan and Bartek 2004). IR-induced DNA damage can cause arrest in S-phase by inhibiting the initiation of

replication at replicative origins (Kastan and Bartek 2004). Inhibition of CDK2 activity via CDC25A degradation after DNA damage can also cause inhibition of CDK2-dependant recruitment of DNA polymerase α at replication origins, restricting the initiation of new DNA replication (Falck *et al.* 2002). In parallel, ATM-mediated activation of structural maintenance of chromosomes 1 (SMC1) after IR can also cause S-phase arrest (Yazdi *et al.* 2002), however the mechanism of SMC1 mediated arrest is still unknown.

The G2-M checkpoint exists to ensure that cells do not enter mitosis until replicative errors and DNA damage is resolved (Kastan and Bartek 2004). Radiation-induced DNA damage can additionally prevent G2-M transition. The mechanisms that arrest in G2 after DNA damage converge upon CDK1 which associates with cyclin-B1 and drives mitotic entry. CDK1 activation has been shown to be inhibited by DNA damage-mediated CDC25 family member inhibition in an ATM- and ATR-dependant manner (Donzelli and Draetta 2003). Furthermore, positive regulators of CDC25 family members such as polo-kinase 1 (Plk1) are negatively regulated in the presence of genomic damage (Smits *et al.* 2000). Other DNA damage response proteins such as breast cancer early onset 1 (BRCA1) (Yarden *et al.* 2002) and p53 binding-protein 1 53BP1 (Fernandez-Capetillo *et al.* 2002) also have roles in establishing a G2-M arrest in response to IR.

The spindle assembly checkpoint (SAC) achieves a block on the metaphase-anaphase transition by inhibiting anaphase promoting complex (APC) until all chromosomes have the appropriate and stable kinetochore-microtubule attachments (Morrow *et al.* 2005). This ensures the faithful segregation of chromosomes during mitosis and there is evidence that the DNA damage response cooperates with the SAC. ATM has been shown to inhibit the formation of the centrosome-associated

mitotic spindles following DNA damage which is likely to induce activation of the SAC (Smith *et al.* 2009). Intra-mitotic activation of ATM has also been shown to be required for the localisation of MDC1 to the kinetochores following DNA damage (Eliezer *et al.* 2014). This localisation of MDC1 was shown to be required for proper localisation and function of the mitotic checkpoint complex that governs the SAC (Eliezer *et al.* 2014). This however, contradicts a previous report that found that MDC1 promotes mitotic progression by directly targeting APC, in both a BUBR1 and ATM/ATR independent manner (Townsend *et al.* 2009), making the link between MDC1 and SAC function in the DNA damage response contentious. Nevertheless, there is also evidence that IR can promote localisation of SAC effector Mad2 to the kinetochores to inhibit APC activity (Collins *et al.* 2015), providing a clear link between the SAC and the DNA damage response.

Subsequently, the integrity of cell cycle checkpoints is important in determining an appropriate response to IR-induced DNA damage (see Figure 1.3).

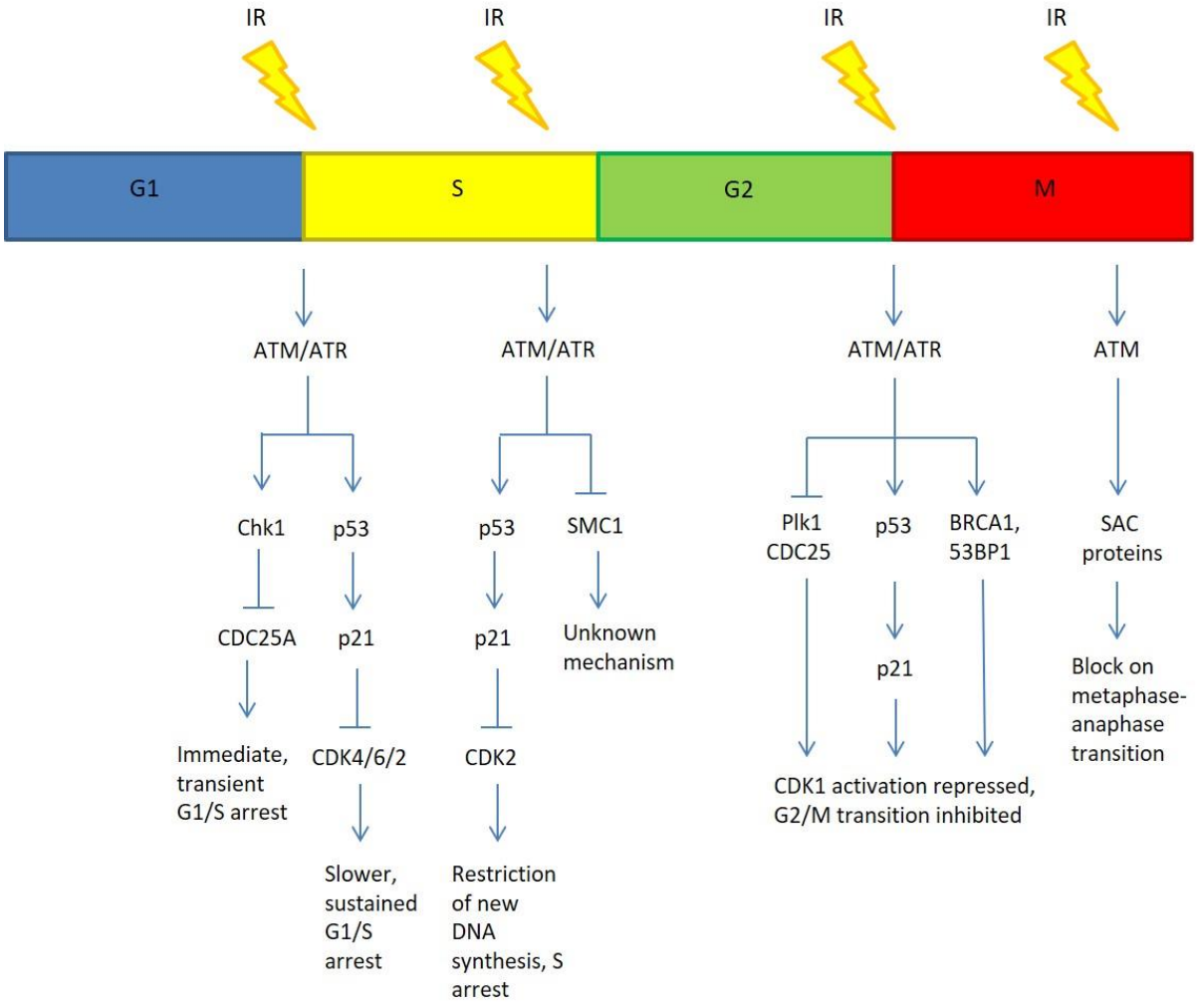

Figure 1.3. **Cell cycle checkpoints invoked by ionising radiation (IR)**. The mechanisms by which cell cycle checkpoints are enforced after ionising radiation (labelled here as IR) exposure in human cells is summarised. Adapted with permission from: Morgan & Lawrence (2015).

In the event of incomplete DNA repair and prolonged p53 activation cellular death, rather than arrest, can be induced (Zhang *et al.* 2011). The current evidence suggests that ATM drives pulses of p53 activity through stabilising phosphorylation of serine-15/serine-20 that promote cell cycle arrest before phosphatase and tensin homolog (PTEN) signalling axis predominates leading to phosphorylation of p53 at serine-46 promoting pro-apoptotic p53 activity (Zhang *et al.* 2011).

1.2.3. Radiation and cell death

The intrinsic apoptotic pathway predominates post-IR and converges upon the release of cytochrome c from the mitochondria (Maier *et al.* 2016). The intrinsic apoptotic pathway is regulated by a balance between expression of pro-apoptotic and anti-apoptotic B-cell lymphoma 2 (BCL2) proteins (Del Gaizo Moore and Letai 2013). The pro-apoptotic and anti-apoptotic BCL2 proteins compete to activate or sequester the pro-apoptotic BCL-2 associated X protein (BAX) and BCL-2 homologous antagonist/killer (BAK) proteins (Del Gaizo Moore and Letai 2013). BAX and BAK once activated, oligomerise and form pores in the outer mitochondrial membrane, facilitating the release of cytochrome c into the cytosol (Wei *et al.* 2001). Release of cytochrome c into the cytosol then irreversibly commits a cell to apoptotic death through the caspase cascade (Li *et al.* 1997). Prolonged activation of p53 by DNA damage post-IR allows nuclear translocation of p53 allowing it to drive the expression of the pro-apoptotic BCL2 proteins p53-upregulated modulator of apoptosis (PUMA), BAX and NOXA (Oda *et al.* 2000; Kuribayashi *et al.* 2011). Increased BAX expression is directly pro-apoptotic whilst PUMA and NOXA act as sensitiser BCL2 proteins serving to indirectly activate BAX/BAK through inhibition of anti-apoptotic BCL2 family members (Del Gaizo Moore and Letai 2013). In addition, the ROS formed through IR-induced radiolysis of water can also promote loss of mitochondrial membrane integrity, release of cytochrome c to the cytosol and a commitment to apoptosis (Maier *et al.* 2016).

IR may also promote apoptosis via the extrinsic apoptotic pathway which are transduced from extracellular stimuli through death receptors. IR-induced p53 activation can allow p53 to drive the expression of both the death CD95 and its ligand CD95L (Sheard 2001). Binding of CD95 by CD95L causes trimerization of

CD95 and conformational changes to the intracellular domains of CD95 resulting in downstream activation of a caspase cascade signalling commitment to apoptosis (Sheard 2001). IR-induced oxidative damage to the plasma membrane may also promote apoptosis in the absence of DNA damage (Liao *et al.* 1999). p53 dependent expression of p21 post-IR can also promote permanent cell cycle exit in the form of senescence (Roninson *et al.* 2001). p21 expression provides an initial block on G1/S progression before p16 expression, a CDK4/6 inhibitor, dominates and provides enduring inhibition of G1/S progression (Stein *et al.* 1999). DNA damage-induced senescence has mechanistic similarities to replicative senescence and can contribute to IR response by limiting the proliferative pool of tumour cells (Roninson *et al.* 2001).

Conversely, cellular pro-survival pathways are also activated following IR. The transmembrane HER1, HER2, HER3 and HER4 receptor tyrosine kinases are potently activated by IR (Yan *et al.* 2015). HER2 activation following IR has been shown to contribute to establishment of the G2-M checkpoint through inhibition of CDK1 (Yan *et al.* 2015), whilst HER1 activation following IR targets DNA-dependent protein kinase (DNA-PK), an important component of c-NHEJ, to the nucleus to participate in repair (Dittmann *et al.* 2005). This works to promote DNA repair in opposition to cell death signalling. Additionally, the activation of HER receptor tyrosine kinases has pro-survival consequences through downstream activation of PI3K/AKT and ERK1/2 pathways (Hein *et al.* 2014). HER3 activation post-IR can recruit PI3K to the plasma membrane (Soltoff *et al.* 1994), subsequently activating a range of proteins such as phosphoinositide-dependent kinase 1 (PDK1) (Marone *et al.* 2008). PDK1 is then able to phosphorylate AKT activating AKT and priming AKT for further activating phosphorylation (Alessi *et al.* 1997). In addition, AKT is

activated by DNA-PK, ATM and ATR post-IR (Xu *et al.* 2012). Activated AKT can then promote cellular survival through inhibitory phosphorylation of pro-apoptotic BCL2 family BAX and BAD proteins (Yamaguchi and Wang 2001), indirect reduction of pro-apoptotic BIM and NOXA expression (J.-Y. Yang *et al.* 2006; Obexer *et al.* 2007), whilst targeting the expression of anti-apoptotic BCL-2 and BCL-XL expression through NF-κB signalling (Ozes *et al.* 1999; Hein *et al.* 2014). Activated AKT has also been shown to promote cell survival through activation of DNA-PK promoting c-NHEJ mediated DNA repair (Toulany *et al.* 2008). p53-induced expression of PTEN occurs following IR (Stambolic *et al.* 2001), counters AKT activation by negatively regulating PI3K signalling (Stambolic *et al.* 1998) and promotes IR-induced apoptosis (Pappas *et al.* 2007), indicating that pro-survival AKT signalling is tightly regulated following IR.

Similarly, IR also induces activation of the mitogen activated protein kinase (MAPK) pathway with pro-survival consequences through ERK1/2 signalling (Dent *et al.* 2003). ERK1/2 has been shown to be activated by upstream MEK1/2 following radiation (Dent *et al.* 2003) and is positively regulated by HER family member activation (Lee *et al.* 2008) and ATM signalling (Golding *et al.* 2007). ERK1/2 activation can promote cell survival by indirectly promoting the expression of anti-apoptotic proteins Bcl-2, Bcl-xL and Mcl-1 (Boucher *et al.* 2000) whilst directly inhibiting the activity of BAD and caspase 9 (Bonni *et al.* 1999; Allan *et al.* 2003). ERK1/2 signalling can also promote DNA repair following IR by positively regulating G2-M cell cycle checkpoint activation (Yan *et al.* 2007), nucleotide excision repair (Yacoub *et al.* 2003), c-NHEJ (Golding *et al.* 2009) and HRR (Golding *et al.* 2007; Golding *et al.* 2009), thus opposing cell death. In summary, there is a delicate

equilibrium between DNA repair, cell cycle arrest and cell death mechanisms following IR.

Mitosis is particularly prone to the effects of radiation and is classically known as the most radiosensitive phase of the cell cycle (International Atomic Energy Agency 2010). Progression into and through mitosis following irradiation has been shown to be important as premature mitotic entry, especially when G2/M checkpoint integrity is compromised, has been associated with mitotic catastrophe, a form of cell death (Ianzini *et al.* 2006). Given that mitotic catastrophe is considered the most common form of cell death post-irradiation (Cohen–Jonathan *et al.* 1999), its regulation is likely important in determining the response of tumours to radiotherapy.

1.2.4. Radiation and mitotic catastrophe

Mitotic catastrophe is defined as a oncosuppressive mechanism that exists to recognise mitotic failure and functions to push cells towards the irreversible states of senescence, apoptosis and necrosis (Vitale *et al.* 2011). Mitotic catastrophe is however distinct from apoptosis, even though it can precede it, and has been shown to occur in intrinsically apoptotic resistant cells (Ianzini *et al.* 2006; Amornwichet *et al.* 2014). Additionally, mitotic catastrophe is associated with intra-mitotic arrest prior to apoptosis, senescence or necrosis which occur during mitosis or in the following G1 phase (Vitale *et al.* 2011). Mitotic catastrophe may arise when there is premature mitotic entry through override or inhibition of the G2/M checkpoint (Cogswell *et al.* 2000; Ianzini *et al.* 2006; Bucher and Britten 2008). Compromised G2/M checkpoint allows cells to enter mitosis with unrepaired DNA damage which results in segregation errors and p53-dependent mitotic catastrophe (Imreh *et al.* 2011).

Perturbation of the mitotic spindles, through microtubule poisons for example (Roninson *et al.* 2001), can also cause mitotic catastrophe through extended activation of the SAC (Vitale *et al.* 2010). Extended SAC activation can result in mitotic slippage, whereby cyclin B degradation over time during mitotic arrest allows abortive completion of mitosis in the absence of proper chromosome segregation (Brito and Rieder 2006). This results in tetraploid progeny which often undergo death in the following G1 phase (Gascoigne and Taylor 2008; Huang *et al.* 2009). Centrosomal amplification may also predispose to mitotic catastrophe through multipolar mitoses that result in aneuploidy and micronuclei formation (Dodson *et al.* 2007). There is evidence that centrosomal amplification occurs after radiation and is a product of prolonged G2 arrest in the presence of DNA damage (Dodson *et al.* 2004). Furthermore, mitotic catastrophe can occur in the progeny of cells undergoing multipolar or abortive mitosis and may manifest after rounds of cellular division (Ianzini *et al.* 2006; Dodson *et al.* 2007; Gascoigne and Taylor 2008; Vitale *et al.* 2010). Subsequently, cellular enlargement with multinucleation and/or multiple micronuclei as a result of aberrant/abortive mitosis are considered hallmarks of mitotic catastrophe (Vitale *et al.* 2011).

Mitotic catastrophe, as defined before, can be caused by radiation (Ianzini and M. A. Mackey 1997; Ianzini *et al.* 2006; Dodson *et al.* 2007; Amornwichet *et al.* 2014), DNA damaging agents (Eom *et al.* 2005; Vakifahmetoglu *et al.* 2008), microtubule poisons (Jordan and Wilson 2004) and biological agents that target the mitotic machinery *in vitro* (Zhou *et al.* 2013). However, mitotic catastrophe is difficult to quantify *in vivo*, but delayed cellular response to radiation *in vivo* suggests that re-entry to the cell cycle is important and implicates mitotic catastrophe (J Merritt *et al.* 1997).

Additionally, radiation induced cellular death *in vivo* with evidence of mitotic aberration indicates that mitotic catastrophe is relevant to radiation response (H Falkvoll 1990). Mitotic catastrophe is an ideal outcome post-radiotherapy because it can eliminate apoptosis-resistant cancer cells (Amornwichet *et al.* 2014) and tumour cells typically have significant tetraploid/aneuploid populations which are inherently more sensitive to mitotic aberration and therefore mitotic catastrophe (Janssen *et al.* 2009). Given this, combinational strategies that disrupt the mitotic process and exacerbate the degree of mitotic catastrophe following radiation are of therapeutic interest.

1.3. Aurora kinase A (AURKA)

1.3.1. The aurora kinase family of proteins

Aurora kinase A (AURKA) is a kinase involved in controlling cell cycle progression through G2 phase to the end of mitosis (Goldenson and Crispino 2015), and thus is under investigation as a potential target for radiosensitisation. Dysregulated expression of AURKA has been suggested to affect the integrity of cell cycle checkpoints and radiosensitivity in a range of cancers including NSCLC (Guan *et al.* 2007; Tao *et al.* 2007; Lin *et al.* 2014; Woo *et al.* 2015). The gene encoding AURKA maps to chromosome 20q13.2 in the human genome (Goldenson and Crispino 2015) and AURKA belongs to the aurora kinase (AURK) family of proteins. Aurora kinase B (AURKB) and aurora kinase C (AURKC) are the other family members. All three AURK family members are serine-threonine kinases sharing a high degree of amino acid sequence homology (Marumoto *et al.* 2005) but each with distinct function in regulating cellular division (see Figure 1.4).

All the AURK family share a highly conserved catalytic site, with a conserved activation loop (Bischoff *et al.* 1998; Carmena and Earnshaw 2003). Each family member has a threonine residue within their activation loop upon which (auto)phosphorylation is a requirement for stable-kinase activity, these are threonine-288 (T288) (Littlepage *et al.* 2002), threonine-232 (T232) (Yasui *et al.* 2004) and threonine-195 (T195) (Goldenson and Crispino 2015) in AURKA, AURKB and AURKC respectively (see Figure 1.4). All three family members also share a C-terminal destruction D-box domain which is important at least in AURKA, for recognition of by E3 ubiquitin ligases and targeting for degradation in late mitosis (Floyd *et al.* 2008). The D-box domain of AURKB is also targeted when it is degradation in late mitosis (Stewart and Fang 2005), and is likely to function similarly in AURKC but this has not been demonstrated. The AURK family members share less amino acid similarity at their N-terminal domains and this allows for specificity of function, via integration with AURKA, AURKB or AURKC specific interacting proteins, and determines cellular localisation during the cell cycle (Giet and Prigent 2001; Zimniak *et al.* 2012). AURKA and AURKB also have N-terminal KEN (APC-recognition signal) and activating D-box motifs which are targeted by ubiquitination during negative regulation (Castro *et al.* 2002; Littlepage and Ruderman 2002; Min *et al.* 2013).

AURKB is a chromosomal passenger protein that is required for ensuring proper spindle-microtubule binding dynamics (and hence proper chromosomal segregation), completion of mitosis and enforcement of the spindle checkpoint in mitosis (Hauf *et al.* 2003). AURKC is exclusively expressed by the tissues of the testis in males and in the oocytes of females co-operates with AURKB to regulate centrosomal function

and chromosome organisation during meiosis (Kimura *et al.* 1999; Nguyen *et al.* 2018).

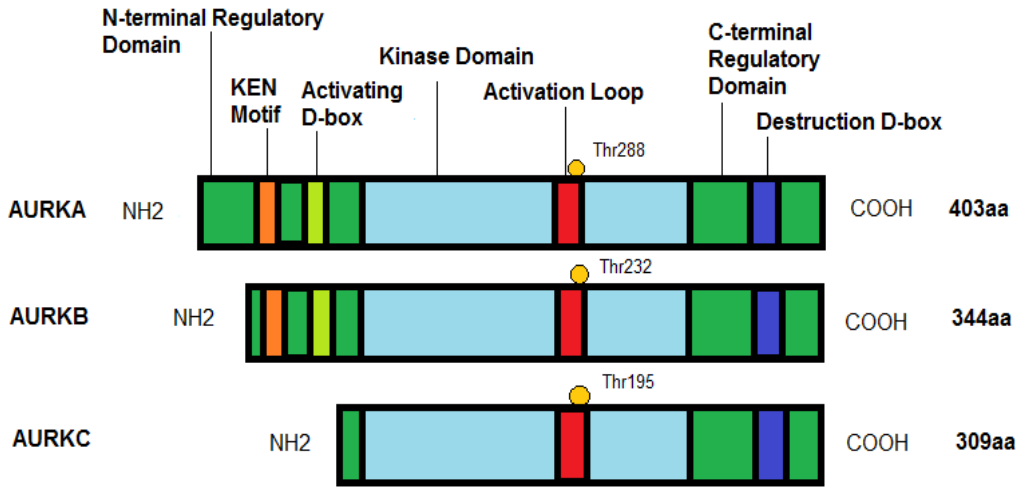

Figure 1.4. **The 2D protein domain structure of the aurora kinase family members**. Adapted with permission from: Goldenson and Crispino (2015).

1.3.2. The mitotic function of AURKA

Following its discovery, expression levels and enzymatic function of AURKA were shown to peak in early M-phase after initially rising in G2 (Bischoff *et al.* 1998) (see section 1.3.2.1). Subsequently established roles for the AURKA gene product include regulating G2-M transition (Hirota *et al.* 2003) mitotic progression and mitotic exit (Marumoto *et al.* 2003; Wang *et al.* 2014b; Ye *et al.* 2016), centrosomal maturation (Hirota *et al.* 2003; Joukov *et al.* 2010) and separation (Marumoto *et al.* 2003), bipolar mitotic spindle assembly (Zhang *et al.* 2008), kinetochore-spindle attachment (Ma *et al.* 2011) with correct chromosomal alignment and segregation.

Specifically, AURKA has been shown to be integral for promoting G2-M transition at the centrosomes. Activated AURKA is able to attract Cyclin B1-CDK1 to the

centrosome, promoting CDK1 activation and subsequent centrosomal maturation (Hirota *et al.* 2003) which is indispensable for mitotic entry. This is achieved by AURKA activating Plk1 through phosphorylation of threonine 210 (Macurek *et al.* 2008; Seki *et al.* 2008; Asteriti *et al.* 2015). Active Plk1 subsequently acts to directly phosphorylate centrosomal cyclin-B1 promoting cyclin-B1 translocation to the nucleus and mitotic entry (Toyoshima-Morimoto *et al.* 2001). Plk1 also relieves the suppression of cyclin B1-CDK1 activity by promoting the degradation of inhibitory kinase Wee1 (van Vugt *et al.* 2004). AURKA further drives mitotic entry by phosphorylating and activating CDC25B, serving to further promote Cyclin-B1-CDK1 activation and cyclin-B1 translocation to the nucleus (Cazales *et al.* 2005). Mutually activating interactions at the centrosomes between Arpc1b, a member of an actin modulating complex, and AURKA have also been shown to be required for mitotic entry and centrosomal activation (Molli *et al.* 2010).

During prophase, AURKA promotes localisation of γ-tubulin (Hirota *et al.* 2003), large tumour suppressor 2 (LATS2) (Toji *et al.* 2004) and nuclear distribution protein nudE-like 1 (NDEL1) (Mori *et al.* 2007) to the centrosomes. The net effect of this is to further promote centrosomal maturation, preparing the centrosome for microtubule nucleation. Upon centrosomal maturation AURKA has been shown to be essential, through an unknown mechanism, for separation of sister centrosomes to opposing poles of the cell, after prior but incomplete separation before nuclear envelope breakdown (Hannak *et al.* 2001; Barr and Gergely 2007; Asteriti *et al.* 2015).

AURKA supports the development of the spindle microtubules which begin to emanate from the mature centrosomes and kinetochores during prophase and prometaphase (Kufer *et al.* 2002). AURKA phosphorylates and co-operates with transforming acidic coiled coil (TACC) family member 3. It has been shown that

phosphorylation of TACC3 by AURKA is critical for targeting this protein to the centrosome (Kinoshita *et al.* 2005). Centrosomal TACC3 can then promote centrosomal spindle formation by co-ordinating the location and function of XMAP215, a protein which stabilises and promotes the polymerisation of the spindle microtubules (Kinoshita *et al.* 2005) (Barros *et al.* 2005). In prophase AURKA also promotes the assembly of the kinetochores via CENP-A interaction (Kunitoku *et al.* 2003). Subsequent to this, AURKA facilitates the nucleation of microtubules from the kinetochores in co-operation with targeted protein for Xklp2 (TPX2) and inner centromeric protein (INCENP) (Katayama *et al.* 2008). The kinetochore-associated microtubules are stabilised by human hepatoma upregulated protein (HURP), which is also positively regulated by AURKA phosphorylation (Barr and Gergely 2007).

Bi-polar spindle dynamics are ensured by active AURKA, as exhibited through inhibition studies (Lioutas and Vernos 2013). It has been suggested that bi-polarity of spindles may be due in part to AURKA acting in complex with BimC-like kinesin Eg5, XMAP215, TPX2 and HURP to promote inter-polar spindle cross-linking and stabilising bi-polar spindle structures (Barr and Gergely 2007). During prometaphase AURKA also mediates centrosomal spindle-kinetochore attachment via interaction with scaffold associated protein A (SAF-A) at the spindle mid-zone (Ma *et al.* 2011). Additionally, AURKA driven separation of centrosome pairs during prometaphase contributes to bi-polar spindle orientation (Barr and Gergely 2007). Maintenance of bi-polar spindle orientation and kinetochore-spindle attachments by AURKA consequently contributes to proper chromosomal alignment on the metaphase plate and chromosomal segregation later in mitosis.

AURKA also controls progression through prometaphase to anaphase by phosphorylating Ras association domain family protein 1 A (RASSF1A) at the

spindle poles (Rong *et al.* 2007). This frees cell division cycle 20 (Cdc20) to act in complex with APC which subsequently drives cells into anaphase when all chromosomes are aligned with appropriate kinetochore-spindle attachments (Song *et al.* 2004). p73 has be shown to be essential for directing SAC effectors BUB1 and BUBR1 to the kinetochores (Tomasini *et al.* 2009; Vernole *et al.* 2009) and is involved in the sequestering of Cdc20 with SAC protein Mad2 preventing APC from driving metaphase-anaphase transition (Katayama *et al.* 2012). AURKA also phosphorylates p73 on S235, which acts to inhibit p73 function in the SAC, promoting dissociation of Cdc20 from Mad2 serving to inactivate the SAC and promoting metaphase-anaphase transition (Katayama *et al.* 2012). Conversely, inhibition of AURKA has also revealed that it is required for Mad2 localisation to unattached kinetochores and thus SAC function during pro-metaphase (Courtheoux *et al.* 2018)

During anaphase and telophase AURKA is subject to negative regulation (see section 1.3.2.2), however some AURKA is localised to the spindle mid-body and may control chromosomal segregation and cytokinesis (Kovarikova *et al.* 2015) (Marumoto *et al.* 2003). In early anaphase segregation of the chromosomes to opposing poles of the cell occurs primarily through depolymerisation of the mitotic spindles, whilst in late anaphase further separation of the chromosomes relies upon the propagation of the central (mid-body) spindles between the segregating chromosomes (Scholey *et al.* 2016). The central spindle also functions to position contractile ring assembly and coordinate abscission at the end of cytokinesis (Glotzer 2009). AURKA activity has been shown to be essential for central spindle production through targeting of TACC3 and P150Glued (Lioutas and Vernos 2013; Reboutier *et al.* 2013). Furthermore, AURKA has been demonstrated to promote the

localisation of HURP and NEDD1 to the spindle mid-zone which are required for central spindle microtubule nucleation and polymerisation (Courthéoux *et al.* 2019). The contribution of AURKA during cytokinesis, however, is not fully understood as AURKA inhibition affects the fidelity but does not fully inhibit cytokinesis (Ye *et al.* 2016). Interestingly, AURKA has additionally been implicated in regulating mitochondrial fission and thus mitochondrial distribution in the two new daughter cells (Kashatus *et al.* 2011). Taken together, activated AURKA is a key regulator of mitotic entry and progression (summarised in Figure 1.5).

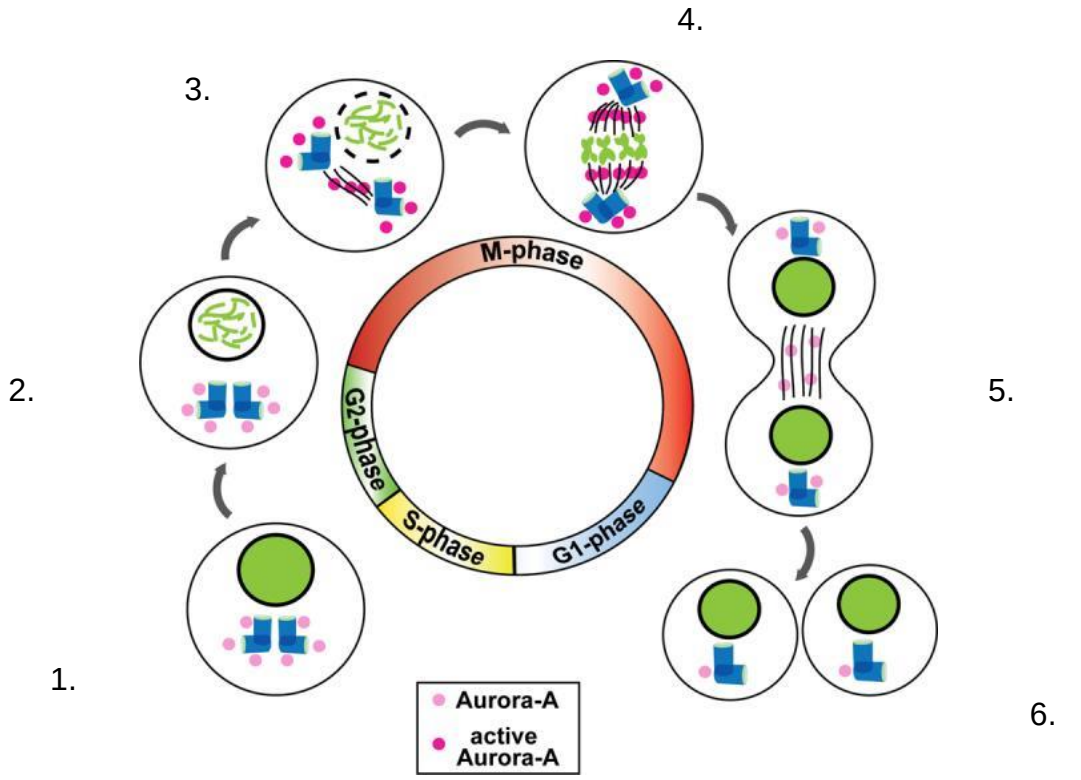

Figure 1.5. **An overview of AURKA function during mitosis**.

1 & 2. Catalytically inactive AURKA begins accumulating at the centrosomes (blue L structures above) during late S and G2. At late G2 levels AURKA T288 auto-phosphorylation is triggered by AURKA-cofactor interactions at the centrosomes. This activates the kinase activity of AURKA and allows AURKA to subsequently drive mitotic entry and centrosomal maturation.

3. After nuclear envelope breakdown at the onset of mitosis, AURKA expression and activation peaks. Now AURKA mediates further centrosomal maturation and centrosomal separation. AURKA also promotes kinetochore formation. Some AURKA is now also targeted to the spindle microtubules and promotes their nucleation, polymerisation and stabilisation as they emanate from the centrosomes and newly formed kinetochores.

4. AURKA then promotes bi-polar spindle dynamics and centrosomal spindle-kinetochore attachments during prometaphase and metaphase.

5 & 6. AURKA drives mitotic progression through to anaphase before it is subject to strong negative regulation. Low levels of AURKA remain at the spindle mid-zone promoting central spindle production before potentially regulating completion of cytokinesis and mitotic exit.

Adapted with permission from: Nikonova *et al* (2014).

1.3.2.1. Positive regulation of AURKA in mitosis

Activation and function of AURKA is controlled by a series of temporally and spatially regulated protein-protein interactions. AURKA has low levels of activity through G1 and S phase of the cell cycle and its activity is kept in check by protein phosphatase 1 (PP1) (Marumoto *et al.* 2002). During S-phase inactive AURKA begins to accumulate at the newly duplicated centrosomes (Roghi *et al.* 1998; Marumoto *et al.* 2005; Rannou *et al.* 2008). However, during late G2-phase centrosomal AURKA interacts with several proteins which alter the conformation of the AURKA activation loop and thus promote T288 auto-phosphorylation. AURKA interacts at the centrosomes with Ajuba (Hirota *et al.* 2003), Bora (Seki *et al.* 2008), human enhancer of filamentation 1 (HEF1/NEDD9) (Pugacheva and Golemis 2005), and p21 activated kinase 1 (PAK1) (Zhao *et al.* 2005). Nucleophosmin (NPM1) also induces auto-phosphorylation of S89 of AURKA during G2 phase which is required for full kinase activity (Reboutier *et al.* 2012). Additionally, the protein kinase D2 (PKD2) has been shown to inhibit AURKA ubiquitination serving to stabilise AURKA at G2-M transition (Roy *et al.* 2018). The net effect is the sustained activation of centrosomal AURKA, allowing AURKA to drive centrosomal maturation and mitotic entry.

Upon mitotic entry the breakdown of the nuclear membrane allows the release of TPX2 from Ran-GTP (Kufer *et al.* 2002). TPX2 and LATS2 now provide further pro-activation signalling to AURKA at the centrosomes (Barr and Gergely 2007). Centrosomal AURKA activity in early mitosis is also maximised by interaction with centrosomal protein 192 (CEP192) which promotes AURKA dimerization and further stabilises active AURKA protein (Joukov *et al.* 2010). TPX2 also begins to target AURKA to the spindle microtubules (Kufer *et al.* 2002). This interaction with TPX2

hinders the access of PP1 to the activation loop of AURKA and subsequent removal of T288 phosphorylation (Bayliss *et al.* 2003) further stabilising activation. In addition, AURKA also undergoes phosphorylation at S51 at its activating D-box during mitosis through an uncharacterised mechanism, promoting even greater stabilisation of AURKA protein (Crane *et al.* 2004; Kitajima *et al.* 2007).

T288 phosphorylation and thus AURKA activation is then maintained throughout mitosis until late-mitosis when AUKRA expression is negatively regulated to allow mitotic exit and cytokinesis (Marumoto *et al.* 2005).

1.3.2.2. Negative regulation of AURKA in mitosis

Like its positive regulation, the negative regulation of AURKA is achieved through interaction with a multitude of factors at mitotic exit. APC in association with its coactivator cadherin1 (Cdh1), recognises the destruction D-box in AURKA and mediates the ubiquitination and subsequent degradation of AURKA protein during anaphase (Floyd *et al.* 2008). However, for the APC/C-Cdh1 interaction with AURKA to occur the stabilising S51 phosphorylation of AURKA must be removed by protein phosphatase 2 A (PP2A) during late mitosis (Horn *et al.* 2007). Another cofactor that acts to negatively regulate the expression of AURKA late in mitosis is AURKA interacting protein 1 (AURKAIP1) which targets AURKA to the proteasome without ubiquitination of AURKA (Kiat *et al.* 2002).

Moreover, S342 auto-phosphorylation of AURKA can inhibit kinase activity of AURKA and provides another mechanism by which AURKA is negatively regulated (Littlepage *et al.* 2002). This phosphorylation is controlled by glycogen synthase kinase 3 (GSK3) and dependant on (micro)environmental stimuli (Sarkissian *et al.* 2004). In summary, a delicate interplay of positive and negative regulation manages

AURKA activity from late G2 through to the completion of mitosis. The mitotic interacting partners of AURKA are summarised in Table 1.2

Cell Cycle Phase	Gene Product	Interaction	Cellular Location	Functionality
G2/M Transition	Ajuba	Promotes T288 auto-phosphorylation of AURKA	Centrosomes	AURKA activation. Centrosomal maturation
	Bora	Promotes T288 auto-phosphorylation of AURKA	Centrosomes	AURKA activation. Centrosomal maturation
	HEF1/NEDD9	Promotes T288 auto-phosphorylation of AURKA	Centrosomes	AURKA activation. Centrosomal maturation
	PAK1	Promotes T288 auto-phosphorylation of AURKA	Centrosomes	AURKA activation. Centrosomal maturation
	Plk1	Mutual activation. Promotes T288 auto-phosphorylation of AURKA	Centrosomes	Activation of Cyclin-B1-CDK1 for mitotic entry. Centrosomal maturation.
	CDC25B	Phosphorylation and activation of CDC25B	Centrosomes	Activation of Cyclin-B1-CDK1 for mitotic entry.
	Arpc1b	Mutual activation. Promotes T288 auto-phosphorylation of AURKA	Centrosomes	Centrosomal maturation. G2-M transition.
	NPM1	Promotes S89 auto-phosphorylation of AURKA	Centrosomes	Centrosomal maturation. G2-M transition.
Prophase-Metaphase	TPX2	Promotes T288 auto-phosphorylation of AURKA	Centrosomes, spindle microtubules	AURKA activation and protection of T288 from PP1. Centrosomal maturation. Targeting of AURKA to spindle

Prophase-Metaphase				microtubules, microtubule polymerisation
	CEP192	Promotes T288 auto-phosphorylation of AURKA and AURKA dimerisation	Centrosomes	Enhanced stability for active AURKA
	γ-tubulin	Co-localisation	Centrosomes	Targeting of γ-tubulin to the centrosomes. Centrosomal maturation
	LATS2	Promotes T288 auto-phosphorylation of AURKA	Centrosomes	Centrosomal maturation
	NDEL1	NDEL1 phosphorylation by AURKA	Centrosomes	Targeting of NDEL1 to the centrosomes. Centrosomal maturation
	TACC3	TACC3 phosphorylation by AURKA	Centrosomes	Targeting of TACC3 to the centrosomes. Spindle microtubule polymerisation and stabilisation
	CENP-A	CENP-A phosphorylation by AURKA	Prophase nuclei	Kinetochore formation
	INCENP	AURKA and INCENP complexing	Kinetochore	Kinetochore-associated microtubule nucleation
	HURP	HURP phosphorylation by AURKA	Spindle microtubules	Stabilisation of kinetochore-associated spindle microtubules
	SAF-A	Co-localisation	Spindle poles	Centrosomal spindle-kinetochore attachment
	Eg5	Complexing with AURKA	Spindle microtubules	Stabilisation of bipolar spindles and spindle cross-linking

	XMAP215	Complexing with AURKA	Spindle microtubules	Stabilisation of bipolar spindles and spindle cross-linking
	RASSF1A	Phosphorylation of RASSF1A by AURKA	Spindle poles	Mitotic progression
Anaphase-Cytokinesis	TACC3	Phosphorylation of TACC3 by AURKA	Spindle mid-body	Assembly and stabilisation of central spindles
	P150Glued	Phosphorylation of P150Glued	Spindle mid-body	Assembly of central spindles
	HURP	Presumed HURP phosphorylation by AURKA	Spindle mid-body	HURP localisation to central spindle microtubules, central spindle polymerisation
	NEDD1	Phosphorylation of NEDD1 by AURKA	Spindle mid-body	NEDD1 localisation to central spindle, microtubule nucleation
	APC-Cdh1	Ubiquitination of AURKA by APC-Cdh1	Spindle mid-body	Proteasomal degradation of AURKA
	PP2A	Removal of ser51 phosphorylation of AURKA by PP2A	Spindle mid-body	De-stabilises AURKA. Allows APC-Cdh1 interaction with AURKA
	AURKAIP1	Targeting of AURKA to the proteasome in ubiquitin-independent manner	Spindle mid-body	Proteasomal degradation of AURKA
	GSK-3β	AURKA ser342 auto-phosphorylation triggered by GSK-3β	Spindle mid-body	Inhibition of AURKA kinase activity

Table 1.2. **The interacting partners and substrates of AURKA in mitosis.** Adapted with permission from: Nikonova *et al* (2014).

1.3.3. Non-mitotic functions of AURKA

Despite a peak of protein expression in G2-M phase of the cell cycle, there is also a literature documenting functions of AURKA outside of mitosis. Indeed, there is evidence that AURKA is involved in the disassembly of primary cilia in cells and is subject to T288 phosphorylation and increased kinase activity in this role (Korobeynikov *et al.* 2017). In keeping with functions in microtubule dynamics, AURKA has also been implicated in cytoskeletal remodelling as neurons extend (Mori *et al.* 2009). There is also an interphase role for AURKA in regulating mitochondrial morphology (Grant *et al.* 2018), fission and energy production (Bertolin *et al.* 2018). Investigations in disease have also shown that AURKA has nuclear transactivating activity in the absence of kinase activity and can promote the expression of a stem-like gene expression programme (N. Yang *et al.* 2017). In keeping with this AURKA has been associated with the maintenance of haematopoietic stem cells (Goldenson *et al.* 2015) and embryonic stem cells (D.-F. Lee *et al.* 2012).

1.3.3.1. AURKA in DNA repair

Investigations, mainly in the field of oncology, have also revealed that AURKA is able to alter the utilisation of DNA repair pathways, which may or may not be related to the mitotic function of AURKA (Sourisseau *et al.* 2010; Yang *et al.* 2010; Wang *et al.* 2014b; Do *et al.* 2017). AURKA in cancer cells has been shown to directly oppose the expression of BRCA1 and BRCA2, known effectors of homologous recombination-based DNA repair, promoting cell cycle progression in the presence of DNA damage (Yang *et al.* 2010; Wang *et al.* 2014b; Do *et al.* 2017). Additionally, AURKA has been shown to promote the utilisation of non-homologous end joining

DNA repair through inhibition of Rad51 recruitment to DNA double-strand breaks in cancer cells (Sourisseau *et al.* 2010). The significance of these interactions between the DNA damage response and AURKA in non-neoplastic cells is not fully understood but hints at a role for establishing a balance between cell cycle progression and DNA repair.

1.3.3.2. AURKA and p53 function

Perhaps one of the most well studied effectors of cell cycle arrest and DNA repair is p53. AURKA has been shown to destabilise p53 expression through phosphorylation of serine 315 of p53, serving to promote p53 interaction with the negative regulator of p53 mouse double minute homolog 2 MDM2 (Katayama *et al.* 2004). AURKA can also phosphorylate serine 215 of p53 causing inhibition of the transactivating function of p53 and downregulation of p53-dependent genes such as p21 and PTEN (Liu *et al.* 2005). AURKA also perturbs interactions between p53 and heterogenous nuclear ribonucleoprotein K (hnRPNK) inhibiting p53 transactivation of DNA repair genes following DNA damage (Hsueh *et al.* 2011). In contrast, AURKA has also been shown to phosphorylate p53 on serine 106 which inhibits MDM2-mediated destabilisation of p53 (Hsueh *et al.* 2013). Conversely, p53 can inhibit AURKA kinase activity through physical interaction (Eyers and Maller 2004) and can inhibit AURKA through multiple transactivation-dependent mechanisms (Sasai *et al.* 2016), clearly linking p53 and AURKA function.

AURKA and p53 have been linked during promotion of centrosomal homeostasis. During G1-S phase of the cell cycle p53 coordinates synchronous DNA replication and centrosomal duplication through a p21-dependent mechanism (Okuda *et al.* 2000). In addition, p53 is recruited to the centrosome and inhibits G1-S progression

when centrosome integrity is affected (Mikule *et al.* 2007; Song *et al.* 2010). p53 recruitment to the centrosomes, however, is reversible and is dissociated from the centrosomes by interactions with Mortalin, releasing the inhibition on centrosomal duplication (Ma *et al.* 2006). AURKA has been shown to promote interaction of p53 with Mortalin (Katayama *et al.* 2012) and has also been shown to oppose p53 and p21 expression promoting G1-S transition (Xu *et al.* 2005). This leads to speculation that AURKA may be involved in promoting p53 dissociation from the centrosome and subsequent centrosomal duplication, but this has not yet been shown.

p53 can also associate with the duplicated centrosomes during G2/M and is involved in establishing G2 arrest following DNA damage through inhibition of cyclin B (Wang *et al.* 2009). Conversely AURKA activation is coupled with the successful duplication of the centrosomes through NPM1 (Reboutier *et al.* 2012). Plk1, a well-known co-operator and substrate of active AURKA in G2, is capable of promoting degradation of p53 and could feasibly affect p53 function at the centrosome at G2 (Yang *et al.* 2009). Convergence of signalling upon Cdk1/Cyclin B at the centrosome during mitotic entry is AURKA dependent. Cyclin B2 activity has been shown to be antagonise p53-dependent inhibition of AURKA activity to coordinate mitotic entry and centrosomal separation (Nam and van Deursen 2014). Therefore, AURKA and p53 act in a mutually antagonistic manner at the centrosomes to regulate centrosome biology and cell cycle progression. This relationship is functionally analogous to that of AURKA and p73 during mitosis, described earlier, which coordinates the balance between spindle assembly checkpoint function and mitotic progression (Katayama *et al.* 2012).

There is also evidence of functional interplay between AURKA and p53 in stem cell maintenance. p53 can associate with NUMB to antagonise the expression of

transcription factors associated with the maintenance of cellular pluripotency (Bric *et al.* 2009) serving to moderate stem cell division. Work in hepatocellular carcinoma cancer stem cells reveals that AURKA, through activation of atypical protein kinase C (aPKC), phosphorylates NUMB, disrupting NUMB p53 interaction and destabilising p53 (Siddique *et al.* 2015). This promoted the maintenance of a pluripotent phenotype (Siddique *et al.* 2015). AURKA has also been shown to maintain cellular pluripotency in embryonic stem cells with evidence of p53 antagonism during this process (D.-F. Lee *et al.* 2012). This suggests that AURKA and p53 establish a balance between the maintenance of a pluripotent phenotype and cellular differentiation.

Critically, AURKA (Zhou *et al.* 1998) and AURKB (Ota *et al.* 2002) have both been implicated in tumourigenesis when their expression is dysregulated. There is an emerging hypothesis that AURKC when overexpressed may also contribute to tumourigenesis (Khan *et al.* 2011; Quartuccio and Schindler 2015), but the mechanism of AURKC mediated tumourigenesis is unclear.

1.4. The Oncogenic Role of AURKA Overexpression

1.4.1. AURKA overexpression in cancers and transforming mechanism

AURKA overexpression has been indicated in a range of solid and haematological malignancies suggesting an oncogenic role for AURKA in cancer (Bischoff *et al.* 1998; Gritsko *et al.* 2003; Lo Iacono *et al.* 2011; Lucena-Araujo *et al.* 2011; Chuang *et al.* 2016; Dawei *et al.* 2018; Guo *et al.* 2018; Subramanian and Cohen 2019). Overexpression of AURKA can result from changes in gene copy number, transcriptional activation, protein modification dynamics and epigenetic dysregulation (Bischoff *et al.* 1998; Reiter *et al.* 2006; Kitajima *et al.* 2007; Lo Iacono *et al.* 2011;

He *et al.* 2018). There is also evidence that AURKA is subject to single nucleotide polymorphisms (SNPs) in cancer with varying effects on tumour behaviour (Necchi *et al.* 2017; Baumann *et al.* 2018; Liao *et al.* 2018). In terms of overexpression, ectopic expression of AURKA in rodent fibroblast cell lines was sufficient for malignant transformation (Zhou *et al.* 1998). The transforming mechanism of AURKA overexpression is due to several downstream effects. AURKA overexpression can contribute to tumourigenesis by causing an override of G2 (Marumoto *et al.* 2002) and spindle assembly (Anand *et al.* 2003) checkpoints. The G2 and spindle checkpoints function to ensure genomic integrity is preserved through critical stages of mitosis and thus AURKA-driven override of these checkpoints enhances the chance of genetic mutations being fixed into the genome. AURKA activity at G2-M has been shown to be normally inhibited by DNA damage (Cazales *et al.* 2005). However, when AURKA is overexpressed it has been associated with a reduction in BRCA1 expression levels (Veerakumarasivam *et al.* 2008), a protein critical for establishing G2/M arrest (Yarden *et al.* 2002). Additionally, AURKA overexpression may drive inappropriate G2-M transition through the stabilisation of cyclin-B1 levels (Qin *et al.* 2009). AURKA overexpression can override the spindle assembly checkpoint resulting in mitotic abortion and tetraploidy, which in the right genetic context (lack of functional p53) can become genetically fixed and may support tumourigenesis (Meraldi *et al.* 2002). Also, AURKA overexpression has cancer promoting consequences upon tumour suppressor and proto-oncogene products. For example, AURKA overexpression has been shown to enhance the interaction between p53 and its negative regulator MDM2 serving to deplete the p53 levels and significantly impair the ability of a cell to instigate checkpoint arrest and apoptosis (Katayama *et al.* 2004). Moreover, in AURKA overexpressing cells p73 was

phosphorylated at S235 by AURKA and this was shown to inhibit the role of p73 in maintaining genomic integrity and appropriate spindle assembly checkpoint (Katayama *et al.* 2012). The expression of pro-apoptotic proteins is also indirectly affected by overexpression of AURKA (Hou *et al.* 2018; Wang-Bishop *et al.* 2018). AURKA overexpression also promotes the stabilisation or activation of other oncogenes such as c-Myc (Lu *et al.* 2014), n-Myc (Otto *et al.* 2009) and c-Src (Do *et al.* 2014). Interestingly, AURKA may act as a nuclear transcription factor, promoting c-Myc expression in a kinase independent mechanism (Zheng *et al.* 2016). AURKA overexpression is additionally implicated in tumour cell metastasis through roles in promoting tumour cell migration and invasion (Eterno *et al.* 2016; Yang *et al.* 2016; Chu *et al.* 2018; Dawei *et al.* 2018) including in NSCLC (Zheng *et al.* 2018). AURKA has also been associated with the maintenance of a cancer stem cell subpopulation (Eterno *et al.* 2016; Zheng *et al.* 2016; N. Yang *et al.* 2017). Therefore AURKA, when overexpressed, can enhance the likelihood of a cell undergoing malignant transformation and promotes malignant behaviour (see Figure 1.6).

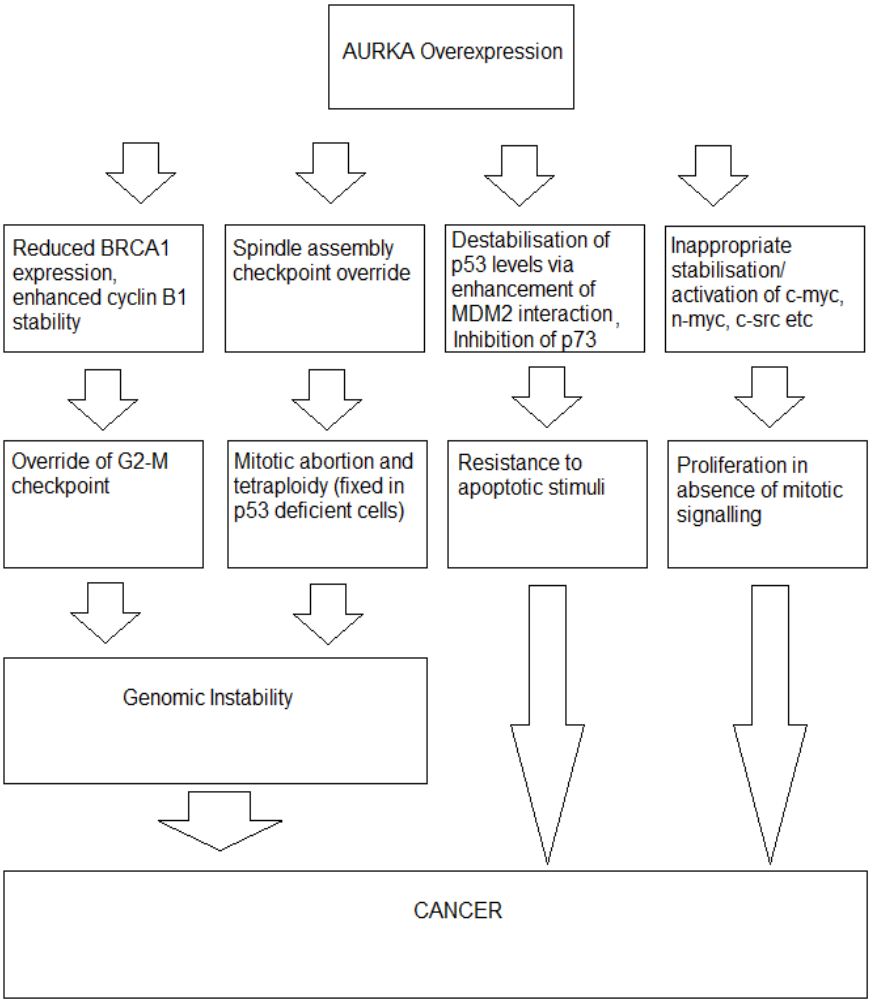

Figure 1.6. **The tumourigenic consequences of AURKA overexpression**. Adapted with permission from: Nikonova *et al* (2014).

1.4.2. AURKA overexpression in NSCLC

AURKA mRNA and protein overexpression has been demonstrated in NSCLC tissue samples when compared to equivalent non-neoplastic tissue (Lo Iacono *et al.* 2011; Al-Khafaji *et al.* 2017). Additionally, it was shown that 1.5-fold increased AURKA mRNA expression is associated with moderate to poor differentiation in lung tumours (Lo Iacono *et al.* 2011). Another study also found an association between high AURKA protein expression in NSCLC tumour samples and worse overall and progression free survival criterion (Xu *et al.* 2014). High AURKA expression, defined

as over 60% tumour tissue staining positive for expression, was detected in 56% of NSCLC samples (Xu *et al.* 2014). Interestingly, combined AURKA and p53 expression in NSCLC tumours has also been shown to confer a poor prognosis post-resection (Li *et al.* 2015). The context of AURKA overexpression in NSCLC however may be important. Ogawa *et al* (2008) found that whilst AURKA protein levels were elevated compared to non-neoplastic pulmonary tissue in nearly 83.6% of NSCLC samples only those with peri-membrane AURKA localisation (22%) conferred a poorer prognosis. Additionally, Ogawa *et al* (2008) and others have found that AURKA overexpression only had significant implications upon criteria such as tumour grade in the SCC NSCLC subtype (Ogawa *et al.* 2008; H.J. Lee *et al.* 2012). This is contrasted by findings that increased AURKA mRNA expression alone and as part of an eight-gene signature was prognostic in lung adenocarcinoma (Li *et al.* 2018; Zhang *et al.* 2018). Therefore, the currently available data suggest that AURKA overexpression is a common and clinically significant occurrence in NSCLC, albeit the importance of this may be restricted to a histological subtype of NSCLC.

1.4.3. The impact of AURKA overexpression on cancer treatment

Aside from a direct oncogenic role, AURKA overexpression has therapeutic implications. AURKA overexpression has been associated with resistance to radiotherapy in laryngeal squamous cell carcinoma *in vitro* (Guan *et al.* 2007). Indeed, it has been shown in cervical squamous cell carcinoma (CSCC) patients treated with definitive radiotherapy that high expression of AURKA in pre-therapy tumour biopsies predicted poorer overall survival and disease recurrence (Ma *et al.* 2017). Critically, this study found that CSCC patients with high pre-therapy AURKA expression in their tumours were less likely to achieve a complete response, and

more likely to have progressive disease in response to definitive radical radiotherapy (Ma *et al.* 2017). This suggests that AURKA expression has a direct effect on the likelihood of a tumour to respond to the deleterious effects of radiation and provides evidence that AURKA may predict radiation response in a patient population. Furthermore, AURKA has been implicated in chemoresistance to DNA damaging agents such as platinum-based agents (Wang *et al.* 2006; Lassmann *et al.* 2007; Mignogna *et al.* 2016) and anthracyclines (Zheng *et al.* 2014) in a range of carcinomas. Moreover, AURKA has been implicated in the resistance to biological therapies, including EGFR inhibitors in NSCLC (Shah *et al.* 2018). Orth *et al* (2018) conversely found that high AURKA mRNA expression was associated with improved overall survival in lung adenocarcinoma patients receiving taxane-based radiochemotherapy, but these findings are limited by small sample size and were not statistically significant. Hence, it is established that AURKA overexpression can affect therapeutic outcome. The relationship between AURKA overexpression and radiotherapy response however has not been fully investigated in primary NSCLC. Due to the emerging role of AURKA overexpression in tumourigenesis and therapeutic response, AURKA has been targeted pharmacologically in AURKA overexpressing cancers.

1.5. The use of AURKA inhibitors

1.5.1. AURKA inhibitor monotherapy

Several pharmacological AURKA specific inhibitors, as well as pan-inhibitors of the aurora kinase family, are now being evaluated in clinical trials in both monotherapy and combinational therapy contexts. ENMD-2076 is a specific inhibitor of AURKA in the aurora kinase family but has other kinase targets with sub-micro molar IC50s

(Tentler *et al.* 2010). A phase I trial in advanced solid tumour patients showed that ENMD-2076 monotherapy had a favourable toxicity profile with few patients experiencing grade 3 toxicities and the most common toxicities such as nausea being clinically manageable (Diamond *et al.* 2011). ENMD-2076 has since been progressed into phase II trials and has 1.shown modest activity in platinum-resistant ovarian cancer with a similar toxicity profile as that seen in phase I (Matulonis *et al.* 2013). Phase II trials in triple negative breast cancer and ovarian clear cell carcinoma have also been performed and indicate clinical benefit from ENMD-2076 monotherapy in a small subset of patients (Diamond *et al.* 2018; Lheureux *et al.* 2018) Another agent MK-5108 is a specific inhibitor of AURKA and has been shown to be well tolerated as a monotherapy but may be more useful in a combinatorial role in solid tumour patients (Minton *et al.* 2010). MLN8054 was an orally available specific AURKA inhibitor that was progressed into phase I clinical trials but abandoned due to dose limiting somnolence (Dees *et al.* 2011). Subsequent to this MLN8237 or Alisertib was developed and is highly specific inhibitor of AURKA without the central nervous system toxicities of MLN8054 (Manfredi *et al.* 2011). Alisertib is now the most extensively tested AURKA specific inhibitor in humans (Malumbres and Pérez de Castro 2014) and has previously shown promising tumour growth inhibition effects in preclinical studies (Manfredi *et al.* 2011; Palani *et al.* 2013). Several phase I dose-escalation studies in patients with advanced solid tumours have shown that Alisertib is generally well-tolerated (Cervantes *et al.* 2012; Dees *et al.* 2012). Alisertib has been tested both as a single-agent and in combination with other agents in a range of solid tumours including NSCLC in phase II (Melichar *et al.* 2015). Alisertib monotherapy failed to induce any significant objective response in NSCLC patients but was well tolerated with drug-related

toxicity being manageable (Melichar *et al.* 2015). Alisertib also entered a phase III clinical trial, as a monotherapy for treating relapsed or refractory peripheral T-cell lymphoma, but was withdrawn as it failed to demonstrate superior efficacy compared to standard of care (Takeda Pharmaceutical Company Ltd 2015; O'Connor *et al.* 2019). Notably phase III failure of Alisertib was not due to safety concerns (Takeda Pharmaceutical Company Ltd 2015). More recent meta-analysis has revealed that Alisertib treatment is associated with haematological toxicity but that these toxicities were mainly manageable (Tayyar *et al.* 2017). Overall, the available clinical trial data suggest that AURKA inhibition is generally well tolerated in solid tumour patients. Given the tolerability of AURKA inhibition in clinical trials, in addition to the *in vitro and in vivo* data suggesting that AURKA reduces the efficacy of certain therapeutics (Wang *et al.* 2006; Guan *et al.* 2007), there is a rationale for use of AURKA inhibitors in combination with other therapeutics in cancer. Indeed, there are now several active phase I and II clinical trials investigating the effect of combining Alisertib in solid tumours with chemotherapy, radiotherapy and other biological agents (see Table 1.3). In fact, recent clinical trial data has indicated that Alisertib Paclitaxel combination enhanced progression-free survival compared to Paclitaxel alone in advanced breast cancer or recurrent ovarian cancer patients (Falchook *et al.* 2019). Furthermore, a recent phase I safety trial in recurrent glioma patients combining stereotactic irradiation and escalating doses of Alisertib indicates that the combination was generally well tolerated (Song *et al.* 2019). This is likely to be followed up by a phase II trial to investigate combinational efficacy of Alisertib and radiation in glioma patients (Song *et al.* 2019). There is no evidence of a combinational trial using AURKA inhibitors and radiotherapy in NSCLC however.

	AURKA Inhibitor Monotherapy Trials				
Inhibitor	**Specificity for AURKA, AURKB and AURKC in cell free assays (IC50 nM)**	**Trial Identifier**	**Phase**	**Disease Type**	**Status**
ENMD-2076	14, 350, N/A (Tentler *et al*. 2010)	NCT01719744	II	Advanced/ metastatic soft tissue sarcoma	Complete (Veitch *et al*. 2019)
ENMD-2076	14, 350, N/A (Tentler *et al*. 2010)	NCT01914510	II	Ovarian clear cell carcinoma	Complete (Lheureux *et al*. 2018)
ENMD-2076	14, 350, N/A (Tentler *et al*. 2010)	NCT00806065	I	Relapsed/ refractory multiple myeloma	Complete
ENMD-2076	14, 350, N/A (Tentler *et al*. 2010)	NCT01104675	II	Platinum resistant ovarian cancer	Complete (Matulonis *et al*. 2013)
ENMD-2076	14, 350, N/A (Tentler *et al*. 2010)	NCT00904787	I	Relapsed/ refractory haematological malignancies	Complete (Yee *et al*. 2016)
ENMD-2076	14, 350, N/A (Tentler *et al*. 2010)	NCT02234986	II	Advanced fibrolamellar carcinoma	Complete
ENMD-2076	14, 350, N/A (Tentler *et al*. 2010)	NCT01639248	II	Previously treated, locally advanced or metastatic triple-negative breast cancer	Complete (Diamond *et al*. 2018)
ENMD-2076	14, 350, N/A (Tentler *et al*. 2010)	NCT00658671	I	Relapsed/ refractory cancers	Complete (Diamond *et al*. 2011)
MK-5108	0.064, 14, 12 (Shimomura et al. 2010)	NCT00543387	I	Advanced/ refractory solid cancers	Complete (Amin *et al*. 2016)
MLN8054	4, 172, N/A (Manfredi *et al*. 2007)	NCT00652158	I	Advanced malignancies	Terminated
MLN8054	4, 172, N/A (Manfredi *et al*. 2007)	NCT00249301	I	Advanced solid tumours	Terminated (Dees *et al*. 2011)
MLN8237 (Alisertib)	1.2, 396.5, N/A (Manfredi *et al*. 2011)	NCT01898078	I	Advanced solid tumours or lymphomas	Complete
MLN8237 (Alisertib)	1.2, 396.5, N/A (Manfredi *et al*. 2011)	NCT02114229	II	Atypical teratoid/rhabdoid tumours	Recruiting
MLN8237 (Alisertib)	1.2, 396.5, N/A (Manfredi *et al*. 2011)	NCT02293005	II	Unresectable malignant pleural mesothelioma	Active, closed to recruitment
MLN8237 (Alisertib)	1.2, 396.5, N/A (Manfredi *et al*. 2011)	NCT00807495	II	Relapsed/ refractory non-Hodgkin lymphoma	Completed (Friedberg *et al*. 2014)
MLN8237 (Alisertib)	1.2, 396.5, N/A (Manfredi *et al*. 2011)	NCT01512758	I	Adcanced solid tumours or lymphomas	Completed (Venkatakrishnan *et al*. 2015)

MLN8237 (Alisertib)	1.2, 396.5, N/A (Manfredi *et al.* 2011)	NCT02860000	II	Locally advanced/ metastatic endocrine resistant breast cancer	Recruiting
MLN8237 (Alisertib)	1.2, 396.5, N/A (Manfredi *et al.* 2011)	NCT01812005	II	Relapsed/ refractory B-cell non-Hogkin lymphoma	Terminated
MLN8237 (Alisertib)	1.2, 396.5, N/A (Manfredi *et al.* 2011)	NCT02530619	I	Myelofibrosis or relapsed/ refractory acute megakaryoblastic leukaemia	Active, closed to recruitment
MLN8237 (Alisertib)	1.2, 396.5, N/A (Manfredi *et al.* 2011)	NCT01714947	I	Advanced solid tumours or lymphomas	Completed
MLN8237 (Alisertib)	1.2, 396.5, N/A (Manfredi *et al.* 2011)	NCT02214147	I	Advanced solid tumours or relapsed/ refractory lymphomas	Completed
MLN8237 (Alisertib)	1.2, 396.5, N/A (Manfredi *et al.* 2011)	NCT01482962	III	Relapsed/ refractory peripheral T-cell lymphoma	Completed (O'Connor *et al.* 2019)
MLN8237 (Alisertib)	1.2, 396.5, N/A (Manfredi *et al.* 2011)	NCT01653028	II	Advanced/ metastatic sarcoma	Completed (Dickson *et al.* 2016)
MLN8237 (Alisertib)	1.2, 396.5, N/A (Manfredi *et al.* 2011)	NCT01637961	II	Recurrent/ persistent leiomyosarcoma of the uterus	Completed (Hyman *et al.* 2017)
MLN8237 (Alisertib)	1.2, 396.5, N/A (Manfredi *et al.* 2011)	NCT01466881	II	Relapsed/ refractory peripheral T-cell lymphoma	Completed (Barr *et al.* 2015)
MLN8237 (Alisertib)	1.2, 396.5, N/A (Manfredi *et al.* 2011)	NCT01154816	II	Paediatric relapsed/ refractory solid tumours or leukaemias	Completed (Mossé *et al.* 2019)
MLN8237 (Alisertib)	1.2, 396.5, N/A (Manfredi *et al.* 2011)	NCT01045421	I/II	Breast cancer, SCLC, NSCLC, head and neck squamous cell carcinoma, gastro-oesphageal adenocarcinoma	Completed (Melichar *et al.* 2015)
MLN8237 (Alisertib)	1.2, 396.5, N/A (Manfredi *et al.* 2011)	NCT02444884	I/II	Paediatric relapsed/ refractory solid tumours	Completed
MLN8237 (Alisertib)	1.2, 396.5, N/A (Manfredi *et al.* 2011)	NCT00962091	I	Advanced solid tumours	Completed (Falchook *et al.* 2016)
MLN8237 (Alisertib)	1.2, 396.5, N/A (Manfredi *et al.* 2011)	NCT00853307	II	Ovarian, fallopian tube or peritoneal carcinoma	Completed

MLN8237 (Alisertib)	1.2, 396.5, N/A (Manfredi *et al*. 2011)	NCT00697346	I	Advanced haematological malignancies	Completed (Kelly *et al*. 2014)
MLN8237 (Alisertib)	1.2, 396.5, N/A (Manfredi *et al*. 2011)	NCT01799278	II	Metastatic catstrate-resistant neuroendocrine prostate cancer	Completed (Beltran *et al*. 2018)
MLN8237 (Alisertib)	1.2, 396.5, N/A (Manfredi *et al*. 2011)	NCT01316692	II	Unresectable stage III-IV melanoma	Terminated
MLN8237 (Alisertib)	1.2, 396.5, N/A (Manfredi *et al*. 2011)	NCT00500903	I	Advanced solid tumours	Completed (Dees *et al*. 2012)
MLN8237 (Alisertib)	1.2, 396.5, N/A (Manfredi *et al*. 2011)	NCT00830518	II	Acute myeloid leukaemia or high-grade myelodysplastic syndrome	Completed (Goldberg *et al*. 2014)
MLN8237 (Alisertib)	1.2, 396.5, N/A (Manfredi *et al*. 2011)	NCT00651664	I	Advanced malignancies	Completed (Cervantes *et al*. 2012)
LY3295668	0.8, 1083, N/A (Gong *et al*. 2019)	NCT03898791	Ib	Extensive stage SCLC	Recruiting
LY3295668	0.8, 1083, N/A (Gong *et al*. 2019)	NCT03955939	I	Metastatic breast cancer	Not yet recruiting
LY3295668	0.8, 1083, N/A (Gong *et al*. 2019)	NCT03092934	I/II	Solid tumours	Active, closed to recruitment
TAS-119	N/A	NCT02448589	I	Advanced solid tumours	Active, closed to recruitment
	AURKA Inhibitor Combination Trials				
Inhibitor	**Combination**	**Trial Identifier**	**Phase**	**Disease Type**	**Status**
MK-5108	Docetaxel	NCT00543387	I	Advanced/ refractory solid cancers	Complete (Amin *et al*. 2016)
MLN8237 (Alisertib)	Rituximab, etoposide, doxorubicin, vincristine, cyclophosphamide and prednisone	NCT02700022	I	Myc-positive B-cell lymphoma	Terminated
MLN8237 (Alisertib)	**Radiation**, methotrexate, cisplatin, carboplatin, cyclophosphamide, etoposide, topotecan, vincristine, surgical resection	NCT02114229	II	Atypical teratoid/rhabdoid tumours	Recruiting
MLN8237 (Alisertib)	Paclitaxel	NCT02109328	II	Relapsed/ refractory urothelial cancer	Completed (Necchi *et al*. 2016)

MLN8237 (Alisertib)	TAK-228	NCT02812056	I	Human papilloma virus associated malignancies	Withdrawn
MLN8237 (Alisertib)	TAK-733	NCT01613261	I	Advanced solid tumours	Withdrawn
MLN8237 (Alisertib)	Paclitaxel	NCT02187991	II	Triple-negative locally recurrent/ metastatic breast cancer	Active, closed to recruitment
MLN8237 (Alisertib)	Cytarabine, idarubicin	NCT01779843	I	Acute myeloid leukaemia	Completed
MLN8237 (Alisertib)	Fluorouracil, leucovorin calcium, oxaliplatin	NCT02319018	I	Gastrointestinal tumours	Completed (Goff *et al*. 2017)
MLN8237 (Alisertib)	**Fractionated stereotactic radiosurgery**	NCT02186509	I	Recurrent high grade gliomas	Completed (Song *et al*. 2019)
MLN8237 (Alisertib)	Paclitaxel	NCT02367352	I	Advanced solid tumours	Terminated
MLN8237 (Alisertib)	Fulvestrant	NCT02860000	II	Locally advanced/ metastatic endocrine resistant breast cancer	Recruiting
MLN8237 (Alisertib)	Abiraterone acetate, prednisone	NCT01848067	I/II	Hormone resistant prostate cancer	Completed (Lin *et al*. 2016)
MLN8237 (Alisertib)	Cytarabine, idarubicin, daunorubicin	NCT02560025	II	Acute myeloid leukaemia	Active, closed to recruitment (Brunner *et al*. 2018)
MLN8237 (Alisertib)	Rituximab	NCT01812005	II	Relapsed/ refractory B-cell non-Hogkin lymphoma	Terminated
MLN8237 (Alisertib)	Fulvestrant	NCT02219789	I	Hormone receptor positive metastatic/locally advanced/ unresectable breast cancer	Completed
MLN8237 (Alisertib)	Itraconazole	NCT02259010	I	Advanced solid tumours or relapsed/ refractory lymohomas	Unknown
MLN8237 (Alisertib)	Esomeprazole, rifampin	NCT01844583	I	Advanced solid tumours or relapsed/ refractory lymohomas	Completed
MLN8237 (Alisertib)	Paclitaxel	NCT02038647	II	SCLC	Completed

MLN8237 (Alisertib)	MLN2480	NCT02327169	Ib	Advanced solid tumours	Completed (Olszanski *et al*. 2017)
MLN8237 (Alisertib)	MLN0128	NCT02719691	I	Advanced solid tumours, metastatic triple-negative breast cancer	Recruiting
MLN8237 (Alisertib)	Romidepsin	NCT01897012	I	Relapsed/ refractory B-cell or T-cell lymphomas	Completed (Strati *et al*. 2019)
MLN8237 (Alisertib)	Gemcitabine	NCT01924260	I	Solid tumours, pancreatic cancer	Active, closed to recruitment (Kim *et al*. 2015)
MLN8237 (Alisertib)	Irinotecan	NCT01923337	I	Solid tumours, colorectal cancer	Completed
MLN8237 (Alisertib)	Bortezomib, rituximab	NCT01695941	I	Relapsed/ refractory mantle cell lymphoma or B-cell low grade non-Hodgkin lymphoma	Active, closed to recruitment
MLN8237 (Alisertib)	Vorinostat	NCT01567709	I	Relapsed/ refractory Hodgkin lymphoma, B-cell non-Hodgkin lymphoma, peripheral T-cell lymphoma	Completed
MLN8237 (Alisertib)	Paclitaxel	NCT01091428	I/II	Advanced breast cancer, recurrent ovarian cancer	Completed (Falchook *et al*. 2019)
MLN8237 (Alisertib)	Docetaxel	NCT01094288	I	Advanced solid tumours, castration-resistant prostate cancer	Completed
MLN8237 (Alisertib)	Pazopanib	NCT01639911	I	Advanced solid tumours	Completed (Shah *et al*. 2019)
MLN8237 (Alisertib)	**Radiotherapy**, cetuximab	NCT01540682	Ib	Head and neck squamous cell carcinoma	Completed
MLN8237 (Alisertib)	Albumin-stabilized nanoparticle formulation paclitaxel	NCT01677559	I	Metastatic/ advanced solid malignancies	Completed (Lim *et al*. 2017)
MLN8237 (Alisertib)	Irinotecan, temozolomide	NCT01601535	I/II	Relapsed/ refractory neuroblastoma	Completed (DuBois *et al*. 2018)
MLN8237 (Alisertib)	Brentuximab vedotin	NCT02780011	I	Relapsed/ refractory CD30 positive lymphomas and solid tumours	Withdrawn

MLN8237 (Alisertib)	Rituximab, vincristine	NCT01397825	I/II	Relapsed/ refractory B-cell lymphoma	Completed (Kelly *et al*. 2018)
MLN8237 (Alisertib)	Bortezomib	NCT01034553	I/II	Relapsed/ refractory multiple myeloma	Completed
MLN8237 (Alisertib)	Erlotinib	NCT01471964	I/II	Recurrent locally advanced or metastatic NSCLC	Terminated after phase I (Godwin *et al*. 2016)
TAS-119	Paclitaxel	NCT02134067	I	Advanced solid tumours	Unknown

Table 1.3 **A summary of historical and ongoing AURKA inhibitor clinical trials as monotherapy or combinational therapy**. Data populated using the clinicaltrials.gov clinical trial database (US National Library of Medicine 2019)

1.5.2. Concurrent use of AURKA inhibitors and radiotherapy

There is emerging support for combining AURKA inhibitors with radiotherapy to potentiate cellular response to IR. Alisertib has been shown to enhance radiation response in glioblastoma and atypical teratoid rhabdoid tumour models respectively *in vitro* (Venkataraman *et al.* 2012; Hong *et al.* 2014). Co-targeting of AURKA and AURKB was also shown to synergise with radiation in cell line and primary glioblastoma cultures *in vitro* (Borges *et al.* 2012). Radio-sensitisation of p53-deficient hepatocellular carcinoma cell lines *in vitro* and *in vivo* has been reported using VE-465 (Lin *et al.* 2014). However this may not indicate that AURKA inhibition alone radio-sensitises as VE-465 inhibits both AURKA and AURKB and there was no validation of singular AURKA inhibition effect on relative radiosensitivity (Lin *et al.* 2014). Another agent Daurinol, which is a plant-derived topoisomerase II inhibitor, has been shown to radio-sensitise three NSCLC cell lines *in vitro* and *in vivo* via the inhibition of transcription of AURKA and AURKB (Woo *et al.* 2015). Critically, Woo *et al* (2015) used short interfering RNA (siRNA) targeted to AURKA and AURKB

individually to validate their findings using Daurinol and demonstrated radio-sensitisation by AURKA inhibition alone in two NSCLC cell lines. Additionally, the AURKA inhibitor Alisertib has shown radiosensitising activity in a p53-dependant manner in a small panel of NSCLC cell lines (Myers *et al.* 2013). This provides some of the first evidence that AURKA can be singularly targeted in NSCLC to enhance response to radiation.

The mechanism by which inhibition of AURKA in AURKA overexpressing cancer reverses the radio-resistant phenotype is subject to speculation. It has been suggested that the radio-sensitising potential of AURKA inhibition lies with interactions between AURKA and mediators of the DNA damage repair response (Wang *et al.* 2014a). In breast, pancreatic and ovarian epithelial cancer cell lines respectively it was shown that AURKA overexpression reduces BRCA1/2, ATR/CHK1, p53 (including S15 phosphorylation of p53), γ-H2A histone family, member X (γH2AX) (S319) and Rad51 expression (Sun *et al.* 2014). It was suggested that AURKA overexpression led to a deficiency in appropriate cell cycle checkpoint arrest and induction of DNA repair in response to IR (Sun *et al.* 2014). Indeed, a role for AURKA opposing homologous recombination based repair of DNA has been shown in breast cancer cell lines whereby forced overexpression of AURKA caused reduced Rad51 foci in response to IR and sensitised cells to PARP inhibitors (Sourisseau *et al.* 2010). Also it has been implied that BRCA1/2, through an unknown interaction, oppose the actions of AURKA in establishing an appropriate pro-arrest/repair/apoptotic response to the DNA damage induced by IR and provides a rationale for inhibiting AURKA alongside radiotherapy (Wang *et al.* 2014b). However, the mechanism is far from understood.

Furthermore, in the context of NSCLC there is little data regarding the proposed mechanisms of radiosensitisation by inhibiting AURKA. The studies by Woo *et al* (2015) and Myers *et al* (2013) only demonstrate a radiosensitisation effect in NSCLC cell lines after AURKA inhibition and do not offer mechanistic explanation of response past AURKA inhibition itself. Also, the work by Sun *et al* (2014), indicating that AURKA overexpression led to a downregulation of certain components of the DNA repair response pathway, only addressed this situation with protein expression and cell cycle data. This work did not appraise the functional consequences of DNA repair downregulation further than γ-H2AX foci formation and was not performed in models of NSCLC.

It could also be argued that Alisertib, alone or in combination with IR could be just as useful in other diseases such as SCLC. Indeed, there is clinical evidence to suggest that SCLCs are more sensitive to Alisertib monotherapy (Melichar *et al.* 2015) which may be related to an increased incidence of MYC amplification (Sos *et al.* 2012), and Alisertib has been shown to improve progression free survival in combination with Paclitaxel in SCLC (Owonikoko *et al.* 2017). Furthermore, radiotherapy is also used flexibly throughout the treatment of SCLC (Glatzer *et al.* 2017) with similar utilisation rates to that in NSCLC historically (Delaney *et al.* 2005). However, NSCLC is a much more prevalent disease compared to SCLC (Jemal *et al.* 2011) thus increasing the pool of patients that could potentially benefit from a combination of Alisertib and IR.

Taken together, NSCLC is a clinically significant problem and is associated with poor overall survival. Radiotherapy is a commonly used and flexible treatment modality in the treatment of NSCLC throughout the different stages of disease but is hindered by radio-resistance and the toxicity of conventional radiotherapy. Moreover, there is a paucity of predictive biomarkers available to identify which NSCLC patients will

benefit most from radiotherapy. The mitotic kinase AURKA is overexpressed in NSCLC and has been shown to associate with a poor prognosis and a poorly differentiated tumour phenotype in some studies. Additionally, AURKA has been shown to, when overexpressed, negatively affect the efficacy of radiotherapy in a range of cancers. Specific inhibitors of AURKA have since been developed, are in clinical trials and are noted for their general tolerability. Given that radiotherapy outcome is sub-optimal in NSCLC and that AURKA may be overexpressed by a proportion of these tumours, there is a rationale that concurrent AURKA inhibition with radiotherapy may improve the therapeutic ratio of radiotherapy in NSCLC patients.

Subsequently, the first hypothesis of this PhD thesis is that inhibiting AURKA in NSCLC cells will sensitise these cells to the effects of IR. The second hypothesis of this thesis is that AURKA expression levels can predict patient response to radiotherapy in primary NSCLC samples.

The aims of this project are to:

1. Generate *in vitro* and *in vivo* proof of concept data for radiosensitisation of NSCLC cells using AURKA inhibitors and AURKA siRNA
2. Examine AURKA expression in primary NSCLC tumours and how expression status predicts radiotherapy response
3. Investigate the molecular mechanism of radiosensitisation

2. Materials & Methods

2.1. Materials

2.1.1. Chemicals

Chemical	Supplied by
Acetone	Fisher Scientific
Agarose	Sigma Aldrich
Amersham enhanced chemiluminescence (ECL) western blotting reagent	GE Life Sciences
Ammonium persulphate (APS)	Fisher Scientific
Bovine serum albumin (BSA)	Sigma Aldrich
Bromophenol blue	Sigma Aldrich
4′,6-Diamidine-2′-phenylindole dihydrochloride (DAPI)	Vector Laboratories
Diaminobenzidine	Vector Laboratories
Dimethyl sulphoxide (DMSO)	Fisher Scientific
Dithiothreitol (DTT)	Fisher Scientific
Dharmafect 1	GE Life Sciences
Ethanol	Fisher Scientific
Ethylenediaminetetraacetic acid (EDTA)	Sigma Aldrich
Glycerol	Fisher Scientific
Glycine	Fisher Scientific
Hydrochloric acid	Sigma Aldrich
45% Hydroxypropyl-β-cyclodextrin (HBC)	Sigma Aldrich
Industrial methylated spirit (IMS)	Fisher Scientific
Isopentane	Sigma Aldrich

Methanol	Fisher Scientific
Methylene Blue	Sigma Aldrich
NP-40	Merck
O.C.T. Compound	Fisher Scientific
4% paraformaldehyde	Boster
Phenylmethanesulfonyl fluoride (PMSF)	Sigma Aldrich
Phosphatase inhibitor cocktails I & II	Sigma Aldrich
Propidium iodide (PI)	Sigma Aldrich
Protease inhibitor	Sigma Aldrich
Protogel (30% acrylamide, 0.8% w/v bis-acrylamide stock solution)	Geneflow
7.5% Sodium bicarbonate ($NaHCO_3$)	Sigma Aldrich
Sodium chloride	Fisher Scientific
Sodium dodecyl sulphate (SDS)	Sigma Aldrich
Sodium deoxycholate	Sigma Aldrich
Sodium hydroxide	Fisher Scientific
Target Retrieval Solution (10x), Citrate pH 6.1	Dako
Tetracycline	Fisher Scientific
Tetramethylethylenediamine (TEMED)	VWR
Tris Base	Fisher Scientific
Triton X-100	Sigma
Tween 20	Acros Organics
Universal x-ray developer	Champion Protochemistry

Universal x-ray fixer	Champion Protochemistry
Xylene	Fisher Scientific
β-mercaptoethanol	Sigma Aldrich

2.1.2. Cell lines

Cell Line	Supplied by	Genotype	p53 Status
A549	PHE	Human lung adenocarcinoma	Wildtype
H520	ATCC	Human lung squamous cell carcinoma	Wildtype
H460	P. Woll (Zhu *et al.* 2008)	Human lung large cell carcinoma	Wildtype
H322	PHE	Human lung adenocarcinoma	Mutant
H1299	ATCC	Human lung large cell carcinoma	Null
SW900	ATCC	Human lung squamous cell carcinoma	Mutant
Lewis Lung Carcinoma (LLC-1)	Dr Will English (Bertram and Janik 1980)	Mouse lung carcinoma	Wildtype
HCT116 p53 +/+	Prof Mark Meuth (Bunz	Human colorectal carcinoma	Wildtype

	et al. 1998)		
HCT116 p53 -/-	Prof Mark Meuth (Bunz *et al.* 1998)	Human colorectal carcinoma	Null

PHE: Public Health England, ATCC: American Type Culture Collection

2.1.3. Cell culture reagents

2.1.3.1. Foetal calf serum (FCS)

Virus, endotoxin and mycoplasma free FCS was supplied by Seralab and stored at -20 ^{o}C until used.

2.1.3.2. Cell culture medium

Cells were cultured in Dulbecco's modified eagles medium (DMEM) containing 4.5 g/L glucose with L-glutamine (A549, HCT116 p53 +/+, HCT116 p53 -/-, LLC-1) or Roswell Park Memorial Institute (RPMI)-1640 medium (H520, H460, H322, H1299, SW900) with L-glutamine. Both culture mediums were from Lonza and stored at 4 ^{o}C. Media was supplemented with 10% foetal calf serum and 1x non-essential amino acids (NEAA) supplied by Lonza.

2.1.3.3. Trypsin and versene/EDTA

Trypsin EDTA with 0.5 g/L Trypsin and 0.2 g/L versene (EDTA) was supplied by Lonza.

2.1.3.4. Matrigel matrix

Growth factor reduced, Phenol Red-free Matrigel® basement membrane matrix was supplied by Corning.

2.1.4. Buffers

2.1.4.1. Phosphate buffered saline (PBS)

PBS was produced by dissolving one Oxoid PBS tablet per every 100 ml of ddH_2O. PBS was sterilised by autoclave and stored at room temperature.

2.1.4.2. Tris-buffered saline (TBS)

10x TBS solution was produced by dissolving 24.2 g Tris Base (200 mM) and 80 g NaCl (1.4 M) in 900 ml ddH_2O. 5 M HCl was then used to adjust solution pH to 7.6 before final volume was adjusted to 1 L with ddH_2O. 10x solution was kept at room temperature. 1x solution was achieved by diluting 10x solution with ddH_2O.

2.1.4.3. 1 M Tris pH 6.8 and 8.0

1 M Tris solution was produced by dissolving 121.1 g of Tris Base in 900 ml ddH_2O. 5 M HCl was then used to adjust solution pH to 6.8 or 8.0 before final volume was adjusted to 1 L with ddH_2O. 1 M Tris pH 6.8 and pH 8.0 were stored at room temperature.

2.1.4.4. 1.5 M Tris pH 8.8

1.5 M Tris solution was produced by dissolving 181.7 g of Tris Base in 700 ml ddH_2O. 5 M HCl was then used to adjust solution pH to 8.8 before final volume was adjusted to 1 L with ddH_2O. 1.5 M Tris pH 8.8 was stored at room temperature.

2.1.4.5. 10 mM Tris 1 mM EDTA solution pH 9.0

10 mM Tris 1 mM EDTA solution was produced by dissolving 1.21 g of Tris Base and 0.37 g EDTA in 900 ml ddH_2O. 5 M HCl was then used to adjust solution pH to 9.0. 0.5 ml Tween 20 (0.05%) was added to the solution before bringing up volume to 1 L with ddH_2O.10 mM Tris 1 mM EDTA solution pH 9.0 was stored at 4 ^oC.

2.1.4.6. 5 x RIPA lysis buffer

100 ml 5 x RIPA lysis buffer was produced by adding 25 ml 1 M Tris pH 8.0 (250mM), 15 ml 5 M NaCl (750mM), 5 ml 10% SDS (0.5%), 5 ml NP-40 (5%), 2.5 g Sodium deoxycholate (2.5%) and ddH_2O to bring volume to 100 ml. 5 x RIPA lysis buffer was stored at room temperature.

2.1.4.7. 5 x SDS sample buffer

100 ml 5 X SDS sample buffer was produced by adding 25 ml 1 M Tris pH 6.8 (250mM), 10 g SDS (10%), 50 ml glycerol (50%), 5 ml β-mercaptoethanol (5%), 20 mg bromophenol blue (0.02%) and ddH_2O to bring volume to 100 ml. 5 x SDS sample buffer was stored at room temperature.

2.1.4.8. 10 x SDS-polyacrylamide gel electrophoresis (SDS-PAGE) running buffer

10 x SDS-PAGE running buffer was produced by dissolving 30 g Tris Base (250 mM) and 144 g Glycine (1.9 M) in 900 ml ddH_2O. Then 100 ml of 10% SDS (1%) was added to bring volume up to 1 L.10 x SDS-PAGE running buffer was stored at room temperature.

2.1.4.9. 1 x SDS-PAGE running buffer

1 x SDS-PAGE running buffer was produced by diluting 100 ml 10 x SDS-PAGE running buffer with 900 ml ddH_2O.

2.1.4.10. 10 x Towbin transfer buffer

10 x Towbin transfer buffer was produced by dissolving 30.3 g Tris Base (250 mM) and 144 g Glycine (1.9 M) in ddH_2O bringing volume to 1 L.

2.1.4.11. 1 x Towbin transfer buffer

1 x Towbin transfer buffer was produced by mixing 100 ml 10 x Towbin buffer, 700 ml of ddH_2O and 200 ml methanol in that order, 1 x Towbin transfer buffer was stored at 4 ^oC on day of use.

2.1.5. Inhibitor Compounds

Compound	Mechanism	Diluent	Storage	Company
MLN8237 (Alisertib)	Inhibits T288 auto-phosphorylation of AURKA	DMSO	-20 ^oC	Selleckchem
Nocodazole	Inhibits microtubule polymerisation	DMSO	-20 ^oC	Sigma Aldrich
Etoposide	Topoisomerase II poison	DMSO	-20 ^oC	Sigma Aldrich

2.1.6. Irradiation

Irradiation of cells was performed using a CIB/IBL 437 CS-137 irradiator. Irradiations were performed in a 3.8 L irradiation canister and were delivered to cells directly in 90 mm^3 dishes (when cells were plated prior to irradiation) or to cells in 15 ml falcon tubes (when cells were to be plated following irradiation).

2.1.7. Short interfering RNA (siRNA) and transfection reagents

siRNA duplexes were made up to 20 μM stock solution in RNAse free siRNA duplex resuspension buffer (Origene) and stored at -20 ^oC:

SR30004 Universal scrambled negative control siRNA duplex (Origene)

AURKA siRNA duplexes (Origene):

AURKA-siRNA 1: 5’ CGAAGAGAGUUAUUCAUAGAGACAT 3’

AURKA-siRNA 2: 5’ GGAACAGUUUAUAGAGAACUUCAGA 3’

AURKA-siRNA 3: 5’ AGCUAGCAAACAGUCUUAGGAAUCG 3’

P53 siRNA duplexes:

s605 (Ambion): GUAAUCUACUGGGACGGAATT

SC-29435 (Santa Cruz Biotechnology): propriety sequence of Santa Cruz Biotechnology.

2.1.8. Antibodies

2.1.8.1. Primary antibodies

Antibody	Host Animal	Manufacturer (Cat number)	Application (Dilution)
pThr288 AURKA, pThr232 AURKB, pThr198 AURKC	Rabbit	Cell Signalling Technology (2914)	WB (1:500)
AURKA	Mouse	Sigma Aldrich (A1231)	WB (1:1000), IHC (1:500-1000)
AURKB	Mouse	Sigma Aldrich (WH0009212M3)	WB (1:1000)
AURKC	Goat	Thermo Fisher Scientific (PA5-19562)	WB (1:1000)
β-tubulin	Mouse	Sigma-Aldrich (T8328)	WB (1:10000)
β-tubulin	Mouse	Sigma-Aldrich (T4026)	IF (1:500)
pSer10 Histone 3	Rabbit	Cell Signalling Technology (9701)	WB (1:20000)
pSer10 Histone 3	Rabbit	Abcam (Ab47297)	FACS (1:500)
pSer10 Histone 3	Rabbit	Abcam (Ab5176)	IHC (1:1000)
p53	Mouse	Santa Cruz Biotechnology (sc-126)	WB (1:1000)
p-Ser9 p53	Rabbit	Cell Signalling Technology (9288)	WB (1:1000)
p-Ser15 p53	Mouse	Cell Signalling Technology (9286)	WB (1:1000)
p-Thr18 p53	Rabbit	Cell Signalling Technology (2529)	WB (1:1000)
p-Ser20 p53	Rabbit	Cell Signalling Technology (9287)	WB (1:1000)
Pericentrin	Rabbit	Abcam (Ab4448)	IF (1:2000)
γH2AX	Rabbit	Cell Signalling Technology (2577)	IF (1:1000)
Chk1	Mouse	Cell Signalling Technology	WB (1:1000)

		(2360)	
p-Ser345 Chk1	Rabbit	Cell Signalling Technology (2348)	WB (1:1000)
Chk2	Rabbit	Cell Signalling Technology (2662)	WB (1:1000)
p-Thr68 Chk2	Rabbit	Cell Signalling Technology (2661)	WB (1:1000)
Akt	Mouse	(BD Biosciences) 610826	WB (1:2000)
p-Ser473 Akt	Rabbit	Abcam (Ab81283)	WB (1:5000)
PTEN	Rabbit	Cell Signalling Technology (9559)	WB (1:2000)
CD31 (mouse)	Rat	Dianova (DIA-310)	IHC (1:200)
Ki67	Rabbit	Abcam (Ab16667)	IHC (1:400)

WB: Western blot, IHC: Immunohistochemistry, IF: Immunofluorescence,

FACS: Fluorescence activated cell sorting

2.1.8.2. Blocking peptides

Peptide	**Host Animal**	**Manufacturer (Cat number)**	**Application (Dilution)**
AURKA blocking peptide	Synthetic peptide	Fitzgerald International Industries (33R-1465)	IHC (1:1000-1:200)

2.1.8.3. Secondary Antibodies

Antibody	**Host Animal**	**Manufacturer (Cat number)**	**Application (Dilution)**
Anti-mouse IgG horse radish peroxidase (HRP)	Horse	Cell Signalling Technology (7076)	WB (1:2000)
Anti-rabbit IgG HRP	Goat	Cell Signalling Technology (7074)	WB (1:2000)

Anti-goat IgG HRP	Rabbit	Dako (P0160)	WB (1:2000)
Anti-mouse Alexa 488	Goat	Life Technologies (A11017)	IF (1:1,000)
Anti-rabbit Alexa 594	Goat	Life Technologies (A11012)	IF (1:1000)
Anti-rabbit Alexa 488	Mouse	Life Technologies (A11008)	FACS (1:200)
Anti-mouse IgG Biotinylated	Goat	Vector Labs (BA-9200)	IHC (1:200)
Anti-rabbit IgG Biotinylated	Goat	Vector Labs (BA-1100)	IHC (1:200)
Anti-rat IgG Biotinylated (mouse adsorbed)	Rabbit	Vector Labs (BA-4001)	IHC (1:200)

WB: Western blot, IHC: Immunohistochemistry, IF: Immunofluorescence, FACS: Fluorescence-activated cell sorting

2.1.9. Mouse models

Male nude CD-1 and C57BL/6 mice aged 4-6 weeks were purchased from Charles River.

2.2. Methods

2.2.1. Mammalian cell culture

2.2.1.1. Passaging cells

NSCLC cell lines were maintained at 37 ^{o}C with 5% CO_2 in T25 or T75 flasks. To passage cells culture media was removed and cells were washed twice in 5 ml PBS. Following washing cells were dislodged from the bottom of the flask by adding 1 ml Trypsin EDTA and returning cells to 37 ^{o}C. Once cells were fully dislodged in trypsin EDTA 9 ml of warm (37 ^{o}C) culture media was used to dilute trypsin. Freshly resuspended cells were then used to seed new flasks.

All experiments were performed when cells were 60-80% confluent to ensure cells were in logarithmic growth phase.

2.2.1.2. Freezing cells

After cells had been suspended in fresh media following trypsin EDTA exposure they were centrifuged in 15 ml falcon tubes at 1200 revolutions per minute (RPM) for 3 minutes. Cellular pellets were resuspended in culture media with 10% DMSO at a density of $1x10^6$ cells per ml. Cells for freezing were distributed into 1 ml cryovials and stored overnight at -80 ^oC in a Mr. Frosty™ Freezing Container supplied by Thermo Fisher Scientific. Following this cells were kept at -80 ^oC for short term storage (< 1 year) and in liquid nitrogen for long term storage (> 1 year).

2.2.1.3. Thawing cells

Resuscitation of frozen cells was achieved by rapidly thawing cells at 37 ^oC in a water bath. Following this cells were transferred from cryovial to a 15 ml falcon tube before 9 ml of warm culture media was gently added in dropwise manner. Cells were then centrifuged at 1200 RPM for 3 minutes before being resuspended in 10 ml media and transferred to a culture flask.

2.2.1.4. Clonogenic survival assays

Plating density of NSCLC cells was varied between 500-5000 cells per condition plated in 90 mm^3 dishes. After appropriate treatment cells were left to form colonies for 10-14 days, following this media was removed and colonies were stained with methylene blue in methanol (4 g/L). Colonies were defined using a threshold of 50 viable cells and counted. Plating efficiency was calculated as number of colonies/number of cells plated. Survival fraction was determined as plating efficiency of condition/plating efficiency of unirradiated control. Unirradiated controls were sham irradiated by rotation in irradiation canister without irradiation exposure.

Minimum of three independent biological repeats were achieved with averages and standard deviations calculated.

2.2.1.4.1. Irradiation/inhibitor alone experiments

Cells were plated and allowed approximately 4 hours to adhere to plate, following this cells were treated as appropriate.

2.2.1.4.2. Irradiation inhibitor combination experiments

When plating pre-treatment cells were allowed approximately 4 hours to adhere to plate, following this cells were treated with AURKA inhibitor for 2 hours before irradiation as appropriate.

When plating post-treatment cells were treated with AURKA inhibitor for 2 hours in flask before being dislodged with trypsin EDTA. Cells were then irradiated in 15ml falcon tubes before being plated. Plated cells were provided with fresh media complemented with/without fresh AURKA inhibitor where appropriate.

2.2.1.4.3. Fractionated irradiation experiments

Cells were plated and allowed approximately 4 hours to adhere to plate before being treated with AURKA inhibitor for 2 hours before cells were irradiated. Cells were then irradiated again 24, 48 and 72 hours following with identical radiation doses. Unirradiated controls were sham irradiated with each set of irradiations.

2.2.2. siRNA transfection

2.25×10^5 H460 cells were seeded per well in 2 ml culture media in 6 well plates 24 hours prior to transfection for approximately 50% confluency at the time of transfection. Per well 2.5 µl of 20 µM siRNA was diluted with 197.5 µl FCS free

RPMI-1640 and left 5 minutes to incubate at room temperature. Simultaneously 5 µl of Dharmafect 1 was diluted with 195 µl FCS free RPMI-1640 and left 5 minutes to incubate at room temperature. Following this siRNA was mixed 1:1 with Dharmafect 1 gently with pipette and incubated for a further 20 minutes at room temperature. During 20-minute incubation cells were removed of media and replaced with 1.6 ml normal serum-containing RPMI-1640. Then 400 µl of siRNA-Dharmafect 1 complex was added dropwise to the media for final concentration of 25nM siRNA and 0.0025% Dharmafect 1 per well. Non-transfected controls achieved by adding 400 µl of serum free RPMI-1640 to cells in place of siRNA-Dharmafect 1 complex. Vehicle controls achieved by mixing Dharmafect 1 in serum free RPMI-1640 1:1 with serum free RPMI alone and adding dropwise to cells as above. Scrambled siRNA controls achieved by using Trilencer 27 Universal scrambled negative control siRNA duplex supplied by Origene.

2.2.3. Western blotting

2.2.3.1. Lysate preparation for western blot

2.2.3.1.1. 2 x SDS sample buffer method

2.2.3.1.1.1. Cell pre-treatment

For analysis of pThr288 AURKA 1-3 x 10^6 NSCLC cells were plated 48 hours prior to lysate production in 90 mm3 dishes. After 24 hours of adherence cells were arrested in mitosis by treating cells overnight with 100 ng/ml Nocodazole. Nocodazole untreated plates were employed for comparison. The following morning all plates were gently removed of media and washed twice with warm culture media, to remove Nocodazole, before re-complementing plates with 10 ml culture media.

Where appropriate cells were treated with AURKA inhibitor for 2 hours prior to lysate production.

2.2.3.1.1.2. Lysate production

Media was removed and cells were gently washed with 1ml ice cold PBS. Cells were then lysed on ice directly in 200 µl 2 x SDS boiling mix with 100 mM DTT (800 µl 5 x SDS sample buffer, 1000 µl ddH2O, 200 µl 1 M DTT per 1 ml). Cell scrapers were then used to collect all cells in lysis buffer on ice before lysate was passed through a 25G needle 20 times with a 1 ml syringe and collected in ice-chilled 1.5 ml Eppendorf tubes. Lysates were then boiled at 90 ^{o}C for 10 minutes before being quickly pulse centrifuged and stored at -20 ^{o}C until required.

2.2.3.1.2. RIPA lysis buffer method

Cells plated at 2.25 x 10^5 per well in a 6-well plate 24, 48, 72 and 96 hours earlier were washed twice with 500 µl PBS and dislodged using 500 µl trypsin EDTA. Trypsin was then diluted with 2 ml warm culture media and cells were collected in 15 ml falcon tubes. Cells were pelleted at 1200 RPM before being resuspended in 1 ml ice cold PBS and transferred to ice-chilled 1.5 ml Eppendorf tubes. Cells were pelleted at 1200 RPM and were lysed in 100 µl 1x RIPA lysis buffer (200 µl 5 x RIPA lysis buffer, 10 µl 100 mM PMSF, 10 µl 100 x SIGMAFAST protease inhibitor, 10 µl each of phosphatase inhibitor cocktail I & II and 770 µl ddH_2O per 1 ml). Pellet was mixed with RIPA lysis buffer by vortexing every 10 minutes for 30 minutes before being passed through a 25G needle 20 times. Lysis mix was centrifuged for 10 minutes at 13400 RPM, of which the supernatant was retained and stored at -20 ^{o}C prior to quantification and analysis via western blot.

2.2.3.2. Protein quantification

Quantification of total protein concentration in lysates achieved with 1x RIPA buffer was performed via the Bradford assay in 1.5 ml Eppendorf tubes. Protein standard curves were made using BSA of known concentration (see Table 2.1).

Total Protein (µg)	0.1 mg/ml BSA (µl)	ddH_2O (µl)	Biorad Protein Assay Dye Reagent Concentrate (µl)
0	0	800	200
1	10	790	200
5	50	750	200
10	100	700	200
15	150	650	200
20	200	600	200

Table 2.1. **Production of a BSA protein standard curve**

1 µl of each lysate was added to 799 µl of ddH_2O. 200 µl of Biorad Protein Assay Dye Reagent Concentrate was added to the lysates and BSA standards after the proteins were diluted in ddH_2O. Diluted lysates and standards were then incubated at room temperature for 15 minutes before optical density (OD) at 595 nm wavelength was measured using the Thermo Scientific Multiskan FC. BSA standards ODs were used to plot protein concentration against OD. The standard curve line from this allowed calculation of total protein in lysates from their OD values. This allowed the amount of protein to be loaded per lane for western blot to be calculated.

Lysates achieved via lysis directly in SDS sample boiling mix could not be quantified. Relative protein concentrations in these samples was approximated by western blotting for β-tubulin.

2.2.3.3. SDS-PAGE

8-12% polyacrylamide resolving gels were produced by using ddH_2O, Protogel 30% w/v acrylamide 0.8% w/v bis-acrylamide stock solution (Gene Flow), 1.5 M Tris pH 8.8, 10% SDS, 10% APS and TEMED. 5% stacking gels were produced by using 1 M Tris pH 6.8 in place of 1.5 M Tris pH 8.8 (see Table 2.2).

	Resolving gel (10 ml)			Stacking gel (ml)	
	8%	10%	12%		5%
ddH_2O (ml)	4.6	4.0	3.3	ddH_2O (ml)	3.4
30% Acrylamide 0.8% bis acrylamide (ml)	2.7	3.3	4.0	30% Acrylamide 0.8% bis acrylamide (ml)	0.83
1.5 M Tris pH 8.8 (ml)	2.5	2.5	2.5	1 M Tris pH 6.8 (ml)	0.63
10% SDS (ml)	0.1	0.1	0.1	10% SDS	0.05
10% APS (ml)	0.1	0.1	0.1	10% APS (ml)	0.05
TEMED (ml)	0.006	0.004	0.004	TEMED (ml)	0.005

Table 2.2. **SDS-PAGE resolving gel and stacking gel recipes**

For lysates achieved via 2 x SDS sample buffer method 5-25 μl of sample was loaded per lane. For lysates achieved via RIPA lysis buffer method 5-30 μg of protein was loaded per lane. 5 μl of Precision Plus Protein Standards (BioRad) was ran

parallel to samples. Proteins were separated by size for 1 hour – 1 hour 30 minutes at 180 V in 1 x SDS-PAGE running buffer.

2.2.3.4. Protein transfer

Proteins were transferred out of the gels onto Protran Nitrocellulose Transfer Membrane. This was achieved in a Criterion Blotter (BioRad) running at 80-100 V for 2 hours in pre-chilled (4 ^{o}C) 1 x Towbin Buffer on ice.

2.2.3.5. Membrane blocking and probing

All membrane incubations and washings were performed on a rocker. Membranes were blocked with 5% milk (Marvel) TBS for 1 hour at room temperature. Membranes were probed with primary antibody diluted in blocking solution at 4 ^{o}C overnight. Following primary antibody incubation membranes were washed three times with TBS-Tween 20 (0.05%) every 10 minutes. Then membranes were incubated with HRP-labelled secondary antibody diluted in blocking solution for 1 hour at room temperature. Following secondary antibody incubation membranes were washed three times with TBS-Tween 20 (0.05%) every 10 minutes before proceeding to enhanced chemiluminescence.

2.2.3.6. Enhanced chemiluminescence (ECL)

2 ml each of detection reagent 1 and 2 from the Amersham ECL Western Blotting Detection Reagent kit was mixed in a 15 ml falcon tube and then applied to the membrane for 1 minute at room temperature. Membranes were then exposed to X-ray film in a dark room and chemiluminescent signal was developed and fixed using RG Universal X-ray Developer and RG Universal X-ray Fixer.

2.2.3.7. Western blot quantification

Films were scanned into JPEG format and band densitometry was performed in ImageJ software. Relative protein expression levels were determined by normalising target protein band density to β-tubulin band density for the same sample. Higher exposures were excluded from densitometry to ensure signal saturation did not occur.

2.2.4. Immunofluorescence

2.2.4.1. Slide preparation

2.2.4.1.1. Mitotic phenotype assessment

1 x 10^5 NSCLC cells were plated directly onto 70% IMS sterilised 22 mm x 22 mm microscope cover slips in 6 well plates. Cells were allowed 4 hours to adhere to coverslips before being treated as appropriate. Cell treatment was terminated after 24 hours and cells were removed of media and gently washed three times with 500 µl pre-warmed (37 ^oC) PBS before being fixed in 500 µl 4% paraformaldehyde for 15 minutes at room temperature. Cells were then permeabilised with 500 µl PBS 0.5% Triton X-100 for 5 minutes at room temperature. Following permeabilisation cells were gently washed three times with 500 µl PBS before being blocked in 500 µl PBS 3% BSA for 30 minutes at room temperature. After blocking coverslips were inverted onto 100 µl PBS 0.5% BSA containing 1:500 dilution of β-tubulin (Sigma Aldrich) and 1:2000 dilution of pericentrin (Abcam) primary antibodies on the 6 well plate lid. Cells were incubated with primary antibody overnight at 4 ^oC in a humidified chamber. Coverslips were then everted into 6 well plates and unbound primary antibody was removed by gently washing three times with 500 µl PBS. After this coverslips were inverted onto 100 µl PBS 0.5% BSA containing 1:1000 Anti-mouse Alexa 488 (Life

Technologies) and 1:1000 dilution of Anti-rabbit Alexa 594 (Life Technologies) secondary antibodies on a fresh 6 well plate lid. Cells were incubated with secondary antibody for 1 hour in a humidified chamber in the dark at room temperature. Coverslips were then everted into 6 well plates and unbound secondary antibody was removed by gently washing three times on a rocker in the dark with 500 µl PBS allowing 10 minutes per wash. Lastly cells were mounted onto microscope slides by inverting coverslips onto Vectorshield hard set mountant with 4′,6-diamidine-2′-phenylindole dihydrochloride (DAPI) (Vector Laboratories) sealing coverslip edges with nail varnish. Coverslips were allowed 2 hours to dry in mountant in the dark at room temperature before being stored at 4 ^{o}C in the dark until required.

2.2.4.1.2. Micronuclei and multinucleate phenotype assessment

5 x 10^4 NSCLC cells were plated and treated as in the mitotic phenotype assays of methods section 2.2.4.1.1. Cell treatment was terminated after 72 hours and slides were prepared as in the mitotic phenotype assays with the exception that pericentrin was not stained for.

2.2.4.1.3. γ-H2AX repair assessment

2 x 10^5 NSCLC cells were plated and treated as in the mitotic phenotype assays of methods section 2.2.4.1.1. Cell treatment was terminated 15 minutes, 1 hour, 6 hours and 24 hours post-irradiation respectively and cells were removed of media and gently washed twice with 500 µl TBS before being fixed in 500 µl 4% paraformaldehyde for 15 minutes at room temperature. Cells were then briefly washed once with 500 µl TBS before washing three times for 10 minutes each with 500 µl TBS 0.2% Tween 20 on a rocker at room temperature. Following this cells were blocked with 500 µl TBS 3% BSA for 1 hour at room temperature. Cells were

then washed two times for 10 minutes each with 500 µl TBS 0.2% Tween 20 on a rocker at room temperature. After washing coverslips were inverted onto 100 µl TBS 0.5% BSA, 0.25% Triton X containing 1:500 dilution of γ-H2AX (cell signalling) primary antibody on the 6 well plate lid. Cells were incubated with primary antibody overnight at 4 ^{o}C in a humidifying chamber. Coverslips were the everted into 6 well plates and unbound primary antibody was removed by gently washing three times for 10 minutes each with 500 µl TBS 0.2% Tween 20. Washing was performed on a rocker at room temperature. Coverslips were then inverted onto 100 µl TBS 0.5% BSA, 0.25% Triton X containing 1:500 dilution of Anti-rabbit Alexa 594 (Life Technologies) secondary antibody on a fresh 6 well plate lid. Cells were incubated with secondary antibody for 1 hour in the dark at room temperature. Coverslips were then everted into 6 well plates and unbound secondary antibody was removed by gently washing cells once with 500 µl TBS 0.2% Tween 20 for 10 minutes and then twice with 500 µl TBS for 10 minutes each. These washes were performed on a rocker, in the dark at room temperature. Lastly cells were mounted onto microscope slides by inverting coverslips onto Vectorshield hard set mountant with 4′,6-diamidine-2′-phenylindole dihydrochloride (DAPI) (Vector Laboratories) sealing coverslip edges with nail varnish. Coverslips were allowed 2 hours to dry in mountant in the dark at room temperature before being stored at 4 ^{o}C in the dark until required.

2.2.4.2. Analysis

2.2.4.2.1. Mitotic phenotype assessment

Images of mitotic cells for assessment of mitotic phenotype were taken using a 60x objective on a Nikon TE200 Inverted Fluorescence and Phase Contrast Microscope. Fluorescent images from separate channels were merged using ImageJ. Pericentrin fragmentation was defined as when pericentrin staining was locally disrupted in a

cell. Centrosomal amplification was defined as when >2 distinct centrosomes were detected within a cell. Mitotic phase was defined in line with previous publication (Zhu *et al.* 2005).

2.2.4.2.2. Micronuclei and multinucleate phenotype assessment

Images of cells for assessment of micro- and or multinucleate phenotype were taken using a 20x objective on a Nikon TE200 Inverted Fluorescence and Phase Contrast Microscope. Fluorescent images from separate channels were merged using ImageJ. A minimum of 100 cells were counted per condition. Micronucleated cells were defined by the presence or absence of micronuclei which had completely budded off of a nucleus within a cell. Multinucleated cells were defined by the presence of >1 nucleus within a single cell membrane. Cells with >3 micronuclei were excluded to exclude dying cells from the analysis (Countryman and Heddle 1976). Cells which satisfied micro- and multinucleate criteria were labelled as dual phenotype.

2.2.4.2.3. γ-H2AX repair assessment

Images of cells for assessment of γ-H2AX repair were taken using a 40x objective on a Nikon TE200 Inverted Fluorescence and Phase Contrast Microscope. Fluorescent images from separate channels were merged using ImageJ. A minimum of 100 cells were counted per condition, counting the number of γ-H2AX foci per nucleus. Mean foci per cell (nucleus) was then calculated.

2.2.5. Flourescence-activated cell sorting (FACS)

2.2.5.1. Cell harvesting

2 x 10^5 NSCLC cells were seeded per 90 mm^3 dish and treated as appropriate. Cells were harvested for FACS analysis 24, 48 and 72 hours post-irradiation by washing plates twice with PBS and dislodging cells with 1 ml trypsin EDTA. Cells were collected in 5 ml ice cold PBS and pooled with media and PBS wash-offs on ice in 50 ml falcon tubes. Cells were pelleted at 1200 RPM for three minutes, washed once in ice cold PBS whilst transferring to 15 ml falcon tubes and resuspended in 1 ml ice cold 100% methanol with vortexing. Cells were stored in 100% methanol for a minimum of 1 hour and a maximum of 2 weeks at -20 ^oC.

2.2.5.2. Propidium iodide (PI) and S10 p-Histone 3 co-staining

Cells were retrieved from -20 ^oC and pelleted at 1200 RPM for 3 minutes before methanol was poured off and cells were washed twice in PBS. Following this cells were resuspended in PBS with 0.5% BSA 0.25% Triton-X100 (Sigma Aldrich) and incubated on ice for 15 minutes. Cells were then pelleted at 1200 RPM, supernatant removed and resuspended in 100 μl of PBS 0.5% BSA (Sigma Aldrich) 0.25% Triton-X100 containing 1:500 dilution of S10 p-Histone 3 (#47297 Abcam) primary antibody. Cells were incubated with primary antibody for 1 hour at room temperature. Cells were washed of unbound primary antibody twice with PBS 0.25% Triton-X100. Cells were then resuspended in 100 μl PBS 1% BSA containing 1:200 dilution of Anti-rabbit Alexa 488 antibody. Cells were incubated for 30 minutes with secondary antibody in the dark at room temperature. Cells were then washed of unbound secondary antibody once with PBS before being resuspended in 200 μl PI/RNAse A solution (18 μg/ml PI, 8 μg/ml RNAse A). Cells were incubated in PI/RNAse A

solution in the dark at 4 ^{o}C for a minimum of 1 hour 30 minutes prior to being analysed with a BD Biosciences FACSCalibur. No primary antibody controls were employed to investigate the extent of non-specific secondary antibody staining.

2.2.5.3. Analysis

Cell doublets were excluded by plotting FL3 (PI)-Area against FL3-Width and gating FL3-Width low cells (see Figure 2.1). 10,000 events were collected in this gating region per sample and a FL3-height (FL3-H) histogram was produced. G1 proportion of cells was defined by gating across the base of the first peak in FL3-H plot (~200 FL3-H), G2-M proportion of cells was defined by gating across the base of the second peak in FL3-H plot (~400 FL3-H). Sub G1 population was defined as all signal to the left of the first peak, S phase population was defined as all signal between first and second peaks. Mitotic population was discriminated by plotting G2-M population FSC-H against FL1-H for S10 p-Histone 3 staining. Mitotic population was discriminated with least 0.5 logs of separation in FL1-H intensity versus G2 population. Polyploid population was defined as all signal the right of the G2-M population.

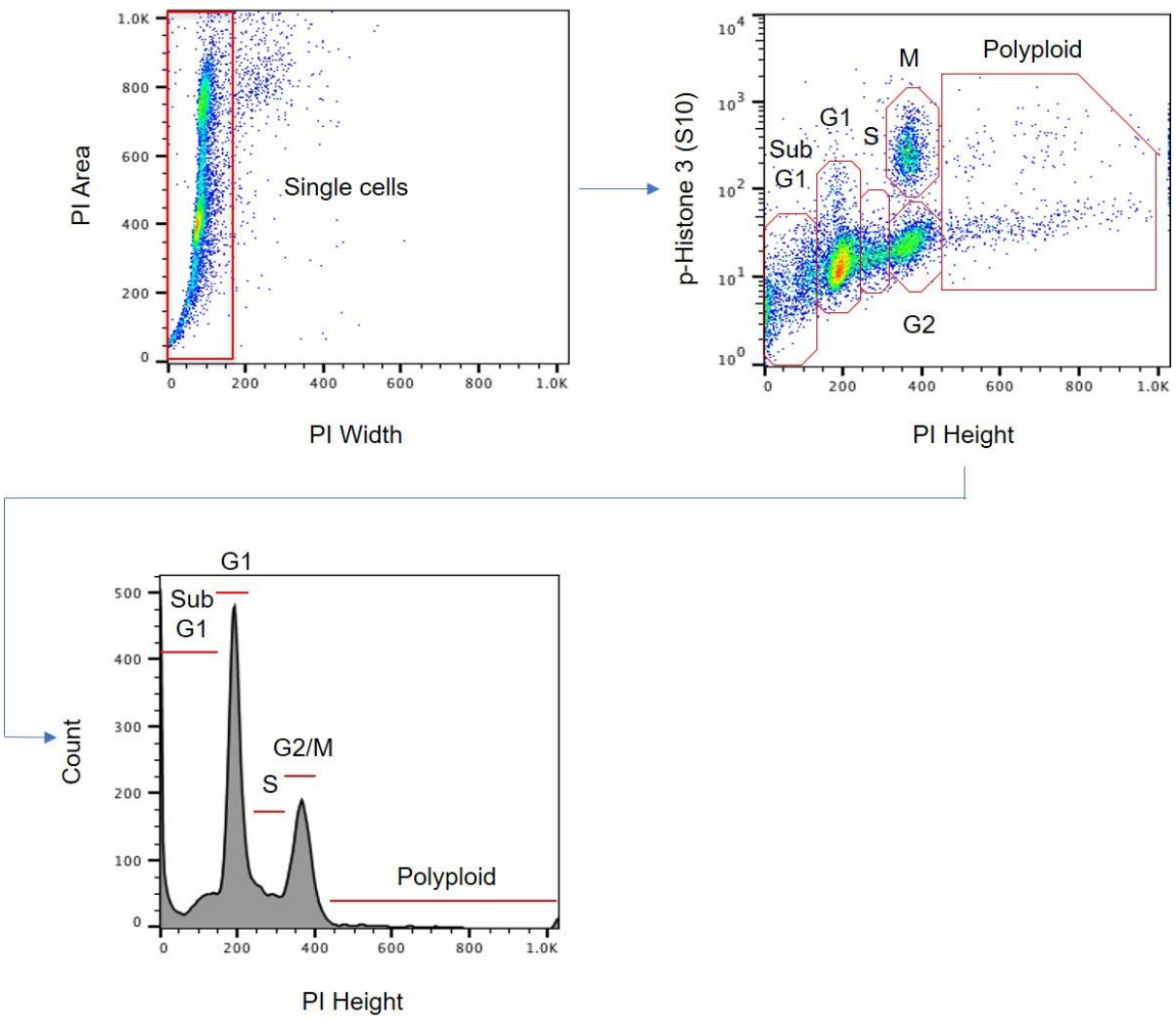

Figure 2.1. **FACS gating strategy outline**. Cell doublets were excluded in the plot of the top left with gate in red. Doublets are visible as a population that stained with greater PI width. Single cell population was taken forward for cell cycle analysis. The plot of the top right illustrates cell cycle profile produced when PI height was plotted against S10 p-Histone 3 positivity allowing discrimination of G2-M population. Bottom left plot shows alternative to the top left when PI height was plotted as a histogram.

2.2.6. Live cell imaging

2.2.6.1. Cell treatment

Cells were treated with AURKA inhibitor in T75 flasks before being transferred to 15 ml falcon tubes for irradiation as appropriate. Then cells were plated at a density of 5

x 10^4 or 2.5 x 10^4 per well in 6 well plate for imaging 24 or 48 hours post-treatment respectively.

2.2.6.2. Imaging

Cells were imaged using a Leica AF6000 Time Lapse microscope with temperature maintained at 37 ^oC and CO_2 plate maintaining 5% CO_2 concentration. Phase contrast images were taken using a 20x phase contrast objective every five minutes overnight. A minimum of five positions were imaged per well with images being focussed on mitotic cells.

2.2.6.3. Analysis

Images were put in sequence producing a time-lapse video using ImageJ. Time through mitosis was defined as the time of nuclear envelope breakdown to the end of cytokinesis (see Appendix Figure 8.1). Cellular death during mitosis was counted (see Appendix Figure 8.2). Aberrant mitoses were defined as mitoses which resulted in < 2 or > 2 daughter cells (see Appendix Figure 8.3). A minimum of 50 mitoses were counted per condition.

2.2.7. Detection of cellular senescence

2.2.7.1. Cell treatment

5 x 10^4 NSCLC cells were plated directly into 6 well plates. Cells were allowed 4 hours to adhere to coverslips before being treated as appropriate. Cell treatment was terminated after 72 hours and cells were removed of media and gently washed twice with 1 ml pre-warmed (37 ^oC) PBS before being fixed and stained in accordance to the manufacturers protocol using the Senescence β-Galactosidase Staining Kit (Cell Signalling Technology #9860). Staining was performed at pH 6 adjusting staining

solution pH with HCl. 12.5 μM Etoposide treatment for 24 hours was used as a positive control for β-galactosidase staining cells. After 24 hours of treatment Etoposide was removed and cells were gently washed twice with 1 ml pre-warmed (37 ^{o}C) PBS before being replaced with 2 ml culture media for remaining 48 hours prior to treatment termination.

2.2.7.2. Imaging

Cells were imaged using a Nikon OPTIPHOT-2 microscope mounted with a Nikon DS-Fi1 digital site. Images were taken using a 10x brightfield objective using Nikon NIS Elements F software.

2.2.7.3. Analysis

Images were analysed using ImageJ. Cells with strong blue staining were considered positive for β-galactosidase expression and were classed as senescent (see Figure 2.2). Cells with weak or absent blue staining were considered as negative for β-galactosidase expression and were classed as non-senescent. The proportion of β-galactosidase expressing cells was calculated counting a minimum of 100 cells per condition.

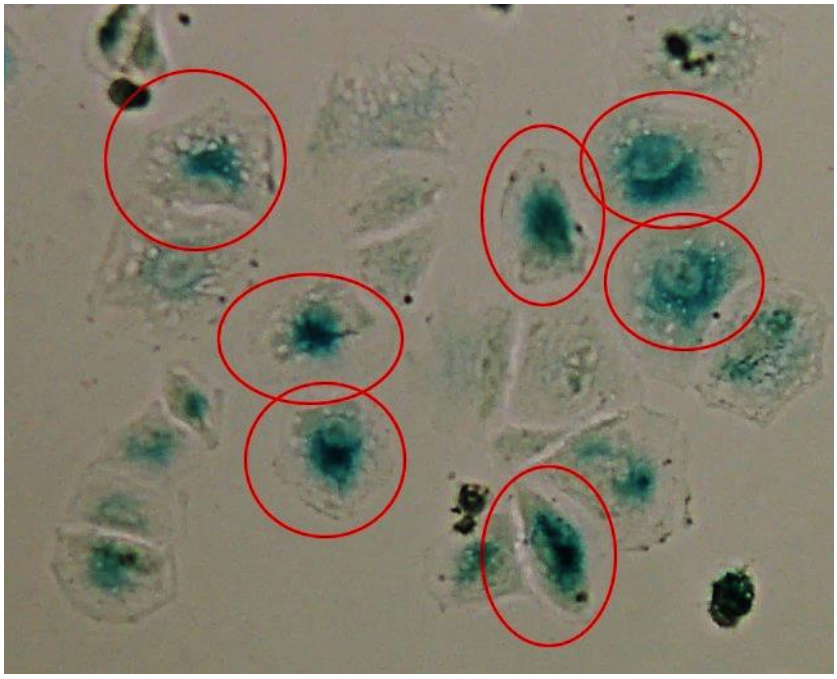

Figure 2.2. **Example scoring of β-galactosidase positive and negative cells**. Cells with dark perinuclear blue staining were defined as β-galactosidase positive (circled red). All other cells with weak or absent blue stain were defined as negative for β-galactosidase

2.2.8. Immunohistochemistry (IHC)

2.2.8.1. Sample preparation

2.2.8.1.1. Cell line pellet preparation

To prepare a cell line pellet for IHC a minimum of two T75 flasks of cells were washed with PBS, dislodged with trypsin EDTA, resuspended in media and pelleted at 1200 RPM for 5 minutes in 50 ml falcon tube. Cells were then washed once with 5 ml PBS and transferred to 15 ml falcon tube before being pelleted again. 1 ml of 4% paraformaldehyde was then slowly dripped down the side of the falcon tube to fix but not disturb the cell pellet. Cells were fixed overnight at 4 ^{o}C before paraformaldehyde was pipetted off and carefully replaced with 1 ml ice cold 70% ethanol and stored at -20 ^{o}C for maximum of 2 weeks.

To embed cell pellets in wax 70% ethanol was removed from cell pellet and pellet was then encased in molten 2% agarose with 4% paraformaldehyde. After agarose had cooled and set agarose encased pellet was placed in a cassette and stored in 70% ethanol at room temperature until processing. Cell pellets were processed using a Leica TP 1020. Processed cell pellets were embedded in wax the following day using a Leica EG1150 wax embedder. 5 µm sections of wax embedded tissue were produced using a Leica RM2125 RTS microtome. Sections were then floated on warm water (approximately 47 ^{o}C) in a floatation bath and manoeuvred onto Menzel-Glaser Superfrost Plus Adhesion microscope slides (Thermo Fisher). Tissue was dried out and fixed to the microscope slide surface through baking in an oven at 37 ^{o}C for 48 hours. Sections were then ready to be stained and were stored at room temperature out of light.

2.2.8.1.2. *In vivo* tissue preparation

Tissues from mouse *in vivo* experiments were taken immediately at the time of culling. Tissues were submerged in O.C.T. compound in Surgipath® clear base moulds (Leica) and were snap frozen in isopentane on dry ice. Samples were kept at -80 ^{o}C until sectioning. 10 µm sections of tissue was produced using a Leica CM3050 cryostat and were electrostatically attracted up to Menzel-Glaser Superfrost Plus Adhesion microscope slides (Thermo Fisher). Samples were then stored at -20 ^{o}C until they were stained.

2.2.8.1.3. NSCLC patient diagnostic biopsy samples

Wax embedded NSCLC patient diagnostic biopsy samples were sectioned and fixed onto microscope slides as performed for cell line pellets above. Five sections were retrieved per sample in line with the clinical study protocol.

2.2.8.2. Staining procedure

2.2.8.2.1. Dewaxing and hydration of tissue (cell line pellets and diagnostic biopsies)

Slides were dewaxed in xylene for 20 minutes, spending 10 minutes each in separate xylene baths. Slides were then gradually hydrated for 3 minutes each in baths of 100% IMS, 100% IMS, 95% IMS, 90% IMS and 70% IMS.

2.2.8.2.2. Fixation and hydration of tissue (O.C.T. frozen tissues only)

Slides were retrieved from -20 ^{o}C and allowed to air dry for 30 minutes before tissues were fixed in ice cold 1:1 mix of methanol and acetone for 20 minutes at -20 ^{o}C. Following fixation, tissues were gently washed twice with PBS to rehydrate, each for 5 minutes, at room temperature.

2.2.8.2.3. Blocking endogenous peroxidase activity

Following tissue hydration slides were incubated in 10% H_2O_2 in methanol for 30 minutes at room temperature to block endogenous peroxidase activity. Following this slides were washed in tap water for 5 minutes.

2.2.8.2.4. Antigen retrieval

2.2.8.2.4.1. Pressure cooker method

Antigen retrieval was achieved by immersing slides in 1x pH 6.1 citrate Target Retrieval Solution (Dako) diluted in ddH_2O or 10 mM Tris 1 mM EDTA pH 9.0 buffer. These slides were then cooked in buffer for 20 minutes in a retriever 2100 pressure cooker (Aptum Biologics) according to the manufacturer's instructions. Slides remained in buffer for a further 2 hours to cool. After antigen retrieval slides were

rinsed once in PBS-Tween 20 (0.1%) before being washed twice for three minutes each in PBS-Tween 20 (0.1%).

2.2.8.2.4.2. Microwave method

1 x Target Retrieval Solution (Dako) diluted in ddH_2O was heated on high setting until boiling in a microwave before slides were cooked in buffer for four minutes in a 700W microwave on high setting. After antigen retrieval slides remained in buffer for a further 10 minutes to cool before being rinsed once in PBS Tween 20 (0.1%) before being washed twice for three minutes each in PBS-Tween 20 (0.1%).

An extended microwave antigen retrieval protocol was used as above but involved retrieval for 10 minutes on high followed by 5 minutes on medium microwave setting.

2.2.8.2.5. Antigenic blocking

Secondary antibody host serum (goat/rabbit) (Vector Laboratories) was diluted 1:10 in PBS 1% BSA 0.1% Tween 20. After antigen retrieval a hydrophobic barrier was drawn around the tissue on the slide using an ImmEdge™ pen (Vector Laboratories). Approximately 250 µl of 10% secondary antibody host serum in PBS 1% BSA 0.1% Tween 20 was dropped onto the tissue section and allowed 1 hour to incubate at room temperature in a humidifying chamber.

2.2.8.2.6. Antibody Incubation

Blocking solution was tapped off slides and was replaced with 250 µl of PBS 1% BSA, 0.1% Tween 20, 2% secondary antibody host serum containing appropriate dilution of primary antibody. Tissue sections were incubated with primary antibody for 1 hour at room temperature or overnight at 4 ^{o}C in a humidified chamber. Controls lacking primary antibody were used to investigate non-specific signal.

Where applicable, blocking peptide was pre-incubated with primary antibody at room temperature for 1 hour with agitation prior to incubation of primary antibody with tissue to test the specificity of staining. Following primary antibody incubation primary antibody was tapped off the slides. Slides were then rinsed once in PBS-Tween 20 (0.1%) before being washed twice for three minutes each in PBS-Tween 20 (0.1%). Biotinylated secondary antibody (Vector Laboratories) was diluted 1:200 in PBS 1% BSA 0.1% Tween 20 2 % secondary antibody host serum and 250 µl of this was dropped onto tissue sections. Secondary antibody incubation was for 1 hour at room temperature in a humidified chamber.

2.2.8.2.7. Avidin-biotin complex (ABC) signal amplification

ABC solution (Vector Laboratories) was prepared 30 minutes prior to its use. ABC solution was made by adding 2 drops of reagent A and 2 drops of reagent B to every 5 ml of PBS-Tween 20 (0.1%) diluent with vortexing after each addition. After secondary antibody incubation slides were rinsed once in PBS-Tween 20 (0.1%) before being washed twice for five minutes each in PBS-Tween 20 (0.1%). 250 µl ABC solution was then added to tissue sections and incubated for 30 minutes at room temperature in a humidified chamber.

2.2.8.2.8. ImmPRESS® signal detection kit

As an alternative to using ABC signal amplification the ImmPRESS Horse anti-mouse HRP Polymer detection kit (Vector Laboratories) was used according to manufacturer's instructions. Sections were blocked for 1 hour in 2.5% ready to use horse serum, before primary antibody incubation in PBS 1% BSA 0.1% Tween 20. After primary antibody incubation, slides were then rinsed once in PBS-Tween 20 (0.1%) before being washed twice for five minutes each in PBS-Tween 20 (0.1%)

before being incubated with ImmPRESS Peroxidase Anti-mouse IgG reagent for 30 minutes before signal development.

2.2.8.2.9. Diaminobenzidine (DAB) signal development

After ABC/ImmPRESS Peroxidase Anti-mouse IgG reagent incubation slides were rinsed once in PBS-Tween 20 (0.1%) before being washed twice for five minutes each in PBS-Tween 20 (0.1%). DAB solution (Vector Laboratories) was prepared by adding 2 drops of buffer, 4 drops of DAB and 2 drops of H_2O_2 per 5 ml H_2O diluent with vortexing after each addition. 250 µl of DAB solution was dropped over tissue sections and signal development in the form of a brown precipitate was allowed to occur between 30 seconds to 15 minutes. After significant signal development this process was halted by washing away DAB from the slides using ddH_2O.

2.2.8.2.10. Haematoxylin counterstain

Slides were counterstained in a bath of Gills haematoxylin for 1 minute. Excess stain was removed by washing slides with running tap water for 5 minutes.

2.2.8.2.11. Dehydration and mounting of slides

Slides were then gradually dehydrated for 3 minutes each in baths of 70% IMS, 90% IMS, 95% IMS, 100% IMS and 100% IMS. Slides were then bathed in mounting xylene for 10 minutes, 5 minutes each in separate baths before being mounted using DPX. Slides were left to dry overnight before being imaged.

2.2.8.3. Imaging

Slides were scanned using a Pannoramic 250 Flash III slide scanner using a 20x brightfield objective. Slide scans were analysed using QuPath software (v0.1.2) (Bankhead *et al.* 2017).

2.2.8.4. Analysis

2.2.8.4.1. Mitotic fraction in xenograft tumour samples

p-Histone 3 (S10) positive cells were defined with DAB positivity after incubation with antibodies for detection p-Histone 3 (S10) detection. Minimum of 9 samplings from the viable tumour regions were used to produce mean mitotic fraction data. Viable regions of xenograft samples were identified by haematoxylin counter-stain intensity with necrotic regions identified by dark staining pattern. Criteria for detection of cells in xenograft tumour sections using QuPath software (v0.1.2) (Bankhead *et al.* 2017) is illustrated in Table 2.3

Parameter	Setting
Detection method	Haematoxylin OD
Requested pixel size	0.5 μm
Background nuclear radius	8 μm
Nuclear Sigma	1.5 μm
Minimum nuclear area	10 μm^2
Maximum nuclear area	400 μm^2
Haematoxylin intensity threshold	0.1
Maximum background intensity	2
Cell expansion (including cell nucleus)	5 μm

Table 2.3. **Criteria for detection of cells in xenograft tumour samples using QuPath software (v.0.1.2)** (Bankhead *et al*. 2017)

Cells positive for DAB were detected using the criteria outlined in Table 2.3 with a stringent single positivity threshold of a cellular DAB OD of 0.95 in QuPath software. An example of the tumour tissues stained for p-Histone 3 (S10) and positive cell detection performed is shown in Figure 2.3.

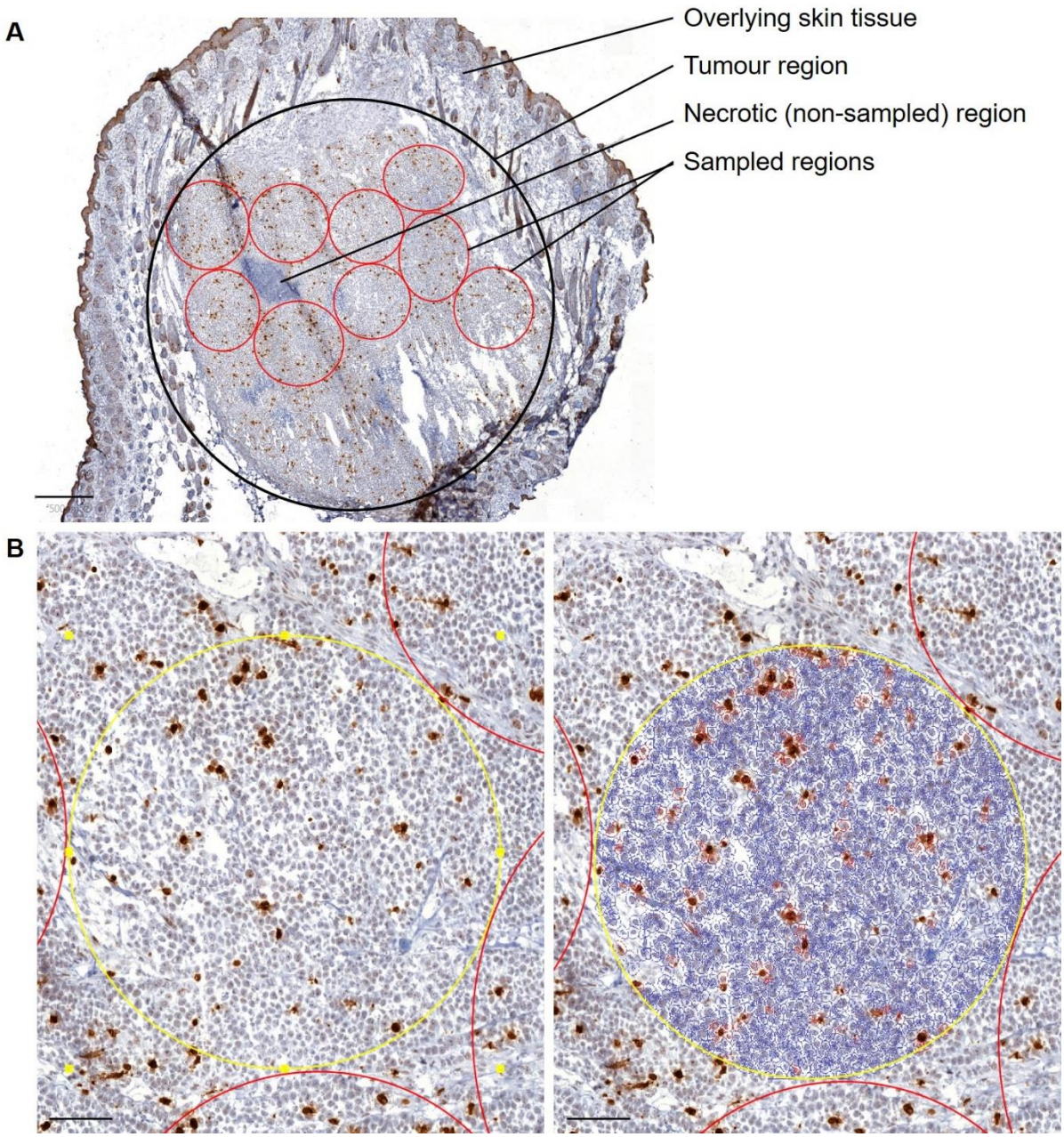

Figure 2.3. **A. Example xenograft section with p-Histone 3 (S10) staining for mitotic fraction sampling**. Only viable tumour tissues were sampled for mitotic fraction. Sampling of a minimum of 9 areas of the tumour ensured sampling of several thousand cells per tumour per condition. Scale bar represents 500 μm **B. Example xenograft section with p-Histone 3 (S10) staining for mitotic fraction sampling prior to positive cell detection analysis (left) and after positive cell detection analysis (right).** Nuclei with inferred cytoplasmic area is shown in righthand image. Red pixels indicate positive cell identification. Swelling of mitotic cells accounted for through cell expansion parameter. Stringent threshold for positivity used to avoid false positive detections. Scale bars represent 100 μm.

2.2.8.4.2. CD31 analysis in xenograft tumour samples

CD31 positive regions were defined with DAB positivity after incubation with antibodies for CD31 detection. The percentage of positive pixels for DAB as a proportion of total pixels of xenograft section was computed using QuPath software (v0.1.2)(Bankhead *et al.* 2017). Pixels only within the viable area of tumour tissues were considered in this analysis. Viable regions of xenograft samples were identified by haematoxylin counter-stain intensity with necrotic regions identified by dark staining pattern. Cell occupied pixels were identified through haematoxylin stain threshold and positive cell pixels were identified through DAB threshold outlined in Table 2.4.

Parameter	**Setting**
Downsample factor	4
Gaussian sigma	2 μm
Haematoxylin threshold	0.02 OD units
DAB threshold	0.1 OD units

Table 2.4. **Criteria for detection of CD31 positive regions in xenograft tumour samples using QuPath software (v.0.1.2)** (Bankhead *et al*. 2017)

An example of the tumour tissues stained for CD31 and positive cell detection performed is shown in Figure 2.4.

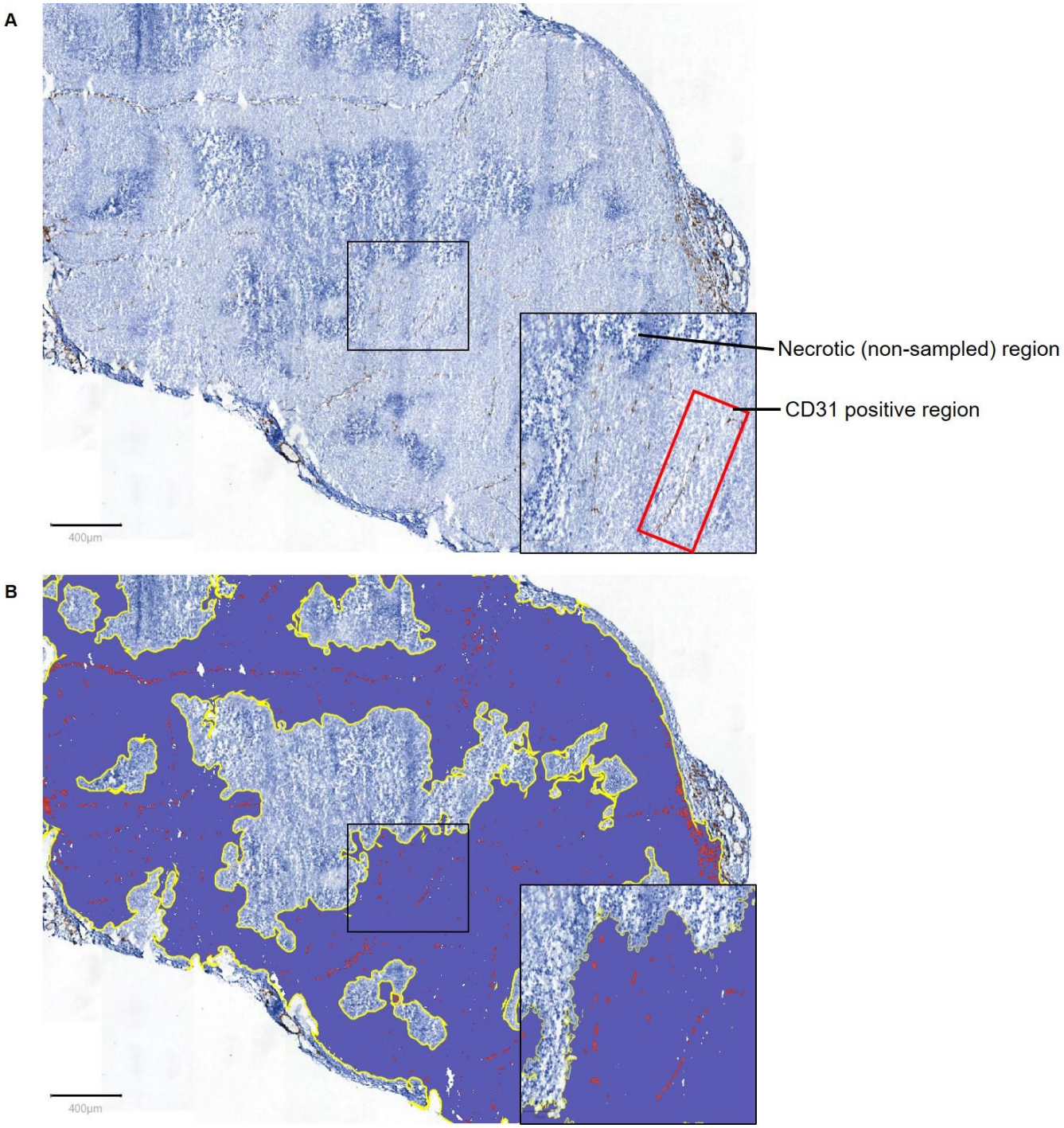

Figure 2.4. **Example xenograft section with CD31 staining A**. Staining example at 2x magnification. **B.** Staining example with positive pixel scoring at 2x magnification. Area within the small rectangle is re-represented in image bottom right corner 5x larger. Only viable tumour tissues sampled for CD31 positivity. Cell occupied pixels scored blue and DAB positive pixels scored red in B respectively. Scale bars represent 400 µm.

2.2.8.4.3. Ki67 analysis in xenograft tumour samples

Ki67 positive regions were defined with DAB positivity after incubation with antibodies for Ki67 detection. The same was performed as in CD31 analysis in xenograft tumour samples with DAB threshold for positivity made more stringent to account for background staining (Bankhead et al. 2017):

Parameter	**Setting**
Downsample factor	4
Gaussian sigma	2 μm
Haematoxylin threshold	0.02 OD units
DAB threshold	0.4 OD units

Table 2.5. **Criteria for detection of Ki67 positive regions in xenograft tumour samples using QuPath sotware (v.0.1.2)** (Bankhead *et al*. 2017)

An example of the tumour tissues stained for Ki67 and positive cell detection performed is shown in Figure 2.5.

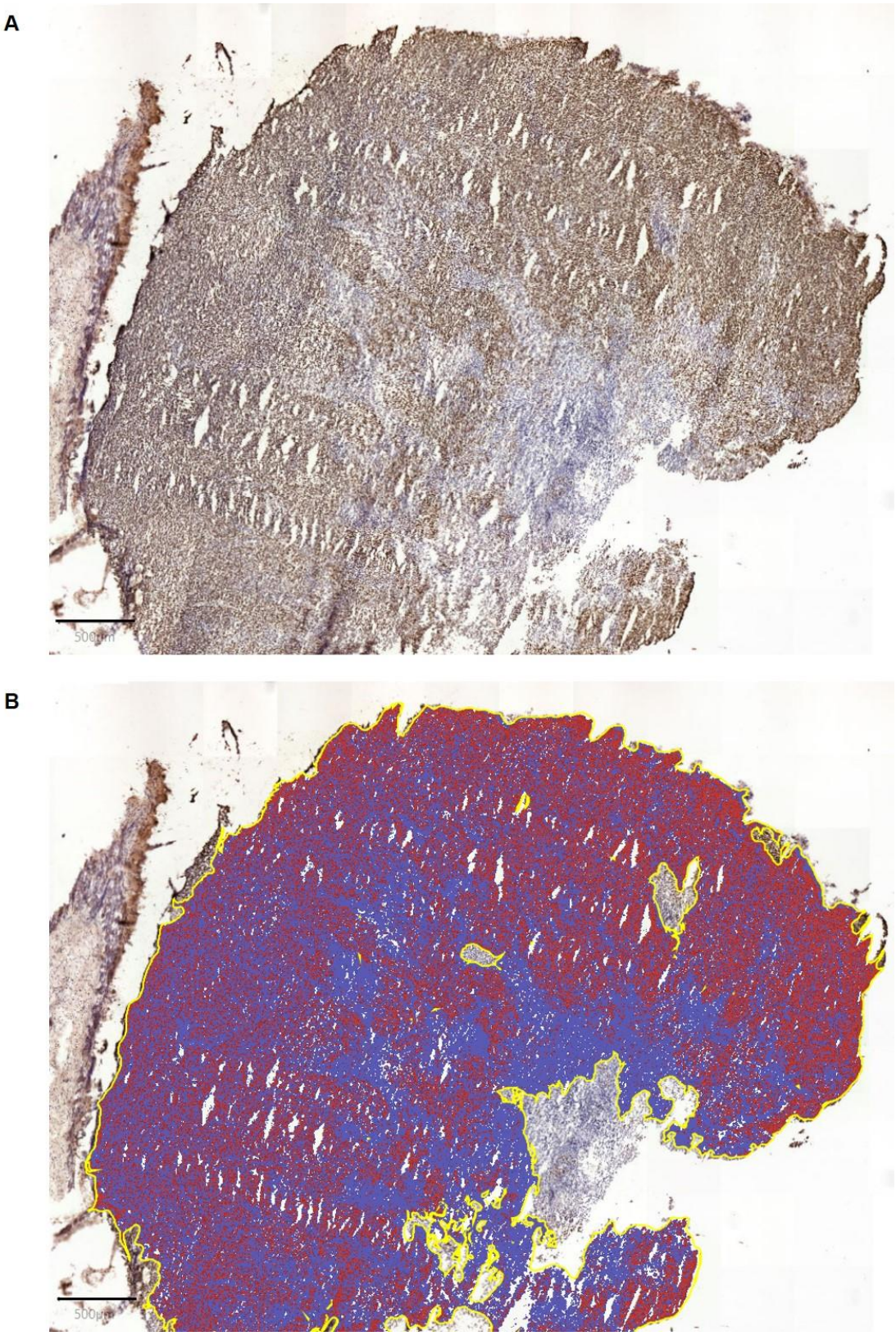

Figure 2.5. **Example xenograft section with Ki67 staining A**. Staining example at 1.5x magnification. **B.** Staining example with positive pixel scoring at 1.5x magnification. Only viable tumour tissues sampled for Ki67 positivity. Cell occupied pixels scored blue and DAB positive pixels scored red in B. Scale bars represent 500 μm

2.2.9. *In vivo* experiments

In vivo experiments were performed under Animals (Scientific Procedures) Act 1986 with local ethical approval on:

Personal license: I7C120AEE

Project license: PDA78C678 (Held by Dr William English)

2.2.9.1. Preparation of Alisertib suspension

Alisertib received from Takeda pharmaceuticals was weighed out and aliquoted into 2 ml Eppendorf tubes. Alisertib powder aliquots were stored at room temperature in the dark until suspension was prepared.

To prepare Alisertib suspension for *in vivo* dosing 20% Hydroxypropyl-β-cyclodextrin (HBC) and 2% sodium bicarbonate were each prepared with ddH_2O. Half of desired volume of HBC was added to Alisertib aliquot and solution was sonicated with a Diogenode Bioruptor® sonicator for 15 minutes. Sonicator was set on high with on and off intervals set at every 30 seconds. After this half of desired volume of 2% sodium bicarbonate was added to tube and solution was sonicated for a further 15 minutes forming an even suspension in 10% HBC 1% sodium bicarbonate vehicle. Suspensions were prepared for a dosing volume of 5 ml/kg (100 µl for a 20g mouse). Suspension preparation was performed under sterile conditions with sterile reagents as final suspension of Alisertib could not be filter sterilised. Suspensions were stored at 4^{o}C for a maximum of 21 days.

2.2.9.2. Tumour implantations

Cells for tumour implantation were trypsinised and resuspended in serum deplete culture media at 2 x 10^6 cells per 50 µl (H460 and LLC-1 models) or 1 x 10^7 per 50 µl (H1299 model). Cells were then transferred to ice and mixed 1:1 with Matrigel® matrix (Corning). For cellular injection procedure mice were anaesthetised with isoflurane gas. 1 x 10^6 cells (50 µl) (H460 and LLC-1 models) or 5 x 10^6 cells (H1299 model) were injected subcutaneously at the hind dorsum of mice with ice chilled 25G needle and 1 ml syringe. Immunocompromised CD-1 nude mice aged 6-8 weeks were subcutaneously injected with H1299 or H460 cells. Immunocompetent C57BL/6 mice aged 6-8 weeks were subcutaneously injected with LLC-1 cells.

2.2.9.3. Tumour measurements

Tumour dimensions were recorded using callipers and tumour volume was determined by 0.52 x d1 (diameter in mm) x d2 (diameter 90^o rotated to d1 in mm) x d3 (tumour base to tumour peak in mm) calculation.

2.2.9.4. Humane endpoints

Humane endpoints were employed to ensure that no animal underwent significant pain, suffering or distress. If animals displayed symptoms of any of the below immediately or for a stated amount of time, then the animal was immediately culled.

2.2.9.4.1. Humane endpoints in all experiments

Significant or chronic piloerection**,** chronic hypothermia**,** chronic hunching, chronic mild dyspnoea, enlarged lymph nodes, anaemia or eating and/or drinking problems for over 48 hours. Body weight reduction of >20% for over 24 hours. Bleeding or discharge from any orifice, hind limb paralysis and weakness, movement difficulties,

severe breathing disturbances, tremors/convulsions or entering a moribund state at any point.

2.2.9.4.2. Humane endpoints specific to tumour bearing experiments

Wet desquamation of the skin overlying the tumour that did not resolve in 48 hours. If tumours ulcerated with signs of self-trauma or deteriorating health at any point. If tumours exceeded a mean diameter of 12 mm at any point.

2.2.9.4.3. Humane endpoints specific to tumour irradiation experiments

Any mice that did not become accustomed to restraint in lead irradiation jigs. If radiodermatitis resulted in superficial infection.

2.2.9.4.4. Humane endpoints specific to experiments involving Alisertib dosing

Minor ailments such as reduction in grooming, poor coat condition and moderate weight loss (<20% of starting weight) progressing to more severe toxicity at any point.

2.2.9.5. Alisertib dose escalation experiments

Non-tumour bearing CD-1 nude mice aged 6-8 weeks were dosed with varying concentrations of Alisertib once per day for 10 consecutive days via oral gavage. 10, 20 and 40 mg/kg daily dosing in line with previously reported maximum tolerated doses (MTD) (Görgün *et al.* 2010; Manfredi *et al.* 2011; Palani *et al.* 2013). There were two animals per experimental group with a sequential experimental design. Depending on the MTD of Alisertib achieved in CD-1 nude mice, the same would be applied to non-tumour bearing C57B/6 mice aged 6-8 weeks. If 10 days of

consecutive dosing (starting day 0) was tolerated animals would be culled on the 10th day. Sequential experimental design is detailed in Table 2.6

Day 0	Day 1	Day 2	Day 3	Day 4	Day 5	Day 6
10 mg/kg	10 mg/kg	10 mg/kg 20 mg/kg	10 mg/kg 20 mg/kg	10 mg/kg 20 mg/kg	10 mg/kg 20 mg/kg	10 mg/kg 20 mg/kg
Day 7	Day 8	Day 9	Day 10	Day 11	Day 12	Day 13
10 mg/kg 20 mg/kg 40 mg/kg	10 mg/kg 20 mg/kg 40 mg/kg	10 mg/kg 20 mg/kg 40 mg/kg	10 mg/kg culled 20 mg/kg 40 mg/kg	20 mg/kg 40 mg/kg C57BL/6	20 mg/kg culled 40 mg/ kg C57BL/6	40 mg/kg C57BL/6
Day 14	Day 15	Day 16	Day 17	Day 18	Day 19	Day 20
40 mg/kg C57BL/6	40 mg/kg C57BL/6	40 mg/kg C57BL/6	40 mg/ kg culled C57BL/6	C57BL/6	C57BL/6	C57BL/6
Day 21						
C57BL/6 culled						

Table 2.6. **Sequential dosing plan for assessment of Alisertib MTD in CD-1 nude mice and C57Bl/6 mice (where stated).**

2.2.9.6. Irradiation dose optimisation experiments

Mice were irradiated once a day for five consecutive days with 200 kV X-rays using an AGO HS X-ray system MP1 irradiator when tumours reached a treatment volume of 100 mm^3. Mice were either irradiated with 4 Gy (H460, H1299 and LLC-1

xenografts) or 8 Gy (LLC-1) per day (total dose of 20 Gy or 40 Gy respectively). Radiation dose rate was 1.33 Gy per minute with a focus-surface distance of 17 cm in all *in vivo* irradiation experiments. Mice were culled when tumours reached a mean tumour diameter of 10 mm or when humane endpoints were reached. Lead jigs were used to restrain animals during irradiation. Additionally, the lead jigs were used to promote hind dorsum tumour irradiation whilst restricting normal tissue irradiation. Lead jig application is summarised in Figure 2.6.

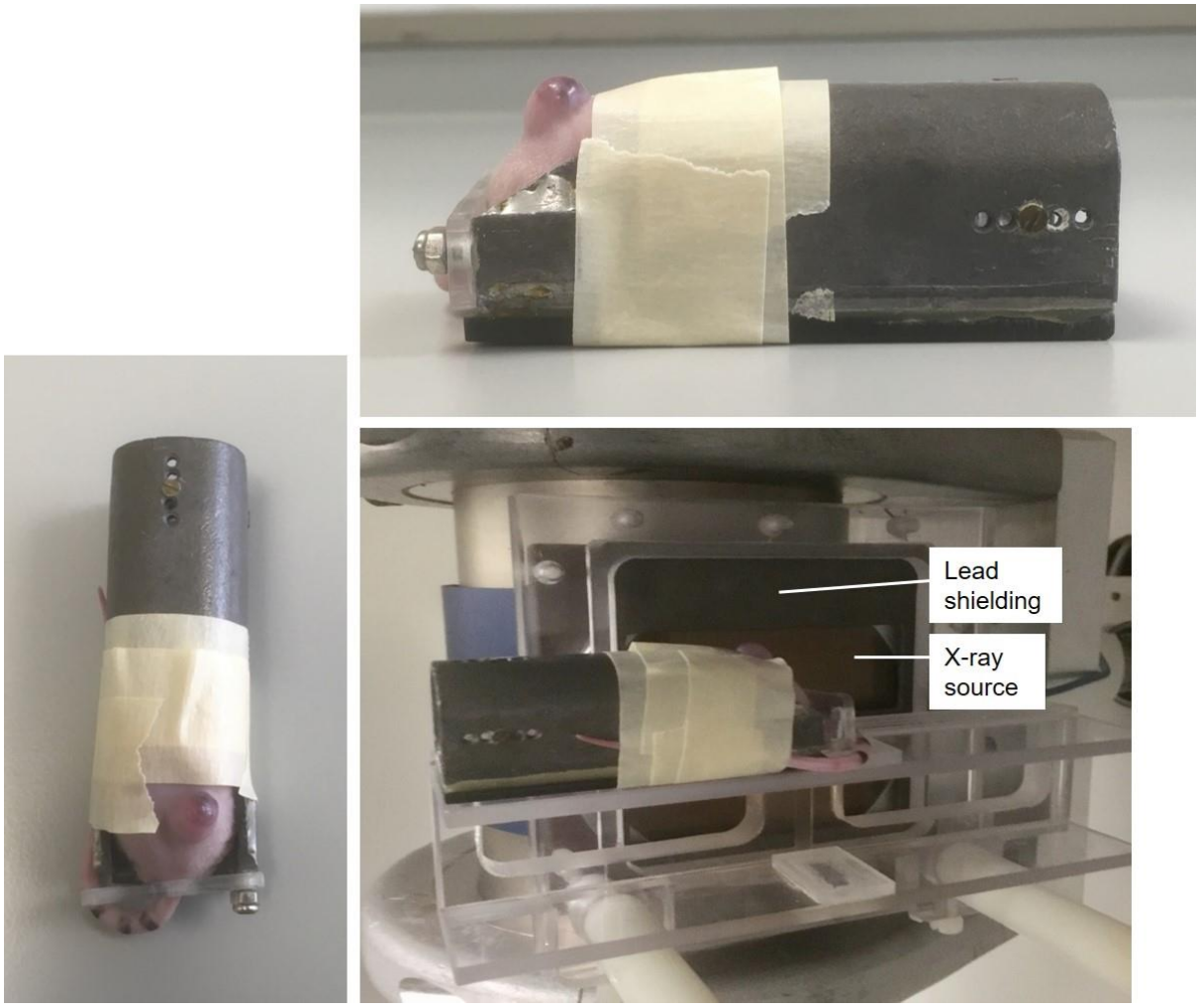

Figure 2.6. **Lead jig set up for mouse tumour irradiation. Left:** Top-down image of jig. Gate mechanism at back of jig prevented exit and movement within the jig. Tape was used to immobilise mouse tail and further immobilise mouse during irradiation. Open back of jig exposed tumour bearing hind dorsum of animal for irradiation. **Top**: Side view of jig demonstrating tumour exposure. **Bottom**: Jig use in irradiator. Lead shielding of both jig and as part of irradiator produced a controlled corridor of irradiation. Irradiator produced x-rays focussed by copper plate.

2.2.9.7. Alisertib dose optimisation experiments

CD-1 nude mice bearing H460 xenografts were treated with 5, 10 or 20 mg/kg Alisertib or vehicle control once a day for 10 consecutive days via oral gavage once tumours reached a treatment volume of 100 mm^3. A dosing volume of 5 ml/kg (100 µl

for a 20 g mouse) was used. Mice were to be culled when tumours reached a mean diameter of 10 mm or when humane endpoints were reached. Prior to culling mice were given a final dose of vehicle/Alisertib appropriate to the treatment group before allowing 6 hours for drug to have a biological effect within the tumours. Mice were then culled, and tumours were harvested and snap frozen immediately in O.C.T. compound.

2.2.9.8. Irradiation Alisertib combination experiments

CD-1 nude mice bearing H460 xenografts were sham irradiated or irradiated with 20 Gy in equal fractions of 4 Gy per day for five days and treated with vehicle control or 5 mg/kg Alisertib for 10 consecutive days once tumours reached a treatment volume of 100 mm^3. Mice received vehicle or 5 mg/kg Alisertib via oral gavage one hour prior to sham irradiation or 4 Gy where appropriate. Half of mice were culled on day 4 after receiving five (sham) irradiations and five days of oral dosing (starting day 0). The tumours from these mice would be harvested for biomarker analysis via IHC during the treatment phase. These tumours were harvested 4 hours after the final oral dosing of vehicle or Alisertib (3 hours after the final sham irradiation or 4 Gy respectively) and snap frozen in O.C.T. compound. The remaining half of mice would be culled when tumours reached a volume of 800 mm^3 or mean diameter of 12 mm or humane endpoints were reached. The tumours from these mice were harvested immediately and snap frozen in O.C.T. compound.

2.2.10. KM plotter analysis

The KM plotter tool KM plotter is an online tool that can be used to query cancer mRNA expression databases GEO, EGA and TCGA whilst simultaneously coupling

patient outcome data with mRNA expression data (Győrffy *et al.* 2013). There are 2437 NSCLC samples with a mean follow-up of 49 months (Győrffy *et al.* 2013).

The relative expression of Affymetrix AURKA mRNA probes 204092_s_at, 208079_s_at and 208080_at were correlated with NSCLC survival outcomes. Dichotomisation of patient cohorts into AURKA high and AURKA low expressers was performed using median probe expression when analysis was unrestricted to the entire available NSCLC database. When restricting analysis to a subset of NSCLC patients who had received radiotherapy (N= 73) (Director's Challenge Consortium for the Molecular Classification of Lung *et al.* 2008; Győrffy *et al.* 2013) both median probe expression and upper and lower tertiles of expression were used to dichotomise patient cohorts into AURKA high and AURKA low expressers. Overall survival and time to first progression were defined from the first day of treatment. Post-progression survival was defined from the day of confirmed progression. Patients surviving at the follow-up thresholds investigated were censored rather than excluded. Biased arrays were excluded from the analysis.

2.2.11. Patients and primary tumour samples

Clinical study was ethically approved by Yorkshire and the Humber Sheffield Research Ethics Committee, sponsored by Sheffield Teaching Hospitals and portfolio adopted by the NIHR (IRAS 174043).

2.2.11.1. Patient population

Eligibility criteria:

- Pathological (cytological or histological) confirmation of NSCLC

- Patients receiving radical or high dose palliative radiotherapy (doses ≥36 Gy in 12 fractions)
- Aged 16yrs or over, no upper limit
- Archived tissue available
- Able to give written informed consent

Exclusion criteria: None

2.2.11.2. Study endpoints

Overall survival was defined following the start date of radiotherapy treatment. Radiotherapy response was assessed via CT scan at approximately 2-3 months post-radiotherapy by radiologist. Tumour radiotherapy response within the irradiated volume was defined according the RECIST criteria (Eisenhauer *et al.* 2009) into complete response (CR), partial response (PR), stable disease (SBD) and progressive disease (PD). Time to tumour progression was defined as the time from start date of radiotherapy treatment to date of confirmed progression.

Around 50% of NSCLC patients achieve a complete or partial response to radiotherapy (Green and Weiss 1992). Assuming equal numbers of cases with strong and weak AURKA protein expression a 100 patient recruitment target was employed to provide 80% power to detect a 20% reduction in drop in response rate in those showing strong AURKA expression.

2.2.12. Statistical Analysis

Data were expressed as means +/- standard deviation (SD) when single data points were derived from each experiment. Data were expressed as means +/- standard error of the mean (SEM) when multiple data points were expressed as a mean from

each experiment resulting in a mean of means after several experiments. The Shapiro-Wilk test was used to test normality of data distribution but was not practical when sample sizes were ≤4N as the test is highly susceptible to type II error with small sample sizes (Ghasemi and Zahediasl 2012). Statistical difference between means was performed using an unpaired two-tailed t-test.

When more than one mean was to be compared statistically with another mean then a one-way ANOVA was performed. When comparisons between multiple means were performed back to the same control condition (many to one comparisons) the Dunnett correction for multiple comparisons was performed. When comparisons between multiple means were performed between treated conditions as well as control conditions the Bonferroni correction for multiple comparisons was performed. When data were not normally distributed the Kruskal-Wallis test with Dunn correction for multiple comparisons was used to compare multiple means.

Radiation dose response data were fitted to the linear quadratic model of cell death in Graphpad Prism v7. Dose enhancement ratios at 10% survival fraction were calculated using these data as: radiation dose (Gy) for 10% survival fraction of IR alone control / radiation dose for 10% survival of an irradiated condition. The extra sum of squares F test was used statistically compare the survival curves of IR alone control compared to other irradiated conditions.

All statistical calculations were performed using Graphpad Prism v7 assuming a cut-off for statistical significance of $p = <0.05$.

Univariate Cox regression was used to calculate a p-value and hazard ratio associated with high and low AURKA mRNA expression and a given clinical outcome using KM plotter.

3. Evaluation of Alisertib as a radiosensitising agent in NSCLC *in vitro*

3.1. Introduction, aims and hypotheses

There is evidence some limited evidence that AURKA inhibitors may be useful as radiosensitising agents in NSCLC (Myers et al., 2013, Woo et al., 2015), however these studies do not account for the whole histological breadth of NSCLC. Given that AURKA inhibitors are in advanced human clinical trials there is likely to be direct translational potential to determining if there is any interaction between AURKA inhibition and IR across NSCLC. Furthermore, there have been conflicting reports that the p53 background of a cancer cell population may determine the radiosensitising efficacy of AURKA inhibitors (Tao *et al.* 2007; Myers *et al.* 2013; Lin *et al.* 2014). Given that p53 aberration is a common occurrence in NSCLC (Kishimoto *et al.* 1992) it must also be determined if p53 status affects the efficacy of AURKA inhibitor IR combination. The first chapter of the thesis will address the question as to whether pharmacological targeting of AURKA enhances IR response in NSCLC.

The aims of this chapter are to assess the following across NSCLC cell line models that represent all histological subtypes of the disease:

1. The doses at which Alisertib inhibits AURKA activating T288 phosphorylation and the cellular toxicity of these doses alone
2. The sensitivity of a range of NSCLC cell lines to radiation alone
3. The effect of combining Alisertib and IR on cell killing *in vitro*
4. The effect of AURKA and p53 expression on Alisertib IR combination
5. The effect of AURKA inhibition timing relative to IR on Alisertib IR combination efficacy

The hypothesis of this chapter is:

Alisertib will enhance IR killing of NSCLC cell lines *in vitro*.

3.2. Results

3.2.1. Effect of Alisertib monotherapy on clonogenic survival and T288 p-AURKA in NSCLC cell lines

A panel of NSCLC cell line was continually exposed to increasing doses of the AURKA inhibitor Alisertib. Baseline clonogenic response to Alisertib was relatively stable across all NSCLC cell lines investigated here, regardless of p53 or histological subtype (see Figure 3.1 A-B). The H520 cell line was the most sensitive to Alisertib monotherapy with a mean lethal median dose (reduce surviving population to 50%) (LD50) of 19.60 nM. The SW900 cell line was the least sensitive to Alisertib monotherapy with a mean LD50 of 41.27 nM.

Inhibition of AURKA by Alisertib was investigated using western blot (see Figure 3.1 C-D). Nocodazole (Noc) was used to in enrich the mitotic population in all tested cell lines so that T288 activating phosphorylation of AURKA could be visualised. After release from Noc treatment Alisertib was added for 2 hours before cell lysis. Here increasing the concentration of Alisertib was associated with increasing inhibition of T288 p-AURKA expression. 25 nM Alisertib was found to consistently and significantly reduce the expression of T288 p-AURKA in all cell lines whilst only having moderate effect on T232 p-AURKB expression after 2 hours of treatment (see Figure 3.1 E-G). 5 nM and 10 nM Alisertib also had modest inhibitory effect on T288 p-AURKA expression in all cell lines but this effect was more variable between cell lines and did not exhibit any increased specificity for T288 p-AURKA inhibition over T232 p-AURKB when compared to 25 nM Alisertib treatment. T198 p-AURKC was

identified in four of the 6 cell lines but relating these findings to Alisertib treatment was hindered by difficulties in reliably detecting AURKC. Note: 25 nM dose was tested on ≥3 occasions while lower doses were tested on fewer occasions limiting statistical testing at lower doses.

A

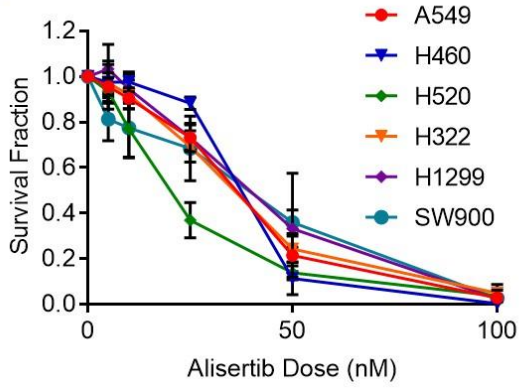

B

Cell Line	NSCLC Subtype	p53 Status	Alisertib LD50 (nM +/- SD)
A549	ADC	Wildtype	36.63 +/- 4.79
H460	LCC	Wildtype	37.50 +/- 1.59
H520	SCC	Wildtype	19.60 +/- 4.53
H322	ADC	Mutant	35.90 +/- 0.99
H1299	LCC	Null	39.33 +/- 1.54
SW900	SCC	Mutant	41.27 +/- 15.23

C

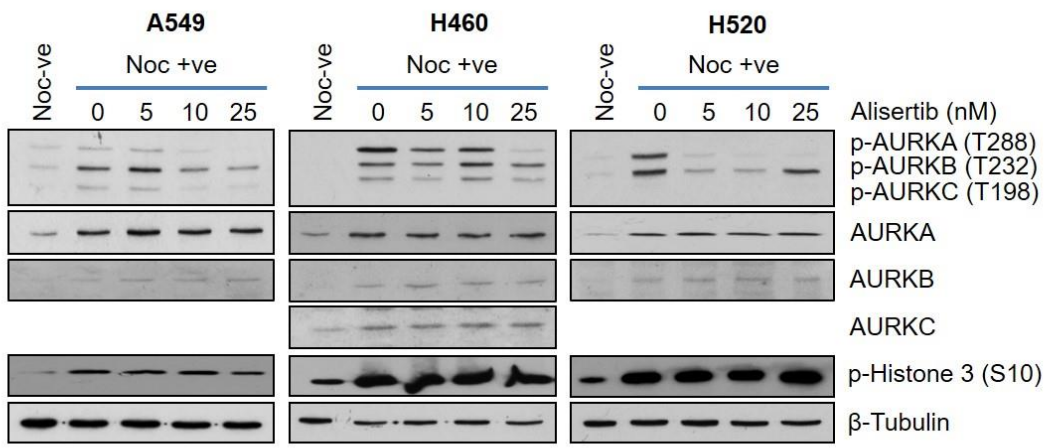

D

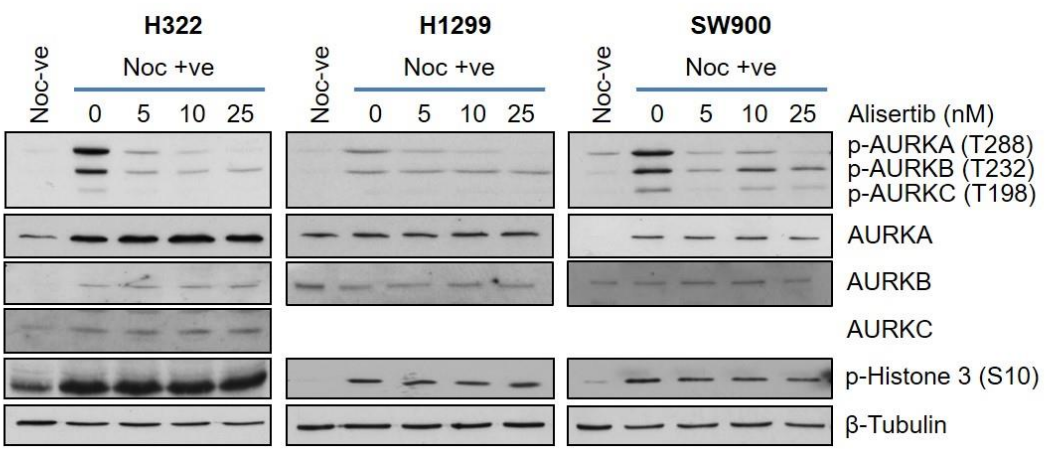

Figure 3.1. **Alisertib monotherapy response in NSCLC cell lines.** Legend overleaf

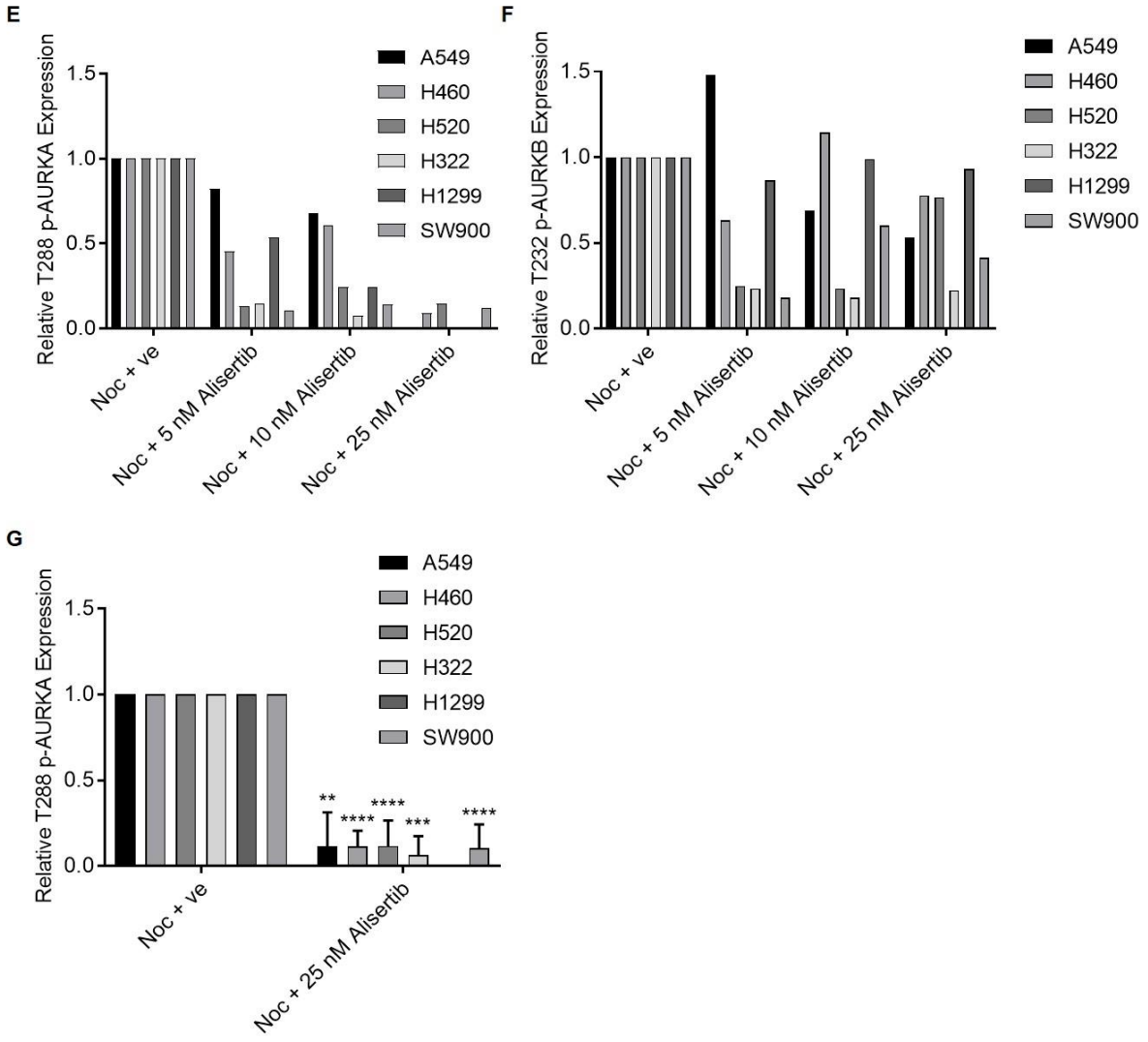

Figure 3.1. **Alisertib monotherapy response in NSCLC cell lines. A**. Survival fraction of NSCLC cell lines after treatment with increasing doses of Alisertib. Data points represent mean survival fraction normalised to untreated control +/- SD (N= 3). **B**. Table of mean Alisertib LD50 values in NSCLC cell lines +/- SD (N= 3). **C**. Representative western blot results for pan p-AURK, AURKA, AURKB, AURKC, p-Histone 3 (S10) levels and β-tubulin in protein extracts from A549, H460 and H520 cells arrested overnight with 100 ng/ml Nococdazole (Noc) and released into increasing concentrations of Alisertib for 2 hours. **D**. As in above in protein extracts from H322, H1299 and SW900 cells. **E**. Quantification of T288 p-AURKA expression normalised to total AURKA levels and adjusted for loading variation with β-tubulin from the western blots in C and D. **F**. Quantification of T232 p-AURKB expression normalised to total AURKB levels and adjusted for loading variation with with β-tubulin from the western blots in C and D. **G.** Mean T288 p-AURKA expression normalised to AURKA and adjusted for loading variation relative to Noc alone control (N= ≥3). * denotes p= ≤0.05, ** denotes p= ≤0.01, *** denotes p=≤0.001 (Student's independent samples two-tailed unpaired t-test) comparing each cell line to Noc control.

3.2.2. Baseline radiosensitivity of NSCLC cell lines

The same panel of NSCLC cell lines was irradiated and then survival was assessed using clonogenic survival assays. There was significant heterogeneity in baseline response to IR in both the p53 wildtype and p53 deficient NSCLC cell lines investigated here, with no apparent correlation between p53 expression status and radiosensitivity (see Figure 3.2 A-B). The A549 cell line was found to the most inherently radio-resistant cell line investigated with the highest mean survival fractions after 2Gy and 4Gy (SF2 and SF4) of 0.82 and 0.41 respectively. This is concordant with the literature which identifies the A549 cell line as the prototypical radio-resistant NSCLC model (Yang *et al.* 2013). The SW900 cell line was found to be the most radio-responsive cell line investigated here with the lowest mean SF2 and SF4 values of 0.36 and 0.06 respectively.

A

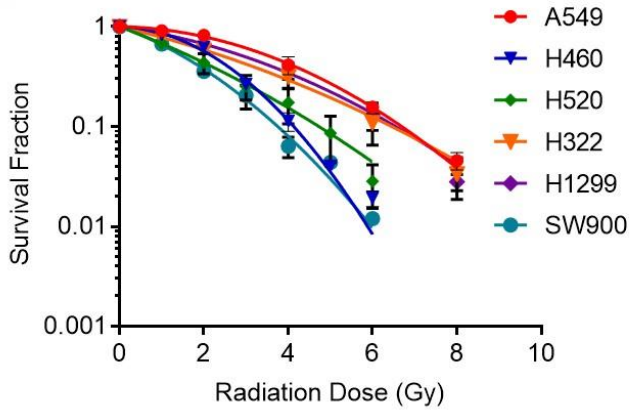

B

Cell Line	NSCLC Subtype	p53 Status	SF2 +/- SD	SF4 +/- SD
A549	ADC	Wildtype	0.82 +/- 0.07	0.41 +/- 0.08
H460	LCC	Wildtype	0.62 +/- 0.05	0.11 +/- 0.02
H520	SCC	Wildtype	0.44 +/- 0.10	0.17 +/- 0.07
H322	ADC	Mutant	0.58 +/- 0.07	0.32 +/- 0.08
H1299	LCC	Null	0.64 +/- 0.08	0.36 +/- 0.07
SW900	SCC	Mutant	0.36 +/- 0.02	0.06 +/- 0.01

Figure 3.2. **Baseline radiation dose-response curves in NSCLC cell lines. A**. Survival fraction of NSCLC cell lines after treatment with increasing doses of IR. Data points represent mean survival fraction normalised to unirradiated control +/- SD (N= ≥3). **B**. Table of SF2 and SF4 values in NSCLC cell lines +/- SD.

3.2.3. Characterisation of NSCLC cell lines – AURKA and p53 protein expression status

Given that AURKA protein expression and p53 aberration have previously been shown to independently affect the radiosensitivity of other cancer cell lines previously (Siles *et al.* 1996; Guan *et al.* 2007) the expression of AURKA and p53 was assessed in NSCLC cell lines. There was a trend for histological subtype to associate with SF2 value in the descending order of ADC>LCC>SCC but this was

limited by sample size and was not tested statistically (see Figure 3.3 A) There was no clear association between histological subtype and baseline AURKA expression. However, the squamous cell carcinoma derived H520 and SW900 cell lines were the lowest mean expressers of baseline AURKA, with approximately half the level seen in the highest expressing H460 cell line (see Figure 3.3 B-C). Interestingly, there was a positive but non-significant correlation between baseline cell line AURKA expression and cell line SF2 value (r= 0.714, p= 0.136 (Spearman correlation)) that is likely limited by sample size (see Figure 3.3 D). There was no pattern of association however between relative expression of AURKA and Alisertib sensitivity (data not shown).

A549, H460 and H520 cells are reported as containing wildtype p53 sequence (Castro *et al.* 2001; S.O. Lee *et al.* 2012; Shen *et al.* 2012), whilst the H1299, SW900 and H322 cells are reported as p53 null or mutant respectively (Nishizaki *et al.* 2004; Shen *et al.* 2012; Korrodi-Gregório *et al.* 2016). The A549 and H460 cell lines were seen to express wildtype p53 as expected, but no wildtype p53 expression was detected in the H520 cell line despite previous reports of, albeit very low, wildtype expression in this cell line (Castro *et al.* 2001) (see Figure 3.3 E). Furthermore, H520 cells could not be seen to express p53 after treatment with 4 Gy, 25 nM Alisertib or 4 Gy + 25 nM Alisertib combination which could be expected to stabilise low level expression (see Figure 3.3 F). p53 expression was also detected in the H322 cell line with multiple banding which is probably explained by expression of mutant p53 in this cell line (Nishizaki *et al.* 2001). No p53 expression was detected in the H1299 and SW900 cell lines. There was no clear association with p53 status and radiation, or indeed Alisertib, sensitivity (data not shown).

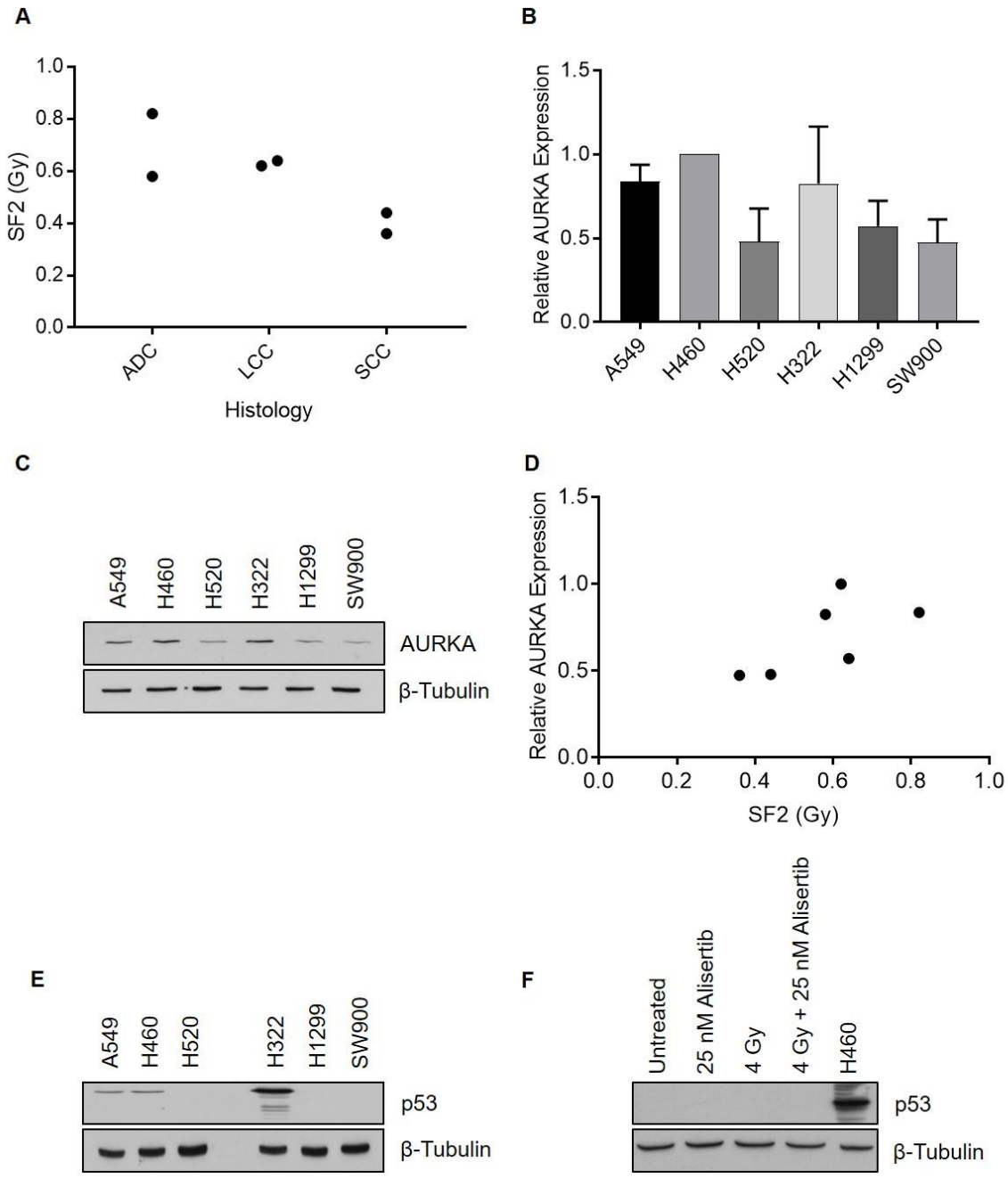

Figure 3.3. **Baseline AURKA and p53 protein expression in the 6 NSCLC cell line panel. A.** Cell line survival fraction after 2 Gy (SF2) plotted against cell line histological subtype. **B.** AURKA expression adjusted for loading with β-tubulin and normalised to H460 expression in NSCLC cell lines +/- SD (N= 4). **C.** Representative western blot for AURKA and β-Tubulin in NSCLC cell lines in logarithmic proliferation phase (N= 4). **D**. Relative cell line expression of AURKA normalised to H460 expression plotted against cell line SF2. **E.** Representative western blot for p53 and β-Tubulin in NSCLC cell lines in logarithmic proliferation phase (N= 2). **F.** Representative western blot for p53 and β-Tubulin in H520 cells after 1 hour treatment with +/- 25 nM Alisertib, 4 Gy or 4 Gy + 25 nM Alisertib. H460 used as a positive control for wildtype p53 expression.

3.2.4. Alisertib enhances response to IR in a dose-dependent manner in p53 wildtype NSCLC cell lines

Given that 25 nM Alisertib was shown to significantly inhibit AURKA T288 phosphorylation after 2 hours and to have little effect on toxicity alone in all NSCLC cell lines investigated, the effect of combining this dose of Alisertib with IR was investigated. Alisertib was given 2 hours prior to irradiation and was present continuously throughout the colony survival assay. Mean dose enhancement ratio when combining 25 nM Alisertib with IR for 10% survival fraction (DER_{10}) indicated that the p53 wildtype A549 and H460 cell lines were radiosensitised by 25 nM Alisertib (see Figure 3.4 A & C). Despite questionable p53 protein expression, the H520 cell line was also radiosensitised by 25 nM Alisertib.

Moreover, the extra sum of squares test revealed that the survival curves for 25 nM Alisertib IR combination were statistically different from the corresponding survival curve for irradiation alone in A549, H460 and H520 cells ($p = <0.0001$ for all three cell lines). Further to this the radiosensitivity of H460 and H520 cell lines was also tested in combination with 10 nM Alisertib. These experiments revealed that 10 nM had a smaller radiosensitising effect on the H460 and H520 cell lines yielding mean DER values of 1.08 and 1.06 respectively at 10% survival fraction (see Figure 3.4 B-C). Both cell lines had altered survival curves when co-treated with 10 nM Alisertib and irradiation resulting in significant statistical differences between that and the irradiation alone survival curves. These data demonstrate a dose-dependent radiosensitising effect of Alisertib in p53 expressing NSCLC cells.

Conversely, 25 nM Alisertib in combination with IR did not cause any statistically significant enhancement of IR cytotoxicity in H322, H1299 and SW900 cells (see

Figure 3.4 A & C). Further to this the extra sum of squares test revealed that the survival curves for 25 nM Alisertib IR combination were not statistically different from the corresponding survival curve for irradiation alone in H322, H1299 and SW900 cells respectively (p= 0.7529, p= 0.949 and p= 0.406).

When radiation is used to treat NSCLC patients it is fractionated into smaller doses which do not tend to exceed 3 Gy per fraction (NICE 2019). Given that single doses of radiation had been used to show combinational effect of Alisertib and radiation in cell lines it was decided that treating cells with smaller fractionated doses of radiation in combination with single dose of Alisertib might be even more clinically relevant. This was tested in the H460 cell line chosen as it was a positive responder to Alisertib combination with single dose IR and because this cell line had high plating efficiency and formed discrete colonies during clonogenic assays. As previously Alisertib was added 2 hours prior to irradiation and present throughout the clonogenic assay. Note: fresh Alisertib was not added prior to further irradiations. There was a statistically significant reduction in survival fraction when H460 cells were treated with single dose of Alisertib two hours prior to 1 Gy irradiation and irradiated with a further three fractions of 1 Gy, once every 24 hours (see Figure 3.4 D). Mean survival fraction for 4 x 1 Gy was 0.432 and fell 2.62-fold to 0.165 when 4 x 1 Gy was combined with a single dosing event of 25 nM Alisertib. This was slightly inferior to the 2.98-fold reduction in mean survival fraction when single dose 4 Gy was combined with 25 nM Alisertib.

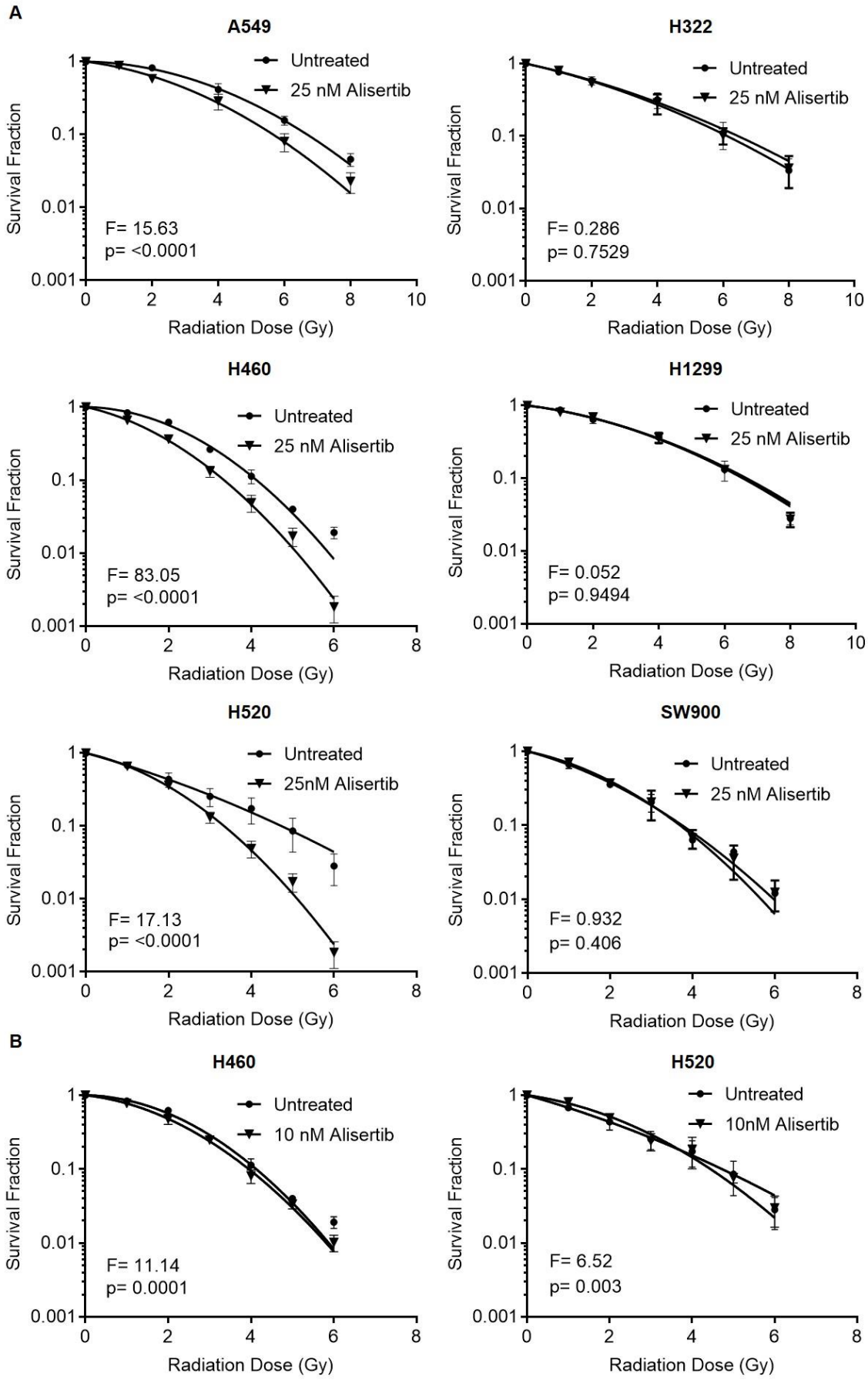

Figure 3.4. **Survival fraction of NSCLC cells after treatment with IR alone or IR in combination with Alisertib.** Legend overleaf

C

Cell Line	NSCLC Subtype	p53 Status	DER_{10} with 25 nM Alisertib +/- SD	DER_{10} with 10 nM Alisertib +/- SD
A549	ADC	Wildtype	1.21 +/- 0.12	
H460	LCC	Wildtype	1.31 +/- 0.07	1.09 +/- 0.05
H520	SCC	Wildtype	1.40 +/- 0.27	1.07 +/- 0.23
H322	ADC	Mutant	1.08 +/- 0.08	
H1299	LCC	Null	1.05 +/- 0.03	
SW900	SCC	Mutant	1.02 +/- 0.23	

D

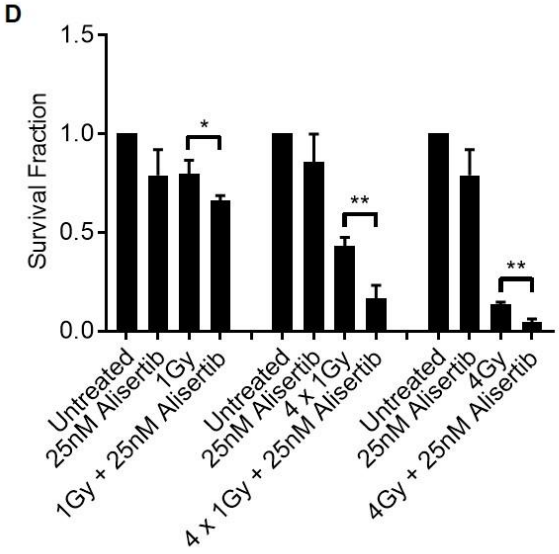

Figure 3.4 **Survival fraction of NSCLC cells after treatment with IR alone or IR in combination with Alisertib. A.** Survival fraction of NSCLC cell lines after treatment with increasing doses of IR +/- 25 nM Alisertib. Data points represent mean survival fraction normalised to unirradiated control +/- SD (N= ≥3). F-value and p-value derived from extra sum of squares test. **B.** Survival fraction of NSCLC cell lines after treatment with increasing doses of IR +/- 10 nM Alisertib. Data points represent mean survival fraction normalised to unirradiated control +/- SD (N= ≥3). F-value and p-value derived from extra sum of squares test. **C.** Table of mean DER_{10} values expressed after combining 25 or 10 nM Alisertib with IR +/- SD (N= ≥3). **D.** Survival fraction of H460 cells after treatment with either fractionated or single dose IR and in combination with 25 nM Alisertib. 4 x 1 Gy represents when four fractions of 1 Gy were given once daily for four consecutive days. Data points represent mean survival fraction normalised to unirradiated control +/- SD (N=3). * denotes p= ≤0.05, ** denotes p= ≤0.01 (Students independent samples unpaired two-tailed t-test). All the above was performed by treating with Alisertib 2 hours prior to irradiation with no drug wash-out post-irradiation.

These data suggest that Alisertib IR combination was effective in enhancing radiation response in a subset of NSCLC cell lines in a dose dependent manner and that the mechanism may be dependent on p53, although this was not clear cut. This corroborated the findings of Myers *et al* (2013) in that H460 cells were radiosensitised by Alisertib. Furthermore, Alisertib IR combination showed efficacy even when IR dosing was split into fractions, although staggering radiation events did not synergise any further with the radiosensitising mechanism of Alisertib IR combination, perhaps because Alisertib was not renewed.

3.2.5. AURKA depletion enhances H460 response to IR

To demonstrate that the radiosensitisation effect was indeed due to AURKA inhibition, H460 cells were plated 24 hours post-transfection with scrambled siRNA or two independent siRNAs against AURKA and irradiated to see if AURKA depletion alone could affect IR response. AURKA siRNA 1 and AURKA siRNA 2 had DER_{10} values of 1.21 and 1.23 when compared to scrambled siRNA control, similar to the DER_{10} achieved with 25 nM Alisertib (see Figure 3.5 A). The extra sum of squares revealed that the survival curves for both AURKA siRNA constructs were different from that of the scrambled curve in a statistically significant manner.

Densitometry of western blots from H460 lysates harvested sequentially post-transfection confirmed that the two AURKA targeted siRNAs used here had similar effects on AURKA protein expression (see Figure 3.5 B-C). Each siRNA caused a mean reduction in AURKA protein expression of 32.3% (siRNA 1) and 57.3 % (siRNA 2) by 24 hours post-transfection and 79.6% (siRNA 1) and 81.4% (siRNA 2) by 48 hours post-transfection relative to scrambled siRNA control.

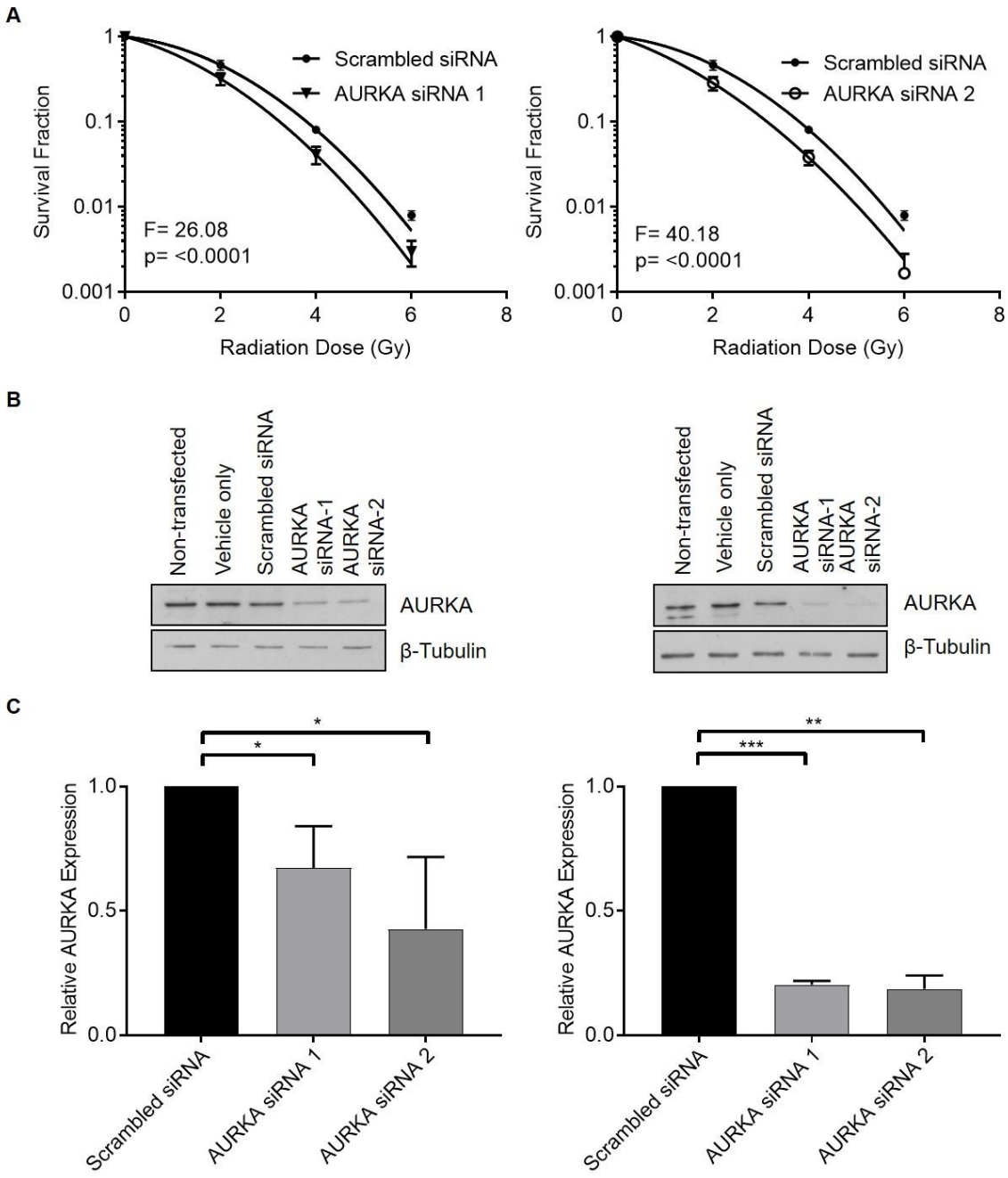

Figure 3.5. **Survival fraction of H460 cells plated and irradiated 24 hours after transfection with scrambled or AURKA siRNA A.** Survival fraction of irradiated H460 cells transfected with scrambled control siRNA, AURKA siRNA 1 (left) or AURKA siRNA 2 (right) Data points represent mean survival fraction normalised to unirradiated control +/- SD. F-value and p-value derived from extra sum of squares test. **B.** Representative western blots of AURKA expression in H460 lysate 24 hours (left) and 48 hours post-transfection (right). **C**. Quantification of AURKA expression in H460 lysate normalised to β-Tubulin expression and relative to scrambled siRNA control 24 hours (left) (N=3) and 48 hours post-transfection (right) (N=2). Data points represent mean relative AURKA expression +/- SD. * denotes p= ≤0.05, ** denotes p= ≤0.01, *** denotes p= ≤0.001 (Student's independent samples unpaired two-tailed t-test).

This suggests that AURKA is a legitimate radiosensitising target in the H460 cell line and supports data from results section 3.2.4. where AURKA was targeted pharmacologically with Alisertib.

3.2.6. p53 depletion attenuates the radiation enhancing effect of Alisertib in NSCLC cells

3.2.6.1. p53 depletion attenuates the radiation enhancing effect of Alisertib in H460 cells

The results section 3.2.4 suggested that functional p53 may be important when determining which cells respond with enhanced IR response after Alisertib IR combination. However, these findings were correlative and did not account for other genetic differences that may be present between NSCLC cell line models. Given this, depletion of p53 expression in the p53 wildtype expressing H460 cell line was performed in combination with irradiation +/- 25 nM Alisertib. H460 cells were plated 48 hours post-transfection with scrambled siRNA or p53 siRNA. p53 depletion attenuated the combinational effect of 25 nM Alisertib and radiation in H460 cells (see Figure 3.6 A-B). Combining 25 nM Alisertib with irradiation when H460 cells were treated with scrambled siRNA control had a mean DER_{10} of 1.35. This was not statistically different from the DER_{10} for non-transfected H460 cells treated with 25 nM Alisertib radiation combination. p53 depletion with p53 siRNA 1 and p53 siRNA 2 in H460 cells caused an attenuation of the mean DER_{10} to 1.12 ($p= 0.057$ Student's t-test) and 1.06 ($p= 0.04$ Student's t-test) respectively when 25 nM Alisertib and radiation were combined. Attenuation of radiosensitising effect when p53 was depleted resulted in p-values >0.05 from the extra sum of squares test indicating that the radiation survival curves +/- 25 nM Alisertib were best described by one dataset.

Densitometry of western blots from H460 lysates harvested sequentially post-transfection revealed that p53 siRNA 2 sourced from Ambion was more efficient in depleting p53 expression when compared to p53 siRNA 1 sourced from Santa Cruz Biotechnology (see Figure 3.6 C). This was consistent with greater attenuation of radiosensitising effect with p53 siRNA 2 compared to p53 siRNA 1. p53 siRNA 2 caused mean depletion of p53 expression, relative to that of scrambled siRNA control, of 83.3% 24 hours post-transfection, 82.6% 48 hours post-transfection, and 75.0% 72 hours post-transfection prior to p53 expression levels returning to levels of 110.5% by 96 hours post-transfection. p53 siRNA 1 caused mean depletion mean depletion of p53 expression, relative to that of scrambled siRNA control, by 50.4% 24 hours post-transfection, 69.5% 48 hours post-transfection, and 38.5% 72 hours post-transfection prior to p53 expression levels returning to levels of 133.3% by 96 hours post-transfection.

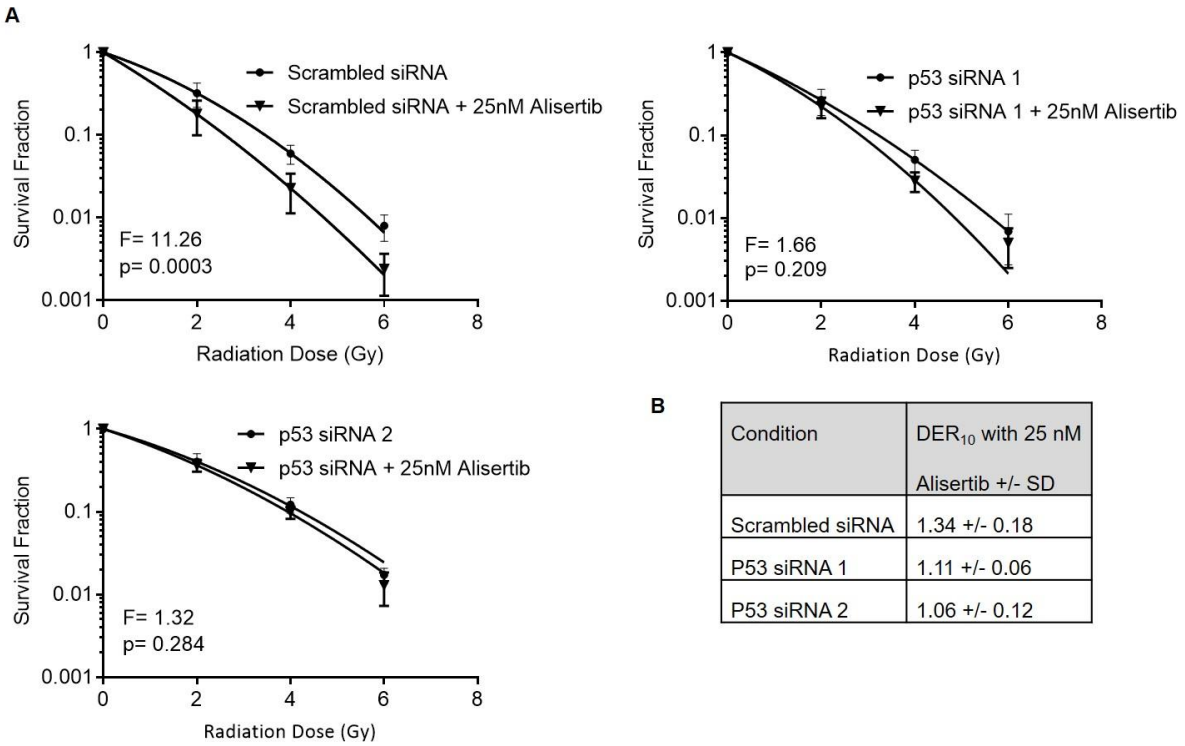

Condition	DER_{10} with 25 nM Alisertib +/- SD
Scrambled siRNA	1.34 +/- 0.18
P53 siRNA 1	1.11 +/- 0.06
P53 siRNA 2	1.06 +/- 0.12

Figure 3.6. **Survival fraction H460 cells plated and irradiated 48 hours after transfection with scrambled or p53 siRNA.** Legend overleaf

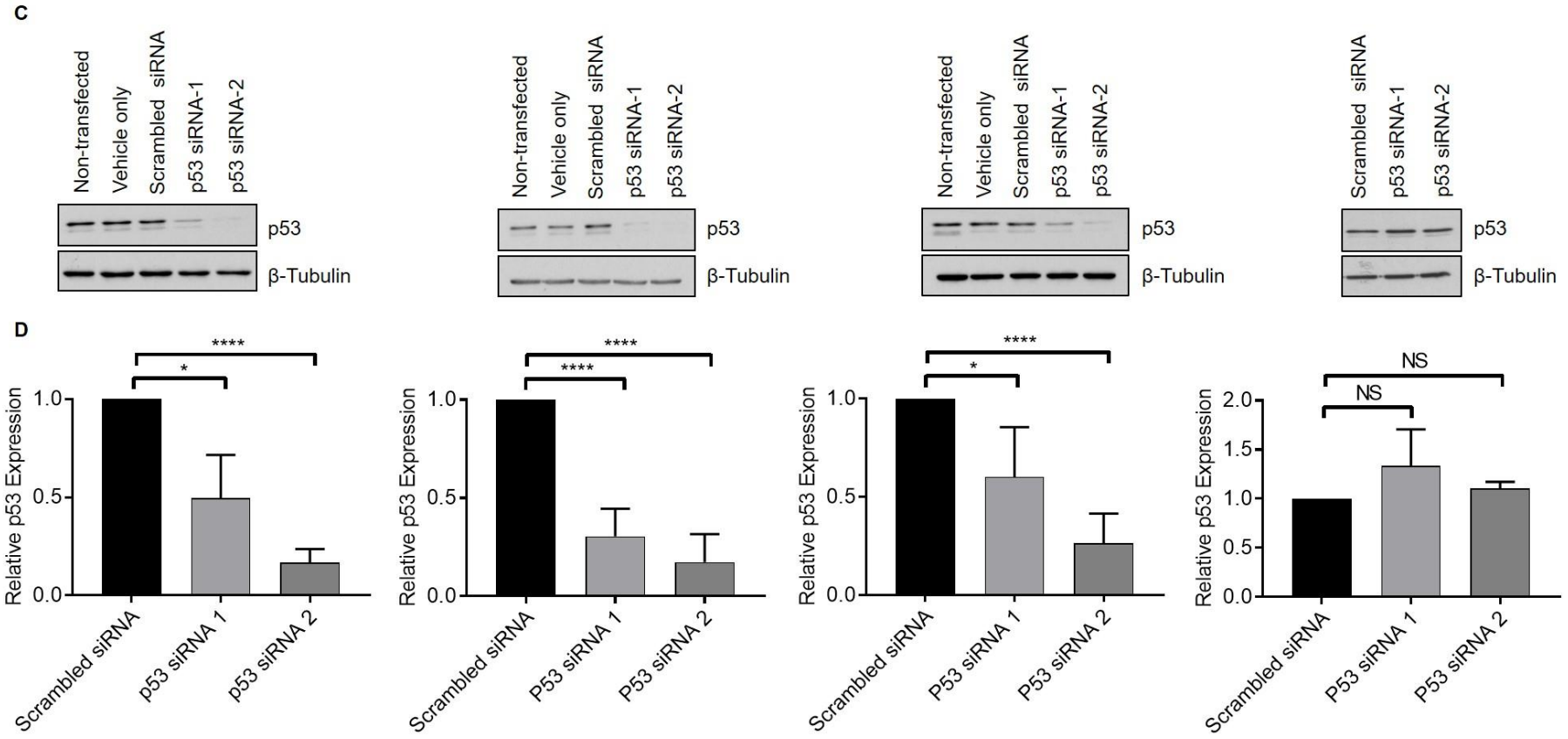

Figure 3.6. **Survival fraction H460 cells plated and irradiated 48 hours after transfection with scrambled or p53 siRNA. A.** Survival fraction of irradiated H460 cells treated transfected with scrambled control siRNA (top left), p53 siRNA 1 (top right) or p53 siRNA 2 (bottom left) and treated with +/- 25 nM Alisertib. Data points represent mean survival fraction normalised to unirradiated control +/- SD. F-value and p-value derived from extra sum of squares test (N= 4). **B.** Table of mean DER_{10} values expressed after combining 25 nM Alisertib with IR in H460 cells transfected with scrambled or p53 siRNA +/- SD (N= 4). **C.** Representative western blots for p53 expression in H460 lysates 24 hours (far left), 48 hours (middle left), 72 hours (middle right) and 96 hours (far right) post-transfection with scrambled or p53 siRNA **D.** Quantification of p53 expression in H460 lysate normalised to β-Tubulin expression and relative to scrambled siRNA control (N= ≥3). Data points represent mean relative p53 expression +/- SD. NS (non-statistically significant) denotes p= >0.05 * denotes p= ≤0.05, ** denotes p= ≤0.01, *** denotes p= ≤0.001 (Student's independent samples unpaired two-tailed t-test).

These data suggest that the mechanism of Alisertib mediated radiosensitisation is p53 dependent.

3.2.6.2. Alisertib radiosensitises both the isogenic HCT116 p53 +/+ and HCT116 p53 -/- colorectal cancer cell lines

The data above suggest that Alisertib only has radiation dose enhancing effects in NSCLC cells in a p53 proficient background and this is in line with the findings of Myers *et al* (2013) in NSCLC models. However considering p53 proficiency and AURKAi + IR combinational effect in a pan-cancer manner, the above data is contradictory to findings in colorectal carcinoma models (Tao *et al.* 2007) and hepatocellular carcinoma models (Lin *et al.* 2014) which suggested that the radiosensitising effect of AURKA inhibition was in fact more pronounced in p53 deficient backgrounds *in vitro* and *in vivo*. These investigations were performed with AURKA inhibitors PHA-680632 and VE465 respectively. We tested the ability of Alisertib to radiosensitise the isogenic colorectal carcinoma HCT116 cell lines which encode either two wildtype TP53 alleles (p53 +/+) or a homozygous deletion of exon 2 in the TP53 gene resulting in no p53 protein expression (p53 -/-) (Bunz *et al.* 1998). This is the same system tested by Tao *et al* (2007). Given that Alisertib was not tested by Tao *et al* (2007) this can help deduce whether p53-dependent radiosensitisation is an Alisertib specific mechanism. This experiment also addresses whether radiosensitisation by Alisertib specifically in p53 proficient backgrounds is a pan-cancer phenomenon or if this effect is more specific to NSCLC. Additionally, the HCT116 isogenic model represents a stable model of p53 wildtype and p53 null expression and overcomes some of the limitations associated with siRNA transfection such as siRNA/transfection reagent-induced toxicity and transient gene expression changes.

As expected p53 was expressed in the p53 +/+ HCT116 model when sampled on three independent occasions and was not detectable in the p53 -/- HCT116 model on the same occasions (see Figure 3.7 A). Additionally, 25 nM Alisertib was shown to provide strong inhibition of T288 p-AURKA, in the absence of significant off target effect on T232 p-AURKB, in Nocodazole released populations in both the HCT116 p53 +/+ and -/- cell lines (see Figure 3.7 B). There is evidence of reduced T288 p-AURKA inhibition by 25 nM Alisertib in the p53 +/+ HCT116 cell line compared to the p53 -/- cell line but this western blot was performed only once. It is unclear if this is a consistent finding.

25 nM Alisertib radiosensitised both cell lines (see Figure 3.7 C-D). The was combined with radiation the HCT116 p53 +/+ had a mean DER_{10} of 1.32 compared to 1.43 in the HCT116 p53 -/- cell line. This difference in mean DER_{10}, however, was not statistically significant (p= 0.506 Student's unpaired two-tailed t-test).

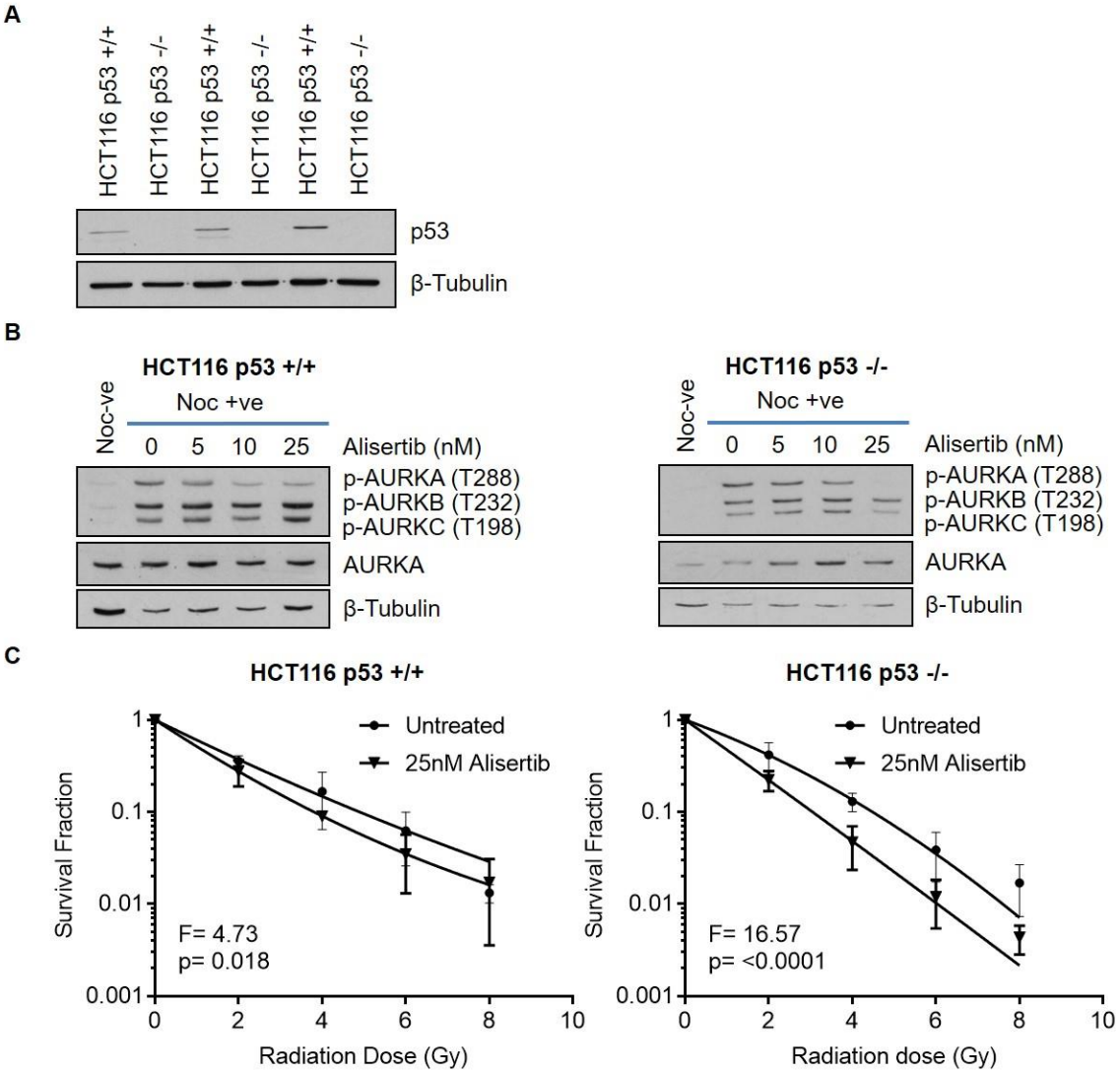

D

Cell line	DER_{10} with 25 nM Alisertib +/- SD
HCT116 p53 +/+	1.32 +/- 0.26
HCT116 p53 -/-	1.43 +/- 0.08

Figure 3.7. **Validation of HCT116 p53 +/+ and HCT116 p53 -/- isogenic model and survival fraction when treated with IR alone or IR in combination with Alisertib. A.** Western blot for p53 and β-tubulin in protein extract from HCT116 p53 isogenic models. **B.** Western blot for pan p-AURK, AURKA and β-tubulin in protein extract from HCT116 p53 +/+ lysates (left) and HCT116 p53 -/- lysates (right) from cells arrested overnight with 100 ng/ml Nocodazole (Noc), released from Noc and treated increasing concentrations of Alisertib for 2 hours. **C.** Survival fraction of irradiated HCT116 p53 +/+ and HCT116 p53 -/- (right) cells after treatment with increasing doses of IR +/- 25 nM Alisertib. Data points represent mean survival fraction normalised to unirradiated control +/- SD (N= 4). F-value and p-value derived from extra sum of squares test. **D.** Table of mean DER_{10} values expressed after combining 25 nM Alisertib with IR +/- SD (N= 4).

These data suggest that Alisertib mediated radiosensitisation is not p53-dependent in HCT116 cells. Although, delineating the genetic determinants of Alisertib IR combinational effect is complicated by the microsatellite instable phenotype of HCT116 cells (Parsons *et al.* 1993). Thus, although it appears that p53 is involved in Alisertib mediated radiosensitisation of NSCLC cells this finding may not be true in all cancers.

3.2.7. Alisertib inhibits background and IR-induced T288 p-AURKA expression

Sequential harvest of proteins from H460 cells post-irradiation was employed to investigate T288 p-AURKA expression changes over time in the presence or absence of 25 nM and/or 4 Gy of irradiation. 25 nM Alisertib or 4 Gy + 25 nM Alisertib treatment alone in H460 cells inhibited T288 p-AURKA to undetectable levels by 1 hour, 4 hours and 24 hours post-irradiation (see Figure 3.8 A-B). In comparison, 4 Gy treatment alone in H460 cells caused moderate reduction in T288 p-AURKA expression levels by 1-hour post-irradiation ($p= 0.01$ Student's t-test), completely abolished expression by 4-hours, before expression rebounded and exceeded those seen in the untreated control by mean 1.93-fold ($p= 0.02$ Student's t-test) after 24 hours. This suggests that activation of AURKA is important at late timepoints post-IR.

Additionally, total AURKA expression itself was variable in the 1 and 4 hours post-irradiation but no change was statistically significant compared to control (see Figure 3.8 A & C). Similar to each treatment alone at 1 and 4 hours post-treatment Alisertib IR combination led to small statistically non-significant increases in AURKA expression levels. Strikingly, at 24 hours post-irradiation in Alisertib IR combination AURKA levels were further increased such that AURKA levels were highly increased

relative to untreated control (p=0.02 Student's t-test) and greatly exceeded the levels seen for 25 nM Alisertib and 4 Gy conditions respectively.

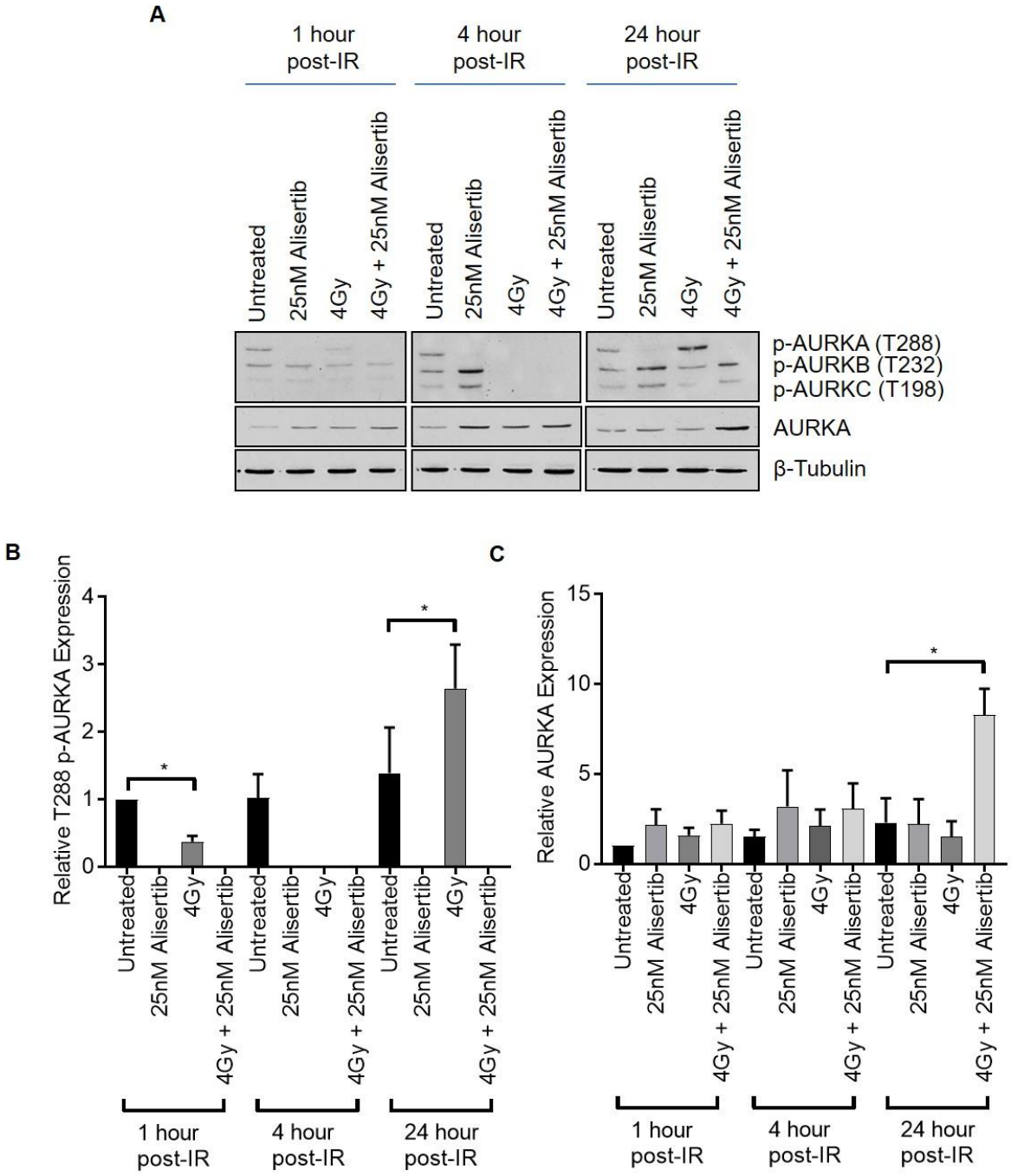

Figure 3.8. **T288 p-AURKA and AURKA protein expression in H460 cells 1-hour, 4-hours and 24-hours post-IR. A.** Representative western blot results for pan p-AURK, AURKA and β-Tubulin in protein extract from H460 cells achieved 1-hour, 4-hours and 24-hours post-irradiation treated with 25 nM Alisertib, 4 Gy or 25 nM Alisertib 4 Gy combination. **B**. Quantification of T288 p-AURKA expression normalised to AURKA levels and adjusted for β-tubulin levels in H460 lysates (N= 3). Data points represent mean T288 p-AURKA expression +/- SD relative to expression in untreated condition 1-hour post-irradiation. **C.** Quantification of AURKA expression β-tubulin levels in H460 lysates (N= 3). Data points represent mean AURKA expression +/- SD relative to expression in untreated condition 1-hour post-irradiation. * denotes p= ≤0.05 (Student's independent samples unpaired two-tailed t-test).

In conclusion to these expression data, 25 nM Alisertib and 25 nM Alisertib in combination with 4 Gy caused abolishment of T288 p-AURKA expression 1-hour, 4-hours and 24-hours post-irradiation in H460 cells. Meanwhile 4 Gy led to a moderate increase in T288 p-AURKA expression by 24-hours post-irradiation after previously reducing/abolishing T288 p-AURKA 1-hour and 4-hours post-irradiation in H460 cells. This suggests that AURKA is activated 24-hour post-irradiation but that this activation is suppressed by Alisertib when combined with 4 Gy. We also found that AURKA protein expression peaked 24-hour post-irradiation in the 4 Gy + 25 nM Alisertib combinational, suggesting that the treatment combination caused an accumulation of inactive AURKA protein.

3.2.8. Alisertib mediated radiosensitisation of H460 cells is dependent on Alisertib dosing after radiation

In previous experiments 2 hour pre-treatment with 25 nM Alisertib followed by continuous exposure post-irradiation caused a statistically significant reduction in H460 cell survival compared to irradiation alone. Given that treatment with 25 nM Alisertib, 4 Gy or 4 Gy + 25 nM Alisertib combination had time dependent effects on T288 p-AURKA and AURKA expression it is possible that the timing Alisertib dosing relative to the point of irradiation could have an impact on sensitisation. Here the dosing regime was altered in H460 cells as depicted in Figure 3.9 A.

Consistent with previous findings 2 hour pre-treatment with 25 nM Alisertib followed by continuous exposure post-IR caused reduction in mean survival fraction from 0.45 to 0.25 for 2 Gy alone ($p= 0.0002$ (One-way ANOVA)) (see Figure 3.9 B). However, when H460 cells were pre-treated for 2 hours with 25 nM Alisertib prior to irradiation but returned to Alisertib free media post-IR there was no significant reduction in

survival fraction compared to 2 Gy alone. This finding was also true when 25 nM Alisertib pre-treatment was extended to 24 hours prior to irradiation before returning cells to Alisertib free media. There were statistically significant reductions in mean survival fraction compared to 2 Gy alone when 25 nM Alisertib was added immediately after irradiation (mean SF: 0.29, p= 0.0017 (One-way ANOVA)) and most interestingly when it was added 24 hours post-irradiation (mean SF: 0.28, p= 0.0012 (One-way ANOVA)) compared to 2 Gy alone.

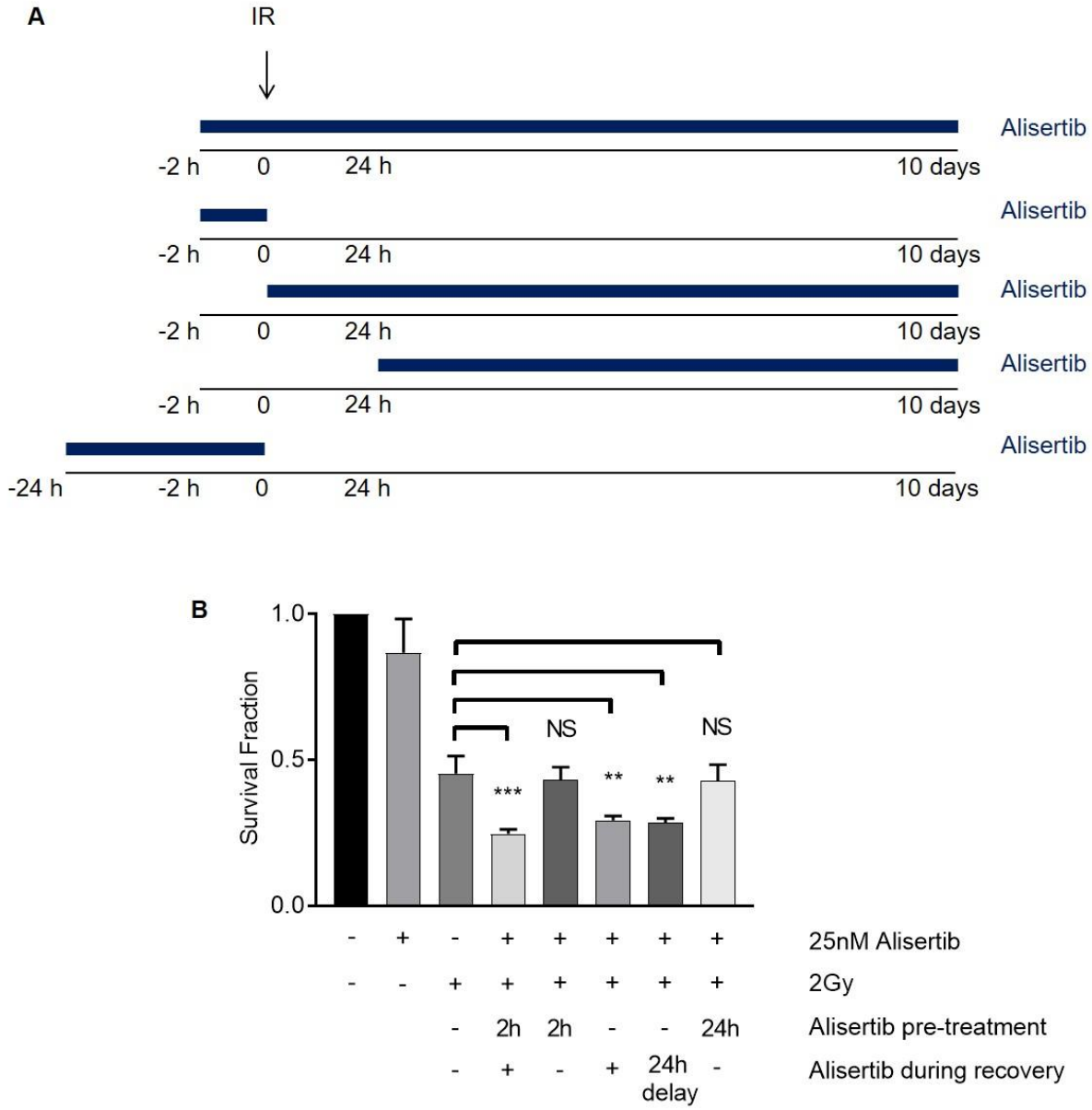

Figure 3.9. **Effect of varying Alisertib IR dosing schedule in H460 cells. A.** Schema of Alisertib dosing regimen changes relative to the point of irradiation. Blue line represents presence of 25 nM Alisertib in the culture media. **B.** Survival fractions of H460 cells after 2 Gy treated with or without 25 nM Alisertib (N=3). Data points represent mean survival fraction normalised to unirradiated control +/- SD. NS (non-statistically significant) denotes p= >0.05, * denotes p= ≤0.05, ** denotes p= ≤0.01, *** denotes p=≤0.001 (One-way ANOVA with Dunnett correction for multiple comparisons).

Given that Alisertib has been shown to cause mitotic accumulation in tumour tissues (Manfredi *et al.* 2011), these data provide evidence against a hypothesis that the

Alisertib IR combination achieves enhancement of IR response through arresting cells in the most radio-responsive phases of the cell cycle prior to irradiation itself. These results indicate that the presence of Alisertib in relation to time of irradiation is most important in the hours after irradiation, during the cellular recovery phase. As radiosensitisation by addition of 25 nM Alisertib is achieved even 24-hours post-irradiation, this suggests that the combinational mechanism is not through immediate recovery effects post-IR. This implicates changes in cell cycle progression and cell death as being responsible for the effects seen.

3.3. Discussion

In this chapter we present evidence that targeting of AURKA with siRNA or Alisertib enhances IR response in NSCLC cells that express wildtype p53 and that the effect with Alisertib is dose-dependent. We also show that the Alisertib IR combination has significant effects on AURKA protein levels and activation (T288) 24 hours post-treatment and that Alisertib presence post-IR, rather than pre-IR, is required for this radiosensitising effect.

3.3.1. Targeting AURKA enhances radiation response in p53 wildtype NSCLC cells

Alisertib only radiosensitised p53 wildtype NSCLC cells *in vitro* in line with the findings of Myers *et al* (2013) with the exception of the H520 cell line which was radiosensitised despite absence of detectable p53 protein in our hands. This may be due to the H520 cell line being hypersensitive to Alisertib monotherapy, with an LD50 value nearly 50% lower compared to the other NSCLC cell lines. Depletion of p53 in the H460 model provided further evidence that targeting AURKA radiosensitised NSCLC cells with a p53 proficient background only. This is an important finding as

p53 aberration is common in NSCLC, between 23% and 73% of tumours harbour p53 mutations (Takahashi *et al.* 1989; Kishimoto *et al.* 1992; Miller *et al.* 1992; Sugimachi *et al.* 1995; Liloglou *et al.* 1997; Mitsudomi *et al.* 2000), and potentially limits the patient population that could benefit from Alisertib IR combination. In contrast, we did not find a significant difference between HCT116 p53 +/+ and HCT116 p53 -/- isogenic cell line response to Alisertib IR combination *in vitro*, with evidence of radiosensitisation in both backgrounds. Our data contradict the findings of Tao *et al* (2007) and Lin *et al* (2014) in colorectal carcinoma and hepatocellular carcinoma who found that targeting AURKA in combination with IR radiosensitised cells with p53 deficient backgrounds more potently than p53 proficient backgrounds *in vitro*. This challenges the pan-cancer mechanism of AURKA inhibitor IR combination, but does not retract from its potential utility. Neither of these studies used Alisertib. Alisertib is 27 times more potent at inhibiting AURKA T288 phosphorylation than PHA-680632 and is 200-fold more specific to AURKA than AURKB, whilst PHA-680632 is only 4.44-fold more specific to AURKA than AURKB (Soncini *et al.* 2006; Manfredi *et al.* 2011). Additionally, VE-465 used by Lin *et al* (2014) is only 30-fold more specific to AURKA than AURKB (Harrington *et al.* 2004). Therefore, mechanistic differences could arise when using Alisertib vs PHA-680632 or VE-465 due to the specificity of the inhibitor. These differences in response in to Alisertib IR combination may also be affected by the genotypic tendencies of the cancer types investigated in Tao *et al* (2007) and Lin *et al* (2014). Additionally, the HCT116 isogenic cell line is microsatellite unstable (Parsons *et al.* 1993), and hence is subject to genomic instability, which may account for differences between our and other published findings using this model. The H1299 H24 cell line, which expresses wildtype p53 protein under a Tetracycline controlled promotor (Chen *et al.* 1996),

would be useful here to test the p53-dependency of Alisertib IR combination in a NSCLC background.

Classically radiosensitising agents should have little or no cytotoxic activity alone whilst enhancing radiation response, however it is now accepted that radiosensitising agents could have either additive or synergistic interactions with radiation provided that the on-target anti-tumour effects outweigh the cost of any additional normal tissue toxicity (Seiwert *et al.* 2007). We propose that because the survival curves of cell lines treated with the Alisertib IR combination were normalised to Alisertib toxicity alone that statistical reductions in survival fraction are at the least additive and indicate radiosensitisation occurred. Isobologram analysis as described by Steel and Peckham could be used to further determine the level of interaction seen between Alisertib and IR (Steel and Peckham 1979).

3.3.2. Alisertib IR combination causes an accumulation of AURKA that is depleted of T288 phosphorylation

Interestingly, we saw that T288 p-AURKA expression levels were increased 24 hours post-irradiation, after initial loss at 4 hours, but were abolished in the presence of Alisertib suggesting that activation of AURKA may be involved in the survival response to IR. AURKA protein levels were significantly increased in Alisertib IR combination but not after irradiation alone, in contrast to previous research which has indicated that AURKA expression, at both mRNA and protein level, increases following IR in NSCLC cells (Woo *et al.* 2015). This may be explained by the use of different NSCLC cell lines and 10 Gy and 20 Gy doses to assess AURKA expression post-IR (Woo *et al.* 2015). We hypothesise that increases in inactive AURKA expression in H460 cells 24 hours post-treatment with Alisertib IR combination could

be due to disrupted cell cycle distribution or altered turnover of AURKA. AURKA expression is greatest during G2/M phases (Bischoff *et al.* 1998), and could therefore be affected by the relative cell cycle distributions 24 hours post-treatment with Alisertib IR combination. Although we did not find similar, there is evidence that Alisertib causes reflexive increases in AURKA expression (Felgenhauer *et al.* 2018), providing evidence against disruption of AURKA protein turnover. AURKA has been shown to enhance the invasiveness of hepatocellular carcinoma cells *in vitro* post-irradiation through epithelial-mesenchymal transition phenotype in a PI3K/AKT dependent manner (Chen *et al.* 2017). Interestingly, this effect was through phosphorylation of AKT, suggesting that AURKA-driven phenotype change post-IR was kinase activity dependent and thus implicates T288 p-AURKA expression in cancer response to IR (Chen *et al.* 2017). Given that T288 p-AURKA expression generally occurs during mitosis (Marumoto *et al.* 2002), this finding could also indicate a recommitment to cell cycle progression following DNA damage.

3.3.3. Alisertib IR combinational effect is time-dependent

Here we present findings that show the timing of Alisertib treatment, relative to irradiation, is important for radiosensitisation. We find that regardless of pre-treatment radiosensitisation only occurs when Alisertib is in the media post-IR. This implicates cellular recovery phase post-IR. However, given that addition of Alisertib 24 hours post-IR radiosensitises H460 cells suggests that the immediate repair phase post-IR is not involved. The majority of IR-induced DNA damage is repaired within 24 hours depending on dose (Redon *et al.* 2009), suggesting that Alisertib-mediated radiosensitisation was not through inhibition of DNA repair, contrary to links between AURKA function and DNA repair (Sourisseau *et al.* 2010; Sun *et al.* 2014; Wang *et al.* 2014a). In addition, Alisertib pre-treatment in the absence of

continued Alisertib treatment post-IR did not radiosensitise H460 cells. This suggests that Alisertib, which has previously been shown to cause mitotic accumulation in cell populations (Manfredi *et al.* 2011), did not enhance IR response by arresting cells in canonically the most radiosensitive phase of the cell cycle. Indeed, given that Alisertib mediated radiosensitisation occurs when dosing 24 hours post-irradiation the radiosensitisng mechanism is likely due to a delayed effect. This potentially implicates altered cell cycle and cell death responses, which may manifest after several aberrant cell divisions (Vitale *et al.* 2011).

3.3.4. Limitations

2D cell culture was used to test the efficacy of Alisertib IR combination in NSCLC cell lines and is advantageous as it is relatively inexpensive compared to *in vivo* models and lends itself to high throughput approaches. But there are limitations to this approach as 2D cell culture does not accurately recapitulate the tumour microenvironment. For example, 2D cell culture does not, without specialist equipment, mimic intra-tumour hypoxia, which is an established negative predictor of radiation response in NSCLC (Li *et al.* 2006). The effect of hypoxia on Alisertib IR combinational efficacy *in vitro* warrants further investigation.

Whilst care has been taken to optimise the dose of Alisertib to provide the maximal amount of on-target effect on T288 p-AURKA with least amount of off-target effect on T232 p-AURKB during radiation, there is evidence of T232 p-AURKB inhibition using 25 nM Alisertib in NSCLC cell lines. Because evidence suggests that AURKB is a radiosensitisation target in its own right (Niermann *et al.* 2011; Woo *et al.* 2015) it is possible that radiosensitisation effect by Alisertib is through off-target AURKA-independent mechanism. It would be interesting to examine if higher concentrations

of Alisertib became more off-target through AURKB inhibition and if this correlated with the degree of radiosensitisation seen.

We used siRNA and the HCT116 stable p53 +/+ p53 -/- isogenic systems to investigate differential p53 expression effects within the same genetic model. These models however only account for changes in wildtype p53 expression or null expression. p53 mutations are common in NSCLC (Miller *et al.* 1992; Sugimachi *et al.* 1995; Liloglou *et al.* 1997; Mitsudomi *et al.* 2000). Additionally, NSCLC samples display frequent overexpression of p53 (Mitsudomi *et al.* 2000) which is suggestive of oncogenic gain of function mutation in p53 (Yue *et al.* 2017). Gain of function p53 mutations have been shown to have biologically distinct effects on cellular phenotype compared to a p53 null background (Olive *et al.* 2004) including radiation response (Li *et al.* 1998). Therefore, using wildtype p53 depletion and p53 null backgrounds in NSCLC oversimplify p53 biology and do not account for a role of p53 gain of function mutation affecting Alisertib IR combination in NSCLC cells. It would be interesting to observe the effect of p53 mutation on Alisertib IR combinational efficacy in NSCLC.

Additionally, assessment of Alisertib IR combination effect on AURKA expression and T288 p-AURKA expression was performed in the H460 cell line only. The significance of these changes in expression following Alisertib IR combination need assessing in more cell lines that do and do not respond to Alisertib IR combinational effect.

4. Evaluation of Alisertib radiosensitising mechanism *in vitro*

4.1. Introduction, aims and hypotheses

Understanding the mechanism by which Alisertib enhances IR response in NSCLC is important. The radiosensitising mechanism may allude to biological markers of Alisertib IR combination efficacy which affect the target patient population and/or can be used as endpoints for *in vitro, in vivo* and clinical studies. This second results chapter will address the biological mechanism for radiosensitisation by Alisertib treatment in NSCLC, using the H460 cells as a model cell line that responded to the treatment combination. In addition, comparison with other NSCLC cell lines will be made to examine the dependency on p53 seen in chapter 3.

The aims of this chapter are to assess the following in NSCLC cell line models *in vitro*:

1. The effect of Alisertib IR combination on cell cycle progression in p53 proficient and p53 deficient NSCLC cell lines
2. The effect of Alisertib IR combination on mitotic phenotype and mitotic progression
3. The effect of Alisertib IR combination on mitotic catastrophe and associated cell death and senescence
4. The effect of Alisertib IR combination on p53 expression and post-translational modifications
5. The effect of Alisertib IR combination on DNA repair, cell cycle arrest and cell death machinery

The hypotheses of this chapter are:

- Cell cycle progression will be affected by Alisertib IR combination leading to increased cell death
- Alisertib IR combination will increase mitotic aberrance in NSCLC cells leading to increased cell death
- Alisertib IR combination will affect DNA repair in NSCLC cell lines leading to increased cell death

4.2. Results

4.2.1. Cell cycle progression is altered in H460 cells treated with Alisertib IR combination

Given that AURKA is important in promoting progression into (Hirota *et al.* 2003), and through (Rong *et al.* 2007) mitosis, and that we observe radiosensitisation of NSCLC cells by Alisertib can occur through a delayed effect, we hypothesised that the mechanism of Alisertib IR combinational effect was through altered cell cycle progression following irradiation. AURKA inhibition with Alisertib has been shown previously to promote G2/M arrest in models of cancer *in vitro* (Görgün *et al.* 2010; Sehdev *et al.* 2013). IR can also perturb cell cycle distribution with DNA damage checkpoints acting in G1, intra-S and G2/M depending on the intactness of cellular checkpoint machinery (Morgan and Lawrence 2015). Lin et al (2014) demonstrated that AURKA inhibition and IR cooperated to reduce the G1 population in hepatocellular carcinoma cell lines in combination with a G2/M arrest. Tao et al (2007) also demonstrated cooperative increases in G2/M populations and noted a reduction in the polyploid cell fraction in PHA680632 IR combination when compared to PHA680632 or IR treatment alone. These data provide evidence of cooperative

changes in cell cycle distribution when co-targeting AURKA with IR. Here we used propidium iodide (PI) staining in combination with p-Histone 3 (S10) to determine the cell cycle profiles of the NSCLC cell line panel following treatment with Alisertib, irradiation or combination. We acknowledge that AURKB has been shown to phosphorylate Histone 3 on serine 10 at the start of mitosis (Baek 2011) and that use of this mitotic marker may be confounded by off-target effects of Alisertib treatment. However, expression of p-Histone 3 at S10 was relatively unaffected by 25 nM Alisertib treatment in our hands in all cell lines via western blot and can occur in the presence of only basal AURKB activity (Le *et al.* 2013). Furthermore, S10 phosphorylation of Histone 3 is required for mitotic entry, still proceeds in the presence of AURKB inhibition, and is performed by other proteins (Keen and Taylor 2009; Baek 2011). Firstly, we investigated cell cycle distribution of the p53 proficient H460 cell line which showed enhancement of radiation response after 25 nM Alisertib + IR combination.

We found that the H460 cell line 24 hours post-irradiation displayed a statistically significant increase in the G1 population in the 4 Gy treatment condition when compared to untreated control, this was not seen in the combination treatment condition which was not different from control or Alisertib alone (see Figure 4.1 A & C). By 72 hours post-irradiation the G1 population in IR treated condition had returned to untreated levels whilst Alisertib alone and Alisertib IR combination had caused significant reduction in G1 population compared to untreated control (see Figure 4.1 A & E). There was a consistent reduction in S phase fraction of H460 cells in all treatment conditions relative to control across all timepoints (see Figure 4.1 A & C-E). This was most apparent in IR alone or in Alisertib IR conditions, but there was no significant difference between either condition. Compared to untreated controls

there was a non-significant trend for an increased G2 fraction in the 25 nM Alisertib condition at 24, 48 and 72 hours post-irradiation. This was also true in the Alisertib IR combination at 24 and 48 hours post-irradiation, but not at 72 hours. Alisertib alone or Alisertib IR combination caused significant increase in mitotic fraction 24 hours post-irradiation when compared to untreated control (see Figure 4.1 A-C). However, in contrast to the increased mitotic population of Alisertib alone, the mitotic population in the Alisertib IR combination was lost by 48 and 72 hours post-irradiation, mimicking IR alone (see Figure 4.1 A-E). There was statistically increased polyploid H460 population by 48 hours post-irradiation in all treatment conditions and in IR and Alisertib IR combination 72 hours post-irradiation, albeit reduced compared to 48 hour timepoint. Consistent with survival data, a sharp statistically significant increase in H460 sub G1 population was observed in all treatment conditions compared to control by 72 hours post-irradiation with greatest increase seen in the combination treatment condition.

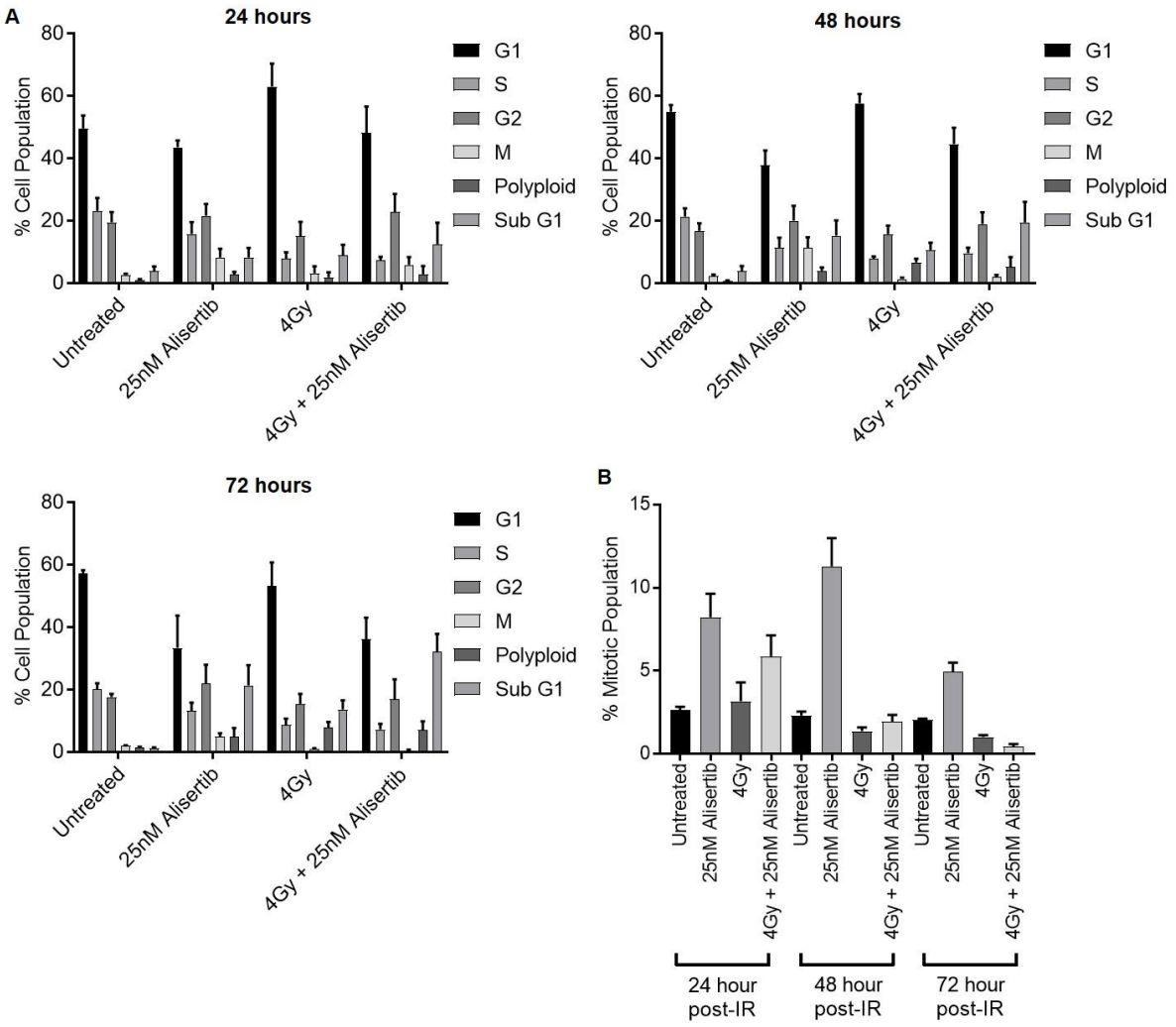

Figure 4.1. **H460 cell cycle distribution 24, 48 and 72 hours following treatment with 25 nM Alisertib, 4 Gy or combination.** Legend on page 147.

C

24 hours	G1				S			
	Untreated	25 nM Alisertib	4 Gy	4 Gy + 25 nM Alisertib	Untreated	25 nM Alisertib	4 Gy	4 Gy + 25 nM Alisertib
Untreated		0.890	0.043	>0.999		0.024	<0.0001	<0.0001
25 nM Alisertib				>0.999				0.010
4 Gy				0.023				>0.999
	G2				M			
	Untreated	25 nM Alisertib	4 Gy	4 Gy + 25 nM Alisertib	Untreated	25 nM Alisertib	4 Gy	4 Gy + 25 nM Alisertib
Untreated		>0.999	0.903	>0.999		0.019	>0.999	0.303
25 nM Alisertib				>0.999				0.779
4 Gy				0.153				0.552
	Polyploid				Sub G1			
	Untreated	25 nM Alisertib	4 Gy	4 Gy + 25 nM Alisertib	Untreated	25 nM Alisertib	4 Gy	4 Gy + 25 nM Alisertib
Untreated		0.865	>0.999	0.705		0.862	0.567	0.065
25 nM Alisertib				>0.999				0.852
4 Gy				>0.999				>0.999

D

48 hours	G1				S			
	Untreated	25 nM Alisertib	4 Gy	4 Gy + 25 nM Alisertib	Untreated	25 nM Alisertib	4 Gy	4 Gy + 25 nM Alisertib
Untreated		>0.999	>0.999	>0.999		0.0008	0.0001	0.0004
25 nM Alisertib				>0.999				>0.999
4 Gy				>0.999				>0.999
	G2				M			
	Untreated	25 nM Alisertib	4 Gy	4 Gy + 25 nM Alisertib	Untreated	25 nM Alisertib	4 Gy	4 Gy + 25 nM Alisertib
Untreated		>0.999	>0.999	>0.999		0.0003	>0.999	>0.999
25 nM Alisertib				>0.999				0.0004
4 Gy				>0.999				>0.999
	Polyploid				Sub G1			
	Untreated	25 nM Alisertib	4 Gy	4 Gy + 25 nM Alisertib	Untreated	25 nM Alisertib	4 Gy	4 Gy + 25 nM Alisertib
Untreated		0.088	0.004	0.022		0.017	0.312	0.004
25 nM Alisertib				>0.999				>0.999
4 Gy				>0.999				0.145

Figure 4.1. **H460 cell cycle distribution 24, 48 and 72 hours following treatment with 25 nM Alisertib, 4 Gy or combination.** Legend on page 147.

E

72 hours	G1				S			
	Untreated	25 nM Alisertib	4 Gy	4 Gy + 25 nM Alisertib	Untreated	25 nM Alisertib	4 Gy	4 Gy + 25 nM Alisertib
Untreated		0.009	>0.999	0.020		0.007	0.0001	<0.0001
25 nM Alisertib				>0.999				0.010
4 Gy				0.045				>0.999
	G2				M			
	Untreated	25 nM Alisertib	4 Gy	4 Gy + 25 nM Alisertib	Untreated	25 nM Alisertib	4 Gy	4 Gy + 25 nM Alisertib
Untreated		>0.999	>0.999	>0.999		0.0004	0.225	0.025
25 nM Alisertib				0.880				<0.0001
4 Gy				>0.999				>0.999
	Polyploid				Sub G1			
	Untreated	25 nM Alisertib	4 Gy	4 Gy + 25 nM Alisertib	Untreated	25 nM Alisertib	4 Gy	4 Gy + 25 nM Alisertib
Untreated		0.408	0.021	0.043		0.0009	0.030	<0.0001
25 nM Alisertib				0.976				0.042
4 Gy				>0.999				0.0009

Figure 4.1. **H460 cell cycle distribution 24, 48 and 72 hours following treatment with 25 nM Alisertib, 4 Gy or combination.** Legend overleaf.

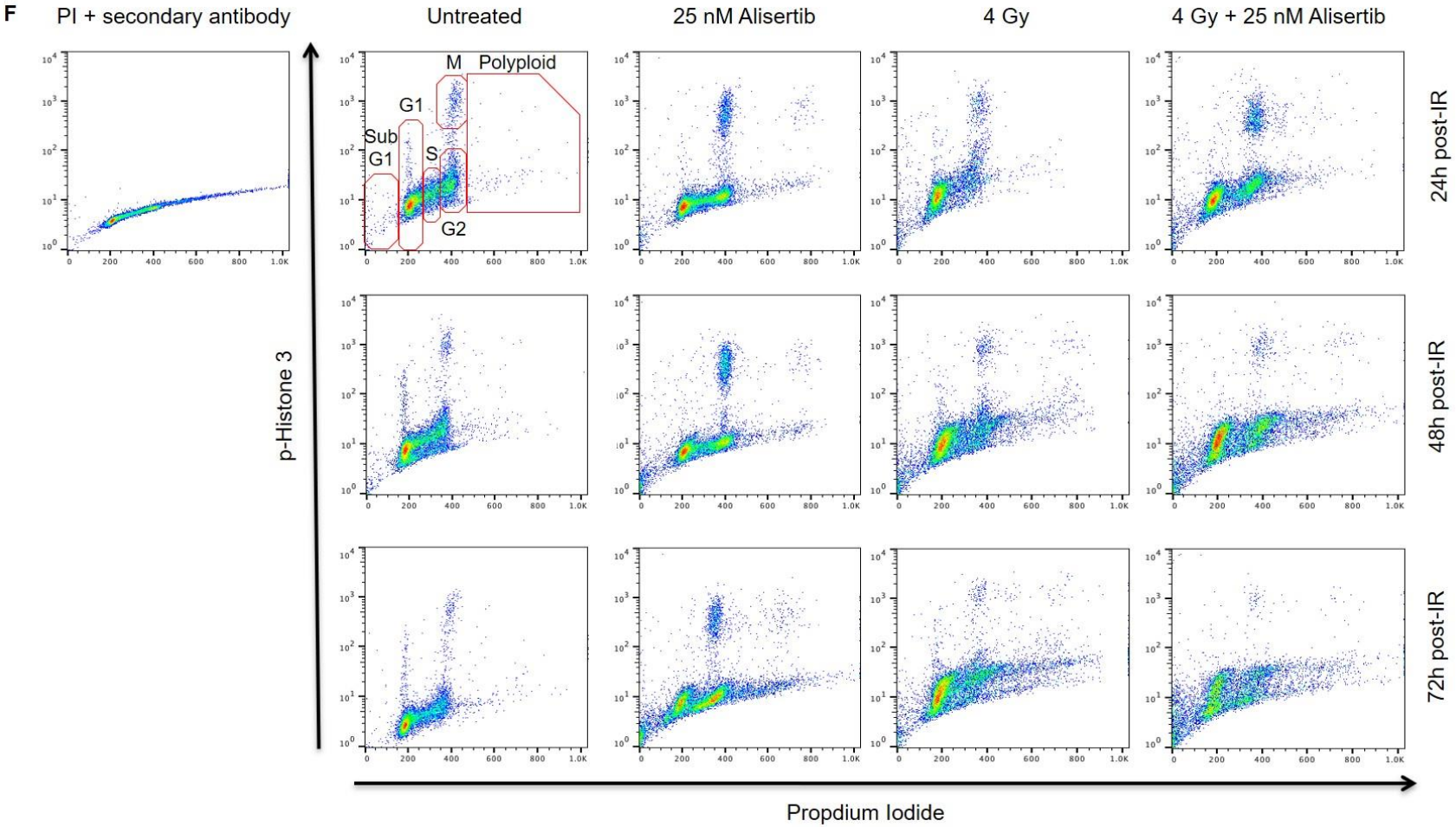

Figure 4.1. **H460 cell cycle distribution 24, 48 and 72 hours following treatment with 25 nM Alisertib, 4 Gy or combination. A.** Mean cell cycle phase distribution 24, 48 and 72 hours post-irradiation. **B.** Mean mitotic distribution 24, 48 and 72 hours post-irradiation re-represented on a different scale for clarity. Data points represent mean cell cycle phase distribution +/- SEM (N= ≥2). Table of p-values from One-way ANOVA tests of cell cycle phase data at **C.** 24 hours, **D.** 48 hours and **E.** 72 hours (bottom) post-irradiation. ANOVA performed with Bonferroni correction for multiple comparisons. **F.** Representative H460 FACS plots for propidium iodide (PI) staining vs p-Histone 3 staining 24, 48 and 72 hours post-irradiation. Gating examples given in red on untreated plot at 24 hour timepoint. Minimum of 10,000 single cell events collected in population isolated through (PI (FL-3) width vs PI (FL-3) height). Mitotic population defined through p-Histone 3 positivity.

These data suggest that Alisertib IR combination altered cell cycle distribution in H460 cells after treatment. At 24 hours Alisertib IR combination inhibited the IR-induced G1 arrest seen in IR alone, instead a mitotic arrest similar to Alisertib alone was induced. However, by 48-72 hours this mitotic arrest was lost in combination therapy and was associated with an increase in sub G1 fraction and reduction in G1 and S phase cells. Furthermore, increases in polyploid population in 25 nM Alisertib, 4 Gy and 4 Gy + 25 nM Alisertib conditions over successive days suggested that the mitotic process was aberrant resulting in > 4N genetic content. Taken together, these data suggest that Alisertib IR combination treated cells were dying from mitotic aberrance.

4.2.2. Live cell imaging reveals that H460 cells are more likely to undergo intra-mitotic death, show increased amount of aberrant mitoses and show trend to spend longer time in mitosis 24 hours post-treatment with Alisertib IR combination

From the data above to help elucidate the consequences of the altered mitotic process in H460 cells treated with Alisertib IR combination, we hypothesised that the effect could be explained by two hypotheses that aren't necessarily mutually exclusive:

- H460 cells die during aberrant mitosis and do not hit the subsequent G1 phase of the following cell cycle
- H460 cells perform aberrant mitosis, undergoing either successful cytokinesis or mitotic slippage processes, before cell death is triggered upon subsequent re-entry to the following cell cycle (G1).

We tested this hypothesis by following mitoses via live cell imaging 24-36 hours and 48-60 hours post-treatment with 25 nM Alisertib, 2 Gy, 4 Gy, 2 Gy + 25 nM Alisertib and 4 Gy + 25 nM Alisertib combinations. Using phase-contrast microscopy mitotic progression was scored, recording percentage of death during mitosis and time spent during mitosis. Additionally, when >2 daughter cells arose, likely during multipolar mitosis, these cells were scored as having undergone “aberrant mitosis”.

Before testing this hypothesis, we adopted an altered approach as live cell imaging of multiple parallel conditions needed performing in a multiple well format. This was important because in the 6 well format we could not differentially sham irradiate and irradiate specific wells, and therefore here we had to plate cells immediately after irradiation rather than plating before which as an approach was used in all other cell line experiments. When H460 cells were re-plated after irradiation we found that 25 nM Alisertib enhanced radiation response with a mean DER at 10% survival fraction of 1.33 (see Figure 4.2 B). The extra sum of squares revealed that the survival curves for irradiation alone compared to Alisertib irradiation combination in H460 cells plated after irradiation were best described by a different curve for each dataset ($p = <0.0001$). This was similar to the mean DER at 10% survival fraction of 1.31 seen in H460 cells plated before irradiation in combination with 25 nM Alisertib (see Figure 4.2 A) and there was no statistical difference between the H460 mean DER at 10% survival fraction between plating methods ($p = 0.807$ (Student’s two-tailed unpaired t-test)). This indicated that despite altered plating method this approach for live cell imaging would be comparable to the other functional cell line data in this thesis.

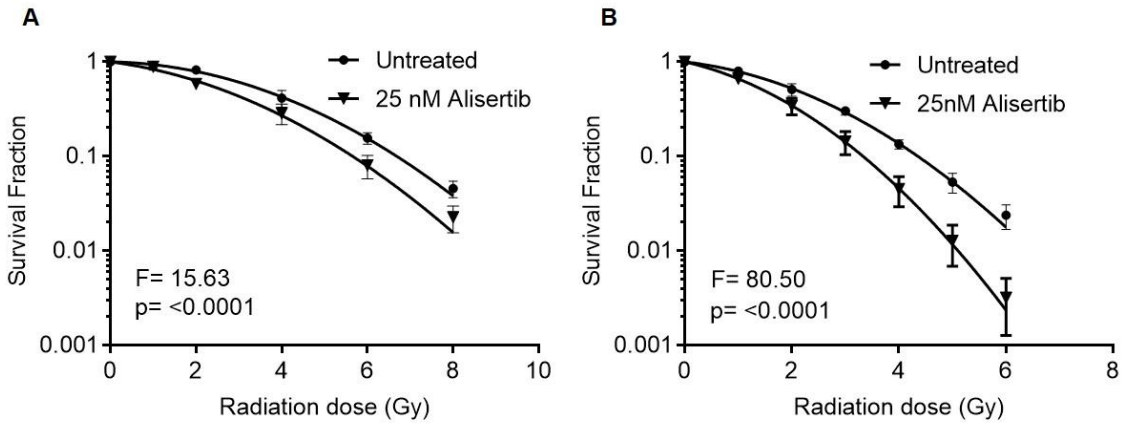

Figure 4.2**. Survival fraction of A. H460 cells plated prior to IR and B. H460 cells plated after IR when treated with IR alone or IR in combination with 25 nM Alisertib.** Data points represent mean survival fraction normalised to unirradiated control +/- SD (N= ≥3). F-value and p-value derived from extra sum of squares test. Survival fraction after +/- IR +/- 25 nM Alisertib when plating prior to IR is re-represented for comparative purposes.

The Shapiro-Wilk test was used accordingly to detect non-normal data distributions and the One-way ANOVA or Kruskal-Wallis tests were used to compare means where appropriate. During live cell imaging there was a trend for increased mean length of mitosis to the point of apparent completion of cytokinesis or death 24-36 hours post-irradiation in all conditions compared to untreated control, but this was only statistically significant in the 2 Gy + 25 nM Alisertib and 4 Gy + 25 nM Alisertib conditions (p= 0.0138 and p= 0.0002 (One-way ANOVA)) (see Figure 4.3 A). There was a greater than additive effect in the 4 Gy + 25 nM Alisertib condition compared to the mean time spent in mitosis in either 25 nM Alisertib or 4 Gy alone (p= 0.011 and p= 0.005 respectively). There was also a trend for H460 cells to spend longer in mitosis until end of cytokinesis or death 48-60 hours post-treatment in all treatment conditions when compared to untreated control, but there was no evidence of

additivity as Alisertib IR combinations mirrored the effect of Alisertib at this timepoint (see Figure 4.4 A).

Similarly, when only scoring mitoses that completed in successful cytokinesis there was a similar trend for increased mean time in mitosis in all treatment conditions 24-36 hours post-irradiation compared to untreated control, but this was only statistically significant in 4 Gy + 25 nM Alisertib condition ($p= 0.0163$ (One-way ANOVA)) (see Figure 4.3 B). There was a greater than additive effect in the 4 Gy + 25 nM Alisertib condition, but this was not statistically different from the mean time in mitosis in either 25 nM Alisertib or 4 Gy alone conditions ($p= 0.164$ and $p= 0.073$ (One-way ANOVA)). At 48-60 hours post-treatment there was a trend for H460 cells to spend longer in mitosis in all treatment conditions when compared to untreated control, but there was no evidence of additivity as Alisertib IR combinations mirrored the effect of Alisertib at this timepoint (see Figure 4.4 B).

There was also an IR dose-dependent increase in mean intra-mitotic death as a percentage of total mitoses in the H460 cells 24-36 hours post-irradiation that was statistically significant in the 2 Gy + 25 nM Alisertib and 4 Gy + 25 nM Alisertib conditions ($p= 0.0110$ and $p= <0.0001$ (One-way ANOVA)) (see Figure 4.3 C). This was a greater than additive effect in the 4 Gy + 25 nM Alisertib condition and was statistically significant from the levels of mean intra-mitotic death in either 25 nM Alisertib or 4 Gy alone ($p= 0.0023$ and $p= 0.0003$ (One-way ANOVA)). At 48-60 hours rates of intra-mitotic death also increased in all treatment conditions when compared to untreated control, but there was no evidence of additivity as Alisertib IR combinations mirrored the effect of Alisertib at this timepoint (see Figure 4.4 C).

The mean fraction of aberrant mitoses (> 2 daughters) as a proportion of all mitoses in the H460 cells 24-36 hours post-irradiation in all treated conditions was increased compared to control but was only statistically significant in the 2 Gy + 25 nM Alisertib and 4 Gy + 25 nM Alisertib conditions ($p= 0.0169$ and $p= 0.0005$ respectively (One-way ANOVA)) (see Figure 4.3 D). There was a greater than additive effect in the 4 Gy + 25 nM Alisertib condition and this increase in fraction aberrant mitoses was statistically significant when compared to 25 nM Alisertib alone condition ($p= 0.006$) but not when compared to 4 Gy ($p= 0.060$ (One-way ANOVA)). We also observed that there were increased levels of aberrant mitoses as a fraction of total mitoses in the H460 cells 48-60 hours post-irradiation in all treated conditions when compared to untreated control, but this was only statistically significant in the 25 nM Alisertib alone 2 Gy + 25 nM Alisertib and 4 Gy + 25 nM Alisertib conditions ($p= 0.0082$, $p= 0.0024$ and $p= <0.0001$ (One-way ANOVA)) (see Figure 4.4 D). There was a trend for less than additive increases in mean percentage of aberrant mitoses in both 2 Gy + 25 nM Alisertib and 4 Gy + 25 nM Alisertib conditions, but neither showed any statistical difference to the mean percentage of aberrant mitoses in 25 nM Alisertib alone ($p= >0.999$ and $p= 0.285$).

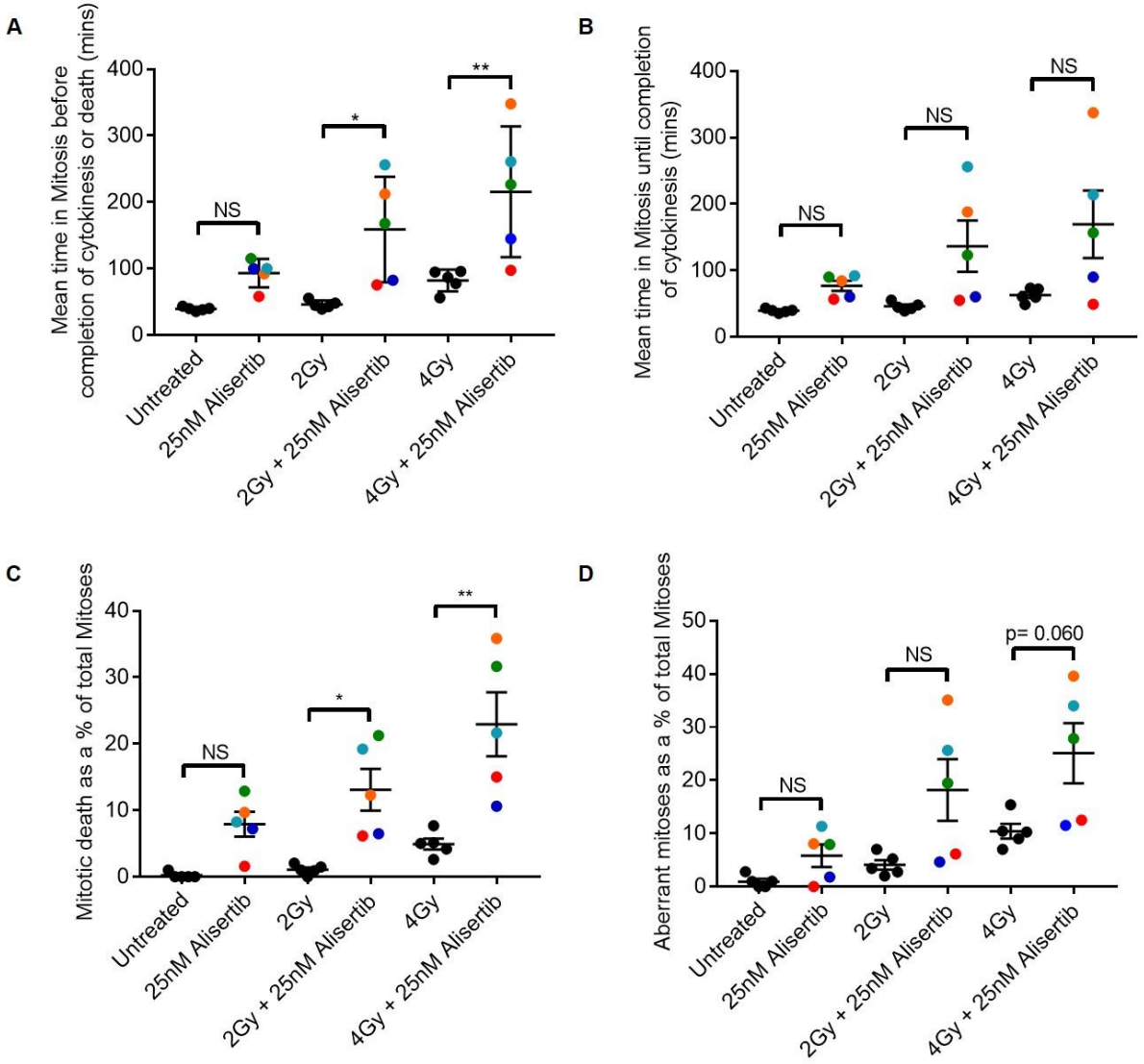

Figure 4.3. **H460 live cell analysis 24-36 hours post-irradiation. A.** Time in mitosis resulting in cytokinesis or death. **B.** Time in mitosis resulting in cytokinesis **C.** Proportion of intra-mitotic death and **D.** Aberrant mitosis resulting in >2 daughter cells. Minimum 50 mitotic cells counted per condition. Data points represent mean proportion of mitotic cells with described outcome +/- SEM (N= 5). Data point colouration represents each independent experiment. NS (non-statistically significant) denotes p= >0.05, * denotes p= ≤0.05, ** denotes p= ≤0.01, *** denotes p= ≤0.001 (One-way ANOVA with Bonferroni correction for multiple comparisons).

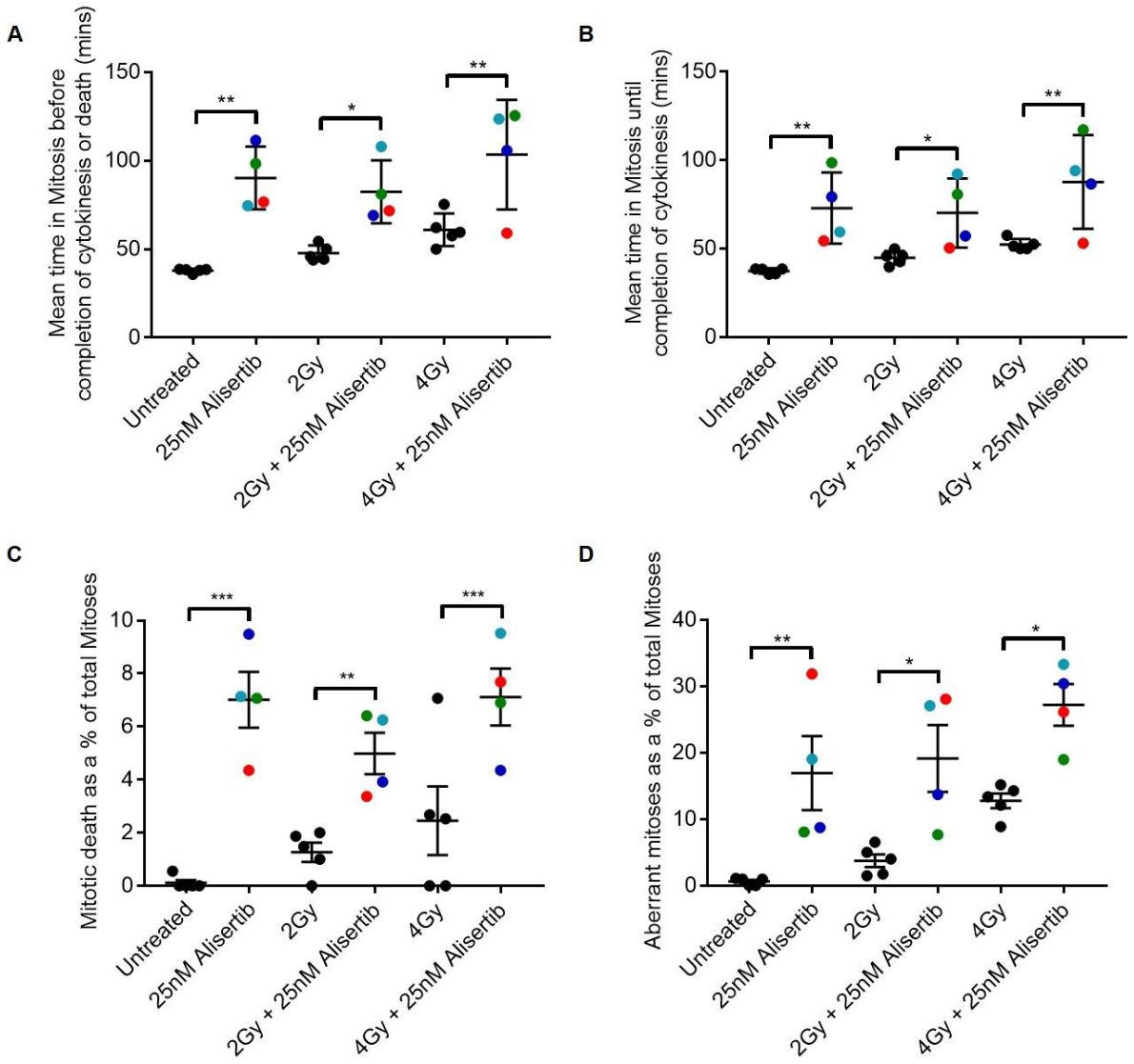

Figure 4.4. **H460 live cell analysis 48-60 hours post-irradiation. A.** Time in mitosis resulting in cytokinesis or death. **B.** Time in mitosis resulting in cytokinesis **C.** Proportion of intra-mitotic death and **D.** Aberrant mitosis resulting in >2 daughter cells. Minimum 50 mitotic cells counted per condition. Data points represent mean proportion of mitotic cells with described outcome +/- SEM (N= 5). Data point colouration represents each independent experiment. NS (non-statistically significant) denotes p= >0.05, * denotes p= ≤0.05, ** denotes p= ≤0.01, *** denotes p= ≤0.001 (Kruskal-Wallis test with Dunn correction multiple comparisons for A. and B. One-way ANOVA with Bonferroni correction for multiple comparisons for C and D).

These data suggest that 24-36 hours post-treatment there is cooperation between Alisertib and IR to slow mitotic progression and that mitosis results more often in

death or aberrant division of daughter cells in an IR dose-dependent manner. Here time in mitosis was increased in the H460 cell time after treatment with Alisertib IR combinations. This was skewed by cells that underwent intra-mitotic death as the effect sizes were reduced when these cells were excluded from the analysis. However, once death was accounted for there remained a non-significant trend for increased time in mitosis in H460 cells that completed cytokinesis implying that Alisertib IR combination was also perturbing mitotic progression. Through examination of variation between independent experiments there was a consistency in that experiments which yielded higher rates of intra-mitotic death in 25 nM Alisertib alone condition also yielded greater effect in Alisertib IR combination conditions. This was also true for proportion of aberrant mitoses and mean time in all mitoses and mean time in mitoses that lead to successful cytokinesis only. This is highlighted by the colouration of data points in Figures 4.3 and 4.4. This suggests that despite inter-experiment variation, the effects observed above 24-36 hours post-irradiation in Alisertib IR combination conditions were Alisertib dependent.

Together these data provide evidence to support the hypothesis that the Alisertib IR combination promotes intra-mitotic death in H460 cells. An increase in aberrant mitosis also provides a mechanism for the increase in polyploidisation that occurs in NSCLC cells after treatment with Alisertib IR combination. These data also suggest that Alisertib IR combination was having the most significant effect on the mitotic process 24-36 hours post-treatment as opposed to 48-60 hours post-treatment. By 48-60 hours post-treatment mean percentage of intra-mitotic death and time in mitosis was indistinguishable from 25 nM Alisertib alone condition, indicating that the cooperative process between Alisertib and IR is diminishing. However, these experiments did not provide adequate or equal cell follow-up periods post-mitosis

and therefore fail to address the hypothesis that polyploid H460 cells were dying via post-mitotic G1 checkpoint activation.

4.2.3. H460 cells exhibit altered mitotic phenotype 24 hours following treatment with Alisertib IR combination

4.2.3.1. H460 cells exhibit aberrant centrosomal phenotype 24 hours following treatment with Alisertib IR combination

Our cell cycle profiling and live cell imaging data indicated that the mitotic process was disrupted in H460 cells treated with Alisertib IR combination, but did not describe the phenotype of mitotic aberration. AURKA is involved in multiple aspects of mitotic regulation to ensure fidelity of the process, and we therefore stained cells with DAPI, β-tubulin and pericentrin to observe mitotic phenotypes. This was investigated in the H460 cell line 24 hours post-treatment as cell cycle profiling data above indicated that increases in polyploid population and mitotic elimination, used here as surrogate products of altered mitosis, were observable by 48 hours post-treatment.

Initial observations revealed obvious changes in centrosomal phenotype and resultant spindle formation. Therefore, we scored for two well documented aberrant centrosomal phenotypes known as centrosomal fragmentation and centrosomal amplification. Centrosomal fragmentation occurs when there is an overduplication of the pericentriolar mass in the absence of centriole duplication (Yabuta *et al.* 2013). Centrosomal amplification occurs when the pericentriolar mass is over duplicated with the centriole (Yabuta *et al.* 2013). Both centrosomal fragmentation and centrosomal amplification are considered aberrant centrosomal phenotypes and

have been shown to contribute to genomic or more specifically chromosomal instability (Yabuta *et al.* 2013).

24 hours post-irradiation the H460 cells treated with 25 nM Alisertib, 4 Gy or 4 Gy + 25 nM Alisertib exhibited increased proportion of mitotic cells with either pericentrin fragmentation or centrosomal amplification when compared to untreated control (p= 0.0146, p= 0.0199 and p= 0.0002 (One-way ANOVA)) (see Figure 4.5). The proportion of cells with either pericentrin fragmentation or centrosomal amplification was less than additive in the combinational treatment arm but was significantly increased when compared to the proportions seen for 25 nM Alisertib or 4 Gy alone conditions (p= 0.025 and p= 0.018 (One-way ANOVA)).

The proportion of H460 cells with pericentrin fragmentation alone increased significantly when treating with 25 nM Alisertib, 4 Gy or 4 Gy + 25 nM Alisertib when compared to untreated control (p= 0.0002, p= 0.0006 and p= 0.0001 (One-way ANOVA)) (see Figure 4.5). The effect of combining 25 nM Alisertib and 4 Gy on the proportion of pericentrin fragmentation positive H460 cells had no additive effect and was statistically non-significant when compared to either treatment alone (p= >0.999 and p= 0.486 (One-way ANOVA)).

There was a trend for the proportion of H460 cells with centrosomal amplification 24 hours post-irradiation to be increased in all treatment conditions when compared to untreated control, but this was only statistically significant in the combinational treatment arm (p= 0.007 (One-way ANOVA)) (see Figure 4.5). There was a greater than additive increase in the proportion of H460 cells with centrosomal amplification in the 4 Gy + 25 nM Alisertib combinational treatment arm and this was statistically different from the proportion of centrosomally amplified H460 cells seen when

treating with 4 Gy alone (p= 0.012), but not significant compared to 25 nM Alisertib alone (p= 0.066).

Considering the proportion of H460 cells that exhibited a dual phenotype of both pericentrin fragmentation and centrosomal amplification 24 hours post-irradiation, there was a trend for this proportion to be increased in all treatment conditions when compared to untreated control, but this was only statistically significant in the combinational treatment arm (p= 0.012 (One-way ANOVA)) (see Figure 4.5). There was a greater than additive increase in dual pericentrin fragmentation positive and centrosomally amplified H460 cells in the 4 Gy + 25 nM Alisertib condition but was however not statistically significant from the proportions of either 25 nM Alisertib or 4 Gy alone (p= 0.071 and p= 0.245 (One-way ANOVA)).

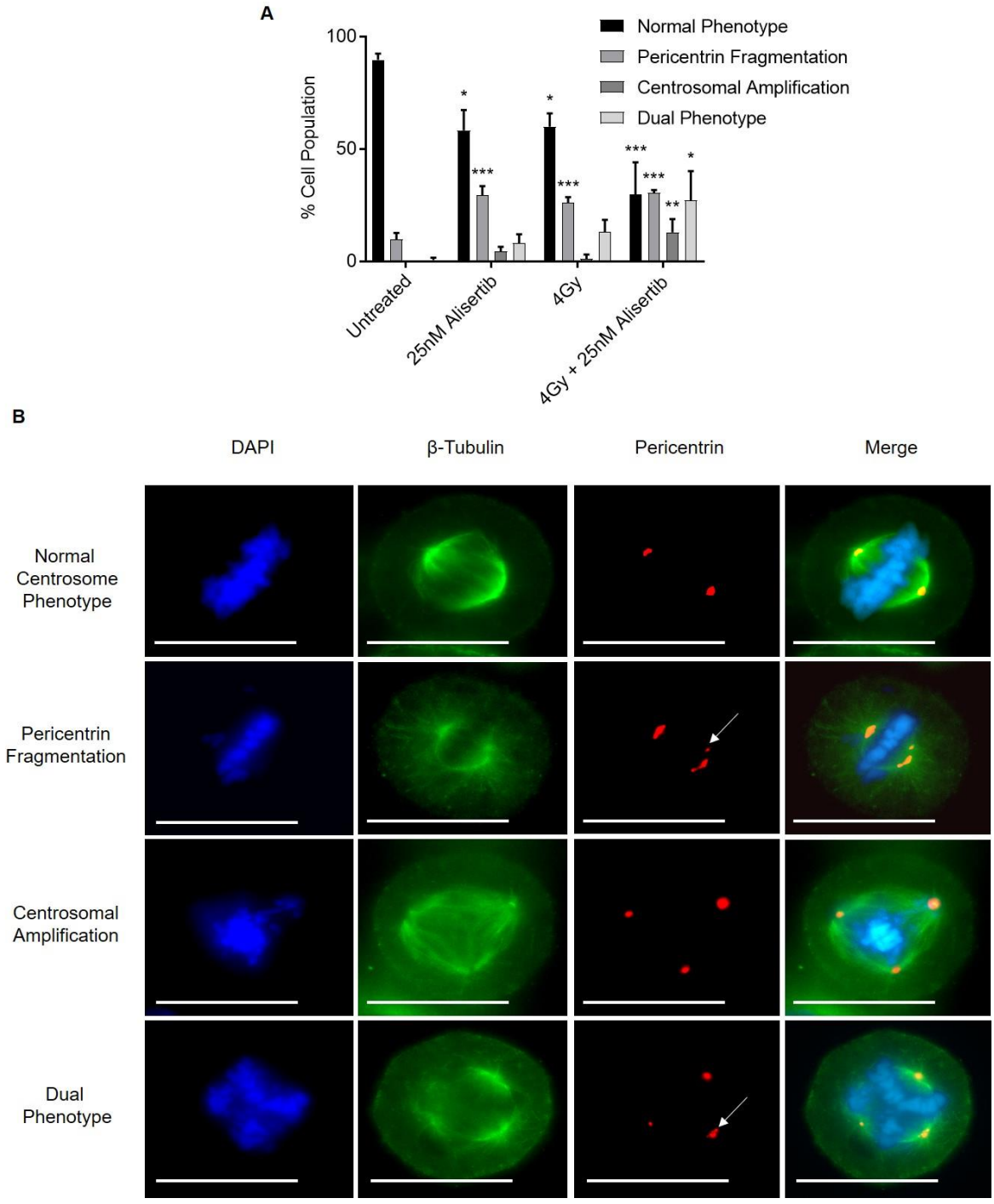

Figure 4.5. **Centrosomal phenotypes in mitotic H460 cells 24 hours post-irradiation. A.** Proportion of mitotic H460 cells with normal centrosomal phenotype, pericentrin fragmentation, centrosomal amplification or both. 30 mitotic cells counted per condition on each of three independent repeats. Data points represent mean proportion of mitotic cells exhibiting given phenotype +/- SEM (N=3) * denotes p= ≤0.05, ** denotes p= ≤0.01, *** denotes p= ≤0.001 compared to corresponding phenotype in untreated control (One-way ANOVA with Bonferroni correction for multiple comparisons). **B.** Representative images of H460 phenotypes scored for aberrant centrosomal phenotype 24 hours post-irradiation. Cells stained for DAPI (cyan), β-Tubulin (green) and pericentrin (red). 30 mitotic cells counted per condition. Imaged with a 60x microscope objective, scale bars represent 120 µm. Arrows indicate pericentrin fragmentation.

These data suggest that Alisertib and IR cooperate to increase the amount of centrosomal aberration seen in H460 cells and could, at least partially, explain why mitotic cell death and polyploidisation occurs following Alisertib IR combination treatment in NSCLC cells.

4.2.3.2. H460 cells exhibit altered mitotic phase distribution following treatment with Alisertib IR condition

There is evidence that progression through mitosis, or lack of it, can determine chemotherapy outcomes (Manfredi *et al.* 2011). Given this and the slowed mitotic progression and altered centrosomal biology we see exacerbated in Alisertib + IR condition, we hypothesised that H460 mitotic phase distribution may also be altered in cells treated with 25 nM Alisertib, 4 Gy and 4 Gy + Alisertib. Scoring of mitotic phase was done in line with previous publication (Zhu *et al.* 2005) 24 hours post-treatment.

When considering the fraction of H460 mitotic cells in prophase, we found there was a trend for reduction in the proportion of cells in prophase in all treated conditions compared to untreated control, but this was only statistically significant for the 4 Gy alone condition ($p= 0.019$ (One-way ANOVA)) (see Figure 4.6).

25 nM Alisertib caused a statistically significant increase in the prometaphase fraction ($p= 0.004$ (One-way ANOVA)), 4 Gy had no effect when compared to untreated control ($p= >0.9999$ (One-way ANOVA)), and the combinational treatment condition had an intermediate effect with modest increase in prometaphase fraction that was not statistically significant ($p= 0.757$ (One-way ANOVA)) (see Figure 4.6).

There was no significant change in the fraction of H460 mitotic cells in metaphase in either 25 nM Alisertib, 4 Gy or 4 Gy + 25 nM Alisertib treatment conditions when compared to untreated control (p= >0.9999, p= >0.9999 and p= >0.9999 (One-way ANOVA)) (see Figure 4.6).

There was a trend for increasing anaphase fraction of H460 mitotic cells in all treated conditions when compared to untreated control, but this increase was only statistically significant in the combinational treatment condition (p= >0.9999, p= 0.168 and p= 0.010 (One-way ANOVA)) (see Figure 4.6). The increase in anaphase fraction of mitotic cells in the combinational treatment condition was greater than additive in effect but the anaphase fraction seen was not statistically different from the anaphase fraction seen in 4 Gy alone condition (p= 0.763 (One-way ANOVA)).

There was a trend with for reduced telophase fraction of H460 mitotic cells 24 hours post-irradiation in the 4 Gy + 25 nM Alisertib condition compared to untreated control, but this was not statistically significant (p= 0.506 (One-way ANOVA), whilst there was no change in either 25 nM Alisertib or 4 Gy alone (see Figure 4.6).

Also, there was a reduction in the fraction of H460 mitotic cells undergoing cytokinesis 24 hours post-irradiation in all treated conditions compared to untreated control, but this was only statistically significant in the 25 nM Alisertib and 4 Gy + 25 nM Alisertib conditions (p= 0.002 and p= 0.001 (One-way ANOVA)) (see Figure 4.6).

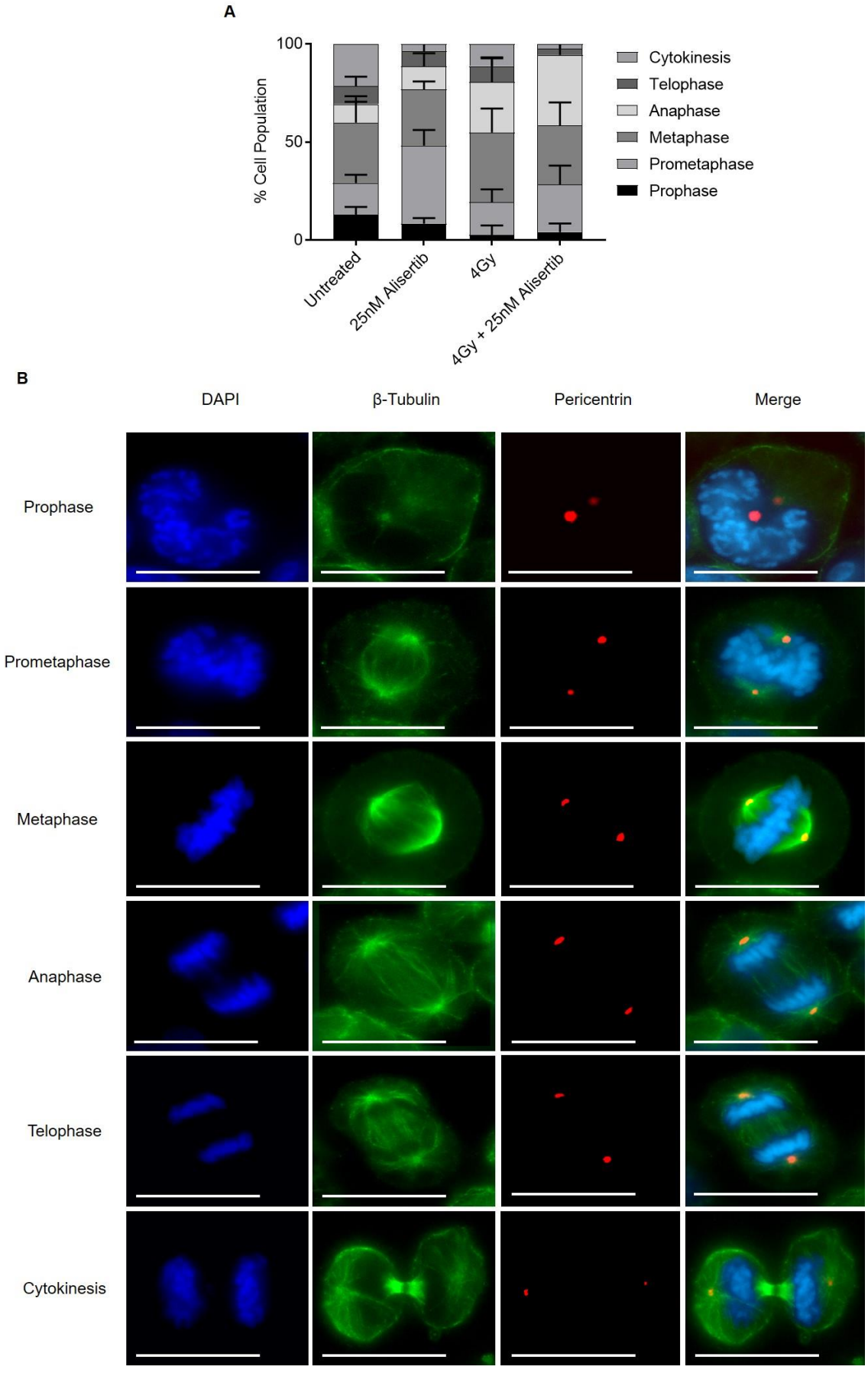

Figure 4.6. **Mitotic distribution of H460 cells 24 hours post-irradiation.** Legend overleaf

Figure 4.6. **Mitotic distribution of H460 cells 24 hours post-irradiation. A.** Mean mitotic phase distribution 24 hours post-irradiation. 30 mitotic cells counted per condition on each of four independent repeats. Data points represent mean proportion of mitotic cells in given phase +/- SEM (N=4), **B.** Representative images of mitotic H460 cells in prophase, prometaphase, metaphase, anaphase, telophase and cytokinesis. Cells stained for DAPI (cyan), β-Tubulin (green) and pericentrin (red). Imaged with a 60x microscope objective, scale bars represent 120 μm.

These data suggest that 24 hours post-treatment H460 cells treated with 25 nM Alisertib alone were more likely to accumulate in prometaphase. Conversely H460 cells treated with 4 Gy + 25 nM Alisertib were cooperatively accumulating in anaphase, with trends for reductions in the proportion of cells in telophase and undergoing cytokinesis. This implied that H460 mitotic progression was being differentially impeded following treatment with Alisertib IR combination.

4.2.4. H460 cells exhibit increased levels of markers of mitotic catastrophe and senescence 72 hours following treatment with Alisertib IR combination

4.2.4.1. H460 cells exhibit increased levels of markers of mitotic catastrophe 72 hours following treatment with Alisertib IR combination

Cell cycle profiling, live cell imaging and mitotic phenotyping data in H460 cells support the hypothesis that Alisertib IR combination may affect normal chromosomal segregation. Therefore, we hypothesised that Alisertib IR combination may increase the likelihood of mitotic catastrophe in NSCLC cells and that this may explain radiosensitising induced cell death. Firstly, we looked in a fixed H460 population 72 hours post-irradiation, providing an extended period for cells to undergo rounds of mitosis and thus accumulation of any divisional aberrations. Cells were stained for DAPI and β-tubulin to stain the DNA and cytoskeletal microtubules respectively.

Micronuclei (Cohen–Jonathan *et al.* 1999) and multinucleation (Ganem *et al.* 2007), as phenotypes, are both considered to be markers of aberrant chromosomal segregation and in turn mitotic catastrophe. Here in the H460 cell line we found that 25 nM Alisertib treatment, 4 Gy and 4 Gy + 25 nM Alisertib treatment all increased the proportion of cells bearing micronuclei or multiple nuclei from mean of 1.56% to 18.37%, 35.50% and 60.81% respectively ($p= 0.065$, $p= 0.001$ and $p= <0.0001$ (One-way ANOVA)) (see Figure 4.7). The proportion of cells bearing micronuclei or multiple nuclei in the combinational treatment arm had a greater than an additive effect between 25 nM Alisertib and 4 Gy and was statistically significant from either treatment alone respectively ($p= 0.0002$ and $p= 0.0069$ (One-way ANOVA)).

The proportion of micronuclei positive H460 cells, when compared to untreated control, increased significantly when treating with 25 nM Alisertib, 4 Gy or 4 Gy + 25 nM Alisertib ($p= 0.009$, $p= 0.002$ and $p= <0.0001$ respectively (One-way ANOVA)) (see Figure 4.7). The effect of combining 25 nM Alisertib and 4 Gy on the proportion of micronuclei positive H460 cells was approximately additive and statistically different from either treatment alone ($p= 0.001$ and $p= 0.004$ (One-way ANOVA)).

When considering the proportion of multinucleate H460 cells we found that this population increased when treated with 25 nM Alisertib, 4 Gy and 4 Gy + 25 nM when compared to untreated control but this was not statistically significant ($p= 0.515$, $p= 0.135$ and $p= 0.069$ respectively (One-way ANOVA)) (see Figure 4.7).

When considering the proportion of cells that exhibited a dual phenotype of both micronuclei positivity and multiple nuclei we found that this proportion was significantly increased when H460 cells were treated with 4 Gy or 4 Gy + 25 nM Alisertib when compared to untreated control ($p= 0.035$ and $p= 0.0004$ respectively

(One-way ANOVA)) (see Figure 4.7). There was a trend for an increase in dual phenotype proportion when treating with 25 nM Alisertib alone compared to untreated control (p= 0.7501 (One-way ANOVA)). There was a greater than additive increase in dual micronuclei positive H460 cells with multinucleation in the 4 Gy + 25 nM Alisertib condition when compared to 25 nM Alisertib and 4 Gy alone (p= 0.002 and p= 0.029 (One-way ANOVA)).

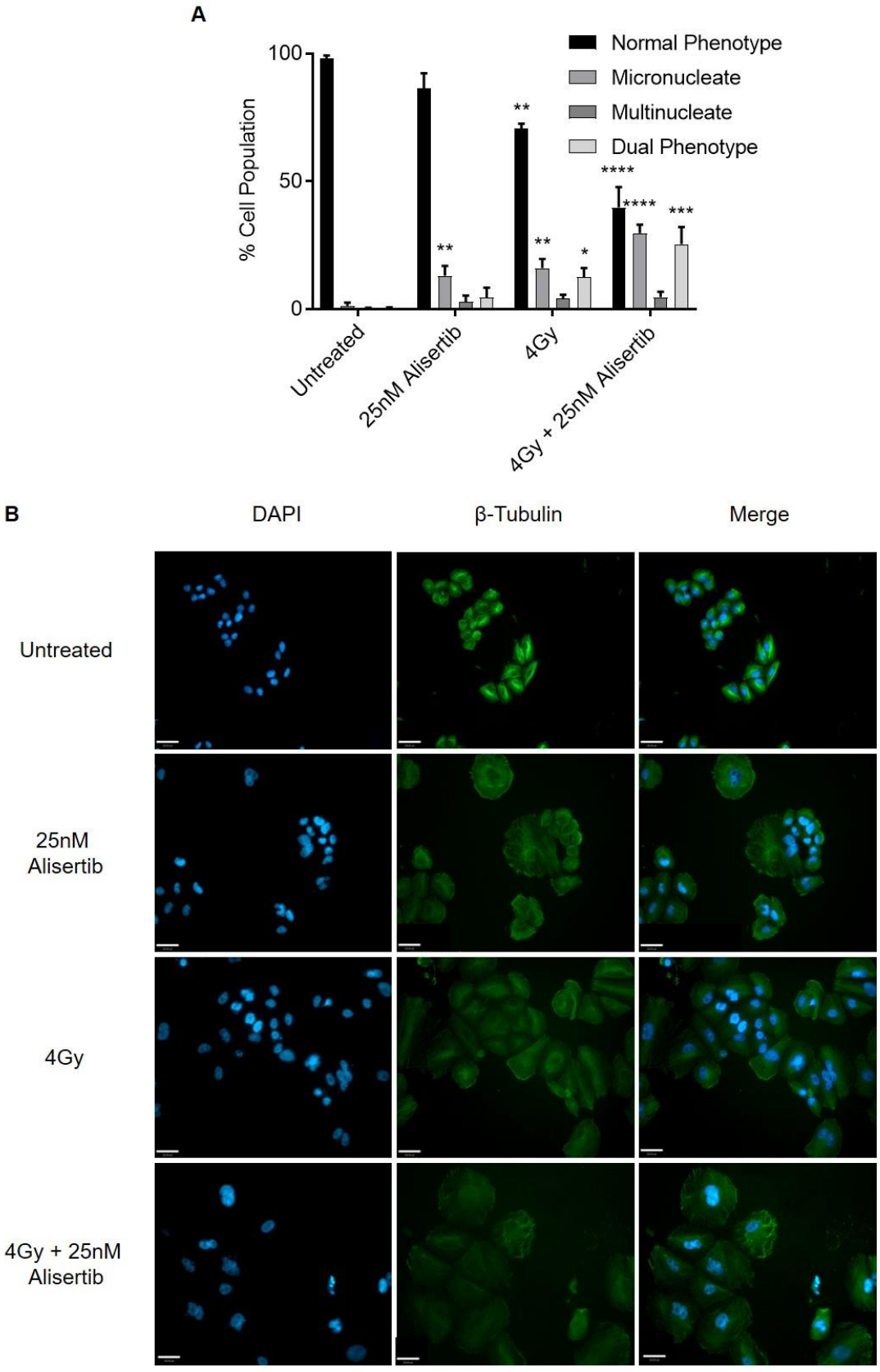

Figure 4.7. **Mitotic catastrophe markers in H460 cells 72 hours post-irradiation.** Legend overleaf.

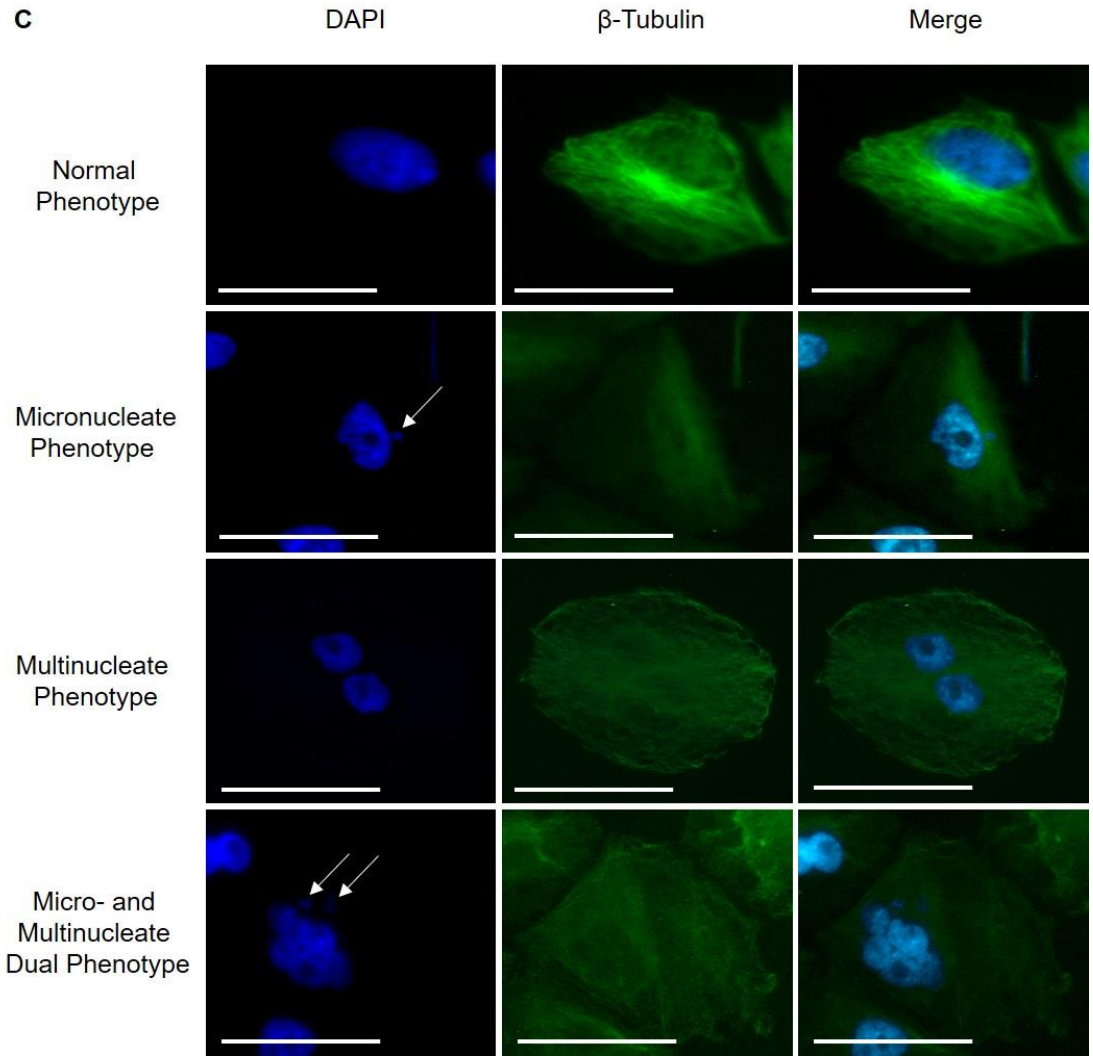

Figure 4.7. **Mitotic catastrophe markers in H460 cells 72 hours post-irradiation. A.** Proportion of H460 cells with normal nuclear phenotype compared with cells with any evidence of micronuclei, multiple nuclei or both (dual phenotype). Micronuclei and nuclei per cell counted. 100 cells counted per condition on each of three independent repeats. Data points represent mean proportion of cells exhibiting given phenotype +/- SEM (N= 3). * denotes p= ≤0.05, ** denotes p= ≤0.01, *** denotes p= ≤0.001 compared to corresponding phenotype in untreated control (One-way ANOVA with Bonferroni correction for multiple comparisons). **B.** Representative images of H460 cells stained for DAPI (cyan) and β-Tubulin (green) 72 hours post-irradiation. Imaged with a 20x microscope objective, scale bars represent 120 μm. **C.** Representative images of H460 phenotypes scored for mitotic catastrophe 72 hours post-irradiation. Cells stained for DAPI (cyan) and β-Tubulin (green). Imaged with a 20x microscope objective, scale bars represent 120 μm. Arrows indicate micronuclei.

These data are consistent with the idea that Alisertib IR combination increased the number of chromosomal abnormalities that are associated with the phenomenon of mitotic catastrophe in H460 cells. This is in line with increasing polyploid fraction following Alisertib IR combination observed by cell cycle profiling.

4.2.4.2. H460 cells exhibit increased levels of senescence 72 hours following treatment with Alisertib IR combination

Mitotic catastrophe can result in irreversible exit from the cell cycle or cellular senescence (Vitale *et al.* 2011) which can limit the proliferative potential of cancer cells following treatment (Luo *et al.* 2013). Given this and that cellular senescence has been shown to occur following irradiation in NSCLC cells in a p53-dependent manner (Luo *et al.* 2013) we hypothesised that induction of cellular senescence following Alisertib IR combination may explain combinational efficacy. β-galactosidase expression is a well-established marker of senescent cells (Dimri *et al.* 1995) and was used as a surrogate of senescence.

Here we demonstrate that the proportion of H460 cells positive for β-galactosidase was significantly increased 72 hours post-treatment with Alisertib IR combination compared to either treatment alone (see Figure 4.8). The etoposide positive control showed that this assay was sensitive enough to detect senescence, despite evidence of significant cytotoxicity in the H460 cells.

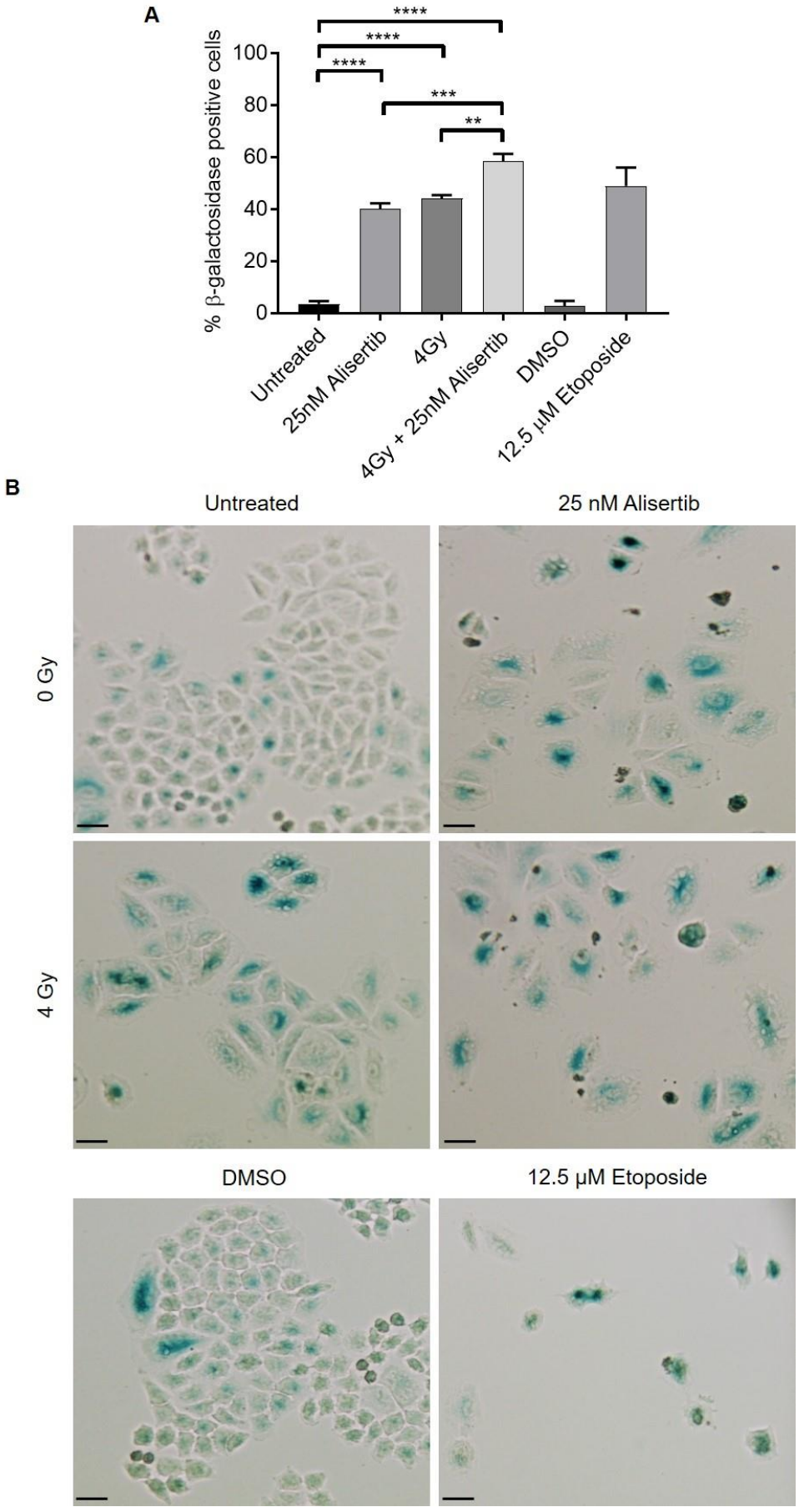

Figure 4.8. **Proportion of H460 cells positive for β-galactosidase expression 72 hours post-irradiation.** Legend overleaf.

Figure 4.8. **Proportion of H460 cells positive for β-galactosidase expression 72 hours post-irradiation. A.** Proportion of cells with dark perinuclear blue staining compared to cells absent of stain. 100 cells counted per condition per repeat. Data points represent mean proportion of cells exhibiting given phenotype +/- SEM (N= 3). NS (non-statistically significant) denotes p= >0.05, * denotes p= ≤0.05, ** denotes p= ≤0.01, *** denotes p= ≤0.001 (One-way ANOVA with Bonferroni correction for multiple comparisons). **B.** Representative images of H460 cells stained for β-galactosidase (blue) 72 hours post-irradiation. 100 cells counted per condition per repeat. Imaged with a 10x microscope objective. Scale bars represent 120 μm.

This suggests that the induction of cellular senescence could contribute the combinational efficacy of Alisertib IR combination.

4.2.5. Comparison of Alisertib IR combination in p53 deficient NSCLC cells

4.2.5.1. Mitotic and polyploid fraction is increased following Alisertib IR combination in p53 depleted H460 cells

We hypothesised that the p53 dependency of the Alisertib induced radiosensitisation may be due to differential cell cycle progression or changes in mitotic elimination post-treatment. To test this hypothesis in an identical genetic system we investigated if transient depletion of p53 in the p53 proficient H460 system affected cell cycle progression post-treatment with Alisertib IR combination. The above hypothesis would be tested in H460 cells depleted of p53 using siRNA 48 and 72 hours post-treatment with Alisertib/IR as this is when H460 polyploid proportions increased in treated conditions and mitotic population was differentially eliminated. H460 cells were re-plated and treated 24 hours post-siRNA transfection to maximise the time cells spent in a state of p53 depletion before being harvested for cell cycle profiling 48 and 72 hours post-treatment with Alisertib/IR (72h and 96h post-transfection respectively). Representative western blots for p53 depletion following siRNA transfection in H460 cells are available in Figure 3.6 (page 118).

Comparing non-transfected H460 cells at 48 hours to cells transfected with scrambled siRNA showed that transfection itself made little difference to the results seen previously such that the predominant effect was loss of cells from G1 and S and mitosis and increase in polyploidy and sub G1 fraction in all conditions compared to control (see Figure 4.9 A). One exception was that scrambled siRNA appeared to prevent mitotic arrest with Alisertib alone, and it was also noted that there was a skew from induction of polyploidy to increased sub G1 in all treated conditions.

Next p53 depleted cells were compared to scrambled siRNA treated cells at the same 48 hour timepoint. Under combination therapy p53 depletion resulted in greater loss of cells from G1 ($p= 0.08$ for p53 siRNA 1 and $p= 0.02$ for p53 siRNA 2 (Student's t-test)), inhibited loss of cells from mitosis ($p= 0.22$ for p53 siRNA 1 and $p= 0.06$ for p53 siRNA 2 (Student's t-test)) and caused increase in polyploidy ($p= 0.13$ for p53 siRNA 1 and $p= 0.01$ for p53 siRNA 2 (Student's t-test)) suggesting a switch from mitotic death to polyploidy (see Figure 4.9 B). The trend for increase in mitotic and polyploid cells was also seen in cells treated with Alisertib or IR alone (see Appendix Figure 8.4 for representative FACS plots).

By 72 hours similar trends were observed when comparing non-transfected cells to scrambled siRNA treated cells with an increase in polyploidy and sub G1 fraction being observed in all treatment conditions when scrambled siRNA was used compared to control (see Figure 4.9 C). Again, scrambled siRNA prevented mitotic arrest via Alisertib alone, and interestingly caused a decrease in G2 fraction after Alisertib treatment.

At 72 hours, depletion of p53 had no statistical effect on the endogenous cell cycle profile compared to scrambled siRNA (see Figure 4.9 D). Similar to 48 hours, p53 depletion combined with Alisertib IR treatment again resulted in greater loss of cells from G1 ($p= 0.017$ for p53 siRNA 1 and $p= 0.001$ for p53 siRNA 2 (Student's t-test)), attenuated mitotic loss ($p= 0.251$ for p53 siRNA 1 and $p= 0.046$ for p53 siRNA 2 (Student's t-test)) and caused an increase in polyploidy ($p= 0.047$ for p53 siRNA 1 and $p= 0.080$ for p53 siRNA 2 (Student's t-test)). Reduced mitotic loss and increased polyploidy in response to p53 depletion was also seen in Alisertib alone and IR alone conditions (see Appendix Figure 8.5 for representative FACS plots).

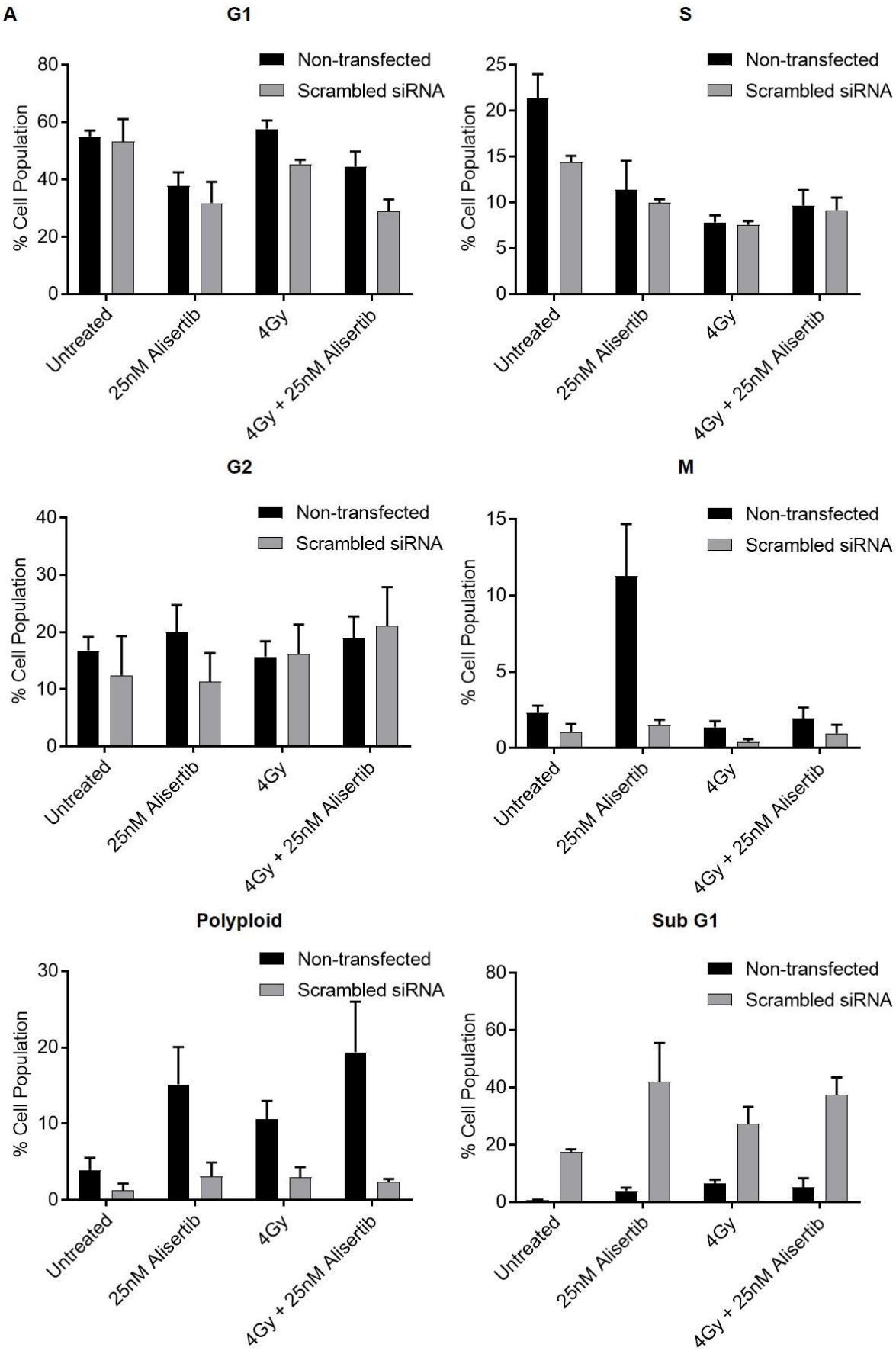

Figure 4.9. **Mean H460 cell cycle distribution following siRNA treatment and treatment with 25 nM Alisertib, 4 Gy or combination.** Legend on page 177.

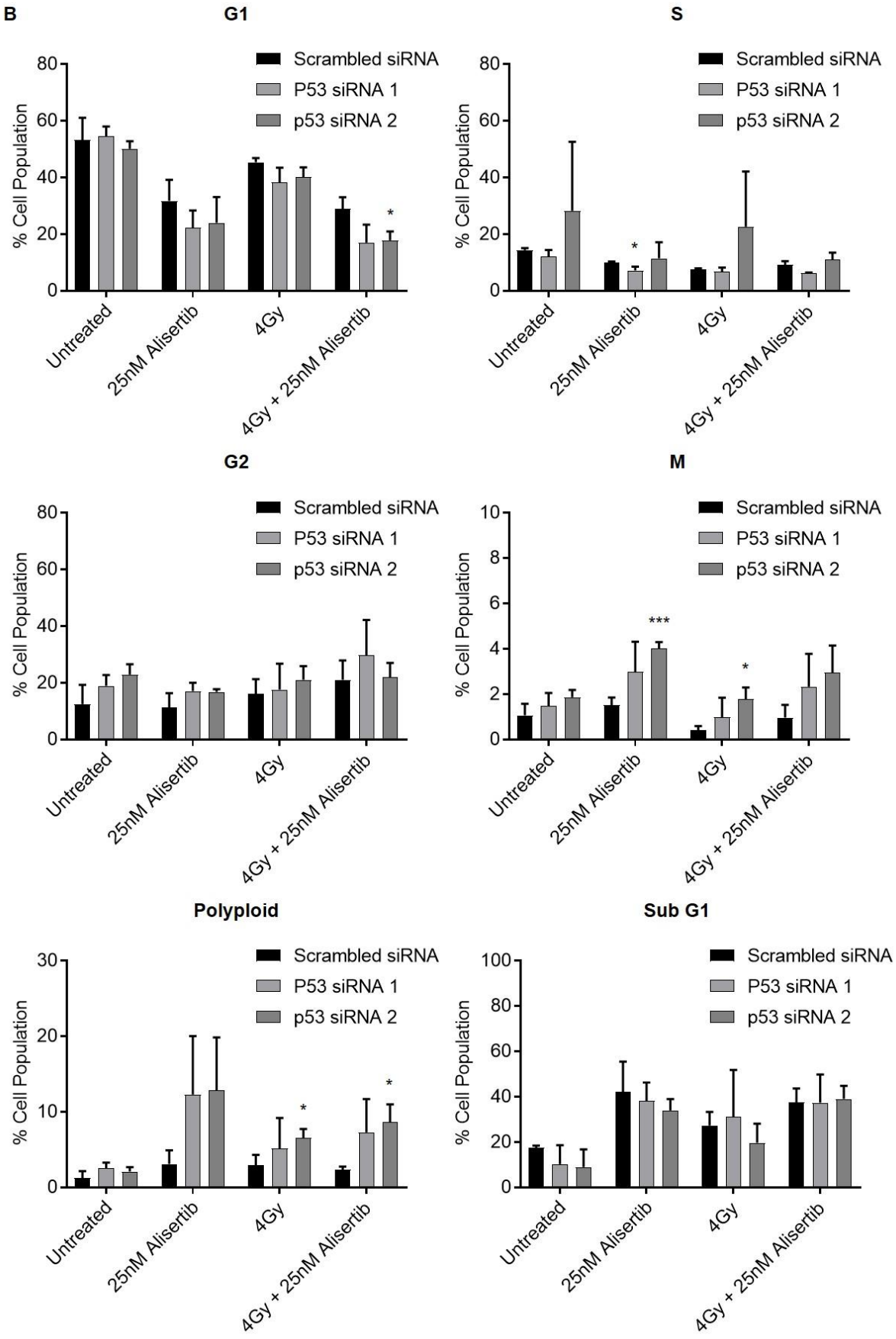

Figure 4.9. **Mean H460 cell cycle distribution following siRNA treatment and treatment with 25 nM Alisertib, 4 Gy or combination.** Legend on page 177.

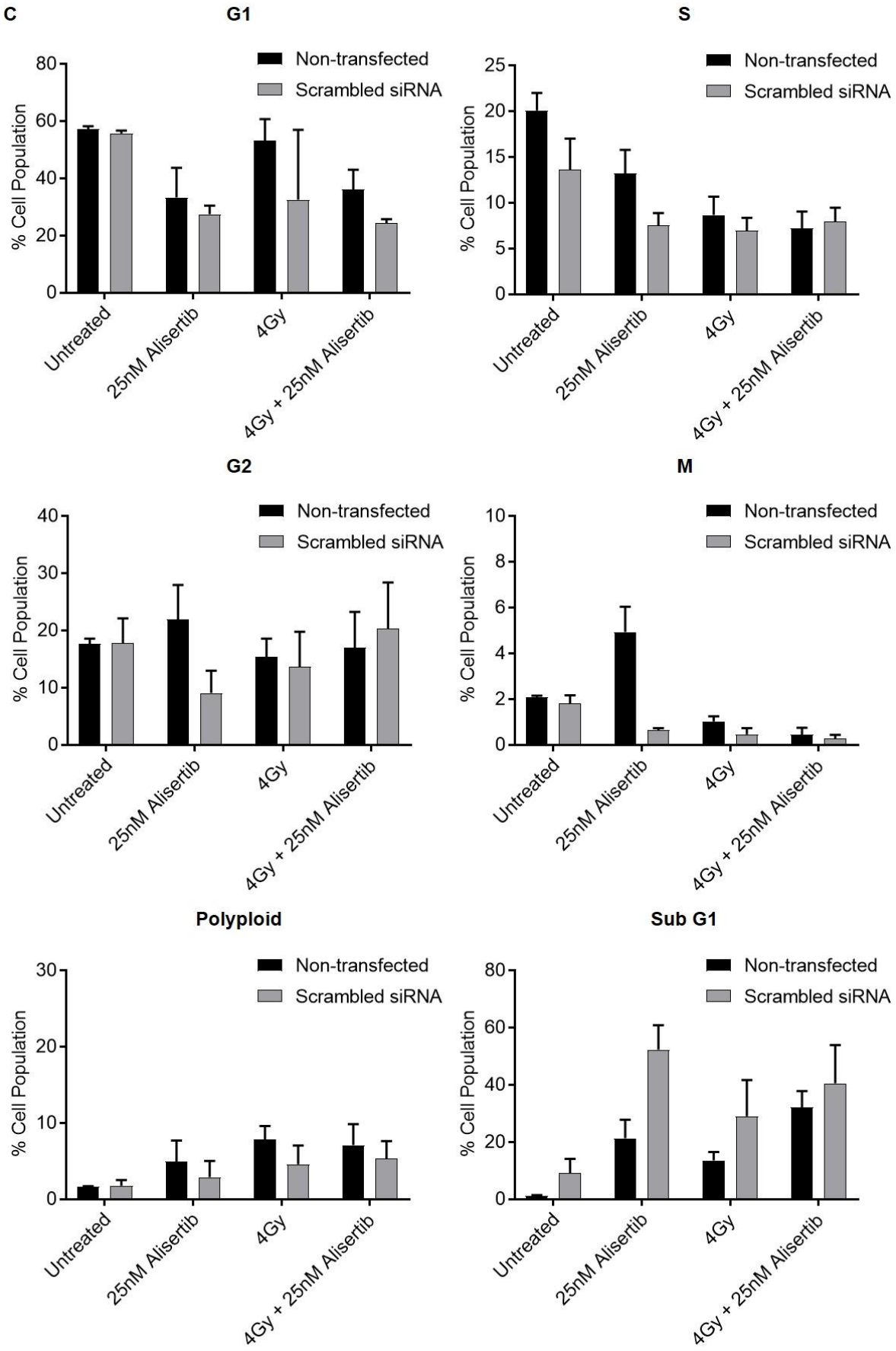

Figure 4.9. **Mean H460 cell cycle distribution following siRNA treatment and treatment with 25 nM Alisertib, 4 Gy or combination.** Legend on page 177.

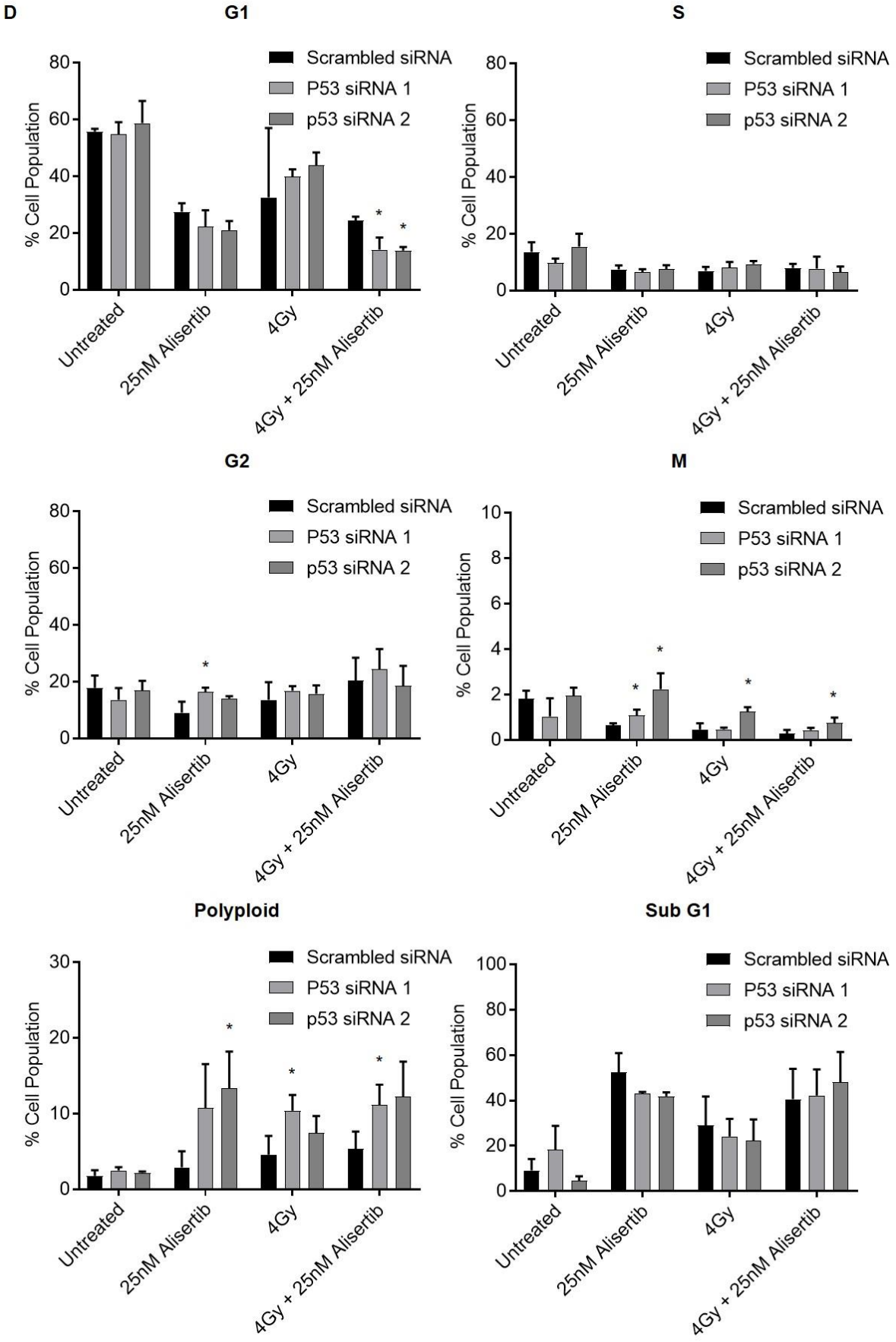

Figure 4.9. **Mean H460 cell cycle distribution following siRNA treatment and treatment with 25 nM Alisertib, 4 Gy or combination.** Legend overleaf.

Figure 4.9. **Mean H460 cell cycle distribution following siRNA treatment and treatment with 25 nM Alisertib, 4 Gy or combination.** Cell cycle profile of non-transfected H460 data re-represented for clarity compared to H460 cells transfected with scrambled siRNA **A.** 48 hours and **C.** 72 hours post-treatment. Cell cycle profile of H460 cells transfected with scrambled siRNA or p53 siRNA **B.** 48 hours and **D.** 72 hours post-treatment. Data points represent mean cell cycle phase distribution +/- SEM (N= ≥2). 10000 events collected per condition within single cell population gate (PI (FL-3) width vs PI (FL-3) height). * denotes p= ≤0.05 and *** denotes p=≤0.001 (Student's independent samples two-tailed unpaired t-test) comparing to scrambled siRNA control

In summary, there were large increases in sub G1 fraction of all transfected H460 cells compared to non-transfected cells even when scrambled siRNA was used. This indicated that transfection alone was having significant toxicity. Additionally, the sub G1 fraction peaked in 25 nM Alisertib alone conditions with an absence of cooperative increases in sub G1 fraction after 4 Gy + 25 nM Alisertib combination seen in non-transfected H460 cells. Thus, inhibiting AURKA in cells stressed by siRNA transfection hinders interpretation of our data. Furthermore, there was consistent reduction in G1 fractions and increase in sub G1 fractions in H460 cells treated with 4 Gy + 25 nM Alisertib, regardless of p53 presence or depletion. This suggests that reduction in G1 fraction and increase in sub G1 fraction again may be reflective of a stress response confusing interpretation of the data. However overall there were trends for increased mitotic fraction and polyploid fraction in H460 cells transfected with p53 siRNA and treated with 25 nM Alisertib or 4 Gy + 25 nM Alisertib when compared to scrambled siRNA control. This suggests that a there may be a switch from mitotic death to polyploidy in the absence of p53 and this potentially may be related to the therapeutic efficacy of Alisertib IR combination.

4.2.5.2. Cell cycle progression is altered in H1299 cells treated with Alisertib IR combination

Although the p53 depletion data were helpful, it should be noted that siRNA transfection in H460 cells was associated with significant toxicity alone and this may potentially confound the effect of Alisertib IR combination on the cell cycle. Given this we used the H1299 cell line as a p53 deficient model of NSCLC that did not respond to Alisertib IR combination, we sought to investigate if the cell cycle distribution following Alisertib + IR could discriminate between the combination responding H460 cell line and the non-responding H1299 cell line.

Firstly, we found that, unlike the H460 cell line, the H1299 cell line did not exhibit a G1 arrest following IR compared to the H460 cell line (see Figure 4.10). However, similar to the H460 cells, there was a time dependent decrease in G1 fraction that was statistically significant compared to control in all treatment conditions by 72 hours ((p= <0.0001, p= 0.0065 and p= <0.0001 One-way ANOVA)) more so in the combinational treatment than either 25 nM Alisertib or 4 Gy alone (conditions (p= 0.0031 and p= <0.0001 (One-way ANOVA)).

A non-significant trend for reduction in H1299 S phase population was observed 24 hours post-irradiation in the 4 Gy condition (p= 0.224) and significant reduction in S phase population in 4 Gy + 25 nM Alisertib condition (p= 0.003) when compared to untreated control (see Figure 4.10). A reduction in S phase fraction in H1299 cells 48 hours post-irradiation was only detected in the combinational treatment arm and this was not statistically significant (p= 0.113). By 72 hours post-irradiation there was a trend for reduction in S phase fraction in H1299 cells in the 25 nM Alisertib, 4 Gy and 4 Gy + 25 nM Alisertib conditions, but this reduction was only significant in the

combinational treatment arm when compared to untreated control (p= 0.247, p= 0.315 and p= 0.007 (One-way ANOVA)). This was similar to the H460 cell line but with reduced effect size.

We could not detect any statistically significant differences in the G2 fractions of H1299 cells in the 25 nM Alisertib, 4 Gy and 4 Gy + 25 nM Alisertib conditions when compared to untreated control across both the 24 and 48 hour timepoints post-irradiation (see Figure 4.10). There was a trend for increasing H1299 G2 fraction in the 25 nM Alisertib, 4 Gy and 4 Gy + 25 nM Alisertib conditions by 72 hours post-irradiation, but this was only statistically significant in the combinational treatment arm when compared to untreated control (p= >0.999, p= 0.119 and p= 0.007 (One-way ANOVA)). This was unlike the H460 cell line which showed consistent increase at all timepoints in 25 nM Alisertib and combination treatment conditions.

H1299 mitotic fraction showed a trend to increase in the 25 nM Alisertib and 4 Gy + 25 nM Alisertib treatment conditions 24, 48 and 72 hours post-irradiation when compared to untreated control (see Figure 4.10). This was statistically significant for 25 nM Alisertib alone at 48 hours post-treatment (p= 0.025 (One-way ANOVA)), and for both 25 nM Alisertib and 25 nM Alisertib + 4 Gy conditions at 72 post-treatment when compared to the untreated control (p= 0.0001 and p= 0.0002 (One-way ANOVA)). This was in contrast to the H460 cell line which saw loss of cells from mitosis 48 and 72 hours post-treatment with combination treatment arm.

There was a trend for polyploid H1299 population to be increased 24 and 48 hours post-irradiation in the 25 nM Alisertib, 4 Gy and 4Gy + 25 nM Alisertib conditions relative to untreated control (see Figure 4.10). By 72 hours post-irradiation the H1299 polyploid population was significantly increased in both the 25 nM Alisertib

and 4 Gy + 25 nM Alisertib conditions relative to untreated control (p= 0.0008 and p= <0.0001 (One-way ANOVA)). The increase in H1299 polyploid population was greater than additive in the combinational treatment arm and was statistically significant from the polyploid fractions seen in the 25 nM Alisertib and 4 Gy alone treatment conditions (p= 0.0054 and p= <0.0001 (One-way ANOVA)). The H1299 cell line exhibited greater polyploid population in combinational treatment arm by 72 hours post-treatment compared to the H460 cell line.

A trend for increased sub G1 H1299 population 24 and 48 hours post-irradiation was observed in all treatment conditions relative to untreated control and was statistically significant in the combinational treatment arm by 48 hours (p= <0.0001 (One-way ANOVA)) (see Figure 4.10). By 72 hours post-irradiation H1299 sub G1 population remained higher in the 25 nM Alisertib, 4 Gy and 4 Gy + 25 nM Alisertib treatment conditions each with statistical significance when compared to untreated control (p= <0.0001, p= 0.008 and p= <0.0001 (One-way ANOVA)). There was no evidence of cooperativity in sub G1 population increase by 72 hours in the H1299 cell line when treated with 25 nM Alisertib + 4 Gy, in contrast to the H460 cell line. Comparative H460 cell cycle data is re-represented for clarity (see Figure 4.10).

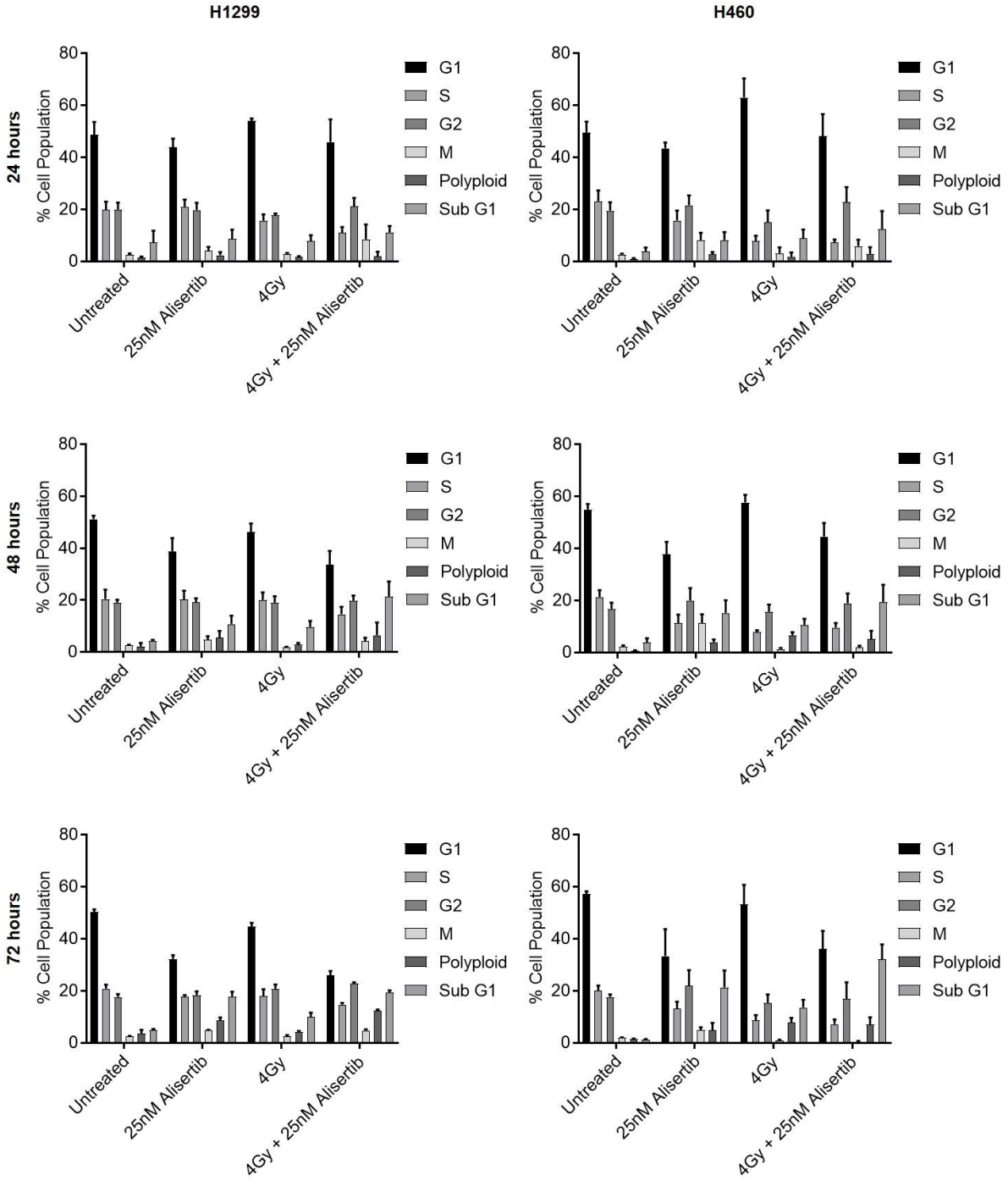

Figure 4.10. **H1299 and H460 cell cycle distribution 24, 48 and 72 hours following treatment with 25 nM Alisertib, 4 Gy or combination.** Mean cell cycle phase distribution 24, 48 and 72 hours post-irradiation. Data points represent mean cell cycle phase distribution +/- SEM (N= ≥2). H460 data are re-represented for clarity

To summarise these data, in p53 deficient H1299 cells reduced G1 and S phase fractions 72 hours post-treatment with 4 Gy + 25 nM Alisertib suggest that, like the H460 cell line, cells were not re-entering subsequent cell cycles. However, in contrast to the H460 cell line, there was not a loss of mitotic cells rather there was a greater increase in polyploidy. Curiously, the H1299 cell line also demonstrated increases in sub G1 fraction that were greatest in the 4 Gy + 25 nM Alisertib combination. Given our long term clonogenic survival data presented earlier, this suggested that sub G1 fraction following Alisertib IR combination may not equate to long term combinational efficacy. Like the cell cycle data in p53 depleted H460 cells, these data suggest that rather than mitotic loss p53 deficient cells become increasingly polyploid in response to Alisertib IR combination.

4.2.5.3. There is a lack of mitotic loss and a greater proportion of polyploid cells in p53 deficient NSCLC cells 48 hours post-treatment with Alisertib IR combination when compared to p53 proficient NSCLC cells

To assess any trends in cell cycle distribution that may be due to p53 the A549 cell line as a p53 proficient model and H322 and SW900 cell lines as p53 deficient models were also subject to cell cycle profiling 48 hours post-treatment with Alisertib IR combination. Here we focus in on mitosis and polyploidy but full cell cycle profiles are shown in Figure 8.6 (see appendix). At 48 hours post-treatment, compared to control, and in line with H460 data there was a trend for loss of cells from mitosis following IR alone or combination treatment in p53 proficient NSCLC cell lines ($p= 0.075$ and $p= 0.194$ (One-way ANOVA)) (see Figure 4.11 A). In contrast, in p53 deficient cells there was no loss of cells from mitosis, in fact there was a trend for increased mitotic fraction following Alisertib IR combination compared to control and IR alone ($p= 0.225$ and $p= 0.192$ (One-way ANOVA)).

Untreated p53 deficient NSCLC cell lines have a trend for increasing polyploidy compared to untreated p53 proficient NSCLC cell lines (p= 0.066 (One-way ANOVA)) (see Figure 4.11 B). There was also a trend for increasing mean proportion of polyploid cells 48 hours post-treatment in IR alone and the combinational treatment arms compared to untreated control in the p53 proficient and p53 deficient NSCLC cell lines although this was only statistically increased in the p53 deficient cell lines (p= 0.025 (One-way ANOVA)). Surprisingly there was no association with sub G1 proportion and Alisertib IR combinational efficacy 48 hours post-treatment (data not shown).

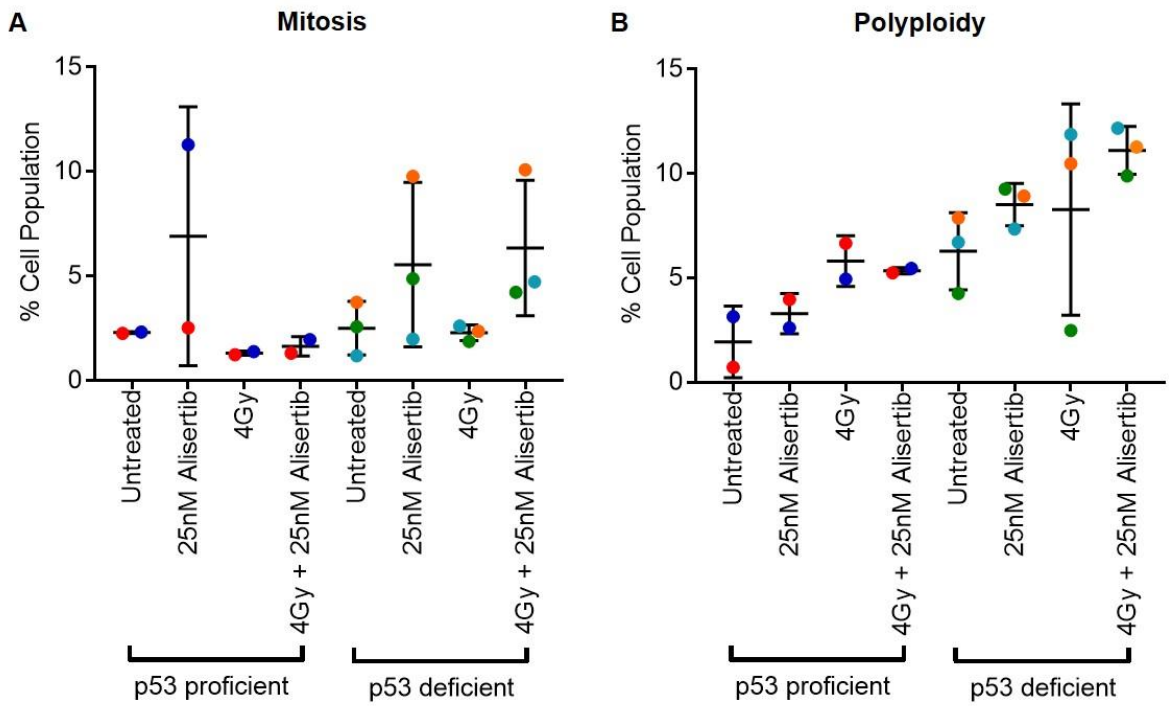

Figure 4.11. **A. Mean mitotic proportion and B. Mean polyploid proportion 48 hours following treatment with 25 nM Alisertib, 4 Gy or combination in NSCLC cell line panel.** Data points represent mean polyploid distribution +/- SEM (N= ≥2) for each cell line tested. 10000 events collected per condition within single cell population gate (PI (FL-3) width vs PI (FL-3) height). Dark blue: A549, Red: H460, Orange: H322, Green: H1299 and Light blue: SW900 respectively

This suggests that the cellular response to IR following Alisertib IR combination is important. There was also evidence of increased polyploidy as a baseline and following Alisertib IR combination in p53 deficient backgrounds. This agrees with previous research which identifies that p53 deficiency is permissive for an increased baseline polyploid population and has been documented previously *in vitro* (Vitale et al. 2010) and *in vivo* (Kurinna et al. 2013). This finding may be partially explained by the role of p53 in regulating a post-mitotic checkpoint which arrests tetraploid cells in G1 (Andreassen et al. 2001). These data showed similar trends to p53 depleted H460 cells and provided further evidence that these effects were both p53-dependent and potentially related to Alisertib IR combinational efficacy.

4.2.5.4. H1299 exhibit increased levels of micronuclei, reduced combined micronuclei and multinucleation and do not show cooperative increase in senescence compared to H460 cells following Alisertib IR combination.

In p53 proficient cells Alisertib IR treatment combination caused cooperative increases in cells with micronuclei alone and in combination with multinucleation as well as increasing β-galactosidase expression, indicating mitotic catastrophe and senescence respectively. Here we asked did p53 expression affect induction of mitotic catastrophe or senescence. We used the H1299 cell line as a model of p53 deficient NSCLC and as previously tested for micronuclei, multinucleation and β-galactosidase expression 72 hours post-treatment with 4 Gy + 25 nM Alisertib.

Like the H460 cell line, in the H1299 cell line 25 nM Alisertib, 4 Gy and 4 Gy + 25 nM Alisertib all increased the proportion of cells bearing either micronuclei or multiple nuclei from 8.76% in untreated control to 25.86%, 39.07% and 58.00% ($p= 0.0637$, $p= 0.0024$ and $p= <0.0001$ (One-way ANOVA)) (see Figure 4.12). However, unlike

the H460 cell line the effect seen in the combinational condition was less than additive although statistically higher than either 25 nM Alisertib or 4 Gy alone (p= 0.002 and p= 0.039 (One-way ANOVA)).

When considering the proportion of micronuclei positive H1299 cells there was an increase in all treatment conditions compared to untreated control, but the increase was only statistically significant when treating with 4 Gy or 4 Gy + 25 nM Alisertib (p= 0.0022 and p= 0.0005 (One-way ANOVA)) (see Figure 4.12). There was a less than additive increase in micronuclei positive H1299 cells when combining 4 Gy and 25 nM Alisertib that was statistically increased compared to 25 nM Alisertib alone but not compared to 4 Gy alone (p= 0.004 and p= >0.999 (One-way ANOVA)). The levels of micronuclei positive H1299 cells following treatment combination exceeded those seen in H460 cells by 1.31-fold (p= 0.156 (Student's independent samples unpaired two-tailed t-test)).

There was a trend to increased proportion of H1299 cells with multiple nuclei in all treatment conditions compared to untreated control, but there was no evidence of statistical increase and is likely reflective of small effect size (see Figure 4.12). Also, similar to the H460 cells, there was no evidence of any cooperative increase in proportion of H1299 cells with multiple nuclei in the combinational treatment condition.

As with the H460 cells, the proportion of H1299 cells exhibiting a dual phenotype of both micronuclei and multiple nuclei was also increased in all treatment conditions compared to untreated control, with statistical increase in the 4 Gy + 25 nM Alisertib conditions (p= 0.0001 (One-way ANOVA)) (see Figure 4.12). There was a greater than additive increase in proportion of H1299 cells with micronuclei and multiple

nuclei in the combinational treatment condition, and this increase was statistically increased compared to 25 nM Alisertib or 4 Gy alone ($p= 0.002$ and $p= 0.002$ respectively (One-way ANOVA)). However, the proportion of H1299 cells with dual micronuclei positive multinucleate phenotype was reduced by 2.15-fold compared to H460 cells ($p= 0.024$ (Student's independent samples unpaired two-tailed t-test)).

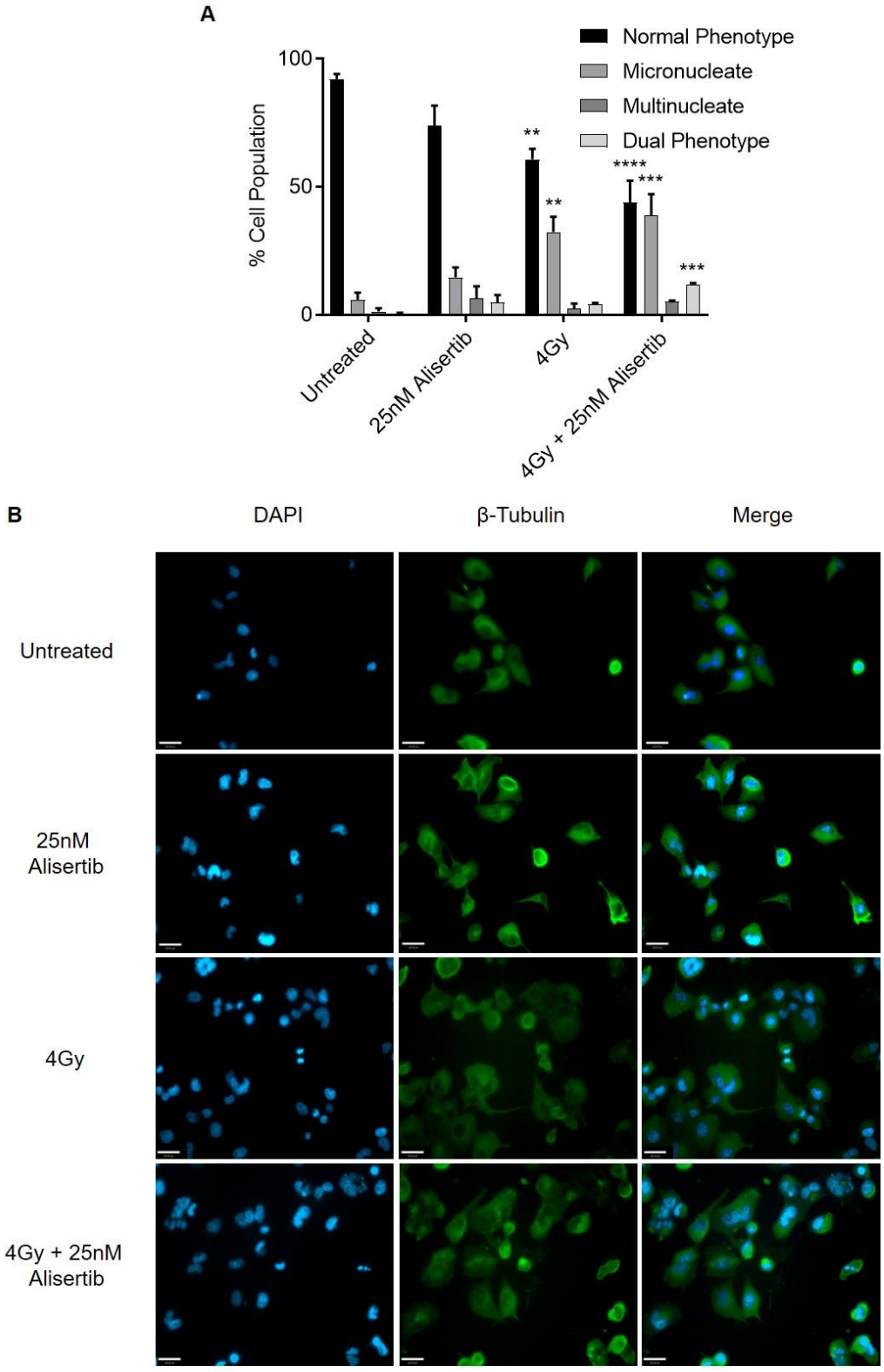

Figure 4.12. **Mitotic catastrophe markers in H1299 cells 72 hours post-irradiation.** Legend overleaf.

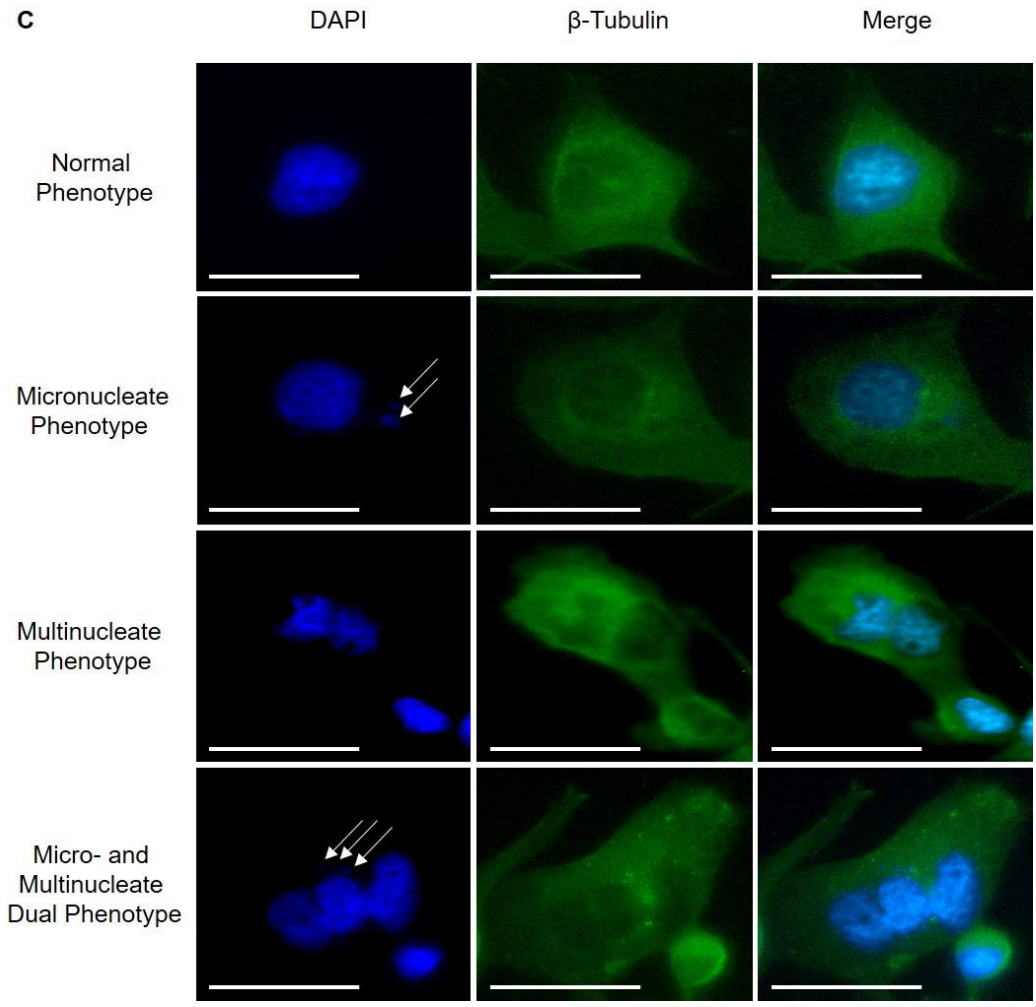

Figure 4.12. **Mitotic catastrophe markers in H1299 cells 72 hours post-irradiation. A.** Proportion of H1299 cells with normal nuclear phenotype compared with cells with any evidence of micronuclei, multiple nuclei or both (dual phenotype). Micronuclei and nuclei per cell counted. 100 cells counted per condition on each of four independent repeats. Data points represent mean proportion of cells exhibiting given phenotype +/- SEM (N= 4). * denotes p= ≤0.05, ** denotes p= ≤0.01, *** denotes p= ≤0.001 compared to corresponding phenotype in untreated control (One-way ANOVA with Bonferroni correction for multiple comparisons). **B.** Representative images of H1299 cells stained for DAPI (cyan) and β-Tubulin (green) 72 hours post-irradiation. Imaged with a 20x microscope objective, scale bars represent 120 μm. **C.** Representative images of H1299 phenotypes scored for mitotic catastrophe 72 hours post-irradiation. Cells stained for DAPI (cyan) and β-Tubulin (green). Imaged with a 20x microscope objective, scale bars represent 120 μm. Arrows indicate micronuclei.

We see increased micronuclei positive cells but reduced dual micronuclei positive/multinucleated H1299 cells compared to the H460 cells. It is possible that the accumulation of micronuclei positive multinucleated cells following Alisertib IR

combination could be related to combinational efficacy. However, these data also suggest that the amount of mitotic aberration in the H1299 cell line following Alisertib IR combination may increase, in the form of micronuclei and multiple nuclei, as in the H460 cell line. This implies that mechanistically, increase in mitotic aberration following Alisertib IR combination occurs in both p53 proficient and p53 deficient NSCLC cell lines. Two hypotheses are therefore possible:

- That mitotic aberration following Alisertib IR combination in NSCLC cells has different consequences in p53 proficient and deficient cells
- Mitotic aberration is not related to efficacy of Alisertib IR combination in NSCLC cells

There is evidence that cellular fate after mitotic catastrophe can be affected by the genetic background of the cell and that these outcomes can be influenced by p53 (Vitale *et al.* 2010; Luo *et al.* 2013) or some of its transcriptional targets (Yun *et al.* 2009). Therefore, it is possible that the cellular fates of NSCLC cells after Alisertib IR combination induced mitotic aberration could be differential based on genetic background, explaining the differing clonogenic responses of the H460 and H1299 cells. Given this, one hypothesis is that the induction of cellular senescence could be differential in cells that are and are not radiosensitised by Alisertib IR combination.

Here we demonstrate that the H1299 cells also showed a trend to increase in β-galactosidase positive proportion following Alisertib IR combination, however unlike the H460 cells this was not statistically different from IR alone (see Figure 4.13).

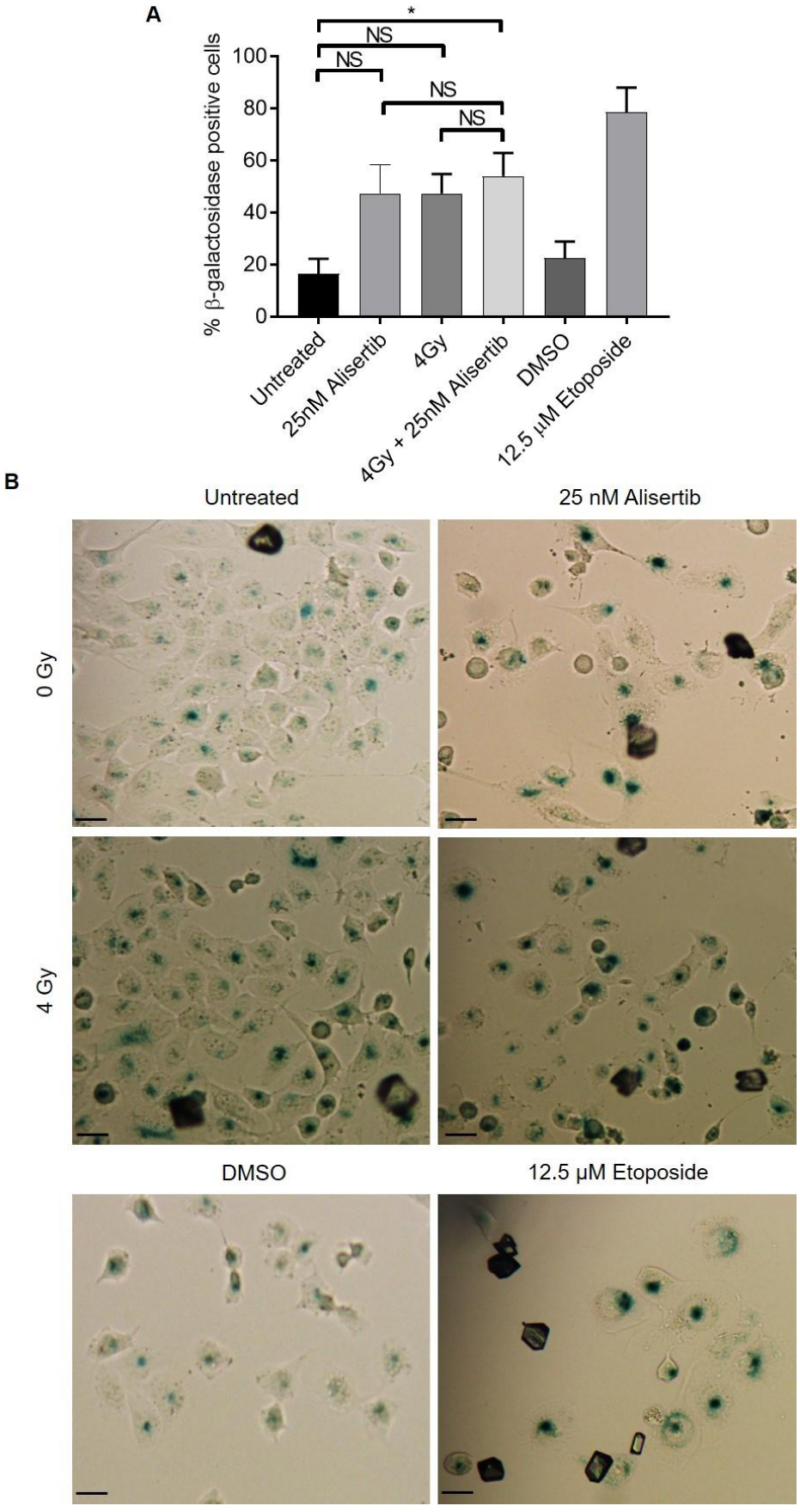

Figure 4.13. **Proportion of H1299 cells positive for β-galactosidase expression 72 hours post-irradiation.** Legend overleaf.

Figure 4.13. **Proportion of H1299 cells positive for β-galactosidase expression 72 hours post-irradiation. A.** Proportion of cells with dark perinuclear blue staining compared to cells absent of stain. 100 cells counted per condition per repeat. Data points represent mean proportion of cells exhibiting given phenotype +/- SEM (N= 3). NS (non-statistically significant) denotes p= >0.05, * denotes p= ≤0.05, ** denotes p= ≤0.01, *** denotes p= ≤0.001 (One-way ANOVA with Bonferroni correction for multiple comparisons). **B.** Representative images of H1299 cells stained for β-galactosidase (blue) 72 hours post-irradiation. 100 cells counted per condition per repeat. Imaged with a 10x microscope objective, scale bars represent 120 μm.

These data show that unlike the H460 cell line there is no cooperative increase in β-galactosidase expression compared to IR alone in H1299 cells treated with Alisertib IR combination. This suggests that induction of senescence following Alisertib IR combination could be related to therapeutic efficacy of the Alisertib IR combination, although the increased effect is small. Overall, it appears that during combination therapy Alisertib alters the cells response to IR induced mitotic aberrance by increasing loss of cells from mitosis, mitotic catastrophe and senescence in a p53-dependent manner.

However, there are also other potential hypotheses for Alisertib IR mechanism. As there is published evidence that AURKA may affect the DNA damage response (Sun *et al.* 2014; Wang *et al.* 2014a), and the main cytotoxic effect of IR is the induction of DSBs (Mladenov *et al.* 2013), we hypothesised that differential DNA damage responses may contribute combinational efficacy of Alisertib IR combination in NSCLC cells. Note this is not mutually exclusive with changes to cell cycle response.

4.2.6. The effect of Alisertib IR combination on the DNA damage response in H460 cells

4.2.6.1. Alisertib IR combination shows trend for increased γ-H2AX foci per cell 24 hours post-treatment

Targeting the many components of the DNA damage response has been shown to be a viable approach for the radiosensitisation of NSCLC (Maier *et al.* 2016). Indeed the CONCORD platform trial in the UK will combine PARP, ATM and ATR inhibitors with conventional radiotherapy in stage III NSCLC patients (Hanna *et al.* 2017). Our data indicate that the Alisertib IR combinational effect in NSCLC models is dependent on the expression of wildtype p53, a well-established regulator of the DNA damage response. This is coupled with previous data that indicated that AURKA can interact with and suppress certain elements of the DNA damage response (Sun *et al.* 2014). Subsequently we hypothesised that Alisertib IR combination could be altering the DNA damage response in irradiated cells, leading to enhanced cellular death. Firstly, we set out to see if DNA damage resolution was affected by staining for γH2AX within the first 24 hours post-irradiation. Serine 139 phosphorylation of histone H2AX has been shown to occur in the locality of DNA DSBs within the first 30 minutes of their induction, attract mediators of the DNA damage response and is de-phosphorylated as the DNA damage is resolved (reviewed in (Kinner *et al.* 2008). Here we used the average number of γH2AX foci per cell as a measure of DNA damage in H460 cells and its repair kinetics over time.

At 15 minutes post-irradiation 4 Gy and 4 Gy + 25 nM Alisertib greatly induced and significantly increased the number of γH2AX foci per cell compared to untreated control ($p= 0.0007$ and $p= 0.0003$ (One-way ANOVA)) (see Figure 4.14 A-B). 25 nM Alisertib alone caused a slight increase in γH2AX per cell, but this was not

significantly different from that seen in untreated cells (p=0.945 (One-way ANOVA)). There was more γH2AX foci per cell in the combinational condition compared to 4 Gy alone, but this effect was less than additive and was not statistically different from IR alone (p= >0.999 (One-way ANOVA)).

At 1 hour post-irradiation the mean foci per cell fell slightly in the 4 Gy and 4 Gy + 25 nM Alisertib conditions, but the amount of foci per cell remained significantly increased compared to control (p= 0.0002 and 0.0002 (One-way ANOVA)) (see Figure 4.14 A & C). Mean γH2AX foci per cell for Alisertib treatment alone remained above untreated control but this remained statistically non-significant (p= 0.775 (One-way ANOVA)). There was no difference between 4 Gy and 4 Gy + 25 nM Alisertib conditions (p= >0.999 (One0way ANOVA)).

By 6 hours post-irradiation the mean amount of γH2AX foci per cell was heavily reduced in the irradiated conditions when compared to 15 minutes post-irradiation (see Figure 4.14 A & D). However, the mean levels of γH2AX foci per cell remained significantly higher in the 4 Gy and 4 Gy + 25 nM Alisertib conditions to control (p= 0.0018 and 0.0003 (One-way ANOVA)). Mean foci per cell in the 25 nM Alisertib alone condition remained stable and above that of the untreated control but this difference was not statistically significant (p= 0.588 (One-way ANOVA)). The mean levels of γH2AX foci per cell was higher in the combinational condition than those seen in the 4 Gy alone condition, but this effect was less than additive and was not statistically significant (p= 0.392 (One-way ANOVA)).

By 24 hours post-irradiation the mean foci per cell in the 25 nM Alisertib alone and 4 Gy alone conditions had resolved to similar levels seen in the control (p= >0.999 and p= >0.999 (One-way ANOVA)) (see Figure 4.14 A & E). Mean γH2AX per cell in the

combinational condition remained nearly double those of the irradiation alone group, but this effect was less than additive and was not statistically different from either control or irradiation alone ($p= 0.077$ and $p= 0.177$ (One-way ANOVA)).

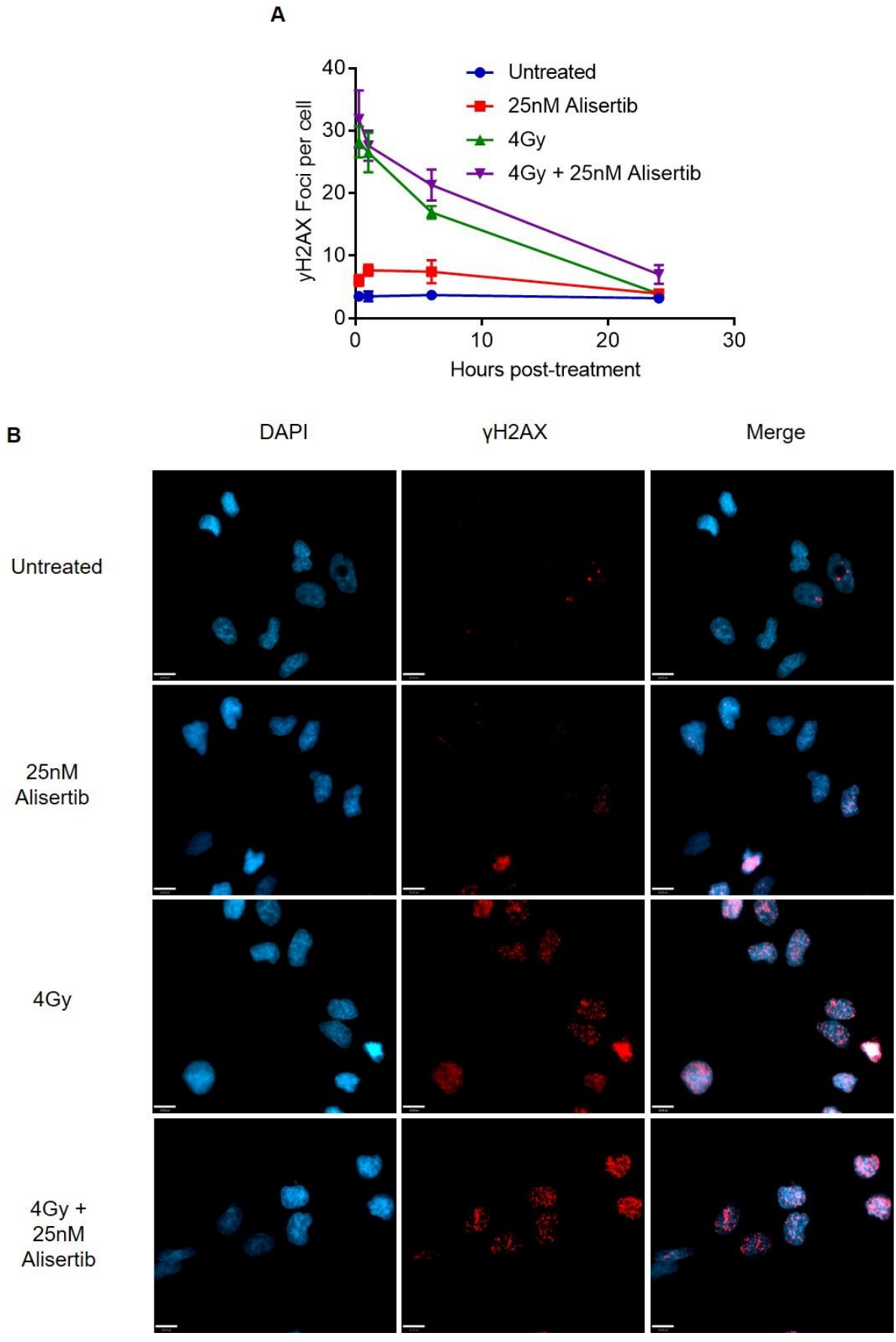

Figure 4.14. **Mean γH2AX foci formation and repair in H460 cells following treatment with 25 nM Alisertib, 4 Gy or combination.** Legend on page 198.

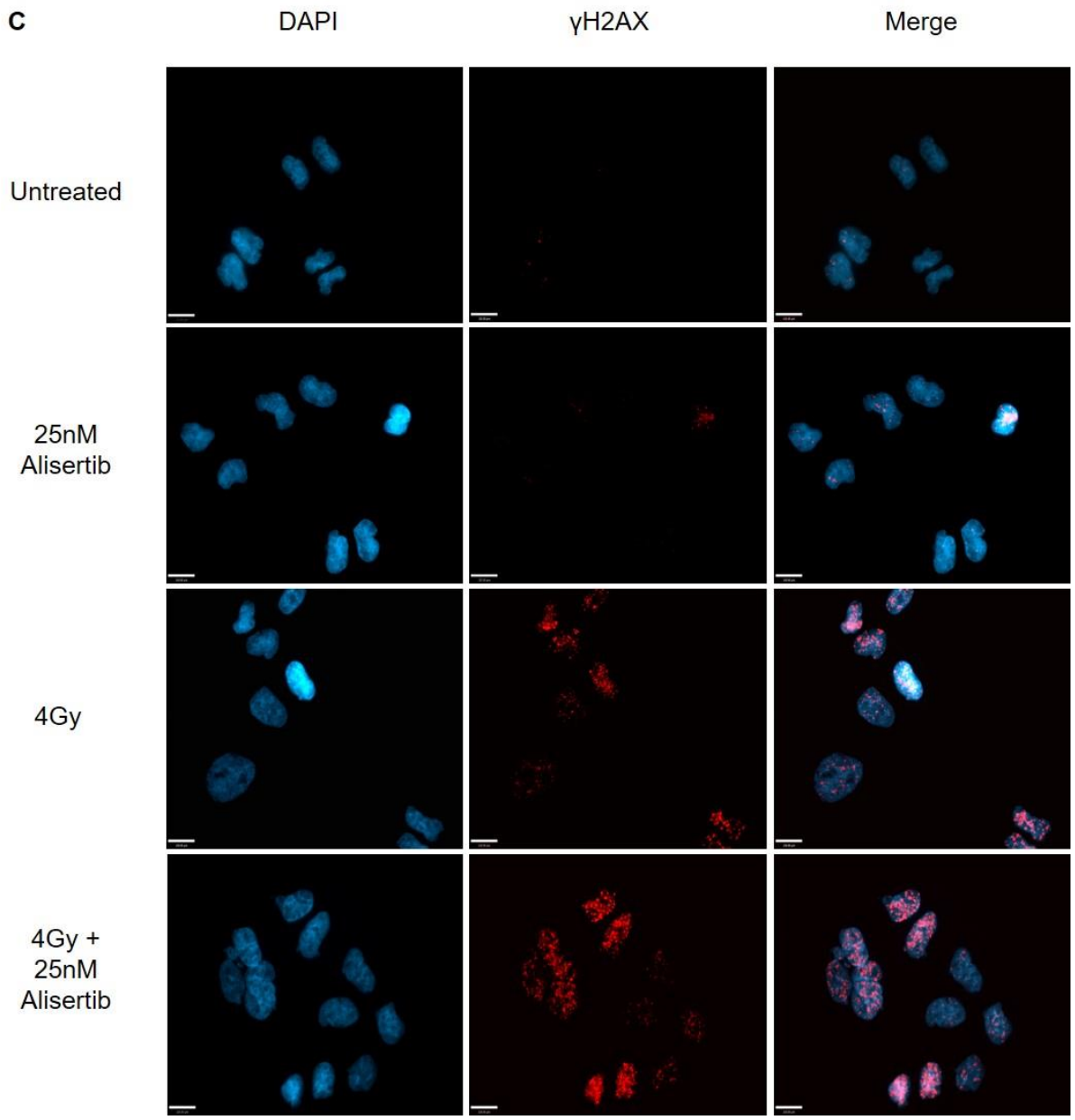

Figure 4.14. **Mean γH2AX foci formation and repair in H460 cells following treatment with 25 nM Alisertib, 4 Gy or combination.** Legend on page 198.

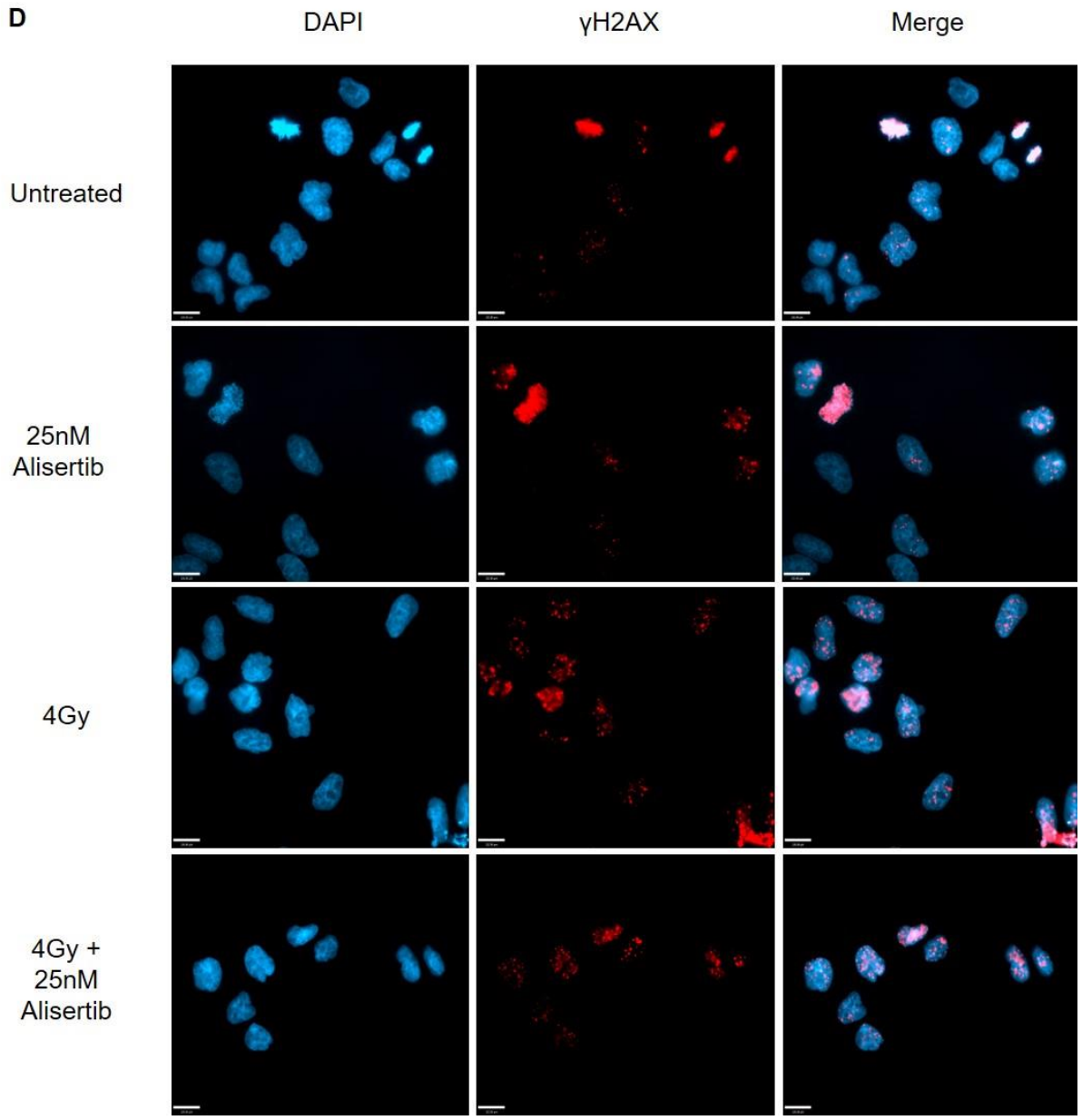

Figure 4.14. **Mean γH2AX foci formation and repair in H460 cells following treatment with 25 nM Alisertib, 4 Gy or combination.** Legend overleaf.

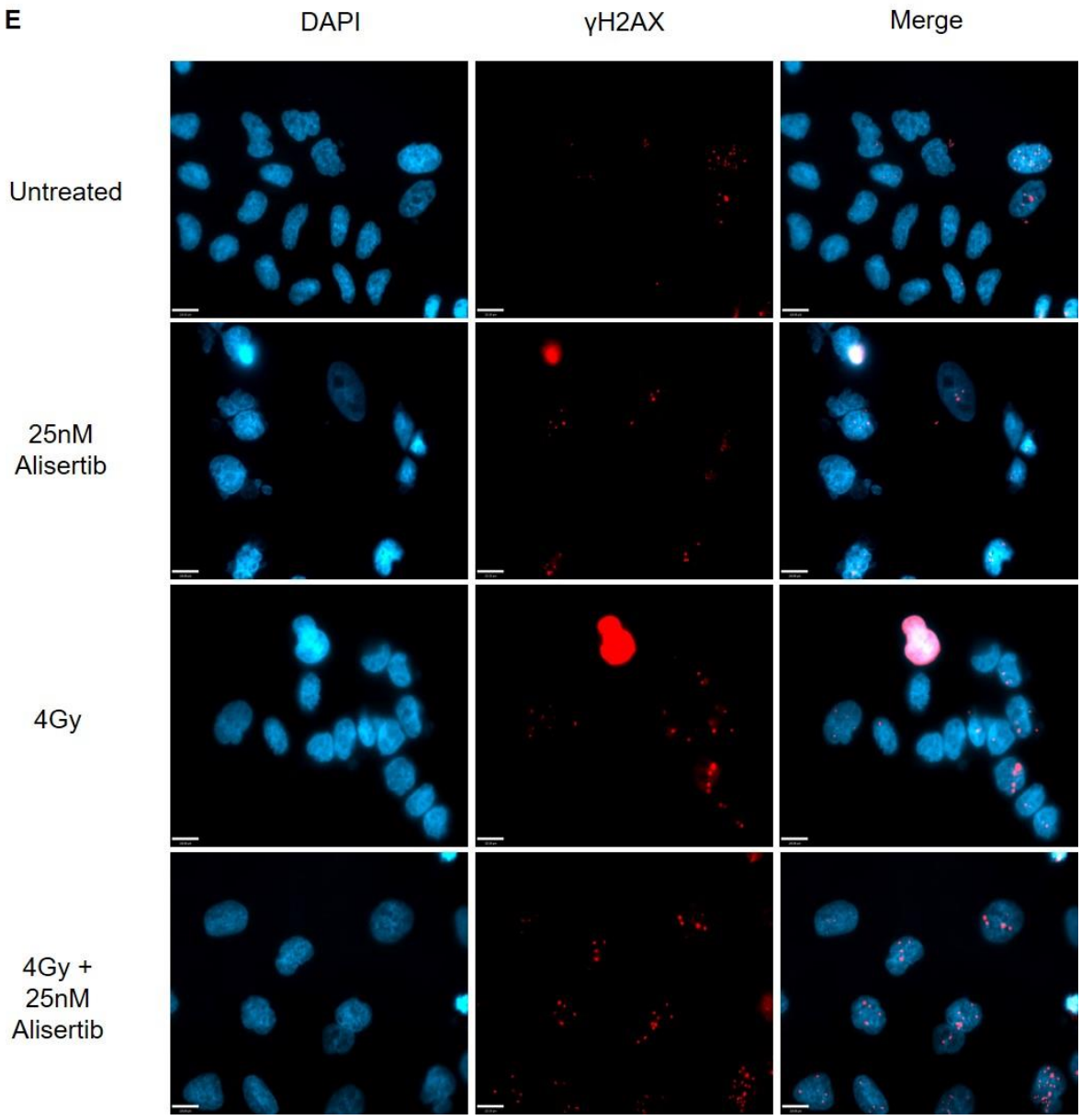

Figure 4.14. **Mean γH2AX foci formation and repair in H460 cells following treatment with 25 nM Alisertib, 4 Gy or combination. A.** Data points represent mean γH2AX foci per cell +/- SEM (N= 3). 100 cells counted per condition per repeat. Representative images of H460 cells stained for DAPI (cyan) and γH2AX (red) **B.** 15 minutes **C.** 1 hour **D.** 6 hours and **E.** 24 hours post-irradiation. Imaged with a 40x microscope objective, scale bars represent 120 μm

These data suggest that 25 nM Alisertib induced low levels of DNA damage but did not show any significant cooperative increases in damage when combined with IR at 15 minutes, 1 hour and 6 hours post-treatment. Additionally, there is limited evidence

of the repair kinetics of γH2AX foci being changed over time in 4 Gy + 25 nM Alisertib combination at these timepoints. This suggests that it is unlikely that general DNA damage repair is being significantly affected by the Alisertib IR combination. However, by 24 hours we see a trend for persistently increased residual DNA damage in cells treated with the Alisertib IR combination compared to IR alone. Although the effect size is small, the persistence of unrepaired DNA damage, especially DNA DSBs 24 hours post-IR has been related to IR efficacy (International Atomic Energy Agency 2010) and therefore could contribute to the therapeutic efficacy of Alisertib IR combination.

4.2.6.2. Alisertib IR combination does not affect the activation of Chk1 or Chk2 in H460 cells

In addition to γH2AX resolution, we sought to address if the modulators of p53 in response to DNA damage such as Chk1 and Chk2 were altered in cells treated with Alisertib IR combination. Chk2 is phosphorylated on T68 by ATM following DNA damage (Ahn *et al.* 2002) and promotes p53 stabilisation through S20 phosphorylation (Chehab *et al.* 2000) and inhibition of destabilising interaction with MDMX (Chen *et al.* 2005). Chk1 is a kinase phosphorylated on S345 after DNA damage which has been shown to promote Chk1 coupling with p53 and subsequent cell cycle arrest (Tian *et al.* 2002). Given this, we examined activating phosphorylation of Chk1 and Chk2 following Alisertib IR combination in p53 proficient H460 cells 1 hour and 4 hours post-IR.

As expected, 4 Gy of irradiation strongly induced p-Chk1 (S345) and p-Chk2 (T68) 1 and 4 hours post-irradiation in H460 cells (see Figure 4.15). There was an increase observed in S345 p-Chk1 expression in combination treatment but this was not

reproduced across two independent repeats. T68 p-Chk2 expression did not differ between 4 Gy and 4 Gy + 25 nM Alisertib conditions at any timepoint. This suggested that in the initial hours post-treatment that Chk1 and Chk2 activation was not consistently differentially affected in the combinational treatment arm in H460 cells.

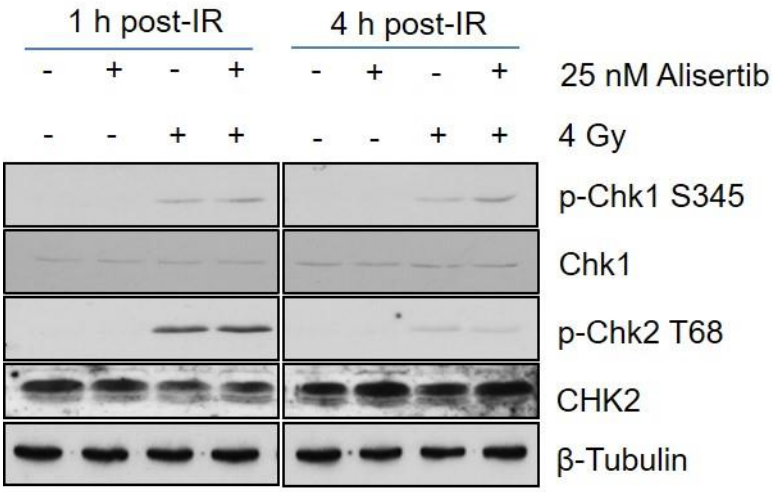

Figure 4.15. **Assessment of p-Chk1 (S345), Chk1, p-Chk2 (T68) and Chk2 expression 1 hour and 4 hours post-treatment in H460 cells.** Representative western blot results for p-p53 (S15), p53, p-Chk1 (S345), Chk1, p-Chk2 (T68), Chk2 and β-tubulin expression 1h and 4h post-treatment in H460 cells (N= 2).

4.2.6.3. p53 phosphorylation following Alisertib IR combination in H460 cells

Given that we observe Alisertib IR combinational effect in a p53-dependent manner in NSCLC cell lines, we hypothesised that p53 could be subject to differential phosphorylation patterns in cells treated with Alisertib IR combination. The stability and function of the transcription factor p53 is affected by post-translational modification of over 40 different amino acids (Gu and Zhu 2012). Under cellular stress, such as DNA damage, p53 is phosphorylated on several residues generally serving to promote the stabilisation of p53 through inhibition of its interaction with its

negative regulator MDM2 (Gu and Zhu 2012). The phosphorylation of different residues on p53, whilst achieving a common goal of p53 stabilisation, can have effects on the specific function of p53 (Gu and Zhu 2012). Furthermore, AURKA directly phosphorylates p53 on S315 (Katayama *et al.* 2004), S215 (Liu *et al.* 2005) and S106 (Hsueh *et al.* 2013) with contrasting effects on p53 stability.

We tested this hypothesis 1 hour and 4 hours post-treatment, as with Chk1/2, and later at 24 hours post-treatment in protein lysates from the p53 proficient H460 cell line. These timepoints of measurement were used because changes in p53 phosphorylation can occur within the first four hours of irradiation (Boehme *et al.* 2008) whilst mitotic effects after Alisertib IR combination in the H460 cells were observed 24 hours post-irradiation.

There was a biphasic p53-based response to Alisertib IR combination in H460 cells (see Figure 4.16). p53 expression was initially increased, likely through stabilisation, 1 and 4 hours post-treatment in all irradiated conditions with notable phosphorylation of S15, S9 and S20 at these times. Conversely, p53 expression was increased in the 25 nM Alisertib alone condition at 24 hours, with low level increases in S15, S9 and S20 phosphorylation being seen.

This suggests that IR has a more pronounced effect on p53 expression and phosphorylation in the initial hours after irradiation whilst Alisertib alone has more of an effect on p53 expression and phosphorylation only upon prolonged exposure.

T18 phosphorylation of p53 was detected 4 hours post-irradiation in the 25 nM Alisertib condition but this was greatly reduced in the 4 Gy + 25 nM Alisertib condition at the same timepoint. This suggests that T18 phosphorylation was inhibited when combining IR and Alisertib treatment. The only detectable difference

between IR and Alisertib IR combination that could not be accounted for by expression of total p53 was S15 phosphorylation 24 hours post-treatment which was increased in Alisertib IR combination.

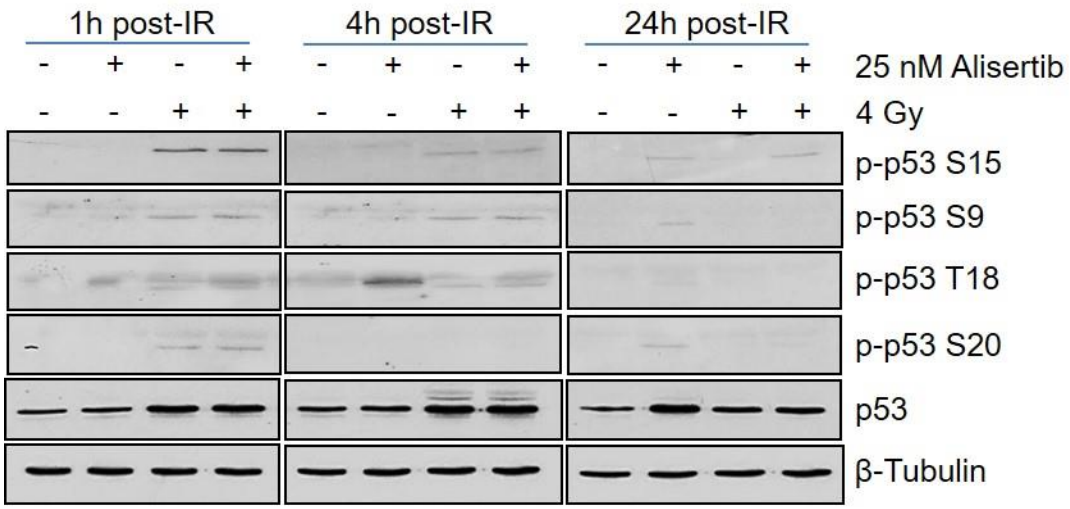

Figure 4.16. **Assessment of p-p53 (S15, S9, T18, S20) and p53 1h, 4h and 24h post-treatment in H460 cells.** Representative western blot results for p-p53 (S15, S9, T18, S20), p53 and β-tubulin expression 1h, 4h and 24h post-treatment in H460 cells (N=2).

These data firstly suggest that there is a biphasic p53-based response to Alisertib IR combination in H460 cells. p53 protein levels are initially increased, likely through stabilisation, 1 and 4 hours post-treatment in irradiated conditions with notable stabilising phosphorylation of S15, S9 and S20 respectively. This is in line with what is reported (Meek 1998; Hofmann *et al.* 2001) and is likely a response to DNA damage. Conversely, p53 expression was increased most in the 25 nM Alisertib alone condition at 24 hours, with low levels of S15, S9 and S20 phosphorylation being seen. However, S9 and S20 phosphorylation of p53 was not apparent in 4 Gy + 25 nM Alisertib condition at 24 hours post-IR perhaps due to reduced expression of total p53 or cell cycle/survival changes. Interestingly, 4 hours post-treatment we see robust and reproducible phosphorylation of T18 of p53 by 25 nM Alisertib treatment

alone, but not in combination treatment. T18 phosphorylation of p53 has been shown to occur after disruption of the mitotic spindles through Mps1 interaction (Huang *et al.* 2009), a component of the SAC, and inhibits the destabilising interaction between p53 and MDM2 (Schon *et al.* 2002). This could suggest that there is differential engagement of the SAC following Alisertib IR combination, compared to Alisertib alone. Alternatively, the H460 mitotic population may be reduced by IR as early as 4 hours post-treatment and lack of T18 phosphorylation in the combination treatment maybe reflective of cell cycle dynamics/cell death.

4.2.7. Alisertib IR combination leads to de-phosphorylation of Akt in H460 cells

Akt is a protein kinase that is able to act upstream of p53, is constitutively active in NSCLC, and can promote cell survival and resistance to chemotherapy and radiation (Brognard *et al.* 2001). Additionally, Akt has been shown to be activated by AURKA *in vitro* and ectopic overexpression of AURKA contributed to resistance to Cisplatin, Etoposide, Doxorubicin and Paclitaxel in p53 proficient-only ovarian cancer cells (H. Yang *et al.* 2006). This mechanism was subsequently shown to be through AURKA mediated inhibition of PTEN expression (Gritsko *et al.* 2003), which when induced by p53 negatively regulates activating phosphorylation of Akt (Stambolic *et al.* 2001). These data align with our demonstration of dependency on wildtype p53 expression for combinational effect of Alisertib IR in NSCLC cell lines.

Consequently, we hypothesised that when we performed the converse, AURKA inhibition rather than overexpression, in NSCLC cells that we may see decrease in Akt activation and an increase in PTEN expression. And furthermore, we hypothesised that decrease in Akt activation and increase in PTEN expression would be greater in Alisertib IR condition than either agent alone. Because Akt is activated

by phosphorylation of threonine 308 and phosphorylation of serine 473 via phosphoinositide 3-kinase (PI3K) signalling pathways (Persad *et al.* 2001) we used S473 p-Akt as a surrogate marker for active Akt. We tested this hypothesis 1 hour, 4 hours and 24 hours post-treatment in protein lysates from the p53 proficient H460 cell line. These timepoints of measurement were used because p53, the positive regulator of PTEN expression, stabilised within the first four hours of irradiation whilst potentially pro-apoptotic mitotic aberrations after Alisertib IR combination were observed 24 hours post-irradiation.

We found that 1 hour post-irradiation there was a trend for reduced expression of S473 p-Akt in all treatment conditions compared to control, but this was only statistically significant in the 4 Gy + 25 nM Alisertib condition ($p= 0.023$ (One-way ANOVA)) (see Figure 4.17). There was increased reduction in S473 p-Akt expression in the 4 Gy + 25 nM Alisertib condition, but this effect was less than additive and was not statistically significant when compared to either 25 nM Alisertib or 4 Gy alone conditions ($p= 0.295$ and $p= 0.263$ (One-way ANOVA)). There was no observable change in PTEN expression at any timepoint.

4 hours post-irradiation a similar trend was observed with statistical reduction in S473 p-Akt expression in the 25 nM Alisertib, 4 Gy and 4 Gy + 25 nM Alisertib conditions compared to control ($p= 0.0026$, $p= 0.0009$ and $p= 0.0001$ (One-way ANOVA)) (see Figure 4.17). There was increased reduction in S473 p-Akt expression in the 4 Gy + 25 nM Alisertib condition that was less than additive but statistically significant when compared to either 25 nM Alisertib or 4 Gy alone conditions ($p= 0.002$ and $p= 0.006$ (One-way ANOVA)).

By 24 hours post-irradiation in H460 cells there was a reduction in S473 p-Akt expression in the 25 nM Alisertib, 4 Gy and 4 Gy + 25 nM Alisertib conditions, each with statistical significance when compared to control ($p= 0.0047$, $p= 0.0031$ and $p= <0.0001$ (One-way ANOVA)) (see Figure 4.17). There was increased reduction in S473 p-Akt expression in the 4 Gy + 25 nM Alisertib condition that was greater than additive and statistically significant when compared to either 25 nM Alisertib or 4 Gy alone conditions ($p= 0.0009$ and $p= 0.0013$ (One-way ANOVA)).

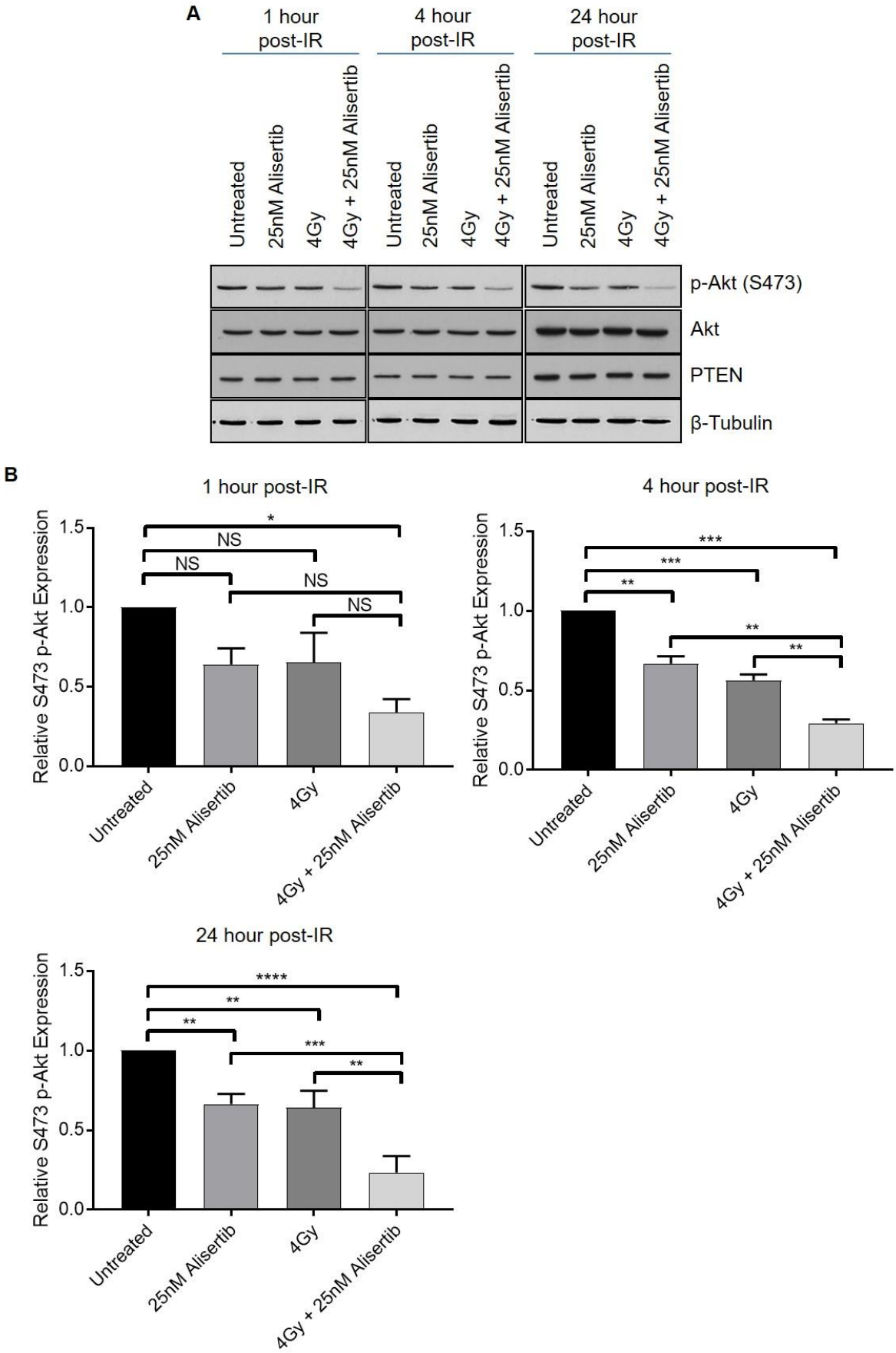

Figure 4.17. **Assessment of p-Akt (S473), Akt, and PTEN expression 1, 4 and 24 hours post-treatment in H460 cells.** Legend overleaf.

Figure 4.17. **Assessment of p-Akt (S473), Akt, and PTEN expression 1, 4 and 24 hours post-treatment in H460 cells. A.** Representative western blot results for p-Akt (S473), Akt, PTEN and β-tubulin expression 1, 4 and 24 hours post-treatment in H460 cells. **B.** Quantification of S473 p-Akt expression 1, 4 and 24 hours post-treatment in H460 cells normalised to total Akt levels and adjusted for loading variation with β-tubulin (N= ≥2). Data points represent mean expression relative to untreated control +/- SD. NS (non-statistically significant) denotes p= >0.05, * denotes p= ≤0.05, ** denotes p= ≤0.01, *** denotes p=≤0.001 (One-way ANOVA with Dunnett correction for multiple comparisons).

These data suggest that Alisertib IR combination cooperated to reduce S473 p-Akt expression. Given that activated Akt is a well-established anti-apoptotic factor in NSCLC (Fumarola *et al.* 2014), this could indicate that the equilibrium between cell survival and apoptosis could be cooperatively shifted towards apoptosis by Alisertib IR combination in NSCLC.

4.3. Discussion

Here we present data indicating that cell cycle progression is altered in NSCLC cells treated with Alisertib IR combination. Furthermore, we show this cell cycle effect differs in NSCLC cells that are radiosensitised by Alisertib IR combination compared to NSCLC cells that do not show radiosensitisation suggesting a dependency on p53. In p53 proficient cells treated with Alisertib IR combination we see mitotic aberrance that results in mitotic catastrophe and senescence, whilst in p53 deficient cells we see greater polyploidy with less cell death and senescence. We also show that Alisertib IR combination does not significantly alter resolution of DNA damage but may promote persistence of residual DNA damage 24 hours post-treatment. Additionally, p53 is subject to biphasic stabilisation following Alisertib IR combination but we do not find any significant change in the activation of DNA damage checkpoint proteins. Lastly, we find cooperative reduction in activated Akt expression

following Alisertib IR combination in NSCLC cells which may promote cell death, again suggesting that the role of p53 is to skew the cellular response towards mitotic death and senescence.

4.3.1. Alisertib IR combination is associated with mitotic cell loss in p53 proficient NSCLC cells but not in p53 deficient cells which show increased polyploidy basally and following Alisertib IR combination

We present cell cycle data, in both a NSCLC cell line panel and in p53 depleted H460 cells that p53 proficient cell lines show mitotic loss by 48 hours post-treatment with both IR alone and Alisertib IR combination, whilst p53 deficiency attenuates this loss of mitotic population. This suggests that AURKA is important in p53 proficient cells. This is counter-intuitive given a range of literature which show that p53 deficiency promotes death by mitotic catastrophe when targeting the mitotic machinery as G2-M checkpoint integrity is compromised (Bunz *et al.* 1998) meaning cells aberrantly enter mitosis (Marxer *et al.* 2013), even in the presence of DNA damage (Nitta *et al.* 2004; Jurvansuu *et al.* 2007). However, we did not find any difference in G2 population in p53 proficient and p53 deficient cell lines 24 and 48 hours post-treatment (data not shown). Indeed there are intra-mitotic functions for p53 including regulation of centrosomal biology (Fukasawa *et al.* 1996) and there is evidence of cooperation between BubR1 and p53, a member of the SAC machinery, to eliminate cells with amplified centrosomes (Oikawa *et al.* 2005). Furthermore, centrosomal amplification has been shown to promote caspase 2 activation, which in turn promotes p53 stabilisation (Fava *et al.* 2017). This coupled with our data that Alisertib IR combination increases centrosomal amplification in H460 mitotic cells, both alone and in combination with centrosomal fragmentation, could explain the difference in mitotic cell populations in p53 proficient and p53 deficient NSCLC cells

following Alisertib IR combination. It is possible that the levels of intra-mitotic death seen in H460 cells by live cell imaging are related to p53-regulated clearance of cells with amplified centrosomes. If so, it would be interesting to investigate if p53 deficient models of NSCLC exhibit differential amounts of intra-mitotic death compared to p53 proficient models following Alisertib IR combination.

Additionally, we show that Alisertib IR combination cooperates to increase the polyploid population in NSCLC cells and that p53 deficiency is permissive for both increased basal polypoid population and increased polyploidy following Alisertib IR combination compared to p53 proficient cells. This provides further evidence that the mitotic process is aberrant in NSCLC cells treated with Alisertib IR combination as polyploidy arises from abortive mitoses (Storchova and Pellman 2004). Furthermore, this suggests that the induction of polyploidy and relative elimination of polyploid cells may be related to the radiosensitising effect of Alisertib IR combination in NSCLC. There is evidence that p53 deficiency is permissive for polyploidy to occur (Vitale *et al.* 2010; Kurinna *et al.* 2013) and that p53 regulates a post-mitotic checkpoint that arrests and promotes apoptosis in tetraploid cells in G1 (Lanni and Jacks 1998; Andreassen *et al.* 2001; Huang *et al.* 2009). There is also evidence escape of polyploid p53 deficient cancer cells from post-mitotic checkpoint following aberrant mitosis post-IR (Erenpreisa *et al.* 2008). Given this, it is a possibility that polyploidy following Alisertib IR combination may lead to differential outcomes depending on p53 status and therefore could explain combinational efficacy. Alternatively, there is also a possibility that mitotic elimination after Alisertib IR combination in p53 proficient NSCLC cells, and lack of in p53 deficient cells, may be related to differences in polyploidy, in that fewer aberrant mitotic cells in p53 proficient cells survive mitosis to form polyploid progeny. It would be interesting to

perform synchronisation studies in p53 proficient and p53 deficient NSCLC models to delineate if mitotic progression or if post-mitotic checkpoint function is more important in determining Alisertib IR combinational outcome.

4.3.2. Alisertib IR combination is associated with aberrant mitotic phenotype

We show that the Alisertib IR combination cooperated to increase time in mitosis, intra-mitotic death and aberrant mitoses (>2 daughters) at 24-36 hours post-treatment but not at 48-62 hours post-treatment. In contrast, we show that by 48-62 hours post-treatment there was a trend for increased aberrant mitoses but time in mitosis and intra-mitotic death was similar to Alisertib alone. This supports 24 hours post-treatment as the critical phase of Alisertib IR combinational effect in line with our previous dose-scheduling data. Increased time in mitosis is suggestive of delay in mitotic progression and potentially implicates the SAC which promotes mitotic delay in the presence of mitotic aberration or DNA damage (Silva *et al.* 2011). Increased intra-mitotic death implicates mitotic catastrophe as the mode of cell death following Alisertib IR combination treatment (Vitale *et al.* 2011), although we see general increases in micronuclei formation and multinucleation in H460 and H1299 cells which respond differently via clonogenic assay. Increasing aberrant mitoses following Alisertib IR combination further implicates mitotic processes as the target of this treatment combination and complements our cell cycle and mitotic phenotype data.

We also present that Alisertib IR combination cooperates to promote centrosomal aberration, especially in the case of centrosomal amplification alone or in combination with pericentrin fragmentation. This is unsurprising given that AURKA functions in establishing centrosome homeostasis (Katayama *et al.* 2012) and

Alisertib treatment has previously been shown to increase multipolar mitoses which can result from centrosomal amplification (Asteriti *et al.* 2014). IR alone has also been shown to promote centrosomal amplification (Dodson *et al.* 2004). This may explain increased aberrant mitoses with >2 daughter cells seen after Alisertib IR combination as centrosomal amplification has been shown to promote multipolar mitosis (Vitale *et al.* 2011). Furthermore, recent evidence suggests that AURKA function is required for centrosome clustering in cells with >2 centrosomes, allowing bipolar division and progeny with capacity to undergo further cell divisions (Navarro-Serer *et al.* 2019). Inhibition of AURKA activity was associated with increased proportion of multipolar mitoses and mitotic catastrophe in cells with centrosomal amplification (Navarro-Serer *et al.* 2019). This could explain why we see increased rates of aberrant mitoses by live cell imaging which result in >2 daughter cells after Alisertib IR combination. It would be interesting to see if this was a consistent effect in both p53 proficient and p53 deficient NSCLC cell lines and if the fate of cells with amplified centrosomes was p53-dependent as observed by Fava *et al* (2017). Furthermore, DNA damage induced centrosome amplification has been shown to be Chk1-dependent (Bourke *et al.* 2007), it would be interesting to see if centrosomal amplification mediated Alisertib IR combinational effect and could be attenuated with Chk1 inhibition.

We also find that mitotic phase distribution is altered following treatment with Alisertib IR combination with H460 cells showing cooperative increase in anaphase population and fewer cells undergoing cytokinesis. This is interesting as it suggests that the SAC has either not been activated, or that the SAC has been unsuccessful in preventing mitotic progression in cells treated with Alisertib IR combination. Indeed, there is evidence that AURKA is required for maintenance of SAC function in

pro-metaphase and that AURKA inhibition with Alisertib in prometaphase inhibits SAC function (Courtheoux *et al.* 2018). Interestingly, IR has been shown to cause activation of the SAC in multipolar mitoses but that these cells can, following mitotic delay, satisfy the SAC and progress into anaphase despite significant mitotic aberrance (Dodson *et al.* 2007). This suggests that multipolar cells, following IR, can escape SAC-induced block on metaphase anaphase transition. Anaphase-telophase transition occurs when the segregated chromosomes decondense and the nuclear envelope begins to reform (Afonso *et al.* 2014). There is evidence that AURKA is required for assembly of the central spindle during anaphase (Lioutas and Vernos 2013; Reboutier *et al.* 2013; Courthéoux *et al.* 2019). Here depletion of AURKA caused defect in anaphase progression, completely inhibited telophase and cytokinesis and resulted in binucleated cells (Reboutier *et al.* 2013) which we also observed after Alisertib IR combination. Furthermore IR can perturb anaphase progression, which results in death or post-mitotic arrest in a p53-dependent manner (Redpath *et al.* 2003). It is possible that AURKA inhibition and IR cooperate to inhibit anaphase progression. Interestingly, AURKA-dependent centrosome clustering for bipolar division in the presence of centrosomal amplification can affect anaphase progression (Navarro-Serer *et al.* 2019) and therefore it is possible that centrosomal aberration in the absence of AURKA activity may be linked to lack of anaphase resolution. Furthermore, mitotic slippage may occur after extensive block on mitotic progression (Brito and Rieder 2006), and cellular fate following slippage could determine Alisertib IR combinational efficacy. It would be useful to see if anaphase is also targeted by Alisertib IR combination in p53 deficient NSCLC cell lines.

4.3.3. Alisertib IR combination is associated with increased in mitotic catastrophe and senescence in NSCLC cells

We show that Alisertib IR combination leads to an increase in mitotic catastrophe in both p53 proficient and p53 deficient NSCLC cells. Mitotic catastrophe results in micronuclei formation or multinucleated cells (Vitale *et al.* 2011), which is corroborated by our findings that polyploidy is increased by Alisertib IR combination. Also, mitotic catastrophe has been shown to occur following perturbation of the mitotic machinery (Vitale *et al.* 2011), including centrosomal amplification (Dodson *et al.* 2007). Given that we see increased centrosomal amplification, alone or in combination with pericentrin fragmentation, in NSCLC cells treated with Alisertib IR combination, it is possible that this contributes to the mitotic catastrophe and polyploidy observed. Additionally, mitotic catastrophe has been shown to occur after perturbation of the mitotic spindles (Roninson et al. 2001), of which function and polymerisation during mitosis is intimately linked to AURKA function (Kinoshita et al. 2005). Whilst we did not assess spindle morphology and function here there is evidence that Alisertib alone (Manfredi *et al.* 2011) and IR alone (P. Li *et al.* 2014) can affect the mitotic spindle. Moreover, centrosomal amplification can result in multipolar mitotic spindle formation (Dodson *et al.* 2007), meaning that is it likely that Alisertib IR combination also affects mitotic spindle function. Interestingly, we find that the proportion of cells bearing micronuclei after Alisertib IR combination was increased in the p53 deficient H1299 cell line, whilst micronuclei in combination with multinucleation was greater in the H460 cell line. Micronuclei may form after incomplete DNA synthesis following IR (Obe *et al.* 1975) or aberrant chromosomal segregation (Vitale *et al.* 2011) whilst multinucleation is an outcome of multipolar or abortive mitosis (Vitale *et al.* 2011). It is unclear if this discrepancy is both consistent

in p53 proficient and deficient NSCLC cell lines and significant in determining Alisertib IR combinational outcome. However, we are confident that Alisertib IR combination causes an increase in mitotic catastrophe markers irrelevant of p53 status and we hypothesise that differential clonogenic response to Alisertib IR combination could be due to differential population response to the same stimulus of mitotic aberration. Given that Alisertib dosing has been shown to be well tolerated once a day for up to 21 days *in vivo* (Palani *et al.* 2013), it would be interesting to see if continuous redosing of Alisertib with irradiation could push p53 deficient NSCLC populations towards a state of aberration that is not compatible with survival.

We also see increased proportion of senescent cells following Alisertib IR combination in both p53 proficient NSCLC cells. Mitotic catastrophe can result in cellular senescence (Vitale *et al.* 2011) and therefore proportions of mitotic catastrophe and senescence seen here could be linked. We did not see induction of further senescence following Alisertib IR combination in p53 deficient H1299 cells compared to IR alone, unlike in the p53 proficient H460 cells, suggesting that induction of senescence may determine the therapeutic efficacy of Alisertib IR combination. Wildtype p53 expression has been shown to be critical for the induction of genotoxic stress-induced senescence (Qian and Chen 2013). Evidence suggests that replicative senescence, distinct from genotoxic stress-induced senescence, is reversible through p53 inactivation (Beauséjour *et al.* 2003; Dirac and Bernards 2003). It is possible that the robustness of senescence induced by Alisertib IR combination could be affected by p53 expression status.

4.3.4. Alisertib IR combination showed trend for increased γ-H2AX foci per cell 24 hours post-treatment

We show that DNA damage resolution using number of γH2AX foci per cell as a surrogate marker of damage following IR is not significantly affected by the addition of Alisertib at 15 minutes, 1 hour and 6 hours post-treatment. However, we see a consistent trend for increased residual DNA damage in the treatment combination, but not IR alone, by 24 hours post-treatment. This suggests that whilst the Alisertib IR combination did not significantly affect the majority of DNA repair, a subset of damage was less likely to be repaired. Unrepaired DNA 24 hours post-IR is understood to be therapeutically significant (International Atomic Energy Agency 2010) and therefore could, at least partially, explain the efficacy of Alisertib IR combination. However, given that we see that radiosensitisation can occur with the addition of Alisertib 24 hours post-irradiation, when most of the DNA damage after IR alone is repaired, it is unlikely that changes to DNA repair are critical mechanistically. It would be interesting to assess the relative repair pathway usage in cells treated with Alisertib IR combination. Sun *et al* (2014) found that targeting AURKA caused statistically more γH2AX foci to be present in combination with IR at 6 hours post-irradiation, and our data follows a similar non-significant trend. However, we did not see evidence of Chk1 or Chk2 expression changes upon targeting AURKA. These discrepancies may be explained by usage of different irradiation doses and the mechanistic differences between AURKA depletion and pharmacological inhibition of AURKA with Alisertib.

4.3.5. p53 is subject to biphasic stabilisation following Alisertib IR combination

We show that p53 expression is increased by 1 and 4 hours post-treatment with IR or Alisertib IR combination, whilst by 24 hours post-treatment p53 is stabilised by 25 nM Alisertib alone but not in 4 Gy + 25 nM Alisertib. This trend was also illustrated by p53 phosphorylation at S9 and S20 which was induced by IR at 1 and 4 hours post-treatment, but was not at 24 hours, whilst the opposite was true in 25 nM Alisertib condition. Given that S9 and S20 have been shown to promote stabilisation of p53 (Meek 1998; Hofmann *et al.* 2001), correlation of p53 expression in combination with S9 and S20 phosphorylation is as expected. This suggests that IR-induced p53 response is dominant in the initial hours post-IR, and Alisertib induces a p53 response in the later recovery period post-IR. Furthermore, IR-induced p53 response which wains by 24 hours post-treatment dominates in the Alisertib IR combination and may explain differential p53 expression by 24 hours. S15 p-p53 expression on the other hand was expressed after IR at 1 and 4 hours post-treatment, and in both Alisertib containing conditions at 24 hours. Furthermore, S15 p-p53 expression 24 hours post-treatment with Alisertib IR combination could not be accounted for by total p53 changes. S15 phosphorylation of p53 is reported to occur after DNA damage through ATM or DNA PK, serves to promote p53 stabilisation and is partially required for the induction p53-dependent apoptosis (Cheng and Chen 2010). It is possible that continued S15 phosphorylation of p53 24 hours post-treatment with Alisertib IR combination could be related to the residual DNA damage we observe (Wittlinger *et al.* 2007).

Interestingly, we see T18 phosphorylation of p53 4 hours following Alisertib treatment but not following Alisertib combination. T18 phosphorylation has been shown to occur through Mps1, a member of the SAC, and allows p53 to mediate a

post-mitotic checkpoint which promotes G1 arrest and apoptosis in cells undergoing mitotic slippage (Huang *et al.* 2009). This potentially indicates that Alisertib treatment is inducing activation of the SAC and mitotic slippage in H460 cells by 4 hours and suggests that, presumably through an IR dominant response on p53 and cell cycle progression, Alisertib IR combination does not induce SAC activation. This is counter-intuitive given that Alisertib mediated inhibition of AURKA in prometaphase has been shown to inactivate the SAC (Courtheoux *et al.* 2018), but may be related to different timepoints and dose of Alisertib used. A lack of SAC activation in the Alisertib IR combination treatment could explain why more cells are observed in anaphase by 24 hours post-treatment. However, we must consider how cell cycle distribution affects S9, S20 and T18 p-p53 expression, especially T18 p-p53 expression which is related to mitotic progression (Huang *et al.* 2009). It is possible that cell cycle distribution is affecting p53 modification and that an IR-dominant response to cell cycle distribution, as we see in H460 mitotic fraction by 48 hours contributes differential p53 stabilisation and phosphorylation. It would be useful to assess H460 cell cycle profile at 1 and 4 hours post-treatment with Alisertib IR combination to help assess if cell cycle distribution is misleading p53 expression data.

4.3.6. Alisertib IR combination causes dephosphorylation of Akt

Here we present data that show that Alisertib IR combination cooperatively reduces expression of S473 p-Akt in H460 cells 1, 4 and 24 hours post-treatment, although this effect did not appear to depend on PTEN stabilisation. Activated S473 p-Akt has been shown to promote cell survival through inhibition or reduction of pro-apoptotic factors (Yamaguchi and Wang 2001; J.-Y. Yang *et al.* 2006) and promotion of anti-apoptotic factors (Ozes *et al.* 1999; Hein *et al.* 2014). Furthermore, activated S473 p-

Akt has been shown to occur in NSCLC and promote cellular survival following IR (Brognard *et al.* 2001). Dephosphorylation of S473 on Akt has been associated with an upregulation of apoptotic markers (Itoh *et al.* 2002; Sun *et al.* 2004). Moreover, AURKA has also been shown to activate Akt in ovarian cancer cells (H. Yang *et al.* 2006). Therefore, it is plausible that combining Alisertib and IR, through targeting of Akt, causes a shift in the equilibrium towards p53-dependent apoptosis. This could explain why we see mitotic aberration in both p53 proficient and deficient NSCLC cell lines following Alisertib IR combination, but differential response via clonogenic assay. However, it remains unclear as to whether Akt dephosphorylation would occur prior to, or as a result of shift towards cell death. Interestingly, Akt has been shown to be required to recruit PTEN to the centrosomes, and Akt inhibition was associated with an increase in centrosomal amplification (Leonard *et al.* 2013). This opens the possibility that centrosomal, and thus mitotic, defects seen in Alisertib IR combination are through targeting of Akt. It would be interesting to see if Alisertib IR combinational efficacy was Akt-dependent.

4.3.7. Limitations

When investigating the p53-dependent effects of Alisertib IR combination on cell cycle progression we depleted p53 using siRNA in the p53 proficient H460 cell line. However, we found significant toxicity in the form of sub G1 peak in cells transfected with siRNA and co-treated with Alisertib, IR or both. This led to Alisertib having dominant effects on sub G1 peak and polyploidy and did not replicate the cooperativity between Alisertib and IR seen previously in non-transfected H460 cells. This indicated that this approach to investigate cell cycle changes was potentially not representative due to the combined toxicities of siRNA transfection and Alisertib or IR dosing. Leading on from this we investigated the efficacy of Alisertib IR

combination in a limited range of cell lines and used the H460 & H1299 cells as p53 proficient and p53 deficient models of NSCLC. This approach is hampered by the genetic differences that may exist between cell lines independent of p53 which may determine response to Alisertib IR combination. It would be useful to repeat these experiments in an isogenic system, such as the H1299 H24 cell line (Chen *et al.* 1996), to test the functional consequences of p53 proficiency and deficiency on Alisertib IR combination in a single genetic background. This system would be of particular use for assessment of intra-mitotic death, which has potential to be differential based upon genetic background (Oikawa *et al.* 2005).

Furthermore, here we demonstrate changes in ploidy through PI staining alone. PI staining with flow cytometric analysis as an indirect measure of ploidy is advantageous as large numbers of cells can be analysed quickly per sample (Darzynkiewicz 2010). However, as a DNA binding fluorochrome, PI staining properties can be influenced by changes to the chromatin structure which occur following treatment with DNA-interacting drugs or radiation (Darzynkiewicz 2010). Therefore, it would be useful to validate our findings with a secondary method of measuring ploidy such as direct assessment through metaphase spread analysis.

Here we use Alisertib to test effect of AURKA inhibition in combination with IR in NSCLC cell lines. It is reported that Alisertib is both the most specific and translationally relevant of the AURKA inhibitors (Malumbres and Pérez de Castro 2014). Additionally, using the 25 nM dose provides optimal on target AURKA effect with minimal off target AURKB effect according to our data. However, there is a risk that observed effects are through Alisertib specific or off target effects. It would be useful to confirm our mechanistic findings using different AURKA inhibitors or through AURKA depletion.

We investigated the effect of Alisertib IR combination on DNA repair using γH2AX foci per cell. Using γH2AX foci as a measure of DNA damage following IR however, whilst sensitive, is limited by also recognising single stranded DNA which can exist during DNA replication and repair and is an indirect measure of damage/damage resolution (Löbrich *et al.* 2010). Moreover, there is evidence that targeting of AURKA can result in a change in the relative contributions of different DNA repair pathways (Sourisseau et al. 2010; Sun et al. 2014; Wang et al. 2014). γH2AX foci staining does not appraise these shifts in pathway usage and therefore we cannot rule out that DNA damage repair is subject to alteration following Alisertib IR combination. It would be interesting to see if the relative contributions of DNA repair pathways were altered by Alisertib IR combination.

We used S473 p-Akt as a surrogate for Akt activity in the H460 cell line as it has been shown to be required in combination with T308 phosphorylation for Akt kinase activity *in vitro* (Alessi *et al.* 1997). There is also evidence that S473 p-Akt is a poor prognostic marker in NSCLC, indicating that this phosphorylation is functionally important (David *et al.* 2004). However, it has also been shown that T308 phosphorylation correlates better with Akt kinase activity when compared to S473 in NSCLC (Vincent *et al.* 2011). It may be useful to assess the effect of Alisertib IR combination on T308 p-Akt expression, to ensure that Akt activity is reduced following treatment.

5. Evaluation of Alisertib as a radiosensitising agent *in vivo*

5.1. Introduction, aims and hypotheses

In vitro assessment of Alisertib IR interaction provides proof of concept and indications of mechanism. Additionally, *in vitro* experiments are flexible and often amenable to high-throughput approaches, and hence have value in cancer research. However, these experiments are limited by the methodology of 2D cell culture which fails to recapitulate the 3D tumour microenvironment and its related selective pressures that are applied to cancer cells during their growth and treatment. For example, intra-tumoural hypoxia has been shown to occur in NSCLC (Le *et al.* 2006; Trinkaus *et al.* 2013), and has been associated with poor prognosis (Li *et al.* 2010) and worse radiotherapy response (Li *et al.* 2006). However, hypoxia does not occur in 2D cell culture without the use of specialised equipment. One approach to address this issue is to use murine models to assess lung cancer growth *in vivo*. We set out to use three *in vivo* models of NSCLC to assess whether Alisertib enhances IR response *in vivo*. Xenografts of either H460 or H1299 human NSCLC cell lines are used in immunocompromised CD-1 nude mice as model responders and non-responders of NSCLC to the Alisertib IR combination *in vitro*. Additionally, mouse LLC-1 cells are grown in immunocompetent C57Bl6 mice as a syngeneic model to consider any effect of an active immune system on Alisertib IR combination.

The aims of this chapter are to assess the following in *in vivo* mouse models of NSCLC:

1. The tolerability and efficacy of Alisertib treatment
2. The sensitivity of NSCLC *in vivo* models to radiation alone
3. The effect of combining Alisertib and IR treatment

4. The biological mechanism of Alisertib IR combinational effect

The hypotheses of this chapter are:

- Alisertib will enhance the radiation response of *in vivo* models of NSCLC
- Alisertib IR combination will target the mitotic population of NSCLC models *in vivo*

5.2. Results

5.2.1. Mouse LLC-1 cells show trend to respond to Alisertib IR combination *in vitro*

LLC-1 cells are p53 proficient (Wu *et al.* 2011) and are a sub-clone derived from the Lewis lung carcinoma cell line which originate from a primary mouse lung SCC (Bertram and Janik 1980). LLC-1 cells are commonly used with immunocompetent C57Bl6 mice as a syngeneic model of NSCLC (Kellar *et al.* 2015). To ensure that the model was suitable prior to *in vivo* testing, the IR enhancing effect of Alisertib was tested on LLC-1 cells *in vitro* using clonogenic survival assays. 25 nM Alisertib induced a mean DER of 1.23 at 20% survival fraction (see Figure 5.1.). Although extra sum of squares analysis revealed that the survival curves for irradiation alone compared to Alisertib irradiation combination in LLC-1 cells were best described by one curve (p= 0.076), this was likely due to the small sample size used (N=2). Encouragingly radiosensitisation was observed on each occasion tested.

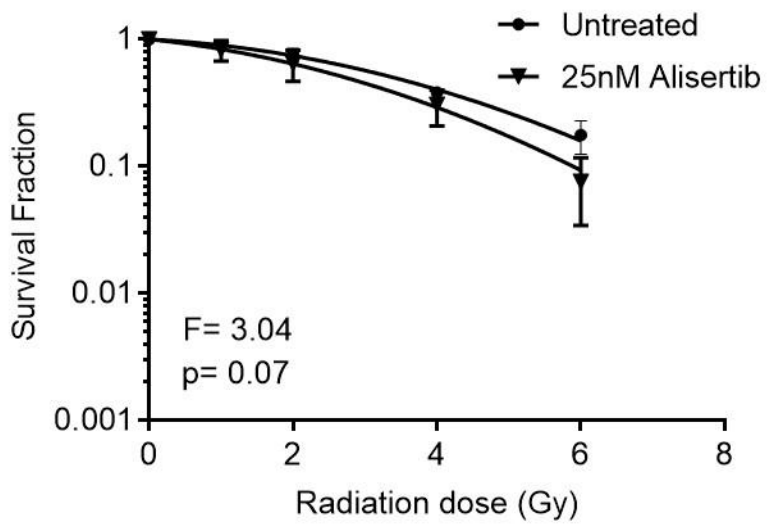

Figure 5.1. **Survival fraction LLC-1 cells after treatment with IR alone or IR in combination with 25 nM Alisertib.** Data points represent mean survival fraction normalised to unirradiated control +/- SD (N=2). F-value and p-value derived from extra sum of squares test.

Thus, co-treatment of LLC-1 *in vivo* was deemed an appropriate model data to assess immune effects that could contribute to the efficacy of the Alisertib IR combination.

5.2.2. Alisertib treatment via oral gavage for 10 consecutive days is well tolerated in both CD-1 nude and C57Bl6 mouse models

The tolerability of Alisertib given in suspension via oral gavage in non-tumour bearing CD-1 nude and C57Bl6 male mice was initially tested. It has been previously been shown that Alisertib treatment via oral gavage is tolerated up to 30 mg/kg once daily for 21 days in female CD-1 nude mice bearing subcutaneous HCT116 xenografts (Manfredi *et al.* 2011). It has also been shown that 98% of Alisertib is excreted by 24 hours post-treatment in mouse systems and therefore a once daily dosing schedule was justified with little risk of any drug accumulation (Palani *et al.* 2013). Here a similar but distinct dosing schedule of once daily for 10 consecutive

days in male CD-1 nude mice was tested. Additionally, the tolerability of Alisertib treatment was tested in the C57Bl6 mouse model as there is evidence that different mouse models can be inherently more or less sensitive to chemotherapeutic agents (Aston *et al.* 2017).

We performed a maximum tolerated dose (MTD) experiment sequentially testing 10 mg/kg Alisertib, then 20 mg/kg Alisertib and finally 40 mg/kg in CD-1 nude mice given once a day for 10 days. The dose was escalated in two independent mice once two mice of the prior lesser dose had successfully received 5 days consecutive of Alisertib (see Materials and Methods Table 2.6). Once the MTD was established in CD-1 model, the same dose of Alisertib with identical dosing schedule was tested in C57Bl6 mouse model. Tolerability of treatment was assessed with daily weighing of mice and checking of behaviour for signs of pain or distress (see Figure 5.2). Here doses up to 40 mg/kg Alisertib were tolerated once daily for 10 consecutive days in both CD-1 Nude and C57Bl6 having no effect on mouse weight.

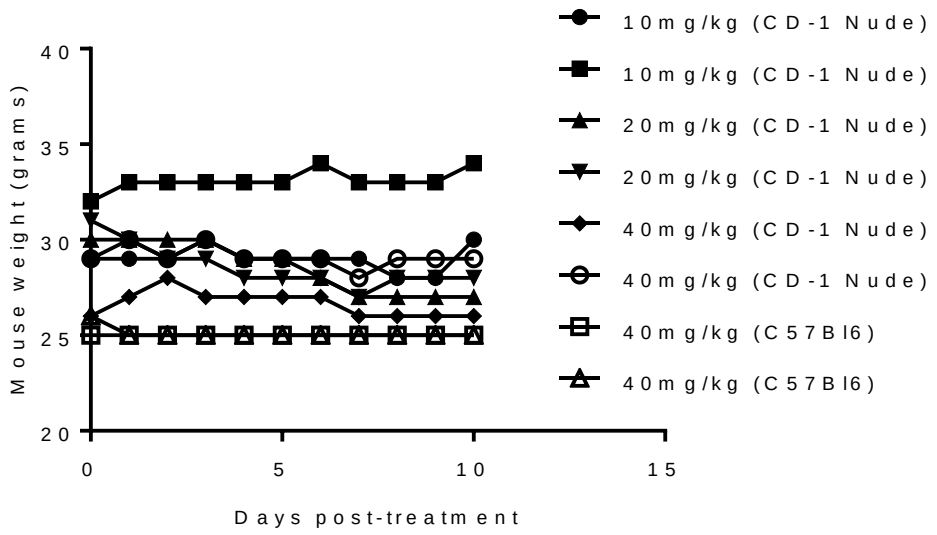

Figure 5.2. **Mouse weight following treatment with increasing doses of Alisertib once a day for 10 consecutive days.** Data points represent individual mouse weights and therefore no error is displayed. Note this experiment was performed entirely by Matthew Fisher.

5.2.3. Four Gy per day for 5 consecutive days causes moderate growth inhibition in H460 and H1299 xenografts but does not inhibit the growth of syngeneic LLC model

In order to test if Alisertib enhances radiation response in the H460, H1299 and LLC models *in vivo* a dose of radiation that causes moderate growth inhibition (20%≤ ≥50% growth inhibition) needed to be established. A dose of radiation too low may not have enough of a biological effect on the tumour to allow any potential combinational effects between Alisertib and radiation to occur. A dose of radiation too high could cause significant tumour growth inhibition and reduce the chance of observing any combinational effect. 20 Gy was given as 4 Gy fractions once a day for 5 days, 24-hours post the final fraction 32.65% and 17.01% mean growth inhibition was seen in H460 and H1299 xenografts respectively (see Figure 5.3 A-B). However, neither mean tumour volume seen was statistically significant (p= 0.099 and 0.255 respectively (Student's independent samples unpaired two-tailed t-test)) from the mean tumour volumes seen in the respective sham irradiated controls. On the other hand, by day 10 post-treatment 20 Gy had caused a mean growth inhibition of 31.78% (p= 0.079 (Student's independent samples unpaired two-tailed t-test)) in the H460 xenograft models and 27.59% (p= 0.127 (Student's independent samples unpaired two-tailed t-test)) in the H1299 xenograft models respectively. We therefore considered that this dosing schedule was adequate to induce a moderate effect and it was taken forward to the combination experiments.

Conversely 20 Gy given over 5 days had little effect on LLC syngeneic model growth rate, recording a mean growth inhibition of 5.14% 24 hours following final irradiation fraction (p= 0.715 (Student's independent samples unpaired two-tailed t-test)) (see Figure 5.3 C). Escalating the radiation dose to 40 Gy over 5 days in the LLC model

caused a mean growth inhibition of 26.93% (p= 0.372 (Student's independent samples unpaired two-tailed t-test)) (see Figure 5.3 D). However, there were problems with tumour ulceration in the LLC model with 2 out of 3 mice being culled after 48 hours of wet desquamation of the tumour after 4- and 12-days post-treatment respectively and this model was not taken forward on ethical grounds.

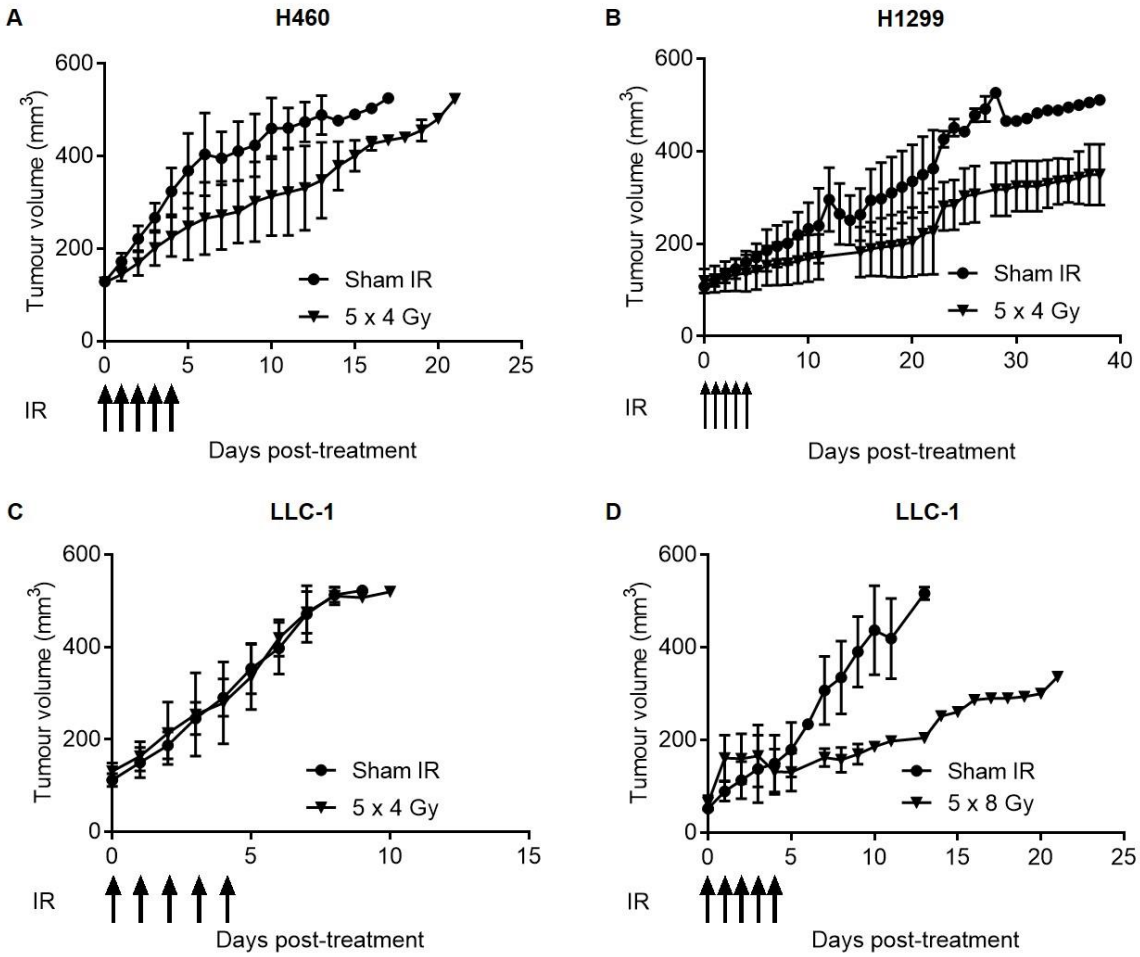

Figure 5.3. **Mean tumour volumes of A. H460 xenografts, B. H1299 xenografts, C. LLC-1 syngeneic models treated with sham irradiation or 20 Gy over 5 days and D. LLC-1 syngeneic models treated with sham irradiation of 40 Gy over 5 days.** Irradiations once a day on days 0-4 indicated by arrows. Data points represent mean tumour volume per condition +/- SD (sham irradiated H460 xenografts N=4, irradiated H460 xenografts N=3, sham irradiated H1299 xenografts N=5, irradiated H1299 N=4, both sham irradiated LLC-1 syngeneic model sets N=4, 20 Gy irradiated LLC-1 N=3 and 40 Gy irradiated LLC-1 N=3). Tumour volumes calculated using d1 x d2 x d3 x 0.52 calculation. Note that tumour implantation and dosing in this experiment was performed in collaboration with Matthew Fisher.

5.2.4. Five mg/kg Alisertib once daily for 10 consecutive days causes moderate growth inhibition in H460 xenografts and increases tumour mitotic fraction

Like radiation dose, the dose of Alisertib used *in vivo* in Alisertib IR combinational experiments should have moderate inhibition of growth with relevant biological effect and thus the dose of Alisertib used *in vivo* in combination with radiation required careful optimisation. This optimisation was performed in the H460 xenografts which more reliably engrafted CD-1 nude mice compared to the H1299 cell line.

There was a dose-dependent inhibition of H460 xenograft in CD-1 nude mice by oral Alisertib given once a day for 10 consecutive days (see Figure 5.4). By day 10, 24 hours after the final dosing event, there was a statistically significant growth inhibition of 47.57%, 61.09% and 70.77% with daily dosing of 5 mg/kg, 10 mg/kg and 20 mg/kg Alisertib respectively when compared to vehicle control ($p = <0.0001$, $p = <0.0001$ and $p = <0.0001$ respectively (One-way ANOVA)).

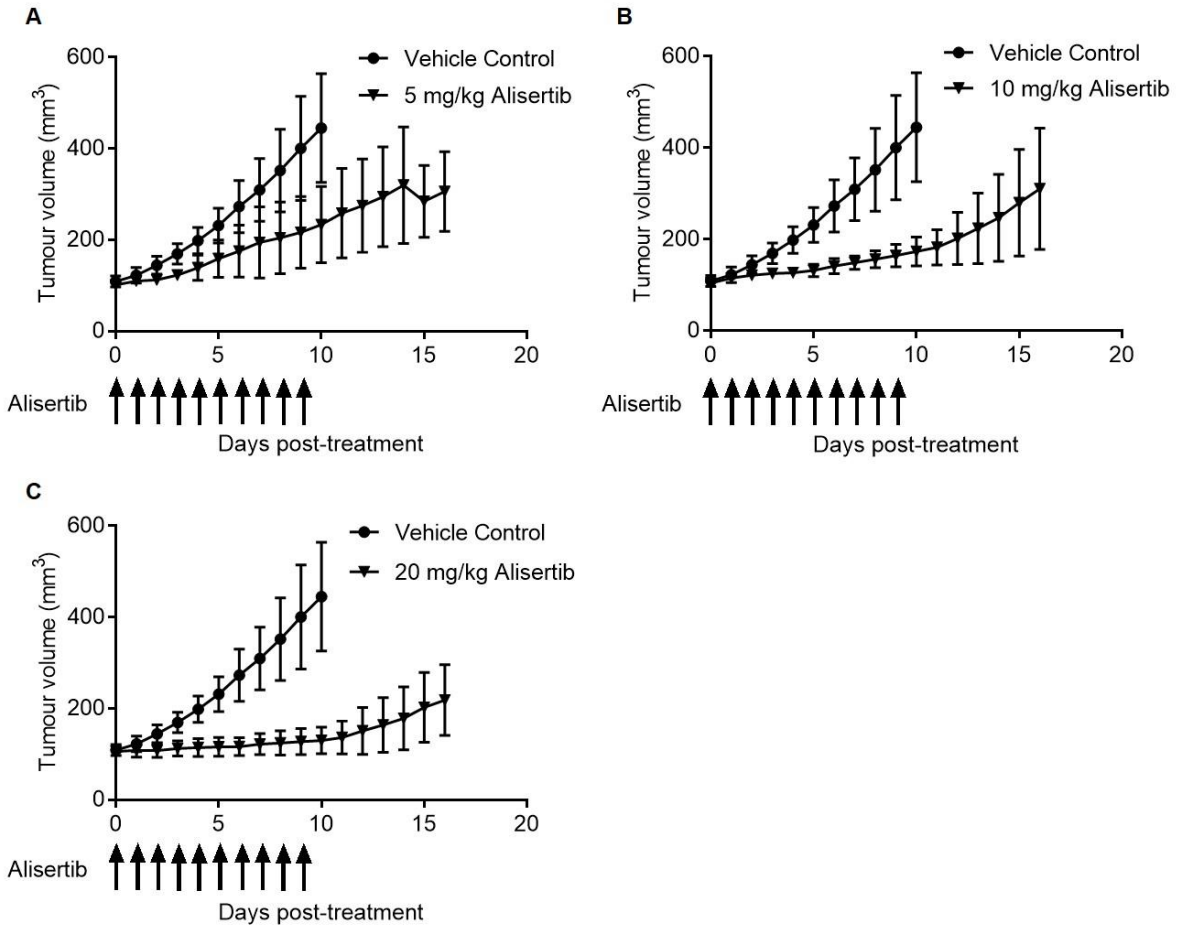

Figure 5.4. **Mean tumour volumes of H460 xenografts treated with vehicle control or A. 5 mg/kg Alisertib, B. 10 mg/kg Alisertib or C. 20 mg/kg Alisertib.** Dosing once per day on days 0-9 indicated by arrows. Data points represent mean tumour volume per condition +/- SD (all conditions N=4). Tumour volumes calculated using d1 x d2 x d3 x 0.52 calculation. Note that tumour implantation and animal dosing in this experiment was performed in collaboration with Matthew Fisher.

Alisertib has been shown to have a short half-life *in vivo* and approximately 98% of Alisertib is excreted by 24 hours post-treatment (Palani *et al.* 2013). Given this, to assess the immediate biological effect of Alisertib treatment, the CD-1 nude mice in the above experiment were also treated once with vehicle control or the relevant dose of Alisertib just prior to tumours hitting 500 mm^3 in volume or on day 16 of the experiment when mice were culled. The tumour tissues from these mice were then harvested 6-hours after the final dosing event. Alisertib treatment has previously

been shown to cause increases in mitotic fraction of xenograft tissues (Manfredi *et al.* 2011). Because of this, immunohistochemistry for p-Histone 3 (S10) was performed to establish the intra-tumour mitotic fraction to assess the biological effect of increasing Alisertib dose. Treatment with 5 mg/kg, 10 mg/kg and 20 mg/kg Alisertib all significantly increased the mitotic fraction in the viable regions of H460 xenograft tumours relative to vehicle control group ($p= 0.0386$, $p= <0.0001$ and $p= 0.0109$ respectively (One-way ANOVA)) (see Figure 5.5). 10 mg/kg Alisertib provided the greatest increase in mean mitotic fraction, followed by 20 mg/kg and then 5 mg/kg respectively. These response kinetics at 6 hours post-treatment are in line with previous findings in HCT116 xenograft models which identified a maximal increase in mitotic fraction with 3 mg/kg Alisertib by 4 hours, with 10 mg/kg Alisertib by 8 hours and a delayed response that peaked at 12 hours with 30 mg/kg Alisertib treatment (Manfredi *et al.* 2011). Furthermore, effects on mitotic fraction were likely to be due to terminal dosing event as opposed to any accumulative effects as 98% of Alisertib has been previously been shown to be eliminated from mouse systems after 24 hours (Palani *et al.* 2013).

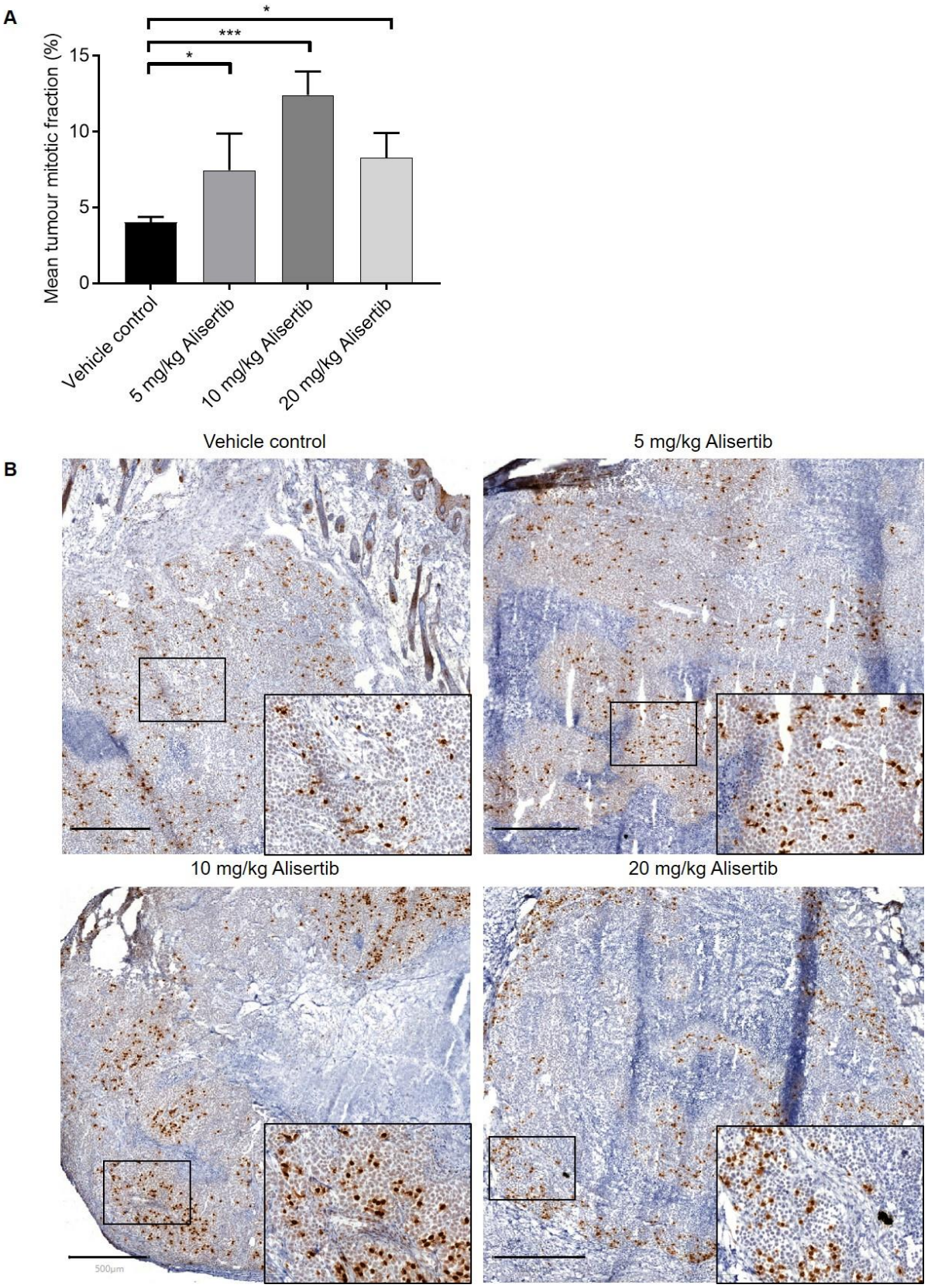

Figure 5.5. **H460 xenograft mitotic fractions 6 hours post-treatment with vehicle control or increasing doses of Alisertib.** Legend overleaf.

Figure 5.5. **H460 xenograft mitotic fractions 6 hours post-treatment with vehicle control or increasing doses of Alisertib. A**. Mean H460 xenograft mitotic fractions 6 hours post-treatment. Data points represent mean mitotic fraction per tumour per condition +/- SEM (N=4 for all conditions). * denotes p= ≤0.05, ** denotes p= ≤0.01, *** denotes p= ≤0.001 (One-way ANOVA with Dunnett correction for multiple comparisons). **B.** Representative H460 xenograft mitotic fraction examples 6-hours post-treatment with vehicle control, 5 mg/kg, 10 mg/kg and 20 mg/kg Alisertib. Mitotic cells stained brown with DAB, defined as positive for p-Histone 3 (S10). Mitotic fraction defined within viable regions of tumour as a percentage of cells present. 9 regions sampled per tumour. Images taken with a Pannoramic 250 Flash III slide scanner 20x objective. Area within the small rectangle is re-represented in image bottom right corner 10x larger. Scale bars represent 500 μm.

Together these indicated that 5 mg/kg Alisertib once daily for 10 consecutive days both had an intra-tumour biological effect and moderate tumour growth inhibition therefore this dose was taken forward for use in combination experiments.

5.2.5. Five mg/kg Alisertib given once daily for 10 consecutive days in combination with 20 Gy given in 5 equal fractions of 4 Gy over 5 days causes temporary regression in H460 xenografts with significant growth inhibition

In combination experiments cells were implanted and xenografts were allowed to grow to an approximate tumour size of 100 mm^3. Five mg/kg oral Alisertib was the given 1-hour prior to 4 Gy IR on 5 consecutive days (days 0-4). Following this 5 mg/kg daily Alisertib was continued for a further 5 days (days 6-10) before tumours were left to grow out to 800 mm^3 or to day 25 whichever came first.

The Shapiro-Wilk test revealed that there was no data skew at any timepoint in any condition indicating that One-way ANOVA comparisons were appropriate. Using the H460 xenograft model we found that at day four Alisertib alone or 5 fractions of 4 Gy alone induced a mean growth inhibition of 35.5% and 28.9% respectively when compared to control group (p= <0.0001 and p= <0.0001 (One-way ANOVA)) (see

Figure 5.6 A, C-D). Encouragingly the Alisertib IR combination had caused a mean tumour regression from 100 mm^3 treatment volume of 12.8% (p= <0.0001 (One-way ANOVA)).

By day 9, after 10 consecutive doses of 5 mg/kg Alisertib, Alisertib alone had induced a mean growth inhibition of 47.8% compared to control group (p= <0.0001 (One-way ANOVA)) (see Figure 5.6 A & C). IR alone also had induced a mean growth inhibition of 52.3% compared to control group (p= <0.0001 (Student's independent samples unpaired two-tailed t-test)). Alisertib IR combination had now caused a mean tumour regression from treatment volume of 40.7% (p= <0.0001 (One-way ANOVA)).

By day 14, 5 days following that last oral dosing of Alisertib, the sham IR + vehicle control group were nearing legal tumour volume limits or had already been culled (see Figure 5.6 A, C-D). At this timepoint the group receiving Alisertib alone showed mean tumour growth inhibition of 58.68% when compared to control group (p= <0.0001 (One-way ANOVA)). Additionally, the group receiving 20 Gy alone had a mean tumour growth inhibition of 62.94% when compared to control group (p= <0.0001 (One-way ANOVA)). Most excitingly the group treated with Alisertib IR combination had a mean tumour regression of 45.1% by day 14 (p= <0.0001 (One-way ANOVA)).

By day 25 mean tumour volume in the Alisertib treated group was like that of the Irradiation alone group at 628.5 mm^3 and 519.2 mm^3 respectively (see Figure 5.6 A, C-D). The mean tumour volume in the Alisertib IR combination group remained significantly reduced when compared to irradiation alone at 228.9 mm^3 (p= 0.003

(One-way ANOVA)). There was, however, evidence of tumour regrowth in the combination treatment group by day 25.

Mouse weight was measured weekly as a crude measure of health and there was no indication of weight loss after treatment with Alisertib, 20 Gy or Alisertib + 20 Gy combination (see Figure 5.6 B). This suggested that Alisertib was tolerated as both a monotherapy and in combination with IR, although this model lacks the anatomical relevance of an orthotopic model.

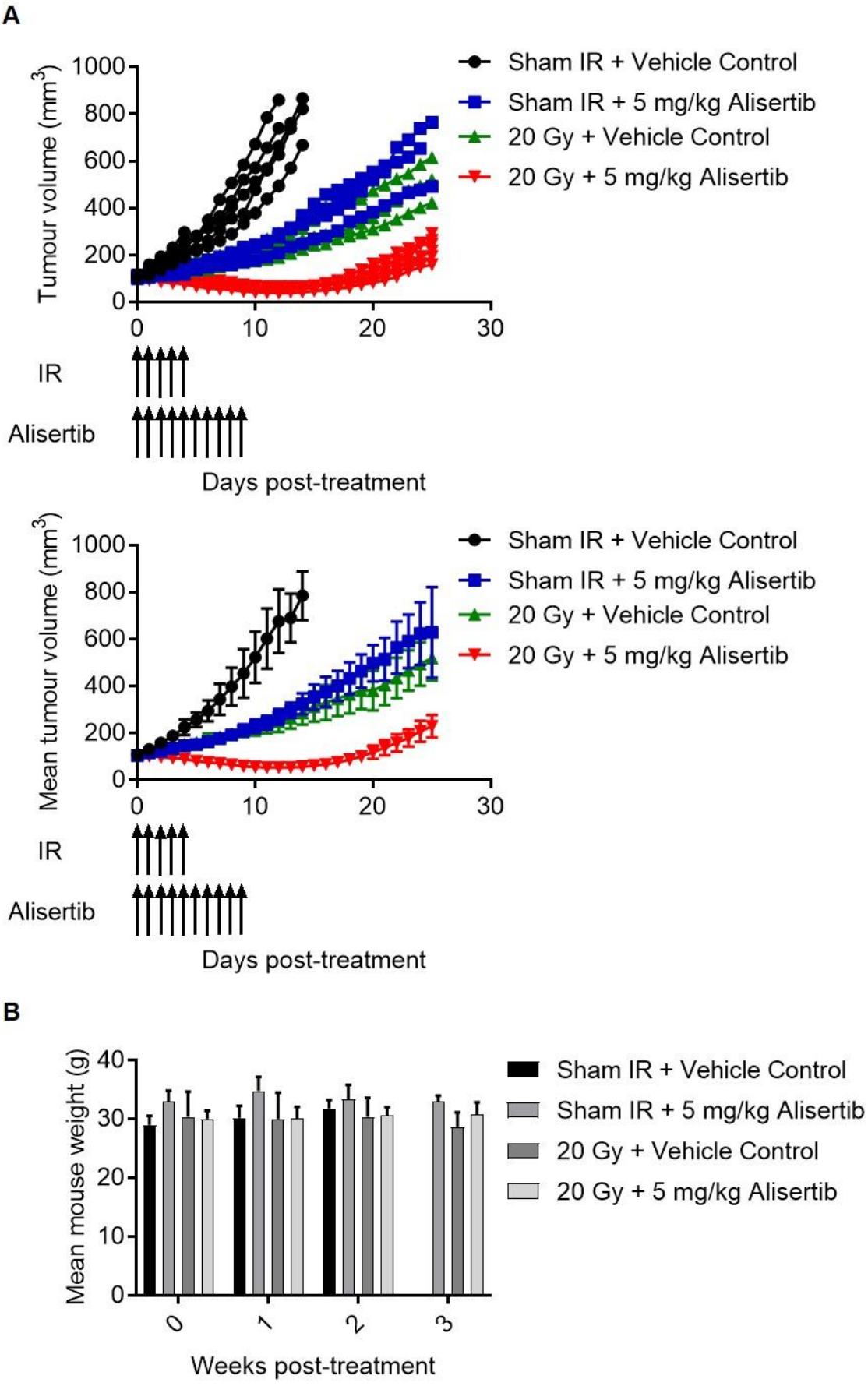

Figure 5.6. **Mean tumour volumes of H460 xenograft tumours treated with sham IR or 20 Gy over 5 days and vehicle control or 5 mg/kg Alisertib once daily for 10 days.** Legend on page 237.

C

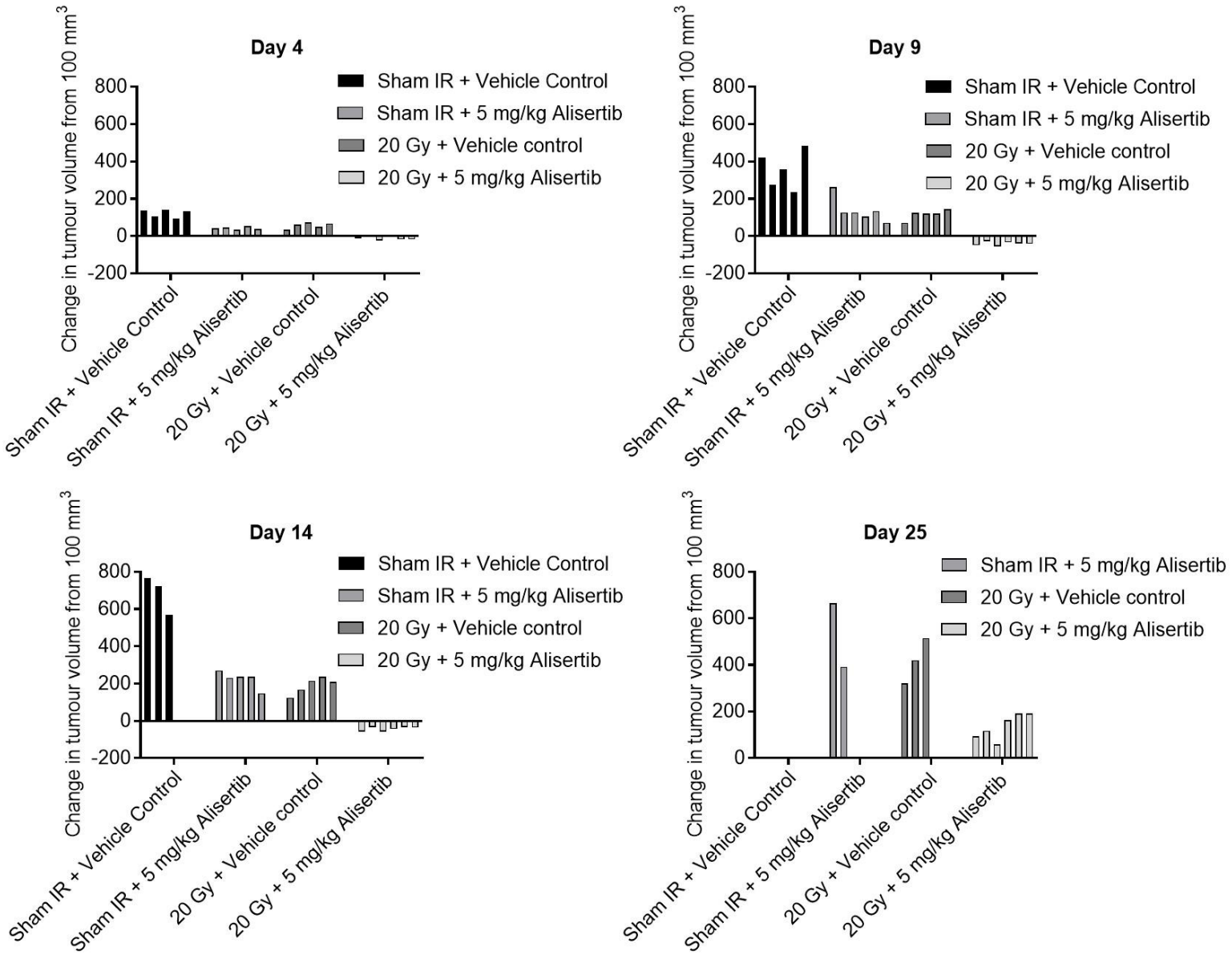

Figure 5.6. **Mean tumour volumes of H460 xenograft tumours treated with sham IR or 20 Gy over 5 days and vehicle control or 5 mg/kg Alisertib once daily for 10 days.** Legend on page 237.

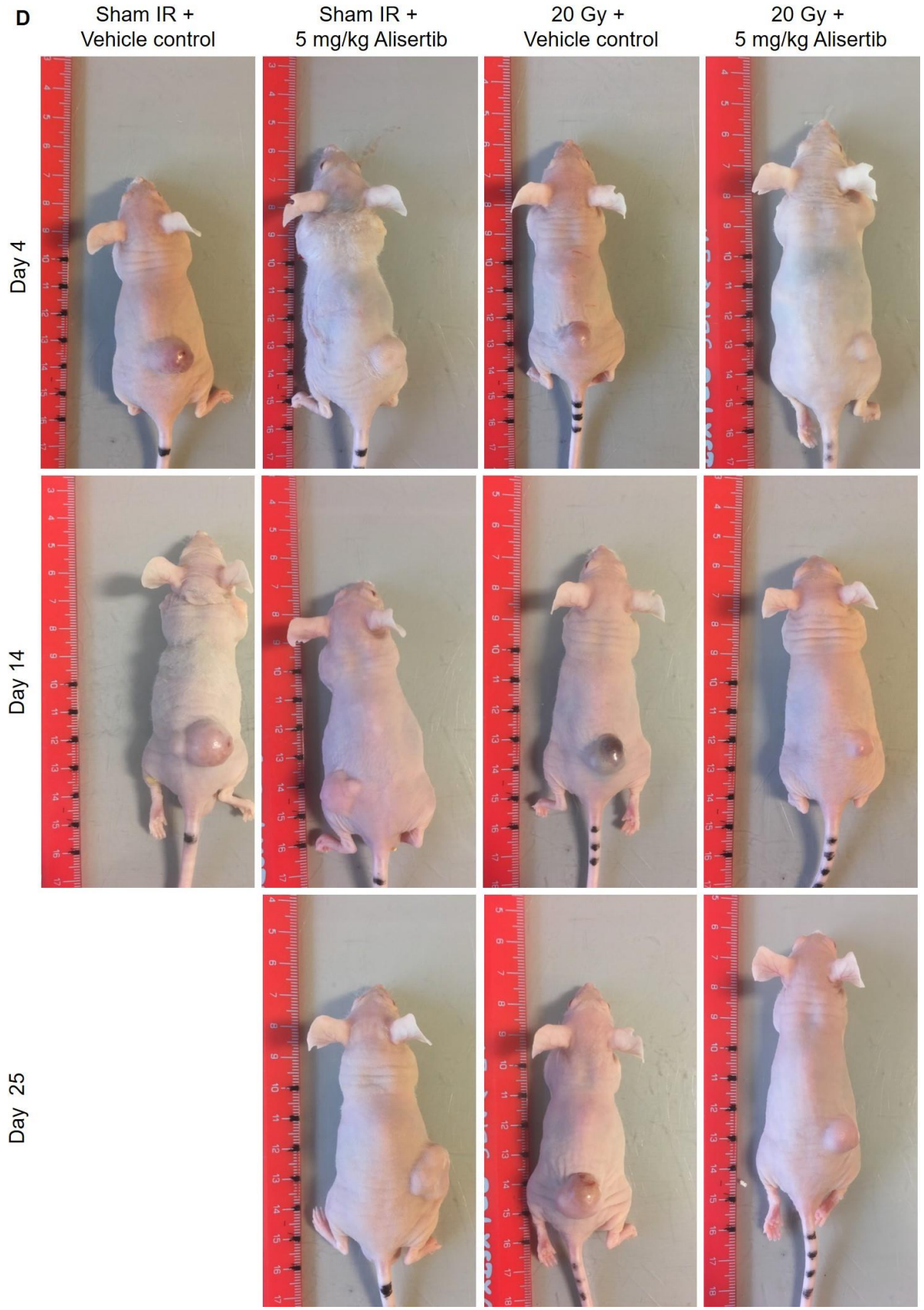

Figure 5.6. **Mean tumour volumes of H460 xenograft tumours treated with sham IR or 20 Gy over 5 days and vehicle control or 5 mg/kg Alisertib once daily for 10 days.** Legend overleaf.

Figure 5.6. **A. Mean tumour volumes of H460 xenograft tumours treated with sham IR or 20 Gy over 5 days and vehicle control or 5 mg/kg Alisertib once daily for 10 days.** Top: Data points represent tumour volume per mouse per condition. Bottom: Data points represent mean tumour volume per condition +/- SD (Sham IR + vehicle control, Sham IR + 5 mg/kg Alisertib and 20 Gy + vehicle control N=5, 20 Gy + 5 mg/kg Alisertib N=6). Tumour volumes calculated using d1 x d2 x d3 x 0.52 calculation. **B.** Mean mouse weights bearing H460 xenografts treated with sham IR or 20 Gy over 5 days and vehicle control or 5 mg/kg Alisertib once daily for 10 days indicated by arrows. Data points represent mean mouse weight +/- SD (Sham IR + vehicle control, Sham IR + 5 mg/kg Alisertib and 20 Gy + vehicle control N=5, 20 Gy + 5 mg/kg Alisertib N=6). **C.** Waterfall plots of H460 xenograft tumour volume changes from 100 mm^3 treatment volume at day 4 (top left), day 9 (top right), day 14 (bottom left) and day 25 (bottom right). Data points represent change from 100 mm^3 treatment volume per mouse per treatment group (no error displayed). **D.** Representative examples of CD-1 nude mice bearing H460 xenografts on day 4 (top row), day 14 (middle row) and day 25 (bottom row) of treatment with sham IR or 20 Gy given once daily in 4 Gy fractions on days 0-4 and vehicle control or 5 mg/kg Alisertib given once daily on days 0-9. Major scale marks in cm, minor scale markings in mm. Images taken with an iPhone SE. Note that tumour implantations were performed in collaboration with Matthew Fisher.

5.2.6. Alisertib IR combination and IR alone reduce H460 xenograft mitotic fraction and Ki67 positivity but do not affect intra-tumour CD31 expression

In combination experiments 50% of mice were culled at day four after completing 5 consecutive days of IR and 5 days or half of oral Alisertib dosing regimen. These mice were culled 4 hours post-Alisertib dosing (3 hours post-IR) and tumours were used to investigate the intra-treatment biological effects of Alisertib IR combination. Given that we see targeting of the mitotic population in H460 cells treated with Alisertib IR combination *in vitro*, we investigated the effect of Alisertib IR combination on the mitotic fraction of H460 xenografts *in vivo*. We found there was no evidence of data skew using the Shapiro-Wilk test. Also, we find that the mitotic fraction of H460 xenografts was significantly increased compared to control in the Alisertib alone

treatment group (p= 0.010 (One-way ANOVA)) (see Figure 5.7). Conversely, the mitotic fraction of H460 xenografts treated with 20 Gy alone or in combination with daily 5 mg/kg Alisertib was significantly reduced compared to control (p= 0.0001 and p= <0.0001 (One-ANOVA)), but there was no statistical difference between IR alone and Alisertib IR combination.

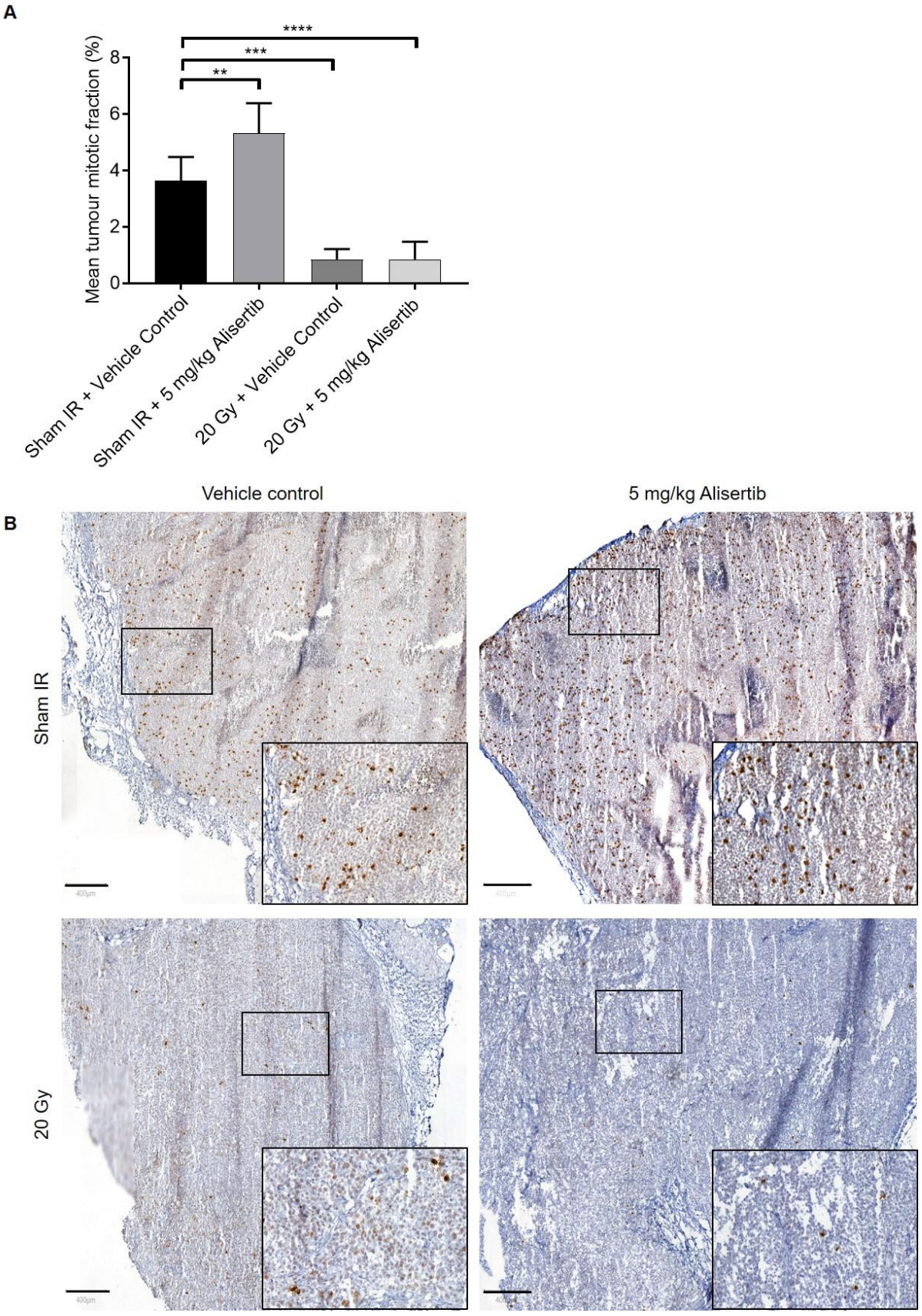

Figure 5.7. **H460 xenograft tumour mitotic fractions 4 hours after final dose of vehicle control or 5 mg/kg Alisertib and 3 hours after final sham IR or 4 Gy treatment after 5 consecutive days of treatment.** Legend overleaf.

Figure 5.7. **H460 xenograft tumour mitotic fractions 4 hours after final dose of vehicle control or 5 mg/kg Alisertib and 3 hours after final sham IR or 4 Gy treatment after 5 consecutive days of treatment. A**. Mean H460 xenograft mitotic fractions 4 hours post-treatment with vehicle control or 5 mg/kg Alisertib. Data points represent mean mitotic fraction per tumour per condition +/- SEM (Sham IR + vehicle control and 20 Gy + 5 mg/kg Alisertib N=6, Sham IR + 5 mg/kg Alisertib N=5 and 20 Gy + vehicle control N=4). ** denotes p= ≤0.01, *** denotes p= ≤0.001, **** p= ≤0.0001 (One-way ANOVA with Bonferroni correction for multiple comparisons). **B.** Representative H460 xenograft mitotic fraction examples 4 hours post-treatment with vehicle control or 5 mg/kg Alisertib and 3 hours post-treatment with sham IR or 4 Gy. Mitotic cells stained brown with DAB, defined as positive for p-Histone 3 (S10). Mitotic fraction defined within viable regions of tumour as a percentage of cells present. 9 regions sampled per tumour. Images taken with a Pannoramic 250 Flash III slide scanner 20x objective. Area within the small rectangle is re-represented in image bottom right corner 10x larger. Scale bars represent 400 μm.

Ki67 is a nuclear marker that is exclusively expressed by actively dividing cells in G1, S, G2 and mitosis and therefore is associated with the proliferative potential, and thus aggression, of tumours (L.T. Li *et al.* 2014). The Shapiro-Wilk test indicated that the distribution of the untreated condition was not normal and therefore comparisons were made using the Kruskal-Wallis test. Here we find that there is no statistical difference in % pixels positive for Ki67 expression between control and Alisertib alone tumours. In contrast, there was a trend for Ki67 staining to be reduced in both 20 Gy alone and 20 Gy + daily 5 mg/kg tumours compared to control (p= 0.042 and p= 0.088 (Kruskal-Wallis test)) (see Figure 5.8). These data indicate that both IR alone and IR + Alisertib reduce the proliferating fraction of NSCLC cells *in vivo*.

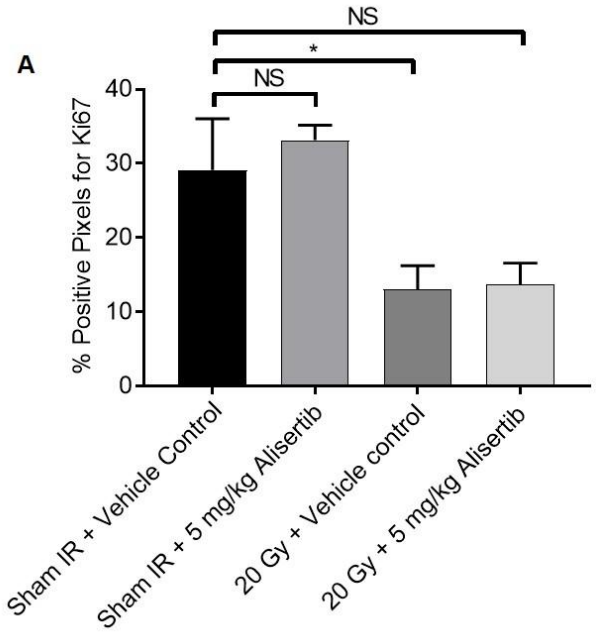

Figure 5.8. **Ki67 expression in H460 xenograft tumours 4 hours after final dose of vehicle control or 5 mg/kg Alisertib and 3 hours after final sham IR or 4 Gy treatment after 5 consecutive days of treatment.** Legend on page 243.

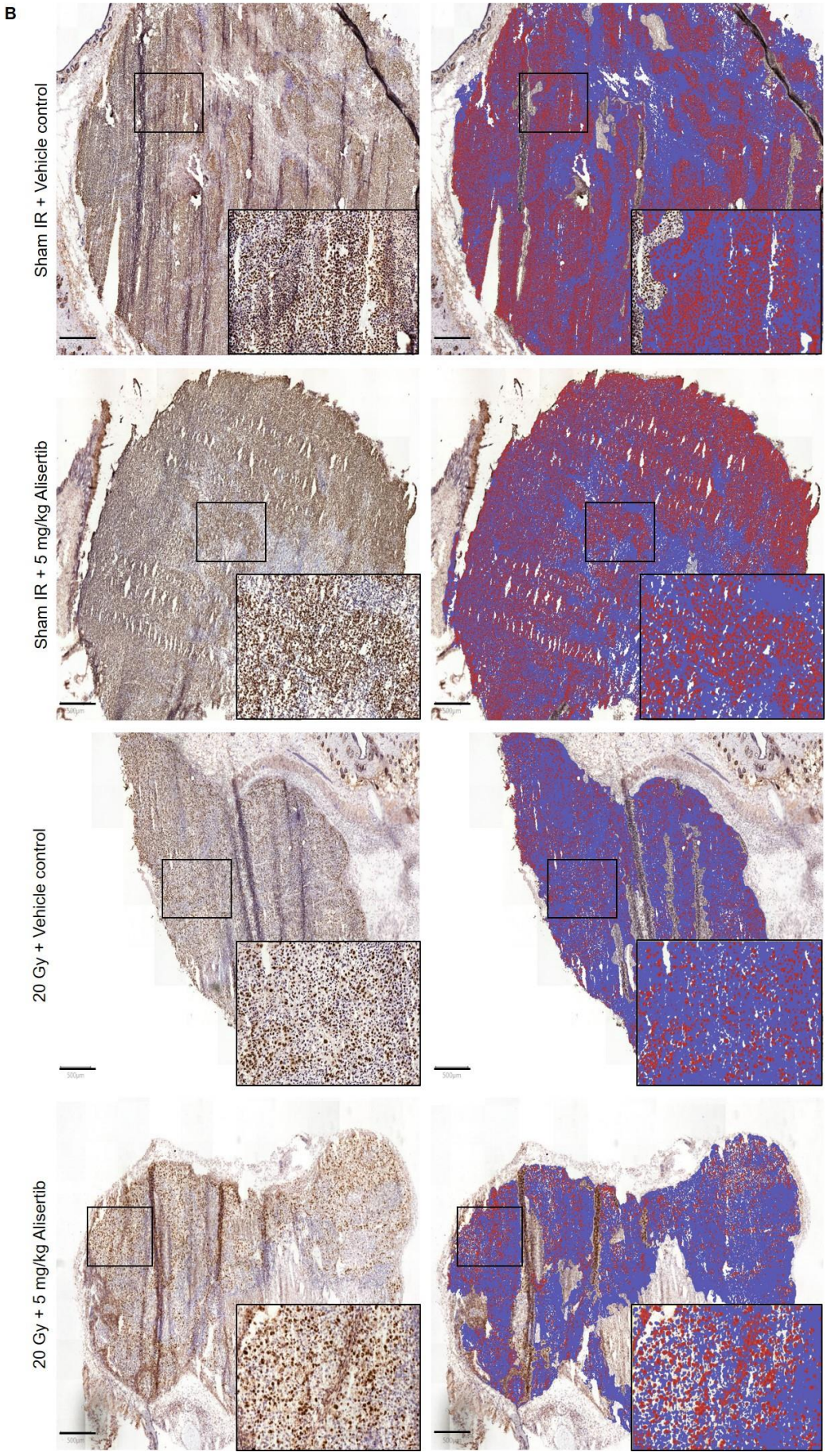

Figure 5.8. **Ki67 expression in H460 xenograft tumours 4 hours after final dose of vehicle control or 5 mg/kg Alisertib and 3 hours after final sham IR or 4 Gy treatment after 5 consecutive days of treatment.** Legend overleaf.

Figure 5.8. **Ki67 expression in H460 xenograft tumours 4 hours after final dose of vehicle control or 5 mg/kg Alisertib and 3 hours after final sham IR or 4 Gy treatment after 5 consecutive days of treatment. A**. Mean % of positive pixels for Ki67 staining in H460 xenograft mitotic fractions 4 hours post-treatment with vehicle control or 5 mg/kg Alisertib. Data points represent mean % positive pixels for Ki67 expression per tumour per condition +/- SEM (Sham IR + vehicle control N=6, Sham IR + 5 mg/kg Alisertib and 20 Gy + 4 mg/kg Alisertib N=4, 20 Gy + vehicle control N=5). NS denotes p= >0.05, * denotes p= ≤0.05 (Kruskal Wallis test with Dunn correction for multiple comparisons). **B.** Representative Ki67 expression (left) and scored Ki67 positive pixels (red) and negative pixels (blue) (right) in H460 xenograft tumours 4-hours post-treatment with vehicle control or 5 mg/kg Alisertib and 3 hours post-treatment with sham IR or 4 Gy. Ki67 positive cells stained brown with DAB. Ki67 positive pixels defined within viable regions of tumour as a percentage of tumour occupied pixels present. Images taken with a Pannoramic 250 Flash III slide scanner 20x objective. Area within the small rectangle is re-represented in image bottom right corner 10x larger. Scale bars represent 500 μm.

Depletion of AURKA has also been shown to shown to reduce angiogenesis in ovarian cancer cell lines (Wang *et al.* 2016), whilst pharmacological targeting of AURKA with Alisertib has been shown to reduce VEGF expression, a pro-angiogenesis signalling protein, in neuroblastoma cells (Romain *et al.* 2014). Given that targeting AURKA with Alisertib may affect angiogenesis, and that targeting angiogenesis has been shown to positively affect radiation response in tumours *in vivo* (Wachsberger *et al.* 2003), we also measured CD31 expression in H460 xenografts. CD31 is expressed by endothelial cells and is essential for new blood vessel formation (DeLisser *et al.* 1997), and therefore we used this marker to identify mouse blood vessel recruitment in the human H460 xenograft tumours. The Shapiro-Wilk test indicated that the both conditions with Alisertib treatment were not normally distributed, so the Kruskal-Wallis test was used to compare mean CD31 expression. Here there was a trend for increased intra-tumour CD31 expression, quantified as % positive pixels, in both sham IR + 5 mg/kg Alisertib and 20 Gy + 5 mg/kg Alisertib

treatment groups when compared to sham IR + vehicle control but neither increase was statistically significant (Kruskal-Wallis test) (see Figure 5.9).

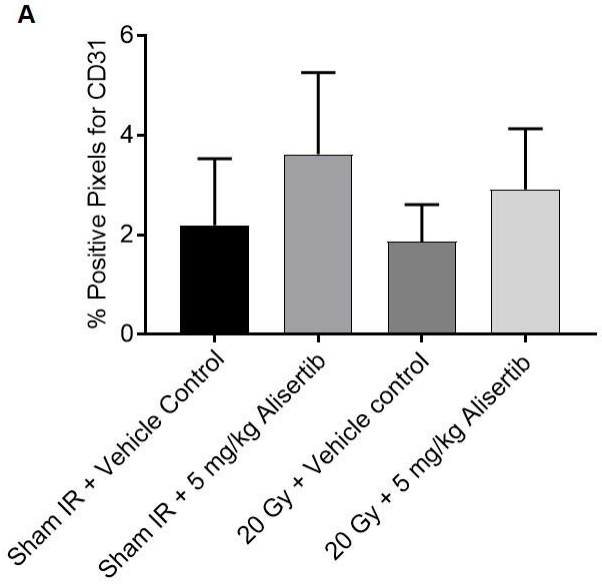

Figure 5.9. **CD31 expression in H460 xenograft tumours 4 hours after final dose of vehicle control or 5 mg/kg Alisertib and 3 hours after final sham IR or 4 Gy treatment after 5 consecutive days of treatment.** Legend on page 246.

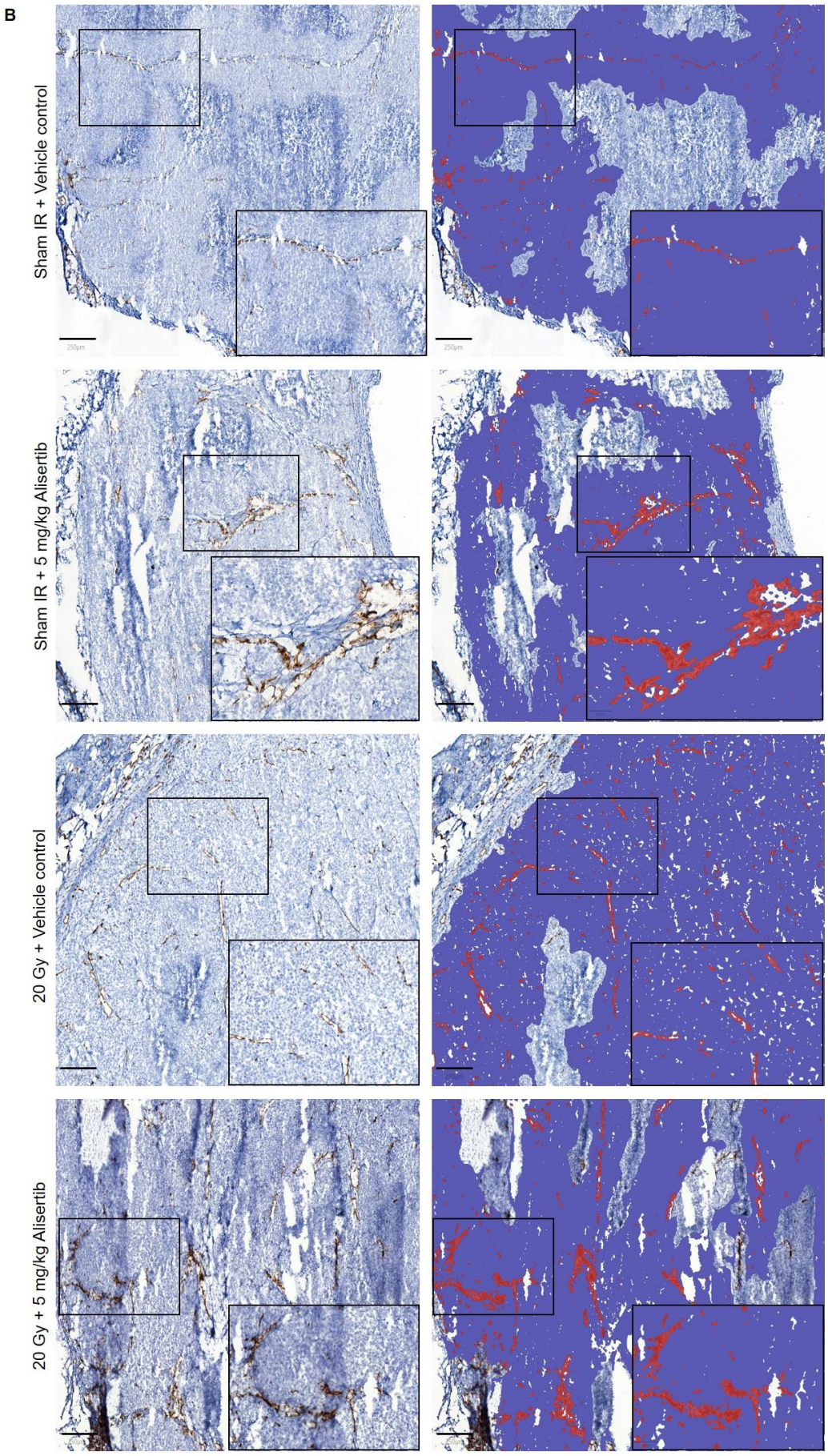

Figure 5.9. **CD31 expression in H460 xenograft tumours 4 hours after final dose of vehicle control or 5 mg/kg Alisertib and 3 hours after final sham IR or 4 Gy treatment after 5 consecutive days of treatment.** Legend overleaf.

Figure 5.9. **CD31 expression in H460 xenograft tumours 4 hours after final dose of vehicle control or 5 mg/kg Alisertib and 3 hours after final sham IR or 4 Gy treatment after 5 consecutive days of treatment. A**. Mean % of positive pixels for CD31 staining in H460 xenograft mitotic fractions 4 hours post-treatment with vehicle control or 5 mg/kg Alisertib. Data points represent mean % positive pixels for CD31 expression per tumour per condition +/- SEM (Sham IR + vehicle control N=4, Sham IR + 5 mg/kg Alisertib, 20 Gy + vehicle control and 20 Gy + 5 mg/kg Alisertib N=5). **B.** Representative CD31 expression (left) and scored CD31 positive pixels (red) and negative pixels (blue) (right) in H460 xenograft tumours 4-hours post-treatment with vehicle control or 5 mg/kg Alisertib and 3-hours post-treatment with sham IR or 4 Gy. CD31 positive cells stained brown with DAB. CD31 positive pixels defined within viable regions of tumour as a percentage of tumour occupied pixels present. Images taken with a Pannoramic 250 Flash III slide scanner 20x objective. Area within the small rectangle is re-represented in image bottom right corner 10x larger. Scale bars represent 250 µm.

5.3. Discussion

In this chapter we present evidence that AURKA inhibitor Alisertib is well tolerated in mouse models and has dose-dependent growth inhibition effect against H460 xenografts. Additionally, we show that targeting AURKA with Alisertib enhances IR response in H460 xenografts and induced almost 50% tumour regression until treatment effect had passed. We also show that Alisertib IR combination *in vivo*, like our *in vitro* investigations, significantly reduces the H460 mitotic population like IR alone, whilst Alisertib treatment increases mitotic fraction *in vivo*.

5.3.1. Alisertib is well tolerated in mouse models and has dose-dependent growth inhibition effect against H460 xenografts

We find that 10 consecutive days of Alisertib treatment up to 40 mg/kg was well tolerated in both C57Bl6 mice and CD-1 nude mice with no obvious toxicities. This is in line with the previously published *in vivo* MTDs for Alisertib (Görgün *et al.* 2010;

Manfredi *et al.* 2011; Palani *et al.* 2013). This suggests that Alisertib may be a useful combinational agent. Furthermore, we find that 5 mg/kg, 10 mg/kg and 20 mg/kg Alisertib given once daily for 10 consecutive days significantly inhibited the growth of H460 xenografts in a dose-dependent manner, as previously published (Palani *et al.* 2013). Daily 20 mg/kg Alisertib nearly completely inhibited growth in H460 xenografts before release from treatment. This suggests that Alisertib monotherapy may be of use in NSCLC, although a lack of efficacy as monotherapy using twice daily 50 mg/kg dose was demonstrated in phase II trials in NSCLC (Melichar *et al.* 2015). This may be explained by dose cycles, which allowed 14 days recovery following 7 days of Alisertib treatment (Melichar *et al.* 2015), which may promote tumour escape from the inhibitory effects of Alisertib. Additionally, H460 xenograft regrowth following treatment release suggested that Alisertib at higher doses of 10 mg/kg and 20 mg/kg was more likely to be having cytostatic, rather than cytotoxic, effect. This replicates previously published work in HCT116 and PC3 xenograft models where cytostatic effect was observed using the molecular precursor to Alisertib MLN8054 (Manfredi *et al.* 2007).

5.3.2. Alisertib IR combination enhances radiation response in H460 xenografts

Daily 5 mg/kg Alisertib significantly enhanced the radiation response in H460 xenografts, causing temporary tumour regression in xenografts treated with Alisertib IR combination. This provides further evidence that co-targeting of AURKA with IR is a valid approach in *in vivo* models of NSCLC (Woo *et al.* 2015), and that Alisertib radiosensitises cancer cells (Venkataraman *et al.* 2012; Hong *et al.* 2014), but is the first example using Alisertib and IR in *in vivo* models of NSCLC. However, additivity or synergy cannot be inferred here as *in vivo* experiments are complicated by

treatment effects on the tumour bed, which can result in the slowed proliferation of tumours in the absence of compromised reproductive potential, leading to overestimation of anti-tumour treatment effects (Stone *et al.* 2016). There was evidence of xenograft regrowth by day 20 onwards in the Alisertib IR combinational treatment group implying that combinational effect on cellular proliferation and survival was temporary. This argues against permanent cell cycle exit as a mechanistic explanation for Alisertib IR combinational efficacy, although there is evidence that treatment-induced senescence may be reversible in cancer (L. Yang *et al.* 2017). Tumour regrowth in the Alisertib IR combinational treatment arm to mean 100 mm^3 tumour volume was achieved by day 19, 10 days post-treatment, and therefore could be related to treatment release.

5.3.3. Alisertib IR combination reduces H460 xenograft mitotic fraction and Ki67 expression but does not affect intra-tumour CD31 expression

We show that 4 hours post-treatment with 5 mg/kg Alisertib, H460 xenograft mitotic fraction was increased compared to control treatment arm, in line with what has been previously published (Manfredi *et al.* 2007). Furthermore, we find that tumour irradiation, both alone and in combination with 5 mg/kg Alisertib, causes significant reduction in mitotic fraction in line with our H460 cell cycle data *in vitro*. Similarly, we find that H460 xenograft Ki67 expression showed trend to be reduced by IR alone and IR in combination with Alisertib with no evidence of cooperativity between Alisertib and IR. This suggests that IR has a dominant role in determining cell cycle response in the H460 cell line following Alisertib IR combination and we speculate that mitotic populations are undergoing cell death. This also suggests that Alisertib IR combination does not have combinational efficacy *in vivo* through cooperative reductions in proliferation. This is in line with our findings in H460 cells *in vitro* which

suggest that proliferation continues in presence of Alisertib IR combination, albeit with more mitotic aberration. It would be interesting to see relative expression of markers of apoptosis is differential between 20 Gy and 20 Gy + daily 5 mg/kg Alisertib treated tumour tissues, despite similarities in proliferative behaviour.

We find there was a trend for increased intra-tumour CD31 expression H460 xenograft tumours treated with 5 mg/kg Alisertib, alone or in combination with IR, but this was not statistically significant. This is counter-intuitive, given that targeting AURKA has been shown to reduce VEGF expression (Romain *et al.* 2014; Wang *et al.* 2016) which is known to positively regulate angiogenesis (Ferrara 2002). The findings of Romain *et al* (2014) were performed using human umbilical vein endothelial cells (HUVEC) cultured with neuroblastoma cell line conditioned media after treating with and without Alisertib. This approach was performed in 2D tissue culture and therefore may not be representative of angiogenesis after targeting AURKA *in vivo*. Furthermore, the functional redundancy of VEGF family members means that reduced VEGF expression by tumour cells may not necessarily result in reduced angiogenesis *in vivo* ((Zhao and Adjei 2015). This however, does not account for the findings by Wang et al (2016) who found that general angiogenesis was inhibited upon AURKA depletion in ovarian xenograft models *in vivo* and warrants further investigation. Currently we are investigating what effect 10 mg/kg and 20 mg/kg Alisertib doses, which were more potent as monotherapy, had on the tumour vasculature. It would also be interesting to assess xenograft tissues for T288 p-AURKA and AURKA expression, polyploidy and centrosomal amplification following treatment with Alisertib IR combination to see if we find similar data trends as previously *in vitro*.

5.3.4. Limitations

Here we used subcutaneous human cell line xenograft models of NSCLC as they reliably engraft, have well established growth kinetics and tumour growth can be monitored superficially without the need for specialist imaging equipment (Kellar *et al.* 2015; L. Yang *et al.* 2017). Also, NSCLC xenografts have been shown to predict efficacy of chemotherapy to reasonable degree in humans suggesting they are useful models, although these were patient derived xenograft models and engrafted under the renal capsules of mice (Dong *et al.* 2010). Subcutaneous xenografts also, at least partially, recapitulate elements of the tumour microenvironment that are not accounted for by 2D cell culture such as hypoxia (Jiang *et al.* 2016) and angiogenesis (Nishikawa *et al.* 2004). However, subcutaneous human cell line xenograft models lack the complexity of NSCLC, cell line models are generated to be genetically identical to a single clone and do not recapitulate the genetic heterogeneity observed in NSCLC (de Bruin *et al.* 2014; Ibarrola-Villava *et al.* 2018). Intra-tumour genetic heterogeneity has been shown to influence radiotherapy response in cancer (Cooke *et al.* 2011) including NSCLC (Das *et al.* 2010). There is a trend towards patient-derived xenograft models in the literature (Ibarrola-Villava *et al.* 2018), these better recapitulate the genetic heterogeneity of NSCLC (Kang *et al.* 2018) and could be useful to assess efficacy of Alisertib IR combination in NSCLC further. Also, subcutaneous xenograft models do not recapitulate the lung microenvironment unlike orthotopic models. Lung microenvironment factors have been shown to affect radiation response in NSCLC (Altorki *et al.* 2019). This also makes it difficult to assess normal tissue responses following Alisertib IR combination as neither the lung tissue or oesophagus are irradiated in these models, both of which may produce dose-limiting normal tissue toxicities after thoracic

irradiation (Kwint *et al.* 2012; Palma *et al.* 2013). It would be interesting to investigate the incidence of normal tissue toxicities and if Alisertib IR combination retained efficacy using orthotopic mouse models of NSCLC.

Human xenografts models require immunocompromised host mouse models to reduce the chance of immune rejection of human cell transplants (Kellar *et al.* 2015). There is evidence that the immune system plays a significant role in determining NSCLC behaviour and treatment response including radiotherapy (Altorki *et al.* 2019). Given that the immune response post-IR has been shown to affect radiotherapy outcomes in NSCLC, the lack of a functional immune system in our models reduce the translational relevance of our findings. It would have been useful to assess Alisertib IR combinational efficacy in the LLC syngeneic model, but this was limited by ethical means.

Additionally, the administration of radiation to the tumour here was crude, whereby radiation fractions were applied in two equal parts, half of dose being given to one face of the tumour and half of dose to the opposite tumour face. This approach lacked the precision of CT guided radiotherapy and did not adapt to the shape of tumours meaning that radiation dose may not have been equally distributed across the tumour. This increases the chance that some tumour cells were insufficiently irradiated and potentially dilutes any observed treatment effects.

6. Evaluation of AURKA expression as a predictive biomarker for NSCLC response to radiation

6.1. Introduction, aims and hypotheses

Lung cancer kills more people annually than any other cancer in the UK, however there has been little improvement in 10-year survival since the 1970s (CRUK 2018). These data suggest that the current treatment options for lung cancer, including radiotherapy, are suboptimal, and this is in part due to a lack of predictive biomarkers for therapeutic response. AURKA is overexpressed, relative to non-neoplastic tissue equivalents, in a large range of cancers (Bischoff *et al.* 1998; Gritsko *et al.* 2003; Lo Iacono *et al.* 2011; Lucena-Araujo *et al.* 2011; Chuang *et al.* 2016; Ma *et al.* 2017). AURKA overexpression is also a well-documented indicator of a poor prognosis in a range of cancers (Lucena-Araujo *et al.* 2011; Ma *et al.* 2017; Yan *et al.* 2018), including NSCLC (Xu *et al.* 2014; Al-Khafaji *et al.* 2017; Koh *et al.* 2017; Schneider *et al.* 2017) and this demonstrates the potential utility of AURKA as a biomarker. There is also evidence linking AURKA expression and radiation response. Ectopic over-expression of AURKA *in vitro* has been shown to reduce the radiosensitivity of laryngeal squamous cell carcinoma cell lines (Guan *et al.* 2007). Furthermore, in cervical squamous cell carcinoma high AURKA expression in pre-therapy tumour biopsies correlated with poorer overall survival and disease recurrence in patients receiving radical radiotherapy (Ma *et al.* 2017). Importantly, high pre-therapy AURKA expression in cervical squamous cell carcinoma was associated with reduced likelihood to achieve a complete response and increased likelihood to have progressive disease in response to definitive radical radiotherapy (Ma *et al.* 2017). This provides evidence that AURKA expression status may predict

radiation response in a patient population. This chapter will address if AURKA expression status in NSCLC is predictive of clinical outcome post-radiotherapy.

The aims of this chapter are to assess the following:

1. The predictive value of AURKA mRNA expression in NSCLC patients treated with radiotherapy using public datasets
2. The sensitivity and specificity of AURKA staining in cell line pellets and NSCLC patient pre-therapy diagnostic tumour samples
3. AURKA protein expression in NSCLC patient pre-therapy diagnostic tumour samples and association with overall survival, radiotherapy response and time to tumour progression in patients treated with radical or high dose palliative radiotherapy

The hypothesis of this chapter is:

- High AURKA expression is associated with poorer clinical outcomes following radiotherapy

6.2. Results

6.2.1. Kaplan Meier (KM) Plotter data reveals AURKA mRNA expression is a negative prognostic marker in NSCLC and is associated with worse overall survival, reduced time to first tumour progression and worse post-progression survival in NSCLC patients that received radiotherapy

6.2.1.1. AURKA mRNA is overexpressed in NSCLC samples and is associated with a poor prognosis that is disease subtype specific

KM plotter is an online tool that can be used to query cancer mRNA expression databases GEO, EGA and TCGA whilst simultaneously coupling patient outcome data with mRNA expression data (Győrffy *et al.* 2013) There are 2437 NSCLC samples with a mean follow-up of 49 months (Győrffy *et al.* 2013). This database was queried to assess the prognostic and predictive value of AURKA in NSCLC.

There were three Affymetrix probes that were used to assess AURKA mRNA expression in NSCLC samples: 204092_s_at, 208079_s_at and 208080_at. When assessed for expression in the NSCLC cohort with it was found that median expression of 204092_s_at and 208079_s_at probes were significantly upregulated in NSCLC tissues when compared to normal lung tissues (data not shown). There was a reduction in median expression of the 208080_at probe in NSCLC samples when compared to normal lung tissues which was not in line with what is accepted about AURKA mRNA expression in NSCLC (Lo Iacono *et al.* 2011; Li *et al.* 2015; Al-Khafaji *et al.* 2017; Li *et al.* 2018; Zhang *et al.* 2018), therefore this probe (208080_at) was not carried forward for further analysis.

Overall survival is considered the gold standard for outcome when assessing the impact of cancer treatment (Mauguen *et al.* 2013). Subsequently when dichotomising

the NSCLC samples, based on median expression, into high and low expressers of AURKA mRNA high expression was associated with worse overall survival in NSCLC patients (see Figure 6.1 A & D). In addition, when disease subtype was considered, high AURKA mRNA expression was associated with worse overall survival in lung adenocarcinoma patients (see Figure 6.1 B & D). In contrast, in lung squamous cell carcinoma patients high AURKA mRNA expression was found that have no effect on overall survival (see Figure 6.1 C-D).

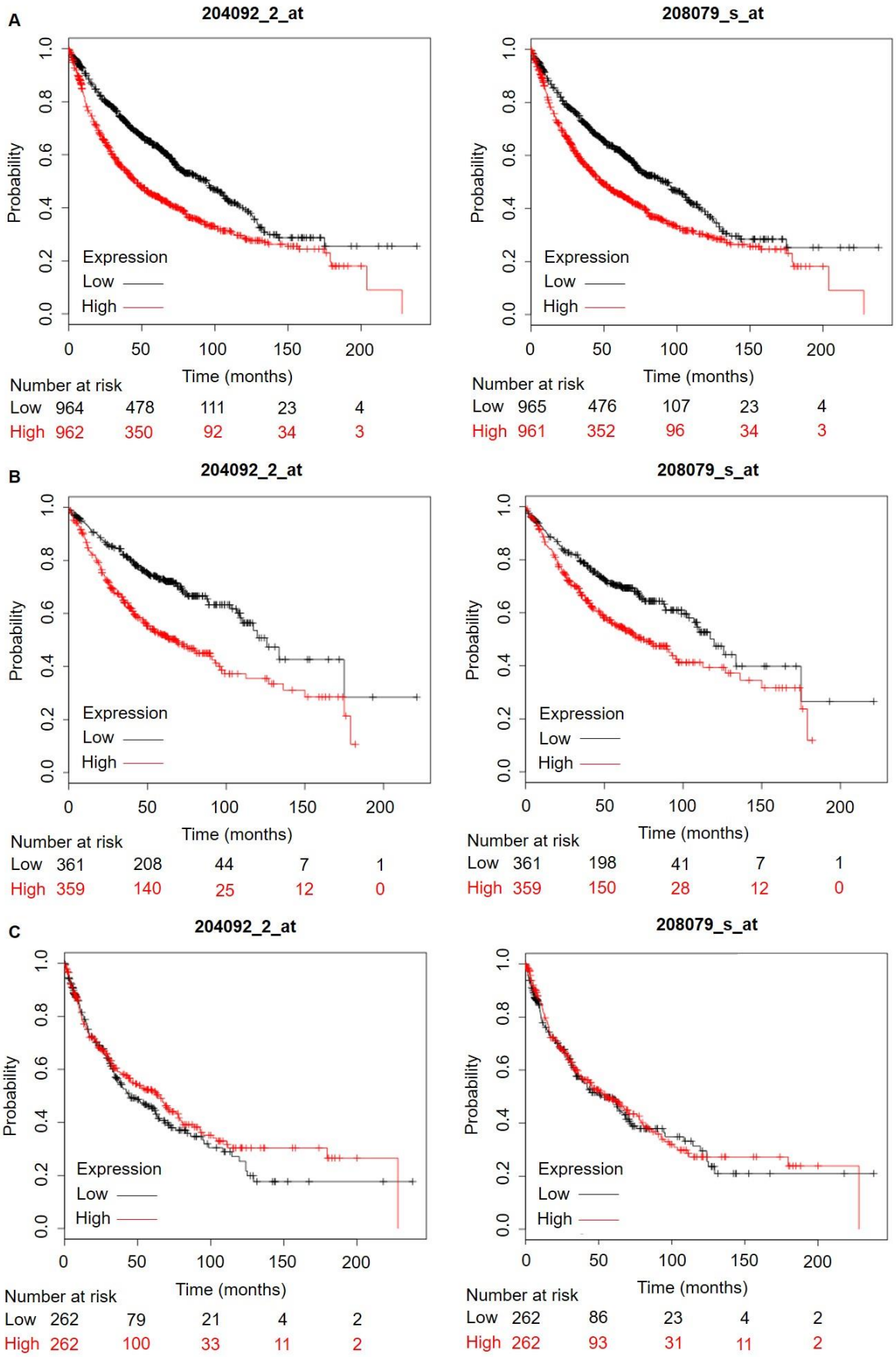

Figure 6.1. **Prognostic Impact of AURKA mRNA expression probes 204092_s_at and 208079_s_at in A. Total NSCLC B. Lung ADC and C. Lung SCC.** Legend overleaf

D

		Median Survival (Months)		Hazard Ratio (HR) (95% CI)		p-value	
	Expression	204092_2_at	208079_s_at	204092_2_at	208079_s_at	204092_2_at	208079_s_at
All NSCLC	High	45.3	48.0	1.63 (1.44-1.86)	1.52 (1.33-1.72)	3.3×10^{-14}	1.2×10^{-10}
	Low	94.5	92.6				
Lung ADC only	High	68.0	73.3	1.94 (1.53-2.46)	1.59 (1.26-2.01)	3.0×10^{-8}	1.0×10^{-4}
	Low	125.8	119.9				
Lung SCC only	High	64.1	54.6	0.88 (0.70-1.12)	0.96 (0.76-1.21)	0.29	0.73
	Low	44	52				

Figure 6.1. **Prognostic Impact of AURKA mRNA expression probes 204092_s_at and 208079_s_at in A. Total NSCLC B. Lung ADC and C. Lung SCC.** Overall survival presented. Cutoff for high vs low expression status was median probe expression. Follow-up threshold was 240 months, patients surviving over this threshold were censored. **D.** Table of median survival in populations, Hazard ratios (HR) with 95% confidence intervals (CI) stated. Survival distributions compared, and p-value derived from logrank test. (All NSCLC group N= 1926, Lung ADC only group N= 720 and Lung SCC only group N= 524).

These data suggest a prognostic role for AURKA expression in lung adenocarcinoma patients. This contrasts with the findings of Lee et al (2012) who found no association with AURKA expression status and overall survival in either lung squamous cell carcinoma or lung adenocarcinoma subtypes respectively. The findings by Lee et al (2012) were however based upon protein AURKA expression, unlike the mRNA-based approach here.

6.2.1.2. High AURKA mRNA expression is associated with worse overall survival, reduced time to tumour progression and showed trend for worse post-progression survival in NSCLC adenocarcinoma patients treated with radiotherapy

To assess the predictive impact of high AURKA expression on NSCLC radiotherapy response KM plotter was again used to assess outcomes in a small cohort of patients (N= 70) that had received radiotherapy (Director's Challenge Consortium for the Molecular Classification of Lung *et al.* 2008; Győrffy *et al.* 2013). This cohort is comprised of lung ADCs of stages I, II and III (Director's Challenge Consortium for the Molecular Classification of Lung *et al.* 2008). Unfortunately, there is no accompanying information pertaining to the dose of radiotherapy received, the modality of radiotherapy and whether radiotherapy was used alone or in conjunction with surgery or chemotherapy (Director's Challenge Consortium for the Molecular Classification of Lung *et al.* 2008). However, this dataset can provide a first investigation into a NSCLC ADC cohort that has received radiotherapy and association of AURKA mRNA expression with patient outcomes.

Using median probe expression as a cut-off for high and low expression of AURKA mRNA there was a non-significant trend for reduced 5-year survival (see Figure 6.2 A & D). Statistical non-significance here, however, may be accounted for by small sample size (N= 70) and a median expression cut-off may dilute effect size. Given this, the 1st and 3rd tertiles of AURKA mRNA expression were used to dichotomise patients into AURKA high and low expressers (see Figure 6.2 B & D). This resulted in further separation of 5-year survival curves that were close to statistical significance. Convergence of survival curves when assessing at the 60 month point of follow-up, despite differences in survival in the intermediate months, implied that

by 5-years survival rates were levelling off. Choosing 36-month follow-up as an intermediate point of assessment revealed that overall survival in patients with AURKA mRNA expression in the upper tertile was significantly reduced when compared to patients with expression in the lower tertile (see Figure 6.2 C-D).

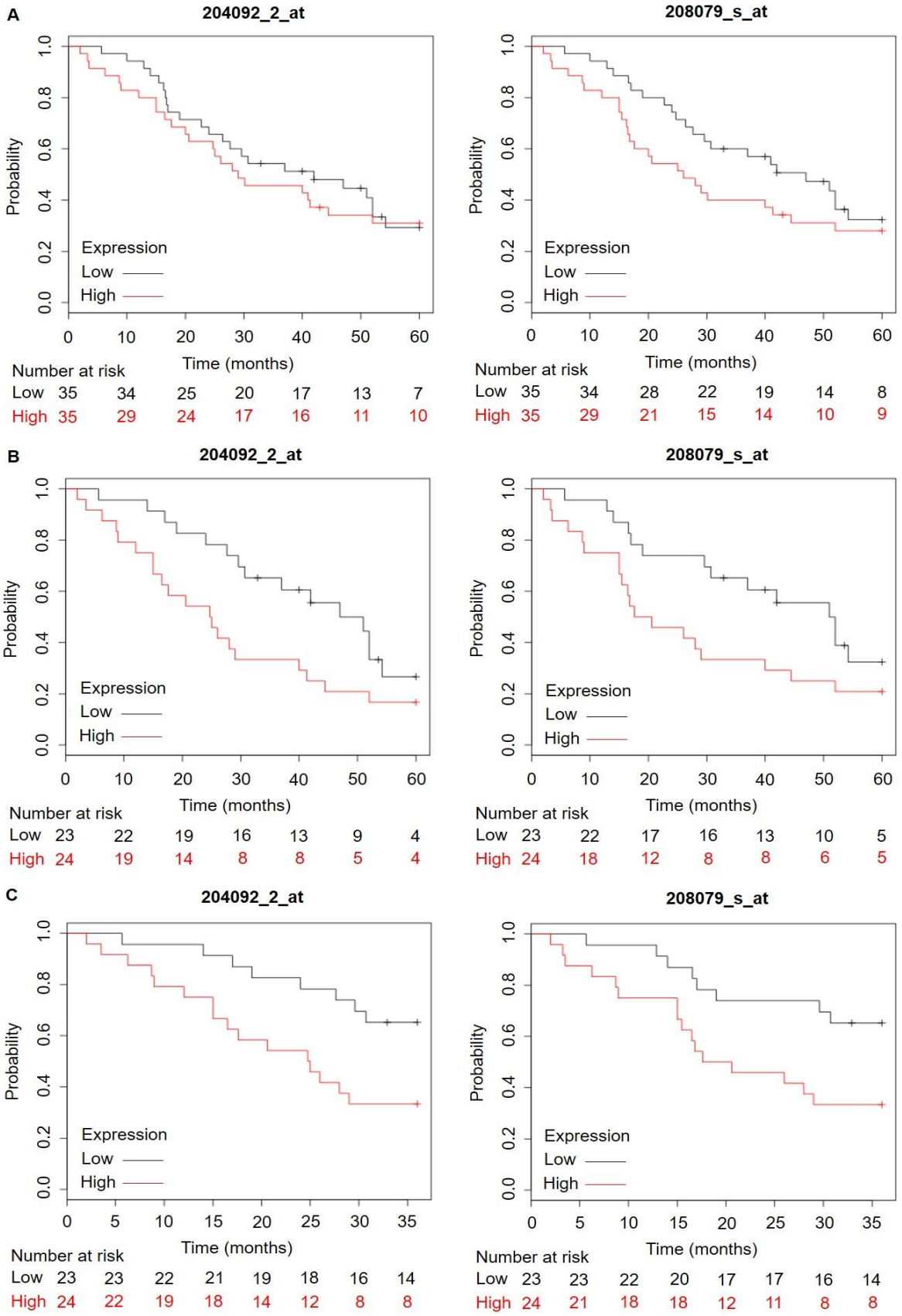

Figure 6.2. **Overall survival of NSCLC ADC patients receiving radiotherapy when AURKA mRNA expression was high or low through probes 204092_s_at and 208079_s_at using A. Median expression cut-off and 60-month follow-up threshold, B. Upper and lower tertile expression cut-off and 60-month follow-up threshold & C. Upper and lower tertile expression cut-off and 36-month follow-up threshold.** Legend overleaf

D

			Median Survival (Months)		Hazard Ratio (HR) (95% CI)		p-value	
Dichotomisation	Follow-up	Expression	204092_2_at	208079_s_at	204092_2_at	208079_s_at	204092_2_at	208079_s_at
Median expression	60 months	High	29.0	26.0	1.15 (0.63-2.04)	1.45 (0.82-2.57)	0.62	0.2
		Low	42.0	47.0				
Upper vs lower tercile	60 months	High	25.0	20.6	1.93 (0.99-3.79)	1.87 (0.93-3.74)	0.051	0.073
		Low	47.0	51.0				
Upper vs lower tercile	36 months	High	15.0	15.0	2.72 (1.16-6.39)	2.66 (1.13-6.25)	0.017	0.019
		Low	27.6	19.0				

Figure 6.2. **Overall survival of NSCLC ADC patients receiving radiotherapy when AURKA mRNA expression was high or low through probes 204092_s_at and 208079_s_at using A. Median expression cut-off and 60-month follow-up threshold, B. Upper and lower tertile expression cut-off and 60-month follow-up threshold & C. Upper and lower tertile expression cut-off and 36-month follow-up threshold.** Patients surviving over follow-up thresholds were censored. **D.** Table of median survival in populations, Hazard ratios (HR) with 95% confidence intervals (CI) stated. Survival distributions compared, and p-value derived from logrank test. (N= 70).

Whilst overall survival is considered a gold standard for assessing NSCLC treatment outcomes it is limited by length of follow-up time required and can be affected by the occurrence of non-cancer deaths (Mauguen *et al.* 2013). Given this, surrogate endpoints associated with tumour progression, with the advantage of requiring reduced follow-up, are also considered useful endpoints in NSCLC patients post-radiotherapy (Mauguen *et al.* 2013). NSCLC ADC patients receiving radiotherapy were also more likely to experience first tumour progression earlier when AURKA mRNA expression was high. 36-month follow-up showed that there was a trend for NSCLC ADC patients receiving radiotherapy to experience earlier first tumour progression when AURKA expression was high (see Figure 6.3 A & D). As 36-month follow threshold for time to first progression was affected by convergence of

probability curves an earlier 18-month follow-up threshold was investigated (see Figure 6.3 B & D). This revealed that when AURKA mRNA expression was high NSCLC ADC patients receiving radiotherapy were significantly more likely to experience earlier first tumour progression.

Post-progression survival is the time between progression free survival and overall survival and has been shown to correlate with overall survival in NSCLC patients following chemoradiotherapy (Kasahara *et al.* 2015). When using a 36-month follow up threshold, there was a non-significant trend for reduced post-progression survival when expression of AURKA mRNA expression was high (see Figure 6.3 C-D).

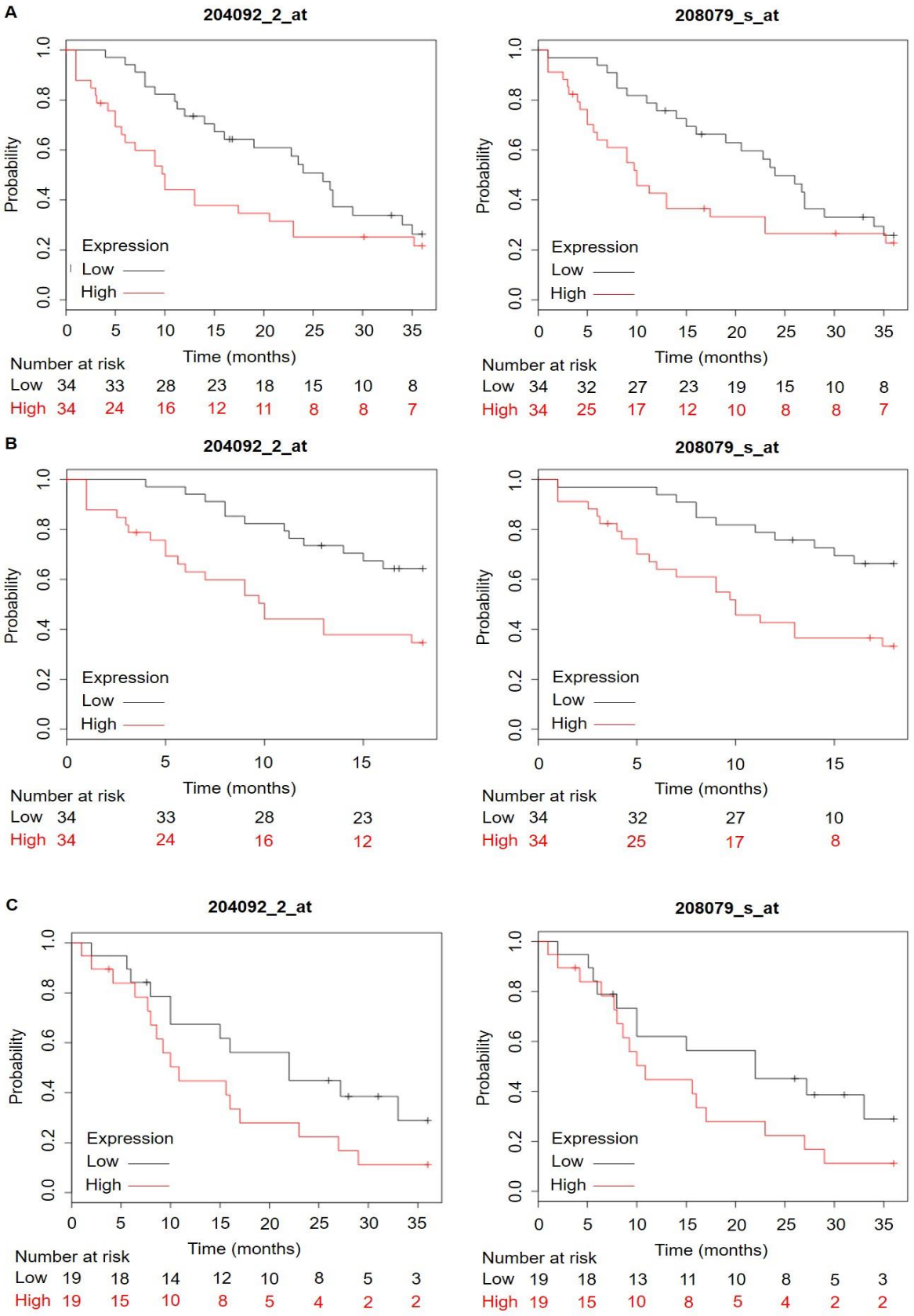

Figure 6.3. **Time to first tumour progression and post-progression survival of NSCLC ADC patients receiving radiotherapy when AURKA mRNA expression was high or low through probes 204092_s_at and 208079_s_at A. Time to first tumour progression using 36-month follow-up threshold. B. Time to first tumour progression using 18-month follow-up threshold. C. Post-progression survival using 36-month follow-up threshold**. Legend overleaf

D

Outcome	Follow-up	Expression	Median Time to Event/Survival (Months)		Hazard Ratio (HR) (95% CI)		p-value	
			204092_2_at	208079_s_at	204092_2_at	208079_s_at	204092_2_at	208079_s_at
First tumour progression	36 months	High	10.0	10.0	1.68 (0.95-2.97)	1.62 (0.91-2.86)	0.07	0.10
		Low	26.0	24.0				
First tumour progression	18 months	High	5.0	5.0	2.68 (1.32-5.47)	2.87 (1.39-5.94)	0.005	0.003
		Low	12.0	14.0				
Post-progression survival	36 months	High	10.9	10.9	1.81 (0.87-3.93)	1.76 (0.83-3.73)	0.1	0.14
		Low	22.0	22.0				

Figure 6.3. **Time to first tumour progression and post-progression survival of NSCLC ADC patients receiving radiotherapy when AURKA mRNA expression was high or low through probes 204092_s_at and 208079_s_at A. Time to first tumour progression using 36-month follow-up threshold. B. Time to first tumour progression using 18-month follow-up threshold. C. Post-progression survival using 36-month follow-up threshold**. Upper and lower tertile expression cut-off used. Patients surviving over follow-up thresholds were censored. **D.** Table of median time to event survival in populations, Hazard ratios (HR) with 95% confidence intervals (CI) stated. Survival distributions compared, and p-value derived from logrank test. (N= 70 for first tumour progression N= 57 for post-progression survival).

These data suggest that high AURKA mRNA expression in NSCLC patients treated at least once with radiotherapy was associated with worse overall survival, earlier first tumour progression and had a trend for reduced post-progression survival. Data showing that AURKA mRNA expression status was associated tumour progression following treatments indicate that AURKA may influence treatment efficacy. However, these data are limited to lung adenocarcinomas and are further limited by a lack of radiotherapy dose data to accompany clinical outcome data. Finally, these investigations were restricted to clinical outcome associations with AURKA mRNA expression only. AURKA regulation, is complex and AURKA protein overexpression can be driven through post-translational stabilisations in an mRNA independent manner (Kitajima *et al.* 2007). Therefore, the above data derived from KM plotter

needs complementing with data that considers radiotherapy dosing specifics and AURKA expression at the protein level to provide support to the hypothesis that AURKA expression can predict radiotherapy response in NSCLC.

6.2.2. Optimisation of AURKA staining via IHC

6.2.2.1. AURKA staining in NSCLC cell line pellets and patient biopsy samples using pressure cooker antigen retrieval, pH 6.1 citrate target retrieval buffer and avidin-biotin (ABC) signal amplification

When staining patient NSCLC biopsy samples for AURKA there must be evidence that the stain is sensitive and specific. Cell line pellets are useful tools for optimisation of IHC staining because gene expression is easily altered *in vitro*. Modulating gene expression *in vitro* using siRNA and IHC staining for that target using cell line pellets can provide indications about the sensitivity and specificity of the staining protocol. Here we used a standard IHC protocol using pressure cooker-based antigen retrieval, pH 6.1 citrate target retrieval solution for antigen retrieval, overnight primary antibody incubation and ABC signal amplification prior to detection.

When the H460 cell line was depleted of AURKA using AURKA siRNA 1 or 2 and harvested 24 hours post-transfection we found that AURKA staining was reduced when compared to H460 cell pellet transfected with scrambled siRNA control when using 1:500 and 1:1000 primary antibody (see Figure 6.4 A). Also sampling of H460 populations prior to fixation for western blot analysis confirmed relative depletion of AURKA expression by 65.8% and 53.3% when transfecting with AURKA siRNA 1 or 2 compared to scrambled siRNA control (see Figure 6.4 B). However, using 1:1000 AURKA blocking peptide with AURKA primary antibody in cell line pellets however

revealed that a proportion of stain via this methodology was likely non-specific (see Figure 6.4 C). The same protocol using 1:1000 primary antibody in diagnostic patient samples was also associated with background stain as well as suspected positive stain (see Figure 6.4 D).

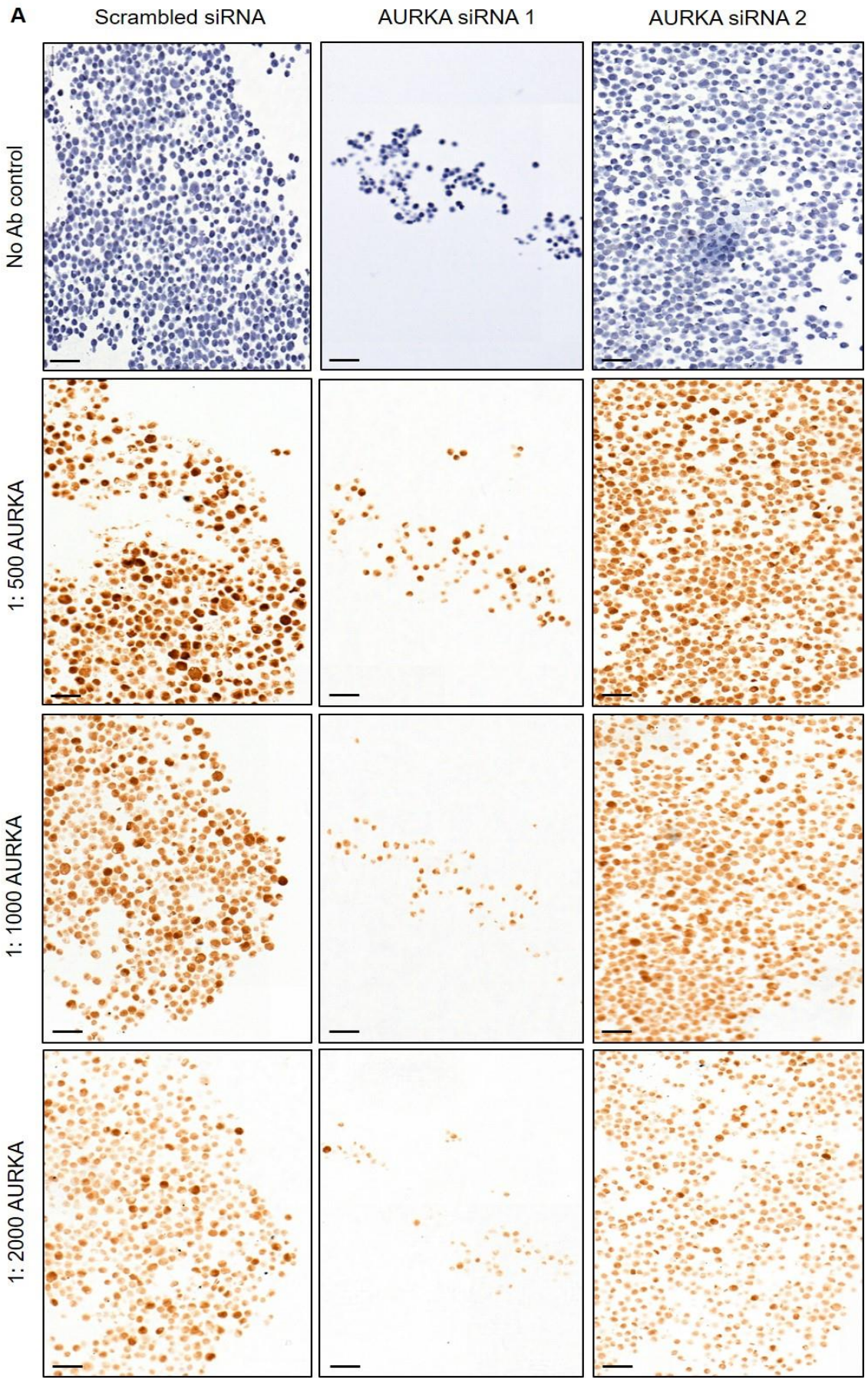

Figure 6.4. **AURKA IHC staining in H460 cell line pellets transfected with scrambled or AURKA siRNA and patient biopsy samples using pressure cooker antigen retrieval, citrate retrieval buffer and ABC signal amplification.** Legend on page 269.

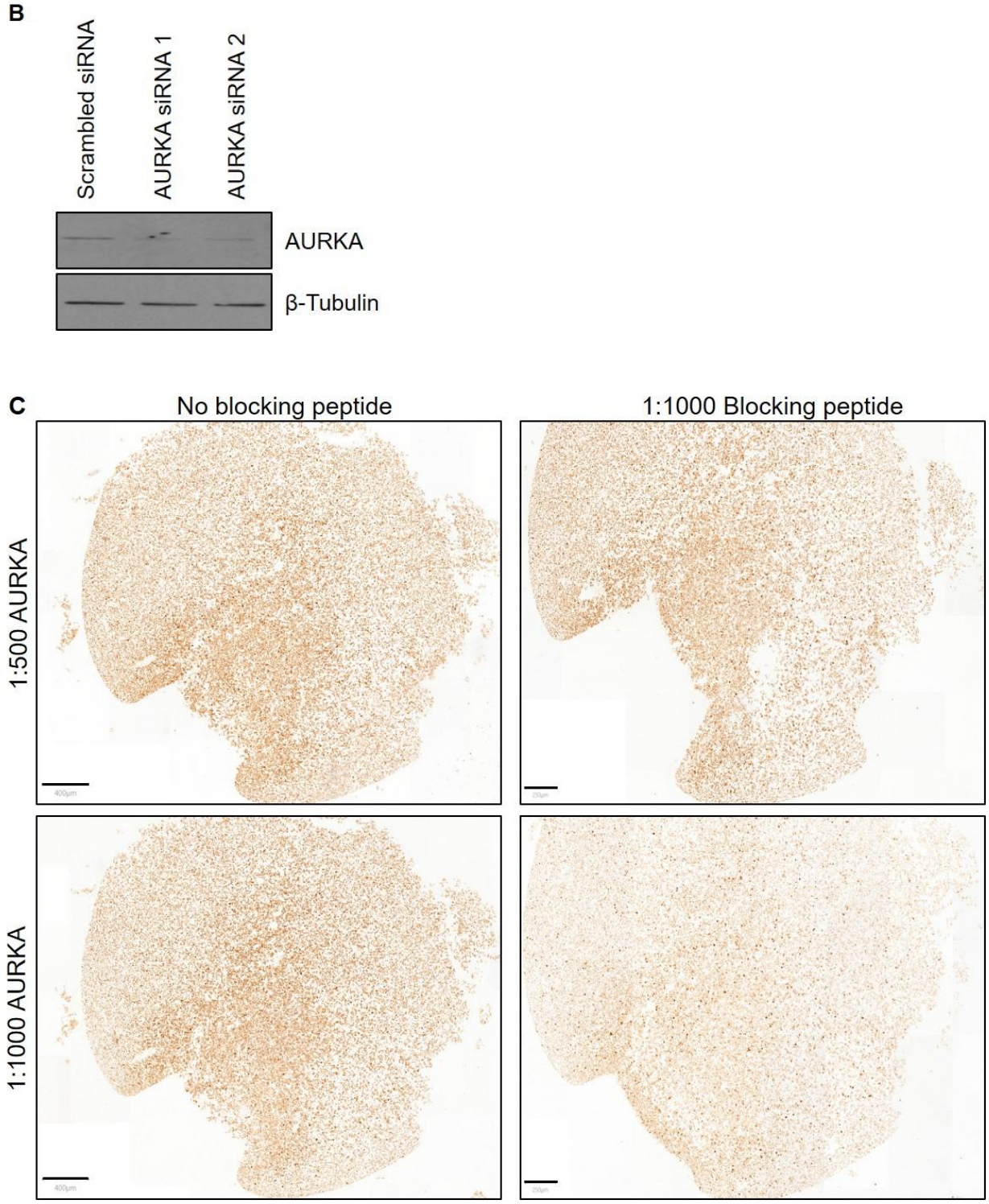

Figure 6.4. **AURKA IHC staining in H460 cell line pellets transfected with scrambled or AURKA siRNA and patient biopsy samples using pressure cooker antigen retrieval, citrate retrieval buffer and ABC signal amplification**
Legend overleaf

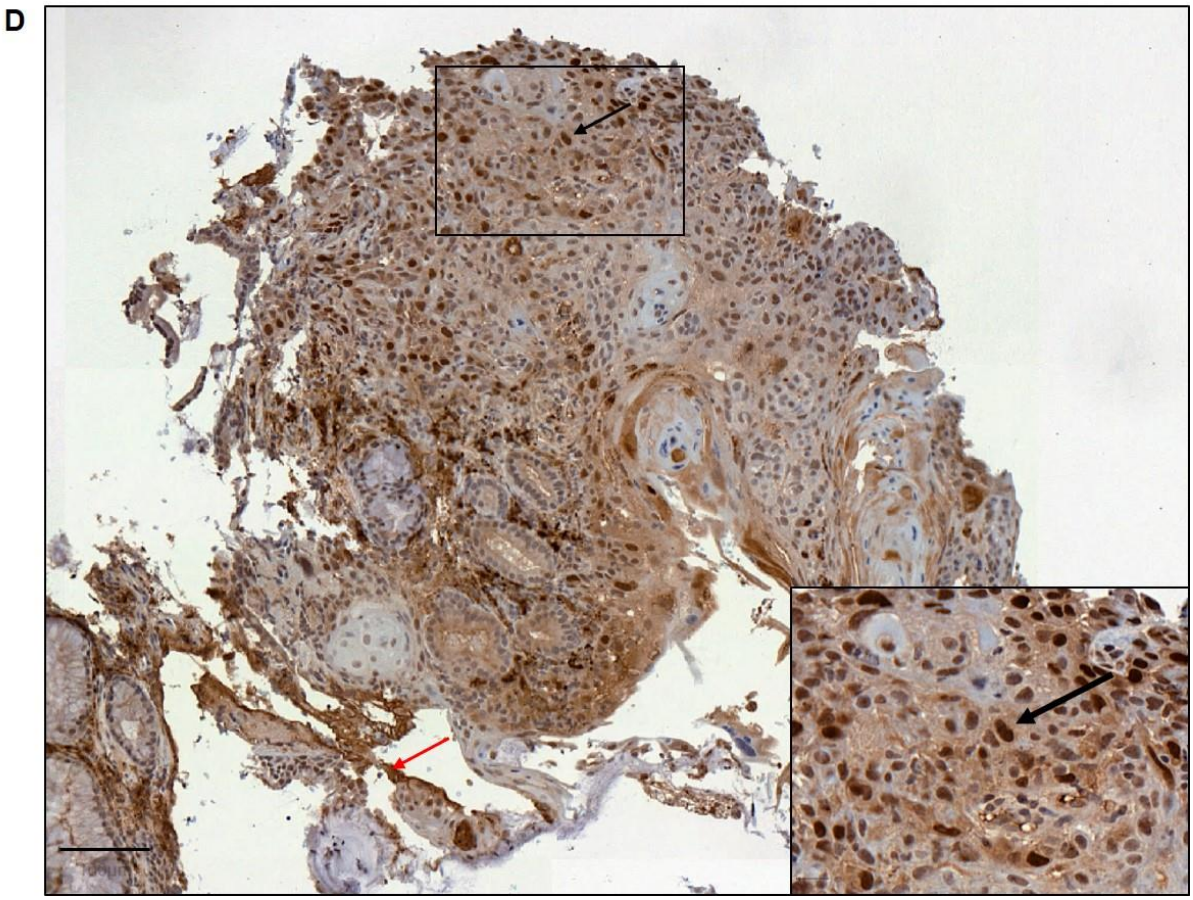

Figure 6.4. **AURKA IHC staining in H460 cell line pellets transfected with scrambled or AURKA siRNA and patient biopsy samples using pressure cooker antigen retrieval, citrate retrieval buffer and ABC signal amplification. A.** Representative images of AURKA IHC staining in H460 cell line pellets. No antibody controls were counterstained with Gill's haematoxylin. Antibody signal on stained cells was developed with DAB for 3 minutes 30 seconds (N=1). Scale bars represent 50 μm. **B.** Western blot for AURKA in H460 lysates from cells 24-hours post-transfection with scrambled siRNA or AURKA siRNA 1/2. Lysates sampled from populations that were used to create cell line pellets in A (N=1). **C**. IHC staining for AURKA in H460 cell line pellets transfected with scrambled siRNA +/- 1:1000 blocking peptide (N=1). Scale bars represent 400 μm (- blocking peptide) and 250 μm (+ blocking peptide) respectively. **D**. AURKA staining in the diagnostic biopsy of a SCC NSCLC patient using 1:1000 primary antibody. DAB exposure was for 3 minutes 30 seconds. Cells were counterstained with haematoxylin. Scale bar represents 100 μm. Area within the small rectangle is re-represented in image bottom right corner 5x larger. Black arrow indicates epithelial cancer cell with positive nuclear and cytoplasmic staining. Red arrow indicates area of non-specific stain. All slides were scanned using a panoramic 250 slide scanner using a 20x objective.

These results suggest that AURKA staining protocol was potentially successful in detecting AURKA but improvements to the signal:background ratio were required to ensure the specificity of stain in biopsy samples.

6.2.2.2. AURKA staining in NSCLC cell line pellets and patient biopsy samples optimising primary antibody incubation and concentration, antigen retrieval method and buffer and signal detection system

To improve the sensitivity of the staining protocol 1:200 primary antibody was used in line with a published example using the same antibody for IHC in NSCLC samples (Xu *et al.* 2014). Initial protocol optimisations would use this concentration of antibody, pressure cooker antigen retrieval, pH 6.1 citrate target retrieval solution for antigen retrieval and ABC signal amplification for signal detection as a baseline of comparison. The length of primary antibody incubation (1 hour vs 18 hours), antigen retrieval method (pressure cooker vs microwave), antigen retrieval buffer (pH 6.1 citrate target retrieval solution vs pH 9.0 Tris EDTA buffer) and signal detection system (ABC vs ImmPRESS® kits) was then altered to see which protocol provided best trade-off between sensitivity and specificity in the H460 cell line pellets described above.

Here we show that the baseline protocol with 1:200 primary antibody was associated with significant background stain both with 1 hour and overnight incubations and poorly discriminated cell line pellet expression levels (see Figure 6.5 A-B). Microwave antigen retrieval, compared to pressure cooker method, was associated with increased specificity after 1 hour primary antibody incubation, producing staining consistent with siRNA depletion data, although this specificity was lost when incubating primary antibody overnight (see Figure 6.5 A-B). The pH 9.0 Tris EDTA

buffer, compared to pH 6.1 citrate target retrieval solution, did not provide any superior specificity with either 1 hour or overnight primary antibody incubation (see Figure 6.5 A-B). The ImmPRESS® detection system, compared to ABC kit, demonstrated improved correlation of staining with gene expression data after 1 hour primary antibody incubation but specificity was lost when antibody incubation was overnight (see Figure 6.5 A-B).

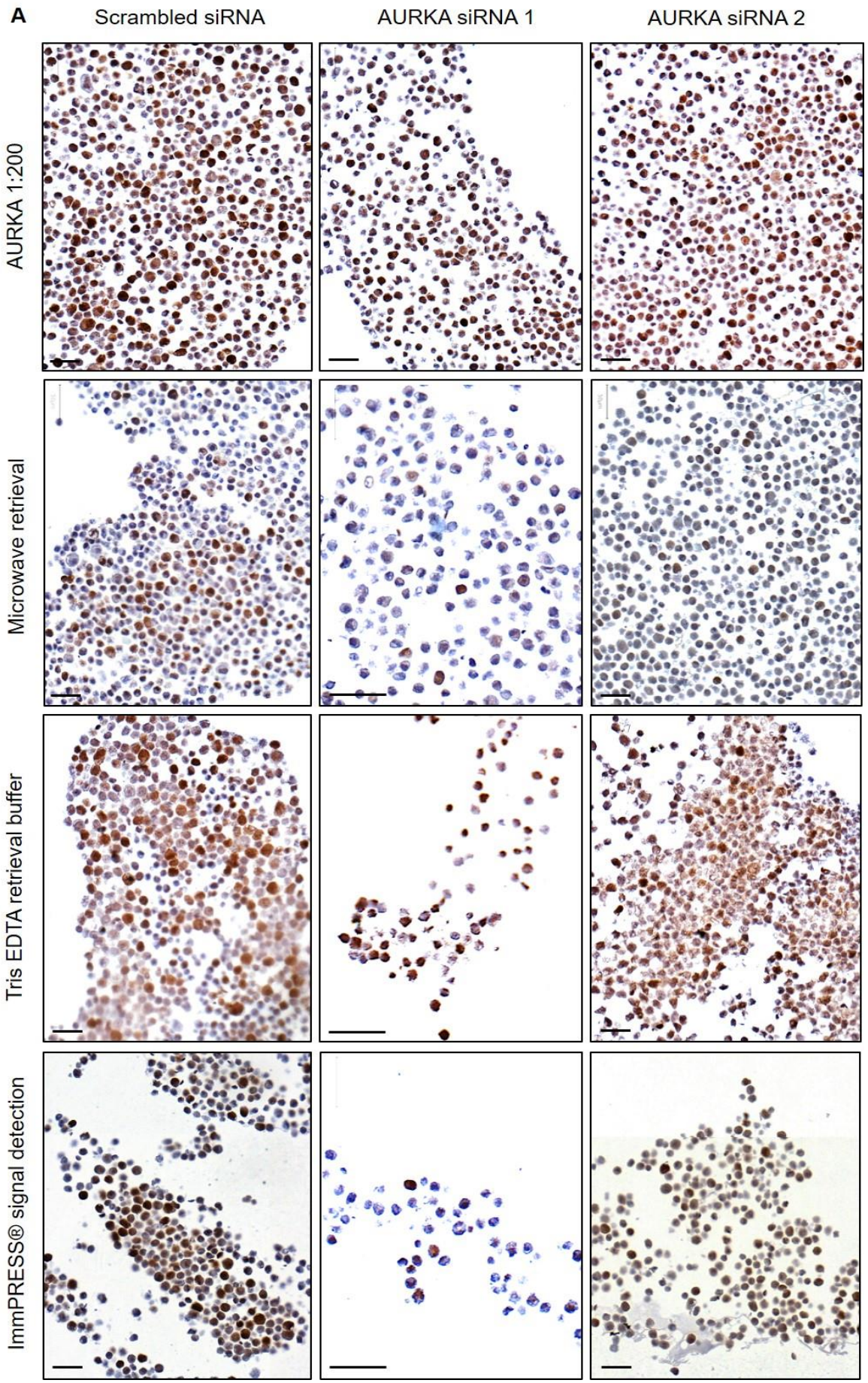

Figure 6.5. **AURKA IHC staining in H460 cell line pellets transfected with scrambled or AURKA siRNA after varying antigen retrieval method, antigen retrieval buffer and signal detection system.** Legend on page 274.

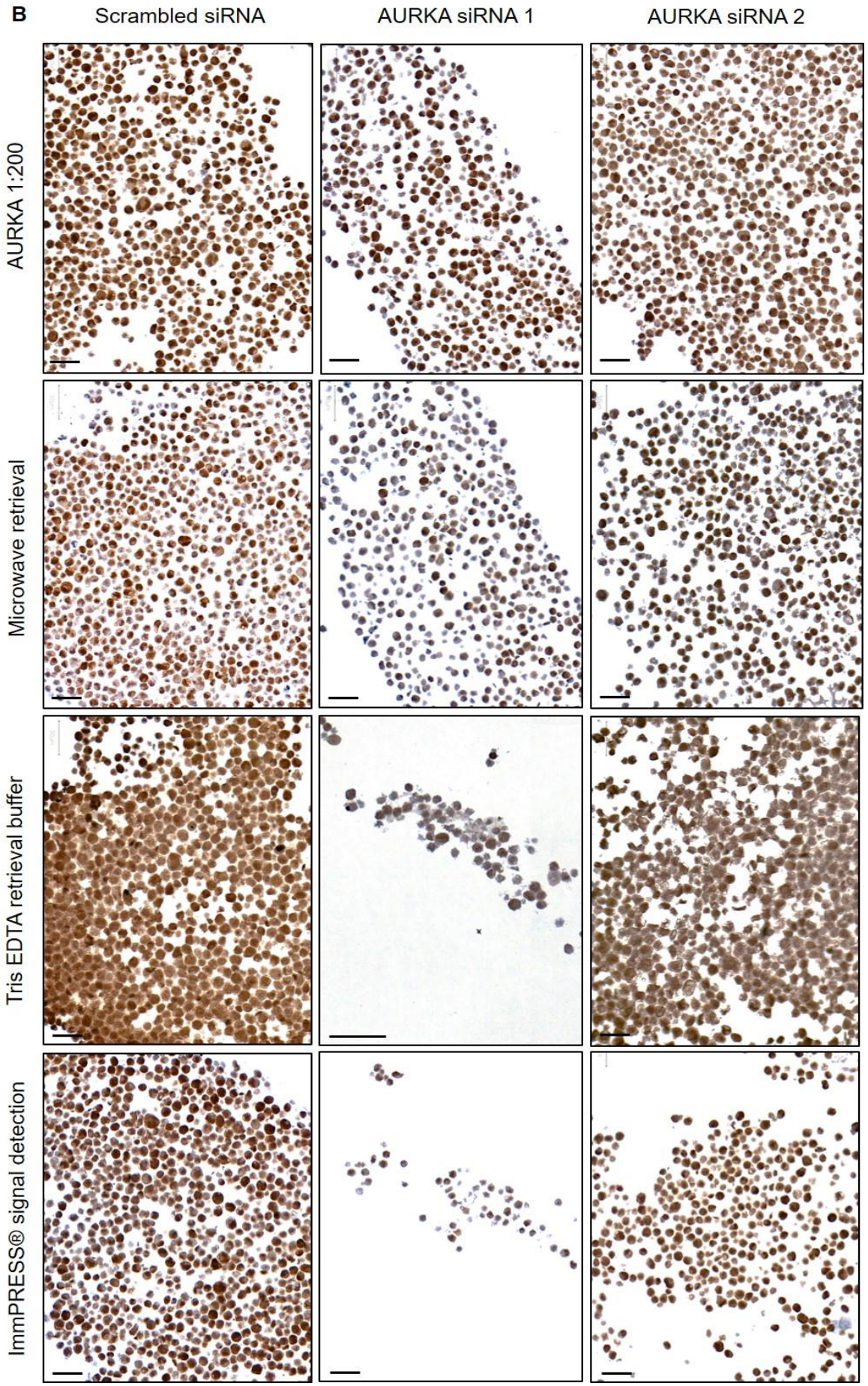

Figure 6.5. **AURKA IHC staining in H460 cell line pellets transfected with scrambled or AURKA siRNA after varying antigen retrieval method, antigen retrieval buffer and signal detection system.** Legend overleaf

Figure 6.5. **AURKA IHC staining in H460 cell line pellets transfected with scrambled or AURKA siRNA after varying antigen retrieval method, antigen retrieval buffer and signal detection system.** Representative images of AURKA IHC staining in H460 cell line pellets after **A.** 1 hour primary antibody incubation and **B.** overnight primary antibody incubation. Standard comparative protocol using labelled 1:200 AURKA used pressure cooker retrieval, pH 6.1 citrate target retrieval solution and ABC detection system. Antibody signal on stained cells was developed with DAB for 3 minutes 30 seconds and cells were counterstained with Gill's haematoxylin (N=1). Scale bars represent 50 μm. All slides were scanned using a panoramic 250 slide scanner using a 20x objective.

These data suggest that using microwave retrieval method or ImmPRESS® signal detection system with 1 hour primary antibody incubation enhanced the specificity of the AURKA staining protocol compared to the standard protocol. Given this we investigated using microwave retrieval in combination with the ImmPRESS system, using 1 hour primary antibody incubation, microwave retrieval method, pH 6.1 citrate target retrieval solution and ABC signal detection as standard. We also used an increased concentration of 1:200 AURKA blocking peptide to compare the specificity of staining protocols.

Here we found that both microwave retrieval alone and microwave retrieval with ImmPRESS® detection method achieved staining consistent with gene expression data in cell line pellets (see Figure 6.6 A-B). However, when using the AURKA blocking peptide we see greater reduction in signal in the protocol combining microwave retrieval and ImmPRESS® signal detection, suggesting that this protocol provided superior specificity. Using the combined protocol with microwave retrieval and ImmPRESS® signal detection to stain patient biopsies also significantly reduced background compared to the first attempt, with evidence of a small number of weakly positive tumour cells (see Figure 6.6 C-D).

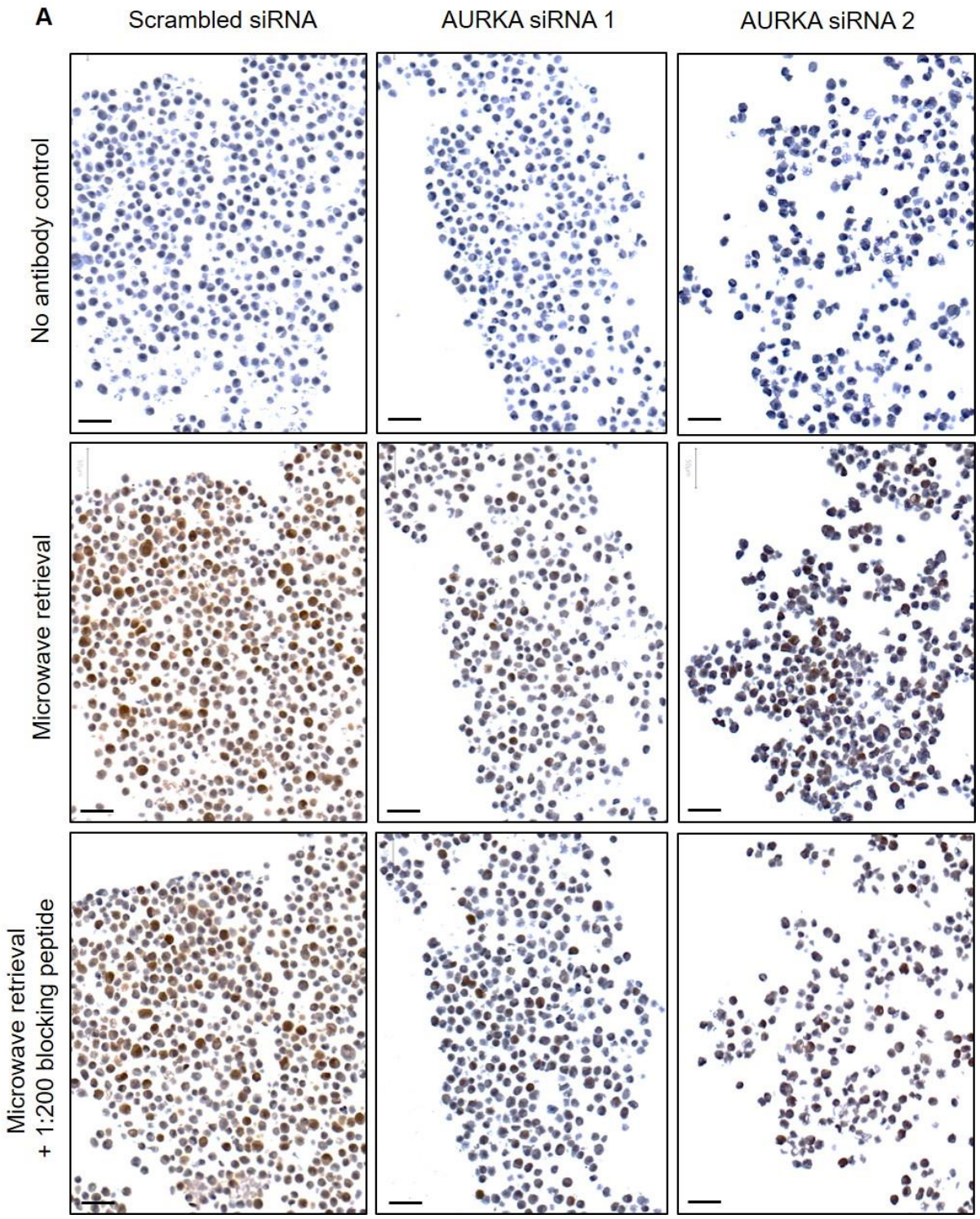

Figure 6.6. **AURKA IHC staining in H460 cell line pellets transfected with scrambled or AURKA siRNA and patient biopsy samples after microwave retrieval method and ImmPRESS® detection system.** Legend on page 278.

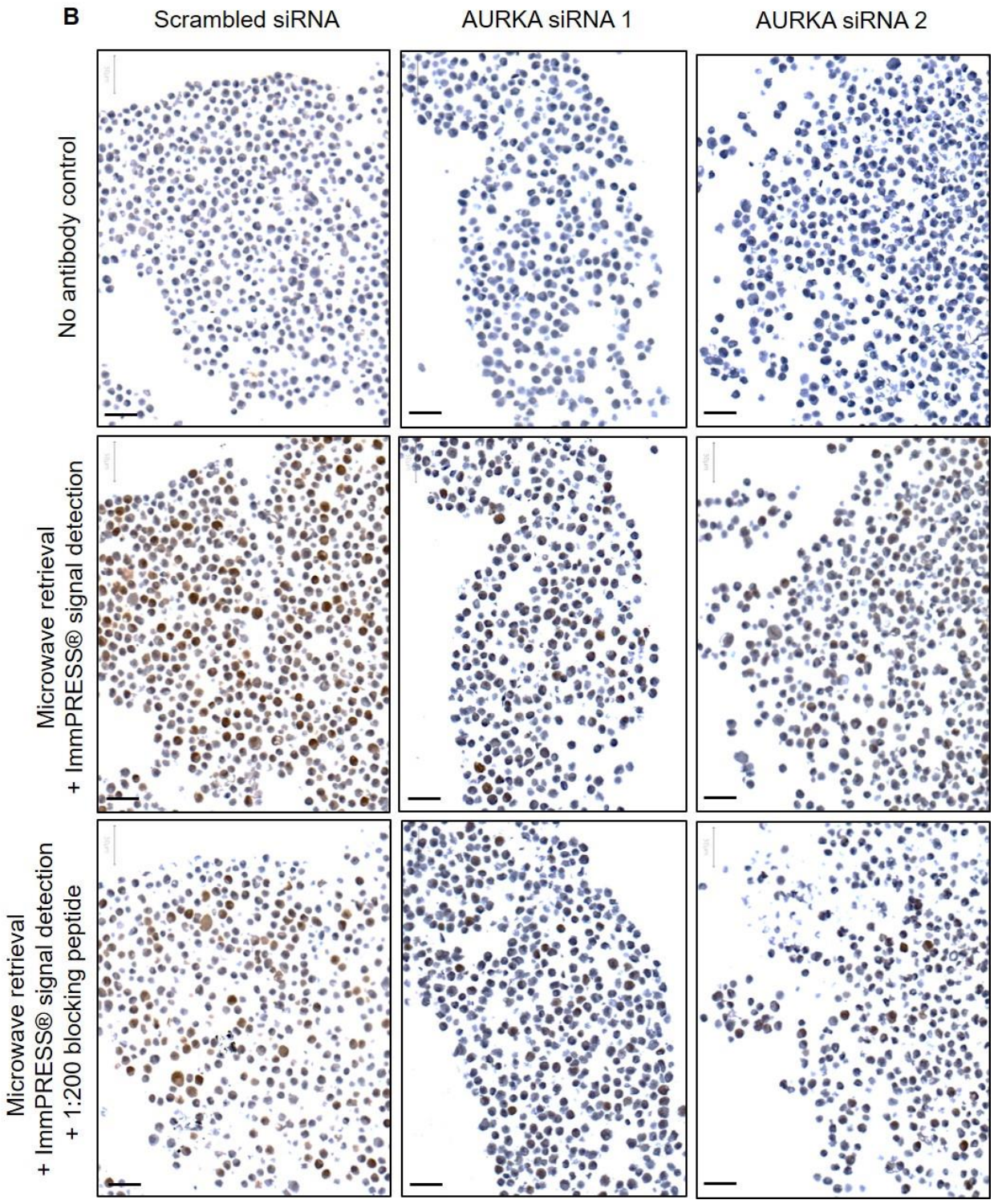

Figure 6.6. **AURKA IHC staining in H460 cell line pellets transfected with scrambled or AURKA siRNA and patient biopsy samples after microwave retrieval method and ImmPRESS® detection system.** Legend on page 278.

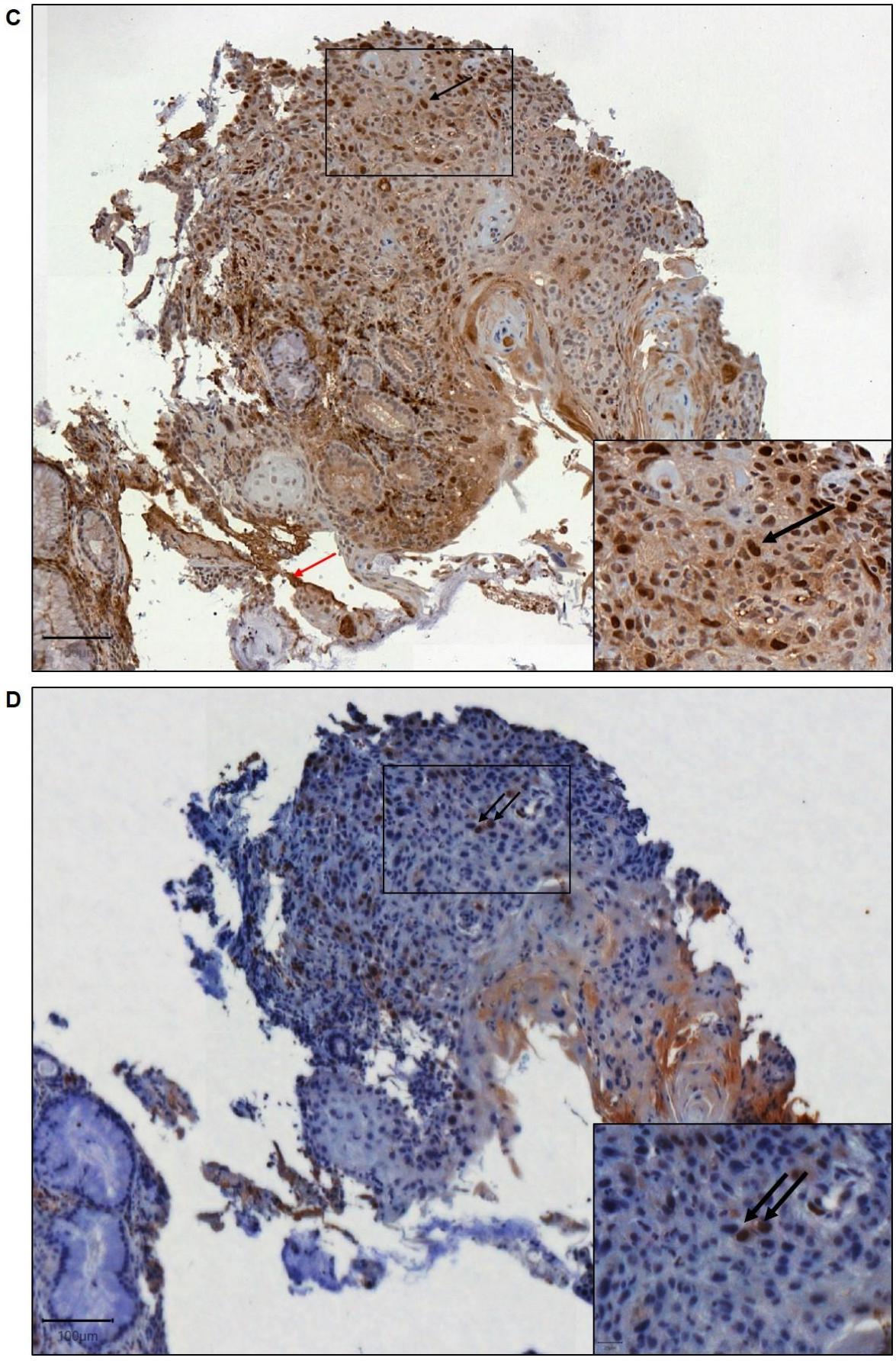

Figure 6.6. **AURKA IHC staining in H460 cell line pellets transfected with scrambled or AURKA siRNA and patient biopsy samples after microwave retrieval method and ImmPRESS® detection system.**

Legend overleaf

Figure 6.6. **AURKA IHC staining in H460 cell line pellets transfected with scrambled or AURKA siRNA and patient biopsy samples after microwave retrieval method and ImmPRESS® detection system.** Representative images of AURKA IHC staining using in H460 cell line pellets after **A.** microwave retrieval with ABC signal detection system and **B.** microwave retrieval with ImmPRESS® signal detection system. Tissues stained with 1:200 AURKA primary antibody +/- blocking peptide. Antibody signal on stained cells was developed with DAB for 3 minutes 30 seconds and cells were counterstained with Gill's haematoxylin (N=1). Scale bars represent 50 μm **C.** AURKA staining in the diagnostic biopsy of a SCC NSCLC patient using 1:1000 primary antibody with overnight incubation, pressure cooker retrieval and ABC signal detection system re-represented for comparative purposes. DAB exposure was for 3 minutes 30 seconds. **D.** AURKA staining in a section from the same diagnostic biopsy in C, using 1:200 primary antibody with 1 hour incubation, microwave antigen retrieval and ImmPRESS® signal detection system. DAB exposure was for 15 minutes. Cells were counterstained with haematoxylin. Scale bars represent 100 μm. Area within the small rectangle is re-represented in image bottom right corner 5x larger. Black arrow indicates epithelial cancer cells with positive nuclear and cytoplasmic staining. All slides were scanned using a panoramic 250 slide scanner using a 20x objective.

This suggested that using microwave antigen retrieval with ImmPRESS signal detection had increased the specificity of AURKA staining in both cell line pellets and diagnostic NSCLC tumour samples. However, whilst positive signal was clear in cell line pellets we observed reduced sensitivity for AURKA detection in diagnostic NSCLC tumour samples. Whilst measures were taken to mimic fixation procedures in cell line pellets as in diagnostic biopsy material, this discrepancy in staining sensitivity may be explained by extent of fixation (Ramos-Vara 2005). Therefore, we investigated using increased primary antibody concentration and extended antigen retrieval time with the optimised protocol so see if we could achieve enhanced staining sensitivity in the absence of increasing background. This was firstly tested in cell line pellets, despite adequate staining sensitivity in this material, due to the precious nature of diagnostic biopsy material.

Increasing primary antibody concentration to 1:100 and 1:50 was associated with increasing positive signal that still discriminated well between cell line pellet AURKA protein expression levels (see Figure 6.7 A). However, use of the blocking peptide revealed that increasing the antibody concentration to 1:100 and 1:50 was also associated with increased non-specific signal (see Figure 6.7 B). Using extended microwave antigen retrieval also resulted in increased positive signal that was in line with levels of AURKA protein known to be present in the cell line pellets (see Figure 6.7 C). Extended microwave antigen retrieval with blocking peptide incubation resulted in general reduction of signal intensity indicating that this protocol was specific. Combining extended microwave antigen retrieval with increased primary antibody concentration resulted in significant non-specificity that did not discriminate AURKA protein expression in cell line pellets and thus was not a useful approach (see Appendix Figures 8.7 and 8.8). Extended microwave antigen retrieval in patient samples resulted in superior sensitivity, compared to the standard microwave retrieval protocol, in the absence of excessive background signal (see Figure 6.7 D-E).

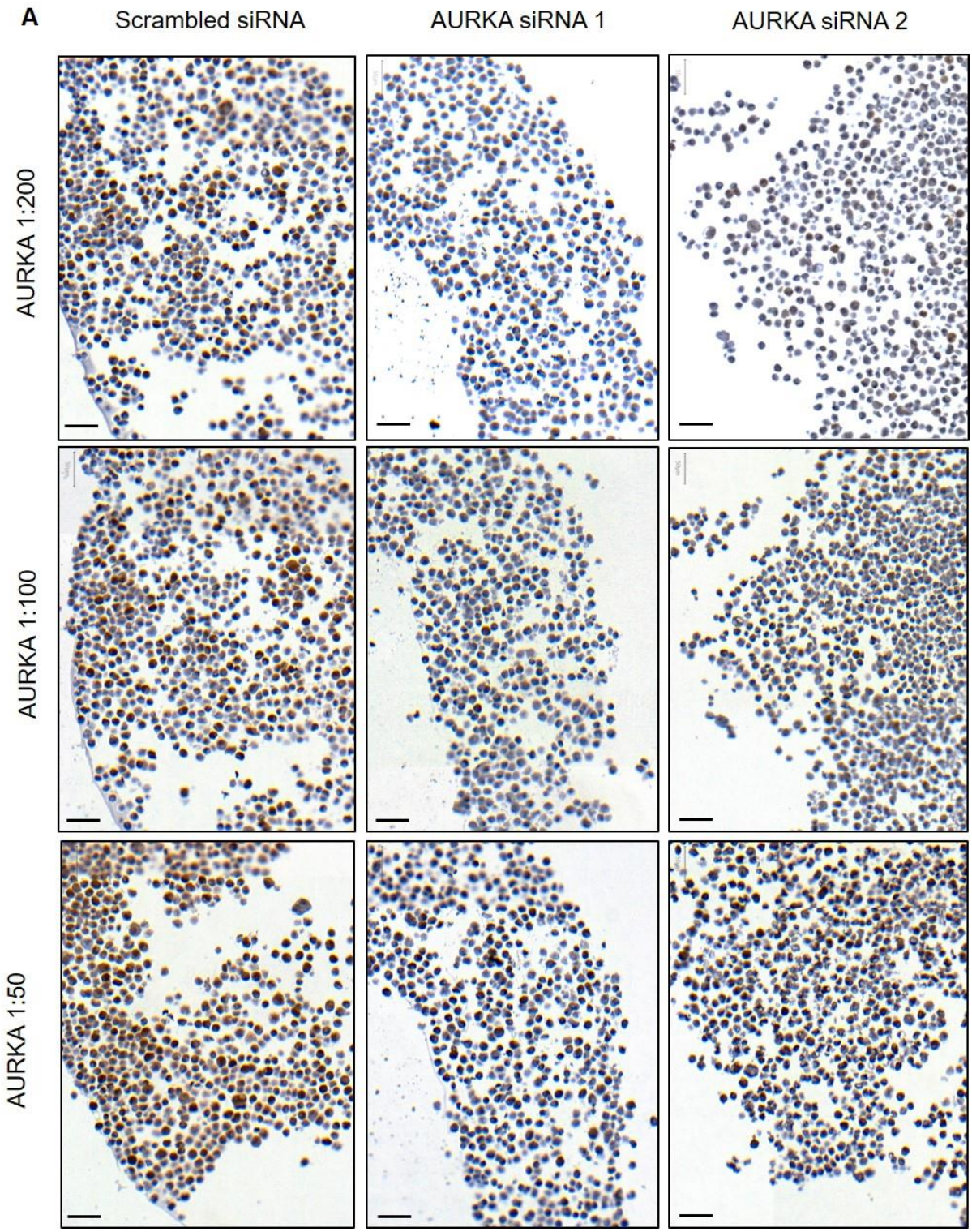

Figure 6.7. **AURKA IHC staining in H460 cell line pellets transfected with scrambled or AURKA siRNA and patient biopsy samples using increased primary antibody concentration or extended microwave retrieval method.**
Legend on page 284.

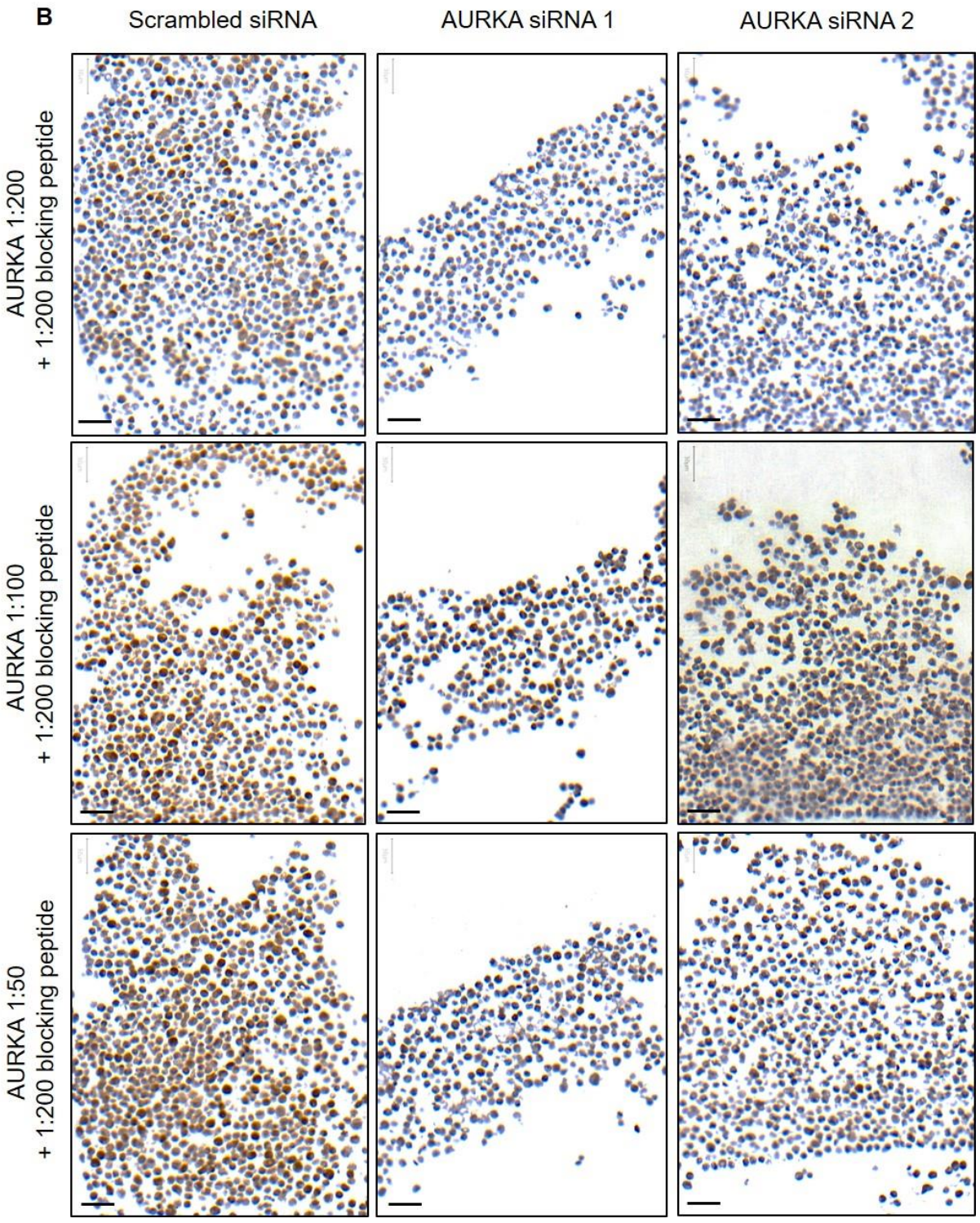

Figure 6.7. **AURKA IHC staining in H460 cell line pellets transfected with scrambled or AURKA siRNA and patient biopsy samples using increased primary antibody concentration or extended microwave retrieval method.** Legend on page 284.

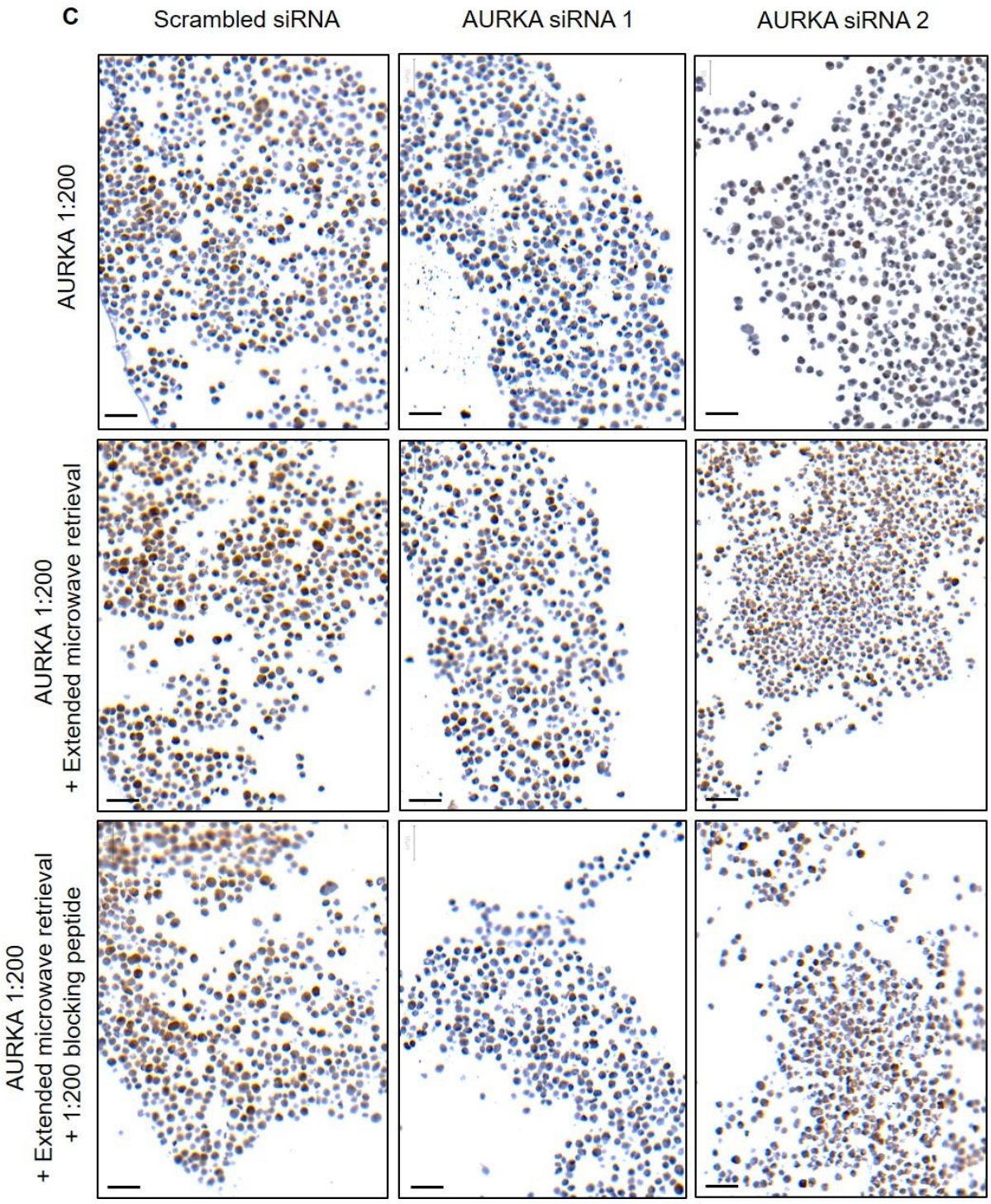

Figure 6.7. **AURKA IHC staining in H460 cell line pellets transfected with scrambled or AURKA siRNA and patient biopsy samples using increased primary antibody concentration or extended microwave retrieval method.** Legend on page 284.

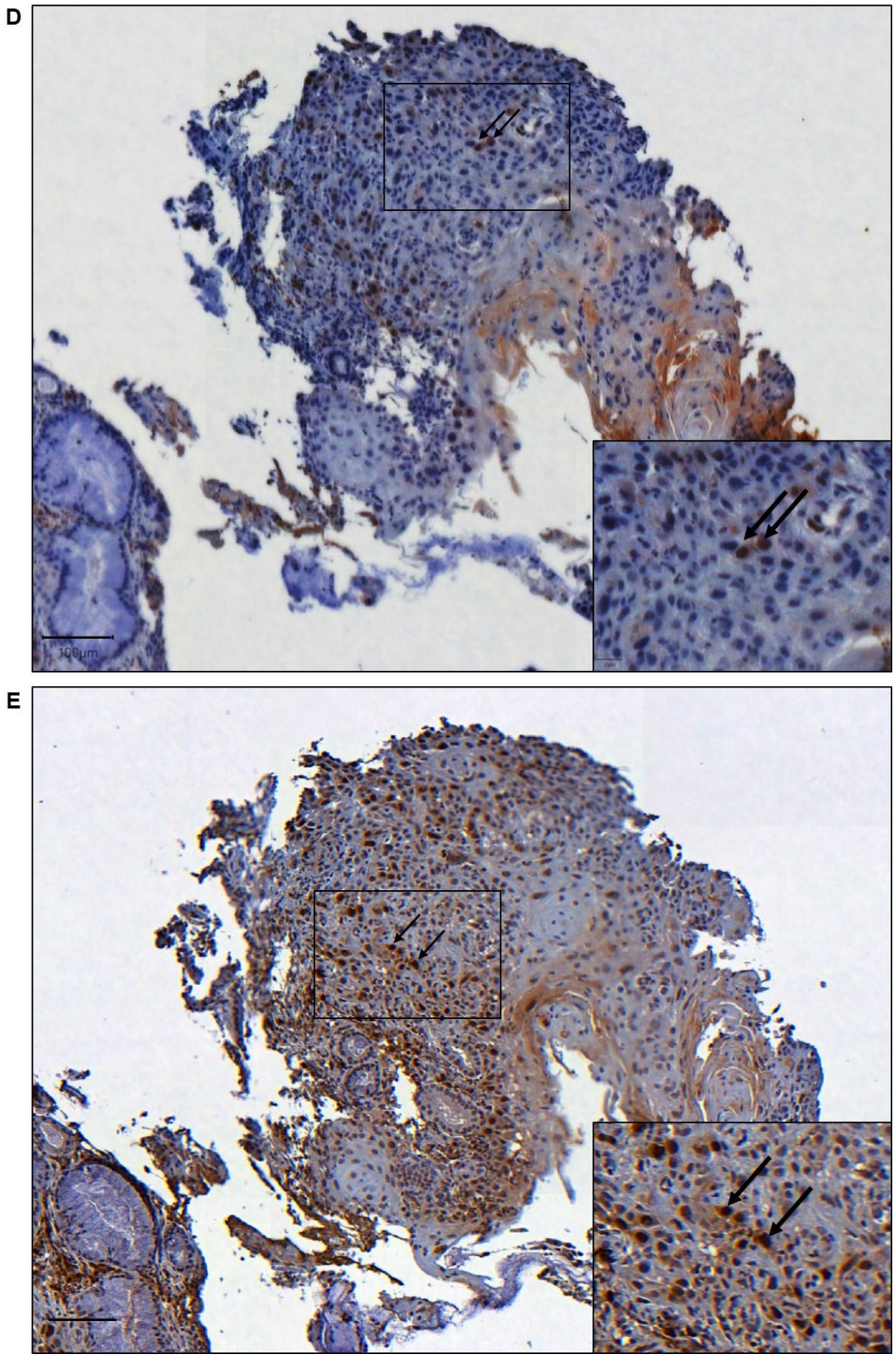

Figure 6.7. **AURKA IHC staining in H460 cell line pellets transfected with scrambled or AURKA siRNA and patient biopsy samples using increased primary antibody concentration or extended microwave retrieval method.** Legend on overleaf.

Figure 6.7. **AURKA IHC staining in H460 cell line pellets transfected with scrambled or AURKA siRNA and patient biopsy samples using increased primary antibody concentration or extended microwave retrieval method.** Representative images of AURKA IHC staining using in H460 cell line pellets after **A.** Microwave retrieval with ImmPress® signal detection system and increasing primary antibody concentration **B.** As in A with blocking peptide. **C.** With extended microwave retrieval protocol with ImmPRESS® signal detection system +/- blocking peptide. Antibody signal on stained cells was developed with DAB for 3 minutes 30 seconds and cells were counterstained with Gill's haematoxylin (N=1). Scale bars represent 50 μm. **D.** AURKA staining in the diagnostic biopsy of a SCC NSCLC patient section using 1:200 primary antibody with 1 hour incubation, standard microwave antigen retrieval and ImmPRESS® signal detection system re-represented for comparative purposes. DAB exposure was for 15 minutes. **E.** AURKA staining in a section from the same diagnostic biopsy in C, using extended microwave antigen retrieval. DAB exposure was for 7 minutes. Cells were counterstained for haematoxylin. Scale bars represent 100 μm. Area within the small rectangle is re-represented in image bottom right corner 5x larger. Black arrow indicates epithelial cancer cells with positive nuclear and cytoplasmic staining. All slides were scanned using a panoramic 250 slide scanner using a 20x objective.

Taken together these data indicate that using extended microwave antigen retrieval time along with our optimised AURKA staining protocol improves protocol sensitivity in both cell line pellets and patient diagnostic biopsy samples without reduction in signal specificity.

6.3. Discussion

In this chapter we present data that illustrates that high AURKA mRNA expression is associated with associated with a poor prognosis in NSCLC ADC patients but not SCC patients. We also show that in a cohort of NSCLC patients receiving radiotherapy that high AURKA mRNA expression is associated with poorer clinical outcomes. Finally, we show that AURKA protein expression can be detected with specificity in cell line pellets using an optimised protocol, and that with further

optimisation an acceptable signal:background ratio could be achieved in NSCLC biopsy samples.

6.3.1. High AURKA mRNA expression is associated with a poor prognosis in ADC but not SCC NSCLC patients

We present data that high AURKA mRNA expression is associated with poorer overall survival in NSCLC, which when tissue histology was accounted for was only true in NSCLC ADC but not SCC. This corroborates other published data that supports a prognostic role for high AURKA mRNA expression in NSCLC ADC (Li *et al.* 2018; Zhang *et al.* 2018) but contrasts with data that suggest that AURKA protein overexpression is prognostic in NSCLC SCC only (Ogawa *et al.* 2008) or in neither subtype (H.J. Lee *et al.* 2012). These discrepancies may be accounted for by the mRNA approach adopted here compared to the protein detection by Ogawa *et al* (2008) and Lee *et al* (2012). Ogawa *et al* (2008) found that only peri-membrane overexpression of AURKA was of prognostic importance in SCC and this biological complexity is not accounted for by mRNA expression. It would be interesting to see if there is a prognostic/predictive role for high AURKA (mRNA/protein) expression in NSCLC LCC, despite this subtype being less common compared to ADC and SCC (Chen *et al.* 2014).

6.3.2. High AURKA mRNA expression is associated with poorer clinical outcomes in NSCLC patients receiving radiotherapy

Our data also show that in a NSCLC ADC patient cohort receiving radiotherapy, high AURKA mRNA expression was associated poorer overall survival, reduced time to first progression and a trend for reduced post-progression. These data suggest that treatment outcomes post-radiotherapy in NSCLC ADC are poorer when AURKA

mRNA expression is high which is in line with a predictive role suggested in cervical squamous cell carcinoma (Ma *et al.* 2017). Further investigations are needed to see if these findings are validated when detecting AURKA at the protein level, and if shorter-term radiotherapy response is also affected by AURKA expression status as seen by Ma *et al* (2017).

6.3.3. AURKA protein staining protocol is sensitive and specific in cell line pellets and in NSCLC patient diagnostic biopsy samples

Here we show that our optimised AURKA staining protocol is sensitive and specific and discriminates well between AURKA protein expression levels in cell line pellets. We show that use of our primary antibody at 1:200, in line with previous reports (Xu *et al.* 2014), provided adequate sensitivity whilst microwave antigen retrieval method, pH 6.1 citrate target retrieval solution and ImmPRESS signal detection system all contributed to the specificity of the staining protocol. However, in NSCLC patient diagnostic biopsies we found that our improved protocol lacked sensitivity. Alteration of this protocol, by using extended microwave antigen retrieval, improved the signal sensitivity of AURKA staining without reducing specificity in both cell line pellets and patient biopsy samples. This suggests that fixation procedure may be an important factor in any future studies of AURKA in NSCLC (Ramos-Vara 2005) and may require fresh or frozen tissue specimens to ensure that fixation procedure is consistent between samples. The extended microwave antigen retrieval protocol produced both cytoplasmic and nuclear staining pattern in NSCLC epithelial cells consistent with previous reports (Lo Iacono *et al.* 2011; Xu *et al.* 2014). We are now prepared to assess AURKA protein expression in our NSCLC cohort and will correlate AURKA staining status with three month radiological response to radiotherapy, time to tumour progression and overall survival. This will give an

indication of the predictive utility of AURKA expression in NSCLC patients receiving radical radiotherapy or high dose palliative radiotherapy. It will also be important in any future clinical trials of AURKA where AURKA staining can be assessed as a biomarker of response to AURKA inhibition/radiation response. Additionally, given that we see that AURKA inhibition radiosensitised NSCLC cell lines in a p53-dependent manner *in vitro,* assessment of both p53 and AURKA protein expression in pre-therapy samples may be of predictive utility when combining AURKA inhibitors and radiotherapy in NSCLC patients.

6.3.4. Limitations

One weakness associated with our KM plotter data is a lack of patient/treatment associated information. Whilst the prognostic impact of high AURKA mRNA expression stands in a large cohort of NSCLC patients, a lack of dosing information is limiting in the subset of patients receiving radiotherapy. The NSCLC cohort analysed is comprised of early stage (I and II) ADC patients (Director's Challenge Consortium for the Molecular Classification of Lung *et al.* 2008). It is therefore possible that radiotherapy treatment was used in a combinational/adjuvant setting and therefore our findings in this smaller cohort are particularly at risk to confounding variables. Another weakness associated with our KM plotter data is that it only appraises AURKA expression at the mRNA level. It is well-established that mRNA levels do not always equate to protein expression levels (de Sousa Abreu *et al.* 2009) and AURKA overexpression has been demonstrated through transcription-independent mechanisms (Kitajima *et al.* 2007). Therefore, AURKA protein expression, in the absence of mRNA overexpression, could affect our KM plotter data and highlight the importance of our clinical study with control for extraneous variables and appraisal of AURKA expression at the protein level.

It is also possible that our findings using KM plotter AURKA mRNA expression data, and any potential future correlations between AURKA protein data and NSCLC radiotherapy outcomes, are related to the prognostic impact of AURKA expression and unrelated to specific therapeutic outcome. A true predictive biomarker identifies patients who are most likely to respond positively to a given treatment (Paesmans 2012) and is best exemplified by Her2 positivity for Trastuzumab treatment for breast cancer (Slamon *et al.* 2011). High AURKA mRNA/protein expression is a well-established marker of malignancy and poor prognosis in multiple cancer types (Lucena-Araujo *et al.* 2011; Ma *et al.* 2017; Yan *et al.* 2018), including NSCLC (Xu *et al.* 2014; Al-Khafaji *et al.* 2017; Koh *et al.* 2017; Schneider *et al.* 2017). The prognostic impact of AURKA may therefore be misleading a potential predictive role. It is postulated that predictive biomarkers need validation through randomised clinical trials to demonstrate the specificity of prediction towards a specific treatment (Paesmans 2012) and this is outside of the scope of this study. It will be interesting to see if AURKA expression status affects three month radiotherapy response in our study, as this could provide the first indication as to whether expression status affects immediate treatment response and could hint at predictive utility. Additionally, although not performed in our study, it would useful to see if NSCLC AURKA expression changes during treatment are predictive of radiotherapy response. Like the RADAR study (Walker *et al.* 2015), this approach would have potential to identify treatment-related changes in biology which we would expect to have increased predictive utility. Moreover, staining for activated T288 p-AURKA may be a useful approach, although this would not account for kinase-independent AURKA activity which has been evidenced in breast cancer (Zheng *et al.* 2016).

Cell line pellets are useful models for IHC staining optimisation because gene expression is easily manipulated *in vitro* to provide material with varying target expression and are potentially endless sources of material. Cell line pellets do not recapitulate the tissue complexity, such as the stromal component, of NSCLC patient diagnostic samples which could affect staining properties (Gedda *et al.* 2010). We found that signal intensity, once acceptable staining was achieved in cell line pellets, was much reduced in NSCLC patient diagnostic biopsy samples. This highlights the poor translation of IHC staining between cell line pellets and biopsy samples and is potentially a consequence of prolonged fixation in patient samples, which is known to reduce antigenicity (Ramos-Vara 2005). It would be useful to have access to a biopsy sample known positive control for AURKA protein such as a normal colonic mucosa sample (Xu *et al.* 2014) to further ensure our staining protocol is adequately sensitive and specific in formalin-fixed tissue specimens.

7. Discussion

7.1. Targeting AURKA radiosensitises NSCLC cells

In this thesis we provide evidence that increased AURKA protein expression is associated with decreased radiosensitivity in NSCLC cell lines whilst increased mRNA expression was associated with a poor prognosis following radiotherapy in NSCLC patients using a publicly available database. This suggests that AURKA expression contributes to the radioresistance of NSCLC and is line with previous reports in different cancer types (Guan *et al.* 2007; Ma *et al.* 2017). We also show that AURKA is activated by IR alone 24 hours post-IR which suggests that AURKA is directly involved in the radiation response of NSCLC cells. This provides further evidence that AURKA activity following IR contributes to the cellular radiation response *in vitro* (Chen *et al.* 2017).

We find that targeting AURKA pharmacologically with Alisertib has significant anti-tumour effects in both *in vitro* and *in vivo* models of NSCLC. Importantly, we present data that demonstrate that targeting AURKA, both pharmacologically with Alisertib and with siRNA, radiosensitises NSCLC cell lines *in vitro* using single dosing events of Alisertib and IR respectively. Furthermore, we find that Alisertib monotherapy potently inhibited H460 xenograft growth and remarkably induced temporary tumour regressions in combination with IR *in vivo*. Taken together these data provide further evidence identifying AURKA as a radiosensitisation target in NSCLC *in vitro* (Myers *et al.* 2013; Woo *et al.* 2015) and *in vivo* (Woo *et al.* 2015) and that Alisertib is capable of radiosensitising cancer *in vivo* (Venkataraman *et al.* 2012; Hong *et al.* 2014). However, this is the first example of Alisertib radiosensitising NSCLC *in vivo*. We predict that this striking effect *in vivo* may be related to repeated IR and Alisertib dosing events. We show that radiosensitising effect of targeting AURKA is p53-

dependent in NSCLC cell lines *in vitro*, as previously reported (Myers *et al.* 2013), which may restrict the patient population that can benefit from this treatment combination.

We demonstrate that the radiosensitising potential of Alisertib is time-dependent requiring presence of Alisertib 24 hours post-IR. This, along with delayed activation of AURKA post-IR, provides evidence of a delayed radiosensitising mechanism and has important implications for combining Alisertib and radiation in further preclinical and human studies. In addition, this provides evidence of a pre-treatment independent effect, and therefore counters the hypothesis that the radiosensitising mechanism is through irradiation of a mitotically enriched population of cells (Manfredi *et al.* 2011). Moreover, we present that 24-hours post-treatment Alisertib inhibits IR-induced activation of AURKA and causes an accumulation of inactive AURKA protein, consistent with a function of AURKA for cell survival during recovery from IR.

7.2. Radiosensitising mechanism of the Alisertib IR combination

In this thesis we also present an evaluation of the radiosensitising mechanism/mode of cell death following Alisertib IR combination. Consistent with a delayed radiosensitising effect, we observed p53-dependent changes in NSCLC cell cycle profiles 48 hours post-treatment with Alisertib IR combination *in vitro*. By 48 hours post-treatment we observe loss of the mitotic population in p53 proficient NSCLC cell lines, but not in p53 deficient cell lines which showed greater polyploidy as a basal population and following Alisertib IR combination. In agreement with this finding, we also find that mitotic population was eliminated in p53 proficient H460 cells *in vivo* following Alisertib IR combination. H460 xenograft Ki67 staining was also reduced

following IR alone or Alisertib IR combination *in vivo*, showing that cell cycle progression was perturbed.

Additionally, we also show that H460 cells underwent increased intra-mitotic death, aberrant mitotic divisions and spent longer in mitosis 24-36 hours but not 48-62 hours following Alisertib IR treatment. This provides evidence of a time-dependent window of effect on the H460 mitotic population and may be related to time-dependent radiosensitising effect observed in the same cell line. Phenotyping of H460 mitotic cells following Alisertib IR combination highlights cooperative increases in centrosomal amplification, with or without pericentrin fragmentation, and increased anaphase population 24 hours post-treatment. There is evidence that cells with centrosome amplification are eliminated via p53-dependent mechanism (Oikawa *et al.* 2005) and this could explain the p53-dependency of radiosensitisation. Given that AURKA activity is required for centrosome clustering after centrosomal amplification (Navarro-Serer *et al.* 2019) and anaphase progression (Reboutier *et al.* 2013; Courthéoux *et al.* 2019), we speculate that AURKA is important for the integrity of mitotic progression following IR. This could explain why we see IR-induced AURKA activation, and AURKA accumulation 24 hours post-treatment in Alisertib IR combination as mitotic progression becomes impeded. Furthermore, a lack of centrosome clustering capability in Alisertib IR combination can provide the mechanistic basis for increased multipolar mitoses observed. We also observed increases in the incidence of micronuclei and multinucleation 72 hours following Alisertib IR combination in both the p53 proficient H460 and p53 deficient H1299 cell lines, indicative of increased mitotic aberrance (Vitale *et al.* 2011). Taken together, this suggests inhibition of AURKA following IR causes cell death, as seen in clonogenic survival, not due to mitotic aberrance per se but due to differential

response to a consistent stimulus. One potential outcome following mitotic aberration is senescence and we see cooperative increases in β-galactosidase expression in H460 cells following Alisertib IR combination, but not in H1299 cells. This allows us to speculate that the induction of cellular senescence following mitotic aberrance may contribute to the efficacy of the Alisertib IR combination. This is plausible given that the induction and maintenance of stress-induced senescence has been shown to occur in a p53-dependent manner (Beauséjour *et al.* 2003; Dirac and Bernards 2003; Qian and Chen 2013). The induction of cellular senescence following Alisertib IR combination treatment *in vivo* has not yet been tested.

We also demonstrate that the addition of Alisertib does not significantly alter DNA damage induction or damage resolution in the initial hours following IR but does show trend for increased residual damage 24 hours post-irradiation. This has potential to contribute to the therapeutic efficacy of the Alisertib IR combination, as persistent DNA damage is highly cytotoxic (International Atomic Energy Agency 2010). We have yet to determine if the Alisertib IR treatment combination changes the relative contributions of the different DNA damage repair pathways following IR. However, we do not predict that this effect is significant in determining the efficacy of the Alisertib IR combination as our data show that radiosensitisation occurs when Alisertib is given 24 hours post-IR, by which point the DNA damage from IR alone is mostly resolved. We show that p53 is subject to biphasic stabilisation following Alisertib IR combination, stabilising initially through IR treatment, before Alisertib mediated stabilisation predominates by 24 hours post-treatment. We also see phosphorylation of p53 at T18, which is related to SAC activation and the p53 post-mitotic checkpoint (Huang *et al.* 2009), 4 hours post-treatment with Alisertib alone but not after Alisertib IR combination. However, we currently do not understand the

functional consequences of this differential phosphorylation and if it is linked to Alisertib IR efficacy nor have we assessed direct activation of the SAC. We also do not see consistent changes to Chk1 and Chk2 activation following Alisertib IR treatment, contrary to a previous report (Sun *et al.* 2014). Overall, we find that changes to mitotic biology following Alisertib IR combination were more striking compared to any changes to the DNA damage response and therefore conclude the former is likely a greater contributor to combinational efficacy.

We present data that demonstrates greater than additive de-phosphorylation of Akt at S473 by 24 hours post-treatment with Alisertib IR combination. We hypothesise that could be the result of an equilibrium shift towards cell death as constitutively S473 phosphorylated Akt in NSCLC is associated with promotion of cellular survival (Brognard *et al.* 2001). Dephosphorylation of Akt has been shown to occur prior to apoptosis (Itoh *et al.* 2002; Sun *et al.* 2004) supporting the argument that cell death, potentially in the form of p53-dependent apoptosis, is being initiated. Akt could also could be the molecular target for induction of centrosome amplification as Akt activity is required for maintenance of centrosome homeostasis (Leonard *et al.* 2013). Given that AURKA interacts with Akt post-IR (Chen *et al.* 2017), we predict that Akt de-phosphorylation is involved in the response to Alisertib IR combination.

In summary, we hypothesise that Alisertib and IR cooperate to promote centrosomal amplification in NSCLC cells in a potentially Akt-dependent mechanism, however in the presence of AURKA inhibition centrosomal clustering and anaphase progression does not occur. This leads to increased intra-mitotic death in p53 proficient cells but not in p53 deficient cells which exit aberrant mitoses and form polyploid cells. Given we observe increased time in mitosis, it is possible that mitotic exit may be through mitotic slippage (Brito and Rieder 2006; Vitale *et al.* 2011) and thus explains the

increase in polyploid cells. We also see increased multipolar mitoses which are the result of a lack of centrosomal clustering promoting micronuclei formation and multinucleation in daughter cells. In this case we hypothesise that the extent of genomic aberration results in cooperative increases in senescence in a p53-dependent manner.

7.3. AURKA as a predictive biomarker for radiotherapy response in NSCLC

We illustrate that high AURKA mRNA expression data may be associated with poorer outcomes in a NSCLC patient cohort that received radiotherapy. However, without information about the radiotherapy given to these patients there may be confounding factors at play. Also, without initial radiotherapy response data poorer outcomes could be reflective of the well documented prognostic impact of high AURKA mRNA expression (Li *et al.* 2015; Li *et al.* 2018; Zhang *et al.* 2018) and unrelated to radiotherapy response. In cell line pellets we demonstrate that immunohistochemical detection of AURKA can be achieved and that microwave antigen retrieval combined with ImmPRESS signal detection system provided the best contrast in signal when AURKA was expressed or depleted. However, the same protocol, despite acceptable background stain, was not sensitive enough in NSCLC diagnostic biopsies. Extended microwave retrieval enhanced the sensitivity of the staining protocol in biopsy samples without reducing specificity and is suitable for staining our cohort of biopsy samples. If the Alisertib IR treatment combination is progressed to human clinical trials in NSCLC, then our data and staining optimisation will be important in accurately identifying patients with tumours evidencing high AURKA expression. Our data and others (Ma *et al.* 2017) indicate that high AURKA expression is associated with poorer radiotherapy outcomes, and therefore accurate

AURKA detection in NSCLC tumours has predictive potential and may allow for patient selection in clinical trials combining Alisertib and radiotherapy.

7.4. Future Work

We demonstrate the efficacy of the Alisertib IR combination *in vitro* and *in vivo* and support investigation of this treatment combination in human clinical trials. Inclusion of an agent into the CONCORDE platform trial in NSCLC requires evidence of an agent's synergy with radiotherapy *in vitro* and *in vivo*, assessment of additional toxicity following thoracic irradiation *in vivo* to predict toxicity patterns as well as dosing and toxicity information of said agent monotherapy in humans (Hanna *et al.* 2017). Alisertib monotherapy is well characterised in humans including NSCLC patients (Malumbres and Pérez de Castro 2014; Melichar *et al.* 2015) and therefore has immediate translational potential. Furthermore, there is pre-existing data pertaining to the use of Alisertib in a combinational context (Falchook *et al.* 2019), even with radiotherapy (Song *et al.* 2019) and can guide the design of Alisertib IR combinational trials in NSCLC patients.

Encouragingly it appears that Alisertib IR combination has an acceptable safety profile in gliomas (Song *et al.* 2019), further supporting a combinational trial in NSCLC. It would be important to further develop an AURKA staining protocol in NSCLC patients to complement any potential human trial as it could allow for patient selection/stratification. Additionally, fixation likely contributed to the requirement for extended antigen retrieval protocol (Ramos-Vara 2005) and future clinical studies should standardise the tissue fixation method, or indeed acquire fresh tissue to promote staining consistency between tissue samples.

Given the incidence of p53 aberration of NSCLC, it is essential that the p53-dependency of Alisertib IR efficacy is further examined as this will impact patient selection in any future potential clinical studies. This would be best investigated using an isogenic NSCLC system such as the H1299 H24 system (Chen *et al.* 1996) *in vitro* and *in vivo* and could be used to test the p53-dependency of the Alisertib IR combinational effects in NSCLC. Identifying the specific molecular mediators of the radiosensitising effect of Alisertib IR combination is also important. This could be achieved by assessing the phospho-proteome following Alisertib IR combination using mass spectrometry. Identifying the mediators of the radiosensitising effect of the Alisertib IR combination have predictive potential in both pre-clinical and human trials using this treatment combination.

The normal tissue effects of the Alisertib IR combination must also be appraised to inform any potential human studies, as exacerbation of normal tissue toxicities following thoracic irradiation is to be avoided. We predict that targeting AURKA in combination with radiation will be most effective in the tumour tissues which are more likely to be high AURKA expressing and enriched for mitotic/cycling cells (Lo Iacono *et al.* 2011). However, there is a risk that targeting a mitotic kinase such as AURKA will radiosensitise all proliferative tissues within the field of irradiation including normal tissues such as the oesophagus (Fountain *et al.* 2015). It is accepted that the use of platinum agents as broad radiosensitising agents in NSCLC, whilst improving overall survival (Aupérin *et al.* 2010) have increased the incidence of radiation oesophagitis and pneumonitis (Verma *et al.* 2017). It must be established if Alisertib also does the same in a preclinical setting, especially given that clinical trials such as the CONCORDE trial require a preclinical appraisal of normal tissue effects of treatment combination to predict organs at risk (Hanna *et al.*

2017). This requires at least thoracic irradiation, ideally in orthotopic models of NSCLC, in combination with Alisertib *in vivo*. This could further help guide Alisertib dosing and toxicity endpoints in any potential human clinical trials combining Alisertib and IR in NSCLC.

8. Appendix

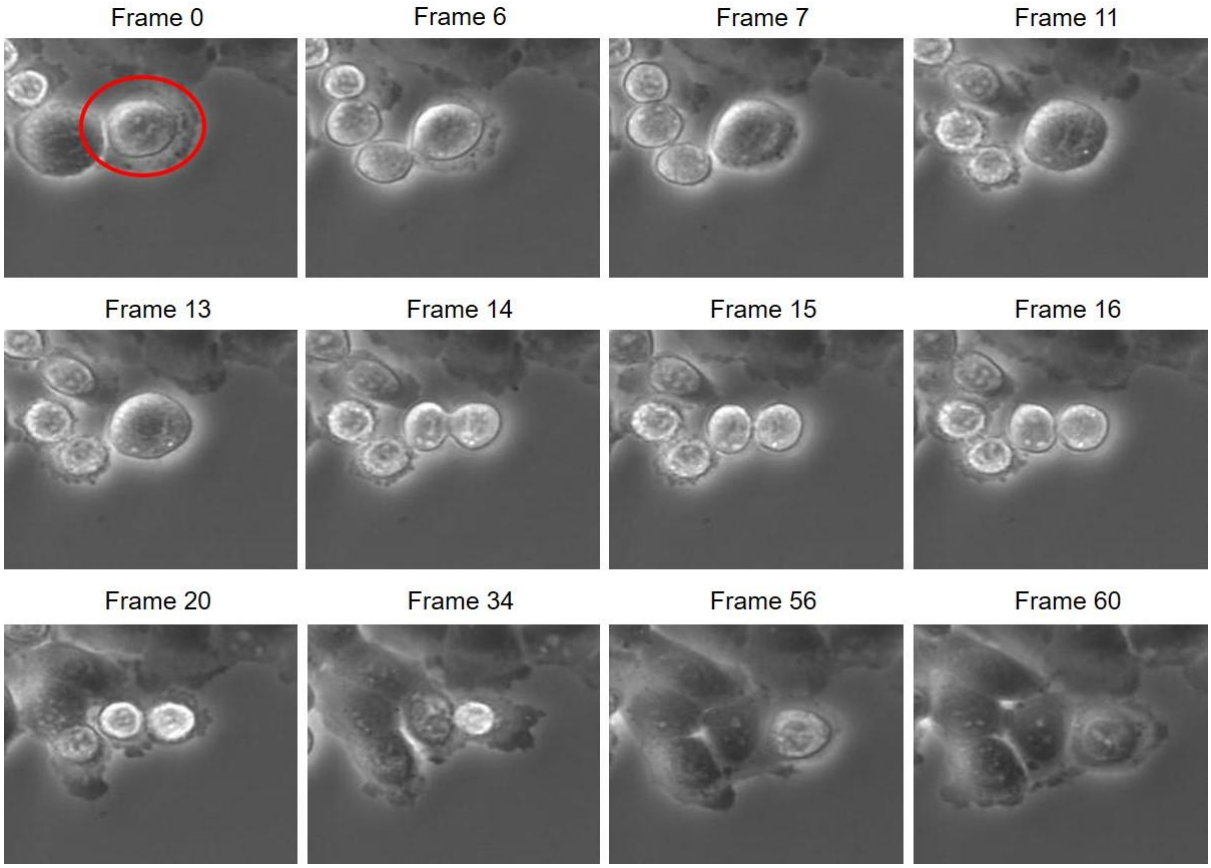

Figure 8.1. **Representative images of a H460 cell undergoing mitosis.** Circled in red is the subject cell of this video. By frame 7 the subject has swollen as the nuclear envelope breaks down. By frame 7 and 11 chromosomes can be seen aligning at the metaphase plate. By frame 14 two daughters can be visualised as the cell performs cytokinesis. By frame 20 there are two distinct daughter cells, indicating that this mitosis took approximately 13 frames (7 – 20) or 65 seconds. Cells imaged with time-lapse phase contrast microscopy and with a 20x microscope objective. Each frame was captured after 5 minute intervals.

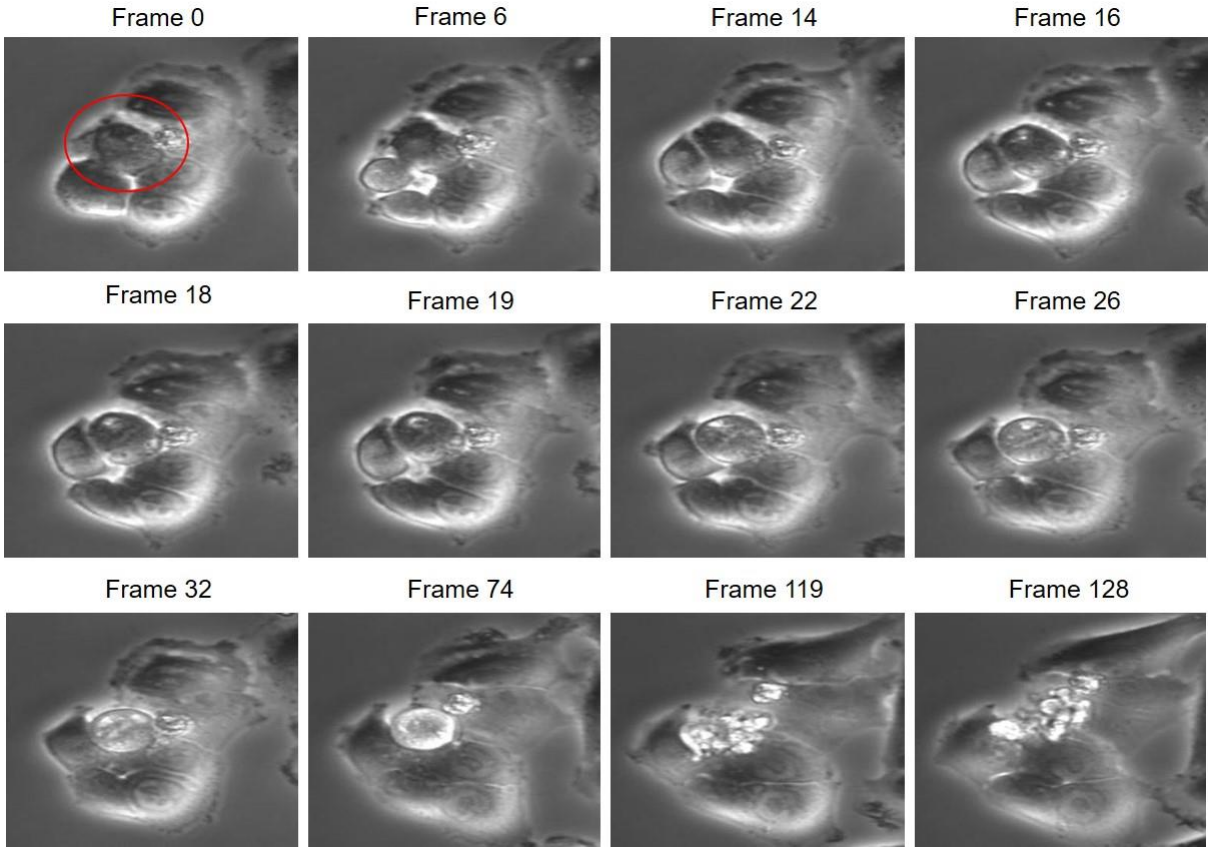

Figure 8.2. **Representative images of a H460 cell that undergoes intra-mitotic death.** Circled in red is the subject cell of this video. By frame 16 the subject has swollen as the nuclear envelope breaks down. By frame 18 the chromosomes aligning at the metaphase plate can be observed in subject. By frame 74 subject appears fully detached from well surface before cell undergoes cellular obliteration seen in frame 119 and frame 128. Cells imaged with time-lapse phase contrast microscopy and with a 20x microscope objective. Each frame was captured after 5 minute intervals.

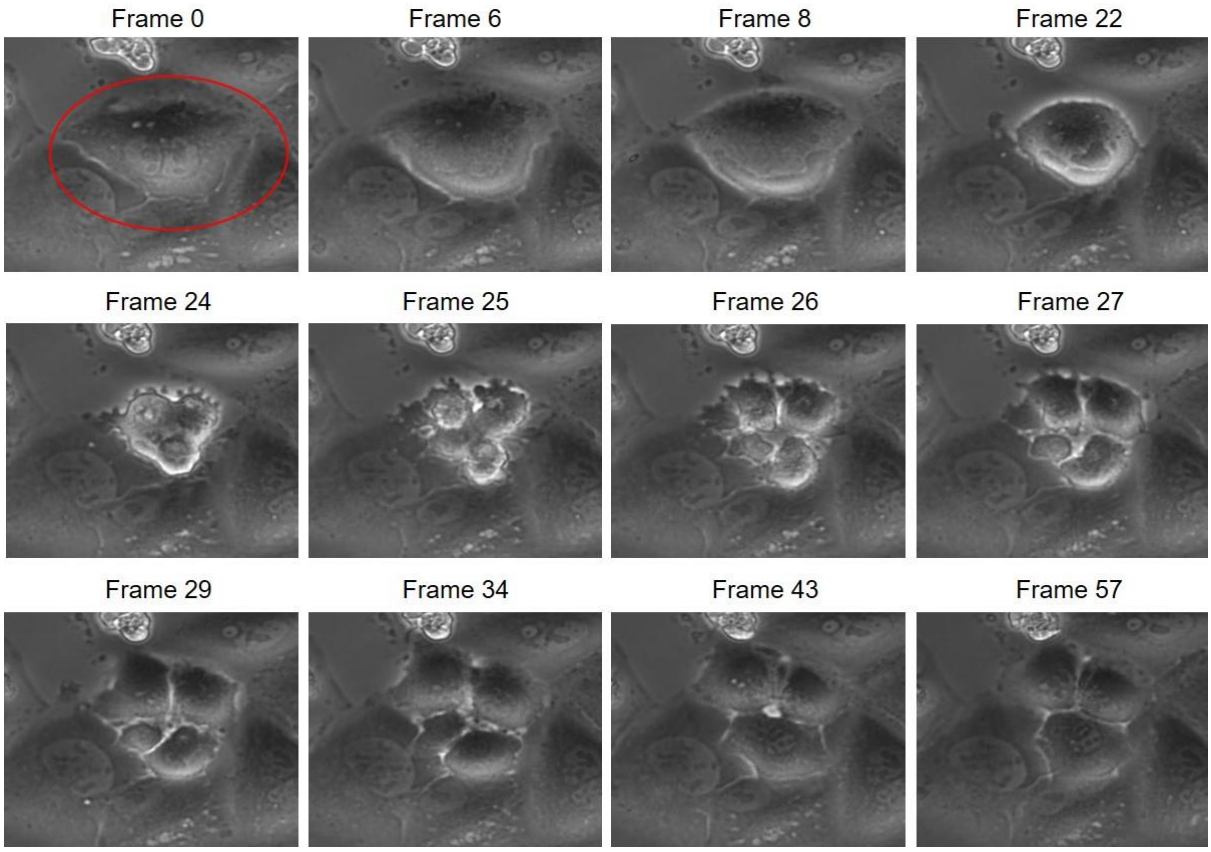

Figure 8.3. **Representative images of a H460 cell that undergoes aberrant mitosis resulting in >2 daughter cells.** Circled in red is the subject cell of this video, seen visible with multiple nuclei. By frame 6 the subject has swollen as the nuclear envelope breaks down. By frame 24-27 multipolar mitosis is occurring. By frame 43 an initial 4 daughters cells has become three as bottom left and bottom right fuse, indicative of dysfunctional cytokinesis. By frame 57 there remains three viable daughter cells. Cells imaged with time-lapse phase contrast microscopy and with a 20x microscope objective. Each frame was captured after 5 minute intervals.

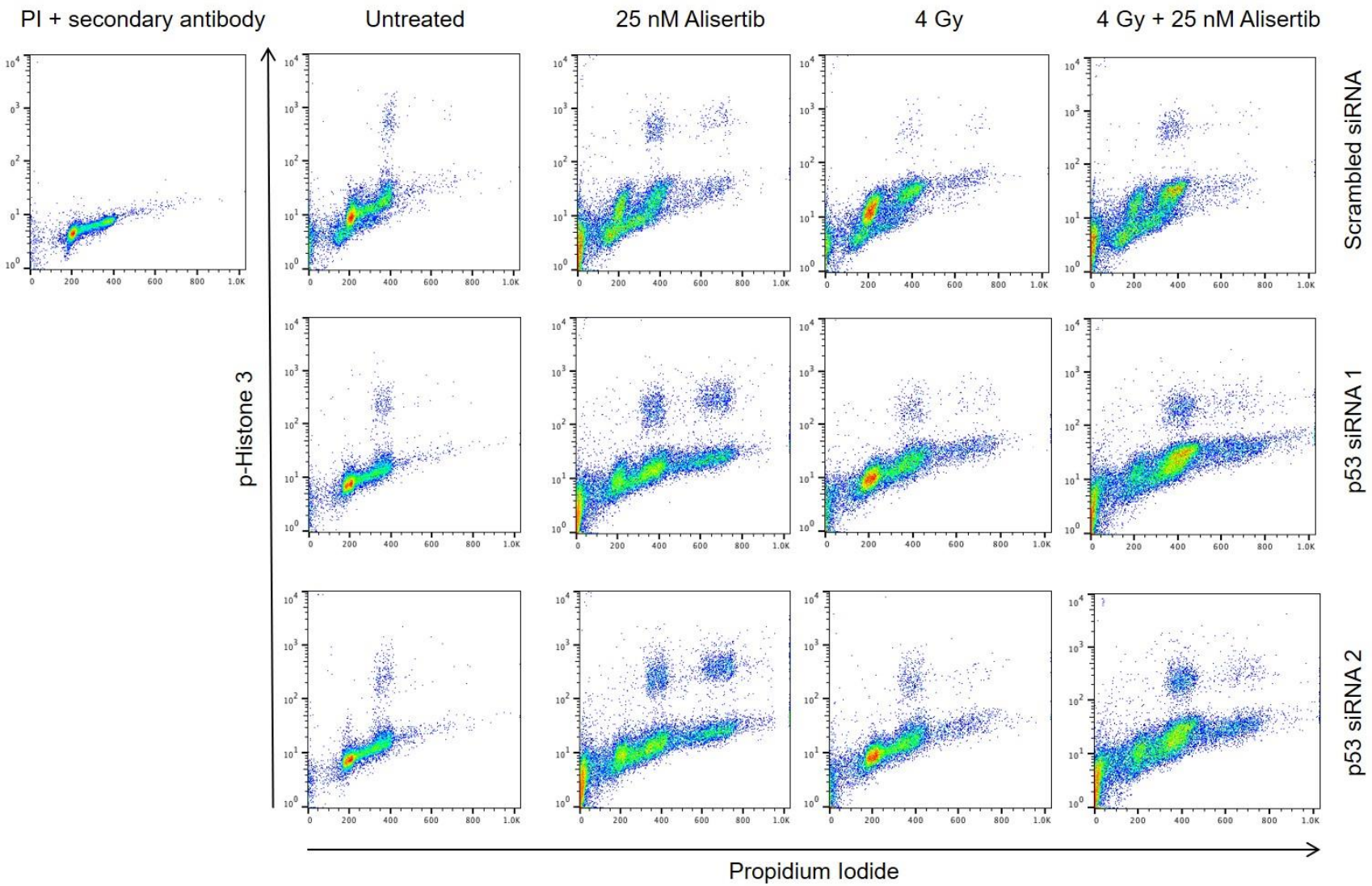

Figure 8.4. **Representative H460 FACS plots for propidium iodide (PI) staining vs p-Histone 3 staining in cells transfected with scrambled siRNA control or p53 siRNA 1/p53 siRNA 2 48 hours post-irradiation (72 hours post-transfection).** Minimum of 10,000 single cell events collected in population isolated through (PI (FL-3) width vs PI (FL-3) height). Mitotic population defined through p-Histone 3 positivity

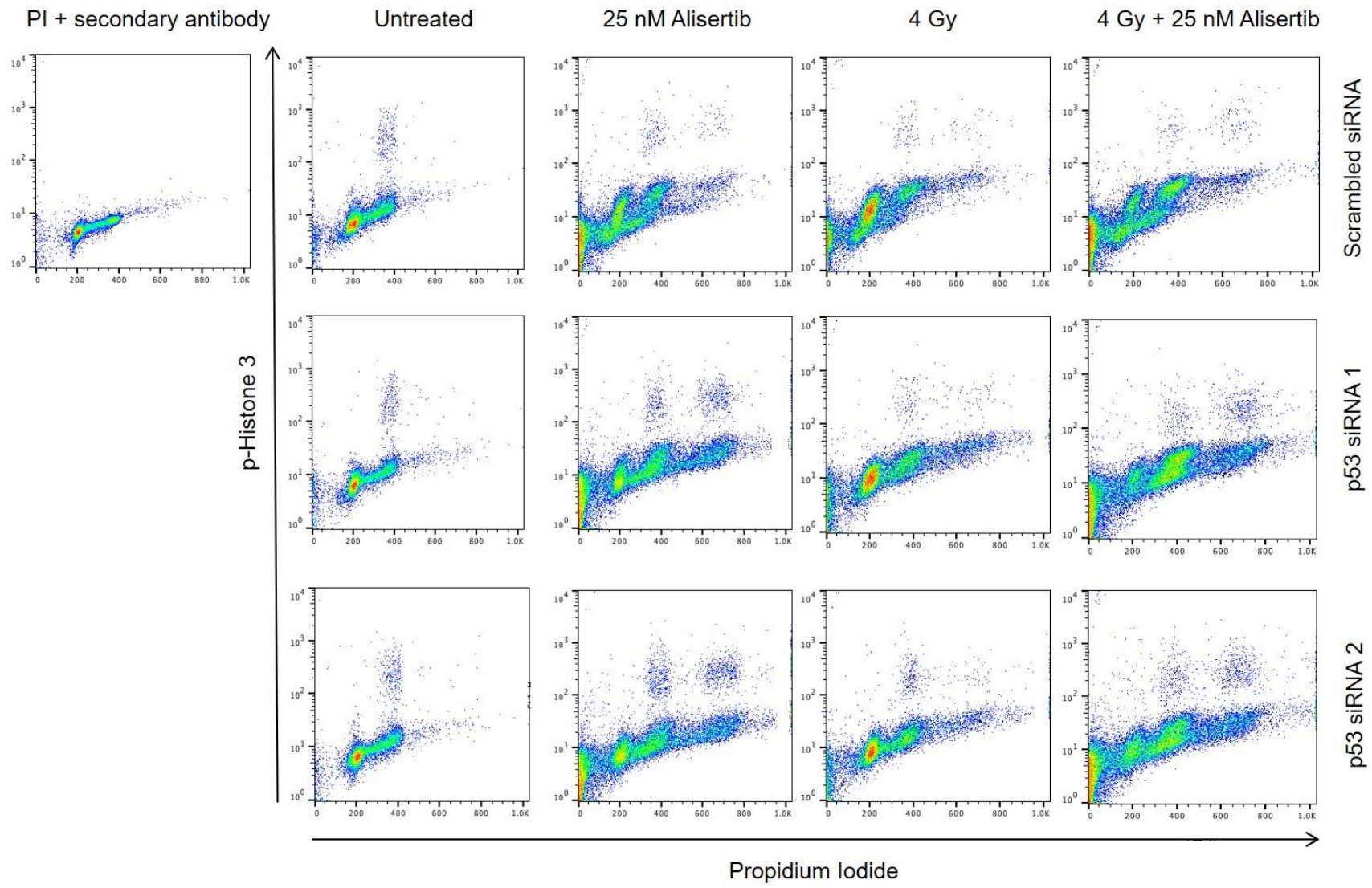

Figure 8.5. **Representative H460 FACS plots for propidium iodide (PI) staining vs p-Histone 3 staining in cells transfected with scrambled siRNA control or p53 siRNA 1/p53 siRNA 2 72 hours post-irradiation (96 hours post-transfection).** Minimum of 10,000 single cell events collected in population isolated through (PI (FL-3) width vs PI (FL-3) height). Mitotic population defined through p-Histone 3 positivity

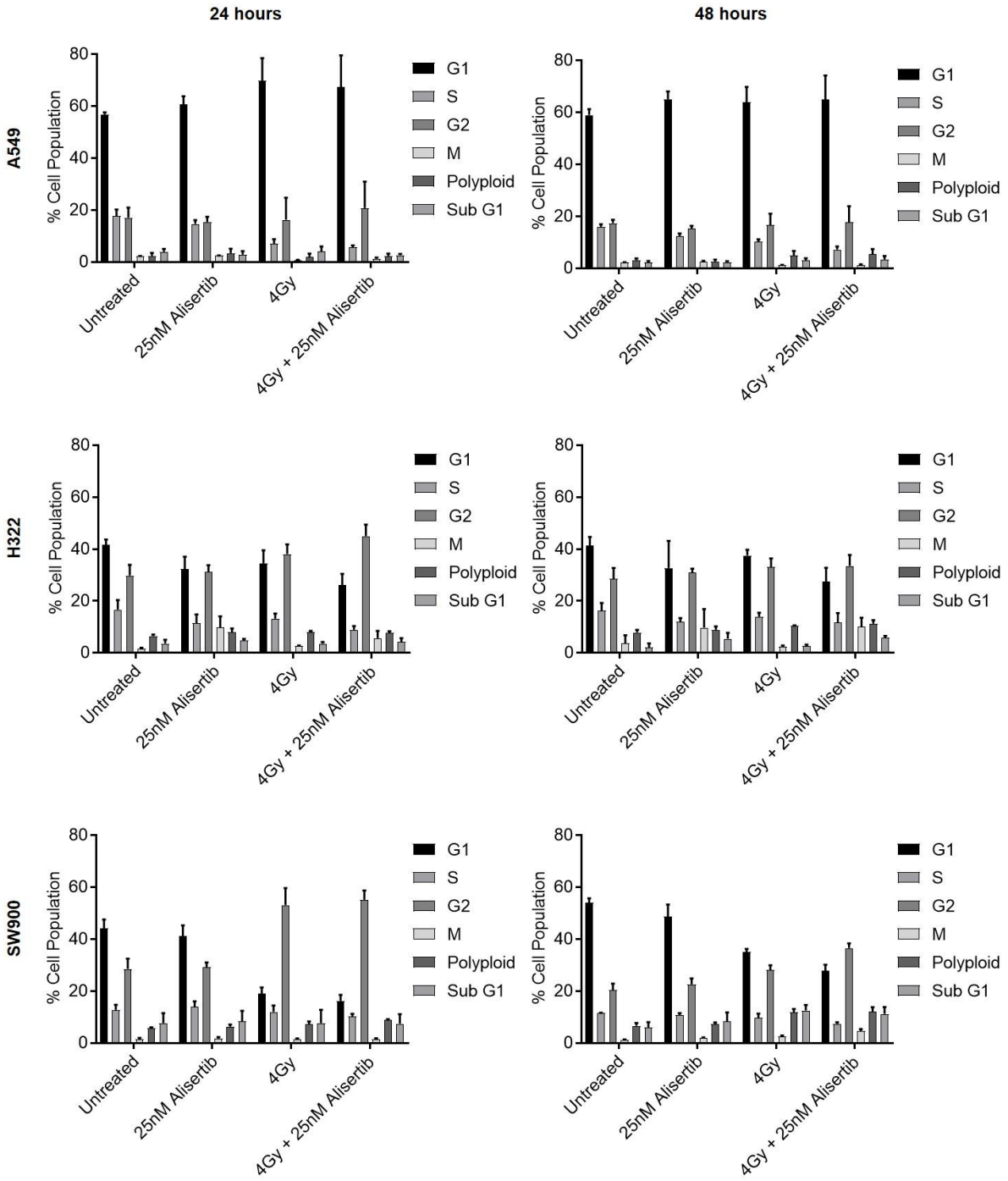

Figure 8.6. **A549, H322 and SW900 cell cycle distribution 24 and 48 hours following treatment with 25 nM Alisertib, 4 Gy or combination.** Mean cell cycle phase distribution 24 and 48 hours post-irradiation. Data points represent mean cell cycle phase distribution +/- SEM (N= ≥2).

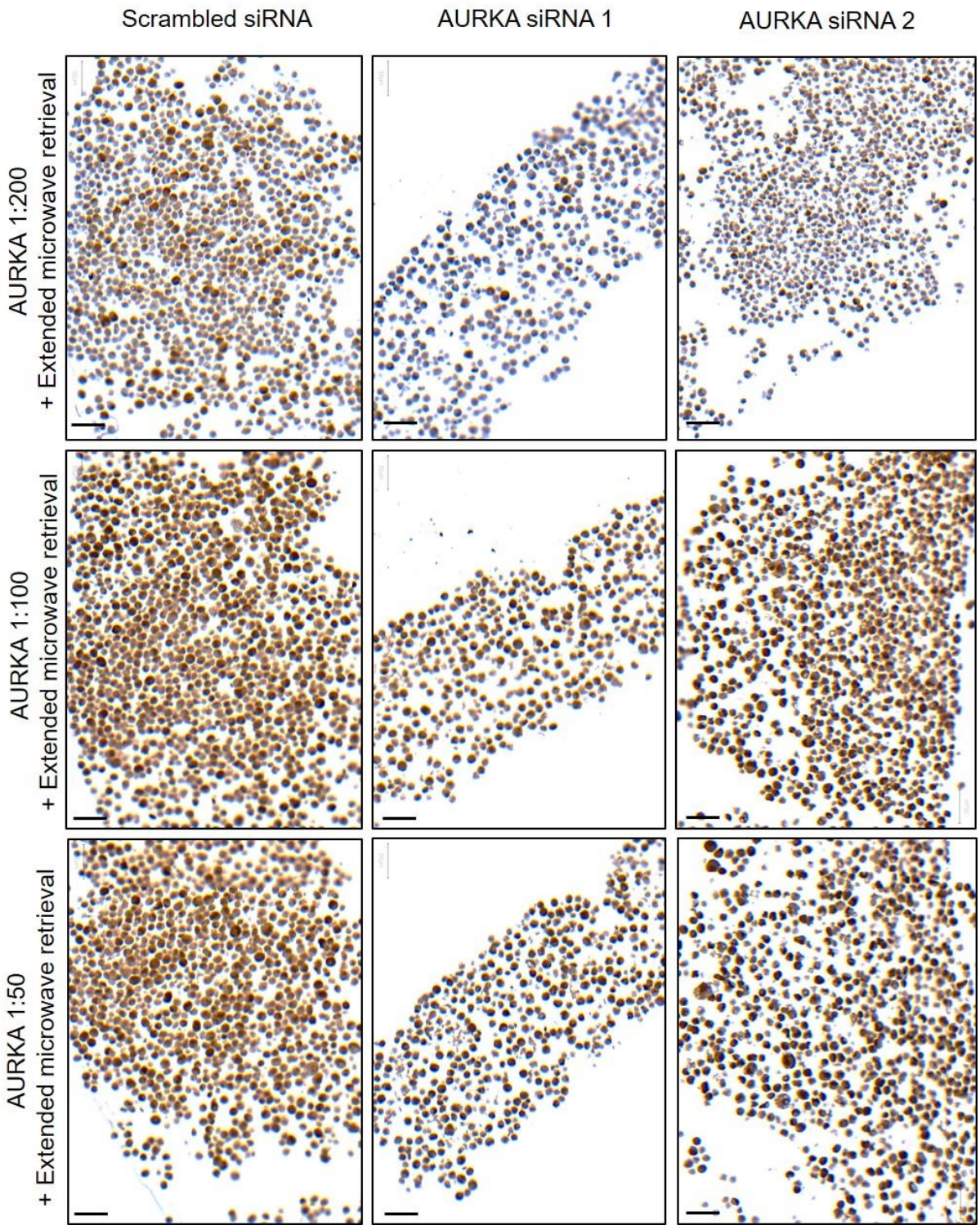

Figure 8.7. **AURKA IHC staining in H460 cell line pellets transfected with scrambled or AURKA siRNA and patient biopsy samples using increased primary antibody concentration and extended microwave retrieval method.** Representative images of AURKA IHC staining using in H460 cell line pellets after extended microwave antigen retrieval with ImmPress® signal detection system and increasing primary antibody concentration. Antibody signal on stained cells was developed with DAB for 3 minutes 30 seconds and cells were counterstained with Gill's haematoxylin (N=1). Scale bars represent 50 µm.

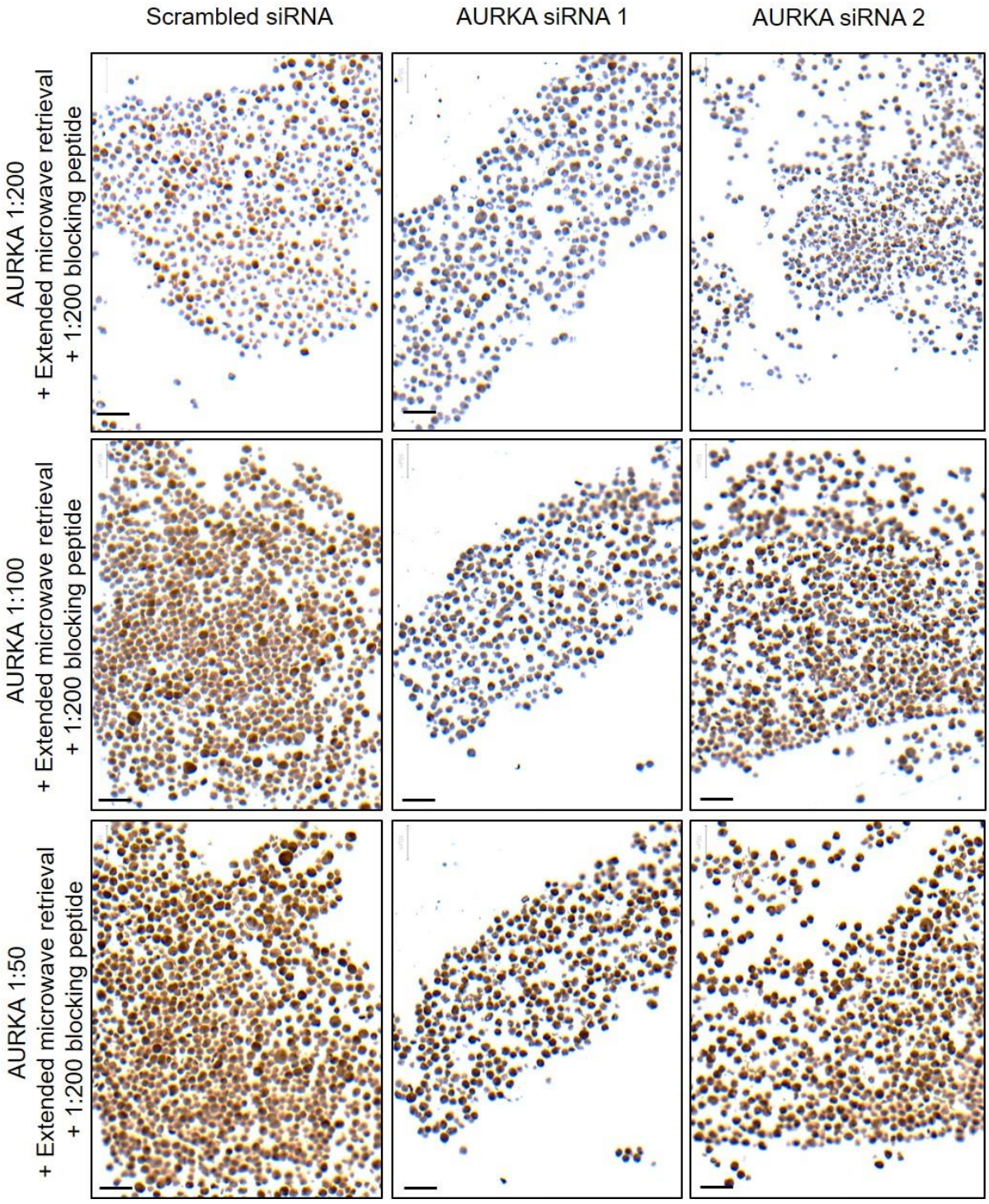

Figure 8.8. **AURKA IHC staining in H460 cell line pellets transfected with scrambled or AURKA siRNA and patient biopsy samples using increased primary antibody concentration and extended microwave retrieval method + blocking peptide.** Representative images of AURKA IHC staining using in H460 cell line pellets after extended microwave antigen retrieval with ImmPress® signal detection system and increasing primary antibody concentration + blocking peptide. Antibody signal on stained cells was developed with DAB for 3 minutes 30 seconds and cells were counterstained with Gill's haematoxylin (N=1). Scale bars represent 50 µm.

References

Afonso, O., Matos, I. and Maiato, H. (2014) 'Spatial control of the anaphase-telophase transition', *Cell cycle*, 13(19), 2985-2986, available: http://dx.doi.org/10.4161/15384101.2014.959853.

Ahn, J.-Y., Li, X., Davis, H.L. and Canman, C.E. (2002) 'Phosphorylation of Threonine 68 Promotes Oligomerization and Autophosphorylation of the Chk2 Protein Kinase via the Forkhead-associated Domain', *Journal of Biological Chemistry*, 277(22), 19389-19395.

Al-Khafaji, A.S.K., Marcus, M.W., Davies, M.P.A., Risk, J.M., Shaw, R.J., Field, J.K. and Liloglou, T. (2017) 'AURKA mRNA expression is an independent predictor of poor prognosis in patients with non-small cell lung cancer', *Oncol Lett*, 13(6), 4463-4468, available: http://dx.doi.org/10.3892/ol.2017.6012.

Alessi, D.R., James, S.R., Downes, C.P., Holmes, A.B., Gaffney, P.R., Reese, C.B. and Cohen, P. (1997) 'Characterization of a 3-phosphoinositide-dependent protein kinase which phosphorylates and activates protein kinase Balpha', *Curr Biol*, 7(4), 261-9.

Allan, L.A., Morrice, N., Brady, S., Magee, G., Pathak, S. and Clarke, P.R. (2003) 'Inhibition of caspase-9 through phosphorylation at Thr 125 by ERK MAPK', *Nat Cell Biol*, 5(7), 647-54, available: http://dx.doi.org/10.1038/ncb1005.

Altorki, N.K., Markowitz, G.J., Gao, D., Port, J.L., Saxena, A., Stiles, B., McGraw, T. and Mittal, V. (2019) 'The lung microenvironment: an important regulator of tumour growth and metastasis', *Nature Reviews Cancer*, 19(1), 9-31, available: http://dx.doi.org/10.1038/s41568-018-0081-9.

Amin, M., Minton, S.E., LoRusso, P.M., Krishnamurthi, S.S., Pickett, C.A., Lunceford, J., Hille, D., Mauro, D., Stein, M.N., Wang-Gillam, A., Trull, L. and Lockhart, A.C. (2016) 'A phase I study of MK-5108, an oral aurora a kinase inhibitor, administered both as monotherapy and in combination with docetaxel, in patients with advanced or refractory solid tumors', *Investigational New Drugs*, 34(1), 84-95, available: http://dx.doi.org/10.1007/s10637-015-0306-7.

Amornwichet, N., Oike, T., Shibata, A., Ogiwara, H., Tsuchiya, N., Yamauchi, M., Saitoh, Y., Sekine, R., Isono, M., Yoshida, Y., Ohno, T., Kohno, T. and Nakano, T. (2014) 'Carbon-ion beam irradiation kills X-ray-resistant p53-null cancer cells by inducing mitotic catastrophe', *PloS one*, 9(12), e115121-e115121, available: http://dx.doi.org/10.1371/journal.pone.0115121.

Anand, S., Penrhyn-Lowe, S. and Venkitaraman, A.R. (2003) 'AURORA-A amplification overrides the mitotic spindle assembly checkpoint, inducing resistance to Taxol', *Cancer Cell*, 3(1), 51-62.

Andreassen, P.R., Lohez, O.D., Lacroix, F.B. and Margolis, R.L. (2001) 'Tetraploid state induces p53-dependent arrest of nontransformed mammalian cells in G1', *Molecular biology of the cell*, 12(5), 1315-1328, available: http://dx.doi.org/10.1091/mbc.12.5.1315.

Antonia, S.J., Villegas, A., Daniel, D., Vicente, D., Murakami, S., Hui, R., Yokoi, T., Chiappori, A., Lee, K.H., de Wit, M., Cho, B.C., Bourhaba, M., Quantin, X., Tokito, T., Mekhail, T., Planchard, D., Kim, Y.-C., Karapetis, C.S., Hiret, S., Ostoros, G., Kubota, K., Gray, J.E., Paz-Ares, L., de Castro Carpeño, J., Wadsworth, C., Melillo, G., Jiang, H., Huang, Y., Dennis, P.A. and Özgüroğlu, M. (2017) 'Durvalumab after Chemoradiotherapy in Stage III Non–Small-Cell Lung Cancer', *New England Journal of Medicine*, 377(20), 1919-1929, available: http://dx.doi.org/10.1056/NEJMoa1709937.

Asteriti, I.A., De Mattia, F. and Guarguaglini, G. (2015) 'Cross-Talk between AURKA and Plk1 in Mitotic Entry and Spindle Assembly', *Frontiers in oncology*, 5, 283-283, available: http://dx.doi.org/10.3389/fonc.2015.00283.

Asteriti, I.A., Di Cesare, E., De Mattia, F., Hilsenstein, V., Neumann, B., Cundari, E., Lavia, P. and Guarguaglini, G. (2014) 'The Aurora-A inhibitor MLN8237 affects multiple mitotic processes and induces dose-dependent mitotic abnormalities and aneuploidy', *Oncotarget*, 5(15), 6229-6242, available: http://dx.doi.org/10.18632/oncotarget.2190.

Aston, W.J., Hope, D.E., Nowak, A.K., Robinson, B.W., Lake, R.A. and Lesterhuis, W.J. (2017) 'A systematic investigation of the maximum tolerated dose of cytotoxic chemotherapy with and without supportive care in mice', *BMC Cancer*, 17(1), 684, available: http://dx.doi.org/10.1186/s12885-017-3677-7.

Aupérin, A., Le Péchoux, C., Rolland, E., Curran, W.J., Furuse, K., Fournel, P., Belderbos, J., Clamon, G., Ulutin, H.C., Paulus, R., Yamanaka, T., Bozonnat, M.-C., Uitterhoeve, A., Wang, X., Stewart, L., Arriagada, R., Burdett, S. and Pignon, J.-P. (2010) 'Meta-Analysis of Concomitant Versus Sequential Radiochemotherapy in Locally Advanced Non–Small-Cell Lung Cancer', *Journal of Clinical Oncology*, 28(13), 2181-2190, available: http://dx.doi.org/10.1200/JCO.2009.26.2543.

Baek, Sung H. (2011) 'When Signaling Kinases Meet Histones and Histone Modifiers in the Nucleus', *Molecular Cell*, 42(3), 274-284, available: http://dx.doi.org/10.1016/j.molcel.2011.03.022.

Ball, D., Mai, G.T., Vinod, S., Babington, S., Ruben, J., Kron, T., Chesson, B., Herschtal, A., Vanevski, M., Rezo, A., Elder, C., Skala, M., Wirth, A., Wheeler, G., Lim, A., Shaw, M., Schofield, P., Irving, L. and Solomon, B. (2019) 'Stereotactic ablative radiotherapy versus standard radiotherapy in stage 1 non-small-cell lung cancer (TROG 09.02 CHISEL): a phase 3, open-label, randomised controlled trial', *Lancet Oncol*, 20(4), 494-503, available: http://dx.doi.org/10.1016/s1470-2045(18)30896-9.

Bankhead, P., Loughrey, M.B., Fernández, J.A., Dombrowski, Y., McArt, D.G., Dunne, P.D., McQuaid, S., Gray, R.T., Murray, L.J., Coleman, H.G., James, J.A., Salto-Tellez, M. and Hamilton, P.W. (2017) 'QuPath: Open source software for digital pathology image analysis', *Scientific Reports*, 7(1), 16878, available: http://dx.doi.org/10.1038/s41598-017-17204-5.

Barr, A.R. and Gergely, F. (2007) 'Aurora-A: the maker and breaker of spindle poles', *J Cell Sci*, 120(Pt 17), 2987-96, available: http://dx.doi.org/10.1242/jcs.013136.

Barr, P.M., Li, H., Spier, C., Mahadevan, D., LeBlanc, M., Ul Haq, M., Huber, B.D., Flowers, C.R., Wagner-Johnston, N.D., Horwitz, S.M., Fisher, R.I., Cheson, B.D., Smith, S.M., Kahl, B.S., Bartlett, N.L. and Friedberg, J.W. (2015) 'Phase II Intergroup Trial of Alisertib in Relapsed and Refractory Peripheral T-Cell Lymphoma and Transformed Mycosis Fungoides: SWOG 1108', *J Clin Oncol*, 33(21), 2399-404, available: http://dx.doi.org/10.1200/jco.2014.60.6327.

Barros, T.P., Kinoshita, K., Hyman, A.A. and Raff, J.W. (2005) 'Aurora A activates D-TACC–Msps complexes exclusively at centrosomes to stabilize centrosomal microtubules', *The Journal of Cell Biology*, 170(7), 1039-1046, available: http://dx.doi.org/10.1083/jcb.200504097.

Bartek, J. and Lukas, J. (2001) 'Pathways governing G1/S transition and their response to DNA damage', *FEBS Lett*, 490(3), 117-22.

Basler, L., Kroeze, S.G.C. and Guckenberger, M. (2017) 'SBRT for oligoprogressive oncogene addicted NSCLC', *Lung Cancer*, 106, 50-57, available: http://dx.doi.org/https://doi.org/10.1016/j.lungcan.2017.02.007.

Baumann, A., Buchberger, A.M.S., Piontek, G., Schuttler, D., Rudelius, M., Reiter, R., Gebel, L., Piendl, G., Brockhoff, G. and Pickhard, A. (2018) 'The Aurora-Kinase A Phe31-Ile polymorphism as possible predictor of response to treatment in head and neck squamous cell carcinoma', *Oncotarget*, 9(16), 12769-12780, available: http://dx.doi.org/10.18632/oncotarget.24355.

Bayliss, R., Sardon, T., Vernos, I. and Conti, E. (2003) 'Structural Basis of Aurora-A Activation by TPX2 at the Mitotic Spindle', *Molecular Cell*, 12(4), 851-862, available: http://dx.doi.org/http://dx.doi.org/10.1016/S1097-2765(03)00392-7.

Beauséjour, C.M., Krtolica, A., Galimi, F., Narita, M., Lowe, S.W., Yaswen, P. and Campisi, J. (2003) 'Reversal of human cellular senescence: roles of the p53 and p16 pathways', *The EMBO journal*, 22(16), 4212-4222, available: http://dx.doi.org/10.1093/emboj/cdg417.

Beltran, H., Oromendia, C., Danila, D.C., Montgomery, B., Hoimes, C., Szmulewitz, R.Z., Vaishampayan, U., Armstrong, A.J., Stein, M., Pinski, J., Mosquera, J.M., Sailer, V., Bareja, R., Romanel, A., Gumpeni, N., Sboner, A., Dardenne, E., Puca, L., Prandi, D., Rubin, M.A., Scher, H.I., Rickman, D.S., Demichelis, F., Nanus, D.M., Ballman, K.V. and Tagawa, S.T. (2019) 'A Phase II Trial of the Aurora Kinase A Inhibitor Alisertib for Patients with Castration-resistant and Neuroendocrine Prostate Cancer: Efficacy and Biomarkers', *Clinical Cancer Research*, 25(1), 43, available: http://dx.doi.org/10.1158/1078-0432.CCR-18-1912.

Bernier, J., Hall, E.J. and Giaccia, A. (2004) 'Radiation oncology: a century of achievements', *Nat Rev Cancer*, 4(9), 737-747.

Bertolin, G., Bulteau, A.-L., Alves-Guerra, M.-C., Burel, A., Lavault, M.-T., Gavard, O., Le Bras, S., Gagné, J.-P., Poirier, G.G., Le Borgne, R., Prigent, C. and Tramier, M. (2018) 'Aurora kinase A localises to mitochondria to control organelle dynamics and energy production', *eLife*, 7, e38111, available: http://dx.doi.org/10.7554/eLife.38111.

Bertram, J.S. and Janik, P. (1980) 'Establishment of a cloned line of Lewis Lung Carcinoma cells adapted to cell culture', *Cancer Lett*, 11(1), 63-73.

Bhargava, R., Onyango, D.O. and Stark, J.M. (2016) 'Regulation of Single-Strand Annealing and its Role in Genome Maintenance', *Trends in Genetics*, 32(9), 566-575, available: http://dx.doi.org/https://doi.org/10.1016/j.tig.2016.06.007.

Bischoff, J.R., Anderson, L., Zhu, Y., Mossie, K., Ng, L., Souza, B., Schryver, B., Flanagan, P., Clairvoyant, F., Ginther, C., Chan, C.S.M., Novotny, M., Slamon, D.J. and Plowman, G.D. (1998) 'A homologue of Drosophila aurora kinase is oncogenic and amplified in human colorectal cancers', *The EMBO Journal*, 17(11), 3052-3065.

Boehme, K.A., Kulikov, R. and Blattner, C. (2008) 'p53 stabilization in response to DNA damage requires Akt/PKB and DNA-PK', *Proceedings of the National*

Academy of Sciences of the United States of America, 105(22), 7785-7790, available: http://dx.doi.org/10.1073/pnas.0703423105.

Bonni, A., Brunet, A., West, A.E., Datta, S.R., Takasu, M.A. and Greenberg, M.E. (1999) 'Cell survival promoted by the Ras-MAPK signaling pathway by transcription-dependent and -independent mechanisms', *Science*, 286(5443), 1358-62.

Borges, K.S., Castro-Gamero, A.M., Moreno, D.A., da Silva Silveira, V., Brassesco, M.S., de Paula Queiroz, R.G., de Oliveira, H.F., Carlotti, C.G., Jr., Scrideli, C.A. and Tone, L.G. (2012) 'Inhibition of Aurora kinases enhances chemosensitivity to temozolomide and causes radiosensitization in glioblastoma cells', *J Cancer Res Clin Oncol*, 138(3), 405-14, available: http://dx.doi.org/10.1007/s00432-011-1111-0.

Boucher, M.J., Morisset, J., Vachon, P.H., Reed, J.C., Laine, J. and Rivard, N. (2000) 'MEK/ERK signaling pathway regulates the expression of Bcl-2, Bcl-X(L), and Mcl-1 and promotes survival of human pancreatic cancer cells', *J Cell Biochem*, 79(3), 355-69.

Bourke, E., Dodson, H., Merdes, A., Cuffe, L., Zachos, G., Walker, M., Gillespie, D. and Morrison, C.G. (2007) 'DNA damage induces Chk1-dependent centrosome amplification', *EMBO reports*, 8(6), 603-609, available: http://dx.doi.org/10.1038/sj.embor.7400962.

Bric, A., Miething, C., Bialucha, C.U., Scuoppo, C., Zender, L., Krasnitz, A., Xuan, Z., Zuber, J., Wigler, M., Hicks, J., McCombie, R.W., Hemann, M.T., Hannon, G.J., Powers, S. and Lowe, S.W. (2009) 'Functional Identification of Tumor-Suppressor Genes through an In Vivo RNA Interference Screen in a Mouse Lymphoma Model', *Cancer Cell*, 16(4), 324-335, available: http://dx.doi.org/10.1016/j.ccr.2009.08.015.

Brito, D.A. and Rieder, C.L. (2006) 'Mitotic checkpoint slippage in humans occurs via cyclin B destruction in the presence of an active checkpoint', *Curr Biol*, 16(12), 1194-200, available: http://dx.doi.org/10.1016/j.cub.2006.04.043.

Brognard, J., Clark, A.S., Ni, Y. and Dennis, P.A. (2001) 'Akt/Protein Kinase B Is Constitutively Active in Non-Small Cell Lung Cancer Cells and Promotes Cellular Survival and Resistance to Chemotherapy and Radiation', *Cancer Research*, 61(10), 3986.

Brunner, A.M., Blonquist, T.M., DeAngelo, D.J., McMasters, M., Winer, E.S., Hobbs, G.S., Amrein, P.C., Hock, H., Steensma, D.P., Garcia, J.S., Luskin, M.R., Stone, R.M., Ballen, K.K., Rosenblatt, J., Avigan, D.E., McAfee, S.L., Moran,

J.A., Bergeron, M., Foster, J., Bertoli, C., McGregor, K., Fishman, K., Macrae, M., Burke, M., Behnan, T.T., Som, T.T., Ramos, A.Y., Vartanian, M.K., Nelson, N., Logan, E., Lombardi Story, J., Connolly, C., Neuberg, D.S., Chen, Y.-B., Graubert, T.A. and Fathi, A.T. (2018) 'Phase II Clinical Trial of Alisertib, an Aurora a Kinase Inhibitor, in Combination with Induction Chemotherapy in High-Risk, Untreated Patients with Acute Myeloid Leukemia', *Blood*, 132(Suppl 1), 766, available: http://dx.doi.org/10.1182/blood-2018-99-115145.

Bucher, N. and Britten, C.D. (2008) 'G2 checkpoint abrogation and checkpoint kinase-1 targeting in the treatment of cancer', *British journal of cancer*, 98(3), 523-528, available: http://dx.doi.org/10.1038/sj.bjc.6604208.

Bunz, F., Dutriaux, A., Lengauer, C., Waldman, T., Zhou, S., Brown, J.P., Sedivy, J.M., Kinzler, K.W. and Vogelstein, B. (1998) 'Requirement for p53 and p21 to sustain G2 arrest after DNA damage', *Science*, 282(5393), 1497-501.

Cane, P., Linklater, K.M., Nicholson, A.G., Peake, M.D. and Gosney, J. (2015) 'Morphological and genetic classification of lung cancer: variation in practice and implications for tailored treatment', *Histopathology*, 67(2), 216-24, available: http://dx.doi.org/10.1111/his.12638.

Carmena, M. and Earnshaw, W.C. (2003) 'The cellular geography of Aurora kinases', *Nat Rev Mol Cell Biol*, 4(11), 842-854.

Castro, A., Vigneron, S., Bernis, C., Labbé, J.-C., Prigent, C. and Lorca, T. (2002) 'The D-Box-activating domain (DAD) is a new proteolysis signal that stimulates the silent D-Box sequence of Aurora-A', *EMBO Reports*, 3(12), 1209-1214, available: http://dx.doi.org/10.1093/embo-reports/kvf241.

Castro, M.A.A., Schwartsmann, G. and Moreira, J.C. (2001) 'Intercellular contact-dependent survival of human A549, NCI-H596 and NCI-H520 non-small cell lung carcinoma cell lines', *Braz J Med Biol Res*, 34(8), 1007-13, available: http://dx.doi.org/10.1590/S0100-879X2001000800006.

Cazales, M., Schmitt, E., Montembault, E., Dozier, C., Prigent, C. and Ducommun, B. (2005) 'CDC25B phosphorylation by Aurora-A occurs at the G2/M transition and is inhibited by DNA damage', *Cell Cycle*, 4(9), 1233-8.

Cervantes, A., Elez, E., Roda, D., Ecsedy, J., Macarulla, T., Venkatakrishnan, K., Rosello, S., Andreu, J., Jung, J., Sanchis-Garcia, J.M., Piera, A., Blasco, I., Manos, L., Perez-Fidalgo, J.A., Fingert, H., Baselga, J. and Tabernero, J. (2012) 'Phase I pharmacokinetic/pharmacodynamic study of MLN8237, an investigational, oral, selective aurora a kinase inhibitor, in patients with

advanced solid tumors', *Clin Cancer Res*, 18(17), 4764-74, available: http://dx.doi.org/10.1158/1078-0432.ccr-12-0571.

Chapman, J.R., Taylor, M.R. and Boulton, S.J. (2012) 'Playing the end game: DNA double-strand break repair pathway choice', *Mol Cell*, 47(4), 497-510, available: http://dx.doi.org/10.1016/j.molcel.2012.07.029.

Chaudhuri, A.A., Tang, C., Binkley, M.S., Jin, M., Wynne, J.F., von Eyben, R., Hara, W.Y., Trakul, N., Loo, B.W., Jr. and Diehn, M. (2015) 'Stereotactic ablative radiotherapy (SABR) for treatment of central and ultra-central lung tumors', *Lung Cancer*, 89(1), 50-6, available: http://dx.doi.org/10.1016/j.lungcan.2015.04.014.

Chehab, N.H., Malikzay, A., Appel, M. and Halazonetis, T.D. (2000) 'Chk2/hCds1 functions as a DNA damage checkpoint in G(1) by stabilizing p53', *Genes & development*, 14(3), 278-288.

Chen, C., Song, G., Xiang, J., Zhang, H., Zhao, S. and Zhan, Y. (2017) 'AURKA promotes cancer metastasis by regulating epithelial-mesenchymal transition and cancer stem cell properties in hepatocellular carcinoma', *Biochemical and Biophysical Research Communications*, 486(2), 514-520, available: http://dx.doi.org/https://doi.org/10.1016/j.bbrc.2017.03.075.

Chen, L., Gilkes, D.M., Pan, Y., Lane, W.S. and Chen, J. (2005) 'ATM and Chk2-dependent phosphorylation of MDMX contribute to p53 activation after DNA damage', *The EMBO journal*, 24(19), 3411-3422, available: http://dx.doi.org/10.1038/sj.emboj.7600812.

Chen, X.B., Ko, L.J., Jayaraman, L. and Prives, C. (1996) 'p53 levels, functional domains, and DNA damage determine the extent of the apoptotic response of tumor cells', *Genes & Dev*, 10, 2438-51, available: http://dx.doi.org/10.1101/gad.10.19.2438.

Chen, Z., Fillmore, C.M., Hammerman, P.S., Kim, C.F. and Wong, K.-K. (2014) 'Non-small-cell lung cancers: a heterogeneous set of diseases', *Nat Rev Cancer*, 14(8), 535-546, available: http://dx.doi.org/10.1038/nrc3775.

Cheng, Q. and Chen, J. (2010) 'Mechanism of p53 stabilization by ATM after DNA damage', *Cell cycle (Georgetown, Tex.)*, 9(3), 472-478, available: http://dx.doi.org/10.4161/cc.9.3.10556.

Chu, T.L.H., Connell, M., Zhou, L., He, Z., Won, J., Chen, H., Rahavi, S.M.R., Mohan, P., Nemirovsky, O., Fotovati, A., Pujana, M.A., Reid, G.S.D., Nielsen, T.O., Pante, N. and Maxwell, C.A. (2018) 'Cell Cycle-Dependent Tumor

Engraftment and Migration Are Enabled by Aurora-A', *Mol Cancer Res*, 16(1), 16-31, available: http://dx.doi.org/10.1158/1541-7786.mcr-17-0417.

Chuang, T.-P., Wang, J.-Y., Jao, S.-W., Wu, C.-C., Chen, J.-H., Hsiao, K.-H., Lin, C.-Y., Chen, S.-H., Su, S.-Y., Chen, Y.-J., Chen, Y.-T., Wu, D.-C. and Li, L.-H. (2016) 'Over-expression of AURKA , SKA3 and DSN1 contributes to colorectal adenoma to carcinoma progression', *Oncotarget; Advance Online Publications: Page 5*.

Cogswell, J.P., Brown, C.E., Bisi, J.E. and Neill, S.D. (2000) 'Dominant-Negative Polo-like Kinase 1 Induces Mitotic Catastrophe Independent of cdc25C Function', *Cell Growth Differentiation*, 11(12), 615-623.

Cohen–Jonathan, E., Bernhard, E.J. and McKenna, W.G. (1999) 'How does radiation kill cells?', *Current Opinion in Chemical Biology*, 3(1), 77-83, available: http://dx.doi.org/https://doi.org/10.1016/S1367-5931(99)80014-3.

Collins, J.K., Lane, S.I.R., Merriman, J.A. and Jones, K.T. (2015) 'DNA damage induces a meiotic arrest in mouse oocytes mediated by the spindle assembly checkpoint', *Nature communications*, 6, 8553-8553, available: http://dx.doi.org/10.1038/ncomms9553.

Conibear, J., Chia, B., Ngai, Y., Bates, A.T., Counsell, N., Patel, R., Eaton, D., Faivre-Finn, C., Fenwick, J., Forster, M., Hanna, G.G., Harden, S., Mayles, P., Moinuddin, S. and Landau, D. (2018) 'Study protocol for the SARON trial: a multicentre, randomised controlled phase III trial comparing the addition of stereotactic ablative radiotherapy and radical radiotherapy with standard chemotherapy alone for oligometastatic non-small cell lung cancer', *BMJ Open*, 8(4), e020690, available: http://dx.doi.org/10.1136/bmjopen-2017-020690.

Cooke, S.L., Temple, J., Macarthur, S., Zahra, M.A., Tan, L.T., Crawford, R.A.F., Ng, C.K.Y., Jimenez-Linan, M., Sala, E. and Brenton, J.D. (2011) 'Intra-tumour genetic heterogeneity and poor chemoradiotherapy response in cervical cancer', *British journal of cancer*, 104(2), 361-368, available: http://dx.doi.org/10.1038/sj.bjc.6605971.

Countryman, P.I. and Heddle, J.A. (1976) 'The production of micronuclei from chromosome aberrations in irradiated cultures of human lymphocytes', *Mutation Research/Fundamental and Molecular Mechanisms of Mutagenesis*, 41(2), 321-331, available: http://dx.doi.org/https://doi.org/10.1016/0027-5107(76)90105-6.

Courtheoux, T., Diallo, A., Damodaran, A.P., Reboutier, D., Watrin, E. and Prigent, C. (2018) 'Aurora A kinase activity is required to maintain the spindle assembly checkpoint active during pro-metaphase', *Journal of Cell Science*, jcs.191353, available: http://dx.doi.org/10.1242/jcs.191353.

Courthéoux, T., Reboutier, D., Vazeille, T., Cremet, J.-Y., Benaud, C., Vernos, I. and Prigent, C. (2019) 'Microtubule nucleation during central spindle assembly requires NEDD1 phosphorylation on Serine 405 by Aurora A', *Journal of Cell Science*, jcs.231118, available: http://dx.doi.org/10.1242/jcs.231118.

Crane, R., Kloepfer, A. and Ruderman, J.V. (2004) 'Requirements for the destruction of human Aurora-A', *Journal of Cell Science*, 117(25), 5975-5983.

Cron, K.R., Zhu, K., Kushwaha, D.S., Hsieh, G., Merzon, D., Rameseder, J., Chen, C.C., D'Andrea, A.D. and Kozono, D. (2013) 'Proteasome Inhibitors Block DNA Repair and Radiosensitize Non-Small Cell Lung Cancer', *PLoS One*, 8(9), available: http://dx.doi.org/10.1371/journal.pone.0073710.

CRUK (2017) *Lung cancer statistics*, available: http://www.cancerresearchuk.org/health-professional/cancer-statistics/statistics-by-cancer-type/lung-cancer#heading-One [accessed 10 August 2017].

CRUK (2018) *Tackle cancers with substantial unmet need: our research strategy*, available: https://www.cancerresearchuk.org/funding-for-researchers/our-research-strategy/tackle-cancers-with-substantial-unmet-need [accessed 14 July 2018].

Darzynkiewicz, Z. (2010) 'Critical aspects in analysis of cellular DNA content', *Current protocols in cytometry*, Chapter 7, Unit7.2-Unit7.2, available: http://dx.doi.org/10.1002/0471142956.cy0702s52.

Das, A.K., Bell, M.H., Nirodi, C.S., Story, M.D. and Minna, J.D. (2010) 'Radiogenomics Predicting Tumor Responses to Radiotherapy in Lung Cancer', *Seminars in Radiation Oncology*, 20(3), 149-155, available: http://dx.doi.org/https://doi.org/10.1016/j.semradonc.2010.01.002.

David, O., Jett, J., LeBeau, H., Dy, G., Hughes, J., Friedman, M. and Brody, A.R. (2004) 'Phospho-Akt overexpression in non-small cell lung cancer confers significant stage-independent survival disadvantage', *Clin Cancer Res*, 10(20), 6865-71, available: http://dx.doi.org/10.1158/1078-0432.ccr-04-0174.

Dawei, H., Honggang, D. and Qian, W. (2018) 'AURKA contributes to the progression of oral squamous cell carcinoma (OSCC) through modulating

epithelial-to-mesenchymal transition (EMT) and apoptosis via the regulation of ROS', *Biochem Biophys Res Commun*, 507(1-4), 83-90, available: http://dx.doi.org/10.1016/j.bbrc.2018.10.170.

de Bruin, E.C., McGranahan, N., Mitter, R., Salm, M., Wedge, D.C., Yates, L., Jamal-Hanjani, M., Shafi, S., Murugaesu, N., Rowan, A.J., Grönroos, E., Muhammad, M.A., Horswell, S., Gerlinger, M., Varela, I., Jones, D., Marshall, J., Voet, T., Van Loo, P., Rassl, D.M., Rintoul, R.C., Janes, S.M., Lee, S.-M., Forster, M., Ahmad, T., Lawrence, D., Falzon, M., Capitanio, A., Harkins, T.T., Lee, C.C., Tom, W., Teefe, E., Chen, S.-C., Begum, S., Rabinowitz, A., Phillimore, B., Spencer-Dene, B., Stamp, G., Szallasi, Z., Matthews, N., Stewart, A., Campbell, P. and Swanton, C. (2014) 'Spatial and temporal diversity in genomic instability processes defines lung cancer evolution', *Science*, 346(6206), 251, available: http://dx.doi.org/10.1126/science.1253462.

de Sousa Abreu, R., Penalva, L.O., Marcotte, E.M. and Vogel, C. (2009) 'Global signatures of protein and mRNA expression levels', *Mol Biosyst*, 5(12), 1512-26, available: http://dx.doi.org/10.1039/b908315d.

Dees, E.C., Cohen, R.B., von Mehren, M., Stinchcombe, T.E., Liu, H., Venkatakrishnan, K., Manfredi, M., Fingert, H., Burris, H.A. and Infante, J.R. (2012) 'Phase I Study of Aurora A Kinase Inhibitor MLN8237 in Advanced Solid Tumors: Safety, Pharmacokinetics, Pharmacodynamics, and Bioavailability of Two Oral Formulations', *Clinical Cancer Research*, 18(17), 4775-4784.

Dees, E.C., Infante, J.R., Cohen, R.B., O'Neil, B.H., Jones, S., von Mehren, M., Danaee, H., Lee, Y., Ecsedy, J., Manfredi, M., Galvin, K., Stringer, B., Liu, H., Eton, O., Fingert, H. and Burris, H. (2011) 'Phase 1 study of MLN8054, a selective inhibitor of Aurora A kinase in patients with advanced solid tumors', *Cancer chemotherapy and pharmacology*, 67(4), 945-954, available: http://dx.doi.org/10.1007/s00280-010-1377-y.

Del Gaizo Moore, V. and Letai, A. (2013) 'BH3 profiling--measuring integrated function of the mitochondrial apoptotic pathway to predict cell fate decisions', *Cancer letters*, 332(2), 202-205, available: http://dx.doi.org/10.1016/j.canlet.2011.12.021.

Delaney, G., Jacob, S., Featherstone, C. and Barton, M. (2005) 'The role of radiotherapy in cancer treatment - Estimating optimal utilization from a review of evidence-based clinical guidelines', *Cancer*, 104, 1129-37, available: http://dx.doi.org/10.1002/cncr.21324.

DeLisser, H.M., Christofidou-Solomidou, M., Strieter, R.M., Burdick, M.D., Robinson, C.S., Wexler, R.S., Kerr, J.S., Garlanda, C., Merwin, J.R., Madri, J.A. and Albelda, S.M. (1997) 'Involvement of endothelial PECAM-1/CD31 in angiogenesis', *The American journal of pathology*, 151(3), 671-677.

Dent, P., Yacoub, A., Fisher, P.B., Hagan, M.P. and Grant, S. (2003) 'MAPK pathways in radiation responses', *Oncogene*, 22(37), 5885-96, available: http://dx.doi.org/10.1038/sj.onc.1206701.

Detterbeck, F.C., Boffa, D.J., Kim, A.W. and Tanoue, L.T. (2017) 'The Eighth Edition Lung Cancer Stage Classification', *CHEST*, 151(1), 193-203, available: http://dx.doi.org/10.1016/j.chest.2016.10.010.

Diamond, J.R., Bastos, B.R., Hansen, R.J., Gustafson, D.L., Eckhardt, S.G., Kwak, E.L., Pandya, S.S., Fletcher, G.C., Pitts, T.M., Kulikowski, G.N., Morrow, M., Arnott, J., Bray, M.R., Sidor, C., Messersmith, W. and Shapiro, G.I. (2011) 'Phase I safety, pharmacokinetic, and pharmacodynamic study of ENMD-2076, a novel angiogenic and Aurora kinase inhibitor, in patients with advanced solid tumors', *Clin Cancer Res*, 17(4), 849-60, available: http://dx.doi.org/10.1158/1078-0432.ccr-10-2144.

Diamond, J.R., Eckhardt, S.G., Pitts, T.M., van Bokhoven, A., Aisner, D., Gustafson, D.L., Capasso, A., Sams, S., Kabos, P., Zolman, K., Colvin, T., Elias, A.D., Storniolo, A.M., Schneider, B.P., Gao, D., Tentler, J.J., Borges, V.F. and Miller, K.D. (2018) 'A phase II clinical trial of the Aurora and angiogenic kinase inhibitor ENMD-2076 for previously treated, advanced, or metastatic triple-negative breast cancer', *Breast Cancer Res*, 20(1), 82, available: http://dx.doi.org/10.1186/s13058-018-1014-y.

Dickson, M.A., Mahoney, M.R., Tap, W.D., D'Angelo, S.P., Keohan, M.L., Van Tine, B.A., Agulnik, M., Horvath, L.E., Nair, J.S. and Schwartz, G.K. (2016) 'Phase II study of MLN8237 (Alisertib) in advanced/metastatic sarcoma', *Ann Oncol*, 27(10), 1855-60, available: http://dx.doi.org/10.1093/annonc/mdw281.

Dimri, G.P., Lee, X., Basile, G., Acosta, M., Scott, G., Roskelley, C., Medrano, E.E., Linskens, M., Rubelj, I. and Pereira-Smith, O. (1995) 'A biomarker that identifies senescent human cells in culture and in aging skin in vivo', *Proceedings of the National Academy of Sciences of the United States of America*, 92(20), 9363-9367.

Dirac, A.M.G. and Bernards, R. (2003) 'Reversal of Senescence in Mouse Fibroblasts through Lentiviral Suppression of p53', *Journal of Biological Chemistry*, 278(14), 11731-11734.

Director's Challenge Consortium for the Molecular Classification of Lung, A., Shedden, K., Taylor, J.M.G., Enkemann, S.A., Tsao, M.-S., Yeatman, T.J., Gerald, W.L., Eschrich, S., Jurisica, I., Giordano, T.J., Misek, D.E., Chang, A.C., Zhu, C.Q., Strumpf, D., Hanash, S., Shepherd, F.A., Ding, K., Seymour, L., Naoki, K., Pennell, N., Weir, B., Verhaak, R., Ladd-Acosta, C., Golub, T., Gruidl, M., Sharma, A., Szoke, J., Zakowski, M., Rusch, V., Kris, M., Viale, A., Motoi, N., Travis, W., Conley, B., Seshan, V.E., Meyerson, M., Kuick, R., Dobbin, K.K., Lively, T., Jacobson, J.W. and Beer, D.G. (2008) 'Gene expression-based survival prediction in lung adenocarcinoma: a multi-site, blinded validation study', *Nature medicine*, 14(8), 822-827, available: http://dx.doi.org/10.1038/nm.1790.

Dittmann, K., Mayer, C., Fehrenbacher, B., Schaller, M., Raju, U., Milas, L., Chen, D.J., Kehlbach, R. and Rodemann, H.P. (2005) 'Radiation-induced epidermal growth factor receptor nuclear import is linked to activation of DNA-dependent protein kinase', *J Biol Chem*, 280(35), 31182-9, available: http://dx.doi.org/10.1074/jbc.M506591200.

Do, T.-V., Hirst, J., Hyter, S., Roby, K.F. and Godwin, A.K. (2017) 'Aurora A kinase regulates non-homologous end-joining and poly(ADP-ribose) polymerase function in ovarian carcinoma cells', *Oncotarget*, 8(31), 50376-50392, available: http://dx.doi.org/10.18632/oncotarget.18970.

Do, T.-V., Xiao, F., Bickel, L.E., Klein-Szanto, A.J., Pathak, H.B., Hua, X., Howe, C., O'Brien, S., Maglaty, M., Ecsedy, J.A., Litwin, S., Golemis, E.A., Schilder, R.J., Godwin, A.K. and Connolly, D.C. (2014) 'Aurora Kinase A Mediates Epithelial Ovarian Cancer Cell Migration and Adhesion', *Oncogene*, 33(5), 539-549, available: http://dx.doi.org/10.1038/onc.2012.632.

Dodson, H., Bourke, E., Jeffers, L.J., Vagnarelli, P., Sonoda, E., Takeda, S., Earnshaw, W.C., Merdes, A. and Morrison, C. (2004) 'Centrosome amplification induced by DNA damage occurs during a prolonged G2 phase and involves ATM', *The EMBO journal*, 23(19), 3864-3873, available: http://dx.doi.org/10.1038/sj.emboj.7600393.

Dodson, H., Wheatley, S. and Morrison, C. (2007) 'Involvement of Centrosome Amplification in Radiation-Induced Mitotic Catastrophe', *Cell Cycle*, 6(3), 364-70, available: http://dx.doi.org/10.4161/cc.6.3.3834.

Dong, X., Guan, J., English, J., Flint, J., Yee, J., Evans, K., Murray, N., Macaulay, C., Ng, R., W Gout, P., Lam, W., Laskin, J., Ling, V., Lam, S. and Wang, Y. (2010) 'Patient-Derived First Generation Xenografts of Non-Small Cell Lung Cancers: Promising Tools for Predicting Drug Responses for Personalized Chemotherapy', *Clin Cancer Res*, 16, 1442-51, available: http://dx.doi.org/10.1158/1078-0432.CCR-09-2878.

Donzelli, M. and Draetta, G.F. (2003) 'Regulating mammalian checkpoints through Cdc25 inactivation', *EMBO reports*, 4(7), 671-677, available: http://dx.doi.org/10.1038/sj.embor.embor887.

DuBois, S.G., Mosse, Y.P., Fox, E., Kudgus, R.A., Reid, J.M., McGovern, R., Groshen, S., Bagatell, R., Maris, J.M., Twist, C.J., Goldsmith, K., Granger, M.M., Weiss, B., Park, J.R., Macy, M.E., Cohn, S.L., Yanik, G., Wagner, L.M., Hawkins, R., Courtier, J., Lai, H., Goodarzian, F., Shimada, H., Boucher, N., Czarnecki, S., Luo, C., Tsao-Wei, D., Matthay, K.K. and Marachelian, A. (2018) 'Phase II Trial of Alisertib in Combination with Irinotecan and Temozolomide for Patients with Relapsed or Refractory Neuroblastoma', *Clinical Cancer Research*, 24(24), 6142, available: http://dx.doi.org/10.1158/1078-0432.CCR-18-1381.

Eisenhauer, E.A., Therasse, P., Bogaerts, J., Schwartz, L.H., Sargent, D., Ford, R., Dancey, J., Arbuck, S., Gwyther, S., Mooney, M., Rubinstein, L., Shankar, L., Dodd, L., Kaplan, R., Lacombe, D. and Verweij, J. (2009) 'New response evaluation criteria in solid tumours: revised RECIST guideline (version 1.1)', *Eur J Cancer*, 45(2), 228-47, available: http://dx.doi.org/10.1016/j.ejca.2008.10.026.

Eliezer, Y., Argaman, L., Kornowski, M., Roniger, M. and Goldberg, M. (2014) 'Interplay between the DNA damage proteins MDC1 and ATM in the regulation of the spindle assembly checkpoint', *The Journal of biological chemistry*, 289(12), 8182-8193, available: http://dx.doi.org/10.1074/jbc.M113.532739.

Eom, Y.W., Kim, M.A., Park, S.S., Goo, M.J., Kwon, H.J., Sohn, S., Kim, W.H., Yoon, G. and Choi, K.S. (2005) 'Two distinct modes of cell death induced by doxorubicin: apoptosis and cell death through mitotic catastrophe accompanied by senescence-like phenotype', *Oncogene*, 24(30), 4765-77, available: http://dx.doi.org/10.1038/sj.onc.1208627.

Erenpreisa, J., Ivanov, A., Wheatley, S.P., Kosmacek, E.A., Ianzini, F., Anisimov, A.P., Mackey, M., Davis, P.J., Plakhins, G. and Illidge, T.M. (2008) 'Endopolyploidy in irradiated p53-deficient tumour cell lines: persistence of cell division activity in giant cells expressing Aurora-B kinase', *Cell biology international*, 32(9), 1044-1056, available: http://dx.doi.org/10.1016/j.cellbi.2008.06.003.

Eterno, V., Zambelli, A., Villani, L., Tuscano, A., Manera, S., Spitaleri, A., Pavesi, L. and Amato, A. (2016) 'AurkA controls self-renewal of breast cancer-initiating cells promoting wnt3a stabilization through suppression of miR-128', *Sci Rep*, 6, 28436, available: http://dx.doi.org/10.1038/srep28436.

Eyers, P.A. and Maller, J.L. (2004) 'Regulation of Xenopus Aurora A Activation by TPX2', *Journal of Biological Chemistry*, 279(10), 9008-9015.

Falchook, G., Coleman, R.L., Roszak, A., Behbakht, K., Matulonis, U., Ray-Coquard, I., Sawrycki, P., Duska, L.R., Tew, W., Ghamande, S., Lesoin, A., Schwartz, P.E., Buscema, J., Fabbro, M., Lortholary, A., Goff, B., Kurzrock, R., Martin, L.P., Gray, H.J., Fu, S., Sheldon-Waniga, E., Lin, H.M., Venkatakrishnan, K., Zhou, X., Leonard, E.J. and Schilder, R.J. (2019) 'Alisertib in Combination With Weekly Paclitaxel in Patients With Advanced Breast Cancer or Recurrent Ovarian Cancer: A Randomized Clinical Trial', *JAMA Oncol*, 5(1), e183773, available: http://dx.doi.org/10.1001/jamaoncol.2018.3773.

Falck, J., Petrini, J.H., Williams, B.R., Lukas, J. and Bartek, J. (2002) 'The DNA damage-dependent intra-S phase checkpoint is regulated by parallel pathways', *Nat Genet*, 30(3), 290-4, available: http://dx.doi.org/10.1038/ng845.

Fava, L., Schuler, F., Sladky, V., D. Haschka, M., Soratroi, C., Eiterer, L., Demetz, E., Weiss, G., Geley, S., Nigg, E. and Villunger, A. (2017) 'The PIDDosome activates p53 in response to supernumerary centrosomes', *Genes & Development*, 31, 34-45, available: http://dx.doi.org/10.1101/gad.289728.116.

Felgenhauer, J., Tomino, L., Selich-Anderson, J., Bopp, E. and Shah, N. (2018) 'Dual BRD4 and AURKA Inhibition Is Synergistic against MYCN-Amplified and Nonamplified Neuroblastoma', *Neoplasia*, 20(10), 965-974, available: http://dx.doi.org/https://doi.org/10.1016/j.neo.2018.08.002.

Fernandez-Capetillo, O., Chen, H.-T., Celeste, A., Ward, I., Romanienko, P.J., Morales, J.C., Naka, K., Xia, Z., Camerini-Otero, R.D., Motoyama, N., Carpenter, P.B., Bonner, W.M., Chen, J. and Nussenzweig, A. (2002) 'DNA damage-induced G2-M checkpoint activation by histone H2AX and 53BP1', *Nat Cell Biol*, 4(12), 993-997, available: http://dx.doi.org/http://www.nature.com/ncb/journal/v4/n12/suppinfo/ncb884_S1.html.

Ferrara, N. (2002) 'Role of vascular endothelial growth factor in physiologic and pathologic angiogenesis: Therapeutic implications', *Seminars in Oncology*, 29(6, Supplement 16), 10-14, available: http://dx.doi.org/https://doi.org/10.1016/S0093-7754(02)70064-X.

Floyd, S., Pines, J. and Lindon, C. (2008) 'APC/CCdh1 Targets Aurora Kinase to Control Reorganization of the Mitotic Spindle at Anaphase', *Current Biology*, 18(21), 1649-1658, available: http://dx.doi.org/http://dx.doi.org/10.1016/j.cub.2008.09.058.

Folkert, M.R. and Timmerman, R. (2015) 'Review of Treatment Options for Oligometastatic Non-Small Cell Lung Cancer', *Clinical Advances in Haematology & Oncology*, 13(3), 186-193.

Fountain, M.D., Abernathy, L.M., Lonardo, F., Rothstein, S.E., Dominello, M.M., Yunker, C.K., Chen, W., Gadgeel, S., Joiner, M.C. and Hillman, G.G. (2015) 'Radiation-Induced Esophagitis is Mitigated by Soy Isoflavones', *Frontiers in oncology*, 5, 238-238, available: http://dx.doi.org/10.3389/fonc.2015.00238.

Franken, N.A.P., Oei, A.L., Kok, H.P., Rodermond, H.M., Siminia, P., Crezee, J., Stalpers, L.J.A. and Barendson, G.W. (2013) 'Cell survival and radiosensitisation: modulation of the linear and quadratic parameters of the LQ model', *International Journal of Oncology*, 42(5), 1501-1515.

Friedberg, J.W., Mahadevan, D., Cebula, E., Persky, D., Lossos, I., Agarwal, A.B., Jung, J., Burack, R., Zhou, X., Leonard, E.J., Fingert, H., Danaee, H. and Bernstein, S.H. (2014) 'Phase II study of alisertib, a selective Aurora A kinase inhibitor, in relapsed and refractory aggressive B- and T-cell non-Hodgkin lymphomas', *Journal of clinical oncology : official journal of the American Society of Clinical Oncology*, 32(1), 44-50, available: http://dx.doi.org/10.1200/JCO.2012.46.8793.

Fukasawa, K., Choi, T., Kuriyama, R., Rulong, S. and Woude, G.F.V. (1996) 'Abnormal Centrosome Amplification in the Absence of p53', *Science*, 271(5256), 1744, available: http://dx.doi.org/10.1126/science.271.5256.1744.

Fumarola, C., Bonelli, M.A., Petronini, P.G. and Alfieri, R.R. (2014) 'Targeting PI3K/AKT/mTOR pathway in non small cell lung cancer', *Biochemical Pharmacology*, 90(3), 197-207, available: http://dx.doi.org/https://doi.org/10.1016/j.bcp.2014.05.011.

Ganem, N.J., Storchova, Z. and Pellman, D. (2007) 'Tetraploidy, aneuploidy and cancer', *Current Opinion in Genetics & Development*, 17(2), 157-162, available: http://dx.doi.org/https://doi.org/10.1016/j.gde.2007.02.011.

Gascoigne, K.E. and Taylor, S.S. (2008) 'Cancer cells display profound intra- and interline variation following prolonged exposure to antimitotic drugs', *Cancer Cell*, 14(2), 111-22, available: http://dx.doi.org/10.1016/j.ccr.2008.07.002.

Gaya, A., Hawkins, M., Kirby, A., Ahmed, M., Van As, M., Syndikus, I., Franks, K., Jain, S., Hall, E. and Khoo, V. (2016) 'CORE - Randomised trial of Conventional care versus Radioablation (stereotactic body radiotherapy

(SBRT)) for Extracranial metastases', in *Radiosurgery Society's SRS/SBRT Scientific Meeting June 2016*, June 2016.

Gedda, L., Björkelund, H. and Andersson, K. (2010) 'Real-time immunohistochemistry analysis of embedded tissue', *Applied Radiation and Isotopes*, 68(12), 2372-2376, available: http://dx.doi.org/https://doi.org/10.1016/j.apradiso.2010.06.003.

Giet, R. and Prigent, C. (2001) 'The non-catalytic domain of the Xenopus laevis auroraA kinase localises the protein to the centrosome', *Journal of Cell Science*, 114(11), 2095-2104.

Glatzer, M., Schmid, S., Radovic, M., Früh, M. and Putora, P.M. (2017) 'The role of radiation therapy in the management of small cell lung cancer', *Breathe*, 13(4), e87, available: http://dx.doi.org/10.1183/20734735.009617.

Glotzer, M. (2009) 'The 3Ms of central spindle assembly: microtubules, motors and MAPs', *Nature reviews. Molecular cell biology*, 10(1), 9-20, available: http://dx.doi.org/10.1038/nrm2609.

Godwin, J.L., Mehra, R., Litwin, S., Olszanski, A.J., Bauman, J.R. and Borghaei, H. (2016) 'A phase I/II study of MLN-8237 (alisertib), an oral aurora kinase inhibitor, in combination with erlotinib in patients with recurrent or metastatic EGFR wild-type non-small cell lung cancer', *Journal of Clinical Oncology*, 34(15_suppl), e20588-e20588, available: http://dx.doi.org/10.1200/JCO.2016.34.15_suppl.e20588.

Goff, L.W., Azad, N.S., Stein, S., Whisenant, J., Vaishampayan, U.N., Hochster, H.S., Connolly, R.M., Weise, A.M., LoRusso, P., El-Rifai, W. and Berlin, J. (2017) 'Phase I study combining the aurora kinase A (AURKA) inhibitor alisertib (Ali) with mFOLFOX in gastrointestinal (GI) cancer', *Journal of Clinical Oncology*, 35(15_suppl), 2593-2593, available: http://dx.doi.org/10.1200/JCO.2017.35.15_suppl.2593.

Goldberg, S.L., Fenaux, P., Craig, M.D., Gyan, E., Lister, J., Kassis, J., Pigneux, A., Schiller, G.J., Jung, J., Jane Leonard, E., Fingert, H. and Westervelt, P. (2014) 'An exploratory phase 2 study of investigational Aurora A kinase inhibitor alisertib (MLN8237) in acute myelogenous leukemia and myelodysplastic syndromes', *Leukemia research reports*, 3(2), 58-61, available: http://dx.doi.org/10.1016/j.lrr.2014.06.003.

Goldenson, B. and Crispino, J.D. (2015) 'The Aurora Kinases in Cell Cycle and Leukemia', *Oncogene*, 34(5), 537-545, available: http://dx.doi.org/10.1038/onc.2014.14.

Goldenson, B., Kirsammer, G., Stankiewicz, M.J., Wen, Q.J. and Crispino, J.D. (2015) 'Aurora kinase A is required for hematopoiesis but is dispensable for murine megakaryocyte endomitosis and differentiation', *Blood*, 125(13), 2141-50, available: http://dx.doi.org/10.1182/blood-2014-12-615401.

Golding, S.E., Morgan, R.N., Adams, B.R., Hawkins, A.J., Povirk, L.F. and Valerie, K. (2009) 'Pro-survival AKT and ERK signaling from EGFR and mutant EGFRvIII enhances DNA double-strand break repair in human glioma cells', *Cancer Biol Ther*, 8(8), 730-8.

Golding, S.E., Rosenberg, E., Neill, S., Dent, P., Povirk, L.F. and Valerie, K. (2007) 'Extracellular signal-related kinase positively regulates ataxia telangiectasia mutated, homologous recombination repair, and the DNA damage response', *Cancer Res*, 67(3), 1046-53, available: http://dx.doi.org/10.1158/0008-5472.can-06-2371.

Gomez-Casal, R., Bhattacharya, C., Ganesh, N., Bailey, L., Basse, P., Gibson, M., Epperly, M. and Levina, V. (2013) 'Non-small cell lung cancer cells survived ionizing radiation treatment display cancer stem cell and epithelial-mesenchymal transition phenotypes', *Molecular Cancer*, 12, 94-94, available: http://dx.doi.org/10.1186/1476-4598-12-94.

Gong, X., Du, J., Parsons, S.H., Merzoug, F.F., Webster, Y., Iversen, P.W., Chio, L.-C., Van Horn, R.D., Lin, X., Blosser, W., Han, B., Jin, S., Yao, S., Bian, H., Ficklin, C., Fan, L., Kapoor, A., Antonysamy, S., Mc Nulty, A.M., Froning, K., Manglicmot, D., Pustilnik, A., Weichert, K., Wasserman, S.R., Dowless, M., Marugán, C., Baquero, C., Lallena, M.J., Eastman, S.W., Hui, Y.-H., Dieter, M.Z., Doman, T., Chu, S., Qian, H.-R., Ye, X.S., Barda, D.A., Plowman, G.D., Reinhard, C., Campbell, R.M., Henry, J.R. and Buchanan, S.G. (2019) 'Aurora A Kinase Inhibition Is Synthetic Lethal with Loss of the RB1 Tumor Suppressor Gene', *Cancer Discovery*, 9(2), 248, available: http://dx.doi.org/10.1158/2159-8290.CD-18-0469.

Grant, R., Abdelbaki, A., Bertoldi, A., Gavilan, M.P., Mansfeld, J., Glover, D.M. and Lindon, C. (2018) 'Constitutive regulation of mitochondrial morphology by Aurora A kinase depends on a predicted cryptic targeting sequence at the N-terminus', *Open biology*, 8(6), 170272, available: http://dx.doi.org/10.1098/rsob.170272.

Green, S. and Weiss, G.R. (1992) 'Southwest Oncology Group standard response criteria, endpoint definitions and toxicity criteria', *Investigational New Drugs*, 10(4), 239-253, available: http://dx.doi.org/10.1007/BF00944177.

Gritsko, T.M., Coppola, D., Paciga, J.E., Yang, L., Sun, M., Shelley, S.A., Fiorica, J.V., Nicosia, S.V. and Cheng, J.Q. (2003) 'Activation and Overexpression of Centrosome Kinase BTAK/Aurora-A in Human Ovarian Cancer', *Clinical Cancer Research*, 9(4), 1420-1426.

Gu, B. and Zhu, W.-G. (2012) 'Surf the Post-translational Modification Network of p53 Regulation', *International Journal of Biological Sciences*, 8(5), 672-684, available: http://dx.doi.org/10.7150/ijbs.4283.

Guan, Z., Wang, X.-r., Zhu, X.-f., Huang, X.-f., Xu, J., Wang, L.-h., Wan, X.-b., Long, Z.-j., Liu, J.-n., Feng, G.-k., Huang, W., Zeng, Y.-x., Chen, F.-j. and Liu, Q. (2007) 'Aurora-A, a Negative Prognostic Marker, Increases Migration and Decreases Radiosensitivity in Cancer Cells', *Cancer Research*, 67(21), 10436-10444.

Guo, M., Lu, S., Huang, H., Wang, Y., Yang, M.Q., Yang, Y., Fan, Z., Jiang, B. and Deng, Y. (2018) 'Increased AURKA promotes cell proliferation and predicts poor prognosis in bladder cancer', *BMC Syst Biol*, 12(Suppl 7), 118, available: http://dx.doi.org/10.1186/s12918-018-0634-2.

Győrffy, B., Surowiak, P., Budczies, J. and Lánczky, A. (2013) 'Online survival analysis software to assess the prognostic value of biomarkers using transcriptomic data in non-small-cell lung cancer', *PloS one*, 8(12), e82241-e82241, available: http://dx.doi.org/10.1371/journal.pone.0082241.

Görgün, G., Calabrese, E., Hideshima, T., Ecsedy, J., Perrone, G., Mani, M., Ikeda, H., Bianchi, G., Hu, Y., Cirstea, D., Santo, L., Tai, Y.-T., Nahar, S., Zheng, M., Bandi, M., Carrasco, R.D., Raje, N., Munshi, N., Richardson, P. and Anderson, K.C. (2010) 'A novel Aurora-A kinase inhibitor MLN8237 induces cytotoxicity and cell-cycle arrest in multiple myeloma', *Blood*, 115(25), 5202.

H Falkvoll, K. (1990) 'The occurrence of apoptosis, abnormal mitoses, cells dying in mitosis and micronuclei in a human melanoma xenograft exposed to single dose irradiation', *Strahlentherapie und Onkologie*, 166(7), 487-92.

Hanna, G., McDonald, F., Greystoke, A., Forester, M., Brown, S., Hall, E., Faivre-Finn, C., Harrow, S., Hatton, M. and Chalmers, A. (2017) 'EP-1228: UK NCRI CTRad consensus on drug and radiotherapy combination platform studies in NSCLC', *Radiotherapy and Oncology*, 123, S662-S663, available: http://dx.doi.org/10.1016/S0167-8140(17)31663-8.

Hannak, E., Kirkham, M., Hyman, A.A. and Oegema, K. (2001) 'Aurora-A kinase is required for centrosome maturation in Caenorhabditis elegans', *The Journal of*

Cell Biology, 155(7), 1109-1116, available: http://dx.doi.org/10.1083/jcb.200108051.

Harrington, E.A., Bebbington, D., Moore, J., Rasmussen, R.K., Ajose-Adeogun, A.O., Nakayama, T., Graham, J.A., Demur, C., Hercend, T., Diu-Hercend, A., Su, M., Golec, J.M. and Miller, K.M. (2004) 'VX-680, a potent and selective small-molecule inhibitor of the Aurora kinases, suppresses tumor growth in vivo', *Nat Med*, 10(3), 262-7, available: http://dx.doi.org/10.1038/nm1003.

Harrow, S., Hanna, G.G., Faivre-Finn, C., McDonald, F. and Chalmers, A.J. (2016) 'The Challenges Faced in Developing Novel Drug Radiation Combinations in Non-small Cell Lung Cancer', *Clinical Oncology*, 28(11), 720-725, available: http://dx.doi.org/https://doi.org/10.1016/j.clon.2016.08.004.

Hauf, S., Cole, R.W., LaTerra, S., Zimmer, C., Schnapp, G., Walter, R., Heckel, A., van Meel, J., Rieder, C.L. and Peters, J.M. (2003) 'The small molecule Hesperadin reveals a role for Aurora B in correcting kinetochore-microtubule attachment and in maintaining the spindle assembly checkpoint', *J Cell Biol*, 161(2), 281-94, available: http://dx.doi.org/10.1083/jcb.200208092.

He, W., Ju, D., Jie, Z., Zhang, A., Xing, X. and Yang, Q. (2018) 'Aberrant CpG-methylation affects genes expression predicting survival in lung adenocarcinoma', *Cancer Med*, 7(11), 5716-5726, available: http://dx.doi.org/10.1002/cam4.1834.

Hein, A.L., Ouellette, M.M. and Yan, Y. (2014) 'Radiation-induced signaling pathways that promote cancer cell survival (review)', *International journal of oncology*, 45(5), 1813-1819, available: http://dx.doi.org/10.3892/ijo.2014.2614.

Hirota, T., Kunitoku, N., Sasayama, T., Marumoto, T., Zhang, D., Nitta, M., Hatakeyama, K. and Saya, H. (2003) 'Aurora-A and an Interacting Activator, the LIM Protein Ajuba, Are Required for Mitotic Commitment in Human Cells', *Cell*, 114(5), 585-598, available: http://dx.doi.org/10.1016/S0092-8674(03)00642-1.

Hofmann, T.G., Möller, A., Sirma, H., Zentgraf, H., Taya, Y., Dröge, W., Will, H. and Schmitz, M.L. (2001) 'Regulation of p53 activity by its interaction with homeodomain-interacting protein kinase-2', *Nature Cell Biology*, 4, 1, available: http://dx.doi.org/https://doi.org/10.1038/ncb715.

Hong, X., O'Donnell, J.P., Salazar, C.R., Van Brocklyn, J.R., Barnett, K.D., Pearl, D.K., deCarvalho, A.C., Ecsedy, J.A., Brown, S.L., Mikkelsen, T. and Lehman, N.L. (2014) 'The selective Aurora-A kinase inhibitor MLN8237 (alisertib)

potently inhibits proliferation of glioblastoma neurosphere tumor stem-like cells and potentiates the effects of temozolomide and ionizing radiation', *Cancer chemotherapy and pharmacology*, 73(5), 983-990, available: http://dx.doi.org/10.1007/s00280-014-2430-z.

Horn, V., Thélu, J., Garcia, A., Albigès-Rizo, C., Block, M.R. and Viallet, J. (2007) 'Functional Interaction of Aurora-A and PP2A during Mitosis', *Molecular Biology of the Cell*, 18(4), 1233-1241, available: http://dx.doi.org/10.1091/mbc.E06-12-1152.

Hou, D., Che, Z., Chen, P., Zhang, W., Chu, Y., Yang, D. and Liu, J. (2018) 'Suppression of AURKA alleviates p27 inhibition on Bax cleavage and induces more intensive apoptosis in gastric cancer', *Cell Death Dis*, 9(8), 781, available: http://dx.doi.org/10.1038/s41419-018-0823-3.

Hsueh, K.-W., Fu, S.-L., Chang, C.-B., Chang, Y.-L. and Lin, C.-H. (2013) 'A novel Aurora-A-mediated phosphorylation of p53 inhibits its interaction with MDM2', *Biochimica et Biophysica Acta (BBA) - Proteins and Proteomics*, 1834(2), 508-515, available: http://dx.doi.org/https://doi.org/10.1016/j.bbapap.2012.11.005.

Hsueh, K.-W., Fu, S.-L., Huang, C.-Y.F. and Lin, C.-H. (2011) 'Aurora-A phosphorylates hnRNPK and disrupts its interaction with p53', *FEBS Letters*, 585(17), 2671-2675, available: http://dx.doi.org/https://doi.org/10.1016/j.febslet.2011.07.031.

Huang, Y.F., Chang, M.D. and Shieh, S.Y. (2009) 'TTK/hMps1 mediates the p53-dependent postmitotic checkpoint by phosphorylating p53 at Thr18', *Mol Cell Biol*, 29(11), 2935-44, available: http://dx.doi.org/10.1128/mcb.01837-08.

Huertas, P. and Jackson, S.P. (2009) 'Human CtIP mediates cell cycle control of DNA end resection and double strand break repair', *The Journal of biological chemistry*, 284(14), 9558-9565, available: http://dx.doi.org/10.1074/jbc.M808906200.

Hwang In, G., Ahn Myung, J., Park Byeong, B., Ahn Yong, C., Han, J., Lee, S., Kim, J., Shim Young, M., Ahn Jin, S. and Park, K. (2008) 'ERCC1 expression as a prognostic marker in N2(+) nonsmall-cell lung cancer patients treated with platinum-based neoadjuvant concurrent chemoradiotherapy', *Cancer*, 113(6), 1379-1386, available: http://dx.doi.org/10.1002/cncr.23693.

Hyman, D.M., Sill, M., Cho, J.K., Lankes, H.A., Piekarz, R. and Hensley, M.L. (2015) 'A phase II study of alisertib (MLN8237) in recurrent or persistent uterine leiomyosarcoma: An NRG Oncology/Gynecologic Oncology Group Study

(GOG-0231D)', *Journal of Clinical Oncology*, 33(15_suppl), e16512-e16512, available: http://dx.doi.org/10.1200/jco.2015.33.15_suppl.e16512.

Ianzini and M. A. Mackey, F. (1997) 'Spontaneous premature chromosome condensation and mitotic catastrophe following irradiation of HeLa S3 cells', *International Journal of Radiation Biology*, 72(4), 409-421, available: http://dx.doi.org/10.1080/095530097143185.

Ianzini, F., Bertoldo, A., Kosmacek, E.A., Phillips, S.L. and Mackey, M.A. (2006) 'Lack of p53 function promotes radiation-induced mitotic catastrophe in mouse embryonic fibroblast cells', *Cancer cell international*, 6, 11-11, available: http://dx.doi.org/10.1186/1475-2867-6-11.

Ibarrola-Villava, M., Cervantes, A. and Bardelli, A. (2018) 'Preclinical models for precision oncology', *Biochimica et Biophysica Acta (BBA) - Reviews on Cancer*, 1870(2), 239-246, available: http://dx.doi.org/https://doi.org/10.1016/j.bbcan.2018.06.004.

Imreh, G., Vakifahmetoglu Norberg, H., Imreh, S. and Zhivotovsky, B. (2011) 'Chromosomal breaks during mitotic catastrophe trigger H2AX-ATM-p53-mediated apoptosis', *J Cell Sci*, 124, 2951-63, available: http://dx.doi.org/10.1242/jcs.081612.

International Agency for Research on Cancer (2019) *Estimated age-standardized incidence and mortality rates (World) in 2018, worldwide, both sexes, all ages*, available: http://gco.iarc.fr/today/online-analysis-multi-bars?v=2018&mode=cancer&mode_population=countries&population=900&populations=900&key=asr&sex=0&cancer=39&type=0&statistic=5&prevalence=0&population_group=0&ages_group%5B%5D=0&ages_group%5B%5D=17&nb_items=10&group_cancer=1&include_nmsc=1&include_nmsc_other=1&type_multiple=%257B%2522inc%2522%253Atrue%252C%2522mort%2522%253Atrue%252C%2522prev%2522%253Afalse%257D&orientation=horizontal&type_sort=0&type_nb_items=%257B%2522top%2522%253Atrue%252C%2522bottom%2522%253Afalse%257D&population_group_globocan_id= [accessed 05 April 2019].

International Atomic Energy Agency (2010) *Radiation Biology: A Handbook for Teachers and Students, Training Course Series No. 42*, IAEA, available: https://www-pub.iaea.org/MTCD/Publications/PDF/TCS-42_web.pdf.

Itoh, N., Semba, S., Ito, M., Takeda, H., Kawata, S. and Yamakawa, M. (2002) 'Phosphorylation of Akt/PKB is required for suppression of cancer cell apoptosis and tumor progression in human colorectal carcinoma', *Cancer*, 94(12), 3127-3134, available: http://dx.doi.org/10.1002/cncr.10591.

Iyengar, P., Kavanagh, B.D., Wardak, Z., Smith, I., Ahn, C., Gerber, D.E., Dowell, J., Hughes, R., Abdulrahman, R., Camidge, D.R., Gaspar, L.E., Doebele, R.C., Bunn, P.A., Choy, H. and Timmerman, R. (2014) 'Phase II trial of stereotactic body radiation therapy combined with erlotinib for patients with limited but progressive metastatic non-small-cell lung cancer', *J Clin Oncol*, 32(34), 3824-30, available: http://dx.doi.org/10.1200/jco.2014.56.7412.

J Merritt, A., Allen, T., S Potten, C. and Hickman, J. (1997) 'Apoptosis in small intestinal epithelia from p53-null mice: Evidence for a delayed, p53-indepdendent G2/M-associated cell death after γ-irradiation', *Oncogene*, 14, 2759-66, available: http://dx.doi.org/10.1038/sj.onc.1201126.

Janssen, A., Kops, G.J.P.L. and Medema, R.H. (2009) 'Elevating the frequency of chromosome mis-segregation as a strategy to kill tumor cells', *Proceedings of the National Academy of Sciences*, 106(45), 19108, available: http://dx.doi.org/10.1073/pnas.0904343106.

Jemal, A., Bray, F., Center, M.M., Ferlay, J., Ward, E. and Forman, D. (2011) 'Global cancer statistics', *CA: A Cancer Journal for Clinicians*, 61(2), 69-90, available: http://dx.doi.org/10.3322/caac.20107.

Ji, X., Ji, J., Shan, F., Zhang, Y., Chen, Y. and Lu, X. (2015) 'Cancer-associated fibroblasts from NSCLC promote the radioresistance in lung cancer cell lines', *Int J Clin Exp Med*, 8(5), 7002-8.

Jiang, Y., Verbiest, T., Devery, A.M., Bokobza, S.M., Weber, A.M., Leszczynska, K.B., Hammond, E.M. and Ryan, A.J. (2016) 'Hypoxia Potentiates the Radiation-Sensitizing Effect of Olaparib in Human Non-Small Cell Lung Cancer Xenografts by Contextual Synthetic Lethality', *International journal of radiation oncology, biology, physics*, 95(2), 772-781, available: http://dx.doi.org/10.1016/j.ijrobp.2016.01.035.

Jordan, M.A. and Wilson, L. (2004) 'Microtubules as a target for anticancer drugs', *Nature Reviews Cancer*, 4, 253, available: http://dx.doi.org/10.1038/nrc1317.

Joukov, V., De Nicolo, A., Rodriguez, A., Walter, J.C. and Livingston, D.M. (2010) 'Centrosomal protein of 192 kDa (Cep192) promotes centrosome-driven spindle assembly by engaging in organelle-specific Aurora A activation', *Proceedings of the National Academy of Sciences of the United States of America*, 107(49), 21022-21027, available: http://dx.doi.org/10.1073/pnas.1014664107.

Jurvansuu, J., Fragkos, M., Ingemarsdotter, C. and Beard, P. (2007) 'Chk1 Instability Is Coupled to Mitotic Cell Death of p53-deficient Cells in Response to Virus-induced DNA Damage Signaling', *Journal of Molecular Biology*, 372(2), 397-406, available: http://dx.doi.org/https://doi.org/10.1016/j.jmb.2007.06.077.

Kang, H.N., Choi, J.W., Shim, H.S., Kim, J., Kim, D.J., Lee, C.Y., Hong, M.H., Park, S.Y., Park, A.Y., Shin, E.J., Lee, S.Y., Pyo, K.-H., Yun, M.R., Choi, H.M., Lee, S.S., Kim, S.-Y., Lee, H., Paik, S., Cho, B.C., Lee, J.G. and Kim, H.R. (2018) 'Establishment of a platform of non-small-cell lung cancer patient-derived xenografts with clinical and genomic annotation', *Lung Cancer*, 124, 168-178, available: http://dx.doi.org/https://doi.org/10.1016/j.lungcan.2018.08.008.

Kasahara, N., Imai, H., Kaira, K., Mori, K., Wakuda, K., Ono, A., Taira, T., Kenmotsu, H., Harada, H., Naito, T., Murakami, H., Endo, M., Nakajima, T., Yamada, M. and Takahashi, T. (2015) 'Clinical impact of post-progression survival on overall survival in patients with limited-stage disease small cell lung cancer after first-line chemoradiotherapy', *Radiology and oncology*, 49(4), 409-415, available: http://dx.doi.org/10.1515/raon-2015-0037.

Kashatus, D.F., Lim, K.-H., Brady, D.C., Pershing, N.L.K., Cox, A.D. and Counter, C.M. (2011) 'RalA and RalBP1 regulate mitochondrial fission at mitosis', *Nature cell biology*, 13(9), 1108-1115, available: http://dx.doi.org/10.1038/ncb2310.

Kastan, M.B. and Bartek, J. (2004) 'Cell-cycle checkpoints and cancer', *Nature*, 432(7015), 316-23, available: http://dx.doi.org/10.1038/nature03097.

Katayama, H., Sasai, K., Kawai, H., Yuan, Z.M., Bondaruk, J., Suzuki, F., Fujii, S., Arlinghaus, R.B., Czerniak, B.A. and Sen, S. (2004) 'Phosphorylation by aurora kinase A induces Mdm2-mediated destabilization and inhibition of p53', *Nat Genet*, 36(1), 55-62, available: http://dx.doi.org/10.1038/ng1279.

Katayama, H., Sasai, K., Kloc, M., Brinkley, B.R. and Sen, S. (2008) 'Aurora kinase-A regulates kinetochore/chromatin associated microtubule assembly in human cells', *Cell Cycle*, 7(17), 2691-2704, available: http://dx.doi.org/10.4161/cc.7.17.6460.

Katayama, H., Wang, J., Treekitkarnmongkol, W., Kawai, H., Sasai, K., Zhang, H., Wang, H., Adams, Henry P., Jiang, S., Chakraborty, Sandip N., Suzuki, F., Arlinghaus, Ralph B., Liu, J., Mobley, James A., Grizzle, William E., Wang, H. and Sen, S. (2012) 'Aurora Kinase-A Inactivates DNA Damage-Induced Apoptosis and Spindle Assembly Checkpoint Response Functions of p73', *Cancer Cell*, 21(2), 196-211, available: http://dx.doi.org/https://doi.org/10.1016/j.ccr.2011.12.025.

Keen, N. and Taylor, S. (2009) 'Mitotic drivers--inhibitors of the Aurora B Kinase', *Cancer Metastasis Rev*, 28(1-2), 185-95, available: http://dx.doi.org/10.1007/s10555-009-9184-9.

Kellar, A., Egan, C. and Morris, D. (2015) 'Preclinical Murine Models for Lung Cancer: Clinical Trial Applications', *BioMed research international*, 2015, 621324, available: http://dx.doi.org/10.1155/2015/621324.

Kelly, K.R., Friedberg, J.W., Park, S.I., McDonagh, K., Hayslip, J., Persky, D., Ruan, J., Puvvada, S., Rosen, P., Iyer, S.P., Stefanovic, A., Bernstein, S.H., Weitman, S., Karnad, A., Monohan, G., VanderWalde, A., Mena, R., Schmelz, M., Spier, C., Groshen, S., Venkatakrishnan, K., Zhou, X., Sheldon-Waniga, E., Leonard, E.J. and Mahadevan, D. (2018) 'Phase I Study of the Investigational Aurora A Kinase Inhibitor Alisertib plus Rituximab or Rituximab/Vincristine in Relapsed/Refractory Aggressive B-cell Lymphoma', *Clinical Cancer Research*, 24(24), available: http://dx.doi.org/10.1158/1078-0432.CCR-18-0286.

Kelly, K.R., Shea, T.C., Goy, A., Berdeja, J.G., Reeder, C.B., McDonagh, K.T., Zhou, X., Danaee, H., Liu, H., Ecsedy, J.A., Niu, H., Benaim, E. and Iyer, S.P. (2014) 'Phase I study of MLN8237--investigational Aurora A kinase inhibitor--in relapsed/refractory multiple myeloma, non-Hodgkin lymphoma and chronic lymphocytic leukemia', *Invest New Drugs*, 32(3), 489-99, available: http://dx.doi.org/10.1007/s10637-013-0050-9.

Khan, J., Ezan, F., Crémet, J.-Y., Fautrel, A., Gilot, D., Lambert, M., Benaud, C., Troadec, M.-B. and Prigent, C. (2011) 'Overexpression of Active Aurora-C Kinase Results in Cell Transformation and Tumour Formation', *PLoS ONE*, 6(10), e26512, available: http://dx.doi.org/10.1371/journal.pone.0026512.

Khosravi, R., Maya, R., Gottlieb, T., Oren, M., Shiloh, Y. and Shkedy, D. (1999) 'Rapid ATM-dependent phosphorylation of MDM2 precedes p53 accumulation in response to DNA damage', *Proceedings of the National Academy of Sciences of the United States of America*, 96(26), 14973-14977.

Kiat, L.S., Hui, K.M. and Gopalan, G. (2002) 'Aurora-A kinase interacting protein (AIP), a novel negative regulator of human Aurora-A kinase', *J Biol Chem*, 277(47), 45558-65, available: http://dx.doi.org/10.1074/jbc.M206820200.

Kim, E.J.-h., Semrad, T.J., Gandara, D.R., Riess, J., Li, T., Yu, A., Matsukuma, K., Mack, P.C. and Kelly, K. (2015) 'Phase I study of the combination of alisertib (MLN8237) and gemcitabine in advanced solid tumors', *Journal of Clinical Oncology*, 33(15_suppl), 2526-2526, available: http://dx.doi.org/10.1200/jco.2015.33.15_suppl.2526.

Kimura, M., Matsuda, Y., Yoshioka, T. and Okano, Y. (1999) 'Cell cycle-dependent expression and centrosome localization of a third human aurora/Ipl1-related protein kinase, AIK3', *J Biol Chem*, 274(11), 7334-40.

Kinner, A., Wu, W., Staudt, C. and Iliakis, G. (2008) 'γ-H2AX in recognition and signaling of DNA double-strand breaks in the context of chromatin', *Nucleic Acids Research*, 36(17), 5678-5694, available: http://dx.doi.org/10.1093/nar/gkn550.

Kinoshita, K., Noetzel, T.L., Pelletier, L., Mechtler, K., Drechsel, D.N., Schwager, A., Lee, M., Raff, J.W. and Hyman, A.A. (2005) 'Aurora A phosphorylation of TACC3/maskin is required for centrosome-dependent microtubule assembly in mitosis', *J Cell Biol*, 170(7), 1047-55, available: http://dx.doi.org/10.1083/jcb.200503023.

Kishimoto, Y., Murakami, Y., Shiraishi, M., Hayashi, K. and Sekiya, T. (1992) 'Aberrations of the p53 Tumor Suppressor Gene in Human Non-Small Cell Carcinomas of the Lung', *Cancer Research*, 52(17), 4799-4804.

Kitajima, S., Kudo, Y., Ogawa, I., Tatsuka, M., Kawai, H., Pagano, M. and Takata, T. (2007) 'Constitutive Phosphorylation of Aurora-A on Ser51 Induces Its Stabilization and Consequent Overexpression in Cancer', *PLoS ONE*, 2(9), e944, available: http://dx.doi.org/10.1371/journal.pone.0000944.

Koh, H.M., Jang, B.G., Hyun, C.L., Kim, Y.S., Hyun, J.W., Chang, W.Y. and Maeng, Y.H. (2017) 'Aurora Kinase A Is a Prognostic Marker in Colorectal Adenocarcinoma', *J Pathol Transl Med*, 51(1), 32-39, available: http://dx.doi.org/10.4132/jptm.2016.10.17.

Korobeynikov, V., Deneka, A.Y. and Golemis, E.A. (2017) 'Mechanisms for nonmitotic activation of Aurora-A at cilia', *Biochem Soc Trans*, 45(1), 37-49, available: http://dx.doi.org/10.1042/bst20160142.

Korrodi-Gregório, L., Soto-Cerrato, V., Vitorino, R., Fardilha, M. and Pérez-Tomás, R. (2016) 'From Proteomic Analysis to Potential Therapeutic Targets: Functional Profile of Two Lung Cancer Cell Lines, A549 and SW900, Widely Studied in Pre-Clinical Research', *PloS one*, 11(11), e0165973-e0165973, available: http://dx.doi.org/10.1371/journal.pone.0165973.

Kovarikova, V., Burkus, J., Rehak, P., Brzakova, A., Solc, P. and Baran, V. (2015) 'Aurora kinase A is essential for correct chromosome segregation in mouse zygote', *Zygote*, 1-12, available: http://dx.doi.org/10.1017/s0967199415000222.

Kriegs, M., Gurtner, K., Can, Y., Brammer, I., Rieckmann, T., Oertel, R., Wysocki, M., Dorniok, F., Gal, A., Grob, T.J., Laban, S., Kasten-Pisula, U., Petersen, C., Baumann, M., Krause, M. and Dikomey, E. (2015) 'Radiosensitization of NSCLC cells by EGFR inhibition is the result of an enhanced p53-dependent G1 arrest', *Radiotherapy and Oncology*, 115(1), 120-127, available: http://dx.doi.org/https://doi.org/10.1016/j.radonc.2015.02.018.

Kufer, T.A., Sillje, H.H., Korner, R., Gruss, O.J., Meraldi, P. and Nigg, E.A. (2002) 'Human TPX2 is required for targeting Aurora-A kinase to the spindle', *J Cell Biol*, 158(4), 617-23, available: http://dx.doi.org/10.1083/jcb.200204155.

Kunitoku, N., Sasayama, T., Marumoto, T., Zhang, D., Honda, S., Kobayashi, O., Hatakeyama, K., Ushio, Y., Saya, H. and Hirota, T. (2003) 'CENP-A phosphorylation by Aurora-A in prophase is required for enrichment of Aurora-B at inner centromeres and for kinetochore function', *Dev Cell*, 5(6), 853-64.

Kuribayashi, K., Finnberg, N., Jeffers, J.R., Zambetti, G.P. and El-Deiry, W.S. (2011) 'The relative contribution of pro-apoptotic p53-target genes in the triggering of apoptosis following DNA damage in vitro and in vivo', *Cell Cycle*, 10(14), 2380-9, available: http://dx.doi.org/10.4161/cc.10.14.16588.

Kurinna, S., Stratton, S.A., Coban, Z., Schumacher, J.M., Grompe, M., Duncan, A.W. and Barton, M.C. (2013) 'p53 REGULATES A MITOTIC TRANSCRIPTION PROGRAM AND DETERMINES PLOIDY IN NORMAL MOUSE LIVER', *Hepatology (Baltimore, Md.)*, 57(5), 2004-2013, available: http://dx.doi.org/10.1002/hep.26233.

Kwint, M., Uyterlinde, W., Nijkamp, J., Chen, C., de Bois, J., Sonke, J.-J., van den Heuvel, M., Knegjens, J., van Herk, M. and Belderbos, J. (2012) 'Acute Esophagus Toxicity in Lung Cancer Patients After Intensity Modulated Radiation Therapy and Concurrent Chemotherapy', *International Journal of Radiation Oncology*Biology*Physics*, 84(2), e223-e228, available: http://dx.doi.org/https://doi.org/10.1016/j.ijrobp.2012.03.027.

Lanni, J.S. and Jacks, T. (1998) 'Characterization of the p53-dependent postmitotic checkpoint following spindle disruption', *Mol Cell Biol*, 18(2), 1055-64.

Lassmann, S., Shen, Y., Jütting, U., Wiehle, P., Walch, A., Gitsch, G., Hasenburg, A. and Werner, M. (2007) 'Predictive Value of Aurora-A/STK15 Expression for Late Stage Epithelial Ovarian Cancer Patients Treated by Adjuvant Chemotherapy', *Clinical Cancer Research*, 13(14), 4083-4091.

Le, L.-T.-T., Vu, H.-L., Nguyen, C.-H. and Molla, A. (2013) 'Basal aurora kinase B activity is sufficient for histone H3 phosphorylation in prophase', *Biology open*, 2(4), 379-386, available: http://dx.doi.org/10.1242/bio.20133079.

Le, Q.-T., Chen, E., Salim, A., Cao, H., S Kong, C., Whyte, R., Donington, J., Cannon, W., Wakelee, H., Tibshirani, R., Mitchell, J., Richardson, D., J O'Byrne, K., C Koong, A. and J Giaccia, A. (2006) 'An Evaluation of Tumor Oxygenation and Gene Expression in Patients with Early Stage Non-Small Cell Lung Cancers', *Clin Can Res*, 12(5), 1507-14, available: http://dx.doi.org/10.1158/1078-0432.CCR-05-2049.

Lee, D.-F., Su, J., Ang, Y.-S., Carvajal-Vergara, X., Mulero-Navarro, S., Pereira, C.F., Gingold, J., Wang, H.-L., Zhao, R., Sevilla, A., Darr, H., Williamson, A.J.K., Chang, B., Niu, X., Aguilo, F., Flores, E.R., Sher, Y.-P., Hung, M.-C., Whetton, A.D., Gelb, B.D., Moore, K.A., Snoeck, H.-W., Ma'ayan, A., Schaniel, C. and Lemischka, I.R. (2012) 'Regulation of embryonic and induced pluripotency by aurora kinase-p53 signaling', *Cell stem cell*, 11(2), 179-194, available: http://dx.doi.org/10.1016/j.stem.2012.05.020.

Lee, H.C., An, S., Lee, H., Woo, S.H., Jin, H.O., Seo, S.K., Choe, T.B., Yoo, D.H., Lee, S.J., Hong, Y.J., Park, M.J., Rhee, C.H., Park, I.C. and Hong, S.I. (2008) 'Activation of epidermal growth factor receptor and its downstream signaling pathway by nitric oxide in response to ionizing radiation', *Mol Cancer Res*, 6(6), 996-1002, available: http://dx.doi.org/10.1158/1541-7786.mcr-08-0113.

Lee, H.J., Koh, E.S., Kwak, J.J., Kim, H.K., Park, S.-M. and Choi, I.-H. (2012) 'Clinicopathologic significance of Aurora kinase A expression in non-small cell lung cancer', *Basic and Applied Pathology*, 5(1), 8-14, available: http://dx.doi.org/10.1111/j.1755-9294.2011.01120.x.

Lee, S.O., Andey, T., Jin, U.H., Kim, K., Singh, M. and Safe, S. (2012) 'The nuclear receptor TR3 regulates mTORC1 signaling in lung cancer cells expressing wild-type p53', *Oncogene*, 31(27), 3265-3276, available: http://dx.doi.org/10.1038/onc.2011.504.

Leonard, M.K., Hill, N.T., Bubulya, P.A. and Kadakia, M.P. (2013) 'The PTEN-Akt pathway impacts the integrity and composition of mitotic centrosomes', *Cell cycle (Georgetown, Tex.)*, 12(9), 1406-1415, available: http://dx.doi.org/10.4161/cc.24516.

Lheureux, S., Tinker, A., Clarke, B., Ghatage, P., Welch, S., Weberpals, J.I., Dhani, N.C., Butler, M.O., Tonkin, K., Tan, Q., Tan, D.S.P., Brooks, K., Ramsahai, J., Wang, L., Pham, N.A., Shaw, P.A., Tsao, M.S., Garg, S., Stockley, T. and Oza, A.M. (2018) 'A Clinical and Molecular Phase II Trial of Oral ENMD-2076 in Ovarian Clear Cell Carcinoma (OCCC): A Study of the Princess Margaret

Phase II Consortium', *Clin Cancer Res*, 24(24), 6168-6174, available: http://dx.doi.org/10.1158/1078-0432.ccr-18-1244.

Li, L., Hu, M., Zhu, H., Zhao, W., Yang, G. and Yu, J. (2010) 'Comparison of 18F-Fluoroerythronitroimidazole and 18F-Fluorodeoxyglucose Positron Emission Tomography and Prognostic Value in Locally Advanced Non–Small-Cell Lung Cancer', *Clinical Lung Cancer*, 11(5), 335-340, available: http://dx.doi.org/https://doi.org/10.3816/CLC.2010.n.042.

Li, L., Yu, J., Xing, L., Ma, K., Zhu, H., Guo, H., Sun, X., Li, J., Yang, G., Li, W., Yue, J. and Li, B. (2006) 'Serial hypoxia imaging with 99mTc-HL91 SPECT to predict radiotherapy response in nonsmall cell lung cancer', *Am J Clin Oncol*, 29(6), 628-33, available: http://dx.doi.org/10.1097/01.coc.0000242345.71582.e0.

Li, L.T., Jiang, G. and Chen, Q. (2014) 'Ki67 is a promising molecular target in the diagnosis of cancer (review)', *Mol. Med. Report. Mar.*, 11(3), 1566-1572.

Li, P., Nijhawan, D., Budihardjo, I., Srinivasula, S.M., Ahmad, M., Alnemri, E.S. and Wang, X. (1997) 'Cytochrome c and dATP-Dependent Formation of Apaf-1/Caspase-9 Complex Initiates an Apoptotic Protease Cascade', *Cell*, 91(4), 479-489, available: http://dx.doi.org/https://doi.org/10.1016/S0092-8674(00)80434-1.

Li, P., Zhou, L., Liu, X., Jin, X., Zhao, T., Ye, F., Liu, X., Hirayama, R. and Li, Q. (2014) 'Mitotic DNA damages induced by carbon–ion radiation incur additional chromosomal breaks in polyploidy', *Toxicology Letters*, 230(1), 36-47, available: http://dx.doi.org/https://doi.org/10.1016/j.toxlet.2014.08.006.

Li, R., Sutphin, P.D., Schwartz, D., Matas, D., Almog, N., Wolkowicz, R., Goldfinger, N., Pei, H., Prokocimer, M. and Rotter, V. (1998) 'Mutant p53 protein expression interferes with p53-independent apoptotic pathways', *Oncogene*, 16, 3269, available: http://dx.doi.org/10.1038/sj.onc.1201867.

Li, S., Xuan, Y., Gao, B., Sun, X., Miao, S., Lu, T., Wang, Y. and Jiao, W. (2018) 'Identification of an eight-gene prognostic signature for lung adenocarcinoma', *Cancer Manag Res*, 10, 3383-3392, available: http://dx.doi.org/10.2147/cmar.s173941.

Li, X., Liu, N., Ren, P., Cao, Q., Wang, P., Zhao, L. and Lu, B. (2015) '[Prognostic value of combined expression of Aurora A, p53 and p21 WAF1 in patients after curative resection of non-small cell lung cancer]', *Zhonghua Zhong Liu Za Zhi*, 37(7), 512-6.

Liao, W.C., Haimovitz-Friedman, A., Persaud, R.S., McLoughlin, M., Ehleiter, D., Zhang, N., Gatei, M., Lavin, M., Kolesnick, R. and Fuks, Z. (1999) 'Ataxia telangiectasia-mutated gene product inhibits DNA damage-induced apoptosis via ceramide synthase', *J Biol Chem*, 274(25), 17908-17.

Liao, Y., Liao, Y., Li, J., Li, J., Fan, Y. and Xu, B. (2018) 'Polymorphisms in AURKA and AURKB are associated with the survival of triple-negative breast cancer patients treated with taxane-based adjuvant chemotherapy', *Cancer management and research*, 10, 3801-3808, available: http://dx.doi.org/10.2147/CMAR.S174735.

Lieber, M.R. (2010) 'The mechanism of double-strand DNA break repair by the nonhomologous DNA end-joining pathway', *Annu Rev Biochem*, 79, 181-211, available: http://dx.doi.org/10.1146/annurev.biochem.052308.093131.

Liloglou, T., Ross, H., Prime, W., Donnelly, R.J., Spandidos, D.A., Gosney, J.R. and Field, J.K. (1997) 'p53 gene aberrations in non-small-cell lung carcinomas from a smoking population', *British journal of cancer*, 75(8), 1119-1124.

Lim, K.-H., Lockhart, A.C., Waqar, S.N., Govindan, R., Morgensztern, D., Picus, J., Tan, B.R., Baggstrom, M.Q., Ratchford, E., Marquez, S. and Wang-Gillam, A. (2017) 'Phase I study combining MLN8237 with nab-paclitaxel in patients with advanced solid malignancies', *Journal of Clinical Oncology*, 35(15_suppl), 2553-2553, available: http://dx.doi.org/10.1200/JCO.2017.35.15_suppl.2553.

Lin, J., Patel, S.A., Sama, A.R., Hoffman-Censits, J.H., Kennedy, B., Kilpatrick, D., Ye, Z., Yang, H., Mu, Z., Leiby, B., Lewis, N., Cristofanilli, M. and Kelly, W.K. (2016) 'A Phase I/II Study of the Investigational Drug Alisertib in Combination With Abiraterone and Prednisone for Patients With Metastatic Castration-Resistant Prostate Cancer Progressing on Abiraterone', *The oncologist*, 21(11), 1296-1297e, available: http://dx.doi.org/10.1634/theoncologist.2016-0297.

Lin, Z.-Z., Chou, C.-H., Cheng, A.-L., Liu, W.-L. and Chia-Hsien Cheng, J. (2014) 'Radiosensitization by combining an aurora kinase inhibitor with radiotherapy in hepatocellular carcinoma through cell cycle interruption', *International Journal of Cancer*, 135(2), 492-501, available: http://dx.doi.org/10.1002/ijc.28682.

Lioutas, A. and Vernos, I. (2013) 'Aurora A kinase and its substrate TACC3 are required for central spindle assembly', *EMBO Reports*, 14(9), 829-836, available: http://dx.doi.org/10.1038/embor.2013.109.

Littlepage, L.E. and Ruderman, J.V. (2002) 'Identification of a new APC/C recognition domain, the A box, which is required for the Cdh1-dependent destruction of the kinase Aurora-A during mitotic exit', *Genes Dev*, 16(17), 2274-85, available: http://dx.doi.org/10.1101/gad.1007302.

Littlepage, L.E., Wu, H., Andresson, T., Deanehan, J.K., Amundadottir, L.T. and Ruderman, J.V. (2002) 'Identification of phosphorylated residues that affect the activity of the mitotic kinase Aurora-A', *Proceedings of the National Academy of Sciences of the United States of America*, 99(24), 15440-15445, available: http://dx.doi.org/10.1073/pnas.202606599.

Liu, Q., Kaneko, S., Yang, L., I Feldman, R., Nicosia, S., Chen, J. and Cheng, J. (2005) 'Aurora-A Abrogation of p53 DNA Binding and Transactivation Activity by Phosphorylation of Serine 215', *J Biol Chem*, 279, 52175-82, available: http://dx.doi.org/10.1074/jbc.M406802200.

Lo Iacono, M., Monica, V., Saviozzi, S., Ceppi, P., Bracco, E., Papotti, M. and Scagliotti, G.V. (2011) 'Aurora Kinase A expression is associated with lung cancer histological-subtypes and with tumor de-differentiation', *Journal of Translational Medicine*, 9, 100-100, available: http://dx.doi.org/10.1186/1479-5876-9-100.

Lu, L., Han, H., Tian, Y., Li, W., Zhang, J., Feng, M. and Li, Y. (2014) 'Aurora kinase A mediates c-Myc's oncogenic effects in hepatocellular carcinoma', *Molecular Carcinogenesis*, n/a-n/a, available: http://dx.doi.org/10.1002/mc.22223.

Lucena-Araujo, A.R., de Oliveira, F.M., Leite-Cueva, S.D., dos Santos, G.A., Falcao, R.P. and Rego, E.M. (2011) 'High expression of AURKA and AURKB is associated with unfavorable cytogenetic abnormalities and high white blood cell count in patients with acute myeloid leukemia', *Leukemia Research*, 35(2), 260-264, available: http://dx.doi.org/10.1016/j.leukres.2010.07.034.

Luo, H., Yount, C., Lang, H., Yang, A., Riemer, E.C., Lyons, K., Vanek, K.N., Silvestri, G.A., Schulte, B.A. and Wang, G.Y. (2013) 'Activation of p53 with Nutlin-3a radiosensitizes lung cancer cells via enhancing radiation-induced premature senescence', *Lung cancer (Amsterdam, Netherlands)*, 81(2), 167-173, available: http://dx.doi.org/10.1016/j.lungcan.2013.04.017.

Löbrich, M., Shibata, A., Beucher, A., Fisher, A., Ensminger, M., Goodarzi, A.A., Barton, O. and Jeggo, P.A. (2010) 'γH2AX foci analysis for monitoring DNA double-strand break repair: Strengths, limitations and optimization', *Cell Cycle*, 9(4), 662-669, available: http://dx.doi.org/10.4161/cc.9.4.10764.

Ma, N., Matsunaga, S., Morimoto, A., Sakashita, G., Urano, T., Uchiyama, S. and Fukui, K. (2011) 'The nuclear scaffold protein SAF-A is required for kinetochore-microtubule attachment and contributes to the targeting of Aurora-A to mitotic spindles', *J Cell Sci*, 124(Pt 3), 394-404, available: http://dx.doi.org/10.1242/jcs.063347.

Ma, Y., Yang, J., Wang, R., Zhang, Z., Qi, X., Liu, C. and Ma, M. (2017) 'Aurora-A affects radiosenstivity in cervical squamous cell carcinoma and predicts poor prognosis', *Oncotarget*, 8(19), 31509-31520, available: http://dx.doi.org/10.18632/oncotarget.15663.

Ma, Z., Izumi, H., Kanai, M., Kabuyama, Y., G Ahn, N. and Fukasawa, K. (2006) 'Mortalin controls centrosome duplication via modulating centrosomal localization of p53', *Oncogene*, 25, 5377-90, available: http://dx.doi.org/10.1038/sj.onc.1209543.

Macurek, L., Lindqvist, A., Lim, D., Lampson, M.A., Klompmaker, R., Freire, R., Clouin, C., Taylor, S.S., Yaffe, M.B. and Medema, R.H. (2008) 'Polo-like kinase-1 is activated by aurora A to promote checkpoint recovery', *Nature*, 455(7209), 119-23, available: http://dx.doi.org/10.1038/nature07185.

Maier, P., Hartmann, L., Wenz, F. and Herskind, C. (2016) 'Cellular Pathways in Response to Ionizing Radiation and Their Targetability for Tumor Radiosensitization', *International journal of molecular sciences*, 17(1), 102, available: http://dx.doi.org/10.3390/ijms17010102.

Malumbres, M. and Pérez de Castro, I. (2014) 'Aurora kinase A inhibitors: promising agents in antitumoral therapy', *Expert Opinion on Therapeutic Targets*, 18(12), 1377-1393, available: http://dx.doi.org/10.1517/14728222.2014.956085.

Manfredi, M.G., Ecsedy, J.A., Chakravarty, A., Silverman, L., Zhang, M., Hoar, K.M., Stroud, S.G., Chen, W., Shinde, V., Huck, J.J., Wysong, D.R., Janowick, D.A., Hyer, M.L., LeRoy, P.J., Gershman, R.E., Silva, M.D., Germanos, M.S., Bolen, J.B., Claiborne, C.F. and Sells, T.B. (2011) 'Characterization of Alisertib (MLN8237), an Investigational Small-Molecule Inhibitor of Aurora A Kinase Using Novel *In Vivo* Pharmacodynamic Assays', *Clinical Cancer Research*, 17(24), 7614.

Manfredi, M.G., Ecsedy, J.A., Meetze, K.A., Balani, S.K., Burenkova, O., Chen, W., Galvin, K.M., Hoar, K.M., Huck, J.J., LeRoy, P.J., Ray, E.T., Sells, T.B., Stringer, B., Stroud, S.G., Vos, T.J., Weatherhead, G.S., Wysong, D.R., Zhang, M., Bolen, J.B. and Claiborne, C.F. (2007) 'Antitumor activity of MLN8054, an orally active small-molecule inhibitor of Aurora A kinase', *Proceedings of the National Academy of Sciences of the United States of*

America, 104(10), 4106-4111, available: http://dx.doi.org/10.1073/pnas.0608798104.

Marone, R., Cmiljanovic, V., Giese, B. and Wymann, M.P. (2008) 'Targeting phosphoinositide 3-kinase: moving towards therapy', *Biochim Biophys Acta*, 1784(1), 159-85, available: http://dx.doi.org/10.1016/j.bbapap.2007.10.003.

Marumoto, T., Hirota, T., Morisaki, T., Kunitoku, N., Zhang, D., Ichikawa, Y., Sasayama, T., Kuninaka, S., Mimori, T., Tamaki, N., Kimura, M., Okano, Y. and Saya, H. (2002) 'Roles of aurora-A kinase in mitotic entry and G2 checkpoint in mammalian cells', *Genes Cells*, 7(11), 1173-82.

Marumoto, T., Honda, S., Hara, T., Nitta, M., Hirota, T., Kohmura, E. and Saya, H. (2003) 'Aurora-A kinase maintains the fidelity of early and late mitotic events in HeLa cells', *J Biol Chem*, 278(51), 51786-95, available: http://dx.doi.org/10.1074/jbc.M306275200.

Marumoto, T., Zhang, D. and Saya, H. (2005) 'Aurora-A [mdash] A guardian of poles', *Nat Rev Cancer*, 5(1), 42-50.

Marxer, M., Ma, H.T., Man, W.Y. and Poon, R.Y.C. (2013) 'p53 deficiency enhances mitotic arrest and slippage induced by pharmacological inhibition of Aurora kinases', *Oncogene*, 33, 3550, available: http://dx.doi.org/10.1038/onc.2013.325.

Matulonis, U.A., Lee, J., Lasonde, B., Tew, W.P., Yehwalashet, A., Matei, D., Behbakht, K., Grothusen, J., Fleming, G., Lee, N.K., Arnott, J., Bray, M.R., Fletcher, G., Brokx, R.D., Castonguay, V., Mackay, H., Sidor, C.F. and Oza, A.M. (2013) 'ENMD-2076, an oral inhibitor of angiogenic and proliferation kinases, has activity in recurrent, platinum resistant ovarian cancer', *European Journal of Cancer*, 49(1), 121-131, available: http://dx.doi.org/http://dx.doi.org/10.1016/j.ejca.2012.07.020.

Mauguen, A., Pignon, J.-P., Burdett, S., Domerg, C., Fisher, D., Paulus, R., Mandrekar, S.J., Belani, C.P., Shepherd, F.A., Eisen, T., Pang, H., Collette, L., Sause, W.T., Dahlberg, S.E., Crawford, J., O'Brien, M., Schild, S.E., Parmar, M., Tierney, J.F., Le Pechoux, C., Michiels, S. and Surrogate Lung Project Collaborative, G. (2013) 'Surrogate endpoints for overall survival in chemotherapy and radiotherapy trials in operable and locally advanced lung cancer: a re-analysis of meta-analyses of individual patients' data', *The Lancet. Oncology*, 14(7), 619-626, available: http://dx.doi.org/10.1016/S1470-2045(13)70158-X.

Meek, D.W. (1998) 'Multisite Phosphorylation and the Integration of Stress Signals at p53', *Cellular Signalling*, 10(3), 159-166, available: http://dx.doi.org/https://doi.org/10.1016/S0898-6568(97)00119-8.

Melichar, B., Adenis, A., Lockhart, A.C., Bennouna, J., Dees, E.C., Kayaleh, O., Obermannova, R., DeMichele, A., Zatloukal, P., Zhang, B., Ullmann, C.D. and Schusterbauer, C. (2015) 'Safety and activity of alisertib, an investigational aurora kinase A inhibitor, in patients with breast cancer, small-cell lung cancer, non-small-cell lung cancer, head and neck squamous-cell carcinoma, and gastro-oesophageal adenocarcinoma: a five-arm phase 2 study', *The Lancet Oncology*, 16(4), 395-405, available: http://dx.doi.org/10.1016/S1470-2045(15)70051-3.

Meraldi, P., Honda, R. and Nigg, E.A. (2002) 'Aurora-A overexpression reveals tetraploidization as a major route to centrosome amplification in p53-/- cells', *Embo j*, 21(4), 483-92.

Mignogna, C., Staropoli, N., Botta, C., De Marco, C., Rizzuto, A., Morelli, M., Di Cello, A., Franco, R., Camastra, C., Presta, I., Malara, N., Salvino, A., Tassone, P., Tagliaferri, P., Barni, T., Donato, G. and Di Vito, A. (2016) 'Aurora Kinase A expression predicts platinum-resistance and adverse outcome in high-grade serous ovarian carcinoma patients', *J Ovarian Res*, 9(1), 31, available: http://dx.doi.org/10.1186/s13048-016-0238-7.

Mikule, K., Delaval, B., Kaldis, P., Jurczyk, A., Hergert, P. and Doxsey, S. (2007) 'Loss of centrosome integrity induces p38-p53-p21-dependent G1-S arrest', *Nat Cell Biol*, 9, 160-70.

Miller, C.W., Simon, K., Aslo, A., Kok, K., Yokota, J., Buys, C.H.C.M., Terada, M. and Koeffler, H.P. (1992) '*p53* Mutations in Human Lung Tumors', *Cancer Research*, 52(7), 1695-1698.

Min, M., Mayor, U. and Lindon, C. (2013) 'Ubiquitination site preferences in anaphase promoting complex/cyclosome (APC/C) substrates', *Open Biology*, 3(9), 130097, available: http://dx.doi.org/10.1098/rsob.130097.

Minton, S.E., LoRusso, P., Lockhart, A.C., Saif, M., Krishnamurthi, S.S., Pickett-Gies, C.A., Wang, Y., Guan, S., Roben, E. and Stein, M.N. (2010) 'A phase I study of MK-5108, an oral aurora A kinase inhibitor, in both monotherapy and in combination with docetaxel in patients with advanced solid tumors', *ASCO Meeting Abstracts*, 28(15_suppl), e13026.

Mitsudomi, T., Hamajima, N., Ogawa, M. and Takahashi, T. (2000) 'Prognostic Significance of p53 Alterations in Patients with Non-Small Cell Lung Cancer: A Meta-Analysis', *Clinical Cancer Research*, 6(10), 4055.

Mladenov, E., Magin, S., Soni, A. and Iliakis, G. (2013) 'DNA Double-Strand Break Repair as Determinant of Cellular Radiosensitivity to Killing and Target in Radiation Therapy', *Frontiers in Oncology*, 3, 113, available: http://dx.doi.org/10.3389/fonc.2013.00113.

Molli, P.R., Li, D.-Q., Bagheri-Yarmand, R., Pakala, S.B., Katayama, H., Sen, S., Iyer, J., Chernoff, J., Tsai, M.-Y., Nair, S.S. and Kumar, R. (2010) 'Arpc1b, a centrosomal protein, is both an activator and substrate of Aurora A', *The Journal of Cell Biology*, 190(1), 101-114, available: http://dx.doi.org/10.1083/jcb.200908050.

Morgan, M.A. and Lawrence, T.S. (2015) 'Molecular Pathways: Overcoming Radiation Resistance by Targeting DNA Damage Response Pathways', *Clinical Cancer Research*, 21(13), 2898-2904.

Mori, D., Yamada, M., Mimori-Kiyosue, Y., Shirai, Y., Suzuki, A., Ohno, S., Saya, H., Wynshaw-Boris, A. and Hirotsune, S. (2009) 'An essential role of the aPKC-Aurora A-NDEL1 pathway in neurite elongation by modulation of microtubule dynamics', *Nat Cell Biol*, 11(9), 1057-68, available: http://dx.doi.org/10.1038/ncb1919.

Mori, D., Yano, Y., Toyo-oka, K., Yoshida, N., Yamada, M., Muramatsu, M., Zhang, D., Saya, H., Toyoshima, Y.Y., Kinoshita, K., Wynshaw-Boris, A. and Hirotsune, S. (2007) 'NDEL1 phosphorylation by Aurora-A kinase is essential for centrosomal maturation, separation, and TACC3 recruitment', *Mol Cell Biol*, 27(1), 352-67, available: http://dx.doi.org/10.1128/mcb.00878-06.

Morrow, C.J., Tighe, A., Johnson, V.L., Scott, M.I.F., Ditchfield, C. and Taylor, S.S. (2005) 'Bub1 and aurora B cooperate to maintain BubR1-mediated inhibition of APC/CCdc20', *Journal of Cell Science*, 118(16), 3639-3652.

Mosse, Y.P., Fox, E., Teachey, D.T., Reid, J.M., Safgren, S.L., Carol, H., Lock, R.B., Houghton, P.J., Smith, M.A., Hall, D., Barkauskas, D.A., Krailo, M., Voss, S.D., Berg, S.L., Blaney, S.M. and Weigel, B.J. (2019) 'A Phase II Study of Alisertib in Children with Recurrent/Refractory Solid Tumors or Leukemia: Children's Oncology Group Phase I and Pilot Consortium (ADVL0921)', *Clin Cancer Res*, 25(11), 3229-3238, available: http://dx.doi.org/10.1158/1078-0432.ccr-18-2675.

Myers, C., Liu, N., Ecsedy, J. and Lu, B. (2013) 'Inhibition of Aurora A Increases Sensitivity to Radiation Therapy in Selected Lung Cancer Cell Lines', *International Journal of Radiation Oncology • Biology • Physics*, 87(2), S544, available: http://dx.doi.org/10.1016/j.ijrobp.2013.06.1439.

Nam, H.-J. and van Deursen, J.M. (2014) 'Cyclin B2 and p53 control proper timing of centrosome separation', *Nature cell biology*, 16(6), 538-549, available: http://dx.doi.org/10.1038/ncb2952.

Navarro-Serer, B., Childers, E.P., Hermance, N.M., Mercadante, D. and Manning, A.L. (2019) 'Aurora A inhibition limits centrosome clustering and promotes mitotic catastrophe in cells with supernumerary centrosomes', *Oncotarget*, 10(17), 1649-1659, available: http://dx.doi.org/10.18632/oncotarget.26714.

Necchi, A., Lo Vullo, S., Mariani, L., Raggi, D., Giannatempo, P., Calareso, G., Togliardi, E., Crippa, F., Di Genova, N., Perrone, F., Colecchia, M., Paolini, B., Pelosi, G., Nicolai, N., Procopio, G., Salvioni, R. and De Braud, F.G. (2016) 'An open-label, single-arm, phase 2 study of the Aurora kinase A inhibitor alisertib in patients with advanced urothelial cancer', *Investigational New Drugs*, 34(2), 236-242, available: http://dx.doi.org/10.1007/s10637-016-0328-9.

Necchi, A., Pintarelli, G., Raggi, D., Giannatempo, P. and Colombo, F. (2017) 'Association of an aurora kinase a (AURKA) gene polymorphism with progression-free survival in patients with advanced urothelial carcinoma treated with the selective aurora kinase a inhibitor alisertib', *Invest New Drugs*, 35(4), 524-528, available: http://dx.doi.org/10.1007/s10637-017-0440-5.

Nguyen, A.L., Drutovic, D., Vazquez, B.N., El Yakoubi, W., Gentilello, A.S., Malumbres, M., Solc, P. and Schindler, K. (2018) 'Genetic Interactions between the Aurora Kinases Reveal New Requirements for AURKB and AURKC during Oocyte Meiosis', *Current Biology*, 28(21), 3458-3468.e5, available: http://dx.doi.org/https://doi.org/10.1016/j.cub.2018.08.052.

NICE (2008) *Cetuximab for the treatment of locally advanced squamous cell cancer of the head and neck*, available: https://www.nice.org.uk/guidance/ta145/chapter/1-Guidance [accessed 2nd Jan 2019].

NICE (2019) *Treating non-small-cell lung cancer*, available: https://pathways.nice.org.uk/pathways/lung-cancer#path=view%3A/pathways/lung-cancer/supportive-and-palliative-care-for-lung-cancer.xml&content=view-quality-statement%3Aquality-statements-palliative-interventions [accessed 05 April 2018].

Nicholson, A.G., Kerr, K. and R., G.J. (2015) *Dataset for lung cancer histo-pathology reports*, 3rd ed. Revised, available: https://www.rcpath.org/uploads/assets/uploaded/eac1baf4-9abf-42f3-866dbefbe8988158.pdf [accessed 07 May 2019].

Niermann, K.J., Moretti, L., Giacalone, N.J., Sun, Y., Schleicher, S.M., Kopsombut, P., Mitchell, L.R., Kim, K.W. and Lu, B. (2011) 'Enhanced Radiosensitivity of Androgen-Resistant Prostate Cancer: AZD1152-Mediated Aurora Kinase B Inhibition', *Radiation Research*, 175(4), 444-451, available: http://dx.doi.org/10.1667/RR2317.1.

Nikonova, A.S., Astsaturov, I., Serebriiskii, I.G., Dunbrack, R.L. and Golemis, E.A. (2013) 'Aurora-A kinase (AURKA) in normal and pathological cell growth', *Cellular and molecular life sciences : CMLS*, 70(4), 661-687, available: http://dx.doi.org/10.1007/s00018-012-1073-7.

Nishikawa, T., Ramesh, R., Munshi, A., Chada, S. and Meyn, R.E. (2004) 'Adenovirus-mediated mda-7 (IL24) gene therapy suppresses angiogenesis and sensitizes NSCLC xenograft tumors to radiation', *Molecular Therapy*, 9(6), 818-828, available: http://dx.doi.org/https://doi.org/10.1016/j.ymthe.2004.03.014.

Nishizaki, M., Meyn, R.E., Levy, L.B., Atkinson, E.N., White, R.A., Roth, J.A. and Ji, L. (2001) 'Synergistic Inhibition of Human Lung Cancer Cell Growth by Adenovirus-mediated Wild-Type p53 Gene Transfer in Combination with Docetaxel and Radiation Therapeutics in Vitro and in Vivo', *Clinical Cancer Research*, 7(9), 2887-2897.

Nishizaki, M., Sasaki, J.-i., Fang, B., Atkinson, E.N., Minna, J.D., Roth, J.A. and Ji, L. (2004) 'Synergistic Tumor Suppression by Coexpression of FHIT and p53 Coincides with FHIT-Mediated MDM2 Inactivation and p53 Stabilization in Human Non-Small Cell Lung Cancer Cells', *Cancer Research*, 64(16), 5745, available: http://dx.doi.org/10.1158/0008-5472.CAN-04-0195.

Nitta, M., Kobayashi, O., Honda, S., Hirota, T., Kuninaka, S., Marumoto, T., Ushio, Y. and Saya, H. (2004) 'Spindle checkpoint function is required for mitotic catastrophe induced by DNA-damaging agents', *Oncogene*, 23, 6548, available: http://dx.doi.org/10.1038/sj.onc.1207873.

O'Connor, O.A., Ozcan, M., Jacobsen, E.D., Roncero, J.M., Trotman, J., Demeter, J., Masszi, T., Pereira, J., Ramchandren, R., Beaven, A., Caballero, D., Horwitz, S.M., Lennard, A., Turgut, M., Hamerschlak, N., d'Amore, F.A., Foss, F., Kim, W.S., Leonard, J.P., Zinzani, P.L., Chiattone, C.S., Hsi, E.D., Trumper, L., Liu, H., Sheldon-Waniga, E., Ullmann, C.D., Venkatakrishnan,

K., Leonard, E.J. and Shustov, A.R. (2019) 'Randomized Phase III Study of Alisertib or Investigator's Choice (Selected Single Agent) in Patients With Relapsed or Refractory Peripheral T-Cell Lymphoma', *J Clin Oncol*, 37(8), 613-623, available: http://dx.doi.org/10.1200/jco.18.00899.

Obe, G., Beek, B. and Vaidya, V.G. (1975) 'The human leukocyte test system. III. Premature chromosome condensation from chemically and x-ray induced micronuclei', *Mutat Res*, 27(1), 89-101.

Obexer, P., Geiger, K., Ambros, P.F., Meister, B. and Ausserlechner, M.J. (2007) 'FKHRL1-mediated expression of Noxa and Bim induces apoptosis via the mitochondria in neuroblastoma cells', *Cell Death Differ*, 14(3), 534-47, available: http://dx.doi.org/10.1038/sj.cdd.4402017.

Oda, E., Ohki, R., Murasawa, H., Nemoto, J., Shibue, T., Yamashita, T., Tokino, T., Taniguchi, T. and Tanaka, N. (2000) 'Noxa, a BH3-only member of the Bcl-2 family and candidate mediator of p53-induced apoptosis', *Science*, 288(5468), 1053-8.

Ogawa, E., Takenaka, K., Katakura, H., Adachi, M., Otake, Y., Toda, Y., Kotani, H., Manabe, T., Wada, H. and Tanaka, F. (2008) 'Perimembrane Aurora-A Expression is a Significant Prognostic Factor in Correlation with Proliferative Activity in Non-Small-Cell Lung Cancer (NSCLC)', *Annals of Surgical Oncology*, 15(2), 547-554, available: http://dx.doi.org/10.1245/s10434-007-9653-8.

Oikawa, T., Okuda, M., Ma, Z., Goorha, R., Tsujimoto, H., Inokuma, H. and Fukasawa, K. (2005) 'Transcriptional control of BubR1 by p53 and suppression of centrosome amplification by BubR1', *Molecular and cellular biology*, 25(10), 4046-4061, available: http://dx.doi.org/10.1128/MCB.25.10.4046-4061.2005.

Okuda, M., Horn, H.F., Tarapore, P., Tokuyama, Y., Smulian, A.G., Chan, P.-K., Knudsen, E.S., Hofmann, I.A., Snyder, J.D., Bove, K.E. and Fukasawa, K. (2000) 'Nucleophosmin/B23 Is a Target of CDK2/Cyclin E in Centrosome Duplication', *Cell*, 103(1), 127-140, available: http://dx.doi.org/https://doi.org/10.1016/S0092-8674(00)00093-3.

Olive, K.P., Tuveson, D.A., Ruhe, Z.C., Yin, B., Willis, N.A., Bronson, R.T., Crowley, D. and Jacks, T. (2004) 'Mutant p53 Gain of Function in Two Mouse Models of Li-Fraumeni Syndrome', *Cell*, 119(6), 847-860, available: http://dx.doi.org/https://doi.org/10.1016/j.cell.2004.11.004.

Olszanski, A.J., Middleton, M.R., Bahleda, R., Heist, R.S., Rangachari, L., Zhou, X., Bozón, V., Kneissl, M. and Macarulla, T. (2015) 'A phase Ib study of investigational pan-RAF kinase inhibitor MLN2480 plus investigational TORC1/2 inhibitor MLN0128, investigational Aurora A kinase inhibitor alisertib (MLN8237), or paclitaxel in patients (pts) with advanced solid tumors', *Journal of Clinical Oncology*, 33(15_suppl), TPS2609-TPS2609, available: http://dx.doi.org/10.1200/jco.2015.33.15_suppl.tps2609.

Orth, M., Unger, K., Schoetz, U., Belka, C. and Lauber, K. (2018) 'Taxane-mediated radiosensitization derives from chromosomal missegregation on tripolar mitotic spindles orchestrated by AURKA and TPX2', *Oncogene*, 37(1), 52-62, available: http://dx.doi.org/10.1038/onc.2017.304.

Ota, T., Suto, S., Katayama, H., Han, Z.-B., Suzuki, F., Maeda, M., Tanino, M., Terada, Y. and Tatsuka, M. (2002) 'Increased Mitotic Phosphorylation of Histone H3 Attributable to AIM-1/Aurora-B Overexpression Contributes to Chromosome Number Instability', *Cancer Research*, 62(18), 5168-5177.

Otto, T., Horn, S., Brockmann, M., Eilers, U., Schüttrumpf, L., Popov, N., Kenney, A.M., Schulte, J.H., Beijersbergen, R., Christiansen, H., Berwanger, B. and Eilers, M. (2009) 'Stabilization of N-Myc Is a Critical Function of Aurora A in Human Neuroblastoma', *Cancer Cell*, 15(1), 67-78, available: http://dx.doi.org/http://dx.doi.org/10.1016/j.ccr.2008.12.005.

Owonikoko, T., Nackaerts, K., Csoszi, T., Ostoros, G., Baik, C., Ullmann, C.D., Zagadailov, E., Sheldon-Waniga, E., Huebner, D., Leonard, E.J. and Spigel, D. (2017) 'OA05.05 Randomized Phase 2 Study: Alisertib (MLN8237) or Placebo + Paclitaxel as Second-Line Therapy for Small-Cell Lung Cancer (SCLC)', *Journal of Thoracic Oncology*, 12(1), S261-S262, available: http://dx.doi.org/10.1016/j.jtho.2016.11.253.

Ozes, O.N., Mayo, L.D., Gustin, J.A., Pfeffer, S.R., Pfeffer, L.M. and Donner, D.B. (1999) 'NF-kappaB activation by tumour necrosis factor requires the Akt serine-threonine kinase', *Nature*, 401(6748), 82-5, available: http://dx.doi.org/10.1038/43466.

Paesmans, M. (2012) 'Prognostic and predictive factors for lung cancer', *Breathe*, 9(2), 112, available: http://dx.doi.org/10.1183/20734735.006911.

Palani, S., Patel, M., Huck, J., Zhang, M., Balani, S.K., Yang, J., Chen, S., Mettetal, J., Manfredi, M., Shyu, W.C., Ecsedy, J.A. and Chakravarty, A. (2013) 'Preclinical pharmacokinetic/pharmacodynamic/efficacy relationships for alisertib, an investigational small-molecule inhibitor of Aurora A kinase', *Cancer Chemother Pharmacol*, 72(6), 1255-64, available: http://dx.doi.org/10.1007/s00280-013-2305-8.

Palma, D.A., Senan, S., Tsujino, K., Barriger, R.B., Rengan, R., Moreno, M., Bradley, J.D., Kim, T.H., Ramella, S., Marks, L.B., De Petris, L., Stitt, L. and Rodrigues, G. (2013) 'Predicting Radiation Pneumonitis after Chemoradiotherapy for Lung Cancer: An International Individual Patient Data Meta-analysis', *International journal of radiation oncology, biology, physics*, 85(2), 444-450, available: http://dx.doi.org/10.1016/j.ijrobp.2012.04.043.

Pappas, G., Zumstein, L.A., Munshi, A., Hobbs, M. and Meyn, R.E. (2007) 'Adenoviral-mediated PTEN expression radiosensitizes non-small cell lung cancer cells by suppressing DNA repair capacity', *Cancer Gene Therapy*, 14, 543, available: http://dx.doi.org/10.1038/sj.cgt.7701050.

Pardee, A.B. (1989) 'G1 events and regulation of cell proliferation', *Science*, 246(4930), 603-8.

Parsons, R., Li, G.M., Longley, M.J., Fang, W.H., Papadopoulos, N., Jen, J., de la Chapelle, A., Kinzler, K.W., Vogelstein, B. and Modrich, P. (1993) 'Hypermutability and mismatch repair deficiency in RER+ tumor cells', *Cell*, 75(6), 1227-36.

Perez Carlos, A., Pajak Thomas, F., Rubin, P., Simpson Joseph, R., Mohiuddin, M., Brady Luther, W., Perez-Tamayo, R. and Rotman, M. (1987) 'Long-term observations of the patterns of failure in patients with unresectable non-oat cell carcinoma of the lung treated with definitive radiotherapy report by the radiation therapy oncology group', *Cancer*, 59(11), 1874-1881, available: http://dx.doi.org/10.1002/1097-0142(19870601)59:11<1874::AID-CNCR2820591106>3.0.CO;2-Z.

Persad, S., Attwell, S., Gray, V., Mawji, N., Deng, J.T., Leung, D., Yan, J., Sanghera, J., Walsh, M.P. and Dedhar, S. (2001) 'Regulation of Protein Kinase B/Akt-Serine 473 Phosphorylation by Integrin-linked Kinase: CRITICAL ROLES FOR KINASE ACTIVITY AND AMINO ACIDS ARGININE 211 AND SERINE 343', *Journal of Biological Chemistry*, 276(29), 27462-27469.

Prasanna, P.G.S., Stone, H.B., Wong, R.S., Capala, J., Bernhard, E.J., Vikram, B. and Coleman, C.N. (2012) 'Normal tissue protection for improving radiotherapy: Where are the Gaps?', *Translational cancer research*, 1(1), 35-48.

Pugacheva, E.N. and Golemis, E.A. (2005) 'The focal adhesion scaffolding protein HEF1 regulates activation of the Aurora-A and Nek2 kinases at the centrosome', *Nature cell biology*, 7(10), 937-946, available: http://dx.doi.org/10.1038/ncb1309.

Qian, Y. and Chen, X. (2013) 'Senescence regulation by the p53 protein family', *Methods in molecular biology (Clifton, N.J.)*, 965, 37-61, available: http://dx.doi.org/10.1007/978-1-62703-239-1_3.

Qin, L., Tong, T., Song, Y., Xue, L., Fan, F. and Zhan, Q. (2009) 'Aurora-A interacts with Cyclin B1 and enhances its stability', *Cancer Lett*, 275(1), 77-85, available: http://dx.doi.org/10.1016/j.canlet.2008.10.011.

Quartuccio, S.M. and Schindler, K. (2015) 'Functions of Aurora kinase C in meiosis and cancer', *Front Cell Dev Biol*, 3, 50, available: http://dx.doi.org/10.3389/fcell.2015.00050.

Quintiliani, M. (1986) 'The oxygen effect in radiation inactivation of DNA and enzymes', *Int J Radiat Biol Relat Stud Phys Chem Med*, 50(4), 573-94.

Ramos-Vara, J.A. (2005) 'Technical Aspects of Immunohistochemistry', *Veterinary Pathology*, 42(4), 405-426, available: http://dx.doi.org/10.1354/vp.42-4-405.

Rannou, Y., Troadec, M.-B., Petretti, C., Hans, F., Dutertre, S., Dimitrov, S. and Prigent, C. (2008) 'Localization of aurora A and aurora B kinases during interphase: role of the N-terminal domain', *Cell cycle (Georgetown, Tex.)*, 7(19), 3012-3020, available: http://dx.doi.org/10.4161/cc.7.19.6718.

Reboutier, D., Troadec, M.-B., Cremet, J.-Y., Chauvin, L., Guen, V., Salaun, P. and Prigent, C. (2013) 'Aurora A is involved in central spindle assembly through phosphorylation of Ser 19 in P150Glued', *The Journal of cell biology*, 201(1), 65-79, available: http://dx.doi.org/10.1083/jcb.201210060.

Reboutier, D., Troadec, M.-B., Cremet, J.-Y., Fukasawa, K. and Prigent, C. (2012) 'Nucleophosmin/B23 activates Aurora A at the centrosome through phosphorylation of serine 89', *The Journal of cell biology*, 197(1), 19-26, available: http://dx.doi.org/10.1083/jcb.201107134.

Redon, C.E., Dickey, J.S., Bonner, W.M. and Sedelnikova, O.A. (2009) 'γ-H2AX as a biomarker of DNA damage induced by ionizing radiation in human peripheral blood lymphocytes and artificial skin', *Advances in space research : the official journal of the Committee on Space Research (COSPAR)*, 43(8), 1171-1178, available: http://dx.doi.org/10.1016/j.asr.2008.10.011.

Redpath, J.L., Bengtsson, U., DeSimone, J., Lao, X., Wang, X. and Stanbridge, E.J. (2003) 'Sticky Anaphase Aberrations after G2-Phase Arrest of Gamma-Irradiated Human Skin Fibroblasts: TP53 Independence of Formation and TP53 Dependence of Consequences', *Radiation Research*, 159(1), 57-71,

available: http://dx.doi.org/10.1667/0033-7587(2003)159[0057:SAAAGP]2.0.CO;2.

Reiter, R., Gais, P., Jutting, U., Steuer-Vogt, M.K., Pickhard, A., Bink, K., Rauser, S., Lassmann, S., Hofler, H., Werner, M. and Walch, A. (2006) 'Aurora kinase A messenger RNA overexpression is correlated with tumor progression and shortened survival in head and neck squamous cell carcinoma', *Clin Cancer Res*, 12(17), 5136-41, available: http://dx.doi.org/10.1158/1078-0432.ccr-05-1650.

Rodrigues, G., Macbeth, F., Burmeister, B., Kelly, K.L., Bezjak, A., Langer, C., Hahn, C. and Movsas, B. (2012) 'Consensus statement on palliative lung radiotherapy: third international consensus workshop on palliative radiotherapy and symptom control', *Clin Lung Cancer*, 13(1), 1-5, available: http://dx.doi.org/10.1016/j.cllc.2011.04.004.

Roghi, C., Giet, R., Uzbekov, R., Morin, N., Chartrain, I., Le Guellec, R., Couturier, A., Doree, M., Philippe, M. and Prigent, C. (1998) 'The Xenopus protein kinase pEg2 associates with the centrosome in a cell cycle-dependent manner, binds to the spindle microtubules and is involved in bipolar mitotic spindle assembly', *Journal of Cell Science*, 111(5), 557.

Romain, C., Paul, P., Kim, K.W., Lee, S., Qiao, J. and Chung, D.H. (2014) 'Targeting Aurora kinase-A downregulates cell proliferation and angiogenesis in neuroblastoma', *J Pediatr Surg*, 49(1), 159-65, available: http://dx.doi.org/10.1016/j.jpedsurg.2013.09.051.

Rong, R., Jiang, L.Y., Sheikh, M.S. and Huang, Y. (2007) 'Mitotic kinase Aurora-A phosphorylates RASSF1A and modulates RASSF1A-mediated microtubule interaction and M-phase cell cycle regulation', *Oncogene*, 26(55), 7700-7708, available: http://dx.doi.org/http://www.nature.com/onc/journal/v26/n55/suppinfo/1210575s1.html.

Roninson, I.B., Broude, E.V. and Chang, B.-D. (2001) 'If not apoptosis, then what? Treatment-induced senescence and mitotic catastrophe in tumor cells', *Drug Resistance Updates*, 4(5), 303-313, available: http://dx.doi.org/https://doi.org/10.1054/drup.2001.0213.

Roy, A., Veroli, M.V., Prasad, S. and Wang, Q.J. (2018) 'Protein Kinase D2 Modulates Cell Cycle By Stabilizing Aurora A Kinase at Centrosomes', *Molecular Cancer Research*, 16(11), 1785, available: http://dx.doi.org/10.1158/1541-7786.MCR-18-0641.

Salem, A., Asselin, M.-C., Reymen, B., Jackson, A., Lambin, P., West, C.M.L., O'Connor, J.P.B. and Faivre-Finn, C. (2018) 'Targeting Hypoxia to Improve Non–Small Cell Lung Cancer Outcome', *JNCI: Journal of the National Cancer Institute*, 110(1), 14-30, available: http://dx.doi.org/10.1093/jnci/djx160.

Sarkissian, M., Mendez, R. and Richter, J.D. (2004) 'Progesterone and insulin stimulation of CPEB-dependent polyadenylation is regulated by Aurora A and glycogen synthase kinase-3', *Genes & Development*, 18(1), 48-61, available: http://dx.doi.org/10.1101/gad.1136004.

Sarna, L., Swann, S., Langer, C., Werner-Wasik, M., Nicolaou, N., Komaki, R., Machtay, M., Byhardt, R., Wasserman, T. and Movsas, B. (2008) 'Clinically meaningful differences in patient-reported outcomes with amifostine in combination with chemoradiation for locally advanced non-small-cell lung cancer: an analysis of RTOG 9801', *Int J Radiat Oncol Biol Phys*, 72(5), 1378-84, available: http://dx.doi.org/10.1016/j.ijrobp.2008.03.003.

Sasai, K., Treekitkarnmongkol, W., Kai, K., Katayama, H. and Sen, S. (2016) 'Functional Significance of Aurora Kinases–p53 Protein Family Interactions in Cancer', *Frontiers in Oncology*, 6, 247.

Schneider, M.A., Christopoulos, P., Muley, T., Warth, A., Klingmueller, U., Thomas, M., Herth, F.J., Dienemann, H., Mueller, N.S., Theis, F. and Meister, M. (2017) 'AURKA, DLGAP5, TPX2, KIF11 and CKAP5: Five specific mitosis-associated genes correlate with poor prognosis for non-small cell lung cancer patients', *Int J Oncol*, 50(2), 365-372, available: http://dx.doi.org/10.3892/ijo.2017.3834.

Scholey, M.J., Civelekoglu-Scholey, G. and Brust-Mascher, I. (2016) 'Anaphase B', *Biology*, 5(4), available: http://dx.doi.org/10.3390/biology5040051.

Schon, O., Friedler, A., Bycroft, M., Freund, S.M.V. and Fersht, A.R. (2002) 'Molecular Mechanism of the Interaction between MDM2 and p53', *Journal of Molecular Biology*, 323(3), 491-501, available: http://dx.doi.org/https://doi.org/10.1016/S0022-2836(02)00852-5.

Sehdev, V., Katsha, A., Ecsedy, J., Zaika, A., Belkhiri, A. and El-Rifai, W. (2013) 'The combination of alisertib, an investigational Aurora kinase A inhibitor, and docetaxel promotes cell death and reduces tumor growth in preclinical cell models of upper gastrointestinal adenocarcinomas', *Cancer*, 119(4), 904-914, available: http://dx.doi.org/10.1002/cncr.27801.

Seiwert, T., Salama, J. and Vokes, E. (2007) 'The concurrent chemoradiation paradigm—General principles', *Nature clinical practice. Oncology*, 4, 86-100, available: http://dx.doi.org/10.1038/ncponc0714.

Seki, A., Coppinger, J.A., Jang, C.-Y., Yates, J.R. and Fang, G. (2008) 'Bora and Aurora A Cooperatively Activate Plk1 and Control the Entry into Mitosis', *Science (New York, N.Y.)*, 320(5883), 1655-1658, available: http://dx.doi.org/10.1126/science.1157425.

Senra, J.M., Telfer, B.A., Cherry, K.E., McCrudden, C.M., Hirst, D.G., Connor, M.J., Wedge, S.R. and Stratford, I.J. (2011) 'Inhibition of PARP-1 by Olaparib (AZD2281) Increases the Radiosensitivity of a Lung Tumor Xenograft', *Molecular Cancer Therapeutics*, 10(10), 1949, available: http://dx.doi.org/10.1158/1535-7163.MCT-11-0278.

Shah, H.A., Fischer, J.H., Venepalli, N.K., Danciu, O.C., Christian, S., Russell, M.J., Liu, L.C., Zacny, J.P. and Dudek, A.Z. (2019) 'Phase I Study of Aurora A Kinase Inhibitor Alisertib (MLN8237) in Combination With Selective VEGFR Inhibitor Pazopanib for Therapy of Advanced Solid Tumors', *Am J Clin Oncol*, 42(5), 413-420, available: http://dx.doi.org/10.1097/coc.0000000000000543.

Shah, K.N., Bhatt, R., Rotow, J., Rohrberg, J., Olivas, V., Wang, V.E., Hemmati, G., Martins, M.M., Maynard, A., Kuhn, J., Galeas, J., Donnella, H.J., Kaushik, S., Ku, A., Dumont, S., Krings, G., Haringsma, H.J., Robillard, L., Simmons, A.D., Harding, T.C., McCormick, F., Goga, A., Blakely, C.M., Bivona, T.G. and Bandyopadhyay, S. (2018) 'Aurora kinase A drives the evolution of resistance to third-generation EGFR inhibitors in lung cancer', *Nat Med*, available: http://dx.doi.org/10.1038/s41591-018-0264-7.

Sheard, M.A. (2001) 'Ionizing radiation as a response-enhancing agent for CD95-mediated apoptosis', *Int J Cancer*, 96(4), 213-20.

Shen, H., Dong, W., Gao, D., Wang, G., Ma, G., Liu, Q. and Du, J. (2012) 'MDM2 antagonist Nutlin-3a protects wild-type p53 cancer cells from paclitaxel', *Chinese Science Bulletin*, 57(9), 1007-1012, available: http://dx.doi.org/10.1007/s11434-012-4984-7.

Shimomura, T., Hasako, S., Nakatsuru, Y., Mita, T., Ichikawa, K., Kodera, T., Sakai, T., Nambu, T., Miyamoto, M., Takahashi, I., Miki, S., Kawanishi, N., Ohkubo, M., Kotani, H. and Iwasawa, Y. (2010) 'MK-5108, a Highly Selective Aurora-A Kinase Inhibitor, Shows Antitumor Activity Alone and in Combination with Docetaxel', *Molecular Cancer Therapeutics*, 9(1), 157, available: http://dx.doi.org/10.1158/1535-7163.MCT-09-0609.

Siddique, H.R., Feldman, D.E., Chen, C.-L., Punj, V., Tokumitsu, H. and Machida, K. (2015) 'NUMB phosphorylation destabilizes p53 and promotes self-renewal of tumor-initiating cells by a NANOG-dependent mechanism in liver cancer', *Hepatology*, 62(5), 1466-1479, available: http://dx.doi.org/10.1002/hep.27987.

Siles, E., Villalobos Alonzo, M., T Valenzuela, M., Nuñez, M., Gordon, A., McMillan, T., Pedraza, V. and Ruiz de Almodóvar, J. (1996) 'Relationship between p53 status and radiosensitivity in human tumour cell lines', *Br J Cancer*, 73, 581-8, available: http://dx.doi.org/10.1038/bjc.1996.101.

Silva, P., Barbosa, J., Nascimento, A.V., Faria, J., Reis, R. and Bousbaa, H. (2011) 'Monitoring the fidelity of mitotic chromosome segregation by the spindle assembly checkpoint', *Cell Proliferation*, 44(5), 391-400, available: http://dx.doi.org/10.1111/j.1365-2184.2011.00767.x.

Simone, C.B. (2017) 'Thoracic Radiation Normal Tissue Injury', *Seminars in Radiation Oncology*, 27(4), 370-377, available: http://dx.doi.org/https://doi.org/10.1016/j.semradonc.2017.04.009.

Slamon, D., Eiermann, W., Robert, N., Pienkowski, T., Martin, M., Press, M., Mackey, J., Glaspy, J., Chan, A., Pawlicki, M., Pinter, T., Valero, V., Liu, M.C., Sauter, G., von Minckwitz, G., Visco, F., Bee, V., Buyse, M., Bendahmane, B., Tabah-Fisch, I., Lindsay, M.A., Riva, A. and Crown, J. (2011) 'Adjuvant trastuzumab in HER2-positive breast cancer', *N Engl J Med*, 365(14), 1273-83, available: http://dx.doi.org/10.1056/NEJMoa0910383.

Smith, E., Dejsuphong, D., Balestrini, A., Hampel, M., Lenz, C., Takeda, S., Vindigni, A. and Costanzo, V. (2009) 'An ATM- and ATR-dependent checkpoint inactivates spindle assembly by targeting CEP63', *Nat Cell Biol*, 11(3), 278-85, available: http://dx.doi.org/10.1038/ncb1835.

Smith, J., Tho, L.M., Xu, N. and Gillespie, D.A. (2010) 'The ATM-Chk2 and ATR-Chk1 pathways in DNA damage signaling and cancer', *Adv Cancer Res*, 108, 73-112, available: http://dx.doi.org/10.1016/b978-0-12-380888-2.00003-0.

Smits, V.A., Klompmaker, R., Arnaud, L., Rijksen, G., Nigg, E.A. and Medema, R.H. (2000) 'Polo-like kinase-1 is a target of the DNA damage checkpoint', *Nat Cell Biol*, 2(9), 672-6, available: http://dx.doi.org/10.1038/35023629.

Soltoff, S.P., Carraway, K.L., 3rd, Prigent, S.A., Gullick, W.G. and Cantley, L.C. (1994) 'ErbB3 is involved in activation of phosphatidylinositol 3-kinase by epidermal growth factor', *Mol Cell Biol*, 14(6), 3550-8.

Soncini, C., Carpinelli, P., Gianellini, L., Fancelli, D., Vianello, P., Rusconi, L., Storici, P., Zugnoni, P., Pesenti, E., Croci, V., Ceruti, R., Giorgini, M.L., Cappella, P., Ballinari, D., Sola, F., Varasi, M., Bravo, R. and Moll, J. (2006) 'PHA-680632, a novel Aurora kinase inhibitor with potent antitumoral activity', *Clin Cancer Res*, 12(13), 4080-9, available: http://dx.doi.org/10.1158/1078-0432.ccr-05-1964.

Song, A., Andrews, D.W., Werner-Wasik, M., Kim, L., Glass, J., Bar-Ad, V., Evans, J.J., Farrell, C.J., Judy, K.D., Daskalakis, C., Zhan, T. and Shi, W. (2019) 'Phase I trial of alisertib with concurrent fractionated stereotactic re-irradiation for recurrent high grade gliomas', *Radiotherapy and Oncology*, 132, 135-141, available: http://dx.doi.org/https://doi.org/10.1016/j.radonc.2018.12.019.

Song, L., Dai, T., Xiong, H., Lin, C., Lin, H., Shi, T. and Li, J. (2010) 'Inhibition of centriole duplication by centrobin depletion leads to p38–p53 mediated cell-cycle arrest', *Cellular Signalling*, 22(5), 857-864, available: http://dx.doi.org/https://doi.org/10.1016/j.cellsig.2010.01.009.

Song, M.S., Song, S.J., Ayad, N.G., Chang, J.S., Lee, J.H., Hong, H.K., Lee, H., Choi, N., Kim, J., Kim, H., Kim, J.W., Choi, E.J., Kirschner, M.W. and Lim, D.S. (2004) 'The tumour suppressor RASSF1A regulates mitosis by inhibiting the APC-Cdc20 complex', *Nat Cell Biol*, 6(2), 129-37, available: http://dx.doi.org/10.1038/ncb1091.

Sos, M.L., Dietlein, F., Peifer, M., Schöttle, J., Balke-Want, H., Müller, C., Koker, M., Richters, A., Heynck, S., Malchers, F., Heuckmann, J.M., Seidel, D., Eyers, P.A., Ullrich, R.T., Antonchick, A.P., Vintonyak, V.V., Schneider, P.M., Ninomiya, T., Waldmann, H., Büttner, R., Rauh, D., Heukamp, L.C. and Thomas, R.K. (2012) 'A framework for identification of actionable cancer genome dependencies in small cell lung cancer', *Proceedings of the National Academy of Sciences of the United States of America*, 109(42), 17034-17039, available: http://dx.doi.org/10.1073/pnas.1207310109.

Sourisseau, T., Maniotis, D., McCarthy, A., Tang, C., Lord, C.J., Ashworth, A. and Linardopoulos, S. (2010) 'Aurora-A expressing tumour cells are deficient for homology-directed DNA double strand-break repair and sensitive to PARP inhibition', *EMBO Molecular Medicine*, 2(4), 130-142, available: http://dx.doi.org/10.1002/emmm.201000068.

Stambolic, V., MacPherson, D., Sas, D., Lin, Y., Snow, B., Jang, Y., Benchimol, S. and Mak, T.W. (2001) 'Regulation of PTEN Transcription by p53', *Molecular Cell*, 8(2), 317-325, available: http://dx.doi.org/https://doi.org/10.1016/S1097-2765(01)00323-9.

Stambolic, V., Suzuki, A., de la Pompa, J.L., Brothers, G.M., Mirtsos, C., Sasaki, T., Ruland, J., Penninger, J.M., Siderovski, D.P. and Mak, T.W. (1998) 'Negative regulation of PKB/Akt-dependent cell survival by the tumor suppressor PTEN', *Cell*, 95(1), 29-39.

Steel, G. and Peckham, M.J. (1979) 'Exploitable mechanisms in combined radiotherapy-chemotherapy: The concept of additivity', *International Journal of Radiation Oncology*Biology*Physics*, 5(1), 85-91, available: http://dx.doi.org/https://doi.org/10.1016/0360-3016(79)90044-0.

Stein, G.H., Drullinger, L.F., Soulard, A. and Dulić, V. (1999) 'Differential roles for cyclin-dependent kinase inhibitors p21 and p16 in the mechanisms of senescence and differentiation in human fibroblasts', *Molecular and cellular biology*, 19(3), 2109-2117.

Stewart, S. and Fang, G. (2005) 'Destruction box-dependent degradation of aurora B is mediated by the anaphase-promoting complex/cyclosome and Cdh1', *Cancer Res*, 65(19), 8730-5, available: http://dx.doi.org/10.1158/0008-5472.can-05-1500.

Stone, H.B., Bernhard, E.J., Coleman, C.N., Deye, J., Capala, J., Mitchell, J.B. and Brown, J.M. (2016) 'Preclinical Data on Efficacy of 10 Drug-Radiation Combinations: Evaluations, Concerns, and Recommendations', *Translational Oncology*, 9(1), 46-56, available: http://dx.doi.org/https://doi.org/10.1016/j.tranon.2016.01.002.

Storchova, Z. and Pellman, D. (2004) 'From polyploidy to aneuploidy, genome instability and cancer', *Nature Reviews Molecular Cell Biology*, 5, 45, available: http://dx.doi.org/10.1038/nrm1276.

Strati, P., Nastoupil, L., Davis, R., E. Fayad, L., Fowler, N., Hagemeister, F., Kwak, L., Oki, Y., Wang, M., Westin, J., E. Ruben, C., T. Wesson, E., Piekarz, R., A. Fanale, M. and Ju Lee, H. (2019) 'A phase 1 trial of alisertib and romidepsin for relapsed/refractory aggressive B-cell and T-cell lymphomas', *Haematologica*, 124, 1744, available: http://dx.doi.org/10.3324/haematol.2019.220012.

Subramanian, C. and Cohen, M.S. (2019) 'Over expression of DNA damage and cell cycle dependent proteins are associated with poor survival in patients with adrenocortical carcinoma', *Surgery*, 165(1), 202-210, available: http://dx.doi.org/10.1016/j.surg.2018.04.080.

Sugimachi, K., Mitsudomi, T., Ogami, A., Nishida, K., Sugio, K., Yasumoto, K., Nakanishi, R., Osaki, T. and Oyama, T. (1995) 'p53 nuclear immunostaining

and gene mutations in non-small-cell lung cancer and their effects on patient survival', *Annals of Oncology*, 6(suppl_3), S9-S13, available: http://dx.doi.org/10.1093/annonc/6.suppl_3.S9.

Sun, C.K., Ng, I.O., Ho, J.W., Ng, K.T., Man, K., Xu, R., Fan, S.T., Lee, T.K., Wang, X.H. and Wong, Y.C. (2004) 'FTY720 induces apoptosis of human hepatoma cell lines through PI3-K-mediated Akt dephosphorylation', *Carcinogenesis*, 25(12), 2397-2405, available: http://dx.doi.org/10.1093/carcin/bgh250.

Sun, H., Wang, Y., Wang, Z., Meng, J., Qi, Z. and Yang, G. (2014) 'Aurora-A controls cancer cell radio- and chemoresistance via ATM/Chk2-mediated DNA repair networks', *Biochim Biophys Acta*, 1843(5), 934-44, available: http://dx.doi.org/10.1016/j.bbamcr.2014.01.019.

Sung, P. and Klein, H. (2006) 'Mechanism of homologous recombination: Mediators and helicases take on regulatory functions', *Nat Rev Mol Cell Biol*, 7, 739-50, available: http://dx.doi.org/10.1038/nrm2008.

Takahashi, T., Nau, M.M., Chiba, I., Birrer, M.J., Rosenberg, R.K., Vinocour, M., Levitt, M., Pass, H., Gazdar, A.F. and Minna, J.D. (1989) 'p53: a frequent target for genetic abnormalities in lung cancer', *Science*, 246(4929), 491, available: http://dx.doi.org/10.1126/science.2554494.

Takeda Pharmaceutical Company Ltd (2015) *Takeda Announces Termination of Alisertib Phase 3 Trial in Relapsed or Refractory Peripheral T-cell Lymphoma* [press release], available: [accessed 06 Jan 2019].

Tao, Y., Zhang, P., Frascogna, V., Lecluse, Y., Auperin, A., Bourhis, J. and Deutsch, E. (2007) 'Enhancement of radiation response by inhibition of Aurora-A kinase using siRNA or a selective Aurora kinase inhibitor PHA680632 in p53-deficient cancer cells', *British Journal of Cancer*, 97(12), 1664-1672, available: http://dx.doi.org/10.1038/sj.bjc.6604083.

Tayyar, Y., Jubair, L., Fallaha, S. and McMillan, N.A.J. (2017) 'Critical risk-benefit assessment of the novel anti-cancer aurora a kinase inhibitor alisertib (MLN8237): A comprehensive review of the clinical data', *Crit Rev Oncol Hematol*, 119, 59-65, available: http://dx.doi.org/10.1016/j.critrevonc.2017.09.006.

Tentler, J.J., Bradshaw-Pierce, E.L., Serkova, N.J., Hasebroock, K.M., Pitts, T.M., Diamond, J.R., Fletcher, G.C., Bray, M.R. and Eckhardt, S.G. (2010) 'Assessment of the In vivo Antitumor Effects of ENMD-2076, a Novel Multitargeted Kinase Inhibitor, against Primary and Cell Line–Derived Human

Colorectal Cancer Xenograft Models', *Clinical Cancer Research*, 16(11), 2989-2998.

Tian, H., Faje, A.T., Lee, S.L. and Jorgensen, T.J. (2002) 'Radiation-induced phosphorylation of Chk1 at S345 is associated with p53-dependent cell cycle arrest pathways', *Neoplasia (New York, N.Y.)*, 4(2), 171-180, available: http://dx.doi.org/10.1038/sj/neo/7900219.

Timmerman, R., Paulus, R., Galvin, J., Michalski, J., Straube, W., Bradley, J., Fakiris, A., Bezjak, A., Videtic, G., Johnstone, D., Fowler, J., Gore, E. and Choy, H. (2010) 'Stereotactic body radiation therapy for inoperable early stage lung cancer', *Jama*, 303(11), 1070-6, available: http://dx.doi.org/10.1001/jama.2010.261.

Toji, S., Yabuta, N., Hosomi, T., Nishihara, S., Kobayashi, T., Suzuki, S., Tamai, K. and Nojima, H. (2004) 'The centrosomal protein Lats2 is a phosphorylation target of Aurora-A kinase', *Genes to Cells*, 9(5), 383-397, available: http://dx.doi.org/10.1111/j.1356-9597.2004.00732.x.

Tomasini, R., Tsuchihara, K., Tsuda, C., Lau, S., Wilhelm, M., Ruffini, A., Tsao, M.-S., Iovanna, J., Jurisicova, A., Melino, G. and W Mak, T. (2009) 'TAp73 regulates the spindle assembly checkpoint by modulating BubR1 activity', *PNAS*, 106, 797-802, available: http://dx.doi.org/10.1073/pnas.0812096106.

Toulany, M., Kehlbach, R., Florczak, U., Sak, A., Wang, S., Chen, J., Lobrich, M. and Rodemann, H.P. (2008) 'Targeting of AKT1 enhances radiation toxicity of human tumor cells by inhibiting DNA-PKcs-dependent DNA double-strand break repair', *Mol Cancer Ther*, 7(7), 1772-81, available: http://dx.doi.org/10.1158/1535-7163.mct-07-2200.

Townsend, K., Mason, H., Blackford, A.N., Miller, E.S., Chapman, J.R., Sedgwick, G.G., Barone, G., Turnell, A.S. and Stewart, G.S. (2009) 'Mediator of DNA damage checkpoint 1 (MDC1) regulates mitotic progression', *The Journal of biological chemistry*, 284(49), 33939-33948, available: http://dx.doi.org/10.1074/jbc.M109.009191.

Toyoshima-Morimoto, F., Taniguchi, E., Shinya, N., Iwamatsu, A. and Nishida, E. (2001) 'Polo-like kinase 1 phosphorylates cyclin B1 and targets it to the nucleus during prophase', *Nature*, 410(6825), 215-20, available: http://dx.doi.org/10.1038/35065617.

Trinkaus, M.E., Blum, R., Rischin, D., Callahan, J., Bressel, M., Segard, T., Roselt, P., Eu, P., Binns, D., MacManus, M.P., Ball, D. and Hicks, R.J. (2013) 'Imaging of hypoxia with 18F-FAZA PET in patients with locally advanced non-

small cell lung cancer treated with definitive chemoradiotherapy', *Journal of Medical Imaging and Radiation Oncology*, 57(4), 475-481, available: http://dx.doi.org/10.1111/1754-9485.12086.

US National Library of Medicine (2019) *Clinicaltrials.gov*, available: https://clinicaltrials.gov/ [accessed 17th August 2019].

Vakifahmetoglu, H., Olsson, M., Tamm, C., Heidari, N., Orrenius, S. and Zhivotovsky, B. (2008) 'DNA damage induces two distinct modes of cell death in ovarian carcinomas', *Cell Death Differ*, 15(3), 555-66, available: http://dx.doi.org/10.1038/sj.cdd.4402286.

van Vugt, M.A.T.M., Brás, A. and Medema, R.H. (2004) 'Polo-like Kinase-1 Controls Recovery from a G2 DNA Damage-Induced Arrest in Mammalian Cells', *Molecular Cell*, 15(5), 799-811, available: http://dx.doi.org/http://dx.doi.org/10.1016/j.molcel.2004.07.015.

Veerakumarasivam, A., Goldstein, L.D., Saeb-Parsy, K., Scott, H.E., Warren, A., Thorne, N.P., Mills, I.G., Venkitaraman, A., Neal, D.E. and Kelly, J.D. (2008) 'AURKA overexpression accompanies dysregulation of DNA-damage response genes in invasive urothelial cell carcinoma', *Cell Cycle*, 7(22), 3525-3533, available: http://dx.doi.org/10.4161/cc.7.22.7042.

Veitch, Z., Zer, A., Loong, H., Salah, S., Masood, M., Gupta, A., Bradbury, P.A., Hogg, D., Wong, A., Kandel, R., Charames, G.S. and Abdul Razak, A.R. (2019) 'A phase II study of ENMD-2076 in advanced soft tissue sarcoma (STS)', *Scientific Reports*, 9(1), 7390, available: http://dx.doi.org/10.1038/s41598-019-43222-6.

Venkatakrishnan, K., Kim, T.M., Lin, C.C., Thye, L.S., Chng, W.J., Ma, B., Chen, M.H., Zhou, X., Liu, H., Kelly, V. and Kim, W.S. (2015) 'Phase 1 study of the investigational Aurora A kinase inhibitor alisertib (MLN8237) in East Asian cancer patients: pharmacokinetics and recommended phase 2 dose', *Invest New Drugs*, 33(4), 942-53, available: http://dx.doi.org/10.1007/s10637-015-0258-y.

Venkataraman, S., Alimova, I., Tello, T., Harris, P.S., Knipstein, J.A., Donson, A.M., Foreman, N.K., Liu, A.K. and Vibhakar, R. (2012) 'Targeting Aurora Kinase A enhances radiation sensitivity of atypical teratoid rhabdoid tumor cells', *J Neurooncol*, 107(3), 517-26, available: http://dx.doi.org/10.1007/s11060-011-0795-y.

Vera, P., Thureau, S., Chaumet-Riffaud, P., Modzelewski, R., Bohn, P., Vermandel, M., Hapdey, S., Pallardy, A., Mahe, M.A., Lacombe, M., Boisselier, P.,

Guillemard, S., Olivier, P., Beckendorf, V., Salem, N., Charrier, N., Chajon, E., Devillers, A., Aide, N., Danhier, S., Denis, F., Muratet, J.P., Martin, E., Riedinger, A.B., Kolesnikov-Gauthier, H., Dansin, E., Massabeau, C., Courbon, F., Farcy Jacquet, M.P., Kotzki, P.O., Houzard, C., Mornex, F., Vervueren, L., Paumier, A., Fernandez, P., Salaun, M. and Dubray, B. (2017) 'Phase II Study of a Radiotherapy Total Dose Increase in Hypoxic Lesions Identified by (18)F-Misonidazole PET/CT in Patients with Non-Small Cell Lung Carcinoma (RTEP5 Study)', *J Nucl Med*, 58(7), 1045-1053, available: http://dx.doi.org/10.2967/jnumed.116.188367.

Verma, V., Simone, B.C. and Werner-Wasik, M. (2017) 'Acute and Late Toxicities of Concurrent Chemoradiotherapy for Locally-Advanced Non-Small Cell Lung Cancer', *Cancers*, 9(9), available: http://dx.doi.org/10.3390/cancers9090120.

Vernole, P., Neale, M., Barcaroli, D., Munarriz, E., A Knight, R., Tomasini, R., W. Mak, T., Melino, G. and De Laurenzi, V. (2009) 'TAp73α binds the kinetochore proteins Bub1 and Bub3 resulting in polyploidy', *Cell Cycle*, 8(3), 421-429, available: http://dx.doi.org/10.4161/cc.8.3.7623.

Vincent, E.E., Elder, D.J.E., Thomas, E.C., Phillips, L., Morgan, C., Pawade, J., Sohail, M., May, M.T., Hetzel, M.R. and Tavaré, J.M. (2011) 'Akt phosphorylation on Thr308 but not on Ser473 correlates with Akt protein kinase activity in human non-small cell lung cancer', *British journal of cancer*, 104(11), 1755-1761, available: http://dx.doi.org/10.1038/bjc.2011.132.

Vinod, S.K. (2015) 'International Patterns of Radiotherapy Practice for Non–Small Cell Lung Cancer', *Seminars in Radiation Oncology*, 25(2), 143-150, available: http://dx.doi.org/10.1016/j.semradonc.2014.11.001.

Vitale, I., Galluzzi, L., Castedo, M. and Kroemer, G. (2011) 'Mitotic catastrophe: a mechanism for avoiding genomic instability', *Nature Reviews Molecular Cell Biology*, 12, 385, available: http://dx.doi.org/10.1038/nrm3115.

Vitale, I., Senovilla, L., Jemaa, M., Michaud, M., Galluzzi, L., Kepp, O., Nanty, L., Criollo, A., Rello-Varona, S., Manic, G., Metivier, D., Vivet, S., Tajeddine, N., Joza, N., Valent, A., Castedo, M. and Kroemer, G. (2010) 'Multipolar mitosis of tetraploid cells: inhibition by p53 and dependency on Mos', *Embo j*, 29(7), 1272-84, available: http://dx.doi.org/10.1038/emboj.2010.11.

Wachsberger, P., Burd, R. and Dicker, A.P. (2003) 'Tumor Response to Ionizing Radiation Combined with Antiangiogenesis or Vascular Targeting Agents', *Clinical Cancer Research*, 9(6), 1957.

Walker, M.J., Zhou, C., Backen, A., Pernemalm, M., Williamson, A.J., Priest, L.J., Koh, P., Faivre-Finn, C., Blackhall, F.H., Dive, C. and Whetton, A.D. (2015) 'Discovery and Validation of Predictive Biomarkers of Survival for Non-small Cell Lung Cancer Patients Undergoing Radical Radiotherapy: Two Proteins With Predictive Value', *EBioMedicine*, 2(8), 841-50, available: http://dx.doi.org/10.1016/j.ebiom.2015.06.013.

Wang, C., Yan, Q., Hu, M., Qin, D. and Feng, Z. (2016) 'Effect of AURKA Gene Expression Knockdown on Angiogenesis and Tumorigenesis of Human Ovarian Cancer Cell Lines', *Targeted Oncology*, 11(6), 771-781, available: http://dx.doi.org/10.1007/s11523-016-0436-7.

Wang, X.X., Liu, R., Jin, S.Q., Fan, F.Y. and Zhan, Q.M. (2006) 'Overexpression of Aurora-A kinase promotes tumor cell proliferation and inhibits apoptosis in esophageal squamous cell carcinoma cell line', *Cell Res*, 16(4), 356-366.

Wang, Y., Ji, P., Liu, J., Broaddus, R.R., Xue, F. and Zhang, W. (2009) 'Centrosome-associated regulators of the G2/M checkpoint as targets for cancer therapy', *Molecular Cancer*, 8(1), 8, available: http://dx.doi.org/10.1186/1476-4598-8-8.

Wang, Y., Sun, H., Wang, Z., Liu, M., Qi, Z., Meng, J., Sun, J. and Yang, G. (2014a) 'Aurora-A: a potential DNA repair modulator', *Tumor Biology*, 35(4), 2831-2836, available: http://dx.doi.org/10.1007/s13277-013-1393-8.

Wang, Y., Wang, Z., Qi, Z., Yin, S., Zhang, N., Liu, Y., Liu, M., Meng, J., Zang, R., Zhang, Z. and Yang, G. (2014b) 'The negative interplay between Aurora A/B and BRCA1/2 controls cancer cell growth and tumorigenesis via distinct regulation of cell cycle progression, cytokinesis, and tetraploidy', *Molecular Cancer*, 13(1), 1-12, available: http://dx.doi.org/10.1186/1476-4598-13-94.

Wang-Bishop, L., Chen, Z., Gomaa, A., Lockhart, A.C., Salaria, S., Wang, J., Lewis, K.B., Ecsedy, J., Washington, K., Beauchamp, R.D. and El-Rifai, W. (2018) 'Inhibition of AURKA Reduces Proliferation and Survival of Gastrointestinal Cancer Cells with Activated KRAS by Preventing Activation of RPS6KB1', *Gastroenterology*, available: http://dx.doi.org/10.1053/j.gastro.2018.10.030.

Weaver, H. and Coonar, A.S. (2017) 'Lung cancer: diagnosis, staging and treatment', *Surgery (Oxford)*, 35(5), 247-254, available: http://dx.doi.org/https://doi.org/10.1016/j.mpsur.2017.02.007.

Wei, M.C., Zong, W.X., Cheng, E.H., Lindsten, T., Panoutsakopoulou, V., Ross, A.J., Roth, K.A., MacGregor, G.R., Thompson, C.B. and Korsmeyer, S.J. (2001) 'Proapoptotic BAX and BAK: a requisite gateway to mitochondrial dysfunction

and death', *Science*, 292(5517), 727-30, available: http://dx.doi.org/10.1126/science.1059108.

West, C., Azria, D., Chang-Claude, J., Davidson, S., Lambin, P., Rosenstein, B., De Ruysscher, D., Talbot, C., Thierens, H., Valdagni, R., Vega, A. and Yuille, M. (2014) 'The REQUITE Project: Validating Predictive Models and Biomarkers of Radiotherapy Toxicity to Reduce Side-effects and Improve Quality of Life in Cancer Survivors', *Clinical Oncology*, 26(12), 739-742, available: http://dx.doi.org/https://doi.org/10.1016/j.clon.2014.09.008.

Westra, W.H. (2000) 'Early glandular neoplasia of the lung', *Respiratory Research*, 1(3), 163-9, available: http://dx.doi.org/10.1186/rr28.

Whitsett, T.G., Mathews, I.T., Cardone, M.H., Lena, R.J., Pierceall, W.E., Bittner, M., Sima, C., LoBello, J., Weiss, G.J. and Tran, N.L. (2014) 'Mcl-1 mediates TWEAK/Fn14-induced non-small cell lung cancer survival and therapeutic response', *Mol Cancer Res*, 12(4), 550-9, available: http://dx.doi.org/10.1158/1541-7786.mcr-13-0458.

Wistuba, I.I. and Gazdar, A.F. (2006) 'Lung cancer preneoplasia', *Annu Rev Pathol*, 1, 331-48.

Wittlinger, M., Grabenbauer, G.G., Sprung, C.N., Sauer, R. and Distel, L.V. (2007) 'Time and dose-dependent activation of p53 serine 15 phosphorylation among cell lines with different radiation sensitivity', *Int J Radiat Biol*, 83(4), 245-57.

Woo, J.K., Kang, J.-H., Shin, D., Park, S.-H., Kang, K., Nho, C.W., Seong, J.K., Lee, S.-J. and Oh, S.H. (2015) 'Daurinol Enhances the Efficacy of Radiotherapy in Lung Cancer via Suppression of Aurora Kinase A/B Expression', *Molecular Cancer Therapeutics*, 14(7), 1693-1704.

Wu, C.-T., Lin, T.-Y., Hsu, H.-Y., Sheu, F., Ho, C.-M. and Chen, E.I.T. (2011) 'Ling Zhi-8 mediates p53-dependent growth arrest of lung cancer cells proliferation via the ribosomal protein S7-MDM2-p53 pathway', *Carcinogenesis*, 32(12), 1890-1896, available: http://dx.doi.org/10.1093/carcin/bgr221.

Xiao, Z., Chen, Z., Gunasekera, A.H., Sowin, T.J., Rosenberg, S.H., Fesik, S. and Zhang, H. (2003) 'Chk1 Mediates S and G2 Arrests through Cdc25A Degradation in Response to DNA-damaging Agents', *Journal of Biological Chemistry*, 278(24), 21767-21773, available: http://dx.doi.org/10.1074/jbc.M300229200.

Xu, J., Yue, C.F., Zhou, W.H., Qian, Y.M., Zhang, Y., Wang, S.W., Liu, A.W. and Liu, Q. (2014) 'Aurora-A contributes to cisplatin resistance and lymphatic

metastasis in non-small cell lung cancer and predicts poor prognosis', *J Transl Med*, 12, 200, available: http://dx.doi.org/10.1186/1479-5876-12-200.

Xu, N., Lao, Y., Zhang, Y. and Gillespie, D.A. (2012) 'Akt: a double-edged sword in cell proliferation and genome stability', *Journal of oncology*, 2012, 951724-951724, available: http://dx.doi.org/10.1155/2012/951724.

Xu, Z.-X., Zou, W.-X., Lin, P. and Chang, K.-S. (2005) 'A Role for PML3 in Centrosome Duplication and Genome Stability', *Molecular Cell*, 17(5), 721-732, available: http://dx.doi.org/https://doi.org/10.1016/j.molcel.2005.02.014.

Yabuta, N., Mukai, S., Okamoto, A., Okuzaki, D., Suzuki, H., Torigata, K., Yoshida, K., Okada, N., Miura, D., Ito, A., Ikawa, M., Okabe, M. and Nojima, H. (2013) 'N-terminal truncation of Lats1 causes abnormal cell growth control and chromosomal instability', *Journal of Cell Science*, 126(2), 508.

Yacoub, A., McKinstry, R., Hinman, D., Chung, T., Dent, P. and Hagan, M.P. (2003) 'Epidermal growth factor and ionizing radiation up-regulate the DNA repair genes XRCC1 and ERCC1 in DU145 and LNCaP prostate carcinoma through MAPK signaling', *Radiat Res*, 159(4), 439-52.

Yalman, D. and Selek, U. (2015) 'Stereotactic ablative radiotherapy (SABR) in operable early stage non-small cell lung cancer (NSCLC) patients: challenge to claim being undisputed gold standard', *Ann Transl Med*, 3(11), 150, available: http://dx.doi.org/10.3978/j.issn.2305-5839.2015.06.23.

Yamaguchi, H. and Wang, H.G. (2001) 'The protein kinase PKB/Akt regulates cell survival and apoptosis by inhibiting Bax conformational change', *Oncogene*, 20(53), 7779-86, available: http://dx.doi.org/10.1038/sj.onc.1204984.

Yan, J., Yu, J., Wu, X., Xu, T., Yu, H., Dai, J., Ma, M., Tang, H., Xu, L., Chi, Z., Si, L., Sheng, X., Cui, C., Kong, Y. and Guo, J. (2018) 'Increased AURKA Gene Copy Number Correlates with Poor Prognosis and Predicts the Efficacy of High-dose Interferon Therapy in Acral Melanoma', *J Cancer*, 9(7), 1267-1276, available: http://dx.doi.org/10.7150/jca.24013.

Yan, Y., Black, C.P. and Cowan, K.H. (2007) 'Irradiation-induced G2/M checkpoint response requires ERK1/2 activation', *Oncogene*, 26(32), 4689-98, available: http://dx.doi.org/10.1038/sj.onc.1210268.

Yan, Y., Hein, A.L., Greer, P.M., Wang, Z., Kolb, R.H., Batra, S.K. and Cowan, K.H. (2015) 'A novel function of HER2/Neu in the activation of G2/M checkpoint in response to gamma-irradiation', *Oncogene*, 34(17), 2215-26, available: http://dx.doi.org/10.1038/onc.2014.167.

Yang, C., Huang, W., Yan, L., Wang, L., Wang, W., Liu, D. and Zuo, X. (2015) 'Downregulation of the expression of B-cell lymphoma-extra large by RNA interference induces apoptosis and enhances the radiosensitivity of non-small cell lung cancer cells', *Molecular Medicine Reports*, 12(1), 449-455.

Yang, G., Chang, B., Yang, F., Guo, X., Cai, K.Q., Xiao, X.S., Wang, H., Sen, S., Hung, M.C., Mills, G.B., Chang, S., Multani, A.S., Mercado-Uribe, I. and Liu, J. (2010) 'Aurora kinase A promotes ovarian tumorigenesis through dysregulation of the cell cycle and suppression of BRCA2', *Clin Cancer Res*, 16(12), 3171-81, available: http://dx.doi.org/10.1158/1078-0432.ccr-09-3171.

Yang, H., He, L., Kruk, P., Nicosia, S.V. and Cheng, J.Q. (2006) 'Aurora-A induces cell survival and chemoresistance by activation of Akt through a p53-dependent manner in ovarian cancer cells', *International Journal of Cancer*, 119(10), 2304-2312, available: http://dx.doi.org/10.1002/ijc.22154.

Yang, H.J., Kim, N., Seong, K.M., Youn, H. and Youn, B. (2013) 'Investigation of radiation-induced transcriptome profile of radioresistant non-small cell lung cancer A549 cells using RNA-seq', *PLoS One*, 8(3), e59319, available: http://dx.doi.org/10.1371/journal.pone.0059319.

Yang, J.-Y., Xia, W. and Hu, M.C.T. (2006) 'Ionizing radiation activates expression of FOXO3a, Fas ligand, and Bim, and induces cell apoptosis', *International journal of oncology*, 29(3), 643-648.

Yang, L., Fang, J. and Chen, J. (2017) 'Tumor cell senescence response produces aggressive variants', *Cell Death Discovery*, 3, 17049, available: http://dx.doi.org/10.1038/cddiscovery.2017.49.

Yang, L., Zhou, Q., Chen, X., Su, L., Liu, B. and Zhang, H. (2016) 'Activation of the FAK/PI3K pathway is crucial for AURKA-induced epithelial-mesenchymal transition in laryngeal cancer', *Oncol Rep*, available: http://dx.doi.org/10.3892/or.2016.4872.

Yang, N., Wang, C., Wang, Z., Zona, S., Lin, S.X., Wang, X., Yan, M., Zheng, F.M., Li, S.S., Xu, B., Bella, L., Yong, J.S., Lam, E.W.F. and Liu, Q. (2017) 'FOXM1 recruits nuclear Aurora kinase A to participate in a positive feedback loop essential for the self-renewal of breast cancer stem cells', *Oncogene*, 36(24), 3428-3440, available: http://dx.doi.org/10.1038/onc.2016.490.

Yang, X., Li, H., Zhou, Z., Wang, W.-H., Deng, A., Andrisani, O. and Liu, X. (2009) 'Plk1-mediated phosphorylation of Topors regulates p53 stability', *The Journal*

of biological chemistry, 284(28), 18588-18592, available: http://dx.doi.org/10.1074/jbc.C109.001560.

Yarden, R.I., Pardo-Reoyo, S., Sgagias, M., Cowan, K.H. and Brody, L.C. (2002) 'BRCA1 regulates the G2/M checkpoint by activating Chk1 kinase upon DNA damage', *Nat Genet*, 30(3), 285-289.

Yasui, Y., Urano, T., Kawajiri, A., Nagata, K.-i., Tatsuka, M., Saya, H., Furukawa, K., Takahashi, T., Izawa, I. and Inagaki, M. (2004) 'Autophosphorylation of a Newly Identified Site of Aurora-B Is Indispensable for Cytokinesis', *Journal of Biological Chemistry*, 279(13), 12997-13003.

Yazdi, P.T., Wang, Y., Zhao, S., Patel, N., Lee, E.Y.H.P. and Qin, J. (2002) 'SMC1 is a downstream effector in the ATM/NBS1 branch of the human S-phase checkpoint', *Genes & Development*, 16(5), 571-582, available: http://dx.doi.org/10.1101/gad.970702.

Ye, A.A., Torabi, J. and Maresca, T.J. (2016) 'Aurora A Kinase Amplifies a Midzone Phosphorylation Gradient to Promote High-Fidelity Cytokinesis', *Biol Bull*, 231(1), 61-72, available: http://dx.doi.org/10.1086/689591.

Yee, K.W.L., Chen, H.-W.T., Hedley, D.W., Chow, S., Brandwein, J., Schuh, A.C., Schimmer, A.D., Gupta, V., Sanfelice, D., Johnson, T., Le, L.W., Arnott, J., Bray, M.R., Sidor, C. and Minden, M.D. (2016) 'A phase I trial of the aurora kinase inhibitor, ENMD-2076, in patients with relapsed or refractory acute myeloid leukemia or chronic myelomonocytic leukemia', *Investigational New Drugs*, 34(5), 614-624, available: http://dx.doi.org/10.1007/s10637-016-0375-2.

Yue, X., Zhao, Y., Xu, Y., Zheng, M., Feng, Z. and Hu, W. (2017) 'Mutant p53 in Cancer: Accumulation, Gain-of-Function, and Therapy', *Journal of Molecular Biology*, 429(11), 1595-1606, available: http://dx.doi.org/https://doi.org/10.1016/j.jmb.2017.03.030.

Yun, M., Han, Y.-H., Yoon, S.H., Kim, H.Y., Kim, B.-Y., Ju, Y.-J., Kang, C.-M., Jang, S.H., Chung, H.-Y., Lee, S.-J., Cho, M.-H., Yoon, G., Park, G.H., Kim, S.H. and Lee, K.-H. (2009) 'p31^{comet} Induces Cellular Senescence through p21 Accumulation and Mad2 Disruption', *Molecular Cancer Research*, 7(3), 371.

Zhang, M.Y., Liu, X.X., Li, H., Li, R., Liu, X. and Qu, Y.Q. (2018) 'Elevated mRNA Levels of AURKA, CDC20 and TPX2 are associated with poor prognosis of smoking related lung adenocarcinoma using bioinformatics analysis', *Int J Med Sci*, 15(14), 1676-1685, available: http://dx.doi.org/10.7150/ijms.28728.

Zhang, X., Ems-McClung, S.C. and Walczak, C.E. (2008) 'Aurora A Phosphorylates MCAK to Control Ran-dependent Spindle Bipolarity', *Molecular Biology of the Cell*, 19(7), 2752-2765, available: http://dx.doi.org/10.1091/mbc.E08-02-0198.

Zhang, X.-P., Liu, F. and Wang, W. (2011) 'Two-phase dynamics of p53 in the DNA damage response', *Proceedings of the National Academy of Sciences of the United States of America*, 108(22), 8990-8995, available: http://dx.doi.org/10.1073/pnas.1100600108.

Zhao, Y. and Adjei, A.A. (2015) 'Targeting Angiogenesis in Cancer Therapy: Moving Beyond Vascular Endothelial Growth Factor', *The oncologist*, 20(6), 660-673, available: http://dx.doi.org/10.1634/theoncologist.2014-0465.

Zhao, Z.S., Lim, J.P., Ng, Y.W., Lim, L. and Manser, E. (2005) 'The GIT-associated kinase PAK targets to the centrosome and regulates Aurora-A', *Mol Cell*, 20(2), 237-49, available: http://dx.doi.org/10.1016/j.molcel.2005.08.035.

Zheng, F., Yue, C., Li, G., He, B., Cheng, W., Wang, X., Yan, M., Long, Z., Qiu, W., Yuan, Z., Xu, J., Liu, B., Shi, Q., Lam, E.W.F., Hung, M.-C. and Liu, Q. (2016) 'Nuclear AURKA acquires kinase-independent transactivating function to enhance breast cancer stem cell phenotype', *Nat Commun*, 7, available: http://dx.doi.org/10.1038/ncomms10180.

Zheng, F.M., Long, Z.J., Hou, Z.J., Luo, Y., Xu, L.Z., Xia, J.L., Lai, X.J., Liu, J.W., Wang, X., Kamran, M., Yan, M., Shao, S.J., Lam, E.W., Wang, S.W., Lu, G. and Liu, Q. (2014) 'A novel small molecule aurora kinase inhibitor attenuates breast tumor-initiating cells and overcomes drug resistance', *Mol Cancer Ther*, 13(8), 1991-2003, available: http://dx.doi.org/10.1158/1535-7163.mct-13-1029.

Zheng, X., Chi, J., Zhi, J., Zhang, H., Yue, D., Zhao, J., Li, D., Li, Y., Gao, M. and Guo, J. (2018) 'Aurora-A-mediated phosphorylation of LKB1 compromises LKB1/AMPK signaling axis to facilitate NSCLC growth and migration', *Oncogene*, 37(4), 502-511, available: http://dx.doi.org/10.1038/onc.2017.354.

Zhou, H., Kuang, J., Zhong, L., Kuo, W.-l., Gray, J., Sahin, A., Brinkley, B. and Sen, S. (1998) 'Tumour amplified kinase STK15/BTAK induces centrosome amplification, aneuploidy and transformation', *Nat Genet*, 20(2), 189-193.

Zhou, N., Singh, K., Mir, M.C., Parker, Y., Lindner, D., Dreicer, R., Ecsedy, J.A., Zhang, Z., Teh, B.T., Almasan, A. and Hansel, D.E. (2013) 'The investigational Aurora kinase A inhibitor MLN8237 induces defects in cell viability and cell-cycle progression in malignant bladder cancer cells in vitro and in vivo', *Clinical cancer research : an official journal of the American*

Association for Cancer Research, 19(7), 1717-1728, available: http://dx.doi.org/10.1158/1078-0432.CCR-12-2383.

Zhu, C., Bossy-Wetzel, E. and Jiang, W. (2005) 'Recruitment of MKLP1 to the spindle midzone/midbody by INCENP is essential for midbody formation and completion of cytokinesis in human cells', *Biochemical Journal*, 389(Pt 2), 373-381, available: http://dx.doi.org/10.1042/BJ20050097.

Zhu, Y.M., Azahri, N.S., Yu, D.C. and Woll, P.J. (2008) 'Effects of COX-2 inhibition on expression of vascular endothelial growth factor and interleukin-8 in lung cancer cells', *BMC Cancer*, 8, 218, available: http://dx.doi.org/10.1186/1471-2407-8-218.

Zimniak, T., Fitz, V., Zhou, H., Lampert, F., Opravil, S., Mechtler, K., Stolt-Bergner, P. and Westermann, S. (2012) 'Spatiotemporal Regulation of Ipl1/Aurora Activity by Direct Cdk1 Phosphorylation', *Current Biology*, 22(9), 787-793, available: http://dx.doi.org/http://dx.doi.org/10.1016/j.cub.2012.03.007.